

Springer Series in Chemical Physics 101

Yoshio Ono
Hideshi Hattori

Solid Base Catalysis



Tokyo Institute of Technology
Press



Springer

Springer Series in
CHEMICAL PHYSICS

Series Editors: A. W. Castleman, Jr. J. P. Toennies K. Yamanouchi W. Zinth

The purpose of this series is to provide comprehensive up-to-date monographs in both well established disciplines and emerging research areas within the broad fields of chemical physics and physical chemistry. The books deal with both fundamental science and applications, and may have either a theoretical or an experimental emphasis. They are aimed primarily at researchers and graduate students in chemical physics and related fields.

Please view available titles in *Springer Series in Chemical Physics*
on series homepage <http://www.springer.com/series/676>

Yoshio Ono
Hideshi Hattori

Solid Base Catalysis



Tokyo Institute of Technology
Press



Springer

Yoshio Ono

Professor Emeritus, Tokyo Institute of Technology, Japan

E-Mail: onoy@u01.gate01.com

Hideshi Hattori

Professor Emeritus, Hokkaido University, Japan

E-Mail: hattorih@khaki.plala.or.jp

Series Editors:

Professor A.W. Castleman, Jr.

Department of Chemistry, The Pennsylvania State University
152 Davey Laboratory, University Park, PA 16802, USA

Professor J.P. Toennies

Max-Planck-Institut für Strömungsforschung
Bunsenstrasse. 10, 37073 Göttingen, Germany

Professor K. Yamanouchi

University of Tokyo, Department of Chemistry
Hongo 7-3-1, 113-0033 Tokyo, Japan

Professor W. Zinth

Universität München, Institut für Medizinische Optik
Öttingerstr. 67, 80538 München, Germany

Springer Series in Chemical Physics ISSN 0172-6218

ISBN 978-4-7692-0492-3 (Japan)

ISBN 978-3-642-18338-6

ISBN 978-3-642-18339-3 (eBook)

DOI 10.1007/978-3-642-18339-3

Springer Heidelberg Dordrecht London New York

Library of Congress Control Number:

© Springer-Verlag Berlin Heidelberg and Tokyo Institute of Technology Press 2011

This work is subject to copyright. All rights are reserved, whether the whole or part of the material is concerned, specifically the rights of translation, reprinting, reuse of illustrations, recitation, broadcasting, reproduction on microfilm or in any other way, and storage in data banks. Duplication of this publication or parts thereof is permitted only under the provisions of the German Copyright Law of September 9, 1965, in its current version, and permission for use must always be obtained from Springer. Violations are liable to prosecution under the German Copyright Law.

The use of general descriptive names, registered names, trademarks, etc. in this publication does not imply, even in the absence of a specific statement, that such names are exempt from the relevant protective laws and regulations and therefore free for general use.

Cover: eStudio Calamar Steinen

Printed on acid-free paper

9 8 7 6 5 4 3 2 1

Springer is a part of Springer Science+Business Media (www.springer.com)

Preface

This volume offers a comprehensive survey of solid base catalysts and their applications to chemical reactions. Fewer efforts have been devoted to solid base catalysis in contrast to the enormous number of studies on the catalysis by solid acids. In 1970, Professor Kozo Tanabe published *Solid Acids and Bases*, an epoch-making title which made the term “solid base” more popular in the catalysis community. The work cited important research done in the 1950's and 1960's on catalysis by solid acids and bases. In 1989, *New Solid Acids and Bases* was published by Tanabe, Misono, and the present authors as a follow-up volume to *Solid Acids and Bases*, summarizing new developments in the field in the 1970's and 1980's. The two books dealt with both solid acids and solid bases, but emphasis was more on the former, reflecting the trend in those decades. Since the early 1990's, tremendous developments have been made in both catalytic materials and the solid base-catalyzed reactions. This is because the environmentally benign nature of solid base catalysis has been recognized.

Solid base catalysts have many advantages over liquid bases. Many organic reactions proceed in liquid phase in the presence of soluble bases such as sodium hydroxide. Usually more than a stoichiometric amount of base is required and a stoichiometric amount of a metal salt such as sodium chloride is formed. Furthermore, solid bases present fewer disposal problems, while allowing easier separation and recovery of products, catalysts and solvents. They are also non-corrosive. Another important advantage of solid bases over homogeneous catalysts concerns the solvent. In homogeneous phase reactions, a base catalyst and reactant(s) must be soluble in a solvent. This restricts greatly the selection of the solvent. In solid base-catalyzed reactions, on the other hand, solvents must dissolve only reactants (and products). The reactions can be performed without solvents or even in the gas phase. Release from restrictions in solvent selection opens up more opportunities for finding novel reaction systems. These advantages of solid base catalysis provide much more environmentally benign reaction systems than systems using liquid bases. As a consequence, the application of solid base catalysts in organic synthesis is expanding. The significant role of solid base catalysis in greener chemistry is described through many examples in this volume.

The present work comprises six chapters. In Chapter 1, the concept and importance of solid base catalysis are described. Chapter 2 covers various methods for characterization of solid bases, including spectroscopic methods and test reactions. Chapters 3 and 4 deal with the preparation and properties of solid

base materials. In Chapters 5 and 6, a variety of reactions catalyzed by solid bases are surveyed in detail. Throughout the volume, the reader will gain an overall view of catalysis by solid bases and discover the versatility of the reactions to which solid base catalysts can be applied.

Both authors express deep gratitude to Professor Kozo Tanabe, who opened up the vistas of solid base catalysis and always inspired them through his enthusiasm for the science of catalysis. Y. O. expresses his heartfelt thanks to the late Professor Tominaga Keii for his long-time encouragement.

Specific thanks are also due to Professor Chuah Gaik Khan (National University of Singapore), Dr. Hideto Tsuji (Mitsubishi Chemical Corp.), Professor Toshihide Baba (Tokyo Institute of Technology), and Professor Masaki Okamoto (Tokyo Institute of Technology) for their contribution to the completion of this volume. We also thank Mr. Ippei Ohta of Tokyo Institute of Technology Press, who handled the editing and publication. Last but not least, we are most grateful to the Foundation for the Promotion of Science and Engineering (Rikogaku Shinkokai) for its varied and generous support.

November 2010

Yoshio Ono
Hideshi Hattori

Contents

Preface.....	v
1. Introduction	1
1.1 Solid Bases and Base-catalyzed Reactions.....	1
References	2
1.2 Advantages of Solid Bases	3
References	5
1.3 Role of Solid Base and Basic Sites as a Catalyst	5
1.3.1 Definition of acid and base	5
1.3.2 Abstraction of protons	6
1.3.3 Activation of reactants without proton abstraction	6
Reference.....	6
1.4 Cooperative Action of Acidic and Basic Sites	6
References	8
1.5 Classification of Base Catalysts.....	9
2. Characterization of Solid Base Catalysts	11
2.1 Methods of Characterization	11
Reference.....	11
2.2 Indicator Method	11
2.2.1 Definition of H_- acidity function in homogeneous phase.....	11
2.2.2 H_- Scale of basic sites on solid surfaces.....	12
2.2.3 Determination of the number of solid bases by titration	13
2.2.4 Drawbacks of indicator methods	15
References	16
2.3 Adsorption-Desorption of Probe Molecules.....	16
2.3.1 Adsorption of probe molecules	16
2.3.2 Poisoning method	18
2.3.3 Temperature-programmed desorption	19
2.3.4 Heat of adsorption	22

	References	24
2.4	Spectroscopic Studies of Solid Bases through Interaction with Probe Molecules	24
2.4.1	Infrared spectroscopy of adsorbed carbon dioxide.....	25
2.4.2	Spectroscopic studies of adsorbed pyrrole	29
2.4.3	Infrared and MAS NMR spectroscopy of adsorbed CHCl_3 and CDCl_3	31
2.4.4	Infrared spectroscopy of adsorbed alkynes	33
2.4.5	Adsorption of nitromethane.....	36
2.4.6	^{13}C MAS NMR of adsorbed methyl iodide	37
	References	40
2.5	Test Reactions	41
2.5.1	Characterization of basic sites by test reactions.....	41
2.5.2	Isomerization of butenes.....	42
2.5.3	Dehydration and dehydrogenation of alcohols.....	47
2.5.4	Reaction of 2-methyl-3-buten-2-ol.....	55
2.5.5	Knoevenagel condensation.....	60
2.5.6	Aldol addition of acetone to diacetone alcohol and retroaldolization of diacetone alcohol	63
2.5.7	Cyclization of acetylacetone.....	65
	References	66
3.	Preparation and Catalytic Properties of Solid Base Catalysts—	
	I. Metal Oxides.....	69
3.1	Alkaline Earth Oxides	69
3.1.1	Generation of active sites	69
3.1.2	Preparation.....	72
3.1.3	Characterization of basic sites	75
3.1.4	Type of reaction vs. optimum strength of basic site.....	87
	References	89
3.2	Rare Earth Oxides.....	91
3.2.1	Preparation.....	91
3.2.2	Characterization.....	92
3.2.3	Catalytic properties.....	93
	References	96
3.3	Zirconium Dioxide	96
3.3.1	Preparation and phase change	97
3.3.2	Characterization.....	102

3.3.3	Catalytic properties.....	104
3.3.4	Morphology dependence	108
	References	110
3.4	Titanium Dioxide.....	111
3.4.1	Preparation.....	111
3.4.2	Characterization.....	113
3.4.3	Catalytic properties.....	113
	References	115
3.5	Zinc Oxide	115
3.5.1	Preparation.....	115
3.5.2	Characterization.....	116
3.5.3	Catalytic properties.....	117
	References	118
3.6	Alumina	118
3.6.1	Structure and preparation of alumina	119
3.6.2	Surface properties of alumina.....	121
3.6.3	Catalytic properties.....	124
	References	127
3.7	Mixed Oxides	128
3.7.1	Mixed oxides containing MgO.....	129
3.7.2	Mixed oxides containing CeO ₂	131
3.7.3	Mixed oxides containing Al ₂ O ₃	132
	References	133
3.8	Metal Oxides Loaded with Alkali Metal Compounds.....	133
3.8.1	Alkali metal compounds-loaded Al ₂ O ₃	134
3.8.2	Alkali metal compound-loaded alkaline earth oxides	136
3.8.3	Alkali metal compound-loaded SiO ₂ and other supports	138
3.8.4	KF/Al ₂ O ₃ and CsF/Al ₂ O ₃	141
3.8.5	KNH ₂ /Al ₂ O ₃	146
	References	148
3.9	Metal Oxides and Carbon Materials Loaded with Alkali Metals.....	149
3.9.1	Preparation of alkali metal-modified catalysts	150
3.9.2	State of alkali metal	150
3.9.3	Strength of basic sites.....	151
3.9.4	Model of basic sites	153
3.9.5	Catalytic properties.....	153
	References	156

4. Preparation and Catalytic Properties of Solid Base Catalysts —	
II. Specific Materials for Solid Bases	157
4.1 Hydrotalcite and Mixed Oxides Derived from Hydrotalcite	157
4.1.1 Structure of hydrotalcite	157
4.1.2 Synthesis of hydrotalcite	158
4.1.3 Thermal decomposition of hydrotalcite.....	159
4.1.4 Rehydration of calcined hydrotalcite.....	160
4.1.5 Introduction of anions into interlayers	160
4.1.6 Application of hydrotalcite-derived materials to base catalysis	162
References	168
4.2 Zeolites	170
4.2.1 Alkali cation-exchanged zeolites.....	170
4.2.2 Alkali metal oxide-loaded zeolites	178
4.2.3 Alkali metal-loaded zeolites	184
References	187
4.3 Metal Phosphates.....	188
4.3.1 Metal phosphates	188
4.3.2 Hydroxyapatite, fluoroapatite	189
4.3.3 Natural phosphate	191
References	191
4.4 Metal Oxynitrides.....	192
4.4.1 Preparation.....	192
4.4.2 Nitridation mechanisms.....	194
4.4.3 Characterization of basic sites	196
4.4.4 Catalytic properties.....	196
References	201
4.5 Anion Exchange Resins.....	201
References	205
4.6 Amines and Ammonium Ions Tethered to Solid Surfaces	205
4.6.1 Loading of basic functional groups to high surface-area silica materials	205
4.6.2 Catalysis using basic functional groups tethered to silica materials	211
4.6.3 Acid-base bifunctional catalysis.....	213
4.6.4 Catalysis by occluded structure directing agent	216
References	217

5. Reactions Catalyzed by Solid Bases.....	219
5.1 Isomerization of Alkenes and Alkynes.....	219
5.1.1 Isomerization of alkenes.....	219
5.1.2 Isomerization of alkynes.....	222
References	223
5.2 Aldol Addition and Aldol Condensation.....	223
5.2.1 Condensation of propanal and butanal	223
5.2.2 Condensation of glyceraldehyde acetonide with acetone.....	225
5.2.3 Claisen-Schmidt condensation	225
5.2.4 Mukaiyama aldol reactions.....	228
5.2.5 Reactions of aldehydes and imines with ethyl diazoacetate.....	229
5.2.6 Vapor phase aldol condensation	230
References	231
5.3 Nitroaldol Reactions (Henry Reaction).....	232
References	236
5.4 Knoevenagel Condensation	237
5.4.1 Catalysts	237
5.4.2 Catalytic reactions	242
References	245
5.5 Michael Addition (Conjugated Addition)	246
5.5.1 Addition of active methylene compounds to α,β -unsaturated carbonyl compounds.....	246
5.5.2 Michael addition of H_2S and thiols.....	255
5.5.3 Addition of amines to α,β -unsaturated compounds	258
5.5.4 Addition of amines to butadiene.....	261
5.5.5 Cyanoethylation of alcohols	261
5.5.6 Addition of alcohol to vinyl ketones and vinyl sulfones.....	263
References	264
5.6 Tishchenko Reactions.....	265
References	269
5.7 Alkylation Reactions	269
5.7.1 Alkylation of phenols	269
5.7.2 Side-chain alkylation of alkyl aromatics	276
5.7.3 Synthesis of α,β -unsaturated compounds from activated methylene compounds and methanol	279
5.7.4 Condensation of alcohols (Guerbert reaction).....	282
5.7.5 Alkylation of nitriles (<i>C</i> -alkylation).....	283
5.7.6 <i>N</i> -Alkylation reactions.....	284

5.7.7	<i>S</i> -Methylation of thiols with dimethyl carbonate (<i>S</i> -alkylation)	289
	References	289
5.8	Addition Reactions	291
5.8.1	Addition to epoxides	291
5.8.2	Nucleophilic addition of alkynes	295
5.8.3	Baylis-Hillman reaction	300
5.8.4	Cyano- <i>O</i> -ethoxycarbonylation of carbonyl compounds	302
	References	303
5.9	Hydrogenation Reactions	303
5.9.1	Hydrogenation of alkenes	303
5.9.2	Hydrogenation of butadienes	304
5.9.3	Hydrogenation of benzoic acid	306
	References	307
5.10	Transfer Hydrogenation Reactions (Meerwein-Ponndorf-Verley Reduction and Oppenauer Oxidation)	308
5.10.1	Reaction mechanism over solid base catalysts	308
5.10.2	Hydrogenation of ketones with alcohols	310
5.10.3	Reduction of nitro-compounds and nitriles with alcohols	315
5.10.4	Oppenauer oxidation	315
5.10.5	Reduction with hydrocarbons	318
	References	318
5.11	Esterification and Transesterification	319
5.11.1	Catalysts for esterification and transesterification	319
5.11.2	Reactions of alkyl carbonates with acids and alcohols	324
5.11.3	Reaction of alkyl carbonates with amines	326
5.11.4	Synthesis of monoglyceride	328
5.11.5	Synthesis of polyoxyglycol esters	329
	References	329
5.12	Liquid-phase Oxidation	330
5.12.1	Oxidation with molecular oxygen	330
5.12.2	Epoxidation of alkenes with alkylperoxide	332
5.12.3	Epoxidation of alkenes with hydrogen peroxide	333
5.12.4	Baeyer-Villiger oxidation with hydrogen peroxide	338
5.12.5	Oxidation of thiols, thioethers and pyridines	338
5.12.6	Oxidation of alcohols with molecular oxygen	338
5.12.7	Oxidation of amines with hydrogen peroxide	339
	References	340

6. Solid Base Catalysts for Specific Subjects	343
6.1 Solid Base Catalysts for Environmentally Benign Chemistry	343
6.1.1 Biodiesel synthesis	343
6.1.2 Synthesis of dimethyl carbonate.....	347
6.1.3 Reaction of H ₂ S and SO ₂	350
6.1.4 Environmentally benign synthesis of fine chemicals	351
References	357
6.2 Synthesis and Ring Transformation of Heterocycles	360
6.2.1 Synthesis of heterocycles	360
6.2.2 Ring transformation of heterocycles	365
References	369
6.3 Reactions of Phosphorus Compounds	369
6.3.1 Wittig reactions	369
6.3.2 Wittig-Horner reactions.....	370
6.3.3 Pudovik reactions	373
References	375
6.4 Reactions of Silicon Compounds	375
6.4.1 Substitution reactions at silicon.....	375
6.4.2 Ring opening of epoxides with trimethylsilyl cyanide.....	380
6.4.3 Addition of silanes to double bonds	381
6.4.4 Reaction of silica with dimethyl carbonate	387
References	389
6.5 Asymmetric Synthesis by Solid Base Catalysts	390
6.5.1 Asymmetric synthesis by metal oxide in the presence of chiral auxiliaries	390
6.5.2 Asymmetric synthesis by supported chiral compounds	393
6.5.3 Asymmetric synthesis by chiral zeotype materials	396
References	396
6.6 Solid Bases as Catalyst Support	396
6.6.1 Enhancing effect of solid bases on metal catalysts	396
6.6.2 Bifunctional catalysis	400
References	408
Subject Index	411
Chemical Formula Index.....	419

1.

Introduction

1.1 Solid Bases and Base-catalyzed Reactions

An enormous number of studies have been devoted to heterogeneous acidic catalysts (solid acid catalysts). This is mainly because solid acids have been used as catalysts in many industrially important processes in petroleum refining and the production of petrochemicals. Such processes include naphtha cracking, xylene isomerization, alkylation of aromatics, etc.

In contrast with extensive studies on solid acids, fewer efforts have been devoted to heterogeneous basic catalysts (solid base catalysts). The first study on the heterogeneous base catalyst was reported by Pines and Haag, who showed that the sodium metal dispersed on alumina was an effective catalyst for double-bond isomerization of alkenes.¹⁾ In 1970, Tanabe published a book entitled *Solid Acids and Bases*.²⁾ This was an epoch-making book which made the term “solid base” more popular in the catalysis community. Most of the important works done in the 1950s and 1960s are cited in the book. Since then, studies of solid bases made extensive progress in terms of catalyst materials and catalytic reactions, although the development was slower compared with that of solid acids.

In 1972, Tanabe and coworkers reported that calcium oxide and magnesium oxide exhibited enormously high catalytic activities for 1-butene isomerization when the catalysts were pretreated under vacuum.^{3,4)} This work clearly indicated the importance of the methods of preparation and pretreatment of the base catalysts. In the 1970s, Tanabe and his coworkers studied very extensively the basic properties of various metal oxides and mixed metal oxides and the numerous reactions catalyzed by these compounds. Meantime, various new materials came in as a family of solid bases. For example, Yashima et al. reported that side-chain alkylation of toluene was catalyzed by alkali cation-exchanged X and Y zeolites and the catalytic activities were attributed to the basic properties of zeolites.⁵⁾ Various methodologies for characterizing the basic properties of solid surfaces and for determining the reaction intermediates were also developed. In 1989, Tanabe et al. published *New Solid Acids and Basis*, summarizing the developments in the area in the 1970s and 1980s.⁶⁾

Development of solid base materials and solid-base catalyzed reactions has continued. The comprehensive review articles published in recent years clearly demonstrate that this development is accelerated as the solid bases are recognized to be environmentally friendly or benign catalysts. This will also be easily seen in the lists of the solid bases and the reactions in Chapters 3 to 6.

The followings are representative review articles on solid bases published since 1995.

- * H. Hattori, "Heterogeneous basic catalysis" *Chem. Rev.*, **95**, 527 (1995).
- * D. Barthomeuf, "Basic zeolites: Characterization and uses in adsorption and catalysis" *Catal. Rev.*, **38**, 521 (1996)
- * Y. Ono, T. Baba, "Selective reactions over solid base catalysts" *Catal. Today*, **338**, 21 (1997).
- * J. W. Frail, J. I. Garcia, J. Mayoral, "Base solids in the oxidation of organic compounds" *Catal. Today*, **57**, 3 (2000).
- * Y. Ono, "Catalysis by strong bases" in *Catalysis*, vol. 15, p.1, The Royal Society of Chemistry, John Wiley & Sons, 2000.
- * F. J. Dosocil, S. Bordawekar, R. J. Davis, "Catalysis by solid bases—Industry" in *Catalysis*, vol. 15, p.40, The Royal Society of Chemistry, John Wiley & Sons, 2000.
- * M. Weitkamp, U. Hunger, "Base catalysis on microporous and mesoporous materials: recent progress and perspectives" *Micropor. Mesopor. Mater.*, **48**, 255 (2001).
- * H. Hattori, "Solid base catalysts, generation of basic sites and application to organic synthesis" *Appl. Catal., A*, **222**, 247 (2001).
- * B. F. Sels, D. E. De Vos, P. A. Jacobs, "Hydrotalcite-like anionic clays in catalytic organic reactions" *Catal. Rev.*, **43**, 443 (2001).
- * Y. Ono, "Base and base catalysis" in *Encyclopedia of Catalysis*, John Wiley & Sons, 2003.
- * R. J. Davis, "Base and base catalysis" in *Encyclopedia of Catalysis*, John Wiley & Sons, 2003.
- * R. J. Davis, "New perspectives on basic zeolites as catalysts and catalyst supports" *J. Catal.*, **216**, 396 (2003).
- * Y. Ono, "Solid bases for the synthesis of fine chemicals" *J. Catal.*, **216**, 406 (2003).
- * D. Ticht, B. Coq, "Catalysis by hydrotalcites and related materials" *Cattech*, **7**, 206 (2003).
- * H. Hattori, "Solid base catalysts: generation, characterization and catalytic behavior of basic sites" *J. Jpn. Petrol. Inst.*, **47**, 67 (2003).
- * F. Figueras, "Base catalysts in the synthesis of the fine chemicals" *Topics Catal.*, **29**, 189 (2004).
- * A. Corma, S. Iborra, "Optimization of alkaline earth metal oxide and hydroxide catalysts for base-catalyzed reactions" *Adv. Catal.*, **49**, 239 (2006).
- * F. Figueras, M. L. Kantam, B. M. Choudary, "Solid base catalysts in organic synthesis" *Curr. Org. Chem.*, **10**, 1627 (2006)
- * G. Busca, "Bases and basic materials in industrial and environmental chemistry: A review of commercial process" *Ind. Eng. Chem. Res.*, **48**, 6486 (2009).

References

1. H. Pines, W. O. Haag, *J. Org. Chem.*, **23**, 328 (1958).

2. K. Tanabe, *Solid Acids and Bases*, Kodansha/Academic Press, 1970.
3. K. Tanabe, N. Yoshii, H. Hattori, *Chem. Commun.*, **1971**, 464.
4. H. Hattori, N. Yoshii, K. Tanabe, *Proceedings of the 5th International Congress on Catalysis*, 1972, Miami Beach, p.233.
5. T. Yashima, Y. Sato, T. Hayasaka, N. Hara, *J. Catal.*, **26**, 303 (1972).
6. K. Tanabe, M. Misono, Y. Ono, H. Hattori, *New Solid Acids and Bases*, Kodansha/Elsevier, 1989.

1.2 Advantages of Solid Bases

Carbanions are important intermediates in many organic reactions, such as isomerization, additions, condensations and alkylations. They are formed by the abstraction of a proton from a C-H bond of an organic molecule by bases conventionally in homogeneous phases

These organic reactions often require a stoichiometric amount of liquid bases to generate carbanions and produce a stoichiometric amount of metal salts as by-product. For example, the methylation of phenylacetonitrile with methyl iodide proceeds in the presence of bases under a phase-transfer condition.



In this case, more than a stoichiometric amount of sodium hydroxide is required to neutralize the hydrogen iodide produced and to keep the system basic. Furthermore, a stoichiometric amount of sodium iodide is inevitably formed and has to be disposed in an appropriate manner. Thus, the reaction is non-catalytic. Therefore, the demand for catalytic reactions to avoid these problems is high.

The methylation of phenylacetonitrile can be performed by using methanol or dimethyl carbonate as the methylating agent and alkali-exchanged zeolites as catalysts. The reaction can be performed in vapor phase.¹⁾



Here, the reactions are catalytic; no inorganic salts like sodium iodide are formed. There is no need to use a stoichiometric amount of base compounds. In this sense, the reactions can be free from a large amount of wastes and, thus, atomically more efficient. Furthermore, in this particular system, the use of toxic reagents such as methyl iodide or dimethyl sulfate as a methylating agent can be avoided.

Another big advantage of solid bases over homogeneous bases concerns the solvent. In homogeneous phase reactions, a base catalyst and reactants must be soluble in a solvent. This restricts very much the selection of the solvent. Because of this, toxic solvents such as methyl chloride and dimethyl sulfoxide (DMSO) are often chosen. Otherwise, one has to use a phase-transfer system as in the case of reaction (1.2.1). This may cause tedious problems in the workup processes such as separation. In solid-base catalyzed reactions, solvents must dissolve only reactants (and products). This considerably expands the choice of solvents. It is

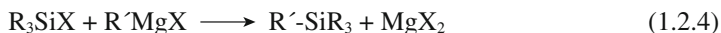
known that the solvent effects in solid-base catalyzed reactions are different from those in the corresponding homogeneous reactions.^{2,3)} For example, in the Knoevenagel condensation of 2-furaldehyde with ethyl cyanoacetate over xonotlite (calcium silicate), the best solvents are water and hydrocarbons such as pentane.²⁾ Furthermore, the reactions can be performed without any solvent.^{3,4)} And as shown in an example above, the reaction can be carried out even in vapor phase. In these cases, obviously, there is no need to separate solvents after the completion of reactions greatly simplifying the process. No wastes based on solvents such as water containing organics or organic solvents containing alkaline water are formed. Simpler separation means reduced energy requirements. Furthermore, solid bases can be used repeatedly after separation. This again serves high atom-economy in catalyst preparation. More importantly, release from restrictions of solvent selection opens up more opportunities to find new reactions.

Solutions containing bases such as sodium hydroxide are corrosive so materials resistant to corrosion must be used for the reactor and the disposal apparatus. This kind of problem does not usually arise in reaction systems using solid base catalysts.

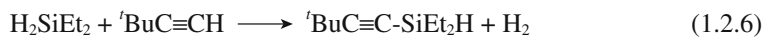
Since most fine chemicals and pharmaceuticals are synthesized either via stoichiometric or homogeneous catalytic processes and those sectors of the chemical industry generate more waste per mass of the desired product, transformation of homogeneous into heterogeneous processes using solid-base (or solid-acid) catalysts is most important in this area because of the advantages described above.

Furthermore, high activities and selectivities are often attained only by solid base catalysts for various kinds of reactions. Cooperative action of acid and basic sites enables many reactions to proceed smoothly. Such examples are found in hydrogenation, transfer hydrogenation, aldol condensation, etc. Reactions over basic catalysts usually do not suffer coking, which is a serious problem in acid-catalyzed reactions. Interaction of functionalized organic compounds such as amines with basic sites is weak compared with that with acidic sites. Thus, these molecules are not trapped on the surface and desorb more easily from the surface. Therefore, reactions involving these molecules proceed more smoothly over solid bases.

Organometallic compounds such as Grignard reagents and alkyl lithium serve as donors of a carbanion-like species. For example, Si-C bond formation can be performed by following types of reactions.



Here again, a stoichiometric use of organometallic reagents is required. Solid bases offer routes for the same products in an easier and more eco-friendly manner.



These two reactions proceed nicely in the presence of $\text{KF}/\text{Al}_2\text{O}_3$ and $\text{KNH}_2/\text{Al}_2\text{O}_3$, respectively, and the reactions are catalytic.^{5,6)}

The features of solid base catalyst systems, as described above, afford much more environmentally benign reaction systems than the systems using liquid bases. But more importantly, there is a high possibility of finding new catalytic reactions which cannot be achieved with the use of homogeneous catalysis.

References

1. Z.-H. Fu, Y. Ono, *J. Catal.*, **145**, 166 (1994).
2. P. Laszlo, *Acc. Chem. Res.*, **19**, 121 (1986).
3. X. Wang, Y.-H. Tseng, J. C. C. Chan, S. Cheng, *J. Catal.*, **233**, 266 (2005).
4. M. J. Climent, A. Corma, S. Iborra, A. Velty, *J. Catal.*, **221**, 474 (2004).
5. T. Baba, A. Kato, H. Yuasa, F. Toriyama, H. Handa, Y. Ono, *Catal. Today*, **44**, 271 (1998).
6. T. Baba, H. Yuasa, H. Handa, Y. Ono, *Catal. Lett.*, **50**, 83 (1998).

1.3 Role of Solid Base and Basic Sites as a Catalyst

1.3.1 Definition of acid and base

There are many kinds of definitions for acids and bases in homogeneous phase.¹⁾ Among them, the definitions by Brønsted-Lowley and Lewis are the most important in relation to the acid-base chemistry of solid surfaces. In the definition by Brønsted and Lowley, an acid (AH) donates a proton and a base (B^-) accepts a proton.

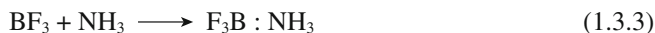


In the reverse reaction, BH is an acid and A^- is a base. The species AH and A^- are referred to as conjugate acid-base pairs. Similarly, BH and B^- are also conjugate pairs. The acids and bases in accordance with this definition are called a Brønsted acid and a Brønsted base, respectively.

In the definition by Lewis, a base ($:\text{B}$) donates a lone pair and an acid (A) accepts a lone pair.



The acids and bases in accordance with this definition are called a Lewis acid and a Lewis base, respectively. In a following reaction, NH_3 is a Lewis base and BF_3 is a Lewis acid.



The solids having the sites which serve as a Brønsted acid and/or a Lewis acid are called solid acids, and the solids having the sites which serve as a Brønsted base and/or Lewis base are called solid bases.

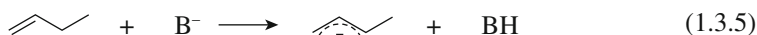
1.3.2 Abstraction of protons

On the surface of solid bases, there are specific sites or centers, which function as a base. Basic sites (centers) abstract protons from the reactant molecules (AH) to form carbanions (A^-).



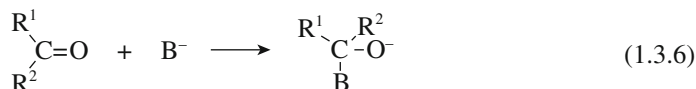
Here, the basic site B^- on the solid surface acts as a Brønsted base. Stronger bases can abstract a proton with molecules with higher pK_a values.

An example is the formation of carbanions from alkenes, which is the first step for alkene isomerization.



1.3.3 Activation of reactants without proton abstraction

Reactants such as ketones and aldehydes are often activated by bases without proton transfer, as expressed by the following equation.



Here, the basic site B^- acts as a Lewis base. This kind of interaction is important in many base-catalyzed reactions such as aldol condensation, Knoevenagel condensation and hydrogen transfer reactions,

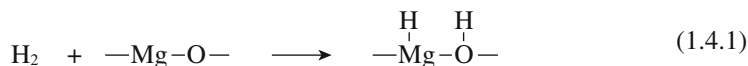
In the definition by Brønsted-Lowley, a base B^- accepts a proton from an adsorbate. In many cases, the same B^- site acts as an electron pair donor to another adsorbate. In this case, the basic site acts as a Lewis base. It should be noted that the same surface site can serve as a Brønsted base (proton acceptor) as well as a Lewis base (electron pair donor), depending on the nature of the adsorbate.

Reference

1. J. Dwyer, H. Schofield, in *Acidity and Basicity of Solids, Theory, Assessment and Utility* (ed. by J. Fraissard, L. Petrakis), NATO ASI Ser., C444, p.13, Kluwer Academic Publishers, 1994.

1.4 Cooperative Action of Acidic and Basic Sites

Magnesium oxide is an active catalyst for the hydrogenation of 1,3-butadiene. It is assumed that hydrogen heterolytically dissociates in the presence of a pair of a coordinatively unsaturated Mg^{2+} and an oxide ion.¹⁾



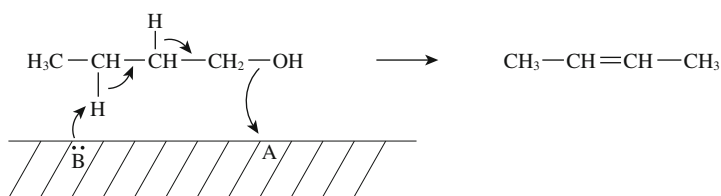


Fig 1.4.1 Concerted mechanism in 1-butanol dehydration.
Reprinted with permission from H. Pines, J. Manassen, *Advances in Catalysis*, **16**, 49 (1966) p. 75.

Here, the Mg ion serves as a Lewis acid and the oxygen ion as a base. The synergy of basic sites and acidic sites is one of the characteristics of solid acid-base catalyzed reactions. For example, dehydration of 1-butanol over alumina is considered to be the concerted action of acid and base sites on the surface (Fig. 1.4.1).²⁾

In some cases, two reactants are activated separately by acid sites and basic sites. Climent et al. proposed the scheme for aldol condensation of benzaldehyde and heptanal over amorphous aluminum phosphate (Fig. 1.4.2).³⁾ Here, the two reactants (benzaldehyde and heptanal) are activated independently by acidic (A^-H^+) and basic (B^-) sites.

Zeidan and Davis prepared mesoporous silica (SBA 15) to which a primary amino group, an acidic group, or both were tethered and carried out aldol condensation of *o*-nitrobenzaldehyde and acetone at 323 K.⁴⁾ The catalysts having both acid and amine components showed high activity. The silica with both carboxy acid and amino groups gave a conversion of 99%, while those with either carboxy or amine groups gave conversions of 0% and 33%, respectively. This again shows

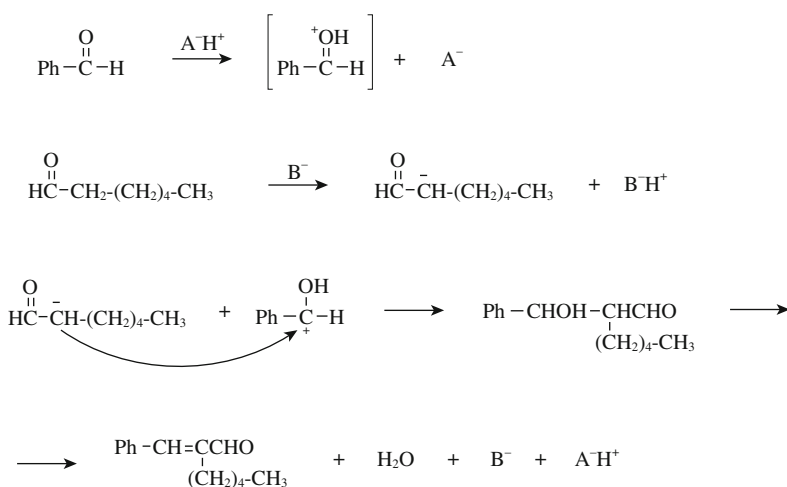


Fig. 1.4.2 Mechanism of aldol condensation.
Reprinted with permission from M. J. Climent, A. Corma, V. Fornes, R. Guil-Lopez, S. Iborra, *J. Catalysis*, **197**, 385 (2001), p.391, Scheme 4.

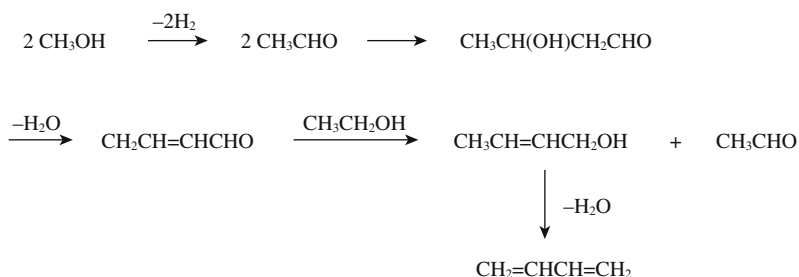
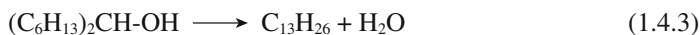


Fig. 1.4.3 Formation of butadiene from ethanol over $\text{SiO}_2\text{-MgO}$.
 Reprinted with permission from H. Niiyama, S. Mohri, E. Echigo, *Bull. Chem. Soc. Jpn.*, **45**, 655 (1972) p.659.

that a combination of weak acid and stronger base is effective in aldol condensation.

In some cases acidic sites and basic sites act at different stages of the reaction scheme. MgO , a solid base with meager acidity, is a good catalyst for transfer hydrogenation between ketones and alcohols. For example, the reaction of 7-tridecanone with 2-propanol affords 7-tridecanol in a 41% yield at 623 K. In addition, a small amount of undecene (7%) is also formed by the dehydration of the alcohol.⁵⁾



When MgO was loaded with H_3PO_4 , the acidic property of the solid developed. This enhances the dehydration of the alcohol. Thus, $\text{H}_3\text{PO}_4/\text{MgO}$ affords exclusively the alkene in a 90% yield at the same temperature.⁶⁾ Similarly, the reaction of acetophenone with 2-propanol directly affords styrene in a 100% yield over $\text{H}_3\text{PO}_4/\text{MgO}$.

In the case of butadiene formation from ethanol over $\text{SiO}_2\text{-MgO}$ mixed oxides at 653 K, a reaction scheme (Fig. 1.4.3) was proposed.⁷⁾ The reaction starts with dehydrogenation of ethanol on basic sites to form acetaldehyde, which undergoes aldol condensation on acidic or basic sites. The condensation product dehydrates on acidic sites. Transfer hydrogenation of croton aldehyde with ethanol requires both acidic and basic sites and the dehydration of crotyl alcohol to butadiene on acidic sites completes the reaction.

Many more examples of the synergy of acidic and basic sites are reviewed by Iglesia et al.⁸⁾

References

1. H. Hattori, *Chem. Rev.*, **95**, 537 (1995).
2. H. Pines, J. Manassen, *Adv. Catal.*, **16**, 49 (1966).
3. M. J. Climent, A. Corma, V. Fornés, R. Guil-Lopez, S. Iborra, *J. Catal.*, **197**, 385 (2001).

4. R. Z. Zeidan, M. E. Davis, *J. Catal.*, **247**, 379 (2007).
5. M. Gliński, A. Gadomska, *React. Kinet. Catal. Lett.*, **65**, 121 (1998).
6. J. Kijeński, M. Gliński, C. W. A. Quiroz, *Appl. Catal., A*, **150**, 77 (1997).
7. H. Niiyama, S. Morii, E. Echigoya, *Bull. Chem. Soc. Jpn.*, **45**, 655 (1972).
8. E. Iglesia, D. G. Barton, J. A. Biscardi, M. J. L. Gines, S. L. Soled, *Catal. Today*, **38**, 339 (1997).

1.5 Classification of Base Catalysts

Many kinds of materials act as solid bases. The most important classes of solid bases are classified in Table 1.5.1. The preparation and characteristics of these materials as a solid base will be described in Chapters 3 and 4.

Table 1.5.1 Classification of solid bases

Metal oxides	MgO, CaO, Al ₂ O ₃ , ZrO ₂ , La ₂ O ₃ , Rb ₂ O
Mixed oxides	SiO ₂ -MgO, SiO ₂ -CaO, MgO-La ₂ O ₃ , MgO-Al ₂ O ₃ (calcined hydrotalcite)
Alkali or alkaline earth oxides on support	Na ₂ O/SiO ₂ , MgO/SiO ₂ , Cs oxides supported on zeolites
Metal oxynitrides and metal nitrides	AlPON, partially nitrated zeolites and mesoporous silica
Alkali compounds on support	KF/Al ₂ O ₃ , K ₂ CO ₃ /Al ₂ O ₃ , KNO ₃ /Al ₂ O ₃ , NaOH/Al ₂ O ₃ , KOH/Al ₂ O ₃
Amides, imines on support	KNH ₂ /Al ₂ O ₃ , K, Y, Eu supported on zeolites from the ammoniacal solution
Alkali metals on support	Na/Al ₂ O ₃ , K/Al ₂ O ₃ , K/MgO, Na/zeolite
Anion exchangers	Anion exchange resins Hydrotalcite and modified hydrotalcite
Zeolites	K, Rb, Cs-exchanged X, Y-zeolites, ETS-10
Clays	Sepiolite, Talc
Phosphates	Hydroxyapatite, metal phosphates, natural phosphates
Amines or ammonium ions tethered to a support	Aminopropyl group/silica, MCM-41, SBA-15 Alkylammonium group/MCM-41

2.

Characterization of Solid Base Catalysts

2.1 Methods of Characterization

In order to predict the capability of solid surface as base catalysts, the basic properties of the surfaces must be clarified. The basic character or basicity includes the following factors: a) the number of basic sites, b) the origin or location of basic sites, and c) the base strength of basic sites.

These are not so easy to determine. Over the solid bases, there are often several kinds of basic sites. For example, on the surface of magnesium oxide, there are oxygen anions with different coordination numbers.¹⁾ Since the basic properties of the oxygen anions depend on the coordination number, the number and base strength of each species must be determined. In some cases, Brønsted and Lewis acid sites coexist on the surface. The heterogeneity of the surface basic sites is one of the complicating factors in determining the basic properties of solid surfaces.

As described below, there is no method that can decisively determine all three factors. Every method has its own advantages and disadvantages. Therefore, it is most desirable to use several methods in different principle.

The methodology for determining the basicity of solid surfaces may be classified as follows: a) indicator/titration methods, b) use of probe molecules; in measurements of adsorption amount, calorimetry and temperature programmed desorption, and spectroscopy of adsorbed molecules, c) test reactions, d) direct spectroscopic observation of solid surface.

Methods a), b) and c) are described in this chapter. Examples of method d) are found throughout Chapters 3 and 4.

Reference

1. H. Hattori, *Chem. Rev.*, **95**, 537 (1995).

2.2 Indicator Method

2.2.1 Definition of H_- acidity function in homogeneous phase

Discussion of the solid bases in many cases is based on the concept developed for acid-base chemistry in solutions. It is appropriate to briefly introduce the defini-

tion of H_- acidity function, one of the most important concepts in the basicity of solutions. This is the counterpart of the acidic function, H_0 , for acidic solutions.

The H_- acidity function is defined as a measure of the ability of the basic solution to abstract a proton from an acidic neutral solute, AH.¹⁾

$$H_- = pK_a - \log ([AH]/[A^-]) \quad (2.2.1)$$

To determine the H_- value of a solution, the concentrations of AH and A^- must be measured accurately. When half of a solute AH is deprotonated in the solution, i.e., $[A^-] = [AH]$, the H_- value of the solution is equal to the pK_a value of AH. The basic strength of a solution is stronger when a neutral molecule of larger pK_a values is deprotonated.

The basic strength of the solution is determined by using indicator molecules, AH, with known pK_a values. Usually, the concentration ratio, $[AH]/[A^-]$, is determined spectrophotometrically. In this way, the H_- values of various basic solutions have been determined.¹⁾ The H_- values of 5.0 mol dm⁻³ aqueous solution of NaOH and KOH at 298 K, are 15.20 and 15.44, respectively. The acidity function, H_- , is originally defined for aqueous solutions. The H_M values of 3.0 mol dm⁻³ KOCH₃ and NaOCH₃ in methanol at ca. 293 K, are 19.99 and 18.30, respectively. (For methanol solution, the term H_M is used instead of H_- ¹⁾)

It is most important to note that the acidity functions H_0 and H_- represent the properties of "solutions". The acidity functions are not a property of individual molecules (or ions), such as NaOH or OH⁻. Obviously, the H_- values are solvent dependent. It is worthy to note that the H_- acidity function is defined for solutions, which act as Brønsted bases, as seen in eq. (2.2.1).

2.2.2 H_- scale of basic sites on solid surfaces

Tanabe proposed to use the H_- scale as a measure of the strength of solid bases.²⁾ Suppose that molecules of an indicator, AH, interact with basic sites B^- on the surface,



The H_- value of the basic site, B^- , is defined as

$$H_- = pK_a - \log ([AH]_s/[A^-]_s) \quad (2.2.3)$$

Here, $[AH]_s$ and $[A^-]_s$ are the surface concentrations of AH and A^- , respectively.

Upon adsorption of AH from the solution, the solid surface exhibits the color of AH when $[AH]_s/[A^-]_s \gg 1$, while it shows the color of A^- when $[AH]_s/[A^-]_s \ll 1$.

When $[AH]_s/[A^-]_s = 1$, the H_- value of the surface basic sites are equal to the pK_a of the indicator molecule, AH.

$$H_- = pK_a \quad (2.2.4)$$

The indicators used for the measurements of basic strength are listed in Table 2.2.1.³⁾ A different set of indicators is also employed.⁴⁾ As solvent, non-polar solvents such as benzene and 2-methylheptane are used.

Table 2.2.1 Indicators used for the measurements of basic properties^{a)}

Indicators	Color		pK_a
	Acid form	Base form	
Bromothymol blue	yellow	green	7.2
Phenolphthalein	colorless	red	9.3
2,4,6-Trinitroaniline	yellow	reddish-orange	12.2
2,4-Dinitroaniline	yellow	violet	15.0
4-Chloro-2-nitroaniline	yellow	orange	17.2
4-Nitroaniline	colorless	orange	18.4
4-Chloroaniline	colorless	pink ^{b)}	26.5
Diphenylmethane	colorless	yellowish-orange	35

^{a)} Based on [reference 3, p. 15 Table 2.3].

^{b)} The color disappears upon addition of benzoic acid.

In practice, it is difficult to determine $[AH]_s$ and $[A^-]_s$. Thus, the H_- of the basic sites is determined as the highest pK_a among the pK_a values of the indicators, which exhibits the color of the conjugate base A^- on the surface. For example, when a solid gives a violet color upon adsorption of 2,4-dinitroaniline, and a yellow color upon adsorption of 4-nitroaniline, the H_- value of the basic sites on the solid lies between 15.0 and 17.2.

Experimental procedures for H_- determination are as follow.⁵⁾ The pre-dried solid (0.1 g) was immersed in dry benzene (2 mL) in a vial. One drop of a 0.1 wt% benzene solution of an indicator was added; the color change of the indicator was judged after 12 h. A more precise description is given by Take et al.⁶⁾ Measurements must be made without exposing the system to ambient air (H_2O , CO_2). Table 2.2.2 shows the list of H_- values for solid base catalysts.

Tanabe named the solid which has basic sites with H_- values higher than +26 superbase.³⁾ This definition of superbase is based on superacids which are defined as acidic solutions with Hammett acidic function H_o value of smaller than -12. This value differs by 19 H_o units from $H_o = 7$, neutral on the acid-base scale. The H_- value of +26 differs by 19 H_- units from $H_- = 7$. According to this definition, alkaline earth oxides (MgO and CaO) and Cs oxides supported on Al_2O_3 , etc., belong to the superbases. Superbases are actually very active for reactions such as alkene isomerization and side-chain alkylation of toluene.

2.2.3 Determination of the number of solid bases by titration

The number of basic sites can be determined by titration with a basic molecule and an indicator. The titration is carried out as follows. The solid is divided into several portions and each of them is dispersed in benzene and an indicator is added to be adsorbed on the basic sites. Finally, to each solution, an acidic molecule, i.e., phenol or benzoic acid, is added, but in different amounts, and the system is maintained until equilibrium is established. Phenol molecules displace the indicator adsorbed on the basic sites. If the amount of phenol is less than that of the basic sites, the surface shows the color of the conjugated base A^- of the indicator. When the amount of phenol added exceeds that of the basic sites, the surface shows the

Table 2.2.2 Basic strength (H_- values) of solid bases

Solid	H_- value	Remarks	Reference
Na/NaOH/Al ₂ O ₃	$H_- \geq +37$		7
	$+37 > H_- \geq +35$		8
KNO ₃ /Al ₂ O ₃	$+18.4 > H_- \geq +15.0$	35 wt% loading, calcined at 773 K	9
	$H_- \geq +27$	14 wt% loading	10
KI/Al ₂ O ₃	$18.4 > H_- > +15.0$	35 wt% loading, calcined at 773 K	11
Na/MgO	$H_- \geq +35$		12
K/MgO	$H_- \geq +35$	K 10%, 15%	13
	$+35.0 > H_- \geq +27$	K10% on MgO, prepared by aerogel method	13
MgO	$+35 > H_- \geq +27$	Mg(OH) ₂ prepared by aerogel procedure, heated under vacuum at 773 K	13
	$+27 > H_- \geq +17.2$	Mg(OH) ₂ heated under vacuum at 773 K	13
	$+26.5 > H_- \geq +22.3$	Mg(OH) ₂ calcined at 773 K	5
	$+26.5 > H_- \geq +18.4$	Mg(OH) ₂ sol-gel, calcined at 1023 K	14
	$+18.4 > H_- \geq +17.2$	Mg(OH) ₂ calcined at 673 K	15
	$+26.5 > H_- \geq +18.4$	basic magnesium carbonate heated at 723 K under vacuum	6
	$+17.2 > H_- \geq +15.0$	basic magnesium carbonate calcined at 723 K	6, 16
CaO	$+33.0 > H_- \geq +26.5$	Ca(OH) ₂ calcined at 773 K	5
	$H_- \geq +26.5$	CaCO ₃ heated at 723 K under vacuum	6
	$+17.2 > H_- \geq +15.0$	CaCO ₃ calcined at 723 K	6
MgO-TiO ₂ (9 : 1, 1 : 1)	$+18.4 > H_- \geq +17.2$	calcined at 673 K, 773 K	15
BaO-ZnO	$+18.4 > H_- > +15.0$	BaO 2.5 mmol/g, calcined at 873 K	17
MgO-Al ₂ O ₃	$+18.0 > H_- \geq +17.2$	hydrotalcite calcined at 723 K	18
Hydroxyapatite	$+18.4 > H_- \geq +15.0$	calcined at 673 K	5
K ₃ PO ₄	$+18.4 > H_- \geq +15.0$	calcined at 453 K	5
Ca(OH) ₂	$+18.4 > H_- \geq +15.0$		5
Mg(OH) ₂	$+9.3 > H_- \geq +7.2$		5
NaX	$+9.3 > H_- \geq +7.2$		19
CsO _x /NaX	$+18.4 > H_- \geq +17.2$	Cs (0.36-1.80 mmol g ⁻¹)-loaded NaX	19
	$+26.5 > H_- \geq +18.4$	Cs (2.60 mmol g ⁻¹)-loaded NaX	19
CsO _x /CsX	$+18.4 > H_- \geq +17.2$		8
Cs ₂ O/Al ₂ O ₃	$H_- \geq +37$		8
Li ₂ O, Na ₂ O, K ₂ O,	$+26.5 > H_- \geq +18.4$	calcined at 1023 K	14
Cs ₂ O/MgO			
KF/Al ₂ O ₃	$+18.4 > H_- > +15.0$	calcined at 773 K	11

color of the indicator, AH. The amount of phenol at just the point where the color change occurs, corresponds to the number of basic sites having an H_- value equal to or higher than the pK_a value of the indicator used.

In many cases, the basic sites on solid surfaces are heterogeneous. Therefore, the number of basic sites depends on the pK_a value of the indicator. In other words, the distribution of sites with different basic strength H_- can be determined.

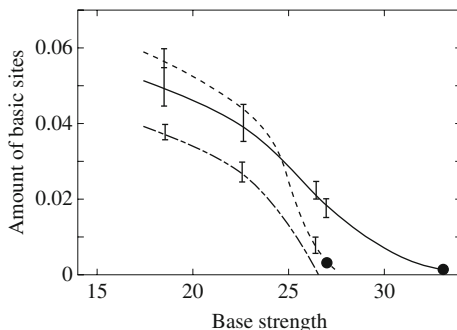


Fig. 2.2.1 Change in the amount of basic sites with pK_a value of indicators

————— Rb₂O evacuated at 643 K

----- Rb₂O evacuated at 573 K

- · - · - · Cs₂O evacuated at 573 K

Reprinted with permission from S. Tsuchiya, S. Takase, H. Imamura, *Chem. Lett.*, **662** (1984); p. 662, Fig. 1.

Figure 2.2.1 shows the number of basic sites with higher than the H_- value for the three alkali oxides.²⁰⁾ Rb₂O has ca. 0.04 mmol g⁻¹ of basic sites stronger than $H_- = 18.4$, while there exists no basic sites stronger than or equal to $H_- = 26.0$. The distributions of basic site strength have been determined for many solid base catalysts.^{3,6)}

2.2.4 Drawbacks of indicator methods

The indicator method described here is based on the method established in the acid-base chemistry in solution. There are several important problems in applying the concept for solutions to the basic sites on the surface.

- The acidity functions in the original concept involve the proton donating/accepting capability of an aqueous solution, but not the properties of individual molecules or ions. However, in the concept transferred into solid acid-base chemistry, the basic strength is expressed as the nature of the individual basic sites. The basic properties of the solid bases are thus expressed by two terms, the number of basic sites and the basic strength (H_-). Heterogeneity of the basic sites is an additional complicating factor.
- As described above, H_- function is based on the nature of the Brønsted acid-base chemistry. Basic sites such as surface oxygen anions act as Lewis bases as well as Brønsted bases. There is, however, no firm guarantee that the basic strength determined by Brønsted-acid type indicators is in parallel with the capability of basic sites as Lewis basic sites.
- There are also experimental drawbacks in the indicator methods. The acidity/basicity is determined by color change of the indicators on the surface. The color change is not so clear and the end point tends to vary depending on the person conducting the experiments. Furthermore, the method is not applicable to colored samples.

- d) Quantitative measurements by titration give very small amounts of basic sites in alkali cation-exchanged faujasites ($< 0.3 \text{ mmol g}^{-1}$) because of the steric hindrance by the metal cations in the zeolite cavities.²¹⁾ The titrating agent and large indicator molecules do not enter easily into the pores. The same holds true for samples having micropore structures.

References

1. C. H. Rochester, *Acidity Functions*, Chapt. 7, p. 234, Academic Press, 1970.
2. K. Tanabe, *Solid Acids and Bases*, Chapt. 3, p.35, Kodansha/Academic Press, 1970.
3. K. Tanabe, M. Misono, Y. Ono, H. Hattori, *New Solid Acids and Bases*, Chapt. 2, p. 5, Kodansha/Elsevier, 1989.
4. S. Malinowski, S. Szczepańska, *J. Catal.*, **2**, 310 (1963).
5. K. Higuchi, M. Onaka, Y. Izumi, *Bull. Chem. Soc. Jpn.*, **66**, 2016 (1993).
6. J. Take, N. Kikuchi, Y. Yoneda, *J. Catal.*, **21**, 164 (1971).
7. G. Suzukamo, M. Fukao, M. Minobe, *Chem. Lett.*, 585 (1987).
8. U. Meyer, H. Gorzowski, W. F. Hölderich, *Catal. Lett.*, **59**, 201 (1999).
9. W. Xie, H. Peng, L. Chen, *Appl. Catal. A*, **300**, 67 (2006).
10. Y. Wang, W. Y. Huang, Y. Chun, J. R. Xia, J. H. Zhu, *Chem. Mater.*, **13**, 670 (2001).
11. W. Xie, H. Li, *J. Mol. Catal.*, **255**, 1 (2006).
12. J. Kijeński, S. Malinowski, *J. Chem. Soc., Faraday Trans.*, **1**, 74, 250 (1978).
13. N. Sun, K. J. Klabunde, *J. Catal.*, **185**, 506 (1999).
14. A. Z. Khan, E. Ruckenstein, *J. Catal.*, **143**, 1 (1993).
15. K. Tanabe, H. Hattori, T. Sumiyoshi, K. Tamaru, T. Kondo, *J. Catal.*, **53**, 1 (1978).
16. T. Matsuda, J. Tanabe, N. Hayashi, Y. Sasaki, H. Miura, K. Sugiyama, *Bull. Chem. Soc. Jpn.*, **55**, 990 (1982).
17. W. Xie, Z. Yang, *Catal. Lett.*, **117**, 159 (2007).
18. T. Nakatsuka, H. Kawasaki, S. Yamashita, S. Kohjiya, *Bull. Chem. Soc. Jpn.*, **52**, 2449 (1979).
19. U. Meier, W. F. Hoelderich, *J. Mol. Catal.*, A, **142**, 213 (1998).
20. S. Tsuchiya, S. Takase, H. Imamura, *Chem. Lett.*, **13**, 661 (1984).
21. D. Barthomeuf, *Catal. Rev.- Sci. Eng.*, **38**, 521 (1996).

2.3 Adsorption-Desorption of Probe Molecules

2.3.1 Adsorption of probe molecules

When acidic molecules are adsorbed on a solid surface, it can be assumed that the solid has basic sites on its surface and that the number of the chemisorbed molecules is equal to that of the basic sites. Benzoic acid, phenol and carbon dioxide are often used as the probe adsorbate. Adsorption is carried out in liquid phase and in gas phase.

(a) Adsorption of acidic molecules from liquid phase

Adsorption of phenol or benzoic acid on suspended solid is carried out at room temperature. The adsorption amount of the adsorbate is determined from the decrease in the concentration of the molecule by various means. The adsorption amount is directly taken as the number of basic sites.¹⁾ In some cases, a Langmuir-type adsorption isotherm is applied and the amount of the saturated adsorption is taken as the number of basic sites.²⁻⁶⁾

Parida and coworkers used two acids with different pK_a values, benzoic acid ($pK_a = 9.9$) and acrylic acid ($pK_a = 4.2$), for determining the amount of basic sites

of zirconia⁴⁾ and MgO-Al₂O₃ mixed oxides (calcined hydrotalcite).⁵⁾ They assume that acrylic acid measures the total number of basic sites, whereas phenol measures only strong basic sites. In the case of zirconia, the number of basic sites measured by phenol and acrylic acid were 39×10^{-3} mmol g⁻¹ and 78×10^{-3} mmol g⁻¹, respectively. In the case of MgO-Al₂O₃ mixed oxides, the corresponding values were 0.16–0.41 mmol g⁻¹ and 7.54–8.87 mmol g⁻¹, depending on the Mg/Al ratio of the oxides.

Campello et al. used three adsorbate, acrylic acid, phenol ($pK_a = 9.9$) and 2,6-di-*t*-butyl-4-methylphenol ($pK_a = 11.1$) for the determination of basic sites on Al₂O₃, AlPO₄, AlPO₄-Al₂O₃ and AlPO₄-SiO₂.²⁾ For all the samples, the numbers of basic sites depended on the acid used, acrylic acid > phenol > 2,6-di-*t*-butyl-4-methylphenol. The adsorption of 2,6-di-*t*-butyl-4-methylphenol may be influenced by the steric effect of ^tBu groups. They also showed that the total basicity as determined by acrylic acid adsorption was the predominant influence on the catalytic activities for retro-aldolization of diacetone alcohol.

The problem in liquid phase adsorption is the possibility that physical adsorption is involved. In fact, an appreciable amount of “basic sites” was found from benzoic acid adsorption on silica.⁶⁾

(b) Adsorption of acidic molecules from gas phase

The number of basic sites can be determined from adsorption of acidic molecules from vapor phase. As molecules, phenol, boron trifluoride and carbon dioxide are often used. Because adsorption temperature can be varied easily, physisorption of the adsorbate can be avoided. On the other hand, the adsorption amount often depends on the choice of adsorption temperature because of the heterogeneity of solid surfaces and the multiple adsorption states of the adsorbate. This kind of information is more easily obtained by using temperature-programmed desorption technique. The use of phenol is questioned since phenol is easily dissociated to adsorb on both acidic and basic sites and hence acidic property affects the adsorption of phenol.⁷⁾

The amount of BF₃ adsorption at 573 K was used as a measure of the basicity for MgO-SiO₂ mixed oxides with different compositions.⁸⁾

A comparative study on the adsorption of phenol and boron trifluoride on MgO and alkaline metal-doped MgO was reported.⁹⁾ Adsorption was done at room temperature and then evacuated at 373 K, 473 K, and 573 K. The amount of adsorbed phenol at 373 K is more than that required for covering the surface with the monolayer, indicating that physical adsorption is involved at this temperature. A fairly good agreement between the adsorption amount of phenol at 573 K and that of boron trifluoride at 473 K was found.

Carbon dioxide is a fairly non-specific adsorbate that titrates both weak and strong basic sites. In fact, carbon dioxide adsorbs in different forms as evidenced by IR spectroscopy. As described later, Barthomeuf concluded that carbon dioxide was not a good probe for zeolites since physical and chemical adsorption occurs simultaneously and various and not well-defined carbonate species may be generated.¹⁰⁾ When the adsorption occurs on very basic oxides the formation of bulk carbonate species is also proposed.

Zotin and Faro Jr. studied the amount of irreversible adsorption of sulfur dioxide on Al_2O_3 and that with modified with Na^+ ions or SO_4^{2-} ions at 373 K.¹¹⁾ The adsorption amount increased by doping with Na^+ ions, while it decreased by doping SO_4^{2-} ions. A linear correlation was found between the catalytic activity for the reaction of $\text{H}_2\text{S} + \text{SO}_2$ and the basic site density in the range of $0.3\text{--}2 \times 10^{14}$ sites cm^{-2} . However, the sample with the highest basicity (3.9% Na^+ on $\gamma\text{-Al}_2\text{O}_3$) exhibited a much lower activity than expected from the correlation, possibly due to too strong adsorption of SO_2 .

2.3.2 Poisoning method

The number of basic sites can be estimated by the addition of an acidic molecule to a catalytic system. The merit of this method is that the number of the basic sites can be determined under the reaction conditions. Fig. 2.3.1 shows the effect of preadsorption of trichloroacetic acid on the catalytic activity of the cyanosilylation of benzophenone (1 mmol) with trimethylsilylnitrile (1.6 mmol) in the presence of hydroxyapatite (0.50 g).¹²⁾



The conversion of benzophenone decreases almost linearly with the preadsorbed amount of trichloroacetic acid. From Fig. 2.3.1, the number of basic sites is estimated as 0.074 mmol per 0.5 g (or 0.15 mmol g^{-1}) of hydroxyapatite. With the same method, the number of basic sites on CaO was estimated as 0.27 mmol g^{-1} of the catalyst.

Isomerization of 1-butene over alumina proceeds via π -allyl anion intermediate. The reaction was poisoned by H_2S .¹³⁾ The number of active sites for the isomerization was estimated as $5.3 \times 10^{13} \text{ cm}^{-1}$ by H_2S titration.

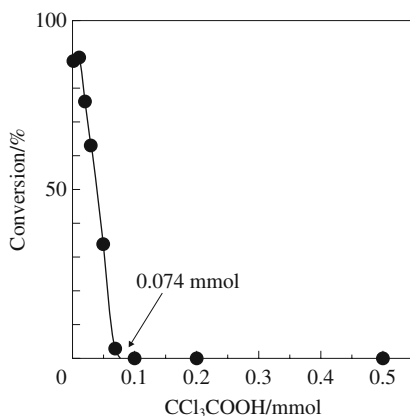


Fig. 2.3.1 Poisoning effect of preadsorbed trichloroacetic acid on the cyanosilylation of benzophenone on hydroxyapatite. Reprinted with permission from K. Higuchi, M. Onaka, Y. Izumi, *Bull. Chem. Soc. Jpn.*, **66**, 2016 (1993) p. 2033, Fig. 5.

Poisoning technique is often used for determining the participation of acidic and/or basic sites to catalytic reactions. In the alkylation of toluene with methanol over alkali cation-exchanged zeolites, addition of hydrogen chloride completely poisons the formation of ethylbenzene and styrene over RbY and CsY, and enhances the formation of xylenes. On the other hand, addition of aniline enhances the formation of ethylbenzene and styrene, and xylenes.¹⁴⁾ These facts lead to the conclusion that xylenes are formed on acidic sites, while ethylbenzene and styrene are formed on basic sites. A similar effect was observed in the ring transformation of γ -butyrolactone into γ -butyrothiolactone.¹⁵⁾ Hydrogen chloride completely retarded the reaction, while pyridine enhanced the reaction rate. The enhancement by pyridine is caused by the induced effect of pyridine adsorbed close to the basic sites.

2.3.3 Temperature-programmed desorption

Temperature-programmed desorption (TPD) of CO_2 is one of the most frequently used methods for evaluating the basic properties of solid surfaces. Typical experimental procedures are divided into two methods. (1) A sample is placed in a flow system. After the sample is treated in helium at 723 K it is exposed to a helium flow containing CO_2 at room temperature until saturation coverage is reached. Weakly adsorbed CO_2 is removed by flushing with helium at room temperature for 0.3–0.5 h. The temperature is then increased at a linear rate of 10–30 K min^{-1} from 298 K to 723–823 K and the rate of CO_2 evolution is monitored with a mass spectrometer.^{16–18)} (2) A sample is placed in a vessel connected to a vacuum system. After the sample is treated at a high temperature under vacuum it is exposed to CO_2 at room temperature. Weakly adsorbed CO_2 is removed by evacuating the system for 30 min at room temperature. Then the sample temperature is increased at a linear rate and the rate of desorption is monitored with a high sensitivity pressure gauge or a mass spectrometer.^{19,20)}

The temperature of desorption represents the strength of the adsorbate-adsorbent interaction. It is presumed that CO_2 desorbs at higher temperatures

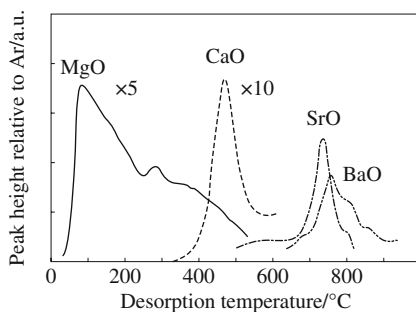


Fig. 2.3.2 TPD profiles of CO_2 desorbed from alkaline earth oxides. Reprinted with permission from G. Zhang, H. Hattori, K. Tanabe, *Appl. Catal.*, **36**, 189 (1988) p. 192, Fig. 3

when the molecule adsorbs at stronger basic sites. The number of basic sites is obtained from the area of the desorption peak. Thus, the TPD method provides a simple method for determining both the strength and the number of basic sites.

The TPD technique does not offer basic strength in a definite scale like the H -function. Information on the exact nature of the basic sites cannot be obtained. A combination with other techniques is essential to elucidate the chemisorbed state of the adsorbate and the nature of the basic sites. Experimentally, it is difficult to get reproducible results, since TPD profiles depend on experimental conditions such as the amount of the sample, flow rate of the carrier gas, the rate of temperature rise in addition to the nature of basic sites. Comparison of data from different authors must be interpreted with caution.

The TPD profiles of CO_2 desorbed from alkaline earth oxides are shown in Fig. 2.3.2, which shows that the basic strength is in the order $\text{BaO} > \text{SrO} > \text{CaO} > \text{MgO}$.²⁰⁾ On the other hand, the number of basic sites per unit weight increases in the order $\text{BaO} < \text{SrO} < \text{CaO} < \text{MgO}$.

Figure 2.3.3 shows the TPD profiles of CO_2 on MgO , Al_2O_3 , and $\text{MgO-Al}_2\text{O}_3$ mixed oxides which were prepared by calcination of hydrotalcite with varying $\text{Mg}/(\text{Al} + \text{Mg})$ ratio, r .¹⁸⁾ The complex TPD profiles suggest that the surfaces of MgO and mixed oxides are not uniform and contain several types of adsorbed CO_2 . The TPD profiles are deconvoluted into three desorption peaks: a low temperature peak (L-peak) at 370–400 K, a middle temperature peak (M-peak) at 460 K and a high temperature peak (H-peak) at 550 K. The densities of the three types of basic sites are given in Table 2.3.1 The M-peak and H-peak are dominant on MgO and $\text{MgO-Al}_2\text{O}_3$ mixed oxide samples with $r \geq 0.5$. For Al-rich samples ($r < 0.5$), the relative contributions of the M- and H-temperature peaks decrease with increasing Al content. Pure Al_2O_3 and $\text{MgO-Al}_2\text{O}_3$ ($r = 0.1$) samples showed no contribution of the high-temperature peak in their TPD profiles. The IR spectrum of adsorbed CO_2 was also studied and bands due to several CO_2 species were observed on the surface. From the thermal stability of each band, the L-, M-, and H-peaks were attributed to hydrogencarbonate, bidentate carbonates and, unidentate carbonates formed on basic OH groups, metal-oxygen pairs and low-coordination oxygen anions, respectively.

Figure 2.3.4 shows the TPD profile of hydrogen from MgO samples heated under vacuum at 773 K and 1123 K.¹⁹⁾ The samples were exposed to 0.73 Pa of H_2 for 2 min at 308 K and gradually cooled to 77 K. Then TPD measurements were started with a heating rate of 19 K min^{-1} . The TPD profile depends very much on the activation temperature of MgO . When activated at 773 K, only one peak was observed at 400 K. With the activation temperature of 1123 K, several active sites with stronger adsorptive force appeared. The difference in adsorption energies was ascribed to the difference in the extent of coordinative unsaturation of both Mg ions and O^{2-} ions on the MgO surface, indicating that highly coordinatively unsaturated pair sites are formed by high temperature heat treatment. More detailed study of H_2 -TPD from MgO has been reported by Ito and coworkers.^{21,22)}

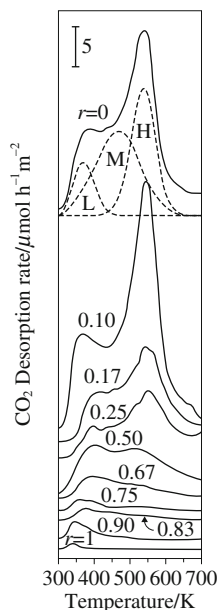


Fig. 2.3.3 TPD profiles of CO₂ on MgO, Al₂O₃, MgO-Al₂O₃ ($r = \text{Al}/(\text{Al} + \text{Mg})$). Reprinted with permission from V. K. Diez, C. R. Apestegula, J. J. Di Cosino, *J. Catal.*, **215**, 220 (2003) p. 224, Fig. 3.

Table 2.3.1 Amounts of CO₂ adsorbed on MgO, Al₂O₃ and MgO-Al₂O₃ mixed oxides

Sample	Density of basic sites/ $\mu\text{mol m}^{-2}$			
	L-peak	M-peak	H-peak	Total evolved CO ₂
MgO	0.79	2.68	2.27	5.74
MgO-Al ₂ O ₃ ($r = 0.9$)	0.81	3.72	2.87	7.40
MgO-Al ₂ O ₃ ($r = 0.83$)	0.33	1.95	1.30	3.58
MgO-Al ₂ O ₃ ($r = 0.75$)	0.29	1.40	0.90	2.59
MgO-Al ₂ O ₃ ($r = 0.5$)	0.37	1.16	0.95	2.48
MgO-Al ₂ O ₃ ($r = 0.33$)	0.25	0.38	0.28	0.91
MgO-Al ₂ O ₃ ($r = 0.25$)	0.14	0.14	0.12	0.40
MgO-Al ₂ O ₃ ($r = 0.17$)	0.26	0.23	0.15	0.64
MgO-Al ₂ O ₃ ($r = 0.10$)	0.16	0.10	0.00	0.26
Al ₂ O ₃	0.04	0.02	0.00	0.06

$$r = \text{Mg}/(\text{Al} + \text{Mg})$$

Reprinted with permission from V. K. Diez, C. R. Apestegula, J. J. Di Cosimo, *J. Catal.*, **215**, 224 (2003) p. 224, Table 2

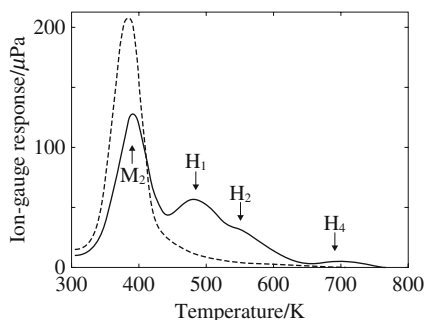


Fig.2.3.4 TPD profiles of H_2 from MgO samples activated at 773 K (---), and at 1123 K (—). Reprinted with permission from T. Ito, T. Sekino, N. Moriai, T. Tokuda, *J. Chem. Soc., Faraday Trans., 1*, **77**, 2181 (1981) p. 2183, Fig. 1.

2.3.4 Heat of adsorption

Heat of adsorption is a direct measure of the interaction of adsorbate and the adsorption sites of solid surfaces. To evaluate the strength of basic sites, the heat of adsorption of carbon dioxide is often used. The measurements of heat of adsorption by microcalorimetry is described in reference 23 and the references therein.²³⁾

The differential heat of adsorption of CO_2 at room temperature and NH_3 at 423 K over a number of metal oxides was determined at 423 K.^{24,25)} The oxides were classified into three groups: acidic oxides (Cr_2O_3 , V_2O_5 , WO_3 , Ta_2O_5 and MoO_3), which adsorb NH_3 but do not chemisorb CO_2 , amphoteric oxides (TiO_2 , ZrO_2 , BeO , Al_2O_3 , Ga_2O_3 and SiO_2), which chemisorb both NH_3 and CO_2 , and basic oxides (Pr_6O_{11} , ThO_2 , Nd_2O_3 , La_2O_3 , ZnO , CaO , MgO) which chemisorb only CO_2 .²⁴⁾ The initial heat of CO_2 adsorption is the highest for Al_2O_3 , higher than 200 kJ mol^{-1} . La_2O_3 and CaO give the initial heat of around 150 kJ mol^{-1} . On MgO , ZrO_2 and TiO_2 , the initial heat of adsorption is about 120 kJ mol^{-1} . The average heat of CO_2 adsorption is correlated with charge/radius ratio of metal ions. It should be noted, however, that the heat of adsorption depends on the preparation method of oxides. Influence of the preparation methods on the heat of adsorption of CO_2 has been reported.²⁶⁻²⁸⁾

The heat of adsorption of CO_2 on MgO , Al_2O_3 , and $MgO-Al_2O_3$ mixed oxides was measured by microcalorimetry²⁹⁾ (Fig. 2.3.5). MgO shows an initial heat of adsorption of about 170 kJ mol^{-1} . In contrast $\gamma-Al_2O_3$ shows a heat of adsorption of about 155 kJ mol^{-1} . The differential heats of adsorption on the mixed oxides were intermediates to the values observed for MgO and $\gamma-Al_2O_3$ and insensitive to the Mg/Al ratio. In every case, the heat of adsorption decreases significantly with the CO_2 coverage. The results for MgO (10 wt%) supported on Al_2O_3 is also shown in Fig. 2.3.5. The sample exhibited basic properties similar to those of $Mg-Al$ mixed oxides. At higher coverages, the differential heat of CO_2 adsorption on the 10% MgO/Al_2O_3 sample is higher than on the mixed oxides. This was attributed to a higher dispersion of MgO on $\gamma-Al_2O_3$ for this sample.

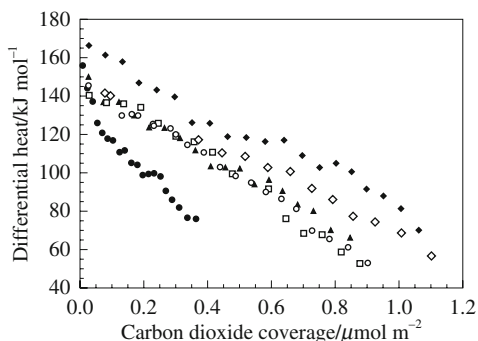


Fig. 2.3.5 Differential heat of adsorption of CO_2 as a function of adsorbed amount on $\gamma\text{-Al}_2\text{O}_3$ (●), $\text{MgO-Al}_2\text{O}_3$ ($r = 0.125$) (▲), $\text{MgO-Al}_2\text{O}_3^*$ ($r = 0.125$) (□), $\text{MgO-Al}_2\text{O}_3$ ($r = 0.923$) (○), MgO (◇), 10% $\text{MgO/Al}_2\text{O}_3$ (◇). Reprinted with permission from J. Shen, J. M. Kobe, Y. Chen, J. A. Domesic, *Langmuir*, **10**, 3902 (1994) p. 3905, Fig. 5.

Cutrufello et al. studied the dehydration of 4-methyl-2-pentanol over ZrO_2 , La_2O_3 , CeO_2 and their mixed oxides and expressed the selectivity toward products as a function of the ratio of the number of basic sites, n_B , and that of acidic sites, n_A , as shown in Fig. 2.3.6.²⁸⁾ Here, n_A is defined as the number of acidic sites, which give the heat of NH_3 adsorption of greater than 38 kJ mol^{-1} as determined by micro-

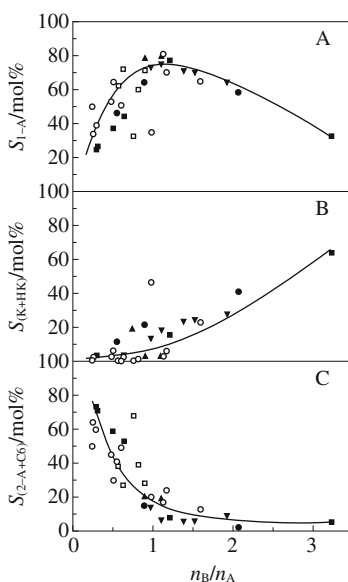


Fig. 2.3.6 Initial selectivity to 4-methyl-1-pentanone (A), 4-methyl-2-pentanone + higher ketones (B) and 4-methyl-2-pentanone + C^{6+} alkenes (C) as a function of the ratio of basic-sites to acid-sites concentration (n_B/n_A) in the reaction of 4-methyl-2-pentanol over ZrO_2 , Li , Na , K , Ba -doped ZrO_2 , CeO_2 , La_2O_3 , $\text{CeO}_2\text{-ZrO}_2$ and $\text{CeO}_2\text{-La}_2\text{O}_3$ mixed oxides. Reprinted with permission from M. G. Cutrufello, I. Ferino, M. Monaci, E. Rombi, V. Salinas, *Top. Catal.*, **19**, 225 (2002) p. 238, Fig. 11.

calorimetry, while n_B is defined the number of basic sites which give the heat of CO_2 adsorption greater than 30 kJ mol^{-1} . At low n_B/n_A ratio, the selectivity for 2-alkene is high. The authors suggest that E1 mechanism prevails at strongly acidic sites. As n_B/n_A increases, the mechanism moves to E1cB through E2. The maximum yield of 1-alkene (E1cB mechanism) was observed at an n_B/n_A ratio of around 1. Further increase of n_B/n_A led to the dehydrogenation of the alcohol. The authors concluded that the combination of strongly basic sites and weakly acidic sites are most favorable for the formation of 1-alkene.

References

1. V. N. Borodin, *Russ. Phys. Chem.*, **51**, 545 (1977).
2. J. M. Campelo, A. Garcia, D. Luna, J. M. Marinas, *Can. J. Chem.*, **62**, 638 (1984).
3. M. A. Aramendia, V. Borau, C. Jimenez, J. M. Marinas, F. J. Romero, *Chem. Lett.*, 279 (1995).
4. K. Parida and H. K. Mishra, *J. Mol. Catal., A*, **139**, 73 (1999).
5. K. Parida and J. Das, *J. Mol. Catal., A*, **151**, 185 (2000).
6. F. M. Bautista, J. M. Campelo, A. García, D. Luna, J. M. Marinas, R. A. Quirós, A. A. Romero, *Appl. Catal., A*, **243**, 93 (2003).
7. K. Tanabe, in *Catalysis Science and Technology Vol. 2* ed. by J. R. Anderson and M. Boudart, Springer-Verlag, chapt. 5 (1981).
8. H. Niiyama, S. Morii, E. Echigoya, *Bull. Chem. Soc. Jpn.*, **45**, 655 (1972).
9. T. Matsuda, Y. Sasaki, H. Miura, K. Sugiyama, *Bull. Chem. Soc. Jpn.*, **58**, 1041 (1985).
10. D. Barthomeuf, *Stud. Surf. Sci. Catal.*, **65**, 157 (1991).
11. J. L. Zotin, A. C. Faro Jr., *Catal. Today*, **5**, 423 (1989).
12. K. Higuchi, M. Onaka, Y. Izumi, *Bull. Chem. Soc. Jpn.*, **66**, 2016 (1993).
13. M. P. Rosynek, F. L. Strey, *J. Catal.*, **41**, 312 (1976).
14. T. Yashima, K. Sato, T. Hayakawa, N. Hara, *J. Catal.*, **26**, 303 (1972).
15. K. Hatada, Y. Takeyama, Y. Ono, *Bull. Chem. Soc. Jpn.*, **51**, 448 (1975).
16. A. L. McKenzie, C. T. Fishel, R. J. Davis, *J. Catal.*, **138**, 547 (1992).
17. J. I. Di Cosimo, V. K. Diez, M. Xu, E. Iglesia, C. R. Apestegua, *J. Catal.*, **178**, 499 (1988).
18. V. K. Díez, C. R. Apestegula, J. J. Di Cosimo, *J. Catal.*, **215**, 220 (2003).
19. T. Ito, T. Sekino, N. Moriai, T. Tokuda, *J. Chem. Soc., Faraday Trans., 1*, **77**, 2181 (1981).
20. G. Zhang, H. Hattori, K. Tanabe, *Appl. Catal.*, **36**, 189 (1988).
21. T. Ito, T. Murakami, T. Tokuda, *J. Chem. Soc., Faraday Trans., 1*, **79**, 913 (1983).
22. T. Ito, M. Kuramoto, M. Yoshioka, T. Tokuda, *J. Phys. Chem.*, **87**, 4411 (1983).
23. V. Solinas, I. Ferino, *Catal. Today*, **41**, 179 (1998).
24. A. Gervasini, A. Auroux, *J. Therm. Anal.*, **37**, 1737 (1991).
25. A. Auroux, A. Gervasini, *J. Phys. Chem.*, **94**, 6371 (1999).
26. A. Auroux, F. Artizzu, I. Ferino, E. Rombi, V. Solinas, G. Petrini, *J. Chem. Soc., Faraday Trans.*, **92**, 2619 (1996).
27. I. Ferino, M. F. Casula, A. Corrias, M. G. Cutrufello, R. Monaci, G. Pachina, *Phys. Chem. Chem. Phys.*, **2**, 1847 (2000).
28. M. G. Cutrufello, I. Ferino, M. Monaci, E. Rombi, V. Solinas, *Top. Catal.*, **19**, 225 (2002).
29. J. Shen, J. M. Kobe, Y. Chen, J. A. Domesic, *Langmuir*, **10**, 3902 (1994).

2.4 Spectroscopic Studies of Solid Bases through Interaction with Probe Molecules

Spectroscopic studies of the adsorbed probe molecules are a direct means of obtaining information on the nature of the adsorption sites and the interactions between reactant molecules and basic sites. By properly selecting the probe molecules and adsorption conditions, one can obtain more specific and detailed infor-

mation on the location of basic sites on surfaces, the basic strength and their reactivity towards adsorbing molecules. Infrared spectroscopy is most frequently used.¹⁻³⁾ MAS NMR and electron spectroscopy are also often utilized.

2.4.1 Infrared spectroscopy of adsorbed carbon dioxide

Carbon dioxide interacts with basic sites in different ways enabling the researcher to distinguish the different types of basic sites.¹⁾ The interaction of CO₂ with hydroxyl groups or oxygen ions on surfaces leads to the formation of carbonate species. The structure of adsorbed carbonate species can be classified as (1) hydrogencarbonate, (2) unidentate carbonate, (3) bidentate carbonate, (4) bridging carbonate, (5) free carbonate, as shown in Fig. 2.4.1. The characteristic IR (and Raman) bands of CO₂ of possible surface species are summarized in Table 2.4.1.³⁾ It should be noted, however, that carbon dioxide is also adsorbed on metal cations on the surface.

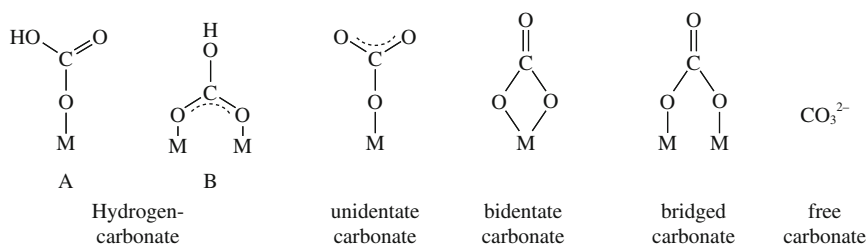


Fig. 2.4.1 Carbonate species on oxide surfaces

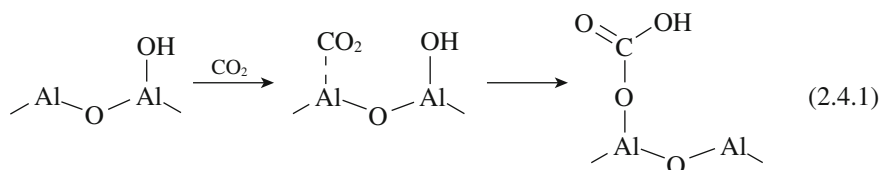
Table 2.4.1 Infrared bands and assignments of carbonate species (frequencies in cm⁻¹)

	Hydrogen-carbonate	Unidentate carbonate	Bidentate carbonate	Bridged carbonate	Free carbonate
$\nu(\text{OH})$	3610-3620				
$\nu_s(\text{O-C-O})$	1440-1450	1350-1420	1260-1350	1800-1870	
$\nu_{as}(\text{O-C-O})$	1645-1670	1490-1560	1620-1680	1130-1280	1440-1450
$\delta(\text{C-O-H})$	1220-1280				

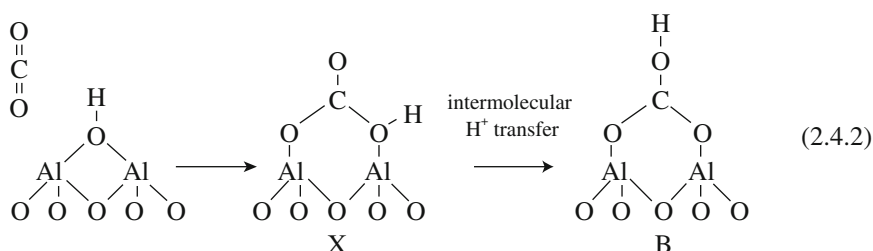
The interaction of CO₂ with basic OH groups on surfaces leads to the formation of hydrogencarbonate species. In the case of $\gamma\text{-Al}_2\text{O}_3$, Haneda et al. observed the bands due to hydrogencarbonate species at 1645, 1480 and 1255 cm⁻¹,⁴⁾ while Partkyns observed the corresponding bands at 1640, 1480 and 1233 cm⁻¹ as well as the band at 3605 cm⁻¹ due to OH stretching vibration.⁵⁾ Among the different types of OH groups on Al₂O₃, OH groups coordinated to only one coordinatively unsaturated cation (3800 cm⁻¹) are mainly involved in the formation of hydrogen-carbonate species.

The structure of hydrogencarbonate species has been studied using the isotope shifts of the bands by using ¹³CO₂ and/or deuteriated Al₂O₃.^{5,6)} The species is

considered to be formed by the insertion of CO₂ weakly-held by Al cation to the surface OH groups. The structure (A) in Fig. 2.4.1 was proposed by Parkyns.⁵⁾



Later, the bridged structure B was proposed by Baltrusaitis et al. based on the isotope shifts of infrared bands and quantum chemical calculations.⁷⁾ In this structure, a proton resides on an oxygen atom originated from CO₂ molecule, but not from an OH group of the surface. The authors proposed the mechanism for hydrogencarbonate formation.



Here, the first step is adsorption of CO₂ on a site next to OH in a linear or bridged configuration. The next step involves nucleophilic attack of the OH on the activated CO₂ molecule to form initial hydrogencarbonate structure (X). The initial structure X is then rearranged into more stable final structure B. The rearrangement does not occur directly (intramolecular rearrangement) because of the high energy barrier, but involves the nearby surface species (OH or carbonate groups). The proton in the initial hydrogencarbonate structure is once transferred into these surface species and then back-transferred into the carbonate, but not in the original position, to form the bridged structure B (intermolecular rearrangement).

Lecher et al. studied CO₂ adsorption on MgO-Al₂O₃ mixed oxides and observed the formation of hydrogencarbonate.⁸⁾ The band position of the symmetric stretching (1417–1450 cm⁻¹) of the hydrogencarbonate species depended on the composition of the mixed oxides, i.e., the downward shift of the wavenumbers with increasing MgO content. They attributed this phenomenon to the increased basic strength with increasing MgO content.

On zirconium oxides, three O-H bands were observed at 3765, 3745 and 3650–3670 cm⁻¹.⁹⁾ These bands were assigned to terminal, bridged, and tribridged OH groups, respectively. The OH groups on tetragonal ZrO₂ are predominantly bibriged, whereas those on monoclinic ZrO₂ are predominantly tribridged. Upon adsorption of CO₂ at room temperature, three types of carbonates were observed;

hydrogencarbonate (1225, 1450, and 1625 cm^{-1}), bidentate carbonate (1325, 1335, 1498, 1556, and 1604 cm^{-1}) and polydentate carbonate (1420 and 1450 cm^{-1}). Hydrogencarbonate species are predominantly formed on tribridged OH groups.⁹ Similar results on the adsorption of CO_2 on ZrO_2 were also reported by Bensitel.¹⁰

Hydrogencarbonate was formed upon adsorption of CO_2 on TiO_2 , Al_2O_3 and ZrO_2 .^{11,12} For example, the bands appeared at 1640, 1440 and 1230 cm^{-1} in the case of Al_2O_3 and 1590, 1435, and 1220 cm^{-1} in the case of TiO_2 . The intensities of $\delta(\text{OH})$ band (ca. 1225 cm^{-1}) of hydrogencarbonate formed on these samples and the catalytic activity for the COS hydrolysis showed a very good correlation (Fig. 2.4.2). Actually, hydrogenthiocarbonate (HSCO_2^-) species formed by the interaction of COS and a basic OH group was proposed as an intermediate for COS hydrolysis.^{13,14}

Oxide ions on surfaces are involved in the formation of unidentate, bidentate and bridged carbonate species, depending on the participation of neighboring metal cations (Fig. 2.4.1). Free carbonate ion (D_{3h} symmetry) presents asymmetric vibration (ν_3) at 1415 cm^{-1} . In the adsorbed state, the symmetry is lowered and the species presents two bands at either side of a wavenumber of ν_3 vibration. The splitting ($\Delta\nu_3$) characterizes the structure of the species formed; it is about 150–200, 250–350, and >400 cm^{-1} for unidentate, bidentate and bridged species, respectively, as shown in Table 2.4.1.¹⁵ On Al_2O_3 , unidentate (1530 and 1370 cm^{-1}), bidentate (1660 and 1230/1270 cm^{-1}) and bridged (1850 and 1180 cm^{-1}) carbonates were observed besides hydrogencarbonate (3605, 1640, 1480, and 1235 cm^{-1}). The relative intensities depend on the pretreatment conditions of the Al_2O_3 samples.^{5,16} Formation of free carbonate is also observed at 1440–1445 cm^{-1} .

Fukuda and Tanabe observed two types of bidentate carbonates (1670, 1315, 1000, and 850 cm^{-1} ; 1630, 1280, 950, and 830 cm^{-1}) and one unidentate carbonate (1550, 1410, 1050, and 860 cm^{-1}) upon adsorption of MgO at room temperature.¹⁷ On CaO , only unidentate species was formed at room temperature. It was noted that the wavenumber difference of the bands between antisymmetric stretching (1540–1580 cm^{-1}) and symmetric stretching (ca. 1420 cm^{-1}) of unidentate carbonate decreased with increasing partial charge of the lattice oxygen of the alkaline earth

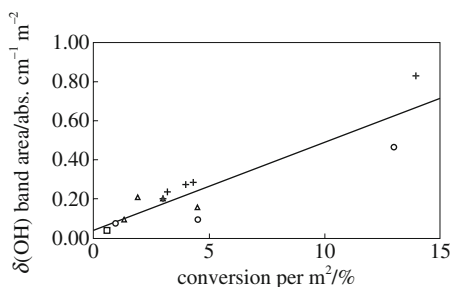


Fig. 2.4.2 Relation between COS hydrolysis activity and the number of hydrogencarbonate species formed from adsorbed CO_2 for $\text{TiO}_2\text{-Al}_2\text{O}_3$ (\square), $\text{TiO}_2\text{-ZrO}_2$ (\circ), and $\text{ZrO}_2\text{-Al}_2\text{O}_3$ (+) catalysts.

Reprinted with permission from C. Lahausse, F. Maugé, J. Bachelier, J. C. Lavalley, *J. Chem. Soc., Faraday Trans.*, **91**, 2907 (1995) p. 2910, Fig. 7.

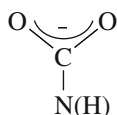
metal oxides.¹⁷⁾ Davylov et al. observed at least four types of carbonates, hydrogen-carbonate, bidentate carbonate, unidentate carbonate and free carbonate (1450 cm^{-1}) on MgO at room temperature.¹⁸⁾ In conformity with the work by Fukuda and Tanabe,¹⁷⁾ only unidentate carbonate was observed on CaO.¹⁸⁾ Phillip et al. reported that unidentate carbonate is the far predominant species upon adsorption of CO_2 both on MgO and CaO at 373 K.¹⁹⁾

On La_2O_3 prepared by dehydration of $\text{La}(\text{OH})_3$ under vacuum at 1073 K, adsorption of CO_2 gave unidentate (a doublet at 1300 and 1500 cm^{-1} , and bands at 1000 and 860 cm^{-1}) at room temperature.²⁰⁾ The number of adsorbed CO_2 corresponds to approximately 1 CO_2 molecule/surface O^{2-} ion. Hydrogencarbonate species was not formed, due to the lack of surface hydroxyl groups on the calcined La_2O_3 . Upon evacuation at 522 K, weak bands appeared at 1310 and 1563 cm^{-1} due to bidentate carbonate species, generated by rearrangement of unidentate structure as their surface population decreased. The unidentate carbonate species disappeared at 573 K and the bidentate disappeared at $\geq 623\text{ K}$.

On MgO- Al_2O_3 mixed oxide, adsorption of CO_2 gave hydrogencarbonate, monodentate carbonate, bidentate carbonate and two species of CO_2 linearly coordinated to metal cations.^{8,21)} Preadsorption of pyridine completely inhibited the formation of linear CO_2 species. The wavenumber difference of the unidentate carbonate showed the same trend as proposed by Fukuda and Tanabe.¹⁷⁾

Diez et al. studied the CO_2 adsorption on Al_2O_3 , MgO and MgO- Al_2O_3 mixed oxides obtained from calcinations of hydrotalcite.²²⁾ As shown in Fig. 2.4.3, three types of adsorption species, hydrogencarbonate, unidentate carbonate, and bidentate carbonate are identified and, as described, the three bands were correlated to the three peaks in the CO_2 -TPD profiles. (Section 2.3.3)

Carbon dioxide interacts with surface amino groups to form carbamate anions.



Thus, when adenine- or guanidine-modified Ti-SBA-15 was exposed to CO_2 , the bands due to carbamate species were observed at 1609 and 1446 cm^{-1} , besides the bands due to carbonate species. The carbamate species was proposed to be an intermediate in the synthesis of cyclic carbonates by the reactions of epoxides with CO_2 .^{23,24)}

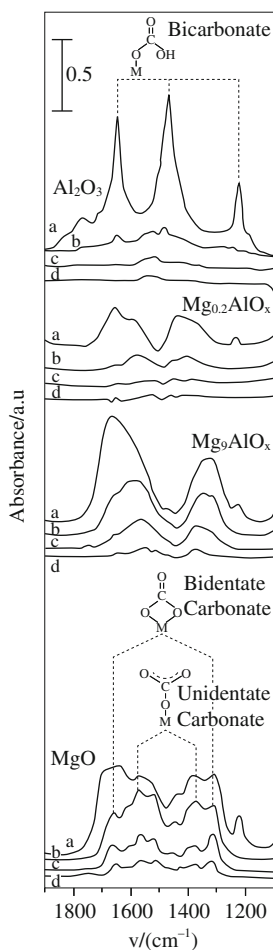


Fig. 2.4.3 Infrared spectra of CO_2 preadsorbed on MgO , Mg_9AlO_x , $\text{Mg}_{0.2}\text{AlO}_x$ samples upon desorption at increasing temperatures (a) 298 K, (b) 373 K (c) 473 K (d) 573 K. CO_2 adsorption at 298 K.

Reprinted with permission from V. K. Díez, C. R. Apesteguía, J. J. Di Cosimo, *J. Catal.*, **215**, 220 (2003) p. 224, Fig. 3.

2.4.2 Spectroscopic studies of adsorbed pyrrole

Adsorption of pyrrole, an acidic molecule, on basic surfaces has been studied by IR, XPS and MAS NMR spectroscopy. In IR spectroscopy, the $\nu(\text{NH})$ frequency shift is used as an evaluation of the basic strength of basic sites interacting with the H atom. The shift of $\nu(\text{NH})$ band to low wavenumbers is related to an increase in basic strength. Scokart and Rouxhet studied the adsorption of pyrrole on Al_2O_3 , MgO and ThO_2 . The $\nu(\text{NH})$ bands were situated at 3230, 3360, 3340 cm^{-1} on Al_2O_3 , MgO and ThO_2 , respectively.^{25,26} This suggests that Al_2O_3 is more basic than MgO and ThO_2 . Fluorination removed the basic sites of Al_2O_3 . Alkali treat-

ment increases the basic strength as indicated by a large frequency shift of the NH band, which appeared at 3200 and 3160 cm^{-1} for Al_2O_3 treated with Na and K, respectively. Mg-treated Al_2O_3 showed a basic character intermediate between Al_2O_3 and MgO. Thus, the basic strength increases in the order $\text{MgO} < \text{Mg-Al}_2\text{O}_3 < \text{Al}_2\text{O}_3$, $\text{ThO}_2 < \text{Na- and K-Al}_2\text{O}_3$. For SiO_2 and $\text{SiO}_2\text{-Al}_2\text{O}_3$, there was no absorption feature indicating the presence of basic sites.

Adsorption of pyrrole on zeolites has been studied extensively by various techniques. Barthomeuf studied the IR spectra of pyrrole adsorbed on X, Y, L, mordenite, ZSM-5.²⁷⁾ The basic strength of cationic mordenite increases in the order $\text{Li} < \text{Na} < \text{K} < \text{Rb} < \text{Cs}$. Zeolites X, Y and L also show similar trends. For any given cation, the basic strength of the zeolites increases with aluminum content ($\text{L} < \text{Y} < \text{X}$), except for mordenite. The basic sites in zeolites are the oxygen anions in the framework. Barthomeuf estimated the negative charges on framework oxygen by using the Sanderson's electronegativity equalization principle.^{27,28)} The charge on the oxygen atom in the zeolites is plotted in Fig. 2.4.4 along with the pyrrole $\nu(\text{NH})$ wavenumber. For each of the zeolites, the shift of the band increases with the negative charge. This indicates that the shift of the $\nu(\text{NH})$ band should be considered as a guide for basicity strength comparison, but only for the zeolites with similar structures. More detailed studies of the interaction of pyrrole with zeolites have been made by using IR, XPS, MASNMR spectroscopy and are described in section 4.2.1.

The major drawback of pyrrole as a probe molecule is that the molecule readily polymerizes or decomposes upon heating. Barthomeuf recommended to record the spectra rapidly after the adsorption with the use of freshly distilled pyrrole.²⁹⁾ Polymerization is usually not observed under these conditions over zeolites while it is observed with basic oxides other than zeolites.

Binet et al. showed that the dissociative adsorption of pyrrole occurred on more basic oxides.³⁰⁾ When pyrrole is adsorbed on ceria (CeO_2) and hydrogen-reduced ceria (Ce_2O_3), the OH stretching bands are observed at 3670 and 3628

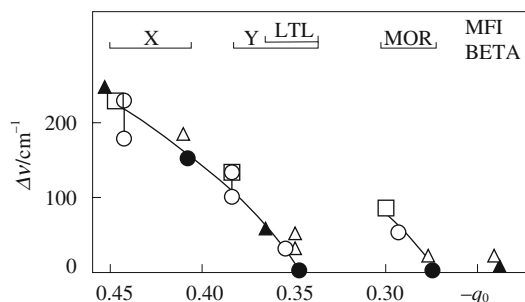


Fig. 2.4.4 Decrease in the NH infrared vibration of pyrrole as the calculated charge on the oxygen decrease for zeolite exchanged with cations.

●: Li, △: Na, ○: K, □: Rb, ▲: Cs.

Reprinted with permission from D. Barthomeuf, in: *Acidity and Basicity of Solids: Theory, Assessment and Utility*, (eds. J. Fraissard, L. Petrakci) NATO ASI ser., C. Vol. 444, P. 181, Kluwer Academic Publishers (1984) p. 189, Fig. 4.

cm^{-1} , respectively, indicating H^+ abstraction by oxygen anions on the surface. In addition, $\nu(\text{ring})$ and $\nu(\text{C-H})$ bands due to pyrrolate anion appeared. The pyrrolate ions are considered to be stabilized by Ce^{4+} or Ce^{3+} ions by electrostatic interaction. The formation of pyrrolate ions was also observed in the adsorption of pyrrole on highly dehydroxylated alumina³⁰⁾ and $\text{MgO-Al}_2\text{O}_3\text{-NiO}$ mixed oxide prepared from hydrotalcite.³¹⁾ Simultaneously, a new band due to a hydrogen-bonded OH band was formed, indicating that the pyrrolate anion is hydrogen-bonded with the OH band formed ($\text{OH}\cdots\text{Py}^-$).

Formation of pyrrolate ions on these oxides indicates that the basic strength of these oxides is much higher than the materials on which pyrrole molecules adsorb only through hydrogen-bonding, i.e., on alkali ion-exchanged zeolites.

2.4.3 Infrared and MAS NMR spectroscopy of adsorbed CHCl_3 and CDCl_3

The C-H stretching vibration of halogenated methanes shifts to lower frequency when they undergo hydrogen bonding. Trichloromethane was proposed as a probe molecule to characterize solid bases by Paukshits et al.³²⁾ The advantage of this method is that CDCl_3 is a weak base and its chemical interaction with aprotic or protic centers is weak. Furthermore, the $\nu(\text{CD})$ bands do not overlap the bands of the surface OH groups, so the complexes of the probes with the base sites can be clearly recognized.

Paukshits et al. studied the adsorption of CHCl_3 and CDCl_3 on various oxides by IR.³²⁾ Spectra of CDCl_3 adsorbed on silica exhibit an absorption band at 2265 cm^{-1} (at 3035 cm^{-1} for CHCl_3), whose position is close to the C-D (or C-H) band in the gaseous adsorbate. The band of SiOH hydroxyl groups at 3740 cm^{-1} is shifted by 45 cm^{-1} close to the shift upon CCl_4 adsorption. Therefore, it was suggested that a chlorine atom of CDCl_3 (or CHCl_3) interacts with a proton of the hydroxyl group and that the D or H atom of the molecule is not bonded to the surface (Type A in Fig. 2.4.5). Upon CDCl_3 adsorption on Al_2O_3 , BeO, and MgO, the spectra exhibit two absorption bands in the range of $2210\text{--}2220$ and $2245\text{--}2250\text{ cm}^{-1}$ with a simultaneous decrease of the OH band frequencies. The former bands were assigned to the adsorption state of Type C, which involves strongly basic

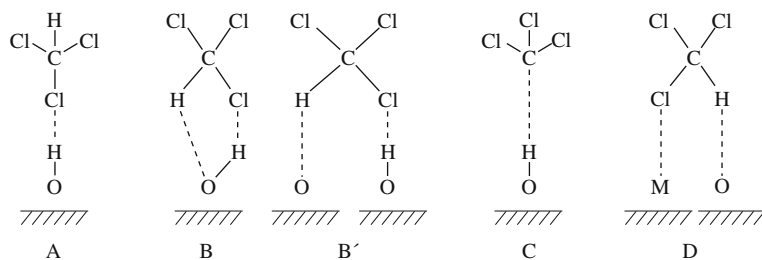


Fig. 2.4.5 Adsorption states of CHCl_3 .

surface oxygen anions, while the latter was assigned the adsorption state of Type B or Type B', which involves weakly basic OH groups.

Barteau et al. studied CDCl_3 adsorption on Al_2O_3 and modified Al_2O_3 .³³⁾ Upon adsorption of CDCl_3 , every sample showed an IR band at 2253 cm^{-1} , which was assigned to CDCl_3 attached to weak basic centers (OH groups). For alumina with Na^+ or Mg^{2+} ions, another band was observed at 2225 cm^{-1} , which was assigned to interaction of CDCl_3 with bridging oxygen atoms (Al-O-Al) on the Al_2O_3 surface.

Davidov et al. also observed two $\nu(\text{CD})$ bands at 2230 and $2190\text{--}2200\text{ cm}^{-1}$ upon adsorption of CDCl_3 on MgO at 293 K .³⁴⁾ They assigned the former band to the CDCl_3 molecules weakly interacting with surface OH groups and the latter to those more strongly interacting with surface oxygen ions.³⁴⁾

Huber and Knözinger observed two sets of bands (3011 and 1240 cm^{-1} , and 2983 and 1216 cm^{-1}) upon adsorption of CHCl_3 on MgO .³⁵⁾ The corresponding bands for CDCl_3 were observed at 2245 cm^{-1} and 2220 cm^{-1} . They assigned the two bands to Type C and Type D. The presence of Type B or B' was refuted because they did not observe a shift of the OH band at 3750 cm^{-1} .

Xie et al. reported that adsorption of CHCl_3 occurred on alkali cation-exchanged X-zeolites.³⁶⁾ Two different C-H stretching bands were observed, one at a constant wavenumber of ca. 2995 cm^{-1} , while the second depended on metal cations. Both bands were assigned to CHCl_3 molecules bonded to the lattice oxygen (Type C). The former results from the interaction of CHCl_3 with oxygen ions adjacent to Na^+ ions, and the latter reflects the adsorption of CHCl_3 on oxygen ions adjacent to K^+ , Rb^+ , or Cs^+ ions. This band shifted to lower frequency in the order Li (3015 cm^{-1}) $>$ Na (2995 cm^{-1}) $>$ K (2966 cm^{-1}) $>$ Rb (2945 cm^{-1}) $>$ Cs (2925 cm^{-1}). Similar results were observed for Y zeolites. Fig. 2.4.6 shows the C-H stretching frequencies as a function of the partial negative charge on the lattice oxygen, calculated

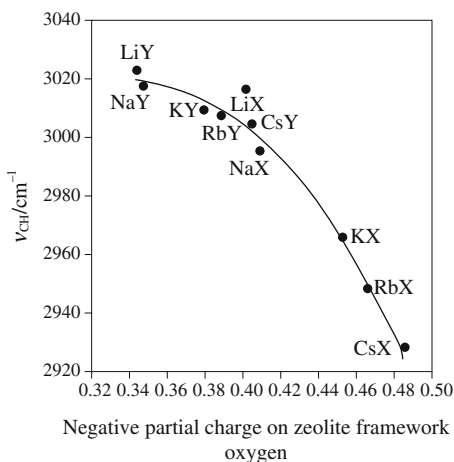


Fig. 2.4.6 C-H frequency of adsorbed CHCl_3 as a function of calculated oxygen charge for X- and Y-Zeolites.

Reprinted with permission from J. Xie, M. Huang, S. Kaliaguine, *React. kinet. Catal. Lett.*, **58**, 217 (1996) p. 226, Fig. 5.

by Sanderson's electronegativity equalization method. The authors concluded that the basicity of zeolites mainly depends on the negative charge of the framework oxygen, while this charge is mainly dependent on the zeolite type and also on the extra framework cations. Similar results were observed for CDCl_3 adsorbed on alkali cation-exchanged X- and Y-zeolites.³⁷⁾

Bosch et al. studied the adsorption of CDCl_3 on a series of alkali cation-exchanged Y zeolites with IR and MAS NMR.³⁸⁾ In the IR spectra, they also observed two bands. For example, in the case of CsNaY , the bands appeared at 2243 cm^{-1} and 2209 cm^{-1} . In contrast to the interpretation by Xie et al.³⁶⁾ and Ryma et al.³⁷⁾, they assigned the two bands to two different adsorption types, Type C (2209 cm^{-1}) and Type D (2243 cm^{-1}). The C-D stretching frequencies of Type C for NaY , RbY , CsNaY are 2225 , 2220 , 2205 , and 2209 cm^{-1} . In the ^1H MAS NMR spectra of CHCl_3 adsorbed on different Y-zeolites, only one peak was observed in contrast with IR spectra. The authors ascribed this to the difference in time scales of the two spectroscopic methods; there must be facile interconversion between Type C and Type D adsorption states. With the exception of KY, the proton chemical shift increases with the size of the alkali metal cation, which reflects the trend of the basic strength. The interaction of Na^+ ions with adsorbed CHCl_3 was also evidenced by ^{23}Na MAS NMR spectroscopy.

Sánchez-Sánchez et al. found similar NMR results for X-zeolites.³⁹⁾ Both the chemical shifts of ^1H MAS NMR and the $\nu(\text{C-H})$ stretching frequency of adsorbed CHCl_3 correlate well with mean negative charge over the framework oxygen as calculated by the method of Sanderson. They also showed that ^{13}C chemical shift of ^{13}C -enriched CHCl_3 is also a measure of framework basicity for zeolite X and Y.

Adsorption of CHCl_3 on alkali cation-exchanged X and Y zeolites was studied also by XPS.⁴⁰⁾

There is a limitation in use of CDCl_3 in some cases. It has been reported that CHCl_3 (CDCl_3) decomposes on the surface of Al_2O_3 to form formate or undergoes the H-D exchange reaction with surface O-H groups even at room temperature.⁴¹⁾

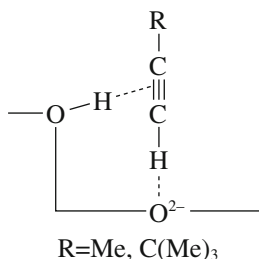
2.4.4 Infrared spectroscopy of adsorbed alkynes

Alkynes are weak C-H acids and interact with basic sites on surfaces. Hydrogen-bonding interaction with surface oxide anions on oxide surfaces induces the red shift of the C-H bond stretching mode. The extent of the red shift depends on the basic strength of oxygen ions. Alkynes may dissociate on the surface.

Adsorption of acetylene at 280 K on MgO revealed a broad asymmetric band at 3150 cm^{-1} due to the CH-stretching mode (ν_3).³⁵⁾ The band is shifted to lower frequency by 137 cm^{-1} from that of gas phase acetylene. The IR silent ν_2 mode became activated and appeared at 1942 cm^{-1} . The appearance of ν_2 -mode and the red shift of the ν_3 -mode are indicative of the H-bonded complex.

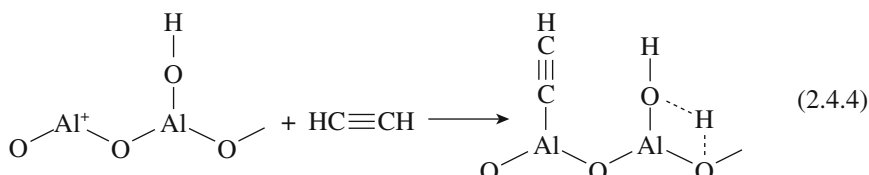
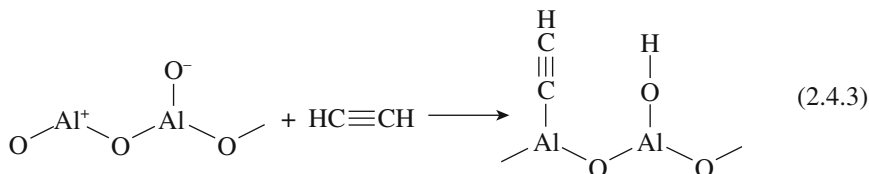
Mordenti et al. studied the adsorption of propyne and 2,2-dimethylbutyne on MgO and silica gel.⁴²⁾ The $\nu(\equiv\text{CH})$ band of propyne red-shifted by 66 cm^{-1} relative to the vapor phase band and had an FWHM of 140 cm^{-1} upon adsorption on MgO. The $\nu(\equiv\text{CH})$ band of 2,3-dimethylbutyne red-shifted 79 cm^{-1} , the FWHM

being 121 cm^{-1} . These observations suggest that acidic C-H groups interact strongly with surface O^{2-} ions. The $\nu(\text{OH})$ band of MgO at 3755 cm^{-1} are red-shifted to two bands at 3693 and 3588 cm^{-1} by adsorption of propyne, while it shifted to three bands at 3082 , 3621 and 3488 cm^{-1} by adsorption of 2,2-dimethylbutyne. These observations indicate the presence of different types of adsorption sites on MgO surface. The authors concluded that the alkyne molecules strongly interact with surface oxygen ions, but they interact simultaneously with surface hydroxyl groups which are preferentially located at the corners on the MgO surface. In the case of adsorption of alkynes on silica gel, the shifts of $\nu(\text{OH})$ band were small. The adsorbed molecules interact weakly with surface OH groups through π -electrons of the $\text{C}\equiv\text{C}$ bonds.⁴²⁾

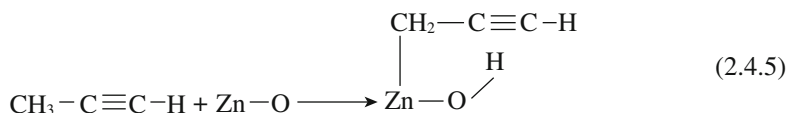


Adsorption of propyne on MgO surface was also studied by Chizallet et al.⁴³⁾ When $0.98\ \mu\text{mol}$ of propyne was introduced to the MgO wafer, the $\nu(\text{C}\equiv\text{C})$ region showed a red shift ($\approx 50\text{ cm}^{-1}$) and the presence of two contributions at 2088 and 2079 cm^{-1} . In the $\nu(\text{OH})$ regions, the 3735 cm^{-1} band decreased and two new bands at 3711 cm^{-1} and 3696 cm^{-1} were formed possibly due to the perturbation of the OH groups. Moreover, a new intense $\nu(\text{OH})$ band at 3441 cm^{-1} also appeared. The bands at 2088 , 2079 and 3441 cm^{-1} were attributed to dissociative adsorption of propyne. The presence of two $\nu(\text{C}\equiv\text{C})$ contributions suggests that two types of basic sites are involved. From the intensity dependence of 3441 cm^{-1} band on the amount of propyne molecules introduced, the number of dissociated propyne is estimated to be $0.046\text{ molecules nm}^{-2}$, suggesting that the dissociation occurs at corners only. When the adsorbed amount of propyne was increased, two new bands appeared at 2098 and 2045 cm^{-1} besides the growth of 2088 and 2079 cm^{-1} in the $\nu(\text{C}\equiv\text{C})$ region. Two $\nu(\equiv\text{CH})$ bands region appeared at 3250 and 3168 cm^{-1} . These bands were assigned to non-dissociative adsorption on two kinds of surface oxygen anions.

Adsorption of acetylene on Al_2O_3 at room temperature was studied by Bhasin et al.⁴⁴⁾ The intensity of the $\nu(\text{C}\equiv\text{C})$ band, infrared inactive in the free acetylene, was as strong as that of the $\nu(\text{C-H stretch})$ band in the chemisorbed state. At the same time, the bands due to isolated OH groups and hydrogen-bonded OH groups were enhanced. The authors ascribed these facts to the dissociative adsorption of acetylene on the pair sites (Al^{3+} and O^- ion) on the Al_2O_3 surface. From the amount of chemisorbed C_2H_2 , the number of pair sites on Al_2O_3 was estimated to be $2\text{--}5 \times 10^{13}\text{ cm}^{-2}$.



Adsorption of C_2H_2 and C_2D_2 on ZnO gives rise to the appearance of new bands at 3550 cm^{-1} and 2622 cm^{-1} , respectively, indicating the dissociative adsorption of acetylene.⁴⁵⁾ Adsorption of propyne gives rise to an OH band at 3515 cm^{-1} . Adsorption of $\text{CH}_3\text{-C}\equiv\text{CD}$, however, also give rise to an OH band at 3515 cm^{-1} , no corresponding OD band is observed. This result suggests that following process occurs. Formation of propargyl anion species was confirmed by adsorption of allene.



Uvarova et al. studied the adsorption of acetylene on Na^+ ion exchanged zeolites. Acetylene was easily and reversibly removed by short evacuation of the zeolites at $300\text{--}370\text{ K}$.⁴⁶⁾ The antisymmetric C-H stretching mode relative to the gas phase frequency (3287 cm^{-1} band) red-shifted by 71, 82, and 107 cm^{-1} for the case of acetylene adsorbed on Na-mordenite, NaY and NaX, respectively. This indicates the formation of hydrogen bonds with framework oxygen and is consistent with the known increase in basic strength in this series. Additional blue-shifted bands were also detected and attributed to π -complexes formed on exchangeable Na^+ ions. The behavior of propyne was found to be analogous.

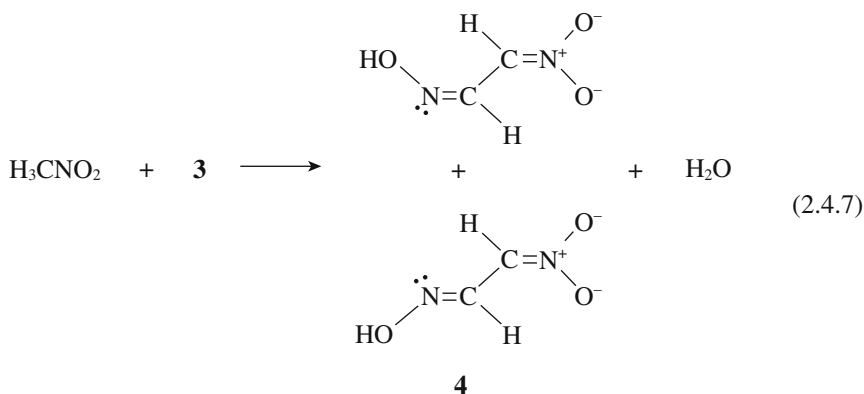
Upon adsorption of acetylene on Cs-Y, two bands were observed in the C-H region at 3242 and 3211 cm^{-1} , the intensities of which are linearly correlated with $\text{C}\equiv\text{C}$ stretching bands at 1958 and 1950 cm^{-1} .⁴⁷⁾ The band pair at 3242 and 1958 cm^{-1} is assigned to an acetylene π -complex, whereas the band pair at 3211 and 1950 cm^{-1} is attributed to an H-bonded species.

Propyne also forms hydrogen-bonded species as indicated by red shifts of the $\text{C}\equiv\text{H}$ stretching mode.⁴⁷⁾ Fig. 2.4.7 shows the correlation of the C-H bond frequency with the cation radius for the series of alkaline cation-exchanged zeolites.

In order to overcome the difficulty due to the presence of two coupled $\nu(\equiv\text{CH})$ vibrations in acetylene, Lavalley et al. used 1-butyne as a probe for the characterization of alkali cation-exchanged zeolites.⁴⁸⁾ The $\nu(\equiv\text{CH})$ bands were observed at

chemical shifts are essentially identical to that of the *aci* anion in solution. The ^{15}N chemical shift of $\text{CH}_3^{15}\text{NO}_2$ adsorbed on MgO was -80 ppm. The upfield shift relative to nitromethane is consistent with the increased negative charge on the adjacent oxygens. At 473 K, the *aci* anion on MgO was converted to a carbonate species. Essentially identical results were obtained upon the adsorption on CaO . A very small amount of *aci* anion formed on CsX . No *aci* anion formed on acidic zeolites.

Lima et al. also studied the adsorption of nitromethane on $\text{MgO-Al}_2\text{O}_3$ -mixed oxides, $\text{MgO-Ga}_2\text{O}_3$ -mixed oxides, MgO , $\gamma\text{-Al}_2\text{O}_3$, NaX , CsX , and Cs -loaded CsX by ^{13}C MAS NMR.^{50,51)} The interaction of nitromethane with the solid surfaces at room temperature is classified into three cases. On zeolites NaX and CsX , only physisorbed nitromethane was observed. Since the pK_a value of nitromethane is 10.2, the H_- value of basic sites on these materials is lower than 10.2. On Al_2O_3 and $\text{MgO-Al}_2\text{O}_3$ mixed oxides *aci* anions were observed besides physisorbed nitromethane, indicating that these materials have basic sites stronger than $H_- = 10.2$. The *aci* anion formed is supposed to be stabilized on Lewis acid sites. On MgO , $\text{MgO-Ga}_2\text{O}_3$ mixed oxides, and Cs -loaded CsX , the species analogous to methazonate anion **4** is formed by the secondary reaction of *aci* anions with nitromethane in addition to *aci* anion and physisorbed nitromethane. The authors suggested that the *aci* anions are less stabilized by Lewis acid sites on these surfaces and undergo a secondary reaction to form methazonate.

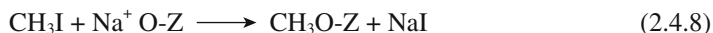


The formation of the *aci* anion on $\text{MgO-Al}_2\text{O}_3$ mixed oxide, MgO , and $\gamma\text{-Al}_2\text{O}_3$ upon adsorption of nitromethane at room temperature was also confirmed by IR spectroscopy.^{52,53)}

2.4.6 ^{13}C MAS NMR of adsorbed methyl iodide

Murray et al. reported that adsorption of CH_3I on CsX readily led to the formation of methoxyl group by ^{13}C MAS NMR at room temperature. The peak was observed at 58 ppm.⁵⁴⁾ Bosáček proposed the use of methyl iodide as a probe to evaluate the basic strength of oxygen ions in the framework of zeolites.⁵⁵⁻⁵⁷⁾ Methyl

iodide molecules dissociatively are adsorbed on alkali ion-exchanged zeolites to form methoxy groups and alkali metal halide.



Here, O-Z denotes the zeolite framework oxygen.

The chemical shift of ^{13}C NMR of the methoxy groups thus formed reflects the basic strength of oxygen ions of the zeolite framework. Fig. 2.4.8 shows the cross-polarization spectra of CH_3I on NaX for different amounts of adsorbed methyl iodide. The spectra contain two signals at about -18.4 ppm and 54 ppm. The former is assigned to physisorbed CH_3I , while the latter is assigned to the bonded methyl formed by reaction (2.4.8). This band has a shoulder at higher loading, indicating the presence of two different kinds of adsorption sites (lattice oxygen ions). The isotropic ^{13}C chemical shift of CH_3I chemisorbed on various zeolites is plotted against electronegativity values of the zeolites (Fig. 2.4.9). The electronegativity values are calculated by Sanderson's electronegativity equalization principle. A linear correlation is found between the chemical shift and the lattice electronegativity. As the electronegativity of the zeolite increases, the NMR signal of the surface-bonded methyl (methoxyl) is shifted to lower fields, indicating the increasing positive charge on the carbon of the methyl. A similar correlation is also found between the ^1H chemical shift of ^1H MAS NMR of chemisorbed methyl iodide and the lattice electronegativity.⁵⁸⁾

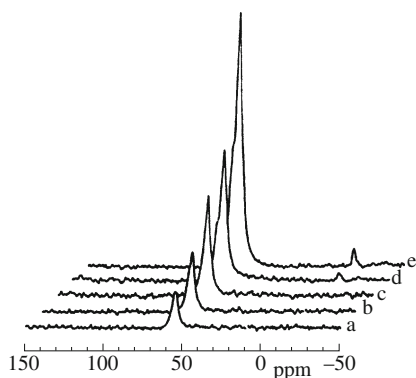


Fig. 2.4.8 ^{13}C CPMAS NMR spectra of methyl iodide adsorbed on NaX at 298 K. Adsorption in mmol g^{-1} (a) 0.07, (b) 0.14 (c) 0.22 (d) 0.4 (e) 0.6 Reprinted with permission from V. Bosáček, *J. Phys. Chem.*, **97**, 10732 (1993) p. 10732, Fig. 2.

Strong solid bases can be prepared by incorporating alkali metal oxides into the zeolite pores [4.2.2]. Hunger et al. examined the effect of the guest compounds on the basic character of the zeolites using ^{13}C MAS NMR of adsorbed CH_3I .^{59,60)} Fig. 2.4.10 shows ^{13}C CP MAS NMR spectra of NaY, CsNaY, and CsOH/CsNaY (CsNaY loaded with 16 CsOH molecules/unit cell) after adsorption of 16 molecules of CH_3I . The zeolites were calcined at 673 K. The signals at -20

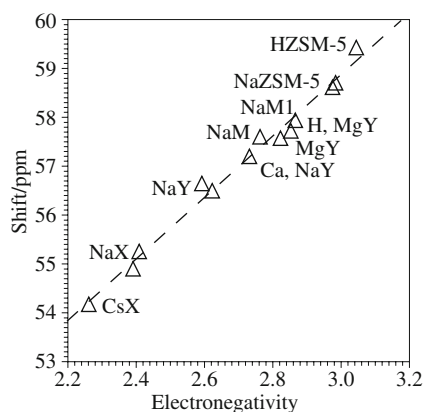


Fig. 2.4.9 Dependence of the chemical shift of the ^{13}C NMR signal assigned to surface methoxy on Sanderson's electronegativity of zeolites. Reprinted with permission from V. Bosáček, *Z. Phys. Chem.*, **189**, 241 (1995) p. 247, Fig. 5A.

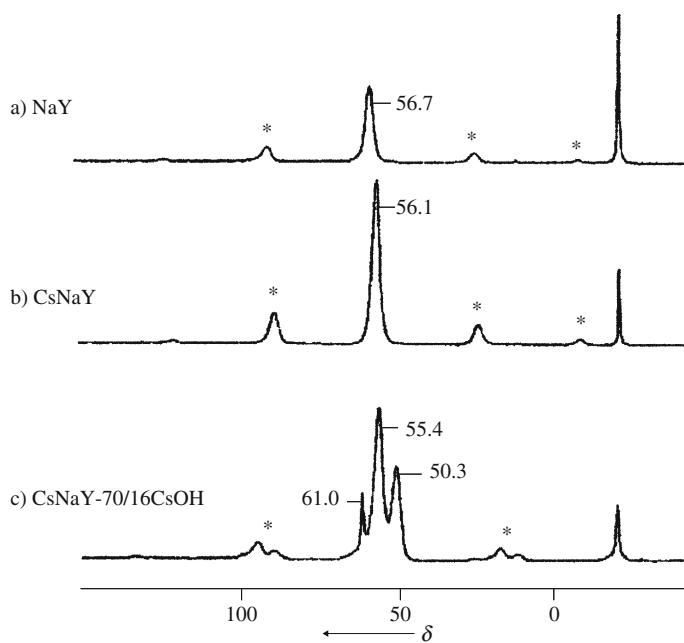


Fig. 2.4.10 ^{13}C CPMAS NMR spectra of dehydrated (at 673 K) zeolites a) NaY, b) CsNaY and c) CsNaY/16CsOH with 16 $\text{CH}_3\text{I}/\text{u.c.}$ Reprinted with permission from M. Hunger, U. Schenk, B. Burger, J. Weitkamp, *Angew. Chem. Int. Ed. Engl.*, **36**, 2504 (1997) p. 2506, Fig. 4.

ppm are due to physisorbed CH_3I . The chemical shifts for NaY (56.7 ppm) and CsNaY (56.1 ppm) are in good agreement with those expected from the relation-

ship shown in Fig. 2.4.9. The spectrum of CsOH/CsNaY consists of large signals at 55.4 and 50.3 ppm due to methoxy groups and a narrow signal at 61 ppm. This latter signal is due to dimethyl ether. The change in the ^{13}C chemical shift from 56.1 ppm for the methoxy group in CsNaY to 55.4 ppm for the methoxy group in CsOH/CsNaY indicates an increased basic strength of the framework oxygen. The signal at 50.3 ppm is assigned to the methoxy group bound to the alkali metal guest introduced upon impregnation. A similar observation has been reported by Schenk et al. for adsorption of CH_3I on CsNaY loaded with CsOH and Cs acetate.⁶¹⁾

Schenk et al. also studied the ^{13}C CP MAS NMR of CH_3I adsorbed on silica gel loaded with alkali metal hydroxides.⁶¹⁾ The loading of CH_3I on dehydrated silica gel does not lead to the formation of a methoxy group. The ^{13}C chemical shift values are 49.6, 49.3, 48.9 and 48.7 ppm for NaOH/SiO_2 , KOH/SiO_2 , RbOH/SiO_2 and CsOH/SiO_2 , respectively. The tendency of the resonance shift from 49.6 ppm for methoxy groups on NaOH/SiO_2 to 48.7 ppm for methoxy groups on CsOH/SiO_2 agrees with the variation of the electronegativities of alkali metals introduced.

References

1. J. C. Lavalley, *Catal. Today*, **27**, 377 (1996).
2. J. Ryczkowski, *Catal. Today*, **68**, 263 (2001).
3. H. Knözinger, *Adv. Catal.*, **25**, 184 (1976).
4. M. Haneda, E. Joubert, J.-C. Ménézo, D. Daprez, J. Barbier, N. Daturi, J. Saussey, J.-C. Lavalley, H. Hamada, *Phys. Chem. Chem. Phys.*, **3**, 1366 (2001).
5. N. D. Parkyns, *J. Chem. Soc. (A)*, **1969**, 410.
6. Y. Amenomiya, Y. Morikawa, G. Pleizier, *J. Catal.*, **46**, 431 (1977).
7. J. Baltrusaltis, J. H. Jemsen, V. H. Grassian, *J. Phys. Chem.*, **110**, 12005 (2006).
8. J. A. Lercher, C. Colombier, N. Noller, *J. Chem. Soc., Faraday Trans., I*, **80**, 949 (1984).
9. K. T. Jung, A. T. Bell, *J. Mol. Catal., A*, **163**, 27 (2000).
10. M. Bensitel, V. Moravek, J. Lamotte, O. Saur, J. C. Lavalley, *Spectrochim. Acta*, **43A**, 1487 (1987).
11. C. Lahousse, A. Aboulayt, F. Maugé, J. Bachelier, J. C. Lavalley, *J. Mol. Catal.*, **84**, 283 (1993).
12. C. Lahousse, F. Maugé, J. Bachelier, J. C. Lavalley, *J. Chem. Soc., Faraday Trans.*, **91**, 2907 (1995).
13. J. Bachelier, A. Aboulay, J. C. Lavalley, O. Legendre, F. Luck, *Catal. Today*, **17**, 55 (1993).
14. F. H. Hoggan, A. Aboulayt, A. Pieplu, P. Nortier, J. C. Lavalley, *J. Catal.*, **149**, 300 (1994).
15. Ya. M. Grigor'ev, D. V. Pozdnyakov, V. N. Filmonov, *Russ. J. Phys. Chem.*, **46**, 183 (1972).
16. N. D. Parkyns, *J. Phys. Chem.*, **75**, 526 (1971).
17. Y. Fukuda and K. Tanabe, *Bull. Chem. Soc. Jpn.*, **46**, 1616 (1973).
18. A. A. Davydov, M. L. Shepot'ko, A. A. Budneva, *Kinet. Katal.*, **35**, 272 (1994).
19. B. Phillip, K. Omata, A. Aoki, K. Fujimoto, *J. Catal.*, **134**, 432 (1992).
20. M. P. Rosynek, *J. Catal.*, **48**, 417 (1977).
21. C. Morterra, G. Ghiotti, F. Boccuzzi, S. Coluccia, *J. Catal.*, **51**, 299 (1978).
22. V. K. Díez, C. R. Apesteguía, J. J. Di Cosimo, *J. Catal.*, **215**, 220 (2003).
23. R. Sivastava, D. Srinivas, P. Ratnasamy, *J. Catal.*, **233**, 1 (2005).
24. R. Sivastava, D. Srinivas, P. Ratnasamy, *Micropor. Mesopor. Mater.*, **90**, 314 (2006).
25. D. Scokart, F. G. Rouxhet, *J. Chem. Soc., Faraday Trans. I*, **76**, 1476 (1980).
26. D. Scokart, F. G. Rouxhet, *J. Colloid Interface Sci.*, **86**, 96 (1982).
27. D. Bartheleuf, *J. Phys. Chem.*, **88**, 42 (1984).
28. D. Bartheleuf, in: *Acidity and Basicity of Solids; Theory, Assessment and Utility* (eds. J. Fraissard and L. Petrakci) NATO ASI ser., C. Vol. 444, p.181, Kuwer Academic Publishers, 1994.
29. D. Bartheleuf, *Catal. Rev. -Sci. Eng.*, **38**, 521 (1996).
30. C. Binet, A. Jadi, J. Lamotte, J. C. Lavalley, *J. Chem. Soc., Faraday Trans.*, **92**, 123 (1996).

31. O. Cairon, E. Dumitriu, C. Guiman, *J. Phys. Chem., C*, **111**, 8015 (2007).
32. E. P. Paukshtis, N. S. Kostsarenko, L. G. Karakchev, *React. Kinet. Catal. Lett.*, **12**, 315 (1979).
33. P. Barteau, M.-A. Kellens, B. Delmon, *J. Chem. Soc., Faraday Trans.*, **87**, 1425 (1991).
34. A. A. Davidov, M.L. Shepořoko, A. A. Yurchenko, K. Jiratova, *Kinet. Catal.*, **12**, 315 (1979).
35. S. Huber, H. Knözinger, *J. Mol. Catal., A*, **141**, 117 (1999).
36. J. Xie, M. Huang, S. Kaliaguine, *React. Kinet. Catal. Lett.*, **58**, 217 (1996).
37. U. Ryma, M. Hunger, H. Knözinger, J. Weitkamp, *Stud. Surf. Sci. Catal.*, **125**, 197 (1999).
38. E. Bosch, S. Huber, J. Weitkamp, H. Knözinger, *Phys. Chem. Chem. Phys.*, **1**, 579 (1999).
39. M. Sánchez-Sánchez, T. Blasco, F. Rey, *Phys. Chem. Chem. Phys.*, **1**, 4529 (1999).
40. J. Xie, M. Huang, S. Kaliaguine, *Appl. Surf. Sci.*, **115**, 157 (1997).
41. T. A. Gordimova, A. A. Davydov, *React. Kinet. Catal. Lett.*, **23**, 233 (1983).
42. D. Mordenti, P. Grotz, H. Knözinger, *Catal. Today*, **70**, 83 (2001).
43. C. Chizallet, M. L. Bailly, G. Costentin, H. Lauron-Pernot, J. M. Kraft, P. Bazin, J. Saussey, M. Che, *Catal. Today*, **116**, 196 (2006).
44. M. M. Bhasin, C. Curran, G. S. John, *J. Phys. Chem.*, **74**, 3973 (1970).
45. C. C. Chang, R. J. Kokes, *J. Am. Chem. Soc.*, **92**, 7518 (1970).
46. E. B. Uvarova, L. M. Kustov, V. B. Kazansky, *Stud. Surf. Sci. Catal.*, **94**, 254 (1995).
47. H. Knözinger, H. Huber, *J. Chem. Soc., Faraday Trans.*, **94**, 2047 (1998).
48. J. C. Lavalley, J. Lamotte, A. Travert, J. Czynievska, M. Ziolk, *J. Chem. Soc., Faraday Trans.*, **94**, 331 (1998).
49. A. A. Kheir, J. F. Haw, *J. Am. Chem. Soc.*, **116**, 817 (1994).
50. E. Lima, L. C. de Ménorval, D. Tichit, M. Laspéras, P. Graffin, F. Fajula, *J. Phys. Chem., B*, **107**, 4070 (2003).
51. E. Lima, M. Laspéras, L. C. de Ménorval, D. Tichit, F. Fajula, *J. Catal.*, **223**, 28 (2004).
52. M. Yamaguchi, *J. Chem. Soc., Faraday Trans.*, **93**, 3581 (1997).
53. N. Nesterenko, E. Lima, P. Griffin, L. C. de Ménorval, M. Laspéras, P. Graffin, D. Tichit, F. Fajula, *New J. Chem.*, **23**, 665 (1999).
54. D. K. Murray, J.-W. Chang, J. F. Haw, *J. Am. Chem. Soc.*, **115**, 4732 (1993).
55. V. Bosáček, *J. Phys. Chem.*, **97**, 10732 (1993).
56. V. Bosáček, *Z. Phys. Chem.*, **189**, 241 (1995).
57. V. Bosáček, R. Klik, F. Genoni, F. Rivetti, F. Figueras, *Magn. Reson. Chem.*, **189**, 241 (1995).
58. V. Bosáček, H. Ernst, D. Freude, T. Mildner, *Zeolites*, **18**, 196 (1997).
59. M. Hunger, U. Schenk, B. Burger, J. Weitkamp, *Angew. Chem. Int. Ed. Engl.*, **36**, 2504 (1997).
60. M. Hunger, U. Schenk, B. Burger, J. Weitkamp, *J. Mol. Catal., A*, **134**, 97 (1998).
61. U. Schenk, M. Hunger, J. Weitkamp, *Magn. Res. Chem.*, **37**, 575 (1999).

2.5 Test Reactions

2.5.1 Characterization of basic sites by test reactions

Test reactions are often used for characterizing the nature of catalysts. One of the advantages of using test reactions is that one can select the test reaction whose reaction conditions such as temperature are close to those of target reactions. However, several points must be noted before the use of test reactions for characterization.

If the reaction involves the abstraction of protons from the reactants, the pK_a value of the reactant is one of the key factors for estimating the basic strength, since the H_- value of the basic sites must be larger than the pK_a value of the reactant. As shown below, the H_- values of alkali cation-exchanged zeolites are estimated to be 10–13 from the rates of Knoevenagel condensations at 363–443 K. However, the zeolites can catalyze the reaction of phenylacetonitrile with dimethyl carbonate at 533 K, while Rb- and Cs-exchanged X-zeolites can catalyze the side-chain alkylation of toluene with methanol at 700 K. These facts clearly show that

these catalysts can activate phenylacetonitrile ($pK_a = 21.9$) and toluene ($pK_a = 37$) at 533 and 700 K, respectively. Base strength of solid bases increases with temperature. Weak bases can be catalysts for a variety of reactions at higher temperatures.

Generally, it is not possible to determine the strength or the number of basic sites only from the rates of reactions. Since the rate depends both on the number of basic sites and turnover frequency, the number of basic sites has to be determined separately to discuss the nature of the basic sites.

By using proper test reactions, one can distinguish basic catalysts from acidic catalysts when the products over basic sites are different from those over acidic sites. For example, the reaction of toluene with methanol over Rb- or Cs-X zeolites gives styrene and ethylbenzene at 700 K, while the reaction over acidic zeolites gives xylenes.

The ratio of the products from different sites, however, cannot be used for the ratio of the amounts of the basic and acidic sites, since the side-chain alkylation and ring-alkylation have different activation energies. Therefore, the ratio of the products is temperature dependent.

It is of the utmost importance that the mechanism of the test reaction be clear. It is highly desirable that the way of participation of the basic sites and the rate-determining step be clarified. For example, if the desorption of the products is the rate-determining step, the reaction rate can not be directly correlated with the reactivity of the reactants or basic strength of active sites.

2.5.2 Isomerization of butenes

n-Butene isomerization is catalyzed by both solid acids and solid bases. The reaction mechanisms are well established for both acid-catalyzed and base-catalyzed reactions, as described below. Accordingly, *n*-butene isomerization is a good test reaction for estimating the nature of active sites as to whether the active sites are acidic or basic. The nature of active sites is reflected on the selectivity of the two isomers produced in the reaction starting from one isomer. The product selectivities in both acid-catalyzed and base-catalyzed isomerization are different from those expected from the equilibrium values listed in Table 2.5.1.¹⁾ In addition, a deuterium tracer experiment can give a definite answer to the question whether

Table 2.5.1 Equilibrium percentages of butene isomers*

Temperature /K	1-Butene	<i>trans</i> -2-Butene /%	<i>cis</i> -2-Butene
273	1.9	78.9	25.7
323	4.2	70.6	25.2
373	6.9	65.4	28.0
423	10.0	60.2	29.8
473	13.3	56.0	30.6
523	16.8	52.1	31.1

* Calculated from equations (1) and (3) in ref. 1.

intermolecular H transfer, which is expected for an acid-catalyzed reaction, or intramolecular H transfer, which is expected for a base-catalyzed reaction, is involved in the isomerization (*vide infra*).

Judging from the pK_a values of 35.5 and 38 for propene and 1-pentene (at α -positions), respectively,²⁾ the pK_a values of butenes should be quite high. Abstraction of an H^+ from butenes needs strong basic sites. The basic sites stronger than ca. 35 in H -scale are required for the reaction at room temperature. Accordingly, the isomerization of butenes is a good test reaction for strongly basic catalysts. Many solid base catalysts show catalytic activity for the isomerization of butenes below room temperature.

It would be helpful to show first the mechanisms for acid-catalyzed *n*-butene isomerization which should be compared to those for the base-catalyzed isomerization. The mechanism for acid-catalyzed isomerization is illustrated in Fig. 2.5.1. Addition of surface H^+ to any of butene isomers results in the formation of 2-butyl cation as a common reaction intermediate. The 2-butyl cation is a metastable species and not an activated complex. In the 2-butyl cation, C_1 , C_2 -H, and C_3 atoms all lie in a plane, parallel to the surface. The C_4 methyl group extends away from the surface, leaving the two hydrogens (labeled H_a and H_b) on C_3 directed toward the surface. The two hydrogen atoms on C_3 are geometrically different, for loss of H_a will result in the formation of *cis*-2-butene, whereas the *trans* isomer will result from loss of H_b . The probability of losing either the H_a or the H_b is equal, and the two C-H bonds are energetically quite similar. Accordingly, the *cis/trans* ratio in the 1-butene isomerization is very near to unity for solid acid catalyst regardless of the reaction temperature.

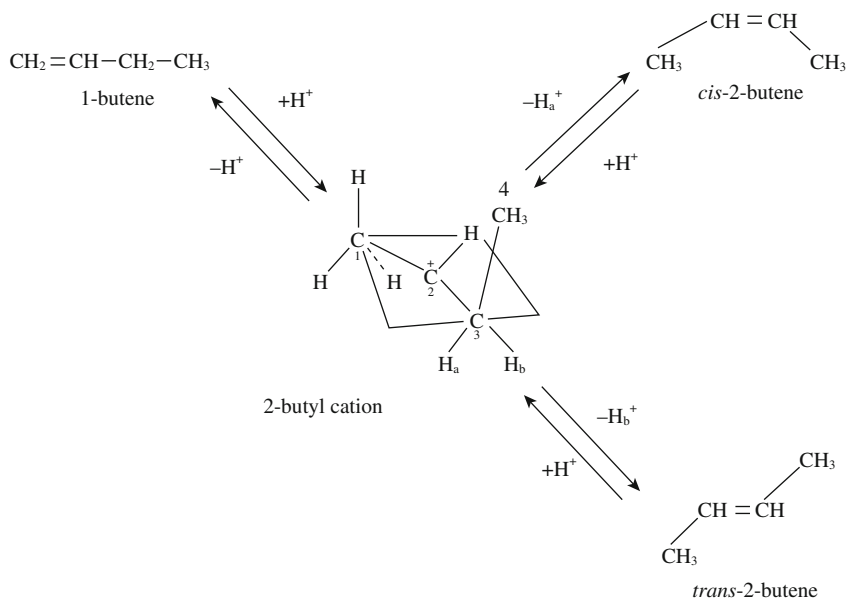


Fig. 2.5.1 Mechanism of acid-catalyzed isomerization of butenes over solid acids.

The 1/*trans* ratio in the *cis*-2-butene isomerization varies with the reaction temperature and perhaps with strength of acid sites. The probability of losing any of three hydrogen atoms on C₁ leading 1-butene is three times higher than that of losing H_b leading to *trans*-2-butene. However, the primary C₁-H bonds are stronger and more difficult to cleave than the secondary C₃-H bonds, and this is reflected in the higher activation energy for the formation of 1-butene than *trans* from the *cis* isomer. The effect of the activation energy difference normally exceeds the effect of the probability difference. In many cases, 1/*trans* ratios are less than unity in the *cis*-2-butene isomerization over solid acid catalysts.

In all interconversions between each of the three isomers, the H⁺ added to a reactant isomer to form the 2-butyl cation is retained in the isomerized products. The H⁺ added to the reactant should originate from the other butene molecules except when the original surface protons interact with the reactant molecules for the first time. The original surface protons are quickly replaced by the protons originating from the reacting molecules. Accordingly, the intermolecular H transfer is involved in the acid-catalyzed isomerization of *n*-butenes.

The mechanisms of base-catalyzed isomerization of butene are shown in Fig. 2.5.2. The intermediates are the *cis* and *trans* forms of allylic carbanion. The characteristic selectivity of the product isomers in base-catalyzed isomerization is due to the relative stability of two allylic carbanions as well as a slow direct interconversion between the two allylic carbanions. Allylic carbanion is more stable in the *cis* form than in the *trans* form. Direct interconversion between the *cis* form of allylic carbanion and the *trans* form of allylic carbanion has a high energy barrier to cross over since the C₂-C₃ bond has a double bond character.

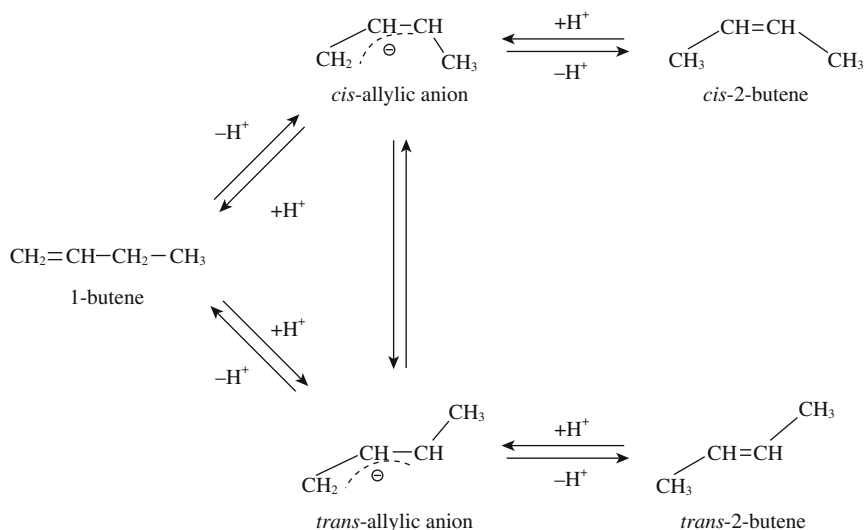


Fig. 2.5.2 Mechanism of base-catalyzed isomerization of butenes over solid bases.

Isomerization is initiated by abstraction of an allylic H from each isomer by basic site. Abstraction of an H^+ from 1-butene results in the formation of both *cis* and *trans* allylic carbanions. Since the *cis* form of allylic carbanion is more stable, the concentration of allylic carbanions is higher in the *cis* form than in the *trans* form on the surface of solid base catalysts. The geometrical structure is retained during the addition of an H^+ to allylic carbanion; addition of an H^+ to the *cis* form and the *trans* form of allylic carbanions results in the formation of *cis*-2-butene and *trans*-2-butene, respectively. Accordingly, *cis*-2-butene is predominantly formed over *trans*-2-butene in the initial stage of 1-butene isomerization. Abstraction of an H^+ from *cis*-2-butene results in the formation of the *cis* form of the allylic carbanion. Interconversion of the *cis* form of allylic carbanion to the *trans* form is slower than the addition of an H^+ to form 1-butene. Accordingly, 1-butene is predominantly formed over *trans*-2-butene in the initial stage of *cis*-2-butene isomerization.

A higher stability of the *cis* form of allylic carbanion as compared to the *trans* form was proposed by Bank et al.^{3,4)} The high stability of the *cis* form of the allylic carbanion was ascribed to the interaction of the dipole of a methyl group with the dipole of the negatively charged π -allyl. The higher stability of the *cis* form of the allylic carbanion was confirmed on the surface of ZnO by IR spectroscopy during isomerization of *n*-butenes.⁵⁾ The observed species were mostly assigned to the *cis* form of the allylic carbanion even when the reaction extended to reach near equilibrium.

Intramolecular H transfer occurs in the base-catalyzed butene isomerization, which is in contrast to intermolecular H transfer for acid-catalyzed isomerization. The H atom that is abstracted from a molecule returns to the same molecule to form the isomerized product.

The deuterium tracer experiment, namely, the coisomerization of a mixture of C_4H_8 (d_0): C_4D_8 (d_8) with a 1 : 1 ratio affords the way to distinguish between intermolecular H transfer and intramolecular H transfer mechanisms. If the reaction involves intermolecular H transfer, the products consist of d_0 , d_1 , d_7 , and d_8 isotopic species. On the other hand, if the reaction involves intramolecular H transfer, the products consist only of d_0 and d_8 isotopic mixtures. This method was proposed by Hightower and Hall, and applied to butene isomerization over $SiO_2-Al_2O_3$ and Al_2O_3 .⁶⁾

The occurrence of intramolecular H transfer can be evidenced by coisomerization of butene- d_0/d_8 . The isomerized butene isomers consist essentially of d_0 and d_8 isomers as seen in Table 2.5.2, which shows the isotopic distribution in the coisomerization of *cis*-2-butene over typical solid base catalyst BaO.⁷⁾ The isotopic distribution in the coisomerization over typical acid catalyst $SiO_2-Al_2O_3$ is also shown in Table 2.5.2 The products (1-butene and *trans*-2-butene) consist essentially of d_0 , d_1 , d_7 , and d_8 , demonstrating occurrence of intermolecular H transfer over $SiO_2-Al_2O_3$.⁶⁾ Large ratios of d_0/d_8 in the product isomers observed for BaO are caused by a kinetic isotope effect, indicating that the C-H (or C-D) bond cleavage (abstraction of an H^+ by basic site) is a slow step. The intramolecular mechanism has also been proven by the tracer method for *cis*-2-butene isomerization

over Y_2O_3 ⁸⁾, La_2O_3 ^{9,10)}, CeO_2 ^{8,10)}, TiO_2 ¹¹⁾, Al_2O_3 ¹²⁾, ZnO ¹²⁾, and ZnO/SiO_2 ¹³⁾, and for 1-butene isomerization over La_2O_3 ⁹⁾ and ZrO_2 ¹⁴⁾.

In Table 2.5.3 are summarized the characteristic features of base-catalyzed isomerization of *n*-butenes in contrast to those of acid-catalyzed isomerization. The selected data for base-catalyzed isomerization of *n*-butenes are listed in Table 2.5.4.

Table 2.5.2 Isotopic distribution of butene isomers in coisomerization of *cis*-2-butene d_0/d_8 over BaO ⁷⁾ and $\text{SiO}_2\text{-Al}_2\text{O}_3$ ⁶⁾

Catalyst (React. temp.)	Product	% each product	Isotopic composition of products / %									
			d_0	d_1	d_2	d_3	d_4	d_5	d_6	d_7	d_8	
BaO (273 K)	1-	3.8	67.8	5.5	3.0	0	0	0	0	0.1	5.8	18.0
	<i>trans</i> -	4.0	76.5	8.9	1.7	0	0	0	0	0	2.2	13.0
	<i>cis</i> -	92.2	47.5	1.0	0	0	0	0	0	0	1.9	49.3
$\text{SiO}_2\text{-Al}_2\text{O}_3$ (292 K)	1-	1.1	33.7	24.4	2.7	0.1	0	0.2	3.8	21.3	13.8	
	<i>trans</i> -	7.5	32.6	18.3	1.4	0.1	0	0.3	2.7	21.4	23.2	
	<i>cis</i> -	91.4	43.4	1.9	0.2	0	0	0	0.4	4.7	49.4	

Table 2.5.3 Reaction features in base- and acid-catalyzed isomerization of *n*-butene

	Base-catalyzed	Acid-catalyzed
Intermediate	Allylic carbanion	2-Butyl cation
<i>cis/trans</i> ratio from 1-butene	Larger than 1	Close to 1
1/ <i>trans</i> from <i>cis</i> -2-butene	Larger than the equilibrium value	Close to the equilibrium value
H transfer involved in the reaction	Intramolecular	Intermolecular
(Isotopic distribution in the product of coisomerization of d_0/d_8)	d_0 and d_8	$d_0, d_1, d_7,$ and d_8
Poisoning effect by CO_2	Strong	None
Poisoning effect by NH_3	Slight	Strong

Table 2.5.4 Selected data of *cis/trans* and *1/trans* ratios in 1-butene isomerization and *cis-2*-butene isomerization, respectively, over solid base catalysts

Catalyst	Pretreat. temp. /K	React. temp. /K	<i>cis/trans</i>	<i>1/trans</i>	Ref.
Li ⁰ /Al ₂ O ₃		303	1		15
Na ⁰ /Al ₂ O ₃		303	4	0.8	15
LiOH		713	1.6	13.3	16
NaOH		673	6.6	∞	16
KOH	593	593	9	27	16
Na ₂ O	420	343	1.7		17
K ₂ O	420	333	2.3		17
Rb ₂ O	573	413	7.1	7.4	18
Cs ₂ O	643	413	5.8	22.3	18
MgO	723	303	16		19
CaO	773	303	6		19
SrO	1273	303	0.75		20
BaO	1273	273	2.3		7
BaO	823	273	6		7
Y ₂ O ₃	973	273	3.9		8
La ₂ O ₃	973	273	2.8	1.5	8
La ₂ O ₃	923	273	7.7	∞	9
CeO ₂	973	473	2.2		8
CeO ₂	973	323	4		10
TiO ₂	723	473	6	13	21
ZrO ₂	773	373	7.3		22
ZrO ₂	723	371	1.6		14
Cr ₂ O ₃	1023	room temp.	50		5
ZnO	753	room temp.	13	0.95	5
Al ₂ O ₃	803	493	6.25	0.22	6
SnO ₂	833	473	19		23
Cs-X	673	423	5		24
K/K-X	673	273	3		24
Rb/Rb-X	673	273	11		24
Cs/Cs-X	673	273	10		24
ZnO-SiO ₂	773	523	1.2	0.6	13
Yb/K-Y ^{a)}	473	273	4.3		25
Eu/K-Y ^{a)}	473	273	10.4		25

^{a)} Supported from the ammoniacal solution of the metal.

2.5.3 Dehydration and dehydrogenation of alcohols

A. Mechanism of alcohol dehydration and dehydrogenation

The mechanism of dehydration (and dehydrogenation) of alcohols over acid-base catalysts can be classified as follows (Fig. 2.5.3).²⁶⁾

Et mechanism The first step of dehydration is the formation of a carbenium ion by the abstraction of an OH group. This mechanism occurs with strongly acidic catalysts such as the H⁺-form of zeolites. The acidic center A may be either Brønsted or Lewis type. In the former case, the carbenium ions may be produced with the intermediacy of oxonium ions. The isomerization occurs at the carbenium

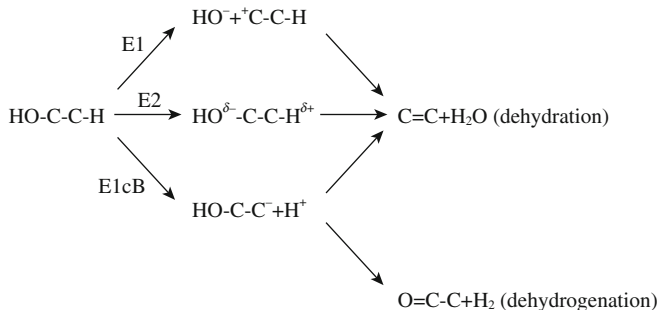


Fig. 2.5.3 Mechanism of alcohol decomposition.

ion stage. Thus, the formation of 2-butene from 1-butanol is indicative of the E1 mechanism.

E2 mechanism The elimination of a proton and a hydroxyl group from alcohols is concerted without the formation of ionic intermediates. Both acidic and basic centers are required in this mechanism. Lack of 2-butene or exclusive formation of 1-butene from 1-butanol is an indication of the E2 mechanism. From 2-butanol, preferential formation of 2-butene (Saytzev orientation) is observed. Alumina is a typical E2 oxide.

E1cB mechanism The first step of dehydration is the formation of a carbanion; a C-H bond is loosened or broken in the first step. This mechanism occurs with strongly basic catalysts such as alkaline earth oxides. High selectivity for 1-butene (Hofmann orientation) from 2-butanol is indicative of E1cB, whereas the E1 and E2 mechanisms give mainly 2-butene. Whenever the E1cB mechanism is found, dehydrogenation is also found in addition to dehydration. The H^- is abstracted from the anion by the surface in the case of dehydrogenation, while OH^- is abstracted in the case of dehydration. Usually stronger bases show higher selectivity for dehydrogenation. Modification of the E1cB mechanism is often proposed. This is exemplified by the mechanism proposed by Diez et al. for 2-propanol reaction as described later.²⁷⁾ Here, dissociative adsorption of alcohol to form surface alkoxide first occurs. Subsequent abstraction of a hydrogen atom at the α or β position by a basic site leads to dehydrogenation or dehydration.

Abstraction of proton by the basic sites to form anionic species is the key step for dehydrogenation as in the case of the E1cB mechanism. In this sense, we use the term “*carbanion mechanism*” to include both the original and modified E1cB mechanism.

Isopropyl ether is often found in the product and its formation is assumed to require acidic sites of medium strength²⁸⁾.

Alumina is a most typical dehydration catalyst and extensive studies on dehydration over alumina have been reviewed by Pines and Manassen.²⁹⁾ Dehydration of butanols shows Al_2O_3 to be a typical E2 catalyst; both acidic and basic sites are involved.³⁰⁾

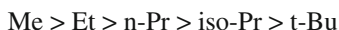
Primary kinetic effect of the gas phase dehydration of *t*-butyl, *s*-butyl, and isobutyl alcohols on Al_2O_3 have been measured in a temperature range between 393 K and 503 K.³¹⁾ The deuteration of the hydroxyl group does not give rise to an isotope effect, whereas substitution of the β -proton by deuterium produces an appreciable effect. From the dependence of the isotope effects on substrate structure and temperature, it was concluded that at temperatures below 473 K, the three alcohols are dehydrated via an E2- like intermediate over Al_2O_3 which presumably contain a certain degree of ionic contributions. With increasing temperature, the ionic contributions are favored so that at elevated temperatures, depending on the reactant structure, the reaction may proceed via the E1 mechanism.

The kinetic isotope effect was studied in the conversion of an equimolar mixture of *t*- $\text{C}_4\text{D}_9\text{OH}$ and *t*- $\text{C}_4\text{H}_9\text{OH}$ and in the conversion of $(\text{CD}_3)_2\text{CH}_3\text{COH}$ to produce $(\text{CD}_3)_2\text{C}=\text{CH}_2$ or $(\text{CH}_3)(\text{CD}_3)\text{C}=\text{CD}_2$ over Al_2O_3 . In both cases, the kinetic isotope effects of 2.1–2.3 ($k_{\text{H}}/k_{\text{D}}$) were obtained.³²⁾ This value is also indicative of the E2 mechanism.

Dautzenberg and Knözinger studied the dehydration of secondary alcohols over alumina.³³⁾



The ratio of 2-alkene and 1-alkene in the product (S_{12}) changes with the substituents R in the sequence



Thus, the substituent alters the reactivity of β -hydrogen and the change in the selectivity S_{12} is due to the inductive effect of the substituents. This indicates that the rupture of $\text{C}^\beta\text{-H}$ bonds is involved in the rate-determining step.

Kibby and Hall studied the decomposition of various alcohols over stoichiometric and calcium-deficient hydroxyapatite catalysts.³⁴⁾ Over the nonstoichiometric (calcium-deficient) hydroxyapatite (NHAP), dehydration was the only reaction that occurred. Both dehydration and dehydrogenation occurred over stoichiometric hydroxyapatite (HAP).

For the dehydration of 15 alcohols over NHAP, the sum of the Taft σ^* values for the alkyl groups at the α -carbon, relative to $\sigma_o^* = \sum \sigma_\alpha^* = 0.49$ for the three groups (two methyl, one hydrogen) of 2-propanol was correlated with the rate constants.

$$\text{Log}(k/k_o) = \rho_\alpha^* (\sigma^* - \sigma_o^*) \quad (2.5.2)$$

The ρ_α^* value were -5 and -4 at 503 and 623 K. The negative value indicates the positive charge at the α -carbon. The concerted mechanism (E2) with the E1 nature is suggested. For the dehydration of primary alcohols over HAP, the ρ_α^* value was also negative (-2.3) at 668 K. On the other hand, the positive value of ρ_α^* of $+1.5$ was obtained for dehydrogenation over HAP. This suggests that a negative charge is developed at the α -carbon in the transition state for dehydrogenation. An alkoxide ion is suggested to be a likely precursor, with hydride transfer as the rate-determining step.

ZrO₂-based catalysts are known to possess a high selectivity towards the formation of 1-alkenes in the dehydration of secondary alcohols. Yamaguchi et al. showed that ZrO₂ gave very high selectivity for 1-butene in the dehydration of 2-butanol.³⁵⁾ The activity and selectivity for dehydration of ZrO₂, however, depends strongly on the method of the preparation and the pretreatment.³⁶⁻³⁸⁾ Doping of NaOH to ZrO₂ increased significantly the selectivity for 1-alkene from 4-methyl-2-pentanol.³⁷⁾

The oxides of lanthanides and actinoids give mainly 1-alkene in the dehydration of 2-hexanol, and 4-methyl-2-pentanol.^{39,40)} The selectivity in the dehydration of 4-methyl-2-pentanol over lanthanides/actinides oxides is given in Table 2.5.5.³⁹⁾

The selectivity in the reaction of 4-methyl-2-pentanol depends strongly on the acid-base properties of oxide catalysts as shown in Fig. 2.3.6. The E1 mechanism prevails at strongly acidic sites. As n_B/n_A increases, the mechanism moves to E1cB through E2. The maximum yield of 1-alkene (E1cB mechanism) was observed at n_B/n_A ratio of around 1. The further increase of n_B/n_A led to the dehydrogenation of the alcohol.

Table 2.5.5 Dehydration of 4-methyl-2-pentanol over metal oxides

Oxide	Temperature /K	LHSV	Conversion /%	Alkenes produced/%	
				1-alkene	2-alkene
Sc ₂ O ₃	680	28	5	95	5
Y ₂ O ₃	685	26	63	96	4
La ₂ O ₃	687	55	39	96	4
CeO ₂	623	50	14	86	14
Pr ₆ O ₁₁	697	55	11	92	8
Nd ₂ O ₃	691	55	25	94	6
Sm ₂ O ₃	688	52	24	94	6
Eu ₂ O ₃	700	46	10	95	5
Gd ₂ O ₃	696	48	23	94	6
Tb ₂ O ₃	700	16	2	90	10
Dy ₂ O ₃	677	45	6	97	3
Ho ₂ O ₃	684	52	47	97	3
Er ₂ O ₃	676	45	6	97	3
Tm ₂ O ₃	676	60	6	95	5
Yb ₂ O ₃	676	50	42	97	3
ThO ₂	672	26	87	97.5	2.5
UO ₂	680	44	49	81	19

Reprinted with permission from A. J. Lundeen, R. van Hoozer, *J. Org. Chem.*, **32**, 3386 (1967); p. 3388, Table VI.

B. Dehydration and dehydrogenation of 2-propanol and butanols

It is often assumed that acidic sites are responsible for the dehydration of alcohols and basic sites are responsible for the dehydrogenation of alcohols. Therefore, the reactions of alcohols have frequently been used for characterizing acid-base sites of solid catalysts. As alcohol, 2-propanol is most often used, but butanols and cyclohexanol have also been used for this purpose. The simple assumption that

acidic sites are responsible for dehydration and basic sites for dehydrogenation is not always valid from a mechanistic viewpoint as described below.

In the reaction of 1-propanol over CaO-SiO_2 , both dehydration and dehydrogenation proceed.⁴¹⁾ Kinetic isotope effects for both reactions were studied with $\text{C}_3\text{H}_7\text{OD}$. For dehydrogenation, the isotope effect of $k_{\text{H}}/k_{\text{D}} = 1.9$, indicating that OH rupture is the rate determining step in the dehydrogenation reaction. On the other hand, for dehydration, no isotope effect was observed. The dehydration is considered to occur via the E1 mechanism on the Brønsted acid sites of the mixed oxide.

Reaction of 2-propanol over $\text{Cd}_3(\text{PO}_4)_2$ affords acetone at 578 K.⁴²⁾ The dehydrogenation to acetone is completely poisoned by co-feeding trichloroacetic acid, while coexistence of pyridine shows no effect on the catalytic performance. These facts indicate that the reaction proceeds on the basic sites of the phosphate.

The selectivity in the reaction of 2-propanol over MgO is controversial. Several groups found both acetone and propene as the products.^{27,43,44)} On the other hand, Gervasini et al. found only propene,⁴⁵⁾ while there is also a report that only dehydrogenation to acetone occurs over alkaline earth oxides at 543–652 K.⁴⁶⁾ Hathaway and Davis found that CO_2 retards both the rates of the formation of acetone and propene upon its addition to the feed in the reaction of 2-propanol over MgO, indicating that both dehydrogenation and dehydration occur on the basic sites.⁴⁴⁾

The decomposition of 2-propanol over MgO, Al_2O_3 , and MgO- Al_2O_3 mixed oxides were studied by Díez et al.²⁷⁾ The mixed oxides were prepared by the decomposition of hydrotalcites of different compositions at 723 K. Fig. 2.5.4 shows the initial rates of formation of the products (propene, isopropyl ether and acetone) as a function of the composition of the catalysts at 533 K. The formation rate of each product strongly depends on the Al content, $m = \text{Al}/(\text{Al}+\text{Mg})$, and the cata-

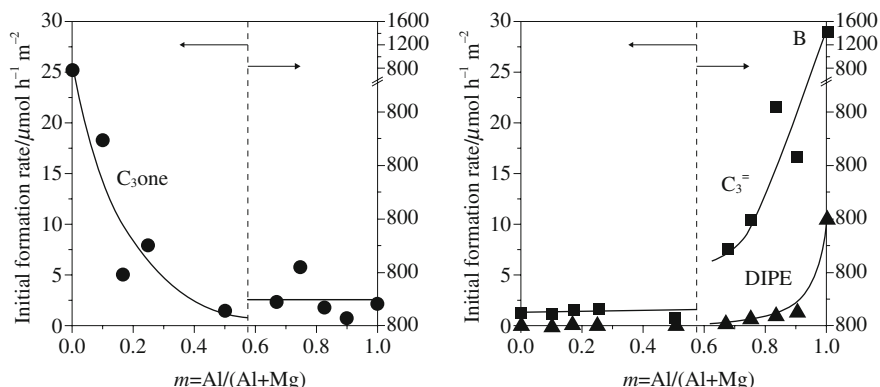


Fig. 2. 5.4 Product distribution for 2-propanol conversion on MgO, Al_2O_3 and MgO- Al_2O_3 mixed oxides. Initial formation rates of acetone (C_3 one) propene ($\text{C}_3=$) and diisopropyl ether (DIPE) at 533 K.

Reprinted with permission from V. K. Díez, C. R. Apesteguía, D. I. Di Cosimo, *J. Catal.*, **215**, 223 (2003); p. 227, Fig. 8.

lysts are divided in two groups. Al_2O_3 and Al-rich samples ($m > 0.5$) were highly active and selective for propene and diisopropyl ether, whereas MgO and Mg-rich oxides ($m < 0.5$) selectively afforded acetone together with a small amount of propene. The formation of propene and diisopropyl ether over Al-rich samples is ascribed to E2-type dehydration involving Al-O pair sites. The formation of both acetone and propene over Mg-rich samples is ascribed to the presence of basic sites, the proposed mechanism being shown in Fig. 2.5.5. The authors supposed that more strongly basic sites are required for formation of propene than for the formation of acetone.

In the first step, 2-propanol is adsorbed through the O-H bond on the acid-base pair site with the formation of a surface propoxide intermediate. The subsequent abstraction of H^α or H^β from the 2-propoxide intermediate leads to acetone or propene. In both routes, a carbanion intermediate is formed as a consequence of the proton detachment by the strongly basic sites. A similar mechanism is also proposed for the reaction of 2-propanol over $\text{TiO}_2\text{-ZrO}_2$ mixed oxides.²⁸⁾ It is suggested that more strongly basic sites are required for the formation of propene than for the formation of acetone.²⁷⁾ Actually, the selectivity for propene over MgO increases when Cs_2O is loaded.⁴⁷⁾ These findings clearly show that propene is formed over strongly basic catalysts. Thus, alcohol dehydration is not a reliable measure

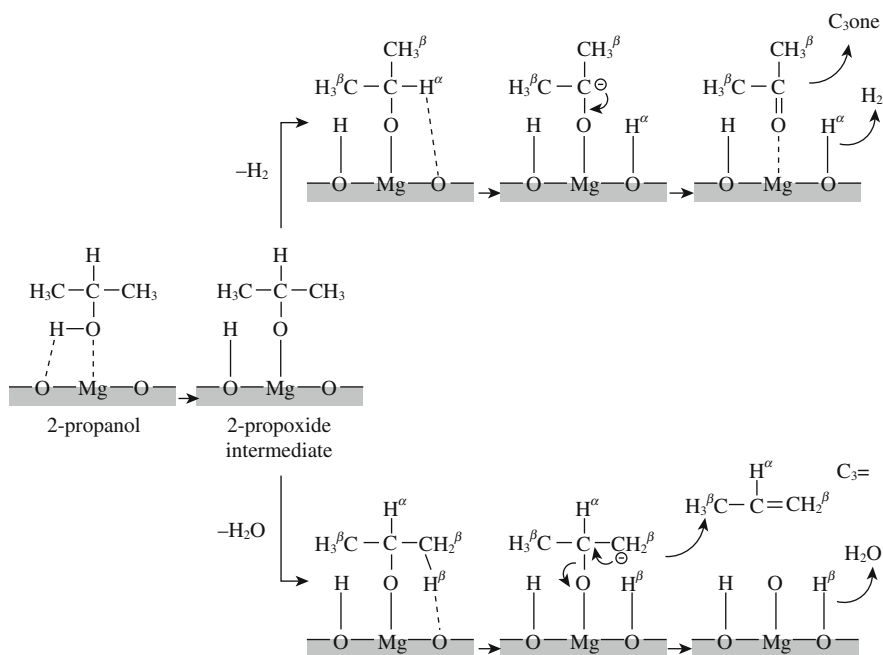


Fig. 2.5.5 Formation of acetone and propene from 2-propanol on MgO and Mg-rich MgO- Al_2O_3 mixed oxides.

Reprinted with permission from V. K. Diez, C. R. Apesteguia, J. I. Di Cosimo, *J. Catal.*, **215**, 220 (2003); p. 228 Scheme 2.

for estimating the acidic property, at least when strongly basic sites exist. It holds true that acetone is formed only on basic sites.

The selectivity depends very much on the reaction conditions such as reaction temperature and the pressure of 2-propanol. In the reaction of 2-propanol over TiO_2 , the dehydrogenation selectivity varies with reaction temperature from nearly 100% and below to 68% at 593 K.⁴⁸⁾ The formation of acetone increases an order of magnitude when the feed contains 10 Torr (1.33 KPa) of oxygen. Addition of relatively small amounts of water produces a profound effect on the selectivity; the rate of acetone formation increases significantly, propene being formed at a nearly constant rate. This indicates that the product of the test reaction, water, alters the nature of the acid-base character of the surfaces.

Yashima et al. studied decomposition of 2-propanol over alkali cation-exchanged X and Y zeolites.⁴⁹⁾ Over Li^+ and Na^+ -exchanged zeolites, 2-propanol underwent mostly dehydration. Over K^+ , Rb^+ , and Cs^+ -exchanged zeolites, both dehydrogenation and dehydration occurred. The dehydration and dehydrogenation of 2-propanol were selectively poisoned by the addition of a basic reagent (pyridine) and an acidic reagent (phenol), respectively. This is one of the first indications that alkali-exchanged zeolites act as solid base catalysts. The yield of acetone increased with increasing ionic radius, except CsX . Since other characterization techniques show that alkali cation-exchanged zeolites are weakly basic, formation of propene via carbanion intermediacy can be ruled out. Jacobs and Uytterhoeven, however, claim that dehydrogenation activity of alkali cation-exchanged zeolites is caused by iron impurities.⁵⁰⁾

The effect of the acid-base properties of metal oxide catalysts for vapor-phase oxidation reactions were extensively studied by Ai.⁵¹⁻⁵³⁾ As a test reaction of acid-base properties, he used decomposition of 2-propanol. By examining the effect of the compositions of oxide catalysts on the adsorption amount of CO_2 (or acetic acid) and the decomposition of 2-propanol over the oxides, the amount of basic sites determined by CO_2 (or acetic acid) on the oxides are better correlated with the ratio of the rate of dehydrogenation (r_a in $\text{mole g}^{-1} \text{h}^{-1}$) and that of dehydration (r_p), rather than with the rate of dehydrogenation (r_a) itself.^{51,52)} On the other hand, the activity for the dehydration is well correlated with the amount of acidic sites determined by pyridine (or ammonia) adsorption. Fig. 2.5.6 shows the dependence of the rate of oxidation of acetic acid per surface area (in $\text{mole m}^{-2} \text{h}^{-1}$) over a series of modified V_2O_5 catalysts on the r_a/r_p values of the catalysts. The author concludes that the basic sites play a crucial role in the oxidation of acidic molecules such as acetic acid.⁵³⁾

The reaction of butanols is also a useful method to characterize surface properties. As described above, formation of 2-butene from 1-butanol is indicative of the E1 mechanism (free carbenium ions) and thus of the presence of strongly acidic sites. From 2-butanol, preferential formation of 2-butene (Saytzev orientation) is observed in the case of the E2 mechanism, in which both acidic and basic sites are required. Over strongly basic catalysts, 1-butene is selectively formed from 2-butanol via carbanion intermediacy.

Table 2.5.6 shows the distribution of butenes in the dehydration of 1-butanol

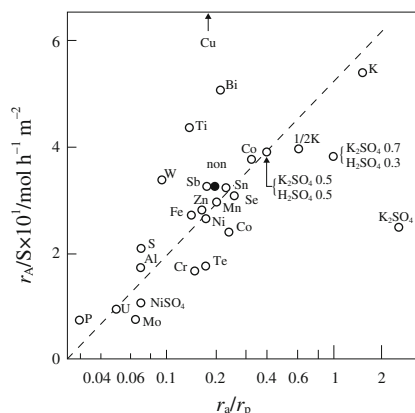


Fig. 2.5.6 Catalytic activities for acetic acid oxidation of metal oxides as a function of r_s/r_p . Reprinted with permission from M. Ai, *Bull. Chem. Soc. Jpn.*, **50**, 2579 (1977); p. 2582, Fig. 6.

Table 2.5.6 Representative butene distributions for evaluation of dehydration mechanisms

Catalyst (mechanism)	Reactant	1-Butene	2-Butene
		%	%
BPO ₄ (E1)	COH-C-C-C	30	70
	C-COH-C-C	30	70
Al ₂ O ₃ (E2)	COH-C-C-C	85	15
	C-COH-C-C	20	80
ThO ₂ (E1cB)	COH-C-C-C	95	5
	C-COH-C-C	90	10

Reprinted with permission from H. Noller, J. A. Lercher, H. Vinek, *Mater. Chem. Phys.*, **18**, 577 (1988); p. 587, Table III.

and 2-butanol over three catalysts, which exhibit typical behavior of the E1, E2 and E1cB mechanisms.²⁶⁾

Zirconium oxide gives mainly 1-butene in the dehydration of 2-butanol, indicating that anionic mechanism is operative as in the case of ThO₂.³⁵⁾

2-Butanol undergoes dehydrogenation over hydroxyapatite to afford 2-butanone in the temperature range 521–605 K.⁵⁴⁾ Dehydrogenation of 2-butanol-2-*d*₁ at 573 K gave 2-butanone free of deuterium, and there was no change in the isotopic composition of the alcohol. All hydrogen from the dehydrogenation of 2-butanol-2-*d*₁ was HD. The kinetic isotope effect on dehydrogenation was 1.8 (k_H/k_D). The proposed mechanism involves the formation of alkoxide followed by abstraction of α -hydrogen.

Alcohols other than 2-propanol and butanols are also used to characterize acid-base properties. Aramendia et al. propose the use of 1-phenylethanol, which gives two products by dehydration and dehydrogenation.⁵⁵⁾ From the correlation between the number of acidic and basic sites as determined by temperature programmed desorption of NH₃ and CO₂, respectively, with the catalytic activities for dehydration and dehydrogenation, the authors concluded that only basic sites are

responsible for dehydrogenation and acidic sites are mainly responsible for the dehydration process, although basic sites can also participate.

2.5.4 Reaction of 2-methyl-3-butyn-2-ol

Lauron-Pernot et al. proposed in 1991 that the vapor-phase reaction of 2-methyl-3-butyn-2-ol (MBOH) could be an effective measure for distinguishing acidic, basic and amphoteric catalysts.⁵⁶⁾ The method was fully reviewed by Lauen-Pernot; reaction conditions, deactivation phenomenon, reaction mechanisms and characteristics as a model reaction being discussed.⁵⁷⁾

The molecule undergoes dehydration over solid acids and decomposition to acetylene and acetone over solid bases. Over amphoteric catalysts, 3-hydroxy-3-methyl-2-butanone (HMB) is mainly formed (Fig. 2.5.7).

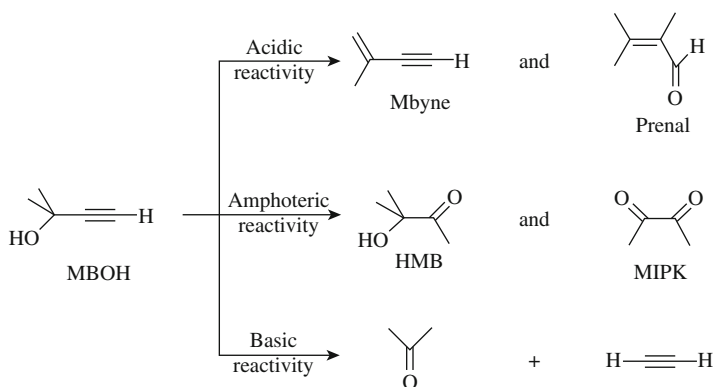


Fig. 2.5.7 The reaction products from MBOH over acidic, amphoteric and basic catalysts. Reprinted with permission from H. Lauron-Pernot, F. Luck, J. M. Popa, *Appl. Catal.*, **78**, 213 (1991); p. 215 Scheme 1.

The product distribution in the decomposition of MBOH on various catalysts reported by Lauron-Pernot is listed in Table 2.5.7.⁵⁶⁾ The reactions were carried out at 453 K with a pulse reactor. The selectivities S_i are defined as $S_i = \alpha_i C_i / (\sum \alpha_i C_i - C_{\text{MBOH}})$, where $\alpha_i = 1$ for all products except for acetylene and acetone, $\alpha_i = 0.5$.

$\text{SiO}_2\text{-Al}_2\text{O}_3$, a typical acid catalyst, gave 90% selectivity to 3-methyl-3-buten-1-yne (Mbyne), 3-methyl-2-butenal (prenal) also being formed. The mechanisms for the dehydration to Mbyne and isomerization to prenal are proposed as shown in Fig. 2.5.8.

Over MgO, a typical solid base, the conversion of MBOH is very high and acetylene and acetone are formed exclusively. Though the conversion is low, ZnO also gave a basic character. The mechanism of the decomposition of MBOH to acetylene and acetone is proposed as shown in Fig. 2.5.9.

Over ZrO_2 , a typical amphoteric oxide, HMB, a hydration product, is mainly formed. The formation of HMB as a main product over ZrO_2 was also

Table 2.5.7 Product distribution in the reaction of MBOH over various catalysts

Catalyst	Calcination Temp./K	Conv./%	Selectivity/%					
			Mbyne	Prenal	C ₂ H ₂	Acetone	HMB	MIPK
SiO ₂ -Al ₂ O ₃	673	25	90	9	0.5	0.5	0	0
MgO	673	70	0	0	52	48	0	0
ZnO	673	20	0	0	50	50	0	0
ZrO ₂	673	8	18.0	0	2	18	76	0
Al ₂ O ₃ (0.025% Na ₂ O)	723	7	16	0	22	23	0	39
Al ₂ O ₃ (0.27% Na ₂ O)	723	9.5	4.5	0	41	43.5	4.5	6.5
Al ₂ O ₃ (4.1% Na ₂ O)	723	100.0	0	0	50	50	0	0

Data reproduced from tables in H. Lauron-Pernot, F. Luck, J. M. Popa, *Appl. Catal.*, **78**, 213 (1991).

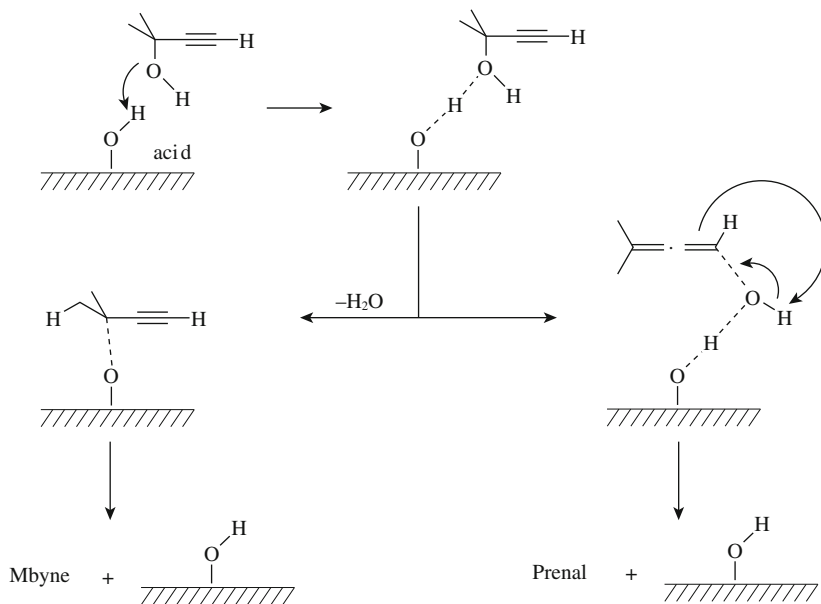


Fig. 2.5.8 Mechanism of MBOH reaction over acidic catalysts. Reprinted with permission from H. Lauron-Pernot, F. Luck, J. M. Popa, *Appl. Catal.*, **A**, **78**, 213 (1991); p. 220, Scheme 2.

confirmed.^{58,59)} Other products are acetylene, acetone, 3-methyl-3-butene-2-one (MIPK) and Mbyne. The distribution of the products depends on the pretreatment of the catalysts and reaction conditions such as reaction temperature. The hydration of MBOH to HMB is presumed to involve the surface hydroxyl groups or traces of water either contained in MBOH or formed by side reactions such as acetone condensation.⁵⁸⁾

Over Al₂O₃ with a low Na₂O content, MIPK is the predominant product, but

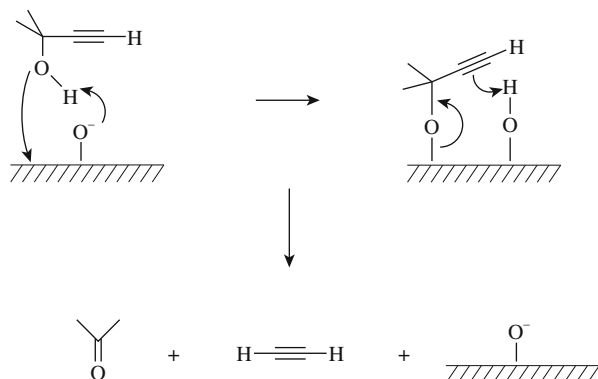


Fig. 2.5.9 Mechanism of MBOH reaction over basic surface. Reprinted with permission from H. Lauron-Pernot, F. Luck, J. M. Popa, *Appl. Catal., A*, **78**, 213 (1991); p. 220, Scheme 2.

C_2H_2 , acetone and MIPK are also formed, indicating that Al_2O_3 has both acidic and basic characteristics. By doping Na_2O onto Al_2O_3 , the products shift to acetylene and acetone, indicating that the material is shifted to a solid base. On the other hand, according to Lahousse et al., Al_2O_3 gave only acetone and acetylene at 523 K, while only dehydration occurred in the decomposition of 2-propanol at 673 K.⁶⁰⁾

ZnO gave acetylene and acetone exclusively in the reaction of MBOH at 523 K, and only acetone in the decomposition of 2-propanol at 673 K, indicating that ZnO is a basic oxide.⁶⁰⁾

$AlPO_4$ gives Mbyne very selectively (>98%). By loading $CsCl$ on the surface, the catalyst turns basic (>91% acetone + acetylene).⁶¹⁾

The reaction of MBOH over various types of zeolites was studied at 453 K by Huang and Kaliaguine.⁶²⁾ Acetone and acetylene are formed exclusively over a series of alkali cation-exchanged zeolites. The initial conversion increased with the counter cations in the order $Li^+ < Na^+ \approx K^+ < Rb^+ \ll Cs^+$. As for a series of Na^+ -exchanged zeolites, NaA, NaX, NaY gave only acetylene and acetone, but Mbyne appeared as another reaction product (6.5%) over NaL. The activity of NaX for the base-catalyzed reaction was greatly enhanced by loading NaN_3 or cesium acetate followed by calcinations.⁶³⁾ Over Na-ZSM-5, Mbyne is the predominant product (95.9%). In contrast to Na-ZSM-5, H-ZSM-5 gave MIPK with the selectivity as high as 45% besides Mbyn (49.6%) and prenal (3.9%). Huang and Kaliaguine propose that the formation of MIBK requires strong Brønsted sites. However, the work by Meir and Hölderich showed that MIBK was a predominant product (>90% selectivity) with a smaller amount of prenal over both Na-ZSM-5 and H-ZSM-5 at 393 K.⁶³⁾

The reaction of MBOH over hydrotalcite (HT) and its calcination products was examined by Costantino and Pinnavaia.^{64,65)} The composition of the starting hydrotalcite was $[Mg_{2.34}Al(OH)_{6.68}][CO_3]_{0.5} \cdot 2.6H_2O$. The material was activated at 353–723 K under a helium stream for 2 h and the catalytic activities for MBOH decomposition were examined at 353–423 K. The products were exclusively equi-

Table 2.5.8 Conversion of MBOH over catalysts by thermal activation of hydrotalcite

Activation temp. /K	Structural assignment	Surface area /m ² g ⁻¹	Reaction temp. /K	Conversion /%	Specific activity /mmol m ⁻² h ⁻¹
353	HT containing pores and interlayer water	-	353	22.4	0.020
423	HT without pore water	89	353	47.7	0.044
			423	100	>0.00930.
523	Anhydrous HT	91	353	25.1	0.024
			423	99.9	>0.093
623	Partially decarbonated HT	107	353	4.7	0.0043
			383	64.6	0.060
			423	93.5	~0.086
723	Amorphous oxide	180	353	4.5	0/0028
			383	38.9	0.060
			423	99.5	>0.061
1013	Spinel and MgO	83	353	2.7	0.0026
			383	39.9	0.038
			423	99.1	>0.096

Reprinted with permission from V. R. L. Constantino, T. J. Pinnavaia, *Catal. Lett.*, **23**, 361 (1994); p. 366, Table 1.

molar amounts of acetylene and acetone for every sample. As shown in Table 2.5.8, all of the samples exhibit MBOH conversions of >95% at a reaction temperature of 423 K. However, at 383 K or 353 K, important structure-dependent differences in the catalytic activity can be distinguished. Most significantly, the material activated below the structural decomposition temperature (≤ 523 K) is an order of magnitude more active than the metal oxides generated at 723 K. Similar results were also reported by Tanner et al.⁶⁶⁾ For most of the catalytic reactions such as the aldol reaction of acetone to diacetonealcohol,⁶⁷⁾ the MgO-Al₂O₃ mixed oxides prepared by calcination of hydrotalcite is highly active, while the hydrotalcite as prepared has nil activity. The reason for this discrepancy remains to be clarified. Rehydrated hydrotalcite, which contains OH⁻ in the interlayers, is more active than the hydrotalcite with CO₃²⁻ for MBOH decomposition.⁶³⁾

The effect of hydration of MgO on the reaction of MBOH was studied by Bailly et al.⁶⁸⁾ MgO was first evacuated at 1273 K. The clean surface was then hydroxylated at 373 K after which the temperature was increased in a flowing nitrogen in 100 °C step to progressively remove physisorbed water and OH groups. The catalytic activities of partially hydrated MgO correlated well with the amount of isolated hydroxyl groups determined by DRIFT, indicating that the isolated OH groups are active centers for MBOH decomposition. Furthermore, this implies that the OH groups are more active than oxide ions on the MgO surface. This is a quite similar to the finding for hydrotalcite materials.⁶⁴⁾

Handa et al. studied the catalytic activities for the reaction of various strong solid bases at 453 K. The results are listed in Table 2.5.9. For all the catalysts, acetylene and acetone were formed exclusively.⁶⁹⁾ The most active catalysts are the alkali metal salts supported on Al₂O₃ (KNO₃/Al₂O₃, K₂CO₃/Al₂O₃, KHCO₃/Al₂O₃,

Table 2.5.9 Catalytic activities of solid base catalysts for the decomposition of 2-methyl-3-butyn-2-ol over alkali compounds supported on alumina^{a)}

Catalyst	W/F /g h mol ⁻¹	MBOH conversion ^{b)} /%		Rate ^{b)} × 10 ⁻¹ /mol h ⁻¹ g ⁻¹	
		5 min	35 min	5 min	35 min
LiOH/Al ₂ O ₃	0.78	10.3	7.4	0.51	0.37
NaOH/Al ₂ O ₃	0.26	26.3	20.9	3.9	3.1
KOH/Al ₂ O ₃	0.13	26.9	24.5	8.5	7.3
RbOH/Al ₂ O ₃	0.094	22.8	18.1	9.5	7.5
CsOH/Al ₂ O ₃	0.088	21.8	17.7	9.7	7.5
KNOH/Al ₂ O ₃	0.12	34.8	23.1	12	7.8
K ₂ OH/Al ₂ O ₃	0.12	36.7	16.9	12	5.6
KHOH/Al ₂ O ₃	0.12	23.1	18.0	7.5	6.0
KFOH/Al ₂ O ₃	0.20	26.5	25.5	5.3	4.9
4MgO · Al ₂ O ₃ ^{c)}	2.07	20.8	19.0	0.39	0.36
4CaO · Al ₂ O ₃ ^{d)}	1.89	15.4	9.1	0.32	0.19
4CaO · Al ₂ O ₃ ^{d),e)}	1.89	12.0	5.3	0.25	0.11
KX	0.78	0.1	0.1	0.0055	0.0049
KX ^{f)}	1.56	6.1	3.9	0.152	0.097
CsX	0.78	0.1	0.1	0.0055	0.0055
CsX ^{f)}	1.56	0.6	0.4	0.00150	0.010
4.2 ^{g)} CsOAc/CsX	0.78	0.47	0.23	0.023	0.012
10.2 ^{g)} CsOAc/CsX	0.78	7.10	4.61	0.35	0.230

^{a)} Reaction conditions: 453 K, MBOH = 39.3 kPa, pretreatment temperature of the catalyst = 673 K, supported amount on alumina = 5 mmol g⁻¹

^{b)} Time on stream.

^{c)} Prepared from Mg₂Al(OH)₆NO₃ · nH₂O.

^{d)} Prepared from 3CaO · Al₂O₃ · Ca(NO₃)₂ · nH₂O at 873 K

^{e)} Prepared from 3CaO · Al₂O₃ · Ca(NO₃)₂ · nH₂O at 1073 K

^{f)} Reaction temperature = 483 K.

^{g)} Supported amount of CsOAc.

Reprinted with permission from H. Handa, Y. Fu, T. Baba, Y. Ono, *Catal. Lett.*, **59**, 195, (1999); p. 197, Table 1.

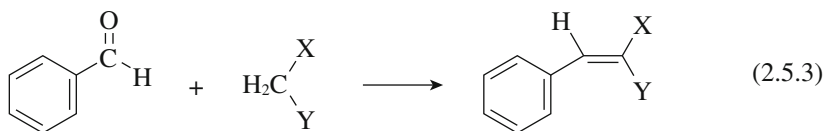
CsOH/Al₂O₃, RbOH/Al₂O₃). The activity of the mixed oxide prepared by calcination of hydrotalcite at 673 K is an order of magnitude lower than metal salts on Al₂O₃, but far more active than zeolites (KX, CsX). The activity of CsX is greatly enhanced by loading Cs(OAc)₂ followed by calcination. These general trends are in good agreement with those found in the activities for liquid-phase isomerization of 2,3-dimethyl-1-butene to 2,3-dimethyl-2-butene. The order of the activities for MBOH reaction over alkali hydroxide is as follows:



This order is the same as that found in the isomerization of 2,3-dimethyl-1-butene at 201 K. However, the relative activities among the catalysts are quite different. For the alkene isomerization, NaOH/Al₂O₃ is totally inactive at this temperature, while CsOH/Al₂O₃ is very active. On the other hand, for the rate of MBOH decomposition at 5 min time on stream, the ratio of the rates over the two catalysts is only 2.5. This indicates that alkene isomerization is a more effective measure of the basic strength for very strong solid bases.

2.5.5 Knoevenagel condensation

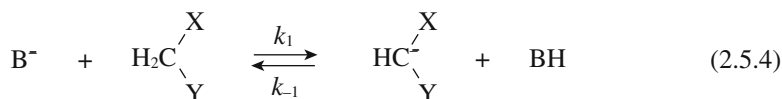
The Knoevenagel condensation is a class of base-catalyzed reactions. The reactions between benzaldehyde and compounds having an active methylene group are usually selected as the test reaction.

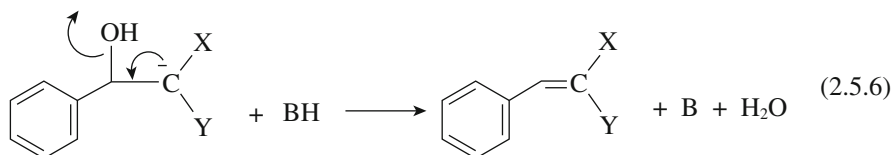
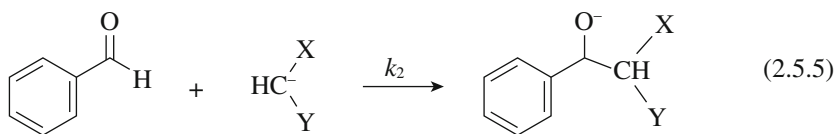


Active methylene compounds of different pK_a values are used. They are ethyl cyanoacetate ($pK_a = 9$), ethyl acetoacetate ($pK_a = 10.7$), malononitrile ($pK_a = 11.0$), diethyl malonate ($pK_a = 13.3$), and ethyl bromoacetate ($pK_a = 16.5$). The reactions are usually very selective. When the basic strength of the catalyst is high, side reactions such as Michael addition are involved. The reaction of benzaldehyde with ethyl cyanoacetate or malononitrile has been studied for a wide variety of solid bases as shown in Table 5.4.1.

Corma et al. proposed Knoevenagel condensation reactions of benzaldehyde with active methylene compounds having different pK_a values for estimating the basic strength of solid bases.⁷⁰⁾ In the reaction of benzaldehyde and ethyl cyanoacetate over a series of alkali metal cation-exchanged X and Y-type zeolites, the order of the catalytic activity was $\text{Li} < \text{Na} < \text{K} < \text{Cs}$ and $\text{Y} < \text{X}$. The orders are in conformity with those determined by the IR band of adsorbed pyrrole. The reaction of benzaldehyde and cyanoacetate were also carried out with homogeneous catalysts, pyridine ($pK_b = 8.8$) and piperidine ($pK_b = 11.12$). Pyridine is less active than any of X zeolites except the Li form, which shows slightly lower activity than pyridine. All Y zeolites show a lower activity than pyridine. Piperidine, however, is more active than any of the zeolites studied. The reaction rate depends on the pK_a values of the compounds having activated methylene groups. In the case of CsX, the rates of benzaldehyde with ethyl acetoacetate and diethyl malonate are 4 times and 30 times lower than the reaction with ethyl cyanoacetate, respectively. These results suggest that most of the basic sites of X- and Y-zeolites have basic sites of $H_- \leq 10.7$ and that only a few sites with $H_- \leq 13$ exist on the more basic CsX zeolite.⁷⁰⁾

The Knoevenagel condensation over basic sites can be expressed as follows.





The reaction rate, r , is expressed by first order kinetics with respect to $[\text{CH}_2\text{XY}]$ when step (2.5.4) is rate-determining.

$$r = k_1[\text{CH}_2\text{XY}] \quad (2.5.7)$$

The rate is directly affected by the ease of the proton abstraction from the active methylene group, thus its $\text{p}K_a$ value. In this case, the rate is not affected by the nature of the aldehyde (or ketone).

When step (2.5.6) is the rate-determining step, the rate is of the second order and expressed as follows.

$$r = k_2 K_1 \frac{[\text{CH}_2\text{XY}][\text{aldehyde}]}{1 + K_1[\text{CH}_2\text{XY}]} \quad K_1 = k_1 / k_{-1} \quad (2.5.8)$$

When $1 \gg K_1[\text{CH}_2\text{XY}]$,

$$r = k_2 K_1 [\text{CH}_2\text{XY}][\text{aldehyde}] \quad (2.5.9)$$

In this case, the rate depends on the properties of both the active methylene compound and the aldehyde (or ketone). In other words, the over-all rate is not a direct measure of the nature of the active methylene group.

In the Knoevenagel reactions over alkali cation-exchanged zeolites, the experimental rates fitted both first and second order kinetics, though a better fit was observed for the latter.⁷⁰⁾ In the Knoevenagel reactions between malononitrile and various ketones in the presence of calcined hydrotalcite and CsX , the rate depended on the ketone in the order, benzophenone > cyclohexanone > *p*-aminoacetophenone.⁷¹⁾

Step (2.5.4), the abstraction of a proton from an active methylene compound by the catalyst, does not proceed if the basic strength of the basic sites is too weak. Thus, for the reaction to proceed, the H value of the basic sites must be equivalent or higher than the $\text{p}K_a$ value of the active methylene group. This is the basis on which the Knoevenagel reaction can be used as a measure of the basic strength of the solid surfaces. It should be noted that the rate of the condensation can also be dependent on the reactivity of the aldehyde (or ketone). Obviously, the rate depends on the number of basic sites. These points must be kept in mind when

one discusses the basic strength of the catalysts from the rate of the Knoevenagel condensation.

Corma et al. studied the various solid base catalysts by the Knoevenagel reactions. Germanium substituted faujasite (Na-GeX) is more active than ordinary NaX for the reaction of benzaldehyde with ethyl cyanoacetate or diethyl malonate.⁷²⁾ For the alkali cation-exchanged sepiolite, the activity order is $\text{Li} < \text{Na} < \text{K} < \text{Cs}$. The activity of $\text{MgO-Al}_2\text{O}_3$ mixed oxide prepared from hydrotalcite ($\text{Mg}/\text{Al} = 3$) is more active than Cs-sepiolite. The activity order is determined as $\text{Mg,Al-mixed oxide} > \text{Cs-sepiolite} > \text{CsX} > \text{CsY}$.^{71,73)} Because of the higher basic strength of the mixed oxide, various side products are formed as a result of Michaels addition, aldol condensation, etc. in the reaction of benzaldehyde and ethyl acetoacetate. These reactions demand stronger bases than the Knoevenagel reaction. The mixed oxide shows also the activity for the Knoevenagel condensation of benzaldehyde and ethyl bromoacetate, indicating that the mixed oxide contains basic sites of H -value up to 16.5.

Rodriguez et al. examined the catalytic activities of Cs-loaded Cs-Y and Cs-X zeolites by using the reaction between benzaldehyde and ethyl cyanoacetate.⁷⁴⁾ The catalysts were prepared by loading cesium acetate with an impregnation method followed by calcination at 823 K. The initial rate of the condensation increased with increase in the loading amount of Cs in the unit cell, indicating that the basic strength and/or amount of basic sites increase with increasing Cs-loading.

Goa et al. compared the catalytic activity of ETS-10 and Y-zeolites for Knoevenagel condensations.⁷⁵⁾ For the reaction of benzaldehyde and ethyl cyanoacetate, alkali cation-exchanged ETS is much more active than alkali cation-exchanged Y-zeolite. For the reaction of acetone with malononitrile, ETS-10 is active, but Y-zeolites are totally inactive. These results indicate that alkali cation-exchanged ETS-10 is more basic than alkali cation-exchanged Y-zeolites.

In the Knoevenagel reaction of benzaldehyde with ethyl malononitrile or ethyl cyanoacetate, the reaction rate is much faster with malononitrile than with ethyl cyanoacetate. (see Table 5.4.1) This is unexpected since the former has higher $\text{p}K_a$ value. Climent et al. attributed this phenomenon to the difference in the stabilization of the carbanion intermediate on the surface.⁷⁶⁾ It should be noted that $\text{p}K_a$ values are dependent on the reaction medium, i.e. solvent used. Climent et al. compared the catalytic activity of four solid bases for Knoevenagel condensation; the reaction of benzaldehyde with malononitrile and dimethyl malonate.⁷⁶⁾ The order of the catalytic activity depended on the reaction studied.

For the reaction of benzaldehyde with malononitrile



For the reaction of benzaldehyde with diethyl malonate



The authors discuss this phenomenon as follows: CsX and AIPON have a higher number of weakly basic sites, and are more active than MgO and the mixed oxide. For the more demanding reaction of benzaldehyde with diethyl malonate, the

catalysts having strong basic sites, MgO and the mixed oxide, are more active than AlPON.

2.5.6 Aldol addition of acetone to diacetone alcohol and retroaldolization of diacetone alcohol

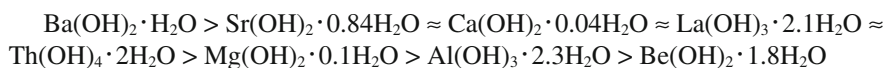
Aldol addition of acetone to diacetone alcohol (DAA) is catalyzed in liquid phase by solid bases.



The reaction is reversible and the acetone conversion at equilibrium has been estimated and is shown in Table 2.5.10.⁷⁷⁾ The reaction has to be carried out under mild conditions to avoid side reactions. In the presence of acid sites, the dehydration of DAA proceeds to form mesityl oxide, which is a strong inhibitor for the aldol reaction.⁷⁸⁾

Barium hydroxide is the conventional catalyst for the aldol reaction of acetone to diacetone alcohol. Raso et al. reported that Ba(OH)₂ obtained by calcination of commercial Ba(OH)₂·H₂O in air at 473 K had a high activity with high selectivity for preparing diacetone alcohol from acetone.⁷⁹⁾ The experimental formula of the catalyst is Ba(OH)₂·0.8 H₂O, the main component being Ba(OH)₂·H₂O.⁸⁰⁾

The catalytic activities of various metal hydroxides were studied at the reflux temperature of acetone.⁸¹⁾ The activity order was as follows.



Zhang et al. studied the aldol addition of acetone over various metal oxides at 273 K.⁸²⁾ Alkaline earth oxides showed high activities and the products consisted mostly of diacetone alcohol and a small amount of mesityl oxide. On a weight basis of catalysts, the activities were in the following order: CaO > BaO > SrO > MgO. The activity order on a unit surface area basis was BaO > SrO > CaO > MgO. This order of the activities coincided with the order of the basic strength of the basic sites as determined by temperature-programmed desorption of carbon dioxide. In the case of MgO, preadsorption of water increased the activity, though the excess amount decreased the activity. The maximum activity was seen at 2.4 mmol water per 1 g of MgO. Preadsorption of water beyond the maximum led to 100% selectivity, formation of the by-product mesityl oxide being completely suppressed. The enhancement of the reaction rate upon addition of water indicates that the surface hydroxyl groups are involved as active sites. La₂O₃ and ZnO were

Table 2.5.10 Equilibrium conversion of acetone to DAA

Temperature /K	273	283	293	303	318	329
Conversion /%	23.1	16.9	12.1	9.3	5.6	4.3

Reprinted with permission from G. G. Podrebarac, F. T. T. Ng, G. I. Rompel, *Chem, Eng, Sci.*, **52**, 2991 (1997); p. 2992, Table 1.

less active than alkaline earth oxides and Nb_2O_5 and SiO_2 showed no activity. A study using isotopic compounds on the reaction in the presence of MgO and La_2O_3 indicates that the C-C bond formation between an acetone molecule and an enolate ion formed on the surface is the rate-determining step.⁸³⁾

An anion exchange resin, Amberlist-900, in the hydroxide form is an effective catalyst for the aldol addition of acetone to DAA.⁷⁷⁾ Mesityl oxide is also formed. The reaction is diffusion controlled. Adding water to the reaction mixture increases the product selectivity toward DAA and the catalyst life time, but slows the rate of the reaction.

The catalytic activities for aldol addition of acetone have been used extensively for estimating the basic properties of hydrotalcite and related materials.^{78,84-89)}

Synthesized hydrotalcite heated at 373 K had no activity, while hydrotalcite calcined at 773 K showed a high activity^{78,86)} The activity of the $\text{MgO-Al}_2\text{O}_3$ mixed oxide formed by calcination depends on the Al/Mg ratio. The main products were diacetone alcohol (96%) and mesityl oxide (4%) at 273 K. The addition of pyridine to the acetone decreases both the activity and selectivity for mesityl oxide, confirming that the acid sites are involved in the dehydration of diacetone alcohol to mesityl oxide. Mesityl oxide is a strong inhibitor of the reaction. The conversion decreased from 11% to 4% when 0.5 wt% of mesityl oxide was added and the reaction was totally inhibited with 3 wt% of mesityl oxide.

Upon treatment of the mixed oxide with water in controlled amounts, the hydrotalcite structure is restored and hydroxide ions (OH^-) are introduced in the interlayers. This reconstructed hydrotalcite showed much higher activity than the mixed oxide.^{84,87)} This indicates that basic OH groups are more active than basic oxide ions. Rehydration is more effective in the liquid phase than in gas phase, the equilibrium conversion being reached in 0.5 h at 273 K.⁸⁸⁾ The OH^- ions near the edges of the hydrotalcite platelets are considered to be the active sites.⁸⁸⁾ The catalytic activity per unit weight of hydrotalcite was much enhanced by supporting hydrotalcite on carbon nanofibers.^{85,89)} The activities of various hydrotalcite-

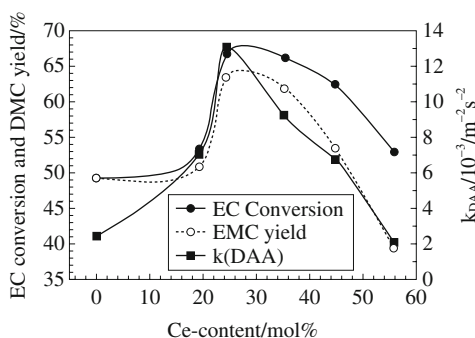


Fig. 2.5.10 Correlation of ethylene carbonate (EC) conversions and dimethyl carbonate (DMC) yields with the first order rate constant $k(\text{DAA})$ in retroaldolization of diacetone alcohol over MgO-CeO_2 catalysts.

Reprinted with permission from H. Abimaynyu, C. S. Kim, B. S. Ahn, K. S. Yoo, *Catal. Lett.*, **118**, 30 (2007); p. 33, Fig. 5.

derived samples were well correlated with the number of basic sites as determined by CO₂ chemisorption.

Retroaldolization of DAA is also used for characterizing the basic properties of solid surfaces.⁹⁰⁻⁹³⁾ A good correlation was observed between the catalytic activities and the number of basic sites, as determined by titration with acrylic acid.⁹²⁾ The first order rate constant of retroaldol reaction of DAA was determined as a function of the composition of MgO-CeO₂ mixed oxides.⁹³⁾ The rate constant is well correlated with the conversion and the yield of dimethyl carbonate in the transesterification of ethylene carbonate with methanol (Fig. 2.5.10).

2.5.7 Cyclization of acetylacetone

Acetylacetone undergoes both acid and base-catalyzed intramolecular cyclizations: Acid catalysis produces 2,5-dimethylfuran (DIMF), whereas base catalysis leads to 3-methyl-2-cyclopenten-1-one (MCPO). The mechanistic scheme for the two reactions is shown in Fig. 2.5.11.⁹⁷⁾ The reaction is carried out in vapor phase at elevated temperatures. The selectivity of the reaction is used for distinguishing acidic and basic surfaces. Some selected data are listed in Table 2.5.11.

Dessau first proposed the use of the transformation of acetylacetone to distinguish the acid-base character of zeolites.⁹⁴⁾ Over H-ZSM-5, DIMF was produced at greater than 97% selectivity at conversions close to 100% at 523–623 K, while over Na-ZSM-5 MCPO was obtained with selectivity of >90% even under complete conversion conditions at 623 K.

MgO shows 100% selectivity for the pentenone, while SiO₂-Al₂O₃ shows 99% selectivity for DIMF at 573 K.⁹⁵⁾ Amorphous aluminophosphate gave 30–38% selectivity for MCPO, the only other product being DIMF, indicating the amphoteric nature of AlPO₄. When AlPO₄ was loaded with cesium acetate and calcined at 873 K, the selectivity for MCPO increased as the loading amount of the Cs compound. The selectivity for MCPO reached 100% when the loading reached 30 wt%.⁹⁵⁾

Hydrated and calcined Nb₂O₅ shows an amphoteric nature.⁹⁶⁾ Al₂O₃ shows a

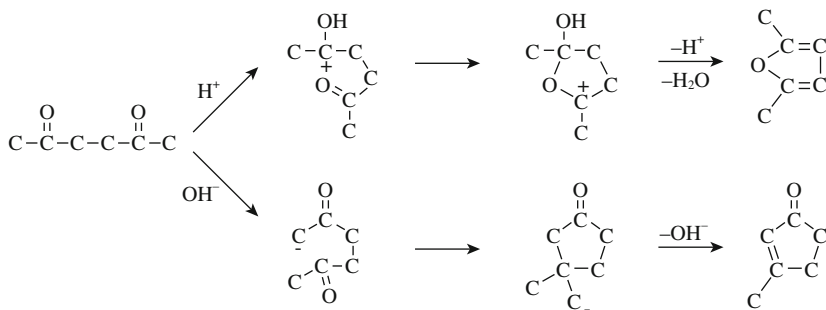


Fig. 2.5.11 Reactions of acetylacetone over acidic and basic catalysts. Reprinted with permission from R. M. Dessau, *Zeolites*, **10**, 205 (1990); p. 206.

Table 2.5.11 Selectivity in the reaction of acetylacetone

Catalyst	Temperature /K	Conversion /%	Selectivity		Reference no.
			DIMF/%	MCPO/%	
H-ZSM-5 (Si/Al = 35)	523	96.8	98.7	1.2	94
H-ZSM-5 (Si/Al = 300)	623	99.9	97.7	1.5	94
Na-ZSM-5 (Si/Al = 300)	623	99.9	4.4	89.1	94
MgO	573	20	0	100	95
SiO ₂ -Al ₂ O ₃	573	20	99.0	1.0	95
AlPO ₄	573	20	67.0	33.0	95
5 wt% CsOAc/AlPO ₄	573	20	60.5	39.5	95
10 wt% CsOAc/AlPO ₄	573	20	49.3	50.7	95
20 wt% CsOAc/AlPO ₄	573	20	17.9	82.0	95
30 wt% CsOAc/AlPO ₄	573	20	2.0	98.0	95
Nb ₂ O ₅ · nH ₂ O	623	20	58	38	96
Nb ₂ O ₅	623	15	54	42	96
Al ₂ O ₃	623	71	13	77	96
K ⁺ /Al ₂ O ₃	623	70	0.4	89	96
Cs ⁺ /Al ₂ O ₃	623	94	1	86	96
MgO-Al ₂ O ₃	573	65	0	100	97
MCM-41	623	18	100	0	98
Li/MCM-41	623	29	12.8	87.2	98
Na/MCM-41	623	30	0	100	98
K/MCM-41	623	79	0	100	98
Rb/MCM-41	623	81	0	100	98
Cs/MCM-41	623	89	0	100	98

basic character rather than acid, though Al₂O₃ shows very high selectivity for 2-propanol dehydration.⁹⁶⁾ The basic character of Al₂O₃ is enhanced by loading alkali metal ions.

MgO-Al₂O₃ mixed oxides prepared from hydrotalcite gave 100% selectivity for MCPO at 573 K.⁹⁷⁾

The effect of alkali-cation loading on MCM-41 was studied by Michalska et al.⁹⁸⁾ The loading was performed by incipient wetness impregnation with alkali metal acetates with a loading of alkali metal element of ca. 5 wt%. The materials were then dried and calcined at 773 K. These treatments caused the destruction of the mesoporous structure. Thus, the surface area of the materials decreased from 990 m² g⁻¹ to 110, 90, 120, 370, and 590 m² g⁻¹ for Li, Na, K, Rb, and Cs-loaded samples, respectively. The acid-base character of the surfaces was studied by the reaction of acetylacetone at 623 K. As shown in Table 2.5.11, MCM-41 gives the DIMF exclusively. Li-loaded MCM-41 developed the activity for the MCPO. K-, Rb- and Cs-loaded materials give the MCPO exclusively.

References

1. E. F. Meyer, D. G. Stroz, *J. Am. Chem. Soc.*, **94**, 6344 (1972).

2. D. J. Cram, *Fundamentals of Carbanion Chemistry*, Academic Press, 1965, New York and London.
3. S. Bank, A. Schriesheim, C. A. Rowe, Jr., *J. Am. Chem. Soc.*, **87**, 3244 (1965).
4. S. Bank, *J. Am. Chem. Soc.*, **87**, 3245 (1965).
5. C. C. Chang, W. C. Conner, R. J. Kokes, *J. Phys. Chem.*, **77**, 1957 (1973).
6. J. W. Hightower, W. K. Hall, *J. Am. Chem. Soc.*, **89**, 778 (1967).
7. H. Hattori, K. Maruyama, K. Tanabe, *J. Catal.*, **44**, 50 (1976).
8. Y. Fukuda, H. Hattori, K. Tanabe, *Bull. Chem. Soc. Jpn.*, **51**, 3150 (1978).
9. M. P. Rosynek, J. S. Fox, J. L. Jensen, *J. Catal.*, **71**, 64 (1981).
10. T. Yamaguchi, N. Ikeda, H. Hattori, K. Tanabe, *J. Catal.*, **67**, 324 (1981).
11. H. Hattori, M. Itoh, K. Tanabe, *J. Catal.*, **41**, 46 (1976).
12. E. A. Lombardo, W. C. Conner, Jr., B. J. Madon, W. K. Hall, V. V. Kharlamov, Kh. M. Minachev, *J. Catal.*, **53**, 135 (1978).
13. T. Sumiyoshi, K. Tanabe, H. Hattori, *Bull. Jpn. Petrol. Inst.*, **17**, 65 (1975).
14. Y. Nakano, T. Iizuka, H. Hattori, K. Tanabe, *J. Catal.*, **51**, 1 (1979).
15. W. O. Haag, H. Pines, *J. Org. Chem.*, **82**, 387 (1960).
16. N. F. Foster, R. J. Cvetanovic, *J. Am. Chem. Soc.*, **82**, 4274 (1960).
17. H. Noumi, T. Misumi, S. Tsuchiya, *Chem. Lett.*, **7**, 439 (1978).
18. S. Tsuchiya, S. Takase, H. Imamura, *Chem. Lett.*, **13**, 661 (1984).
19. H. Hattori, N. Yoshii, K. Tanabe, *Proc. 5th Inter. Conf. Catal. Miami 1972*, p. 233.
20. M. Mohri, K. Tanabe, H. Hattori, *J. Catal.*, **32**, 144 (1974).
21. H. Hattori, M. Itoh, K. Tanabe, *J. Catal.*, **38**, 172 (1975).
22. T. Yamaguchi, H. Sasaki, K. Tanabe, *Chem. Lett.*, **2**, 1017 (1973).
23. M. Itoh, H. Hattori, K. Tanabe, *J. Catal.*, **43**, 192 (1976).
24. H. Tsuji, F. Yagi, H. Hattori, *Chem. Lett.*, **20**, 1881 (1991).
25. T. Baba, G. J. Kim, Y. Ono, *J. Chem. Soc. Faraday Trans.*, **88**, 891.1 (1992).
26. H. Noller, K. Thomke, *J. Mol. Catal.*, **6**, 375 (1979).
27. V. K. Diez, C. R. Apesteguía, J. J. Di Cosimo, *J. Catal.*, **215**, 220 (2003).
28. M. E. Manriquez, T. López, R. Gómez, J. Navarrete, *J. Mol. Catal. A*, **220**, 229 (2004).
29. H. Pines, J. Manassen, *Adv. Catal.*, **16**, 49 (1966).
30. H. Noller, J. A. Lercher, R. Vinex, *Mater. Chem. Phys.*, **18**, 577 (1988).
31. H. Knözinger, A. Scheglila, *J. Catal.*, **17**, 252 (1970).
32. B. Shi, H. A. Dabbagh, B. H. Davis, *Topics Catal.*, **18**, 259 (2002).
33. D. Dautzenberg, H. Knözinger, *J. Catal.*, **33**, 142 (1974).
34. C. L. Kibby, W. K. Hall, *J. Catal.*, **29**, 144 (1973).
35. T. Yamaguchi, H. Sasaki, K. Tanabe, *Chem. Lett.*, **2**, 1017 (1973).
36. B. H. Davis, P. Ganesan, *Ind. Eng. Chem., Prod. Rev. Dev.*, **18**, 191 (1979).
37. A. Auroux, P. Arizzu, L. Ferino, V. Solinass, G. Leofanti, M. Padovan, G. Messina, R. Mansani, *J. Chem. Soc. Faraday Trans.*, **91**, 3263 (1995).
38. I. Ferino, M. F. Casula, A. Corrias, M. G. Cutrufello, R. Monaci, G. Paschina, *Phys. Chem. Chem. Phys.*, **2**, 1847 (2000).
39. A. J. Lundeen, R. van Hoozer, *J. Org. Chem.*, **32**, 3386 (1967).
40. K. Thomke, *Z. Phys. Chem., N. F.*, **106**, 225 (1977).
41. H. Niiyama, E. Echigoya, *Bull. Chem. Soc. Jpn.*, **44**, 1739 (1971).
42. F. Nozaki, H. Ohta, *Bull. Chem. Soc. Jpn.*, **47**, 1307 (1974).
43. M. A. Armendía, V. Borau, C. Jiménez, J. M. Marinas, A. Porras, F. J. Urbano, *J. Catal.*, **161**, 829 (1996).
44. P. E. Hathaway, M. Davis, *J. Catal.*, **116**, 279 (1989).
45. A. Gervasini, J. Fenyvesi, A. Auroux, *Catal. Lett.*, **43**, 219 (1987).
46. Z. G. Szabó, B. Jóvér, R. Ohmacht, *J. Catal.*, **39**, 225 (1975).
47. V. K. Diez, C. R. Apestegula, J. J. Di Cosimo, *Stud. Surf. Sci. Catal.*, **130**, 2219 (2000).
48. J. E. Rekoste, M. A. Barteau, *J. Catal.*, **165**, 57 (1997).
49. T. Yashima, H. Suzuki, N. Hara, *J. Catal.*, **33**, 486 (1974).
50. P. A. Jacobs, J. B. Uytterhoeven, *J. Catal.*, **50**, 109 (1977).
51. M. Ai, *Bull. Chem. Soc. Jpn.*, **49**, 1328 (1976).
52. M. Ai, *J. Catal.*, **40**, 327 (1973).
53. M. Ai, *Bull. Chem. Soc. Jpn.*, **50**, 2579 (1977).
54. C. Kibby, W. K. Hall, *J. Catal.*, **31**, 65 (1973).
55. M. A. Aramendía, V. Borau, C. Jiménez, J. M. Marinas, A. Purras, F. J. Urbano, *React. Kinet. Catal. Lett.*, **65**, 25 (1998).

56. H. Lauron-Pernot, F. Luck, J. M. Popa, *Appl. Catal.*, **78**, 213 (1991).
57. H. Lauron-Pernot, *Catal. Rev.*, **48**, 315 (2006).
58. F. Audry, P. E. Hoggan, J. Saussey, J. C. Lavalley, H. Lauron-Pernot, A. M. Le Govic, *J. Catal.*, **168**, 471 (1997).
59. M. A. Aramendia, V. Boráú, C. Jiménez, J. M. Marinas, A. Marinas, A. Porras, F. J. Urbano, *J. Catal.*, **183**, 240 (1999).
60. C. Llahoussé, J. Bachelier, J.-C. Lavalley, *J. Mol. Catal.*, **87**, 329 (1994).
61. F. M. Bautista, J. M. Campelo, A. Garcia, R. M. Leon, D. Luna, J. M. Marinas, A. A. Romero, *React. Kinet. Catal. Lett.*, **65**, 239 (1998).
62. M. Huang, S. Kaliaguine, *Catal. Lett.*, **18**, 373 (1993).
63. U. Meir, W. F. Hölderich, *J. Mol. Catal. A*, **142**, 213 (1999).
64. V. R. L. Constantino, T. J. Pinnavaia, *Catal. Lett.*, **23**, 361 (1994).
65. V. R. L. Constantino, T. J. Pinnavaia, *Inorg. Chem.*, **34**, 883 (1995).
66. R. Tanner, D. Enache, R. P. K. Wells, G. Kelly, J. Casci, G. J. Hutchings, *Catal. Lett.*, **100**, 259 (2005).
67. F. Prinetto, D. Ticht, R. Teissier, B. Coq, *Cat. Today*, **55**, 103 (2002).
68. M.-L. Bailly, C. Chizallet, G. Constantin, J.-M. Krafft, H. Lauron-Pernot, M. Che, *J. Catal.*, **235**, 413 (2005).
69. H. Handa, Y. Fu, T. Baba, Y. Ono, *Catal. Lett.*, **59**, 195 (1999).
70. A. Corma, V. Fornés, R. M. Martín-Aranda, H. Garcia, J. Promo, *Appl. Catal.*, **59**, 237 (1990).
71. A. Fornés, R. M. Martín-Aranda, F. Rey, *J. Catal.*, **134**, 58 (1992).
72. A. Corma, R. M. Martín-Aranda, F. Sánchez, *J. Catal.*, **126**, 192 (1990).
73. A. Corma, R. M. Martín-Aranda, *J. Catal.*, **130**, 130 (1991).
74. I. Roriguez, H. Cambon, D. Brunel, M. Laspéras, *J. Mol. Catal. A*, **130**, 195 (1998).
75. Y. Goa, P. Wei, T. Tatsumi, *J. Catal.*, **224**, 107 (2004).
76. M. J. Climent, A. Corma, V. Fornés, A. Frau, R. Guil-López, S. Ibbora, J. Primo, *J. Catal.*, **163**, 392 (1996).
77. G. G. Podrebarac, F. T. T. Ng, G. I. Rempel, *Chem. Eng. Sci.*, **52**, 2991 (1997).
78. D. Ticht, M. N. Bennani, F. Figueras, R. Tessier, J. Kervennal, *Appl. Clay Sci.*, **13**, 401 (1998).
79. A. G. Raso, J. V. Sinisterra, J. Marinas, *React. Kinet. Catal. Lett.*, **18**, 33 (1981).
80. A. Aguilera, A. R. Alcantara, J. M. Marinas, J. V. Sinisterra, *Can J. Chem.*, **65**, 1165 (1987).
81. H. Dabbach, B. H. Davis, *J. Mol. Catal.*, **48**, 117 (1988).
82. G. Zhang, H. Hattori, K. Tanabe, *Appl. Catal.*, **A**, **36**, 189 (1988).
83. G. Zhang, H. Hattori, K. Tanabe, *Appl. Catal.*, **A**, **40**, 183 (1988).
84. J. C. A. Roelofs, A. J. van Dillen, K. P. de Jong, *Catal. Today*, **60**, 297 (2000).
85. J. C. A. Roelofs, D. J. Lensveld, A. J. van Dillen, K. P. de Jong, *J. Catal.*, **203**, 184 (2001).
86. P. Kuśtrowski, D. Sulkowska, L. Chmielarz, A. Rafalska-Lasocha, B. Dudek, R. Dziembaj, *Micropor. Mesopor. Mater.*, **78**, 11 (2003).
87. P. Kuśtrowski, D. Sulkowska, L. Chmielarz, P. Olszewski, A. Rafalska-Lasocha, R. Dziembaj, *React. Kinet. Catal. Lett.*, **85**, 383 (2005).
88. S. Abelló, F. Medina, D. Ticht, J. Pérez-Ramírez, J. C. Groen, J. E. Sueiras, P. Salagre, Y. Cesteros, *Chem. Eur. J.*, **11**, 728 (2005).
89. F. Winter, V. Koot, A. J. van Dillen, J. W. Geus, P. de Jong, *J. Catal.*, **236**, 91 (2005).
90. Y. Fukuda, K. Tanabe, S. Okazaki, *Nippon Kagaku Kaishi*, 513 (1972) (in Japanese).
91. A. Tada, *Bull. Chem. Soc. Jpn.*, **49**, 1391 (1975).
92. J. M. Campelo, A. Garcia, D. Luna, J. M. Marinas, *Can. J. Chem.*, **62**, 638 (1984).
93. H. Abimanyu, C. S. Kim, B. S. Ahn, K. S. Yoo, *Catal. Lett.*, **118**, 30 (2007).
94. B. M. Dessau, *Zeolites*, **10**, 205 (1990).
95. F. M. Bautista, J. M. Campelo, A. Garcia, R. M. Leon, D. Luna, J. M. Marinas, A. A. Romero, *Catal. Lett.*, **60**, 145 (1999).
96. V. Calvino-Casilda, R. Martín-Aranda, I. Sobczak, M. Ziolk, *Appl. Catal.*, **A**, **303**, 121 (2006).
97. A. Guida, M. H. Lhouty, D. Ticht, F. Figueras, P. Genste, *Appl. Catal.*, **A**, **164**, 251 (1997).
98. A. Michalska, M. Daturi, J. Saussey, I. Nowak, M. Ziolk, *Micropor. Mesopor. Mater.*, **90**, 362 (2006).

3.

Preparation and Catalytic Properties of Solid Base Catalysts — I. Metal Oxides

3.1 Alkaline Earth Oxides

MgO, CaO, SrO and BaO are representative solid base catalysts that are used for a number of base-catalyzed reactions. The surface basic strength is believed to follow the order: $\text{MgO} < \text{CaO} < \text{SrO} < \text{BaO}$. Among these, MgO has been studied most extensively, probably because samples of definite structure with high surface area are prepared much more easily by thermal pretreatment than samples of CaO, SrO and BaO. The structures of CaO, SrO, and BaO are similar to that of MgO, and thus, the catalytic and surface properties of CaO, SrO, and BaO can be estimated from the results obtained with MgO. Although BeO and RaO are included in the alkaline earth oxides, they have not been studied because of toxicity and radioactivity, respectively.

In this section, generation of basic sites, characterization of active sites, preparation of catalysts for high surface area and definite pore structure are described mostly for MgO, and to a lesser extent for the other alkaline earth oxides. In the final section the catalytic properties of alkaline earth oxides are briefly described focusing on the strength of basic sites relevant to different types of reaction.

3.1.1 Generation of Active Sites

MgO and CaO are normally prepared by thermal decomposition of $\text{Mg}(\text{OH})_2$ and $\text{Ca}(\text{OH})_2$, respectively. On the other hand, SrO and BaO are prepared from SrCO_3 and BaCO_3 , respectively, because $\text{Sr}(\text{OH})_2$ and $\text{Ba}(\text{OH})_2$ melt at low temperatures when temperature is rising. $\text{Sr}(\text{OH})_2$ melts at 648 K in H_2 , and $\text{Ba}(\text{OH})_2$ melts at 351 K. Any commercially available alkaline earth oxides have probably been exposed to the atmosphere and their surfaces may be covered with carbonates, hydroxides, and in some cases, peroxides. Removal of carbon dioxide, water and oxygen from the surfaces is required to reveal the oxide surfaces.

During thermal treatment of commercially available hydroxides and carbonates, water and carbon dioxide are evolved. Fig. 3.1.1 shows the evolution of water and carbon dioxide from $\text{Ca}(\text{OH})_2$ as a function of outgassing temperature. Surface areas and the activities for 1-butene isomerization are also plotted.^{1,2)} Evolution of water and carbon dioxide begins at about 600 K and continues up to about 1000 K. Evolution of water and carbon dioxide results in generation of basic sites on the surfaces which act as catalytically active sites for e.g., 1-butene

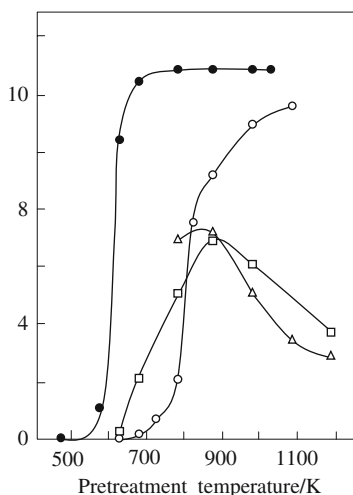


Fig. 3.1.1 Variations in (○) amount of CO₂ evolved/20 mmol g⁻¹, (●) amount of H₂O evolved/mmole g⁻¹, (△) surface area/100 m² g⁻¹, (□) activity for 1-butene isomerization/a.u. as a function of pretreatment temperature of CaO prepared from Ca(OH)₂.

isomerization. The surface area changes with an increase in the outgassing temperature. Essentially the same features for the evolution of water and carbon dioxide are observed for MgO.

When BaO and SrO are prepared from commercially available BaO and SrO, evolution of water and carbon dioxide appears at 673 K for BaO,³⁾ and evolution of water and carbon dioxide at 473 K and 673 K, respectively, for SrO.⁴⁾ The evolution of water and carbon dioxide continues to much higher temperatures for BaO and SrO than for CaO and MgO. In addition to water and carbon dioxide, oxygen begins to evolve above 900 K. BaO and SrO easily form peroxides on contact with oxygen, so removal of oxygen is also required to reveal the oxide surfaces to show active sites for 1-butene isomerization.

The surface model is proposed by Coluccia and Tench for completely dehydrated and decarbonated MgO, as shown in Fig. 3.1.2.⁵⁾ Several Mg²⁺-O²⁻ ion pairs with different coordination numbers are present. Ion pairs with low coordination numbers exist at corners, edges and high Miller index surfaces. Among the ion pairs with different coordination numbers, threefold-Mg²⁺-threefold-O²⁻ (Mg²⁺_{3C}-O²⁻_{3C}) is most reactive and adsorbs carbon dioxide and water most strongly, though it was reported recently that the divacancies of Mg²⁺ and O²⁻ adsorb water most strongly (see section 3.1.3 (F)). To reveal this ion pair, the highest pretreatment temperature is required. By raising the pretreatment temperature, ion pairs with different coordination numbers appear successively according to the adsorption strength of the ion pairs toward water and carbon dioxide, and the most reactive ion pair of Mg²⁺_{3C}-O²⁻_{3C} appears at the highest temperature. The most reactive ion pair is most unstable and tends to rearrange to disappear at high temperature. The appearance of such highly unsaturated ion pairs by removal of

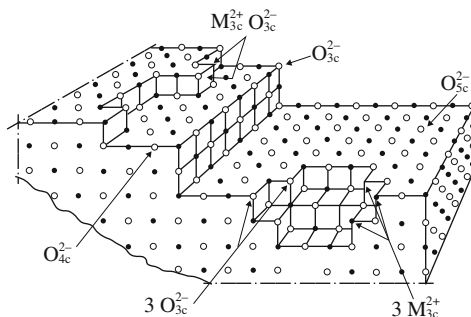


Fig. 3.1.2 Ions in low coordination on the surface of MgO.
 Reproduced with permission from S. Coluccia, A. J. Tench, *Stud. Surf. Sci. Catal.*, **7**, 1160 (1981) Fig. 5.

water and carbon dioxide competes with the elimination of the ion pairs by the rearrangement, which results in the activity maximum with pretreatment temperature.

As the crystalline structures of MgO, CaO, SrO and BaO are all cubic, the surface model proposed for MgO can be applied to the other oxides for understanding the variations of the catalytic activity with pretreatment temperature. The strength of the basic sites required for base-catalyzed reactions varies with the ease

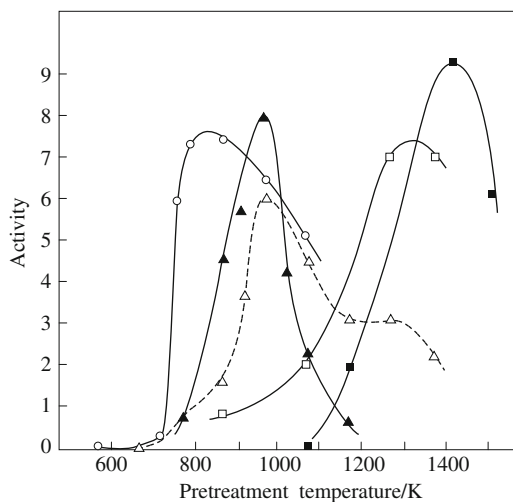


Fig. 3.1.3 Variations in activities of MgO for different types of reactions as a function of pretreatment temperature.
 ○, 1-butene isomerization/ 3.5×10^3 mmHg min⁻¹, 303 K; ▲, CH₄-D₂ exchange/ 4.3×10^3 % s⁻¹ g⁻¹, 673 K; △, amination of 1,3-butadiene with dimethylamine/ 5×10^{17} molecules min⁻¹ g⁻¹, 273 K; □, 1,3-butadiene hydrogenation/ 2.5×10^{-1} % min⁻¹ g⁻¹, 273 K; ■, ethylene hydrogenation/ 0.3 % min⁻¹ g⁻¹, 523 K.
 Reprinted with permission from K. Tanabe, M. Misono, Y. Ono, H. Hattori, *New Solid Acids and Bases*, Kodansha-Elsevier (1985) Fig. 3.11.

of proton abstraction from the reactant under the reaction conditions employed. The reaction of the reactant from which a proton is easily abstracted proceeds even on a weakly basic site, and the reaction of the reactant from which a proton is difficult to abstract proceeds only on a strongly basic site. The optimum pretreatment temperature depends on the type of reaction and the type of alkaline earth oxide.

Figure 3.1.3 shows the variations of the activity for different reactions as a function of the pretreatment temperature of MgO prepared from hydroxide by decomposition in a vacuum.⁶⁾ The optimum pretreatment temperatures are different depending on the type of reaction. For MgO, the temperatures giving the maximum activities are 800K for 1-butene isomerization, 973 K for methane-D₂ exchange and 1300 K for hydrogenation of 1,3-butadiene. The change in the optimum pretreatment temperature reflects the strength of the basic site required for the reaction. Stronger basic sites are required going from 1-butene isomerization to 1,3-butadiene hydrogenation.

3.1.2 Preparation

MgO and CaO are normally prepared by thermal decomposition of hydroxides, and SrO and BaO from carbonates. The thermal decomposition is undertaken in a vacuum or inert gases such as N₂ and Ar. SrO and BaO are also prepared by thermal decomposition of Sr(OH)₂ and commercially available BaO though difficulty in handling samples exists because Sr(OH)₂ and Ba(OH)₂ melt at lower temperatures. The surface areas of the resulting MgO, CaO, SrO and BaO are on the order of 10², 10¹, 10⁰, and 10⁻¹ m² g⁻¹, respectively, if no special preparation methods are employed.

In conversion of Mg(OH)₂ to MgO, a layered structure called brucite changed into a cubic structure called periclase. Change in morphology during the transformation of brucite to periclase was actually observed by TEM.⁷⁾

A. Conventional preparation method for MgO catalyst

Commercially available MgO has low surface area. MgO with high surface area is prepared from a commercially available MgO by the following procedures. The commercially available MgO is boiled in a deionized water overnight with magnetic stirring. Mg(OH)₂ is formed in the slurry which is then filtered, and the filter cake is dried in an oven at 393 K. The dried powder is slowly heated (less than 10 K min⁻¹) to 773 K or above under a vacuum or flowing nitrogen. The resulting MgO has a surface area of 100–250 m² g⁻¹ depending on the final decomposition temperature. Care should be taken to avoid the presence of H₂O during heat treatment at high temperatures, otherwise MgO is sintered and its surface area becomes low.

Transformation of brucite Mg(OH)₂ to periclase MgO occurs over the temperature range 553 - 623 K in a vacuum. An example of the change in XRD pattern with heating temperature is shown in Fig. 3.1.4.⁸⁾ The heating time was 5 h. Transformation of Mg(OH)₂ to MgO is prominent when the temperature is raised from 573 K to 583 K. Transformation of Mg(OH)₂ to MgO is determined not only

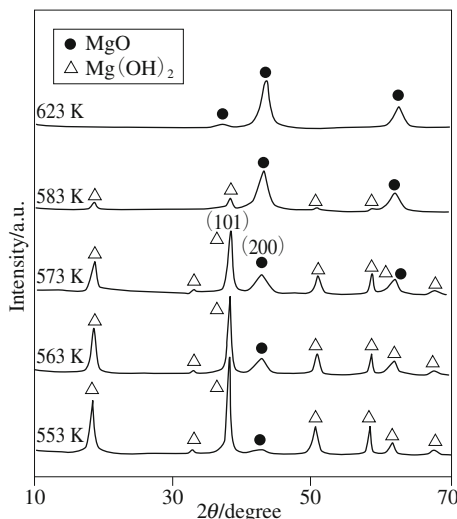


Fig. 3.1.4 XRD patterns of $\text{Mg}(\text{OH})_2$ evacuated at 553–623 K. Reprinted with permission from T. Yoshida, T. Tanaka, H. Yoshida, T. Funabiki, S. Yoshida, *J. Phys. Chem.*, **99**, 10890 (1995) Fig. 2.

by the temperature of heat treatment but also duration of heating. When $\text{Mg}(\text{OH})_2$ was heat treated at 623 K in a vacuum for 1 h, 15% of MgO phase appeared. The percentage of MgO phase increased to 94% after heating for 10 h. The fraction of MgO was estimated by XANES.

When $\text{Mg}(\text{OH})_2$ is calcined in air, the transformation of brucite to periclase occurs in the temperature range 473–673 K.⁹⁾

B. Effects of starting magnesium salt

The type of magnesium salt from which $\text{Mg}(\text{OH})_2$ is prepared by hydrolysis affects the properties of the resulting MgO. Residual anions suppress the basic properties. In particular, chloride ions affect strongly the basicities of the resulting MgO.

Matsuda et al. prepared MgO from magnesium salts of nitrate, sulfate, chloride, carbonate, oxalate and acetate by hydrolysis with aqueous ammonia followed by washing and calcination at 823 K. MgO's prepared from nitrate, oxalate and acetate possessed strong basic sites, relatively large surface area and high activity for 1-butene isomerization, while MgO's prepared from chloride, carbonate and sulfate possessed weak basic sites, small surface area and low activity for 1-butene isomerization. Addition of Cl^- ions greatly suppressed the activity and basicity. It was suggested that Cl^- is retained in the MgO prepared from MgCl_2 and exerts an influence on the surface properties of MgO.¹⁰⁾

Choudhary et al. prepared MgO through hydrolysis of magnesium salts to $\text{Mg}(\text{OH})_2$ followed by calcination under different conditions. The conditions they changed were the type and concentration of magnesium salt, precipitating agent, pH and temperature of precipitation, aging period, and calcination temperature.

All conditions affected the surface properties of the resulting MgO. A prominent effect of low surface area was observed for the MgO prepared from MgCl_2 .¹¹⁾

Aramendia et al. prepared MgO by various synthetic procedures including use of different salts, application of sol-gel technique and precipitation with urea, and measured the catalytic activity for the Meerwein-Ponndorf-Verley reaction of cyclohexanone with 2-propanol. The most active MgO was prepared by rehydration and subsequent calcination of MgO that was previously obtained from commercially available $\text{Mg}(\text{OH})_2$ by calcination at 873 K in air for 2 h.¹²⁾

C. Preparation of MgO with high surface area by sol-gel method

Wang et al. prepared sol-gel MgO by the following procedure.¹³⁾ Oxalic acid ($\text{H}_2\text{C}_2\text{O}_4$) was added to refluxing mixture of $\text{Mg}(\text{OC}_2\text{H}_5)_2$ and ethanol to adjust pH 5 to form gel. After vaporizing excess ethanol, the product was dried in air at 343 K to obtain white powder which was calcined in air at 673, 873 and 1073 K. The surface areas for the samples calcined at 673, 873 and 1073 K were 199, 267 and $163 \text{ m}^2 \text{ g}^{-1}$, respectively. They observed morphological change by TEM for conversion of brucite ($\text{Mg}(\text{OH})_2$) to periclase (MgO) by calcination.¹⁴⁾ Brucite was synthesized by the sol-gel technique using magnesium diethoxide in a homogeneous reaction medium. When the calcination temperature was increased from 540 to 773 K, brucite decomposed to form periclase, which was accompanied by morphology change from a needle shape (hexagonal structure) to small crystallite with the cubic structure.

Gulkova et al. prepared a high surface area MgO by modified sol-gel method in which MgO was treated with methanol/water or ethanol/water followed by simple drying; alcogel of $\text{Mg}(\text{OH})_2$ was obtained. MgO with surface area 310 - 370 $\text{m}^2 \text{ g}^{-1}$ was obtained by calcination of the alcogel at 623–663 K in flowing air.¹⁵⁾

Klabunde's group prepared a high surface area MgO by an aerogel method using the autoclave, and they named the resulting MgO AP-MgO (autoclave preparation MgO).^{16–18)} Clean metal pieces were dissolved in methanol under an inert atmosphere to form metal methoxide, toluene was added, and upon vigorous stirring for a few hours, deionized water was added dropwise to form a hydroxide gel, which was dried of solvent in an autoclave. The hydroxide obtained was heated under a dynamic vacuum (< 0.05 Torr) for 24 h to yield partial transformation to the nanometer-sized metal oxide. The autoclave preparation gives MgO of very high surface areas.

The autoclave preparation can also be applied to CaO preparation.¹⁹⁾ The surface areas of MgO and CaO prepared by the autoclave (aerogel) method and conventional method, together with commercially available samples are summarized as follows: AP-MgO, 250-500; CP-MgO, 130-250; CM-MgO, 10-30; AP-CaO, 120-160; CP-CaO, 50-100; CM-CaO, 1-3 $\text{m}^2 \text{ g}^{-1}$, where AP, CP, and CM represent autoclave (aerogel) preparation, conventional preparation and commercially available sample, respectively.^{20,21)}

D. Preparation of mesoporous MgO

Addition of carboxylic acids in aqueous solution of magnesium salts increases the surface area of the resulting MgO.

Chen et al. used citric acid.²¹⁾ Into an aqueous solution of $\text{Mg}(\text{NO}_3)_2$, citric acid was added. The solution was heated to evaporate the water to form a viscous solution. The viscous solution was moved to an oven and heated at 413–453 K for half an hour to form a fluffy powder. The powder was heated at 1073 K under N_2 flow containing 0.5% O_2 to obtain an amorphous mixture of MgO and carbon. MgO particles were covered with carbon to prevent the aggregation of MgO particles. Then the mixture was heated at 673 K in air to remove carbon. The resulting MgO had a surface area of $230 \text{ m}^2 \text{ g}^{-1}$ and mean pore size of 4.0 nm.

Nakayama et al.²²⁾ also prepared MgO from a mixture of $\text{Mg}(\text{NO}_3)_2$ and citric acid according to the method reported by Marcilly et al.²³⁾ and obtained MgO with a surface area of $172 \text{ m}^2 \text{ g}^{-1}$ and pore size distribution centered at ca. 7 nm after calcination at 673 K in air.

Takenaka et al. used a series of carboxylic acids to be added to $\text{Mg}(\text{NO}_3)_2$ aqueous solution.²⁴⁾ The pore size of the resulting MgO was controllable with the alkyl-chain length of carboxylic acid in the range 13–38 nm. Table 3.1.1 shows the surface areas and pore sizes of the resulting MgO calcined at 673 K with the chain length (n) of carboxylic acids.

Table 3.1.1 Surface area and pore size of MgO prepared with carboxylic acids with different alkyl-chain lengths

n	$\text{SA}/\text{m}^2 \text{ g}^{-1}$	Pore size/nm
10	175	13.2
12	193	14.9
14	171	14.9
16	154	19.5
20	131	37.5

An ordered mesoporous MgO was prepared by exotemplating method in which CMK type carbon was used as an exotemplate.²⁵⁾ CMK type carbon is also prepared by use of mesoporous silica as an exotemplate.²⁶⁾ CMK-3 was dispersed in an aqueous solution of $\text{Mg}(\text{NO}_3)_2$ and stirred for 2 h to impregnate the mesopores with $\text{Mg}(\text{NO}_3)_2$. After filtration and drying in a vacuum, the sample was heated under air atmosphere to 573 K at a constant rate of 2.5 K/min to convert $\text{Mg}(\text{NO}_3)_2$ to MgO within the pores. This procedure was repeated three times. Finally, the carbon was removed by heating to 1073 K at a constant rate of 2 K min^{-1} . The resulting MgO has a surface area of $306 \text{ m}^2 \text{ g}^{-1}$, and possesses ordered mesopores of 5.6 nm diameter as observed by TEM.

3.1.3 Characterization of Basic Sites

Characterization of the surface properties by different methods reveals the structure of basic sites on alkaline earth oxides. The characterization indicates the existence of ion pairs with low coordination numbers, and they act as basic sites.

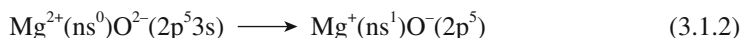
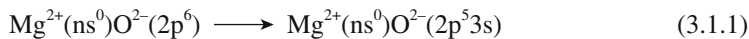
A. Strength of basic sites measured by indicator method

Strength of basic sites was measured by an indicator method in which a series of nitroaniline compounds were used.²⁷⁾ Strength of basic sites varies with the pretreatment conditions. The basic strengths of MgO and CaO calcined at 723 K in air for 2 h were in the H_- range 15.0–17.2 and 15.0–17.2, respectively. The strengths were enhanced to 18.4–26.5 for MgO and >26.5 for CaO by pretreatment at 723 K overnight in a vacuum. SrO showed basic sites of > 26.5 in H_- scale when pretreated at 723 K overnight in a vacuum.

B. UV- absorption

Zecchina et al. measured UV-absorption spectra of MgO and CaO.²⁸⁾ MgO showed two absorptions; 270 and 217 nm (37000 and 46000 cm^{-1}). These frequencies are considerably lower than those of the absorption edges due to bulk excitonic transitions for single crystals of MgO (163 nm, 61500 cm^{-1} , 7.7 eV). The lower the coordination around a surface oxide ion, the lower the frequency of the surface exciton associated with it. This is because the Madelung potential is progressively reduced as the coordination decreases, and the overall process requires less energy. On this basis the absorptions at 270 and 217 nm were attributed to two different coordinations of surface O^{2-} ions, the lower frequency absorption representing the lower coordination.

The absorption was ascribed to the electronic excitation of the oxide ion (Eq. 3.1.1) followed by the charge transfer (Eq. 3.1.2).



Similar absorptions were observed for CaO,²⁸⁾ SrO and BaO.²⁹⁾ Garronne et al. summarized the diffuse reflectance spectra of MgO, CaO, SrO and BaO, as shown in Fig. 3.1.5.³⁰⁾ The energies of the transitions are summarized in Table 3.1.2. Bands I, II, and III were attributed to surface ions in fivefold, fourfold, and three fold coordination, respectively. As shown in Fig. 3.1.2, fivefold coordinated ions exist on the (100) plane, and fourfold and threefold coordinated ions exist at steps, edges or kink sites.

Table 3.1.2 Energies of optical transitions of alkaline earth oxides

	Absorption/nm			
	Bulk	I	II	III
MgO	161	188	216	268
CaO	182	225	280	331
SrO	214	268	316	354
BaO	302	344	375	-

C. Photoluminescence

Coluccia et al. observed photoluminescence from high surface area alkaline earth

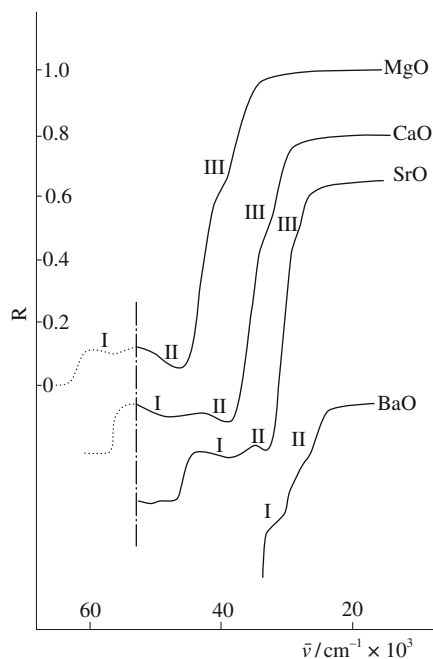


Fig. 3.1.5 Diffuse reflectance spectra of polycrystalline MgO, CaO, SrO and BaO after outgassing at 1073 K. The reflectance scale is displaced vertically in order to avoid overlap of the spectra. Reprinted with permission from E. Garrone, A. Zecchina, F. S. Stone, *Phylos. Mag.*, **42B**, 683 (1980) Fig. 1.

oxides with excitation light of a much lower frequency than that expected from the band gaps of the bulk oxides.³¹⁾ They summarized excitation and emission spectra, together with absorption spectra as shown in Table 3.1.3. Data for absorption spectra were cited from refs. 28 and 29. It was concluded that both excitation and the luminescence spectra arise from excitons in the surface region. The different behavior towards O₂ and H₂ suggested that the excitation site where absorption of light occurs is associated with anions of low coordination, while the luminescence is associated with a cation of low coordination.

Table 3.1.3 Absorption and emission bands for alkaline earth oxides and those of O atoms with different coordinations in MgO

Oxide	Absorption/nm	Excitation/nm	Emission/nm
MgO	218; 271	< 230; 274	390
CaO	225; 281	< 230; 281	405
SrO	267; 313	280; 315	470
BaO	344; 385	335	464
MgO			
O ²⁻ _{4C}		230	380
O ²⁻ _{3C}		270	460
O ²⁻ _{5C}		230	350
H-O _{3C, 4C}		250	410

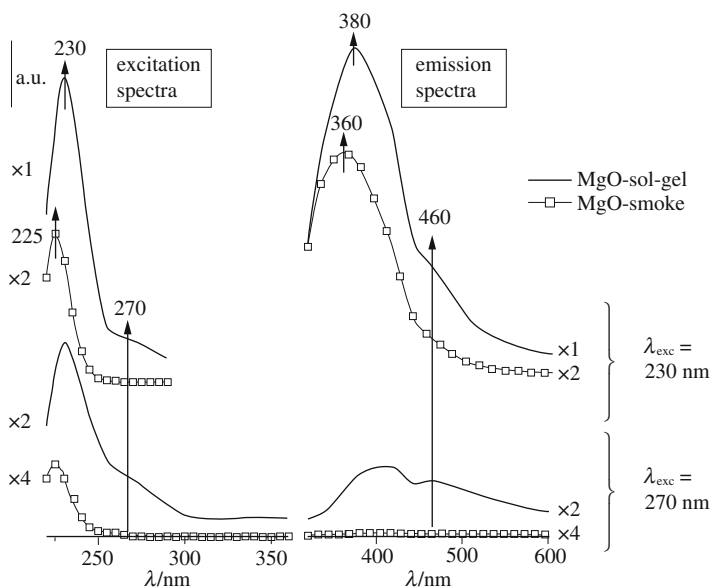


Fig. 3.1.6 Emission spectra monitored at 230 and 270 nm of the clean MgO-sol-gel (—) and MgO-smoke (□) and corresponding excitation spectra monitored at the maximum of emission. Reprinted with permission from M.-L. Bailly, G. Costentin, H. Lauron-Pernot, J. M. Kraft, M. Che, *J. Phys. Chem. B*, **109**, 2404 (2005) Fig. 3.

Recently, Bailly et al. re-examined photoluminescence of MgO with an improved photoluminescence cell. They observed two maxima at 395 and 460 nm when monitored at both 230 and 270 nm. Photoluminescent species excited at 270 nm and emitting at 460 nm were assigned to oxide ions O_{4C}^{2-} (four-coordinated oxide ions at the edges), while those excited at 230 nm and emitting at 395 nm were assigned to oxide ions O_{3C}^{2-} (three-coordinated oxide ions at the corners).^{32,33)}

Emission spectra differed depending on how the MgO was prepared. Fig. 3.1.6 shows emission spectra monitored at 230 and 270 nm of the MgO prepared by sol-gel method (MgO-sol-gel) and the MgO prepared from metallic Mg vapor by air oxidation (MgO-smoke).³³⁾ When MgO-sol-gel was excited by light 230 and 270 nm, two maxima were observed in the emission spectrum at 380 and 460 nm. On the other hand, MgO-smoke gave only one emission peak at 360 nm, no emission was observed when excited by light 270 nm. The ratios O_{3C}^{2-}/O_{4C}^{2-} were estimated to be close to 0 and 0.15 for MgO-smoke and MgO-sol-gel, respectively. The O_{3C}^{2-}/O_{4C}^{2-} ratio was obtained from the ratio of the areas of the deconvoluted excitation peaks at 270 and 230 nm monitored at 460 and 380 nm, respectively.³⁴⁾

D. IR of adsorbed H_2

Appearance of O-H stretching vibration on adsorption of H_2 on MgO was reported by Coluccia and Tench.⁵⁾ A more definite spectrum for the dissociative adsorption of H_2 on the defect sites of MgO was reported by Cavalleri et al.³⁵⁾ IR spectra following hydrogen adsorption at room temperature on MgO outgassed at 1123 K

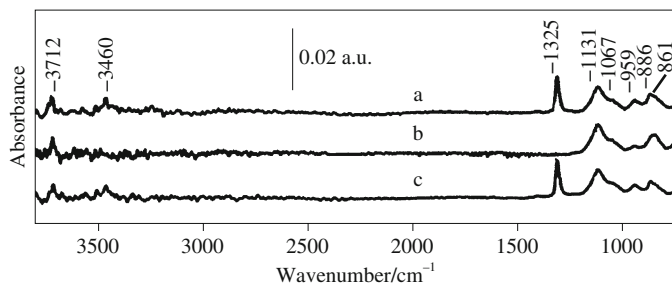
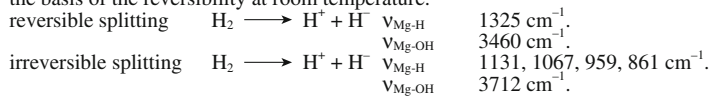


Fig. 3.1.7 IR spectra following hydrogen adsorption at room temperature on MgO pre-outgassed at 1123 K; a) in presence of 200 Torr H₂; b) after outgassing 10 min at room temperature; c) after readmission of 200 Torr H₂.

The two processes and the related most significant bands can be summarized as follows on the basis of the reversibility at room temperature.



Reprinted with permission from M. Cavalleri, A. Pelmenschikov, G. Morosi, A. Gamba, S. Coluccia, G. Marta, *Stud. Surf. Sci. Catal.*, **140**, 131 (2001) Fig. 2.

are shown in Fig. 3.1.7.³⁵⁾ Calculations assigned a band of the reversible species at 1325 cm⁻¹ to the Mg_{3c}-H hydride group and a band of irreversible species at 3712 cm⁻¹ to the O_{3c}-H hydroxyl group. The hydrogen atoms bridging two or three neighboring low coordinated Mg atoms of the surface are suggested to be responsible for the complex bands in the 1130–880 cm⁻¹ region. No IR bands were observed that correspond to the calculated frequencies of the H atoms bound to the 4- or 5- coordinated Mg and O atoms, suggesting that the stabilization of H species at these sites is unfavorable compared to those at the 3-coordinated sites. The calculated adsorption energies confirm that dissociative adsorption can occur only when 3-coordinated cations and/or anions are involved.

IR study of hydrogen adsorption on CaO and SrO indicated that hydrogen is heterolytically adsorbed on CaO and SrO as it occurs on MgO.³⁶⁾

E. TPD of adsorbed H₂

The hydrogen molecule is heterolytically dissociated on the surface of MgO to form H⁺ and H⁻, which are adsorbed on the surface O²⁻ ion and Mg²⁺ ion, respectively. Ito et al. measured temperature-programmed desorption (TPD) of H₂ from MgO. TPD profiles are quite dependent on the pretreatment temperature of MgO. As shown in Fig. 2.3.4 (p.22) for the MgO pretreated at 1123 K, which is regarded to be fully dehydrated MgO. In the TPD profile, seven peaks appear. From observed TPD profiles and H₂ adsorption behavior, a series of the active sites is divided into three groups which differ in adsorptive ability. By comparison of the activation temperature dependence of the site concentration of each group obtained from the TPD profiles with that of the concentration of coordinatively unsaturated surface ions estimated from available reflectance spectra, coordination numbers of the active sites are determined to be O_{4c}²⁻-Mg_{3c}²⁺, O_{3c}²⁻-Mg_{4c}²⁺ and O_{3c}²⁻-Mg_{3c}²⁺

for the weakest, medium and strongest groups, respectively. The number of total adsorption sites was only 67×10^{15} sites m^{-2} , which corresponds to 0.6% of the total number of surface ions. The adsorption occurs only on specific surface sites.³⁷⁻³⁹⁾

F. IR of surface OH groups

The IR spectra of the various types of hydroxyl groups on MgO were measured by a number of researchers. Study of the state of OH groups on MgO surface reveals not only the nature of OH groups but also the surface structure of MgO formed by

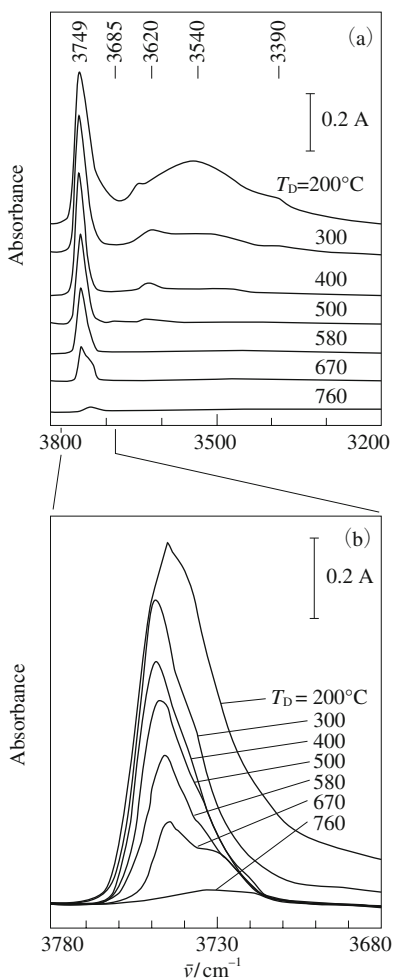


Fig. 3.1.8 OH stretching region of a hydroxylated MgO sample after dehydroxylation at temperature T_D between 200 and 760°C.

Reprinted with permission from E. Knözinger, K.-H. Jacob, S. Singh, P. Hafmann, *Surf. Sci.*, **290**, 388 (1993) Fig. 5.

dehydration and dehydroxylation of $\text{Mg}(\text{OH})_2$. One example of IR spectra in the O-H stretching region is shown in Fig. 3.1.8.⁴⁰⁾ The spectrum is composed of several bands and the fraction of each band depends on the pretreatment temperature. The assignment of each band is controversial. Recently, Chizallet et al. reconsidered the surface topology and ion coordination on MgO surfaces based on the density functional theory (DFT) applied to the IR spectra of OH groups observed on adsorption of water molecules.^{41,42)} They calculated the band positions based on the four types of OH group defined by Knözinger et al. (Fig. 3.1.9).⁴⁰⁾ The assignments of IR bands are summarized in Table 3.1.4 together with the assignments reported in the literature.⁴²⁾ The most distinctive difference of the assignment by Chizallet et al. from those in the literature can be seen in the assignment of the band of the highest frequency. In all reports except that by Anderson et al.⁴³⁾ the highest frequency band was assigned to isolated OH groups. Chizallet et al. assigned the highest frequency band to the monocoordinated hydrogen acceptor OH group.

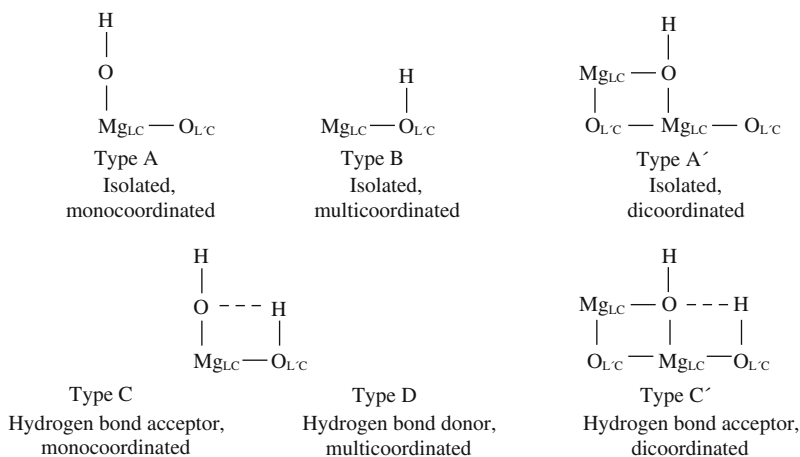
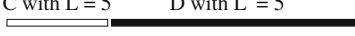
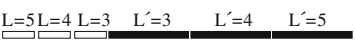

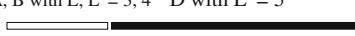

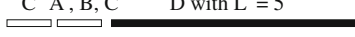
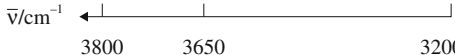


Fig. 3.1.9 The four types of OH group defined by Knözinger et al.⁴⁰⁾ (A, B, C and D) and additional two types of OH group defined by Chizallet et al.⁴²⁾ (A' and C').

The OH groups located at different coordination states are subsequently desorbed as the temperature increases. Chizallet et al. calculated the hydration energies on Mg^{2+} - O^{2-} ion pairs of different coordinations. The hydration energies reflect the strength of the interaction of MgO with water. From the hydration energies, the temperature to give a certain equilibrium water vapor pressure can be estimated. They calculated the temperatures for an evacuation pressure of 10^{-2} Pa. The temperatures were calculated to be 475 K for the edge of high steps, 500 K for $\text{Mg}^{2+}_{3\text{C}}$ -terminated corners, 550 K for O^{2-} -terminated corners, 620 K for monoatomic steps, 740 K for O^{2-} -terminated kinks, 805 K for Mg^{2+} -terminated kinks, and 1110 K for divacancies. The results suggest that the Mg^{2+} - O^{2-} ion pairs appear progressively from the edge of high steps finally to divacancies as the evacuation temperature increases.

Table 3.1.4 Assignment of IR bands in the O-H stretching region of hydroxylated MgO from different authors

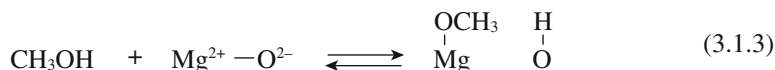
Authors	Year	References	Assignments
Anderson et al.	1965	43	C with L = 5 D with L' = 5 
Shido et al.	1989	44	A with: A with: 
Coluccia et al.	1988	45, 46	A, B with L, L' = 3, 4 C, D with L, L' = 5 
Morrow	1990	47	A, B with L, L' = 3, 4 D with L' = 5 
Knözinger et al.	1993	40	A B, C D 
Chizallet et al.	2007	42	C A', B, C' D with L' = 5 
<i>Experimental spectrum</i>		$\bar{\nu}/\text{cm}^{-1}$	

^{a)} L and L' stand for the coordination numbers of lattice Mg and O, respectively. For A, B, C, D, A' and C', see Fig. 3.1.9. The white and black rectangles relate to the sharp and broad experimental bands, respectively.

Reproduced with permission from C. Chizallet, G. Costentin, M. Che, F. Delbecq, O. Sautet, *J. Am. Chem. Soc.*, **129**, 6442 (2007) Table 1.

G. IR of adsorbed CH₃OH

CH₃OH is adsorbed on MgO in different states: molecular adsorption involving H-bonding, monodentate methoxy and bidentate methoxy. The formation of two types of methoxy groups results from the dissociation of CH₃OH into CH₃O⁻ and H⁺ on Mg²⁺-O²⁻ ion pairs.



The position of the equilibrium of equation (3.1.3) indicates the thermodynamic strength of Brønsted basicity of the ion pair Mg²⁺-O²⁻.⁴⁸⁾

IR spectra of adsorbed CH₃OH on MgO were reported by Binsitel et al.⁴⁹⁾ They assigned the bands at 1060, 1092, and 1114 cm⁻¹ to the molecularly adsorbed CH₃OH, bidentate methoxy and monodentate methoxy, respectively.

The relative intensities of these bands depend on the preparation methods for MgO. Bailly et al. plotted the catalytic activities for MBOH reaction (section 2.5.4) against the integrated band area for the dissociated CH₃OH on MgO cata-

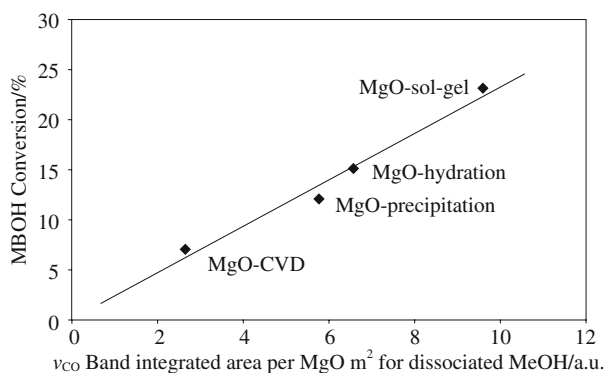


Fig. 3.1.10 Correlation, for different “clean” MgO surfaces, between MBOH conversion and thermodynamic Brønsted basicity evaluated from the integrated area of the ν_{CO} band per $MgO\ m^2$ for dissociated methanol. Reprinted with permission from M.-L. Bailly, C. Chizallet, G. Costentin, J.-M. Kraft, H. Lauron-Pernot, M. Che, *J. Catal.*, **235**, 413 (2005) Fig. 7.

lysts prepared by different methods as shown in Fig. 3.1.10.⁴⁸⁾ A linear correlation is observed between the activity and the Brønsted basicity estimated from the integrated band area for the dissociated CH_3OH .

H. TPD and IR of adsorbed CH_4

Methane is adsorbed dissociatively on MgO to form CH_3^- and H^+ . CH_4 adsorbed on MgO was examined by TPD combined with *ab initio* calculation.⁵⁰⁾ Two types of chemisorption were observed resulting from heterolytically dissociated species $Mg_{LC}^{2+}-CH_3^-$ and $O_{LC}^{2-}-H^+$. The first type occurs on the nearest pair of low-coordinated ions. The second type on the sites consists of Mg_{LC}^{2+} and O_{LC}^{2-} isolated from each other, and is initiated by the adsorption on $Mg^{2+}-O_{3C}^{2-}$, where Mg^{2+} is not in low coordination. The CH_3^- formed on this ion pair migrates to Mg_{LC}^{2+} to be stabilized.

Ferrari et al. studied adsorption of CH_4 on MgO at 88K at which temperature dissociation of methane is not expected.⁵¹⁾ By combining IR spectroscopy and density functional cluster model calculations together with co-adsorption of CO, they indicated that methane is adsorbed mainly on the low-coordinated $Mg^{2+}-O^{2-}$ ion pairs.

I. IR of adsorbed NO

NO is adsorbed on MgO to form a variety of surface complexes such as NO^- , NO_2^- of different configurations, and $(NO)_2^-$. IR study of natural and ^{18}O -enriched NO was reported by Yanagisawa et al.⁵²⁾ Three types of NO adsorption in the region $1500-1000\ cm^{-1}$ were observed. With the help of density functional theory for $(MgO)_n$ -NO cluster, types 1, 2 and 3 were assigned to monodentate, asymmetric and symmetric bidentate geometries, respectively. Type 4, a tridentate model which involves NO_3^- -like species, gives a wavenumber of less than $1000\ cm^{-1}$.

All types of adsorption occur on the ion pairs of low coordination. An on-top

NO adsorption at a four-coordinated $\text{Mg}_{4\text{C}}$ site on an edge forms the type 1 unidentate. An NO adsorption at $\text{O}_{4\text{C}}$ site with a nearby $\text{Mg}_{4\text{C}}$ forms the type 2 asymmetric bidentate NO_2 . An NO adsorption at the $\text{O}_{3\text{C}}\text{-Mg}_{4\text{C}}$ pair at the kink site may form the type 3 symmetric bidentate NO_2 , when $\text{O}_{3\text{C}}$ is left of lattice site. At the particular site, e.g., a cation-anion vacancy pair site at a step, NO may be adsorbed and may be trapped at a cation (N) and anion (O) site, respectively, to form the type 4 tridentate NO_3 -like species.

J. ESR of adsorbed NO

Lunsford observed two kinds of paramagnetic species on adsorption of NO on dehydrated MgO.⁵³⁾ One was observable at 77 K and identified as an adsorbed NO in a molecular form in a strong electric field. The other observable at room temperature was identified as a stable NO_2^{2-} species in which the surface O^{2-} ions are involved. Both species were eliminated by room temperature outgassing.

Valentin et al. measured by ESR the paramagnetic species formed on adsorption of ^{14}NO and ^{15}NO on a high-surface area polycrystalline MgO prepared by chemical vapor deposition.⁵⁴⁾ Only 0.5% of total NO deposited is in a paramagnetic state; out of the paramagnetic species, 98% is physisorbed and only 2% is chemisorbed. On the terrace sites, NO prefers to form dimers $(\text{NO})_2$. Only at defect sites (low-coordinated cations) is the interaction of NO monomers with the MgO surface stronger, preventing the formation of the diamagnetic dimers. A small minority of chemisorbed species is formed only at low coordinated anions (steps, edges, or corners) or oxygen vacancies.

Paganini et al. measured adsorption of NO on CaO by ESR and compared the species formed on CaO and those on MgO. Four distinct types of NO_2^- surface species were formed on CaO by interaction of basic oxygen ions with NO. The number of sites involved in the interaction was very low and amounted to a value in the range of 0.25–0.5% of the whole surface ions (or 2.5–5% of the low coordinated ones). These active sites were low coordination sites present at morphological defects of the polycrystalline solid. The concentration of the basic sites is 25 times greater than that of the corresponding sites on MgO.^{55–57)}

NO adsorption on MgO was examined by use of density functional theory by Xu et al.⁵⁸⁾ NO is weakly adsorbed on MgO(100) terrace site. On steps and corners, NO is adsorbed in the following three forms; (a) NO adspecies with N-end bridging over the step-sitting $\text{Mg}_{\text{XC}}\text{-O}_{\text{YC}}$ (X, Y = 3, 4) ion pairs, (b) NO_2^{2-} with the O-N bond chaining over the step-sitting $\text{Mg}_{\text{XC}}\text{-O}_{\text{YC}}$ (X, Y = 3, 4) ion pairs, (c) $\text{N}_2\text{O}_3^{2-}$ adspecies formed by attaching another NO molecule on the NO_2^{2-} species.

Recently, Higashimoto et al. measured the concentration of two paramagnetic species formed on adsorption of NO on MgO as a function of outgassing temperature of MgO.⁵⁹⁾ They identified two paramagnetic species as NO physisorbed on $\text{Mg}_{\text{LC}}^{2+}$ and NO_2^{2-} formed by adsorption of NO on $\text{O}_{\text{LC}}^{2-}$. The concentrations of the physisorbed NO and NO_2^{2-} are plotted against the outgassing temperature of MgO. Both of the adsorbed species are maximized on the MgO pretreated at 1073 K. The maximum concentration of the physisorbed NO was approximately 8×10^{16} spins m^{-2} , which corresponds to approximately 0.3% of all the surface Mg^{2+}

ions. The maximum concentration of NO_2^{2-} was two orders of magnitude smaller than that of the NO.

K. IR of adsorbed CO_2

Pacchioni et al. used CO_2 as a probe molecule for the basic character of the O^{2-} surface sites of MgO and CaO.⁶⁰⁾ On MgO, CO_2 formed a weakly bound surface complex, while on CaO the formation of a strongly bound carbonate species was observed. A decomposition of the interaction energy into electrostatic, polarization and charge transfer contributions shows that CaO is a stronger base than MgO. The ultimate reason for the different surface reactivities of MgO and CaO can be simply explained in terms of electrostatic stabilization of the surface anion. The O^{2-} anion at the surface is stabilized by the Madelung potential of the ionic crystal. This is smaller for CaO than for MgO (Table 3.1.5), thus leading to a higher basicity and reactivity of CaO. In this respect, a regular surface site of CaO behaves similarly to a low-coordinated site of MgO.

Table 3.1.5 Madelung potential at various sites of MgO and CaO surfaces

Site	Madelung constant	Madelung potential/eV	
		MgO ($r = 0.2106$ nm)	CaO ($r = 0.2399$ nm)
O_{6c}^{2-} bulk	1.747	23.89	20.97
O_{5c}^{2-} surface	1.681	22.98	20.18
O_{4c}^{2-} step	1.591	21.76	19.10
O_{3c}^{2-} corner	1.344	18.38	16.13

Reproduced with permission from G. Pacchioni, J. M. Ricart, F. Illas, *J. Am. Chem. Soc.*, **116**, 10152 (1994) Table 5.

L. TPD of adsorbed CO_2

TPD of CO_2 is most frequently used to measure the number and strength of basic sites.⁶¹⁻⁶³⁾ The strength and the number of basic sites are reflected in the desorption temperature and the peak area, respectively. TPD profiles of CO_2 desorbed from alkaline earth oxides are compared in Fig. 2.3.2 in which the amount of CO_2 adsorbed on the samples was limited.⁶⁴⁾ The strength of basic sites is in the increasing order $\text{MgO} < \text{CaO} < \text{SrO} < \text{BaO}$. The number of basic sites per unit weight that can retain CO_2 under the adsorption condition increases in the order $\text{BaO} < \text{SrO} < \text{MgO} < \text{CaO}$.

TPD study of C^{18}O_2 adsorbed on MgO indicated that CO_2 migrates over the surface of MgO accompanied by O exchange with the lattice O.⁶⁵⁾ It is not possible for unidentate carbonate to exchange its O with lattice O. Bidentate carbonate can undergo exchange by processes I, II and III, as shown in Fig. 3.1.11. TPD results showed that the desorbed CO_2 contained a large fraction of C^{16}O_2 . A single occurrence of process I, II or III should give only one O atom exchange. More than one successive occurrence of any of the processes I, II and III is required for exchange of two O atoms, which results in migration of adsorbed CO_2 over the surface. CO_2 is desorbed from the site different from the site on which CO_2 is ini-

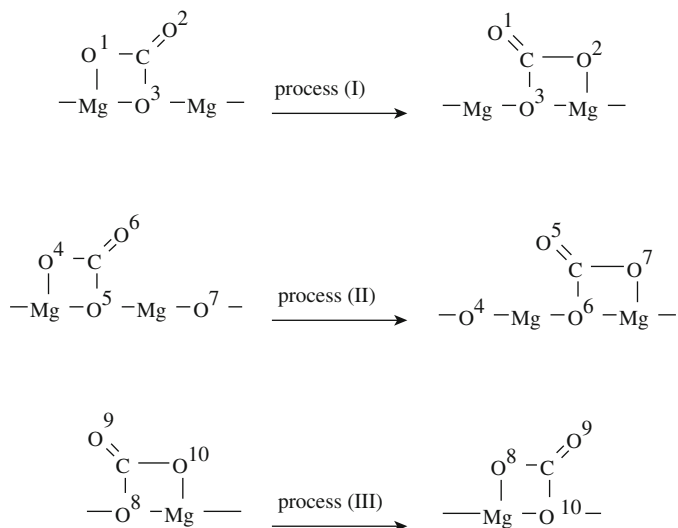


Fig. 3.1.11 Proposed processes for mechanism of migration of surface bidentate carbonate. Reproduced with permission from H. Tsuji, T. Shishido, A. Okamura, Y. Gao, H. Hattori, H. Kita, *J. Chem. Soc., Faraday Trans.*, **90**, 803 (1994) Fig. 6.

tially adsorbed. Accordingly, the local structure of Mg-O site changes on adsorption and desorption of CO₂.

M. ¹H MAS NMR of surface OH groups

Chizallet et al. measured ¹H MAS NMR spectrum of MgO treated at 673 K by single pulse, Hahn-echo and 2D NOESY-like sequences.^{66,67)} The spectrum is shown in Fig. 3.1.12. The MgO was prepared by sol-gel method followed by treatment in N₂ at 1023 K, hydration at 373 K and finally treated in N₂ at 673 K. Six lines were identified at 1.2, 0.7, 0.0, -0.4, -0.7 and -1.8 ppm. These lines were assigned by combining DFT embedded cluster calculations and experiments using single pulse, Hahn-echo and 2D NOESY-like sequences. It was expected that OH groups coming from protonation of O²⁻ ions and being more coordinated would give a signal at a higher chemical shift than the OH groups formed by coordination of a hydroxide ion to a Mg²⁺. Chemical shift calculations suggest the qualitative classification of protons into three main categories. The highest chemical shift ($\delta_{\text{H}} > -0.7$ ppm) is proposed to be characteristic of hydrogen-donor OH groups (threefold O_{3C}-H, fourfold O_{4C}-H, and O_{5C}-H localized on corners, edges and in valleys, respectively). The lowest chemical shifts ($\delta_{\text{H}} < -0.7$ ppm) are associated to isolated and hydrogen-bond acceptor twofold O_{2C}-H and onefold O_{1C}-H, whereas the central signal at ($\delta_{\text{H}} = -0.7$ ppm) would correspond to isolated O_{3C}-H and O_{4C}-H on kinks and divacancies.

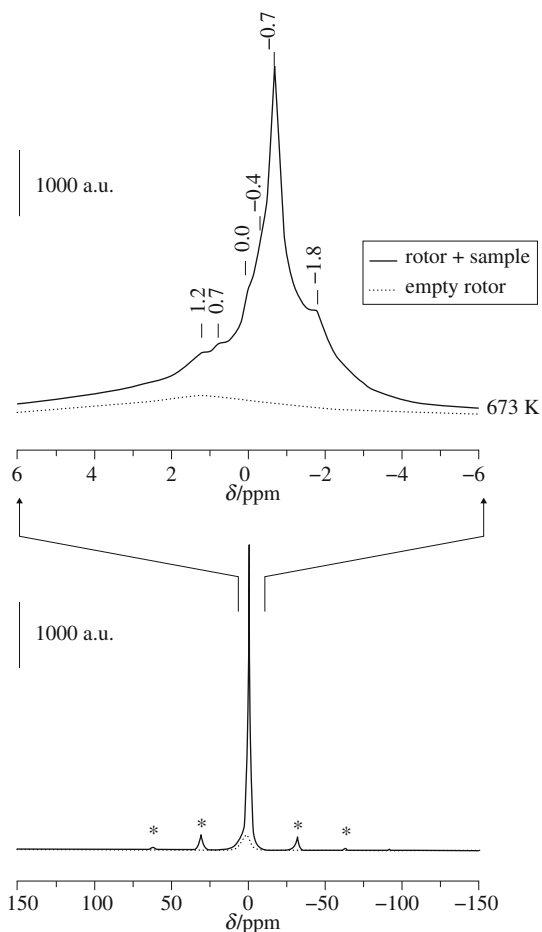


Fig. 3.1.12 ^1H Hahn-echo MASS NMR spectrum of MgO-sol-gel after treatment in flowing nitrogen ($20\text{ cm}^3\text{ min}^{-1}$) at 1023 K for 1 h, hydration at 373 K and subsequent treatment in flowing nitrogen ($20\text{ cm}^3\text{ min}^{-1}$) at 673 K for 2 h. The spectrum of the empty rotor is given in dashed line.

Reprinted with permission from C. Chizallet, G. Costentin, H. Lauron-Pernot, J. Maquet, M. Che, *Appl. Catal.*, **307**, 239 (2006) Fig. 1.

3.1.4 Type of Reaction vs. Optimum Strength of Basic Site

The strength of basic sites required for promoting a certain reaction varies with the type of reaction. Some reactions need strong basic sites, and some other reactions proceed on weak basic sites. As noted above, the strength of basic sites is in the order $\text{MgO} < \text{CaO} < \text{SrO} < \text{BaO}$. In addition, the strength of basic sites appearing on the surfaces also depends on the pretreatment temperature.

Table 3.1.6 lists 19 types of reaction for which a series of alkaline earth oxides were used as catalysts and pretreatment temperature-dependencies of the activity of MgO were measured.⁶⁸⁾ The reactions are characterized by the reaction temper-

Table 3.1.6 Reaction characteristics over alkaline earth oxides

Entry	Reaction	T _{REACT} ^{a)}	Order of activity ^{b)}	T _{MAX} ^{c)}	Relative activity ^{d)}	Ref.
1	Hydrogenation of alkenes	523	SrO > BaO > CaO > MgO	1373	~0	69
2	Hydrogenation of conjugate dienes	273	CaO > SrO > MgO > BaO	1273	~0	70
3	CH ₄ -D ₂ Exchange	573	CaO, MgO > SrO > BaO	1073	~0	2
4	Amination of conjugate dienes	273	CaO > SrO > MgO	1273	~0	71
5	Tishchenko reaction	353	SrO > CaO > MgO > BaO	1073	small	72
6	DBM ^{e)} of 1-butene	273	CaO > MgO > SrO > BaO	873	~0	1, 3, 4
7	DBM ^{e)} of 3-carene	353	CaO > MgO > SrO > BaO	873	~0	73
8	DBM ^{e)} of 5-vinylbicyclo [2.2.1]hept-2-ene	273	CaO > MgO > SrO > BaO	873	~0	74
9	DBM ^{e)} of allylamine	313	CaO, MgO > SrO > BaO	1073	~0.8	75
10	DBM ^{e)} of 2-propenyl ether	273	SrO > CaO > MgO > BaO	-	-	76
11	Aldol addition of butyraldehyde	273	CaO > MgO	873	~0.8	77
12	Transesterification ^{f)} with methanol	273	BaO > SrO > MgO > CaO	-	-	78
13	Transesterification ^{f)} with 2-propanol	273	SrO > BaO > CaO > MgO	-	-	78
14	Cyanoethylation of alcohol	323	SrO > BaO > MgO, CaO	1073	~1	79
15	Aldol addition of acetone	273	CaO > BaO > SrO > MgO	673	1	64
16	Nitroaldol reaction ^{g)}	313	MgO > CaO > SrO > BaO	1073	~1	81
17	Michael dimerization of methyl crotonate	323	MgO ≫ CaO > SrO > BaO	873	~1	80
18	Addition of methanol to 3-butene-2-one	273	MgO > CaO > SrO > BaO	673	1	82
19	Michael addition of nitromethane ^{h)}	273	MgO > CaO ≫ BaO, SrO	-	-	83

a), Reaction temperature; b), Activity order among alkaline earth oxides; c), Pretreatment temperature to give maximum activity of MgO; d), Activity of MgO pretreated at 673 K relative to that of MgO pretreated at T_{MAX}, 0 indicates MgO pretreated at 673 K shows no activity, and 1 indicates T_{MAX} is 673 K; e), Double bond migration; f), Transesterification of ethyl acetate; g), Nitromethane with methyl crotonate; h), Michael addition of nitromethane to α , β -unsaturated compounds.

ature, the order of activities among alkaline earth oxides, the pretreatment temperature to give a maximum activity of MgO and the activity of the MgO pretreated at 673 K relative to that of the MgO pretreated at the temperature to give a maximum activity. The last item represents the contribution of weak basic sites to the activity. This is based on the assumption that MgO pretreated at 673 K possesses weak basic sites. If the value is close to zero, the contribution of weak basic sites

is small, and if the value is close to unity, weak basic sites and strong basic sites contribute to the reaction to a similar extent. The order of activity is based on the unit weight of the catalyst. However, the specific surface areas of alkaline earth oxides are quite different. In particular, the specific surface area of BaO is much lower than that of the others. Therefore, the position of BaO in the activity order contains uncertainty to some extent. Regardless of the uncertainty, the types of reaction are arranged in such a way that the reactions requiring stronger basic sites are listed in the upper rows.

It may be said from Table 3.1.6 that the reactions with hydrocarbons need strongly basic sites. Weak basic sites which are supposed to be present on the MgO pretreated at 673 K are scarcely relevant to the reactions with hydrocarbons. Although not shown, these reactions are very sensitive to the presence of CO₂ and H₂O in the reaction mixture; the reactions are strongly retarded by trace amounts of CO₂ and H₂O.

The reactions with the compounds containing functional groups such as hydroxyl, nitro and carbonyl groups tend to proceed even on weakly basic sites. Perhaps the adsorption of such compounds on the basic sites is strong, and the abstraction of an H⁺ from the compound is relatively easy. Strong adsorption of the compounds causes a small poisoning effect by CO₂ and H₂O. Actually the reactions of entries 12, 13, 16, and 18 are not poisoned by CO₂ as described earlier. The common feature of these reactions is that one of the reactants is an alcohol except for the nitroaldol reaction. The adsorption of alcohol is compatible to or stronger than that of CO₂, and replacement of adsorbed CO₂ by alcohols is possible. The adsorption of nitromethane used for the nitroaldol reaction is also strong.

References

1. H. Hattori, N. Yoshii, K. Tanabe, *Proc. 5th Intern. Congr. Catal. Miami Beach*, 1972, p. 233.
2. M. Utiyama, H. Hattori, K. Tanabe, *J. Catal.*, **53**, 237 (1978).
3. H. Hattori, K. Maruyama, K. Tanabe, *J. Catal.*, **44**, 50 (1976).
4. M. Mohri, K. Tanabe, H. Hattori, *J. Catal.*, **32**, 144 (1974).
5. S. Coluccia, A. J. Tench, *Stud. Surf. Sci. Catal.*, **7**, 1154 (1981).
6. K. Tanabe, M. Misono, Y. Ono, H. Hattori, *New Solid Acids and Bases*, Kodansha-Elsevier, (1989).
7. A. F. Moodie, C. E. Warble, *J. Crystal Growth*, **74**, 89 (1986).
8. T. Yoshida, T. Tanaka, H. Yoshida, T. Funabiki, S. Yoshida, *J. Phys. Chem.*, **99**, 10890 (1995).
9. K. J. D. Mackenzie, R. H. Meinhold, *Thermochim. Acta*, **230**, 39 (1993).
10. T. Matsuda, J. Tanabe, N. Hayashi, Y. Sasaki, H. Miura, K. Sugiyama, *Bull. Chem. Soc. Jpn.*, **55**, 990 (1982).
11. V. R. Choudhary, M. Y. Pandit, *Appl. Catal.*, **71**, 265 (1991).
12. M. A. Aramendía, V. Borau, C. Jiménez, J. M. Marinas, J. R. Ruiz, F. J. Urbano, *Appl. Catal. A*, **244**, 207 (2003).
13. J. A. Wang, X. Bokhimi, O. Novaro, T. López, R. Gómez, *J. Mol. Catal.*, **145**, 291 (1999).
14. J. A. Wang, O. Novaro, X. Bokhimi, T. López, R. Gómez, J. Navarrete, M. E. Llanos, E. López-Salinas, *Mater. Lett.*, **35**, 317 (1998).
15. D. Gulkova, O. Solcova, M. Zdrzil, *Micropor. Mesopor. Mater.*, **76**, 137 (2004).
16. M. S. Mel'gunov, V. B. Fenelov, E. A. Mel'gunova, A. F. Bedilo, K. J. Klabunde, *J. Phys. Chem. B*, **107**, 2427 (2003).
17. S. Utamapanya, K. Klabunde, J. R. Schlup, *Chem. Mater.*, **3**, 175 (1991).
18. H. Itoh, S. Utamapanya, J. V. Stark, K. J. Klabunde, J. R. Schlup, *Chem. Mater.*, **5**, 71 (1993).

19. O. B. Koper, I. Lagadic, A. Volodin, K. J. Klabunde, *Chem. Mater.*, **9**, 2468 (1997).
20. K. J. Klabunde, J. Stark, O. Koper, C. Mohs, D. G. Park, S. Decker, Y. Jiang, I. Lagadic, D. Zhang, *J. Phys. Chem.*, **100**, 12142 (1996).
21. L. Chen, X. Sun, Y. Liu, Y. Li, *Appl. Catal. A*, **265**, 123 (2004).
22. T. Nakayama, S. Sato, F. Nozaki, *Bull. Chem. Soc. Jpn.*, **69**, 2107 (1996).
23. C. Marcilly, P. Courty, B. Delmon, *J. Am. Ceram. Soc.*, **53**, 56 (1970).
24. S. Takenaka, S. Sato, R. Takahashi, T. Sodesawa, *Phys. Chem. Chem. Phys.*, **5**, 4968 (2003).
25. J. Roggenbuck, M. Tiemann, *J. Am. Chem. Soc.*, **127**, 1096 (2005).
26. M. Choi, R. Ryoo, *Nature Mater.*, **2**, 473 (2003).
27. J. Take, N. Kikuchi, Y. Yoneda, *J. Catal.*, **21**, 167 (1971).
28. A. Zecchina, M. G. Lofthouse, F. S. Stone, *J. Chem. Soc. Faraday Trans.*, **71**, 1476 (1975).
29. A. Zecchina, F. S. Stone, *J. Chem. Soc. Faraday Trans. 1*, **72**, 2364 (1976).
30. E. Garrone, A. Zecchina, F. S. Stone, *Phylos. Mag.*, **42B**, 683 (1980).
31. S. Coluccia, A. M. Deane, A. J. Tench, *J. Chem. Soc. Faraday Trans. 1*, **74**, 2913 (1978).
32. M.-L. Bailly, G. Costentin, J. M. Krafft, M. Che, *Catal. Lett.*, **92**, 101 (2004).
33. M.-L. Bailly, G. Costentin, H. Lauron-Pernot, J. M. Kraft, M. Che, *J. Phys. Chem. B*, **109**, 2404 (2005).
34. M.-L. Bailly, C. Chizallet, G. Costentin, J.-M. Krafft, H. Lauron-Pernot, M. Che, *J. Catal.*, **235**, 413 (2005).
35. M. Cavalleri, A. Pelmenchikov, G. Morosi, A. Gamba, S. Coluccia, G. Martra, *Stud. Surf. Sci. Catal.*, **140**, 131 (2001).
36. S. Coluccia, F. Bocuzzi, G. Ghiotti, C. Morterra, *J. Chem. Soc. Faraday Trans.*, **1**, **78**, 2111 (1982).
37. T. Ito, T. Sekino, N. Moriai, T. Tokuda, *J. Chem. Soc. Faraday Trans. 1*, **77**, 2181 (1981).
38. T. Ito, T. Murakami, T. Tokuda, *J. Chem. Soc. Faraday Trans. 1*, **79**, 913 (1983).
39. T. Ito, M. Kusamichi, M. Yoshioka, T. Tokuda, *J. Phys. Chem.*, **87**, 4411 (1983).
40. E. Knözinger, K.-H. Jacob, S. Singh, P. Hofmann, *Surf. Sci.*, **290**, 388 (1993).
41. C. Chizallet, G. Costentin, M. Che, F. Delbecq, P. Sautet, *J. Phys. Chem. B*, **110**, 15878 (2006).
42. C. Chizallet, G. Costentin, M. Che, F. Delbecq, P. Sautet, *J. Am. Chem. Soc.*, **129**, 6442 (2007).
43. P. J. Anderson, R.F. Horlok, J.F. Olivier, *Trans. Faraday Soc.*, **61**, 2754 (1965).
44. T. Shido, K. Asakura, Y. Iwasawa, *J. Chem. Soc. Faraday Trans. 1*, **85**, 441 (1989).
45. S. Coluccia, L. Marchese, S. Lavagnino, M. Anpo, *Spectrochim. Acta*, **43A**, 1573 (1987).
46. S. Coluccia, S. Lavagnino, L. Marchese, *Mat. Chem. Phys.*, **18**, 445 (1988).
47. B. A. Morrow, *Stud. Surf. Sci. Catal.*, **57**, 161 (1990).
48. M.-L. Bailly, C. Chizallet, G. Costentin, J.-M. Krafft, H. Lauron-Pernot, M. Che, *J. Catal.*, **235**, 413 (2005).
49. M. Bensitel, O. Saur, J. C. Lavalley, *Mater. Chem. Phys.*, **28**, 309 (1991).
50. T. Ito, T. Tashiro, M. Kawasaki, T. Watanabe, K. Toi, H. Kobayashi, *J. Phys. Chem.*, **95**, 4476 (1991).
51. A. M. Ferrari, S. Huber, H. Knözinger, K. M. Neyman, N. Roesch, *J. Phys. Chem. B*, **102**, 4548 (1998).
52. Y. Yanagisawa, K. Kuramoto, S. Yamabe, *J. Phys. Chem. B*, **103**, 11078 (1999).
53. J. H. Lunsford, *J. Chem. Phys.*, **46**, 4347 (1967).
54. C. D. Valentini, G. Pacchioni, M. Chiesa, E. Giamello, S. Abbet, U. Heiz, *J. Phys. Chem. B*, **106**, 1637 (2002).
55. E. Giamello, M. C. Paganini, D. M. Murphy, A. M. Ferrari, G. Pacchioni, *J. Phys. Chem. B*, **101**, 971 (1997).
56. M. C. Paganini, M. Chiesa, E. Giamello, S. Coluccia, G. Martra, D. M. Murphy, G. Pacchioni, *Surf. Sci.*, **421**, 246 (1999).
57. M. C. Paganini, M. Chiesa, P. Martino, E. Giamello, *J. Phys. Chem. B*, **106**, 12531 (2002).
58. X. Lu, X. Xu, N. Wang, Q. Zhang, *J. Phys. Chem. B*, **103**, 5657 (1999).
59. S. Higashimoto, G. Costentin, B. Morin, M. Che, *Appl. Catal. B*, **84**, 58 (2008).
60. G. Pacchioni, J. M. Ricart, F. Illas, *J. Am. Chem. Soc.*, **116**, 10152 (1994).
61. E. Giamello, P. Ugliengo, E. Garrone, J. Che, *J. Chem. Soc. Faraday Trans. 1*, **85**, 1373 (1989).
62. C. Satoko, M. Tsukada, H. Adachi, *J. Phys. Soc. Jpn.*, **45** (1978).
63. H. Kobayashi, T. Ito, *Nippon Kagaku Kaishi*, **1996**, 765 (in Japanese).
64. G. Zhang, H. Hattori, K. Tanabe, *Appl. Catal.*, **36**, 189 (1988).
65. H. Tsuji, T. Shishido, A. Okamura, Y. Gao, H. Hattori, H. Kita, *J. Chem. Soc. Faraday Trans.*, **90**, 803 (1994).
66. C. Chizallet, G. Costentin, H. Lauron-Pernot, J. Maquet, M. Che, *Appl. Catal. A*, **307**, 239 (2006).

67. C. Chizallet, G. Costentin, H. Lauron-Pernot, M. Che, C. Bonhomme, J. Maquet, F. Delbecq, P. Sautet, *J. Phys. Chem. C*, **111**, 18279 (2007).
68. H. Hattori, *J. Jpn. Petrol. Inst.*, **47**, 67 (2004).
69. H. Hattori, Y. Tanaka, K. Tanabe, *Chem. Lett.*, **4**, 659 (1975).
70. Y. Tanaka, Y. Imizu, H. Hattori, K. Tanabe, *Proc. 7th Intern. Congr. Catal.*, Tokyo, Kodansha (1981).
71. Y. Kakuno, H. Hattori, *J. Catal.*, **85**, 509 (1984).
72. T. Seki, H. Kabashima, K., Akutsu, H. Tachikawa, H. Hattori, *J. Catal.*, **204**, 393 (2001).
73. K. Shimazu, K. Tanabe, H. Hattori, *J. Catal.*, **45**, 302 (1977).
74. H. Kabashima, H. Tsuji, H. Hattori, *React. Kinet. Catal. Lett.*, **58**, 255 (1996).
75. A. Hattori, H. Hattori, K. Tanabe, *J. Catal.*, **65**, 246 (1980).
76. H. Matsushashi, H. Hattori, *J. Catal.*, **85**, 457 (1984).
77. G. Zhang, H. Hattori, K. Tanabe, *Bull. Chem. Soc. Jpn.*, **62**, 2070 (1989).
78. H. Hattori, M. Shima, H. Kabashima, *Stud. Surf. Sci. Catal.*, **130**, 3507 (2000).
79. H. Kabashima, H. Hattori, *Catal. Today*, **44**, 277 (1998).
80. H. Kabashima, H. Tsuji, H. Hattori, *Appl. Catal. A*, **165**, 319 (1997).
81. K. Akutu, H. Kabashima, T. Seki, H. Hattori, *Appl. Catal. A*, **247**, 65 (2003).
82. H. Kabashima, T. Katou, H. Hattori, *Appl. Catal. A*, **214**, 121 (2001).
83. H. Kabashima, H. Tsuji, T. Shibuya, H. Hattori, *J. Mol. Catal. A*, **155**, 23 (2000).

3.2 Rare Earth Oxides

Although rare earth oxides show strong basic properties, they have not been utilized widely in base-catalyzed reactions. The oxides also show oxidation ability. The catalytic behaviors are reviewed in reference 1.

3.2.1 Preparation

Rare earth oxides are prepared from the hydroxides by calcination in air or by decomposition in a vacuum at high temperatures. The hydroxides are obtained from aqueous nitrates by hydrolysis with aqueous ammonia. Except for those of three elements (Ce, Pr and Tb), rare earth oxides thus prepared are stable in sesquioxide (M_2O_3) stoichiometry. The oxides of the three exceptions are stable in the nominal compositions CeO_2 , Pr_6O_{11} and Tb_4O_7 .

The formation of oxides from hydroxides normally proceeds via three distinct steps. The thermogram of $La(OH)_3$ to La_2O_3 in a vacuum is shown in Fig. 3.2.1.²⁾ Following an initial small weight loss at 373 to 473 K (a – b) due to removal of adsorbed water and/or crystallization water, the first true stage of $La(OH)_3$ decomposition occurs in the temperature range 523 to 623 K, and results in the formation of a well-defined hexagonal $LaO(OH)$ intermediate, represented by the break in the integral TG curve at point c. Subsequent dehydration of oxyhydroxide to La_2O_3 occurs at 523 to 693 K (c – d) and is completed at the latter temperature. The final broad weight loss that occurs in the temperature range 723 to 1073 K (d – e) is due to decomposition of carbonate species that is invariably present in the oxide as a result of interaction of the highly basic trihydroxide precursor with atmospheric carbon dioxide during preparation and handling.

IR measurement during heat treatment of $La(OH)_3$ indicates that CO_2 is strongly adsorbed and retained on the surface following outgassing at 773 K. The IR bands assigned to carbonates almost diminished following outgassing at 923 K.

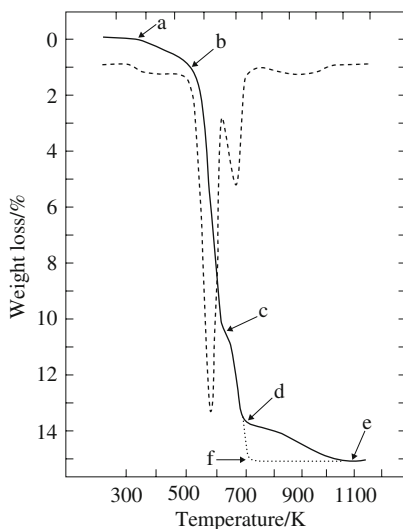


Fig. 3.2.1 Thermogram of prepared $\text{La}(\text{OH})_3$ obtained at 2 K/min in vacuum. solid line, integral weight loss curve; broken line, time/temperature derivative; dotted line, pathway followed by rehydrated La_2O_3 sample during second stage of dehydration. Reproduced with permission from M. P. Rosynek, D. T. Magnuson, *J. Catal.*, **46**, 407 (1977) Fig. 4.

Strong basic sites seem to exist in maximum number at the outgassing temperature of 923 K.

Surface areas of the rare earth oxides prepared by decomposition of hydroxides depend on the decomposition conditions, temperature, atmosphere, etc. The oxides prepared by decomposition of hydroxides at 873 K in a vacuum have specific surface areas in the range 10 to 50 $\text{m}^2 \text{g}^{-1}$.

As the rare earth oxides interact strongly with CO_2 and H_2O , they change their structures during storage in air at room temperature unless special precautions are taken. When a freshly prepared La_2O_3 was stored under normal conditions for five years, La_2O_3 underwent bulk hydration and carbonation, the hexagonal $\text{La}(\text{OH})_3$ and amorphous hydroxycarbonate $\text{La}_2(\text{OH})_4\text{CO}_3 \cdot n\text{H}_2\text{O}$ phase being formed.³⁾ Thermal treatment at about 1100 K is necessary to regenerate the oxide phase.

3.2.2 Characterization

A. Indicator method

Amounts and strength of La_2O_3 were measured by titration with benzoic acid using 2,4,6-trinitroaniline ($\text{p}K_{\text{BH}} = 12.2$) as an indicator.⁴⁾ The maximum basicity upon unit weight basis was observed with the pretreatment temperature at 773 K. The amounts of the basic sites stronger than $H_- = 12.2$ correlated with the catalytic activity for diacetone alcohol decomposition.

B. IR of surface OH groups

Several OH groups differing in IR absorption frequency exist on rare earth oxides. An example is shown in Fig. 3.2.2 for Ho_2O_3 pretreated at 720 K in a vacuum.⁵⁾ The spectrum displays five absorptions at 3775, 3720, 3695, 3655 and 3570 cm^{-1} due to $\nu(\text{OH})$ vibrations of isolated OH groups. The former two absorptions at 3775 and 3720 cm^{-1} are due to terminal OH groups, while the following two absorption bands at 3696 and 3655 cm^{-1} are due to bridging OH groups. The band at 3570 cm^{-1} is due most likely to multicentered OH groups. The IR band at the highest frequency has been assigned to the most basic OH groups. The band was weakened by adsorption of CO_2 and the band at 3620 cm^{-1} assigned to $\nu(\text{H-OCO}_2^-)$ developed. This accounts for involvement of the most basic OH groups in the formation of hydrogencarbonate species.

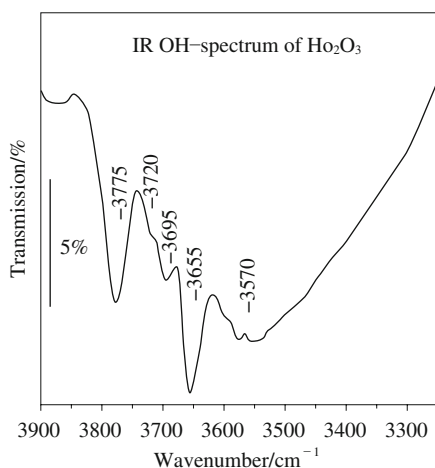


Fig. 3.2.2 IR $\nu(\text{OH})$ spectrum of Ho_2O_3 after outgassing at 720 K. Reprinted with permission from G. A. H. Mekheimer, *Appl. Catal. A*, **275**, 1 (2004) Fig. 2.

C. IR of adsorbed CO_2

Several bands appeared in the range 1700 to 1000 cm^{-1} on adsorption of CO_2 on the rare earth oxides. On Ho_2O_3 pretreated at 720 K, all of hydrogencarbonate, monodentate carbonate, bidentate carbonate, and polydentate carbonate were observed. At high coverage, linear species (2350 and 1380 cm^{-1}) appeared.⁵⁾

On the surface of La_2O_3 dispersed on Si-MCM-41, unidentate carbonate and bidentate carbonate were observed on adsorption of CO_2 .⁶⁾ Unidentate carbonate having bands in the ranges 1510–1550 cm^{-1} and 1360–1400 cm^{-1} was formed on strong basic sites, and bidentate carbonate having bands in the ranges 1610–1630 cm^{-1} and 1320–1340 cm^{-1} was formed on medium basic sites.

3.2.3 Catalytic Properties

The reactions for which basic properties of rare earth oxides are relevant are

hydrogenation of alkenes, double bond isomerization of alkenes, aldol addition of ketones, dehydration of alcohols, Meerwien-Pondorf-Verley reactions (transfer hydrogenation), esterification and H-D exchange between hydrocarbons and hydrogen.

The catalytic activities of rare earth oxides for base-catalyzed reactions are dependent on the temperature of pretreatment of the catalyst. Fig. 3.2.3 shows the variations of the activities of La_2O_3 as a function of the pretreatment temperature for 1-butene isomerization,⁴⁾ 1,3-butadiene hydrogenation,⁷⁾ and methane- D_2 exchange.⁸⁾ Pretreatment at 923 K resulted in the maximum activity for all the reactions. Essentially the same variation was observed for Nd_2O_3 and Sm_2O_3 in that the maximum activity was obtained at the pretreatment temperature of 923 K. This is the temperature required to remove all CO_2 from the surface as detected by IR, indicating that strong basic sites are relevant to the catalytic activities for these reactions.

Rare earth oxides show characteristic selectivity in dehydration of alcohols. In many cases, catalysts of basic character promote dehydrogenation of alcohols rather than dehydration of alcohols. Rare earth oxides, however, promote dehydration. The dehydration over rare earth oxides is dissimilar to those observed over acidic catalysts. 2-Alcohols undergo dehydration to form 1-alkenes (Table 2.5.5). The formation of thermodynamically unstable 1-alkenes contrasts with the formation of 2-alkenes observed in the dehydration over acidic catalysts. Lundeen and Hoozen studied dehydration of 4-methyl-2-pentanol over a series of rare earth oxides (oxides of Sc, Y, La, Ce, Pr, Nd, Sm, Eu, Gd, Tb, Dy, Ho, Er, Tm, Yb, and U) in the temperature range 623 to 700 K.⁹⁾ The selectivities to 1-alkene exceeded 90% for all the catalysts except Pr_6O_{11} (86%) and UO_2 (81%). The cata-

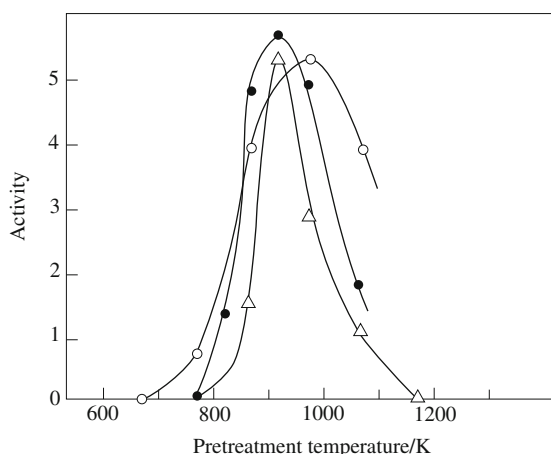


Fig. 3.2.3 Activity variation of La_2O_3 with pretreatment temperature.

○; 1-butene isomerization at 303 K (1 unit: 6.4×10^{20} molecules $\text{min}^{-1} \text{g}^{-1}$).

△; $\text{CH}_4\text{-D}_2$ exchange at 573 K (1 unit: $10^{-2}\% \text{s}^{-1} \text{g}^{-1}$).

●; 1,3-butadiene hydrogenation at 273 K (1 unit: 1.2×10^{20} molecules $\text{min}^{-1} \text{g}^{-1}$).

Reprinted with permission from K. Tanabe, M. Misono, Y. Ono, H. Hattori, *New Solid Acids and Bases*, Kodansha-Elsevier (1985) Fig. 3.16.

lytic activity of rare earth oxides in dehydration of alcohol is similar to that of ZrO_2 in their preferential formation of 1-alkenes from 2-alcohols.

For hydrogenation of alkenes, rare earth oxides show characteristic features. A series of rare earth oxides shows high activity for ethylene hydrogenation.¹⁰⁾ The reaction proceeds at 195 K. In particular, La_2O_3 and Nd_2O_3 have activities comparable to those of transition metal oxides such as Cr_2O_3 . Oxides such as CeO_2 and Pr_6O_{11} with high oxidation states, however, show low activities. Although the participation of basic sites in the reaction mechanism was not pictured, the importance of basic sites for the hydrogenation was suggested.¹⁰⁾ For 1,3-butadiene hydrogenation, 1,4-addition of H atoms to form 2-butene was observed for La_2O_3 , indicating that the reaction proceeds via π -allylic carbanion intermediates.⁷⁾ Hydrogenation of butene to butane did not occur at all under the same reaction conditions. This also supports a carbanionic hydrogenation taking place over La_2O_3 .

For butene isomerization over La_2O_3 , reaction mechanisms were studied mainly by a tracer study in which co-isomerization of a mixture containing perdeuterio butene and non-deuterio butene was undertaken.^{4,11-13)} All the results indicated that the isomerization proceeded via π -allylic carbanion intermediates, and intramolecular H transfer was involved in the reaction. Basic sites on La_2O_3 abstract an H^+ from butene to form π -allylic carbanion to initiate the reaction.

The oxidation state of the metal cations in rare earth oxides affects much the catalytic activities. The activity sequences of a series of rare earth oxides are shown in Fig. 3.2.4 for 1-butene double bond isomerization, 1,3-butadiene hydrogenation and acetone aldol addition.¹⁴⁾ The activity sequence was the same for 1-butene isomerization and 1,3-butadiene hydrogenation, which is different from that of acetone aldol addition. For the former reaction group, one characteristic feature is that the oxides of sesquioxide stoichiometry show the activity while the oxides with metal cations of higher oxidation states are entirely inactive. The situation is different in acetone aldol addition. Three oxides with high oxidation state, CeO_2 , Pr_6O_{11} and Tb_4O_7 , showed considerable activity. Pr_6O_{11} in particular showed activity close to the highest activity among rare earth oxides. It was suggested that the oxides with metal cations of oxidation state higher than 3 possess weak basic sites which function as active sites for aldol addition, but are not strong enough to catalyze hydrogenation and isomerization.

The catalytic properties of CeO_2 change much on the pretreatment with H_2 at high temperatures. The activity for 1-butene isomerization at 323 K was one order of magnitude higher for the CeO_2 pretreated with hydrogen in the range 673 to 1273 K than for the CeO_2 outgassed in the same temperature range. The reaction has characteristic features of base-catalyzed isomerization; high *cis-trans*-2-butene ratio, and an involvement of intramolecular H(orD) transfer.¹⁵⁾ For the transfer-hydrogenation of 1,3-butadiene with cyclohexadienes to butenes, CeO_2 became active when treated with H_2 at 873 K. The hydrogenation of 1,3-butadiene with H_2 proceeded on the reduced CeO_2 , but the rate was three orders of magnitude lower than that with 1,4-cyclohexadiene.¹⁶⁾ Without pretreatment with H_2 , the CeO_2 did not show any activity for the 1,3-butadiene hydrogenation with cyclohexadiene

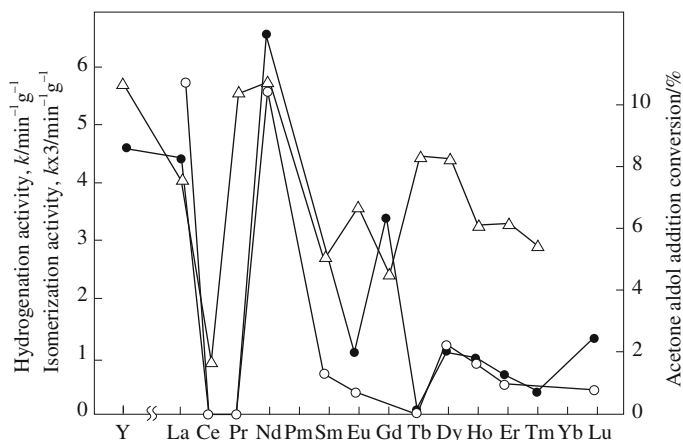


Fig. 3.2.4 Catalytic activities of rare earth oxides for 1-butene isomerization (○), 1,3-butadiene hydrogenation (●) and acetone aldol addition (△). Reprinted with permission from K. Tanabe, M. Misono, Y. Ono, H. Hattori, *New Solid Acids and Bases*, Kodansha-Elsevier (1985) Fig. 3.15.

nor with H₂. It was suggested on the basis of XRD measurements that Ce₂O₃ with the structure of rare earth type-A isomorphous with La₂O₃ is produced by the reduction of CeO₂ with H₂ at high temperatures.¹⁵⁾

References

1. M. P. Rosynek, *Catal. Rev. -Sci. Eng.*, **16**, 111 (1977).
2. M. P. Rosynek, D. T. Magnuson, *J. Catal.*, **46**, 407 (1977).
3. S. Bernal, F. J. Botana, R. Garcia, J. M. Rodriguez-Izquierdo, *Thermochim. Acta*, **66**, 139 (1983).
4. Y. Fukuda, H. Hattori, K. Tanabe, *Bull. Chem. Soc. Jpn.*, **51**, 3150 (1978).
5. G. A. H. Mekhemer, *Appl. Catal. A*, **275**, 1 (2004).
6. S. C. Shen, X. Chen, S. Kawi, *Langmuir*, **20**, 9130 (2004).
7. Y. Imizu, K. Sato, H. Hattori, *J. Catal.*, **76**, 65 (1982).
8. M. Utiyama, H. Hattori, K. Tanabe, *J. Catal.*, **44**, 237 (1978).
9. A. J. Lundeen, R. van Hoozen, *J. Org. Chem.*, **32**, 3386 (1967).
10. K. M. Minachev, Y. S. Khdakov, V. S. Nakhshunov, *J. Catal.*, **49**, 207 (1977).
11. J. Goldwasser, K. W. Hall, *J. Catal.*, **63**, 520 (1980).
12. J. Goldwasser, K. W. Hall, *J. Catal.*, **71**, 53 (1981).
13. M. P. Rosynek, J. S. Fox, J. L. Jensen, *J. Catal.*, **71**, 64 (1981).
14. H. Hattori, H. Kumai, K. Tanaka, G. Zhang, K. Tanabe, *Proc. 8th National Symp. Catal. India, Sindri, 1987*, p. 243.
15. T. Yamaguchi, N. Ikeda, H. Hattori, K. Tanabe, *J. Catal.*, **67**, 324 (1981).
16. T. Yamaguchi, H. Shima, *Chem. Lett.*, **8**, 899 (1979).

3.3 Zirconium Dioxide

Zirconium dioxide (ZrO₂) catalyzes various base-catalyzed reactions. The catalytic behavior of ZrO₂, however, is not the same as those of the other solid base catalysts such as MgO and alkali compound-modified metal oxides. Alcohols undergo dehydrogenation to form ketones or aldehydes over most of the solid base catalysts,

but undergo dehydration over ZrO_2 . The catalytic behaviors that distinguish ZrO_2 from the other solid base catalysts are frequently interpreted by the acid-base bifunctional properties of ZrO_2 .

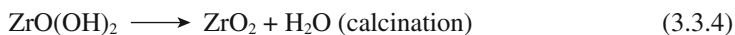
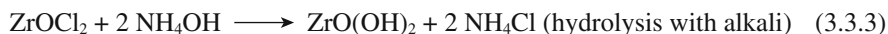
Zirconium oxide is used in industrial processes more frequently than the other solid base catalysts. Dehydration of 1-cyclohexylethanol to cyclohexylethylene,^{1,2)} dehydration of 2-hydroxypropylamine,³⁾ production of diisopropyl ketone from isobutyraldehyde and water,⁴⁾ and hydrogenation of aromatic carboxylic acids to aromatic aldehyde⁵⁾ are the industrial processes in which ZrO_2 is used as a catalyst.

3.3.1 Preparation and Phase Change

Raw materials of zirconium compounds are natural ores such as zircon ($ZrSiO_4$) and baddeleyite (ZrO_2). The ores are treated by alkali fusion, plasma fusion, or carbon reduction method. For ZrO_2 catalyst, $ZrOCl_2$ is widely used as a starting material prepared by the following steps.⁶⁾



$ZrOCl_2$ is hydrolyzed with alkali to form hydrous zirconia followed by calcination at 673–1073 K.



The natural ores contain 1–3% Hf, which is difficult to separate from zirconium compounds. Accordingly, the main impurities possibly contained in the final ZrO_2 prepared by the method described above are Hf, Si, Na and Cl.

Zirconia has three crystalline structures: monoclinic phase, tetragonal phase and cubic phase. The monoclinic phase is stable up to 1473 K, the tetragonal phase is stable up to 2173 K, and the cubic phase is stable above 2173 K. When hydrous zirconia is calcined at progressively higher temperature to obtain ZrO_2 , the phases of the resulting ZrO_2 do not follow the thermodynamic stabilities of the phases. The resulting phases depend on the preparation conditions as described below. The phases of ZrO_2 used for catalyst are amorphous, metastable tetragonal and monoclinic. The surface area of ZrO_2 is small in the form of stable tetragonal and cubic phases.

Tetragonal phase and monoclinic phase can be determined clearly by XRD. Monoclinic phase shows XRD peaks at $\sim 28^\circ$ and 31° in 2θ , for (11 $\bar{1}$) and (111) reflections, respectively, while tetragonal phase shows at 30° for (111) reflection. However, it is difficult to distinguish tetragonal phase from cubic phase by XRD. The XRD patterns of the cubic and the tetragonal zirconia are nearly identical though small differences are observable; the tetragonal phase gives a limited number of additional high order and low intensity reflections due to its lower degree of symmetry. For the sample whose crystallization degree is low, it is not

possible to determine clearly from broad XRD patterns whether the phase is tetragonal or cubic.

The tetragonal and cubic phases may be readily identified and distinguished from one another by means of Raman spectroscopy. Tetragonal zirconia is expected to give a spectrum consisting of six Raman bands with frequency at about 148, 263, 325, 472, 608 and 640 cm^{-1} , while cubic zirconia is expected to give a single Raman band around 490 cm^{-1} .⁷⁾

Figure 3.3.1 shows Raman spectra of ZrO_2 samples prepared by calcination of hydrous zirconia at different temperatures together with a pure monoclinic sample.⁷⁾ ZrO_2 is tetragonal when hydrous zirconia is calcined at 723 K. The tetragonal phase completely converts to monoclinic phase by calcination at 1123 K.

Appearance and transformation of the phases are strongly dependent on the preparation conditions and procedures for ZrO_2 . The main factors determining the crystalline phase are pH of the mother liquid during hydrothermal treatment (aging, digestion), period of hydrothermal treatment, temperature and environment (type of gas(es) in contact with the oxide) during heat treatment to obtain ZrO_2 from hydrous zirconia, and presence of contaminants or additives.

The effects of the pH of the mother liquid are complicated. Denkewicz et al. reported that at a high pH (> 13) of the mother liquid during hydrothermal treatment of the precipitate at about 383 K, tetragonal phase of hydrous zirconia formed predominantly, while at a low pH (< 3), monoclinic hydrous zirconia formed predominantly.⁸⁾ At an intermediate pH (4–12), fraction of tetragonal phase varied very much; in the pH range 4–6, tetragonal phase formed dominantly while in the pH range 7–12, monoclinic phase formed dominantly. At a pH lower

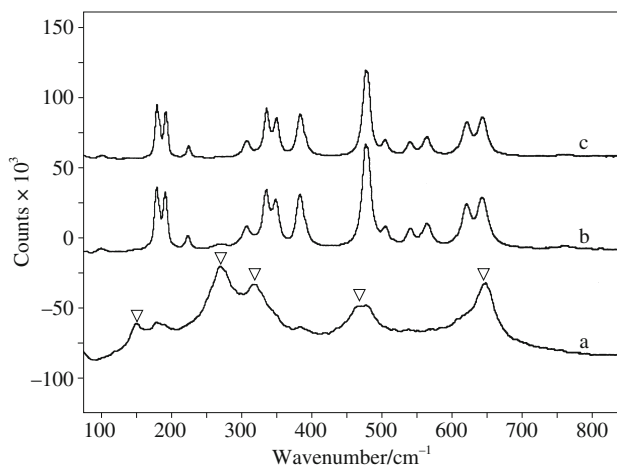


Fig. 3.3.1 Typical Raman spectra of different ZrO_2 samples: (a) a predominantly "metastable" tetragonal sample obtained by calcining hydrous zirconia at 723 K (triangles indicate strongest bands resulting from the "metastable" tetragonal phase); (b) a predominantly monoclinic sample obtained by calcining hydrous zirconia at 1123 K; and (c) a 100% monoclinic sample (CERAC Chemicals, spectro grade monoclinic ZrO_2). Reprinted with permission from P. D. L. Mercera, J. G. Van Ommen, E. B. M. Doesburg, A. J. Burggraaf, J. R. H. Ross, *Appl. Catal.*, **57**, 127 (1990) Fig. 2.

than 3, no precipitation occurred immediately, but occurred after a prolonged hydrothermal treatment. Clearfield et al. reported that on refluxing a 1 M solution of ZrOCl_2 the pH decreased continuously, and precipitation began in about 20 h when the pH became about 0.9.⁹⁾ The precipitate was a colloidal suspension of monoclinic particles. Essentially the same results were reported by others.¹⁰⁻¹²⁾

Without hydrothermal treatment, the hydrous zirconia precipitated at the intermediate pH is amorphous. As the hydrothermal treatment is prolonged at about 373 K, the phase of hydrous zirconia converts successively from amorphous, tetragonal, and finally monoclinic. It is suggested that dewatering is facilitated during hydrothermal treatment. The structures of zirconium polycations change successively from α -type ($\text{Zr}_4(\text{OH})_{16}^{8+}$) to β -type ($\text{Zr}_4\text{O}_2(\text{OH})_{12}^{8+}$), and to γ -type ($\text{Zr}_4\text{O}_4(\text{OH})_8^{8+}$) with hydrothermal treatment period.¹³⁾ The crystalline structure of the hydrous zirconia is retained after calcination at about 573 K.

Type of gas(es) in contact with the oxide during calcination and the temperature affect the crystalline structure of the resulting ZrO_2 . When an amorphous hydrous zirconia was heated at 573 K in a vacuum, in air, and under steaming, the resulting ZrO_2 's were amorphous, tetragonal and monoclinic, respectively.¹⁴⁾ Further increase in a heat treatment temperature brought about a change in the phase of ZrO_2 .

DTA-TG analysis of an amorphous hydrous zirconia in air shows a sharp exothermic peak at about 693 K which is not accompanied by weight change. The peak is attributed to a phase change from amorphous phase to tetragonal phase. The formation of tetragonal phase at this temperature (metastable tetragonal phase) is contradictory to the thermodynamic stabilities of the phases; monoclinic phase is thermodynamically more stable at about 693 K. The monoclinic phase appears when the tetragonal phase is calcined above 1073 K in air and cooled to room temperature.

The presence of contaminants or additives in hydrous zirconia affects the temperature at which the phase transformation from amorphous to tetragonal occurs. The exothermic peak at about 693 K in DTA curve shifts to a higher temperature in the presence of contaminants or additives such as Na, Si, Cr, Cl and SO_4 .⁶⁾ The exothermic peak appears at about 900 K for the hydrous zirconia which has been impregnated with 2 M H_2SO_4 followed by drying at 373 K.

As the thermodynamically stable phase at room temperature is monoclinic, the existence of a low-temperature tetragonal phase seems to be in conflict with the phase diagram of bulk zirconia. However, many of ZrO_2 samples calcined below ca. 900 K have been reported to be in the tetragonal phase at room temperature. The monoclinic phase appears after heat treatment at a higher temperature. Many explanations have been advanced for the initial transformation of amorphous phase to the tetragonal phase and not to the more stable monoclinic phase. One of the explanations is a crystallite size effect.¹⁵⁻¹⁷⁾ While the monoclinic phase has a lower bulk free energy, the tetragonal phase has a lower surface free energy. For crystallites below a certain critical size, the surface energy term dominates the bulk energy term, which results in stabilizing the tetragonal phase. Another explanation is the short range structural similarities between the amorphous phase and

the tetragonal phase. The amorphous phase converts faster to tetragonal phase than to monoclinic phase.

It should be noted that the phase transformation from tetragonal to monoclinic occurs during the cooling period of the calcined ZrO_2 , as clarified by Turrillas et al.¹⁸⁾ They prepared hydrous zirconia from zirconium hydrogensulfate at pH values of 8.37 and 10.35. The hydrous zirconia was heated at a high temperature, and its phase change monitored during the cooling period by *in situ* measurement of energy dispersive diffraction (EDD). The sample heated at 1573 K for 60 min was tetragonal at this temperature and transformed to monoclinic at 1183–1093 K of cooling process. The sample heated at 1173 K for 60 min was also tetragonal at 1173 K and transformed to monoclinic at 693–373 K. The tetragonal-monoclinic transformation temperature varied with the pH value at which hydrous zirconia was precipitated and the period of heating time at top temperature. They concluded two principles. Firstly, the transformation temperature can be greatly increased by the temperature and duration of heating. Secondly, whereas the high-pH-prepared material intrinsically produces high transformation temperatures, it is the low-pH-prepared material that is more sensitive to heat treatment temperature. For the samples calcined below 1273 K, the high-pH material displays the higher transformation temperatures, whereas for the samples calcined above 1273 K, the low-pH material displays the higher transformation temperature. If the material shows a transformation temperature below room temperature, the material obtained by cooling the calcined sample to room temperature will be tetragonal.

Ward and Ko reported essentially the same results as reported by Turrillas et al. in the same year.¹⁹⁾ They prepared amorphous ZrO_2 aerogel by sol-gel method and measured the structure by *in situ* XRD. The ZrO_2 aerogel was heat-treated at different temperatures and its structural change monitored during cooling by *in situ* XRD as shown in Fig. 3.3.2. All the samples heat-treated at 973, 1173 and 1373 K were tetragonal before cooling. The phase transformation from the tetragonal to monoclinic phase occurred when the sample was cooled. The temperature at which the transformation occurs varied with the heat treatment temperature. For the sample heat-treated at 973 K, the tetragonal to monoclinic transformation occurred at a low temperature of 673 K, the room temperature product being a mixture of tetragonal and monoclinic phase. On the other hand, the sample heat-treated at 1373 K, the transformation occurred at a high temperature of 973 K, the room temperature product being a monoclinic phase.

An example of the variations in the surface area and the percentage of monoclinic phase as a function of the calcination temperature is shown in Fig. 3.3.3 for the zirconia prepared from ZrOCl_2 by precipitation at pH 10.⁷⁾ The amorphous phase is not counted in the percentages of these phases. The surface area markedly decreases while the percentage of monoclinic phase increases with the calcination temperature. Essentially the same changes in surface area and fraction of tetragonal phase with calcination temperature were observed by other researchers.¹⁰⁾

As shown in Fig. 3.3.3, the surface area of ZrO_2 decreases markedly with calcination temperature. Several preparation methods were proposed for ZrO_2 of high surface area after calcination at high temperature.

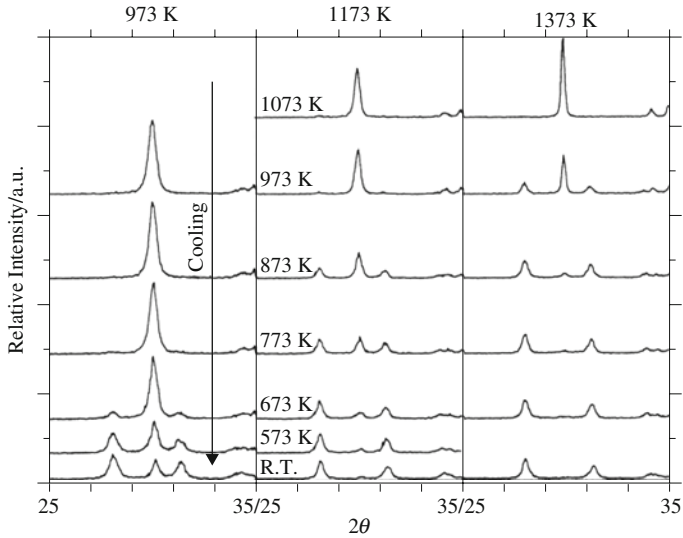


Fig. 3.3.2 *In situ* X-ray diffraction patterns of zirconia aerogel. Each panel represents a sample that was heated to the temperature indicated at the top, held at that temperature for 2 h and cooled.

Reprinted with permission from D. A. Ward, E. I. Ko, *Chem. Mater.*, **5**, 956 (1993) Fig. 11.

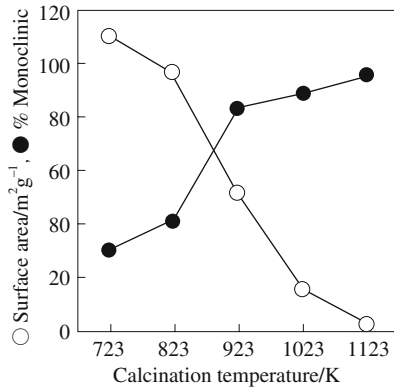


Fig. 3.3.3 Variations in surface area (○) and % monoclinic phase (●) as a function of calcination temperature of hydrous zirconia.

Replotted from the data in reference 7 (P. D. L. Mercera, J. G. Van Ommen, E. B. M. Doesburg, A. J. Burggraaf, J. R. H. Ross, *Appl. Catal.*, **57**, 127 (1990)).

Chuah et al. reported that prolonged hydrothermal treatment (digestion) resulted in a ZrO_2 possessing a high surface area after calcination at high temperature.^{20,21} The hydrous zirconia precipitated with NH_4OH at pH 11 (initial) to 9.4 (final) followed by hydrothermal treatment for 192–500 h produced ZrO_2 possessing a surface area of $240 \text{ m}^2\text{g}^{-1}$ after calcination at 773 K. Without hydrothermal treatment, the ZrO_2 obtained after calcination at 773 K had a surface area of 42.8

m^2g^{-1} . The hydrous zirconias precipitated with NaOH and KOH were more stable to calcination at high temperature. The surface area did not decrease much up to 1073 K but decreased markedly beyond 1073 K. The crystalline phase was exclusively tetragonal for the ZrO_2 calcined below 1273 K. Although Chuah et al. deduced the increased surface area to the prolonged hydrothermal treatment, it turned out that the surface area increase was due primarily to the dissolution of Si from the glass container used in the hydrothermal treatment. It was also revealed, however, that the prolonged hydrothermal treatment caused an increase in surface area, though the effect was not so strong as that caused by the inclusion of Si from the container. Increase in the surface area by prolonged hydrothermal treatment was also reported by other researchers who prepared a hydrous zirconia in a glass container.²²⁾

Sato et al. examined the effects of Si which might be dissolved from the glass container during hydrothermal treatment.²³⁾ A Si component was intentionally added to the mother liquid. The resulting ZrO_2 showed a high surface area. They concluded that the high surface area of the ZrO_2 is primarily due to the inclusion of the Si component into hydrous zirconia during hydrothermal treatment. This conclusion was supported by other researchers.²⁴⁾

It is evident, however, that hydrothermal treatment is effective for the enlargement of the surface area of the resulting ZrO_2 . Sato et al. also reported that the surface area of the ZrO_2 hydrothermal treated for 96 h in a container made of polymethylpentane was $78 \text{ m}^2\text{g}^{-1}$ after calcination at 773 K. Without hydrothermal treatment, the surface area was $44 \text{ m}^2\text{g}^{-1}$. Chang et al. also reported an increase in the surface area by hydrothermal treatment for the sample prepared in a Teflon container.²²⁾ The surface area obtained after calcination at 1173 K was ca. $10 \text{ m}^2\text{g}^{-1}$ for the sample without hydrothermal treatment and ca. $33 \text{ m}^2\text{g}^{-1}$ for the sample with hydrothermal treatment for 15 h.

A high surface area ZrO_2 is also prepared by sol-gel method. Into a mixture containing HNO_3 , 1-propanol, and zirconium tetrapropoxide, a water-1-propanol mixture was added to form a gel. The ratios $\text{H}_2\text{O}/\text{Zr}^{4+}$ and $\text{HNO}_3/\text{Zr}^{4+}$ were 2.0 and 0.761, respectively. The alcohol contained in the gel was removed by supercritical carbon dioxide. The alcohol was completely replaced by CO_2 in ca. 2 h. After removal of the CO_2 , the resulting powder was evacuated at 383 K followed by calcination under flowing O_2 at 773K. The resulting ZrO_2 had a surface area of $134 \text{ m}^2\text{g}^{-1}$.¹⁹⁾

3.3.2 Characterization

A. TPD of adsorbed CO_2 and NH_3

The existence of both acidic sites and basic sites on the surface is a characteristic of ZrO_2 , as evidenced by TPD of NH_3 and CO_2 . TPD plots of NH_3 and CO_2 on the monoclinic ZrO_2 calcined at 1073 K together with those for $\text{SiO}_2\text{-Al}_2\text{O}_3$ and MgO are shown in Fig. 3.3.4.²⁵⁾ ZrO_2 adsorbs both NH_3 and CO_2 , though adsorption of NH_3 and CO_2 on ZrO_2 is not strong compared to the adsorption of NH_3 on $\text{SiO}_2\text{-Al}_2\text{O}_3$ and CO_2 on MgO , respectively. Co-adsorption of NH_3 and CO_2 on ZrO_2

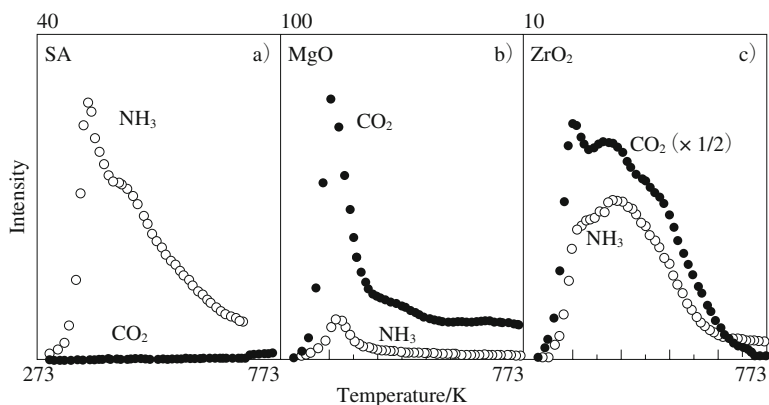


Fig. 3.3.4 TPD profiles of NH₃ and CO₂ on SiO-Al₂O₃ (a), MgO (b) and ZrO₂ (c). Reprinted with permission from B.-Q. Xu, T. Yamaguchi, K. Tanabe, *Chem. Lett.*, **1988**, 1663 Fig. 1.

revealed that there exist, in addition to independent acidic sites and basic sites, pairs of acidic and basic sites located nearby so that the adsorbed NH₃ and adsorbed CO₂ attract and interact with each other.^{25,26)}

B. IR of surface OH groups

Generally from two to four discrete hydroxyl bands are observed in the O-H stretching region of 4000–3500 cm⁻¹. Two main bands appear at 3780 cm⁻¹ and 3680 cm⁻¹. There is no controversy as to the assignment of the band at 3780 cm⁻¹. Although the peak position of this band is not the same in all reported papers, this band is assigned to the OH groups which bind to one Zr atom through O (terminal OH, unidentate type). For the other main band at 3680 cm⁻¹, Bachiller-Baeza et al. assigned it to tribridged OH groups,²⁷⁾ while Yamaguchi et al.,²⁸⁾ Aboulayt et al.,²⁹⁾ Bensitel et al.³⁰⁾ and Ouyang et al.³¹⁾ assigned it to bridged OH groups which bind to two Zr atoms through O.

In addition to the two main bands, the bands at about 3740 cm⁻¹, 3540 cm⁻¹ and 3533 cm⁻¹ were reported in some cases. The band at 3740 cm⁻¹ was assigned to bidentate OH by Bachiller-Baeza et al.²⁷⁾ but terminal OH on tetragonal ZrO₂ by Hertl.³²⁾ The 3740 cm⁻¹ band observed for ZrO₂ containing silica was assigned to bridged OH groups on tetragonal ZrO₂,³³⁾ and the bands at 3540 cm⁻¹ and 3533 cm⁻¹ were assigned to OH groups on tetragonal phase and amorphous phase, respectively.³²⁾

The reactivity toward D₂, D₂O, CO, CO₂, CH₃OH, and HCOOH is higher for the terminal OH groups than for the bridged OH groups. This is due to the stronger basicity of the terminal OH groups as compared to the bridged OH groups. It was also reported that the concentration of OH groups is higher on the monoclinic ZrO₂ than on the tetragonal ZrO₂.³³⁾

C. IR of adsorbed CO₂

Carbon dioxide is adsorbed on ZrO₂ in different forms as described in section

2.4.1^{27, 31–35)}. Carbon dioxide is adsorbed more strongly on monoclinic ZrO₂ than on tetragonal ZrO₂.^{27,33)} The adsorption sites on the monoclinic ZrO₂ with stronger basicity are associated to $\text{cusZr}^{4+}\text{-O}^{2-}$ pairs.²⁷⁾ Unidentate carbonate is formed on cusO^{2-} of high basicity.

For the formation of the ionic hydrogencarbonate species, the terminal OH groups giving a band at the highest frequency ($\sim 3780\text{ cm}^{-1}$) are more reactive than the bridged OH groups giving a band at lower frequency ($\sim 3680\text{ cm}^{-1}$). It is suggested that the terminal OH groups are a stronger base than the bridged OH groups.^{31,32)}

D. IR of adsorbed H₂

Hydrogen is adsorbed on ZrO₂ to give several adsorbed species.^{36–38)} The forms of the surface species depend on the adsorption temperature. Below 173 K, molecularly adsorbed hydrogen was observed by IR, which gave an absorption band at 4029 cm^{-1} and eliminated by outgassing. At 173 K, Zr-H resulting from homolytic dissociative adsorption was also observed as a broad band centered at 1540 cm^{-1} . Above 223 K, heterolytic dissociative adsorption generating Zr-H and O-H species giving bands at 1562 and 3668 cm^{-1} , respectively, were observed. Once heterolytic adsorption occurred, Zr-H and O-H species were irreversibly observed in the temperature range 223–373 K. Heterolytic dissociative adsorption of hydrogen indicates that O^{2-} and Zr^{4+} act as base and acid, respectively. Above 300 K, another type of dissociative adsorption occurred, giving two different OH species at 3668 and 3778 cm^{-1} . Judging from the absorption frequency, these two bands are the terminal OH groups and the bridged OH groups, respectively. When the temperature was raised under hydrogen, the OH bands at 3668 and 3778 cm^{-1} intensified, while the band due to Zr-H species at 1562 cm^{-1} reduced, and the band at 1562 cm^{-1} disappeared at 525 K.

The reactivities of the OH species resulting from hydrogen adsorption are similar to those present on the ZrO₂ pretreated at high temperature. The OH species resulting from hydrogen adsorption reacts with CO to form formate ions at 373 K, and methoxide in addition to the formate at 473 K.

ZrO₂ catalyzes ethylene hydrogenation. However, Domen et al. concluded that Zr-H and O-H formed by adsorption of hydrogen do not participate in the hydrogenation of ethylene.^{39,40)} This is a point which distinguishes ZrO₂ from ZnO on which Zn-H and O-H formed by hydrogen adsorption participate in the hydrogenation of ethylene.⁴¹⁾

3.3.3 Catalytic Properties

Zirconia possesses both acidic sites and basic sites though they are not strong. Many of the catalytic properties of ZrO₂ are explained by bifunctional catalysis in which both acidic sites and basic sites participate. Cooperation of acidic sites with basic sites results in an efficient catalytic property. For the reaction of 2-methyl-3-butyne-2-ol (MBOH), which is a diagnostic reaction to examine the nature of active sites, acidic, basic, or amphoteric, ZrO₂ yields mainly 3-hydroxy-3-methyl-2-

butanone, indicating that the active sites on ZrO_2 are amphoteric.⁴²⁻⁴⁴⁾ The basic OH group reacts with the -OH group of 3-methyl-3-butyn-2-ol to form water, while the vacant Zr *d*-orbital (acidic site) interacts with acetylenic π -bond to yield hydroxymethylbutanone.⁴²⁾

For 1-butene isomerization, which is also a diagnostic reaction, ZrO_2 shows a high *cis-trans*- ratio in 2-butene, indicating a base-catalyzed reaction. The ratio observed by Yamaguchi et al. was 7.3 at a reaction temperature of 373 K.⁴⁵⁾ The reaction was completely retarded by CO_2 which was retained on ZrO_2 after evacuation of adsorbed CO_2 at 373 K. Pajonk and Tanany also reported a high ratio of *cis-trans*- ratio in 2-butene formed in 1-butene isomerization. They suggested the participation of acidic sites from a strong poisoning effect by NH_3 .⁴⁶⁾

Alcohols undergo dehydration to form alkenes over ZrO_2 . This is in contrast with the general trend whereby alcohols undergo dehydrogenation over basic catalyst, but dehydration over acidic catalyst. The selectivity to alkenes over ZrO_2 is not the same as that observed for solid acid catalysts. In the dehydration of 2-alkanols, 1-alkenes are primarily formed over ZrO_2 while 2-alkenes are the main products for solid acid catalysts. The reaction mechanisms for dehydration of alcohols over ZrO_2 (E1cB mechanism) are different from those over solid acid catalysts (E1 or E2 mechanism).

Yamaguchi et al. found that 2-butanol undergoes dehydration over ZrO_2 at 473 K to selectively yield 1-butene; 90.2% 1-butene was formed.⁴⁵⁾ The activity was slightly poisoned by butylamine injection, but gradually recovered with time on stream, suggesting the participation of weak acid sites. Ferino et al. also reported the preferential formation of 1-alkenes in dehydration of 4-methylpentan-2-ol; the selectivity to 4-methyl-1-penten was 77% at a conversion of 63% at 603 K. They suggested an E2-like mechanism with the activated complex having a marked carbanionic character.^{47,48)} Basic sites and acidic sites cooperate in the activation of alcohols in both of the above cases. By utilizing the selective formation of 1-alkenes in dehydration of 2-alcohols over ZrO_2 , the production of cyclohexylethylene by dehydration of 1-cyclohexylethanol has been industrialized.^{1,2)}

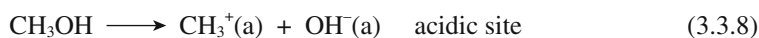
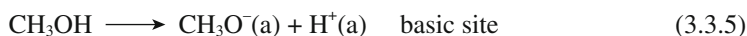
Hydrogenation of conjugated dienes proceeds over ZrO_2 . 1,3-Butadiene underwent hydrogenation at 323 K to produce *n*-butenes, *trans*-2-butene being the major product. A negligible amount of *n*-butane was produced. Deuteration (using D_2 in place of H_2) of 1,3-butadiene yielded exclusively butene isomers-*d*₂, and ¹³C NMR of the produced *trans*-2-butene indicated that the two D atoms were located almost exclusively on the C₁ and C₄ atoms.⁴⁹⁾ 2-Methyl-1,3-butadiene (isoprene) also underwent hydrogenation at 323 K to produce 2-methylbutenes: 60% 2-methyl-2-butene, 35% 2-methyl-1-butene and 5% 3-methyl-1-butene being formed. This means that hydrogenation involves 60% 1,4-addition and 40% 1,2- (and 3,4-) addition of hydrogen. The variation of the activity with the pretreatment temperature of ZrO_2 runs parallel with that of H_2 - D_2 equilibration. It is suggested that the dissociation of hydrogen is the key step for the direct hydrogenation.⁵⁰⁾

ZrO_2 promotes the transfer hydrogenation of conjugated dienes.⁵⁰⁾ Transfer hydrogenation is hydrogenation with the aid of organic molecules as the hydrogen

donor in place of hydrogen. The transfer hydrogenation of 1,3-butadiene with cyclohexadiene proceeded at 323 K over ZrO_2 . The product distribution in *n*-butenes was different for the transfer hydrogenation and for the direct hydrogenation with H_2 , 1-butene (1,2-addition) and *trans*-2-butene (1,4-addition) being the major products in the transfer and direct hydrogenation, respectively. The first step in transfer hydrogenation is the addition of H^+ to form a cationic intermediate, while that in direct hydrogenation is the addition of H^- to form an allylic anion. The H^+ and H^- are provided by the dissociative adsorption of cyclohexadiene and H_2 , respectively.

The intermediate of the hydrogenation is suggested to be of cationic character for the transfer hydrogenation which leads to 1,2-addition of hydrogen atoms, while it is the allylic anion for the direct hydrogenation which leads to 1,4-addition. Variation in the activity of ZrO_2 with pretreatment temperature for the transfer hydrogenation runs parallel with that of 1-butene isomerization. The optimum pretreatment temperature for both reactions is 1073 K. Both the transfer hydrogenation and 1-butene isomerization are initiated with the abstraction of an H^+ from cyclohexadiene and 1-butene, respectively. The abstraction of an H^+ from cyclohexadiene by a basic site is the key step for the transfer hydrogenation, and addition of the H^+ to 1,3-butadiene leads to the formation of the cationic intermediate.

ZrO_2 catalyzes the synthesis of dimethyl carbonate from methanol and CO_2 . The reaction involves the following steps.⁵¹⁾



Basic sites activate methanol and CO_2 to form methylcarbonate anions, while acidic sites activate methanol to form methyl cations. The methylcarbonate anion formed on the basic site reacts with the methyl cation formed on the acidic site to form dimethylcarbonate.^{26,51)} Neighboring acid sites and basic sites are effective for the reaction. Two reactant molecules are activated separately by basic sites and acidic sites.

Jung and Bell proposed slightly different mechanisms for the formation of dimethyl carbonate from methanol and CO_2 based on IR study.¹⁰⁾ The ion pair $\text{Zr}^{4+}\text{-O}^{2-}$ adjacent to the OH group interacts with methanol in two ways; one to form methoxide and the other to split the C-O bond in methanol.

Formation of aldehydes from aromatic carboxylic acids in H_2 is an industrialized process in which ZrO_2 is used. The active sites for the reaction may be

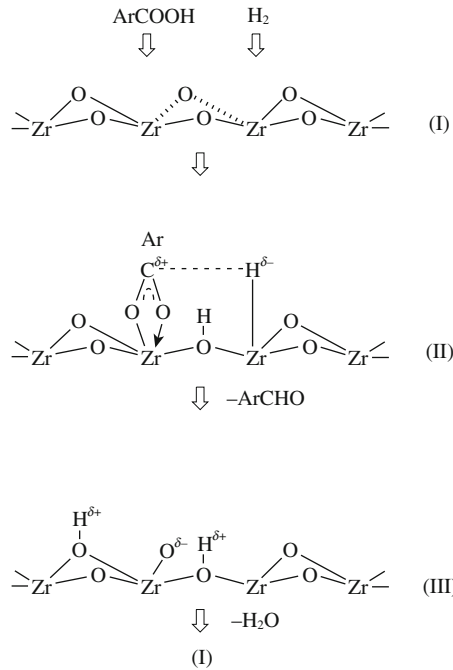


Fig. 3.3.5 Reaction mechanism proposed for reduction of benzoic acid to benzaldehyde over ZrO_2 .

understood by the cooperation of neighboring ion pairs. The reaction mechanisms proposed are shown in Fig. 3.3.5.⁵¹ The bidentate carboxylate is formed by the abstraction of an H^+ from the carboxylic acid by a basic site. On the neighboring ion pair, H_2 is heterolytically dissociated to form an H^+ and H^- . The carboxylate reacts with the H^- to form the aldehyde, leaving O^{2-} on the Zr^{4+} ion. The O^{2-} reacts with two H^+ ions left on the surface O atoms to form H_2O which leaves the surface.

In the decomposition of alkylamines to nitriles over ZrO_2 , acidic sites and basic sites act at different stages of the reaction scheme. Triethylamine and dimethylamine convert to acetonitrile over ZrO_2 catalyst at 673 K, as shown in Fig. 3.3.6.⁵² The location of acid sites and basic sites nearby is efficient because

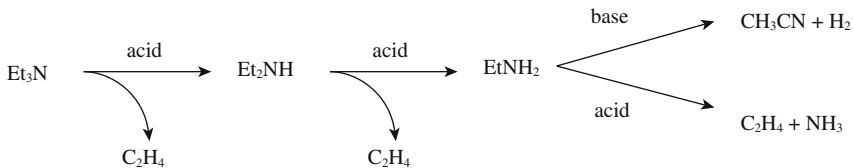


Fig. 3.3.6 Participation of acid sites and basic sites in decomposition of triethylamine.

diethylamine and ethylamine formed on an acidic site can rapidly migrate to a basic site where dehydrogenation takes place to yield acetonitrile.

The first industrial process in which ZrO_2 was used is the production of diisopropyl ketone from a equimolar mixture of isobutyraldehyde and water.⁴⁾ A conversion of 90.8% and a selectivity of 92.3% were obtained at 733 K. The formation of diisopropyl ketone involve five different types of reactions; Tishchenko reaction, hydrolysis, dehydrogenation, decarbonation and dehydration.⁵³⁾ Although ZrO_2 was not recognized as a base catalyst when the process was industrialized, it is now understood that basic sites together with acidic sites on ZrO_2 are relevant to those five types of reactions.

Meerwein-Pondorf-Verley reduction and its reverse reaction Oppenauer oxidation are catalyzed more efficiently by hydrous ZrO_2 than by crystalline ZrO_2 . Hydrous ZrO_2 shows catalytic activities for Meerwein-Pondorf-Verley reduction (transfer hydrogenation) of a wide variety of compounds with 2-propanol.⁵⁴⁻⁵⁶⁾ The compounds include ketones, aldehyde, carboxylic acids, carboxylic acid anhydrides, esters, lactones and nitriles (see section 4.10). For these reactions, the hydrous ZrO_2 obtained by heat treatment at 573 K gave the highest activity. The activities decreased when hydrous zirconia was calcined above 573 K to produce tetragonal or monoclinic phases.

Hydrous ZrO_2 shows catalytic activities also for Oppenauer-type oxidation of alcohols and hydroxyl esters with hydrogen acceptors such as ketones and quinone.⁵⁷⁾ For the Oppenauer-type oxidation of primary alcohols to produce aldehydes, surface modification of hydrous ZrO_2 with trimethylsilylchloride is effective. The modification eliminates the acidic hydroxyl groups on the ZrO_2 that act as active sites for aldol condensation of the hydrogen acceptor. As a result, the selectivity to the target product of aldehyde improves.

3.3.4 Morphology dependence

Catalytic activity dependence on the crystalline phase of ZrO_2 is discussed for a few reactions. All the studies suggest that monoclinic phase is more active than tetragonal phase. Maruya et al. observed that the rate of hydrocarbon formation in the CO hydrogenation correlated well with the fraction of monoclinic phase in ZrO_2 .⁵⁸⁾ The high activity of monoclinic phase is caused by stronger basic sites on monoclinic phase as compared to tetragonal phase. Yamamoto et al. also reported that dehydration of 1,4-butanediol to yield 3-buten-1-ol proceeded over monoclinic phase, while tetrahydrofuran was formed over tetragonal phase.⁵⁹⁾ They interpreted that the selectivity difference is caused by a difference in the densities of acidic sites and basic sites. High densities of acidic sites and basic sites on monoclinic phase make it possible for an acidic site and a basic site to be located close to each other while an acidic site and a basic site are separated on tetragonal phase.

Tomishige et al. reported that the highest activity for the formation of dimethyl carbonate from methanol and CO_2 was observed for the ZrO_2 calcined at 673 K, at which tetragonal phase began to appear in XRD pattern, but monoclinic phase was dominant by Raman spectroscopy.²⁶⁾ Raman spectroscopy is surface sensitive, and

accordingly, the surface phase of the active ZrO_2 is monoclinic. They concluded that the phase of ZrO_2 active for the formation of dimethyl carbonate is monoclinic phase.

The catalytic activity of ZrO_2 varies with the pretreatment temperature at which ZrO_2 is prepared from hydrous ZrO_2 . The temperature for a maximum activity varies with the type of reaction. Examples are shown in Fig. 3.3.7.⁶⁰⁾ Both hydrogenation of 1,3-butadiene and H_2 - D_2 equilibration show the activity maxima at a pretreatment temperature of 873 K, and the activities are eliminated upon pretreatment at 1073 K. On the other hand, isomerization of 1-butene and transfer hydrogenation of 1,3-butadiene with cyclohexadiene show the activity maxima at a pretreatment temperature of 1073 K. The surface area decreases and the fraction of monoclinic phase increases with an increase in the pretreatment temperature, as shown in Fig. 3.3.3. Tanabe and Yamaguchi postulate that the variation in the activity with pretreatment temperature is caused by the variation of bond distance between Zr and O with pretreatment temperature.⁶⁰⁾

An alternative explanation could be as follows. Both isomerization of 1-butene and transfer hydrogenation of 1,3-butadiene with cyclohexadiene involve H^+ abstraction as the initial step. The abstraction of an H^+ from a butene or cyclohexadiene molecule occurs on a strong basic site. Since monoclinic ZrO_2 has strong basic sites, the abstraction of an H^+ proceeds more efficiently on the surface of monoclinic ZrO_2 . On the other hand, hydrogenation of 1,3-butadiene and H_2 - D_2 equilibration involve dissociation of the hydrogen molecule. The sites for the dissociation of hydrogen may have a different cation-anion configuration in a tetragonal structure than the sites corresponding to the monoclinic structure, and such sites may not show strong basicity.

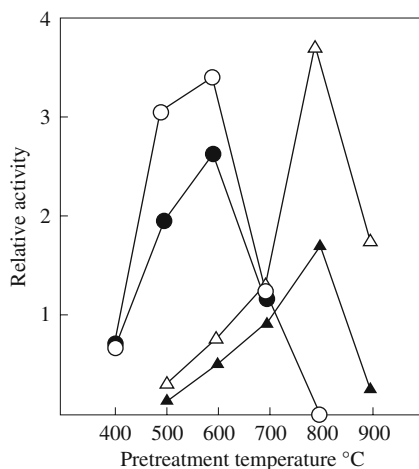


Fig. 3.3.7 Catalytic properties of ZrO_2 pretreated at different temperatures. (○) hydrogenation of 1,3-butadiene with H_2 ; (●) H_2 - D_2 equilibration; (△) isomerization of 1-butene; (▲) hydrogenation of 1,3-butadiene with cyclohexadiene. Reprinted with permission from K. Tanabe, T. Yamaguchi, *Catal. Today*, **20**, 185 (1994) Fig. 2.

References

1. M. Araki, K. Takahashi, T. Hibi, *Eur. Pat.* 0150832 B1 (1985).
2. K. Takahashi, T. Hibi, Y. Higashio, M. Araki, *Shokubai* (Catalyst), **35**, 12 (1993) (in Japanese).
3. Koei Kagaku *Eur. Pat.* 0433959 (1991).
4. M. Fukui, S. Hayashi, K. Okamoto, I. Koga, T. Inoi, *US Pat.* 3966822 (1976).
5. T. Yokoyama, T. Setoyama, N. Fujita, M. Nakajima, T. Maki, K. Fukui, *Appl. Catal. A*, **88**, 149 (1992).
6. T. Yamaguchi, *Catal. Today*, **20**, 199 (1994).
7. P. D. L. Mercera, J. G. Van Ommen, E. B. M. Doesburg, A. J. Burggraaf, J. R. H. Ross, *Appl. Catal.*, **57**, 127 (1990).
8. R. P. Denkwicz, Jr., K. S. Ten, J. H. Adair, *J. Mater. Res.*, **5**, 2698 (1990).
9. A. Clearfield, G. P. D. Serrette, A. H. Khazi-Syed, *Catalysis Today*, **20**, 295 (1994).
10. K. T. Jung, A. T. Bell, *J. Mol. Catal. A: Chemical*, **163**, 27 (2000).
11. R. Srinivasan, B. Davis, O. B. Cavin, C. R. Hubbard, *J. Am. Ceram. Soc.*, **75**, 1217 (1992).
12. K. Matsui, M. Ohgai, *J. Am. Ceram. Soc.*, **83**, 1386 (2000).
13. Y. Murase, E. Kato, *Nippon Kagaku Kaishi*, **86**, 367 (1978) (in Japanese).
14. Y. Murase, E. Kato, *Yogyo-Kyokai-Shi*, **86**, 226 (1978) (in Japanese).
15. R. C. Garvie, *J. Phys. Chem.*, **69**, 1238 (1965).
16. R. C. Garvie, *J. Phys. Chem.*, **82**, 218 (1978).
17. R. C. Garvie, M. F. Goss, *J. Mater. Res.*, **21**, 1253 (1986).
18. X. Turrillas, P. Barnes, D. Häusermann, *J. Mater. Chem.*, **8**, 163 (1993).
19. D. A. Ward, E. I. Ko, *Chem. Mater.*, **5**, 956 (1993).
20. G. K. Chauh, S. Jaenicke, *Appl. Catal. A: General*, **163**, 261 (1997).
21. G. K. Chuah, S. Jaenicke, B. K. Pong, *J. Catal.*, **175**, 80 (1998).
22. H.-L. Chang, P. Shady, W.-H. Shih, *Micropor. Mesopor. Mater.*, **59**, 29 (2003).
23. S. Sato, R. Takahashi, T. Sodesawa, S. Tanaka, K. Oguma, K. Ogura, *J. Catal.*, **196**, 190 (2000).
24. G. Aguila, S. Guerrero, F. Gracia, P. Araya, *Appl. Catal. A: General*, **305**, 219 (2006).
25. B.-Q. Xu, T. Yamaguchi, K. Tanabe, *Chem. Lett.*, **17**, 1663 (1988).
26. K. Tomishige, Y. Ikeda, T. Sakaihiro, K. Fujimoto, *J. Catal.*, **192**, 355 (2000).
27. B. Bachiller-Baeza, I. Rodoríguez-Ramos, A. Guerrero-Ruiz, *Langmuir*, **14**, 3556 (1998).
28. T. Yamaguchi, Y. Nakano, K. Tanabe, *Bull. Chem. Soc. Jpn.*, **51**, 2482 (1978).
29. A. Aboulayt, C. Binet, J.-C. Lavalley, *J. Chem. Soc. Faraday Trans.*, **91**, 2913 (1995).
30. M. Bensitel, V. Moravek, J. Lamotte, O. Saur, J.-C. Lavalley, *Spectrochimica*, **43A**, 1487 (1987).
31. F. Ouyang, A. Nakayama, K. Tabada, E. Suzuki, *J. Phys. Chem. B*, **104**, 2012 (2000).
32. W. Hertl, *Langmuir*, **5**, 96 (1989).
33. K. Pokrovski, K. T. Jung, A. T. Bell, *Langmuir*, **17**, 4297 (2001).
34. C. Morterra, L. Orto, *Mater. Chem. Phys.*, **24**, 247 (1990).
35. D. Bianchi, T. Chafik, M. Khalfallah, S. J. Teichner, *Appl. Catal. A: General*, **112**, 219 (1994).
36. T. Onishi, H. Abe, K. Maruya, K. Domen, *J. Chem. Soc. Chem. Commun.*, **1985**, 617.
37. J. Kondo, Y. Sakata, K. Domen, K. Maruya, T. Onishi, *J. Chem. Soc. Faraday Trans.*, **86**, 397 (1990).
38. K. Domen, J. Kondo, T. Onishi, *Catal. Lett.*, **12**, 127 (1992).
39. J. Kondo, K. Domen, K. Maruya, T. Onishi, *J. Chem. Soc. Faraday Trans.*, **86**, 3021 (1990).
40. J. Kondo, K. Domen, K. Maruya, T. Onishi, *J. Chem. Soc. Faraday Trans.*, **86**, 3665 (1990).
41. R. J. Kokes, A. L. Dent, *Adv. Catal. Relat. Subj.*, **22**, 1 (1972).
42. F. Audry, P. E. Hoggan, J. Saussey, J. C. Lavalley, H. Lauron-Pernot, A. M. Le Govic, *J. Catal.*, **168**, 471 (1997).
43. H. Lanron-Pernot, F. Luck, J. M. Popa, *Appl. Catal.*, **78**, 213 (1991).
44. M. A. Aramandia, V. Boau, C. Jimenez, J. M. Marias, A. Marinas, A. Poras, F. J. Urbano, *J. Catal.*, **183**, 240 (1999).
45. T. Yamaguchi, H. Sasaki, K. Tanabe, *Chem. Lett.*, **2**, 1017 (1973).
46. G. M. Pajonk, A. E. Tanany, *React. Kinet. Catal. Lett.*, **47**, 167 (1992).
47. I. Ferino, M. F. Casula, A. Corrias, M. G. Cutrufello, R. Monaci, G. Paschina, *Phys. Chem. Chem. Phys.*, **2**, 1847 (2000).
48. M. G. Cutrufello, I. Ferino, R. Monaci, E. Rombi, V. Solinas, *Stud. Surf. Sci. Catal.*, **140**, 175 (2001).
49. T. Yamaguchi, J. W. Hightower, *J. Am. Chem. Soc.*, **99**, 4201 (1977).
50. Y. Nakano, T. Yamaguchi, K. Tanabe, *J. Catal.*, **80**, 307 (1983).
51. Y. Ikeda, T. Sakaihiro, K. Fujimoto, *J. Catal.*, **192**, 355 (2000).

52. B.-Q. Xu, T. Yamaguchi, K. Tanabe, *Appl. Catal.*, **75**, 75 (1991).
53. M. Fukui, Y. Urata, *Kouryo*, **215**, 107 (2002) (in Japanese).
54. K. Takahashi, M. Shibagaki, H. Matsushita, *Bull. Chem. Soc. Jpn.*, **65**, 262 (1992).
55. H. Kuno, M. Shibagaki, K. Takahashi, H. Matsushita, *Bull. Chem. Soc. Jpn.*, **66**, 1699 (1993).
56. S. H. Liu, S. Jaenicke, G. K. Chuah, *J. Catal.*, **206**, 321 (2002).
57. H. Kuno, M. Shibagaki, K. Takahashi, H. Matsushita, *Bull. Chem. Soc. Jpn.*, **66**, 1305 (1993).
58. K. Maruya, T. Komiya, M. Yashima, *Stud. Surf. Sci. Catal.*, **101B**, 1401 (1996).
59. N. Yamamoto, S. Sat, R. Takahashi, K. Inui, *J. Mol. Catal. A: Chemical*, **243**, 52 (2006).
60. K. Tanabe, T. Yamaguchi, *Catal. Today*, **20**, 185 (1994).

3.4 Titanium Dioxide

Titanium dioxide has three polymorphs stable at atmospheric pressure, rutile, anatase and brookite. For catalysts and supports, rutile and anatase are commonly used. Anatase converts to rutile when heated in air at about 1073 K or higher temperatures. Titanium dioxide of both anatase and rutile polymorphs shows acidic and basic properties on the surface, and catalyzes the reactions in which acidic sites and/or basic sites are relevant. As compared the acidic character of TiO_2 with those of ZrO_2 and CeO_2 , the order is $\text{TiO}_2 > \text{ZrO}_2 > \text{CeO}_2$ as experimentally shown by infrared spectroscopy of adsorbed probe molecules.¹⁾ The basic character is in the opposite order.²⁾

3.4.1 Preparation

Titanium dioxide is prepared normally from TiCl_4 or titanium alkoxides by hydrolysis followed by calcination. Use of $\text{Ti}(\text{SO}_4)_2$ or TiOSO_4 as a raw material results in inclusion of SO_4^{2-} ions in the resulting TiO_2 even if the precipitate is extensively washed. The TiO_2 containing SO_4^{2-} has a high surface area and possesses strong acid sites on the surface arising from the presence of SO_4^{2-} ions.

One example of preparation of TiO_2 from TiCl_4 is as follows. Into 360 mL of iced water, 62.5 mL of TiCl_4 is added dropwise to avoid temperature increase of the solution. Ammonia water (28%) is added to the solution until pH of the mother solution becomes 7.0. The precipitate is washed with deionized water until no Cl^- ions are detected by 0.1 N AgNO_3 aqueous solution. The precipitate is dried at room temperature then calcined at the desired high temperature. Another example is hydrolysis of TiCl_4 aqueous solution prepared as described above. The TiO_2 aqueous solution is boiled for 7 h to form precipitate. The precipitate is washed with deionized water as above.

An example of preparation of TiO_2 from titanium alkoxides is as follows. Titanium tetraisopropoxide is purified by recrystallization from 2-propanol. Three hundred grams of titanium isopropoxide is dissolved in 300 g of 2-propanol. The isopropanol solution is added at a rate of 30 mL min^{-1} into 5 L of water with stirring. The precipitate is washed with water by decantation until no Cl^- ions are detected, and dried at 393 K. The dried sample is calcined at higher temperature. The crystalline structures are amorphous by calcination below 573 K, anatase by calcination in the temperature range 623–773 K, and rutile by calcination above 873 K.

For a high surface area TiO_2 , a number of methods have been proposed. All of them include a sol-gel process in which titanium alkoxides are used as the starting materials. One type of method does not use structure-directing agent, and the other type uses a structure-directing agent for the mesoporous structure. Two methods of the former type and several examples of the latter type are described here.

Tanaka et al. synthesized a titanium oxide with microporous structure by a salt catalytic sol-gel process of dilute titanium *n*-butoxide and H_2O solution without any template molecule.^{3,4)} Under a nitrogen atmosphere, 10 mL of a butanol solution containing 12.5 mmol of titanium *n*-butoxide and 15 mL of another butanol solution containing 12.5 mmol of ammonium acetate and 12.5 mmol of H_2O were prepared. A sol-gel reaction started when the two butanol solutions were mixed to a total of 25 mL. Reaction temperature was kept constant at 298 K for 24 h and kept at 338 K for a week. The precipitate was dried at 333 K and calcined at a temperature range of 523–773 K for 90 min. The surface areas of the TiO_2 's calcined at 523, 573, 623, 673, 723 and 773 K were 270, 310, 310, 63, 4 and 3 m^2g^{-1} , respectively. The TiO_2 's calcined at 623 K and below were amorphous, and those calcined at 673 K and above were anatase.

Liu et al. prepared mesoporous titanium oxide by a similar procedure in which nitric acid was used in place of ammonium acetate as catalyst for hydrolysis.⁵⁾ The resulting TiO_2 had a surface area of 470 m^2g^{-1} as-prepared, and 106 m^2g^{-1} after calcination at 723 K.

The other method uses active carbon. A certain amount of active carbon of particle size of 100 mesh and surface area of 1400 m^2g^{-1} was settled in ethanol suspension followed by the addition of $\text{Ti}(\text{O}^i\text{Pr})_4$.⁶⁾ Once the suspension was homogenized, the same volume of water was added. Precipitation was achieved by pouring down NH_4OH until pH reached 9. The precipitate was dried at 383 K and calcined at 723 K for 3 h. The surface area of the resulting TiO_2 depended on the content of active carbon and the ratio of carbon weight to total suspension. For the TiO_2 percent relative to active carbon of 20% and the carbon weight to total suspension ratio of 5/200, the surface area was 117 m^2g^{-1} , which is significantly larger than 13 m^2g^{-1} for TiO_2 prepared without the addition of active carbon.

For the mesoporous titanium dioxide, different types of structure-directing

Table 3.4.1 Selected examples of templates and surface areas of resulting mesoporous TiO_2

Templates	Surface area $/\text{m}^2\text{g}^{-1}$	Pretreatment	Ref.
Cetyletrimethylammonium chloride ($\text{C}_{16}\text{TMA}^+\text{Cl}^-$)	ca. 300	Calcined at 537 K	7
β -Cyclodextrin and urea	ca. 250–300	Dried at 373 K	8
Non-ionic surfactant (TX-100)	781	Calcined at 773 K	9
Non-ionic block copolymer (Pluronic P-123)	547	No calcination	10
Block copolymer ($\text{EO}_{20}\text{PO}_{70}\text{EO}_{20}$)	128	Calcined at 673 K	11
Block copolymer surfactant ($\text{EO}_{106}\text{PO}_{70}\text{EO}_{106}$)	135	Calcined at 653 K	12
Dodecylamine	1200		13

agents (templates) are normally used. Selected examples of templates and the surface areas of the resulting TiO₂ are summarized in Table 3.4.1.

3.4.2 Characterization

The adsorption states of CO₂ on TiO₂ were studied by IR spectroscopy. Unidentate carbonate, bidentate carbonate, and hydrogencarbonate were formed on TiO₂. The formation of the carbonates depends on the pretreatment conditions of TiO₂, in particular oxidation and reduction conditions, and dehydroxylation conditions.

Tanaka and White observed the formation of hydrogencarbonate species when CO₂ was adsorbed at room temperature on the oxidized anatase pretreated with oxygen followed by evacuation at 673 K.¹⁴⁾ The hydrogencarbonate species resulted from the reaction of coordinated CO₂ with basic OH⁻ on the surface. Pairs of these hydrogencarbonate species slowly reacted to form bidentate carbonate and water. Room temperature evacuation removed the bidentate carbonate, residual hydrogencarbonate and coordinated CO₂ leaving some adsorbed water and re-forming some adsorbed OH⁻. On a reduced anatase sample, exposure to CO₂ gave only a small amount of coordinated CO₂ which showed no tendency to convert to carbonate of any kind. Surface basicity is reduced by reduction at 673 K with H₂. Essentially the same behavior of TiO₂ on adsorption of CO₂ was reported by Morterra et al.¹⁵⁾

The formation of hydrogencarbonate species on adsorption of CO₂ on TiO₂ was observed by Primet et al. indicating that there are basic OH groups on the surface.¹⁶⁾ The adsorbed hydrogencarbonate was eliminated by evacuation at 298 K. The basicity of the OH groups is weak.

Ferretto et al. observed unidentate carbonate on adsorption of CO₂ on TiO₂ of rutile, in addition to bidentate carbonate and hydrogencarbonate.¹⁷⁾ The formation of unidentate carbonate indicates the presence of basic oxygen sites. Raupp and Dumesic also observed the formation of unidentate carbonate on adsorption of CO₂ on TiO₂ prepared from metallic Ti foil by oxidation.¹⁸⁾ The desorption energy of the unidentate carbonate was 45 kJ mol⁻¹. This value is close to the value 63 kJ mol⁻¹ reported by Goepel et al. for the heat of adsorption of CO₂ at the oxygen anion site on a TiO₂ [110] surface.¹⁹⁾

On the reduced TiO₂, adsorption of CO₂ formed bidentate carbonate, which converted to adsorbed CO and O. The CO was desorbed and the O was retained on the surface.^{14,18)}

3.4.3 Catalytic Properties

2-Propanol undergoes mainly dehydration to propene and dehydrogenation to acetone over TiO₂. The selectivity for dehydration varies with the reaction time and co-presence of oxygen in the feed. Haffad et al. studied decomposition of 2-propanol in the temperature range 423 to 523 K over TiO₂ prepared from titanium isopropoxide by hydrolysis and calcination at 823 K and in the form of anatase.²⁰⁾ The initial product was acetone, but propene then appeared and became predominant

afterward. Selectivity to propene exceeded 95% at 473 K in the reaction time 2–6 h with the conversion ca. 30%. They observed that the conversion increased in the presence of air in the feed, and the selectivity to acetone also increased to ca. 70%. They suggested that an acid-base concerted mechanism is involved in the dehydration over TiO₂ in a helium flow. The acidic OH groups are participating in the reaction together with basic sites which are either surface oxygen or O of the OH groups. In the presence of oxygen in the feed, propene formed by dehydration reacted with oxygen molecule to form acetone .



Han et al. observed the same tendency on the effect of the presence of oxygen in the feed of 2-propanol on the selectivity.²¹⁾ Propene was the main product in the absence of oxygen, while acetone was the main product in the presence of oxygen at a reaction temperature of 553 K.

Aldolization of acetaldehyde to crotonaldehyde occurs more rapidly on rutile than on anatase.²²⁾ At 313 K, the reaction occurred only on rutile, while anatase was inactive at this temperature. At 373 K, the reaction proceeded at almost the same rate over rutile and anatase. Acetaldehyde is adsorbed through the carbonyl oxygen atom on the TiO₂ surface. The OH groups on TiO₂ do not participate in the adsorption of acetaldehyde.

Gandhe and Fernandes prepared TiO₂ of pure rutile structure using urea and compared its activity for alkylation of phenol with methanol with those of a commercial TiO₂ and another TiO₂ prepared without urea which contained considerable amount of anatase structure.²³⁾ The pure rutile was more active and selective for *ortho*-selective alkylation. 100% *ortho*-selectivity was observed at 753 K at 40% conversion for the pure rutile TiO₂, while *ortho*-selectivity was ca. 80% for the TiO₂ prepared without urea. The high selectivity was attributed to the presence of weak basic sites which is unique to the pure rutile TiO₂.

1-Butene isomerization proceeds over TiO₂ at 473 K.²⁴⁾ The activity of TiO₂ as well as the reaction mechanism varied with the pretreatment temperature in a vacuum. As the pretreatment temperature was raised, the activity appeared at 473 K and increased with temperature to reach a maximum at 673 K. Above 673 K, the activity decreased with temperature, but the ratio of *cis*-/*trans*- in the produced 2-butenes increased. On increasing the pretreatment temperature, Ti³⁺ also increased. The intensity of ESR signal assigned to Ti³⁺ run parallel to the *cis*-/*trans*- ratio. A tracer study of the co-isomerization of 1-butene *d*₀/*d*₈ indicated that an intermolecular H(or D) transfer was involved in the isomerization on the TiO₂ pretreated below 673 K, while an intramolecular H(or D) transfer was involved on the TiO₂ pretreated above 673 K.²⁵⁾ Acid-catalyzed isomerization prevailed on the TiO₂ pretreated below 673 K, while base-catalyzed isomerization preferentially occurred on the TiO₂ pretreated above 673 K. By pretreatment above 673 K, TiO₂ was reduced to some extent, and basic sites were generated by reduction. It is plausible that oxide ions adjacent to Ti³⁺ act as basic sites to abstract an H⁺ from 1-butene to form allylic carbanion.

Glucose undergoes dehydration to 1,6-anhydroglucose, and isomerization to

fructose, which further undergoes dehydration to 5-hydroxymethyl-2-furaldehyde.²⁶⁾ Under the reaction conditions of hot-compressed water at 473 K, anatase TiO₂ catalyzed both isomerization and dehydration to form all the products while rutile TiO₂ was inactive for these reactions. By referring to the results obtained for ZrO₂, which promotes only isomerization, it was suggested that anatase TiO₂ promotes isomerization by basic sites, and dehydration by acidic sites.

References

1. G. Busca, *Phys. Chem. Chem. Phys.*, **1**, 723 (1999).
2. D. Haffad, A. Chambellan, J. C. Lavalley, *J. Mol. Catal. A*, **168**, 153 (2001).
3. K. Tanaka, Y. Murakami, T. Imai, T. Matsumoto, S. Furuno, W. Sugimoto, Y. Takasu, *Chem. Lett.*, **30**, 1280 (2001).
4. T. Matsumoto, Y. Murakami, Y. Takasu, *J. Phys. Chem. B*, **104**, 1916 (2000).
5. C. Liu, L. Fu, J. Economy, *J. Mater. Chem.*, **14**, 1187 (2004).
6. G. Colon, M. C. Hidalgo, J. A. Navio, *Catal. Today*, **76**, 91 (2002).
7. D. T. On, *Langmuir*, **15**, 8561 (1999).
8. J.-Y. Zheng, J.-B. Pang, K.-Y. Qiu, Y. Wei, *J. Mater. Chem.*, **11**, 3367 (2001).
9. P. Kluson, P. Kacer, T. Cajthaml, M. Kalaji, *J. Mater. Chem.*, **11**, 644 (2001).
10. G. Calleja, D. P. Serrano, R. Sanz, P. Pizarro, A. Garcia, *Ind. Eng. Chem. Res.*, **43**, 2485 (2004).
11. J. C. Yu, L. Zhang, J. Yu, *Chem. Mater.*, **14**, 4647 (2002).
12. H. Luo, C. Wang, Y. Yan, *Chem. Mater.*, **15**, 3841 (2003).
13. H. Yoshitake, T. Sugihara, T. Tatsumi, *Chem. Mater.*, **14**, 1023 (2002).
14. K. Tanaka, J. M. White, *J. Phys. Chem.*, **86**, 4708 (1982).
15. C. Morterra, A. Chiorino, F. Boccuzzi, *Z. Phys. Chem.*, **124**, 211 (1981).
16. M. Primet, P. Pichat, M.-V. Mathieu, *J. Phys. Chem.*, **75**, 1221 (1971).
17. L. Ferretto, A. Glisenti, *Chem. Mater.*, **15**, 1181 (2003).
18. G. B. Raupp, J. M. Dumesic, *J. Phys. Chem.*, **89**, 5240 (1985).
19. W. Goepel, G. Rocker, R. Feierabend, *Phys. Rev. B*, **28**, 3427 (2983).
20. D. Haffad, A. Chambellan, J. C. Lavalley, *J. Mol. Catal. A*, **168**, 153 (2001).
21. C. Han, B. Liu, H. Zhang, J. Shen, *Acta Phys. -Chim. Sin.*, **22**, 993 (2006).
22. J. E. Rekoske, M. A. Barteau, *Langmuir*, **15**, 2061 (1999).
23. A. R. Gandhe, J. B. Fernandes, *Catal. Commun.*, **5**, 89 (2004).
24. H. Hattori, M. Ito, K. Tanabe, *J. Catal.*, **38**, 172 (1975).
25. H. Hattori, M. Ito, K. Tanabe, *J. Catal.*, **41**, 46 (1976).
26. M. Watanabe, Y. Aizawa, T. Iida, R. Nishimura, H. Inomata, *Appl. Catal. A*, **295**, 150 (2005).

3.5 Zinc Oxide

Zinc oxide is considered to be amphoteric, and the existence of both acidity and basicity have been experimentally shown. As a catalyst, ZnO promotes reactions by the way of base-catalyzed reaction, though acidic sites are involved in the reactions.

3.5.1 Preparation

Zinc oxide is normally prepared by precipitation of the hydroxide upon addition of ammonium hydroxide to an aqueous solution of zinc nitrate at 353 K until precipitation is almost complete.¹⁾ The precipitate is filtered, washed with water, dried and calcined in air in the temperature range 673–773 K. It was reported that the catalytic activity for methanol synthesis varied with the precipitating reagent; the

catalyst prepared using sodium carbonate showed higher activity than that prepared using ammonium hydroxide.²⁾

Zinc oxide is also prepared by ignition of zinc metal. For many catalytic studies, commercial ZnO (Kadox-25) supplied from New Jersey Zinc Co. have been used. Kadox-25 is prepared by ignition of zinc metal.

3.5.2 Characterization

IR spectroscopy of NH₃ adsorbed indicated the presence of Lewis acidity.³⁾ Acid strength of H₀ < 3.3 appears when calcined in the temperature range 573–773 K.⁴⁾ Nagao et al. measured ca. 100 kJ mol⁻¹ for the heat of NH₃ adsorption.⁵⁾ The values ranging 60 - 80 kJ mol⁻¹ were reported by Yasumoto.⁶⁾

IR spectroscopy of adsorbed CO₂ indicated the formation of carbonate.⁷⁾ The heat of adsorption was measured to be 60–120 kJ mol⁻¹ by Yasumoto,⁶⁾ and ca. 80 kJ mol⁻¹ by Nagao et al.⁵⁾ The basicity on the basis of IR study of adsorbed molecules which possess different pK_a values was reported.⁸⁾ Propene (pK_a = 35) is dissociated, but NH₃ (pK_a = 36) is not. The basicity of ZnO is considered to be less than 36 in H₋ scale.

Adsorption of hydrogen on ZnO involves two types: reversible adsorption at room temperature IR active, and irreversible adsorption IR inactive.^{9,10)} The IR spectrum in hydrogen shows two strong bands at 3489 and 1709 cm⁻¹. These bands, first reported by Eischens et al.,¹¹⁾ are assigned to an OH and ZnH species, respectively. Hydrogen is adsorbed in a heterolytic fashion at the highly polar active site.



The hydrogen attached to the oxygen has a protonic character and the hydrogen attached to the zinc has a hydridic character.

Griffin and Yates proposed on the basis of coverage induced frequency shifts of OH and ZnH bands that hydrogen is adsorbed on the Zn-rich ZnO [0001] surface.¹²⁾

Propene is adsorbed on ZnO to form allylic species and hydroxyl species.¹³⁾ Fig. 3.5.1 shows the spectra of chemisorbed CH₃-CH=CD₂ and CD₃-CH=CH₂ in the C-H deformation region. The spectra of the species formed from these two compounds are the same within experimental error. The coincidence of the spectra strongly suggests that propene is adsorbed to form a symmetric allylic species.



On adsorption of CH₃-CH=CD₂ and CD₃-CH=CH₂, O-H and O-D stretching vibrations appear, respectively. It is plausible that an H⁺ (or D⁺) is abstracted from propene by basic O on ZnO to form allylic anions.

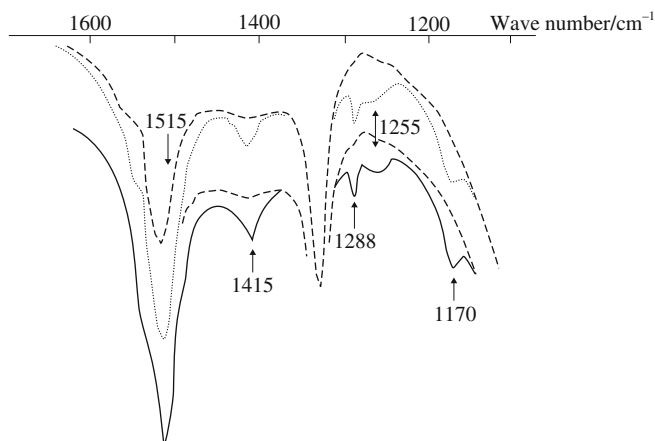


Fig. 3.5.1 Spectrum of chemisorbed propene ($\text{CD}_3\text{-CH}=\text{CH}_2$ and $\text{CH}_3\text{-CH}=\text{CD}_2$): dotted line, chemisorbed $\text{CD}_3\text{-CH}=\text{CH}_2$ on zinc oxide; solid line, chemisorbed $\text{CH}_3\text{-CH}=\text{CD}_2$ on zinc oxide. Reprinted with permission from A. L. Dent, R. J. Kokes, *J. Am. Chem. Soc.*, **92**, 6709 (1970) Fig. 7.

3.5.3 Catalytic Properties

Formic acid decomposes on ZnO into CO_2 and H_2 , indicating that ZnO acts as solid base catalyst. IR study of decomposition of formic acid demonstrated that the reaction proceeds via a formate species.¹⁴⁾



2-Propanol undergoes exclusively dehydrogenation to acetone on ZnO at 483 K, indicating the basic properties of ZnO.¹⁵⁾ Berlowitz and Kung measured the dehydrogenation of 2-propanol on ZnO single crystal, and reported that the rate was highest on the Zn polar surface [0001], 3–5 times higher than on the O polar surface [000 $\bar{1}$] surface.¹⁶⁾ Vohs and Barteau reported essentially the same conclusions that 2-propanol decomposed primarily to acetone on Zn polar surface (0001) through an alkoxide intermediate.¹⁷⁾ On the O polar surface, 2-propanol was adsorbed only in molecular form and desorbed below 300 K by evacuation.

The diagnostic reaction of 2-methyl-3-buten-2-ol (MBOH) proceeds over ZnO at 453 K to yield acetone and acetylene in a ratio 1 to 1, indicating that a base-catalyzed reaction is operating.¹⁵⁾

1-Butene undergoes double bond isomerization on ZnO at room temperature to form *cis*-2-butene and *trans*-2-butene, initial *cis* to *trans* ratio being 13.^{18,19)} The high selectivity to *cis*-2-butene indicates that the isomerization proceeds via the allylic carbanion which is formed by the abstraction of an H^+ by a basic site. *cis*-2-Butene also isomerizes to 1-butene and *trans*-2-butene with an initial 1- to *trans* ratio of unity. IR study of adsorbed *cis*-2-butene together with IR study of

adsorbed propene indicated that the intermediate is an allylic species. Since the initial 1- to *trans* ratio was unity, it was suggested that direct *cis-trans* isomerization occurs.

cis-1,3-Pentadiene undergoes *cis-trans* isomerization over ZnO to yield *trans*-1,3-pentadiene, and no double bond isomerization to 1,4-pentadiene at 293 K.²⁰⁾ 1,3-Pentadiene is more reactive than 1-butene and 1-pentene. The most plausible intermediates for *cis-trans* isomerization of 1,3-pentadiene are allylic carbanions formed by the abstraction of an H⁺ from the methyl group in 1,3-pentadiene. The electron delocalization of the allylic carbanion extends to the terminal double bond to stabilize the intermediates more, which makes 1,3-pentadiene more reactive than 1-butene.

Imizu et al. reported that the activities for isomerization of 1-butene, 1-pentene and 1,3-pentadiene were enhanced by modification of ZnO with alkylsilylation.²⁰⁾ In particular, the activity for 1,3-pentadiene was enhanced by a factor of 89 by modification with triethylsilane. The enhancement was attributed to prevention of irreversible adsorption of the reactant to keep active sites free from self poisoning.

References

1. J. R. Huffman, B. F. Dodge, *Ind. Eng. Chem.*, **21**, 1056 (1929).
2. M. C. Molstad, B. F. Dodge, *Ind. Eng. Chem.*, **27**, 134 (1935).
3. M. C. Kung, H. H. Kung, *Catal. Rev. Sci. Eng.*, **27**, 425 (1985).
4. K. Tanabe, C. Ishiya, I. Matsuzaki, I. Ichikawa, H. Hattori, *Bull. Chem Soc. Jpn.*, **45**, 49 (1972).
5. M. Nagao, M. Kiriki, H. Muraishi, T. Morimoto, *J. Phys. Chem.*, **82**, 2561 (1976).
6. I. Yasumoto, *J. Phys. Chem.*, **88**, 4041 (1984).
7. D. G. Rethwish, J. A. Dumesic, *Langmuir*, **2**, 73 (1986).
8. R. J. Kokes, *Intra-Science Chem. Rep.*, **6**, 77 (1972).
9. R. J. Kokes, A. L. Dent, *Adv. Catal. Relat. Subj.*, **22**, 1 (1972).
10. R. J. Kokes, A. L. Dent, C. C. Chang, L. T. Dixon, *J. Am. Chem. Soc.*, **94**, 4429 (1972).
11. R. P. Eischens, W. A. Pliskin, M. J. D. Low, *J. Catal.*, **1**, 180 (1962).
12. G. L. Griffin, J. T. Yate, Jr., *J. Chem Phys.*, **77**, 3744 (1982).
13. A. L. Dent, R. J. Kokes, *J. Am. Chem. Soc.*, **92**, 6709 (1970).
14. Y. Noto, K. Fukuda, T. Onishi, K. Tamaru, *Trans. Faraday Soc.*, **63**, 3081 (1967).
15. C. Lahousse, J. Bachelier, J. C. Lavalley, *J. Mol. Catal.*, **87**, 329 (1994).
16. P. Berlowitz, H. H. Kung, *J. Am. Chem. Soc.*, **108**, 3532 (1986).
17. J. M. Vohs, M. A. Barteau, *J. Phys. Chem.*, **95**, 297 (1991).
18. C. C. Chang, W. C. Conner, R. J. Kokes, *J. Phys. Chem.*, **77**, 1957 (1973).
19. A. L. Dent, R. Kokes, *J. Phys. Chem.*, **75**, 487 (1971).
20. Y. Imizu, T. Narita, Y. Fujito, H. Yamada, *Stud. Surf. Sci. Catal.*, **130**, 2429 (2000).

3.6 Alumina

Alumina (Al₂O₃) is used both as a catalyst for various kinds of reactions and as a support for metals and metal oxides. Dehydration of alcohols to yield alkenes is a representative reaction for which Al₂O₃ acts as a catalyst. H-D exchange between CH₄ and D₂ is a reaction specific to Al₂O₃; the reaction proceeds even at room temperature. Al₂O₃ is very frequently used as a support of industrial catalysts for its mechanical strength as well as its strong interaction with metals and metal oxides

that enables high dispersion of the supported compounds. As for the surface properties, alumina is generally regarded as acidic rather than basic. However, participation of basic sites in the catalytic behavior of alumina is indispensable.

3.6.1 Structure and Preparation of Alumina

Alumina is prepared from hydroxide ($\text{Al}(\text{OH})_3$) and oxyhydroxide ($\text{AlO}(\text{OH})$) by dehydration at elevated temperatures. The hydroxide, oxyhydroxide and oxide of Al exist in α and γ forms. These Al compounds are commonly referred to by the mineral names.¹⁾

Chemical formula	Form	Mineral name	Form	Mineral name
$\text{Al}(\text{OH})_3$	α	bayerite	γ	gibbsite, hydrargillite, nordstrandite
$\text{AlO}(\text{OH})$	α	diaspore	γ	boehmite
Al_2O_3	α	corundum	γ	–

Al_2O_3 exists in different crystal phases depending on the precursors and the conditions of heat treatment. The most stable crystal form of alumina is α -alumina, and heating the precursors above 1470 K results in the formation of α -alumina. At lower temperatures a variety of phases are formed which are collectively known as γ -alumina, and in various studies most of the Greek alphabet has been used in naming them, e.g., χ , δ , ϵ , γ , η , κ , θ , and ρ . These phases represent various degrees of ordering of Al atoms in an essentially cubic closest packing of O atoms, described as a defect spinel structure, since there are only 21 and 1/3 metal atoms arranged at random in the 16 octahedral and 8 tetrahedral positions of that structure. Among these transition aluminas, γ - and η -aluminas are important as catalysts primarily because of their high surface area.

The pathways for the formation of different transition aluminas proposed

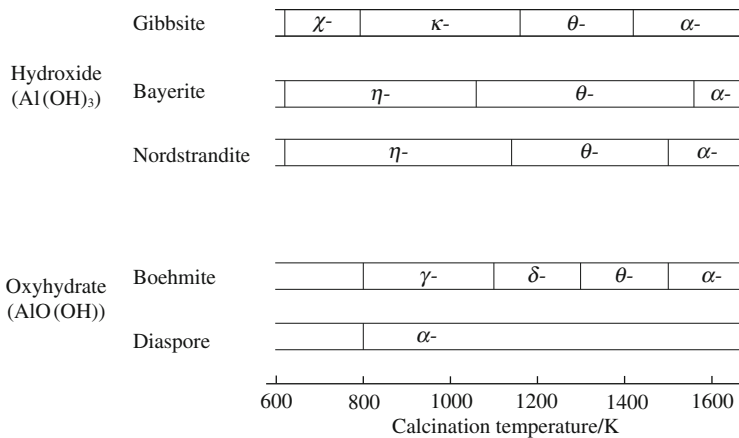


Fig. 3.6.1 Pathways for formation of different transition alumina.

display some discrepancies between researchers, but the following pathways are typical of the schemes postulated as the result of X-ray and DTA studies.²⁾(Fig. 3.6.1)

A. Conventional preparation of η -alumina

One preparation method for η -alumina through bayerite reported by Kul'ko et al. is described below.³⁾ Bayerite was prepared by the precipitation from an aqueous solution of $\text{Al}(\text{NO}_3)_3$ with concentrated aqueous ammonia at constant pH 10.0 ± 0.2 and at 295 ± 2 K, followed by aging the suspension at room temperature for 10 days. After aging, the precipitate was filtered off and washed with distilled water until no NO_3^- ions were detected in the filtrate. The filtered cake was dried at 383 K for one day. The material obtained was bayerite which contained 2.99 mol $\text{H}_2\text{O}/(\text{mol Al}_2\text{O}_3)$, which is close to the theoretical value of 3.0 mol $\text{H}_2\text{O}/(\text{mol Al}_2\text{O}_3)$. η -Alumina was obtained by calcination of the bayerite at 873 K or 1073 K in air for 4 h. The η -alumina thus obtained changed gradually into θ - Al_2O_3 on heat treatment in the range 1173–1273 K, and then into α - Al_2O_3 above ca. 1573K. Surface area of the η -alumina obtained by calcination at 873 K and θ - Al_2O_3 obtained by calcination at 1173 K was 280 and 110 m^2g^{-1} , respectively.

Other preparation methods for η -alumina as well as γ -alumina were reported by MacIver et al.⁴⁾

B. pH swing method

Control of pore structure of alumina by pH swing method was reported by Ono et al.⁵⁾ Into a water kept at 373 K, aluminum nitrate was dissolved followed by addition of sodium aluminate to form particles of alumina hydrate dispersed in the water. Into the aqueous suspension, aluminum nitrate and sodium aluminate were alternatively added. The pH value of the suspension changed alternatively. At a low pH when aluminum nitrate was added, fine particles of the alumina hydrate dissolved and large particles of the alumina hydrate remained. The pH swinging resulted in the formation of well-controlled alumina hydrate particles. Finally, the alumina sol was filtered, washed with water and dried to form alumina hydrate gel. The gel was calcined at 773 K to form γ -alumina with a narrow pore size distribution. The pore size varied with the range of pH swinging and number of pH swinging.⁶⁾

C. Sol-gel preparation of alumina

A sol-gel preparation of Al_2O_3 reported by Wang et al. is as follows.⁷⁾ Aluminum *s*-butoxide (25.73 mL) was dissolved into a given amount of butanol. Oxalic acid (1 g) was added to the solution as a hydrolysis catalyst. pH of the solution was kept at 5. Then 15 mL of water was slowly added into the solution followed by refluxing for 3 h at 343 K with continuous stirring until a gel was formed. The gel was dried at 343 K and calcined at 673, 873 or 1073 K. The Al_2O_3 calcined at 673, 873, and 1073 K had surface areas of 504.7, 346.8 and 172.9 m^2g^{-1} , respectively. The Al_2O_3 calcined at 673 K was composed of boehmite and γ -alumina. The samples of Al_2O_3 calcined at 873 K and 1073 K were composed of γ - and θ -

Al₂O₃. The relative composition of θ -alumina was higher for the 873 K-calcined sample as compared to the 1073 K-calcined sample.

D. Mesoporous alumina

Vaudry et al. prepared mesoporous alumina as follows.⁸⁾ An aluminum hydroxide suspension was obtained by hydrolysis of 43.8 g of aluminum *s*-butoxide with 10.3 g of deionized water in 275 g of 1-propanol. After 60 min of stirring, 10.8 g of lauric acid was added. The mixture was aged for 24 h at room temperature and heated under static condition at 383 K for 2 days. The solid was filtered, washed with ethanol, and dried at room temperature. A mesoporous alumina having pores of 2.1 nm and surface area of 710 m²g⁻¹ was obtained after calcining at 703 K for 2 h in air.

Following Vaudry et al., a number of papers were reported and they were reviewed by Marquez-Alvarez et al.⁹⁾ The synthesis approaches for mesoporous aluminas are based on sol-gel processes of anionic surfactants such as dodecyl-sulfate, cationic surfactants such as alkyltrimethylammonium, or non-ionic surfactants such as di- or triblock copolymers like Triton.

3.6.2 Surface Properties of Alumina

Surface properties of alumina have been studied primarily by IR of the surface OH groups and the adsorbed probe molecules.

A. IR of surface OH groups

The surface hydroxyl groups on transition aluminas were studied by IR, and the exact assignments of the O-H bands have been a subject of discussion.¹⁰⁾

Peri observed five distinct O-H stretching bands; three major OH bands (3800, 3744 and 3700 cm⁻¹) and two minor bands (3780 and 3733 cm⁻¹).^{11,12)} Relative intensities of these bands varied with the temperature of evacuation. Peri proposed the surface model of Al₂O₃ by assuming that the (100) plane of a cubic, close-packed oxide lattice and that aluminum ions are located in all interstices between oxide ions. Based on the model, he assigned the five bands to isolated hydroxyl groups in different environments, each with a different number of oxide ions as nearest neighbors on the surface. The bands at 3800, 3780, 3744, 3733 and 3700 cm⁻¹ were assigned to the OH groups with the number of the nearest neighbor oxide ions of 4, 3, 2, 1 and 0, respectively. The limit of Peri's model is the assumption of the (100) crystal face as the only possible termination for the crystallites of alumina, in that only octahedrally coordinated Al atoms (Al^{VI}) would be present in the uppermost layer.

Tsyganenko and Filimonov examined the ν_{OH} vibrations of a very large number of metal oxides including alumina and grouped according to the crystal structure.^{13,14)} Considering the most probable terminations of the crystallites and the geometry of the OH groups in these terminations, they concluded that the number of nearest neighbors has a negligible effect on the frequency of the OH species, whereas the determining factor is the number of lattice metal atoms that

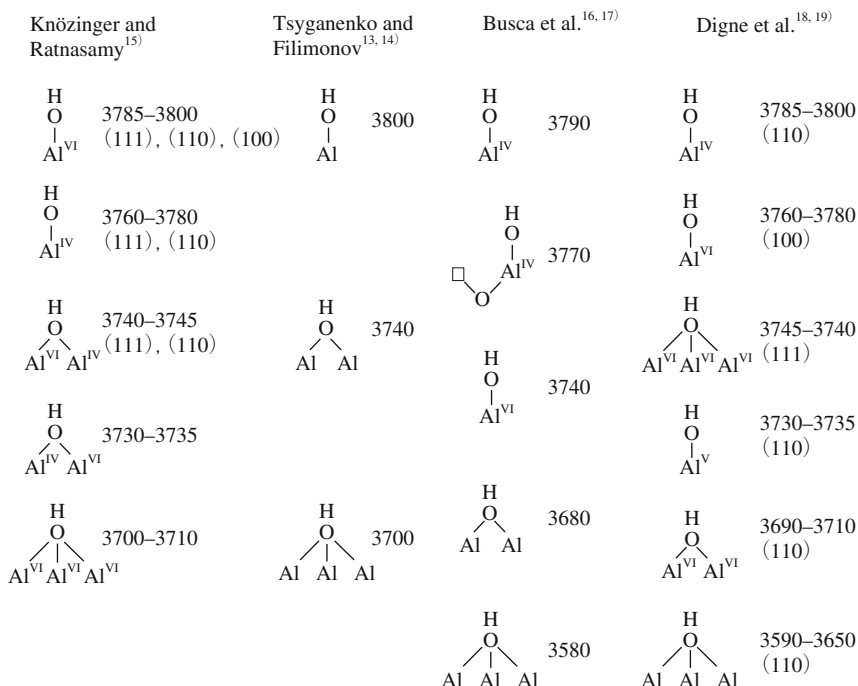


Fig. 3.6.2 Types of OH groups and IR absorption frequencies (cm^{-1}) proposed by researchers.

OH groups are attached to. There exist three types of OH groups of type I, II and III, differing in the coordination number of the OH groups, 1, 2 and 3, respectively (Fig. 3.6.2). They also suggested that the further splitting of the each band could be caused by the difference in the coordination number of the aluminum atoms.

Knözinger and Ratnasamy proposed a very detailed model for the surface of transition alumina.¹⁵⁾ The basic assumptions of the model are: (1) the termination of alumina crystallites occurs along crystal planes, the (111), (110) and (100) planes, and (2) the frequency of OH species is imposed by the net electrical charge at the OH group. The net charge is determined by the coordination number of both OH groups and Al cations. Based on these considerations, they singled out, within the three crystal planes and nine possible OH configurations, five configurations as shown in Fig. 3.6.2 by neglecting possible differences of relative orientation of the OH group with respect to Al.

Busca et al. modified the model of Knözinger and Ratnasamy, who considered only regular surface terminations by taking account of cation vacancies, and reassigned the various OH species as shown in Fig. 3.6.2.^{16,17)}

Digne et al. made the vibrational analysis of the OH groups on (110), (100) and (111) surfaces of the bulk model of $\gamma\text{-Al}_2\text{O}_3$ based on DFT (density functional theory) calculation.^{18,19)} The model they used was also constructed by DFT calculation for the dehydration of boehmite to $\gamma\text{-Al}_2\text{O}_3$. The most stable structure turned out to be nonspinel with 25% tetrahedral Al atoms, which is not a traditional

defective spinel-like structure.²⁰⁾ They calculated OH vibration frequencies for 12 different OH groups. Selected OH groups and their frequencies are included in Fig. 3.6.2.

Although the assignment of the O-H vibration peaks is not always the same for all investigators, they agree on the point that the OH groups giving the bands at higher frequencies are stronger in basic properties than the other OH groups, with some exceptions. Peri suggested that the electron density of the OH group showing IR band at 3800 cm^{-1} is the highest because it is surrounded by 4 O atoms, and therefore, the most basic. Knözinger and Ratnasamy suggested that the net charge of the OH group showing 3785 cm^{-1} is the most negative, and therefore, the basic strength is the highest. In addition, the highest two peaks at 3785 and 3775 cm^{-1} remained almost entirely unaffected by CO, while the three bands at lower frequency, 3725 , 3715 and 3695 cm^{-1} , were completely eroded. CO interacts with acidic OH groups. The strong nucleophilic character of the two OH-groups showing higher frequencies shown by their anion exchange ability with F^- and with molybdate anions supports their strong basic properties. Digne et al. calculated that on introduction of HCl, energetically favorable substitution of OH with Cl occurs on OH groups which show peaks at higher frequencies.¹⁸⁾ Actually, Vigué et al. observed that peaks at 3787 , 3778 and 3722 cm^{-1} disappeared, while peaks at 3675 and 3596 cm^{-1} remained after chlorination.²¹⁾

Morterra et al. pointed out that the OH groups of the second highest frequency are more reactive than the OH groups of the highest frequency.¹⁰⁾ They assumed that the higher reactivity is due to a higher accessibility of the OH species to probe molecules and the possible presence of the OH group in particularly exposed zones of the surface.

B. IR of adsorbed CO_2

The existence of basic OH groups and basic oxide ions is revealed by IR studies of adsorbed CO_2 . As described in Chapter 2.4.1, adsorption of CO_2 on Al_2O_3 results in the formation of several surface species such as linear CO_2 , bridged carbonate, bidentate carbonate, unidentate carbonate and hydrogencarbonate.²²⁻²⁵⁾ The spectra of adsorbed CO_2 reported by various authors differ considerably, due primarily to the degree of dehydration of Al_2O_3 . The phase of alumina does not significantly influence the spectra.²⁶⁾

Below ca. 673 K of heat treatment, the Al_2O_3 surface is full of OH groups, and adsorption of CO_2 results in the predominant formation of hydrogencarbonate species and the formation of linear CO_2 to a small extent. Above ca. 673 K , oxide ions and exposed Al ions exist together with OH groups. Adsorption of CO_2 on alumina heat-treated at high temperatures results in the formation of bidentate carbonate, unidentate carbonate, bridged carbonate, linear CO_2 , and hydrogencarbonate. For the formation of bidentate carbonate and bridged carbonate, the presence of both exposed Al ion and coordinatively unsaturated O ion (O_{CUS}) on the surface is required. For the linear CO_2 , coordinatively unsaturated Al atom of tetrahedral coordination ($\text{Al}^{\text{IV}}_{\text{CUS}}$) or that of octahedral coordination ($\text{Al}^{\text{VI}}_{\text{CUS}}$) is responsible. For the unidentate carbonate, only oxide ions are required. Accordingly, except

for the formation of the linear CO₂, the surface oxide ions in different coordination states are involved in the formation of the carbonates species. In all cases, these oxide ions undergo nucleophilic attack to C in CO₂, and, therefore, act as a base toward CO₂.

The linear CO₂ shows three bands at 2347, 2370 and 2407 cm⁻¹. Morterra et al. measured the dependency of the peak intensity on the CO₂ pressure, co-presence of CO, and the sample heat-treatment temperature.²³⁾ They assigned the band at 2347 cm⁻¹ to CO₂ interacting with a coordinative vacancy on an Al^{VI}, and the two bands at 2370 and 2407 cm⁻¹ to that on an Al^{IV}. Their assignment coincides with Peri's assignment that the band at 2370 cm⁻¹ is ascribed to CO₂ held by a strained Al-O-Al linkage (α site) by ion-quadrupole interaction if Peri's α site is Al^{IV}. In addition, they observed a connection between sites responsible for the strongly held linear CO₂ and those for bridged carbonate as suggested by Peri that the 2370 cm⁻¹ and 1870 cm⁻¹ bands are related through an equilibrium between the linear CO₂ and bridged carbonate.

Hydrogencarbonate species were not formed on adsorption of CO₂ on the Al₂O₃ heat-treated above 973 K,²³⁻²⁷⁾ though Peri observed hydrogencarbonate formation on the Al₂O₃ outgassed at 1073 K. On adsorption of CO₂, hydrogencarbonate is formed at the expense of the OH band at 3770-3780 cm⁻¹, which is the highest frequency band for the Al₂O₃ heat-treated at 773 K.²³⁾ Hydrogencarbonate is formed even on the hydroxylated Al₂O₃ outgassed at 298 K.

The mechanism of hydrogencarbonate formation on the hydroxylated γ -Al₂O₃ was proposed by Baltrusaitis et al. by IR combined with isotope labeling and quantum chemical calculation.²⁸⁾ The mechanism is illustrated in eq. 2.4.2 (p. 26).

Among unidentate, bidentate and bridged carbonates, unidentate carbonate is the most strongly adsorbed.²³⁾ This is due to the formation of unidentate carbonate on a particularly basic O_{cus} ion.

3.6.3 Catalytic Properties

Reactions catalyzed by Al₂O₃ include dehydration of alcohols, isomerization of alkenes, H-D exchange between D₂ and CH₄ or alkenes, H-D exchange between CH₄-CD₄, and among alkenes, and H₂/D₂ equilibration for which different surface sites on Al₂O₃ are involved in different ways. For the diagnostic reaction of 2-methyl-3-buten-2-ol (MBOH), alumina gives a dehydrated product 3-methyl-3-butene-2-one (MIPK) indicating amphoteric properties.

A. Dehydration of alcohol

Alumina catalyzes intramolecular dehydration of alcohols to form alkenes and intermolecular dehydration to form ethers. The selectivity of alkene formation vs. ether formation is primarily determined by the reaction temperature as well as the structure of alcohols. Alkene formation is favored at high temperatures, while ether formation is favored at low temperatures. The alcohols without β -H atoms (such as benzylalcohol) yield only ethers. The tendency toward ether formation is reduced as the chain length and chain branching of alcohols increase; tertiary

alcohols (such as *t*-butyl alcohol) form exclusively alkenes. Reaction mechanisms and, therefore, surface sites involved in the reaction are different for alkene formation and ether formation. Basic sites (O^{2-} ions) participate in both types of dehydration.

Intramolecular dehydration of alcohols on Al_2O_3 proceeds via the E2 mechanism in which elimination of the OH group and β -H of the alcohol is concerted without formation of ionic intermediates. Both surface OH groups and basic sites (O^{2-} ions) are involved. Lewis acid sites (coordinatively unsaturated Al^{3+} ions) do not participate in the reaction. This is based on poisoning experiments with varying amounts of preadsorbed pyridine in dehydration of *t*-butyl alcohol and isobutyl alcohol. The dehydration is not retarded by preadsorption of pyridine, which is adsorbed on Lewis acid site. Preadsorption of TCNE, which is adsorbed on the basic sites, on the other hand, strongly retards the dehydration.²⁹⁾ Oxide ions and OH groups in suitable arrangements and configurations appear to form the active sites for alkene formation.

Knözinger proposed the mechanism of the activation of alcohol as follows.^{30,31)} The activation is assumed to be initiated by proton fluctuations between adsorbed alcohol molecules and the surface, which may result in polarization of the molecule. The alcohol molecule itself is suggested to possess some vibrational or rotational freedom relative to the surface so that the β -H may approach a basic O^{2-} ion while the alcohol is in the antiperiplanar conformation. The rate-determining step is the abstraction of H attached to β -C by basic site on Al_2O_3 (O^{2-}), which is estimated from the primary isotope effect observed when the H attached to β -C is substituted by D.³¹⁾ The mechanism for intramolecular dehydration of alcohols is shown in Fig. 3.6.3.³²⁾

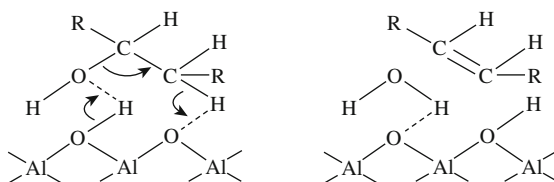


Fig. 3.6.3 Intramolecular dehydration of alcohols.

For intermolecular dehydration of alcohols to ethers, three types of centers are involved; Al-O pair sites and OH groups. Unlike intramolecular dehydration, intermolecular dehydration is strongly poisoned by pyridine, indicating the participation of Lewis acid sites (Al^{3+}). TCNE also retards ether formation, indicating the participation of basic sites. It was shown that as the chain length of alcohol is reduced, the tendency to form alcoholates on Al_2O_3 increases, and the tendency to form ethers also increases, suggesting that alcoholates formed on Al-O pair sites are reaction intermediates. The second molecules to react with the alcoholates are assumed to be the alcohol molecules which are H-bonded to the surface OH groups.

B. Isomerization of alkenes

Butenes undergo double bond and *cis-trans* isomerization over Al_2O_3 above room

temperature. Hightower et al. studied co-isomerization of 1-butene d_0/d_8 and *cis*-2-butene d_0/d_8 on alumina at 300 K, and showed that the *cis-trans* isomerization involves primarily intramolecular H (or D) transfer, but no decision could be reached concerning double bond migration. Reactivity of d_0 butene isomers was higher than d_8 isomers; definite isotope effects were observed for all the isomerization reactions. The *cis* to *trans* ratio in 2-butene produced in 1-butene isomerization was 6.25 at 300 K. The ratio of 1-butene to *trans*-2-butene was 0.22 in *cis*-2-butene isomerization; double bond migration was slower than *cis-trans* isomerization, which is not typical for base-catalyzed *cis*-2-butene isomerization. As they noted, the reaction may proceed by different pathways.³³⁾

Whatever the active sites and mechanisms are, one point has been clearly established: all the isomerization reactions over alumina involve C-H bond cleavage in the rate-determining step. For the main pathway for double bond migration, Gerberich and Hall proposed a cyclic intermediate which is draped over a surface oxide ion in the form of *cis* configuration to explain the high *cis/trans* ratio in 1-butene isomerization.³⁴⁾ Although Gerberich and Hall did not state that the reaction intermediates are carbanion, it is plausible to assume that the double bond migration of 1-butene proceeds via the abstraction of an allylic H^+ by basic site (O^{2-}) to form an allylic carbanion intermediate which then accepts the abstracted H^+ at the terminal C to form primarily *cis*-2-butene.

Peri observed that 1-butene isomerization was poisoned by ammonia.³⁵⁾ He also measured the adsorbed ammonia on alumina by IR spectroscopy. Adsorption of ammonia occurs in several ways. Certain sites that adsorb ammonia as NH_2^- and hydroxyl ions appear essential for butene isomerization. The sites are suggested to be "acid-base" or "ion-pair" sites. He proposed the reaction occurs through transient formation of a carbanion.

Gati and Knözinger reported isomerization of substituted alkenes over Al_2O_3 .³⁶⁾ Based on the reactivity of substituted alkenes and product distribution, they proposed carbanion-like intermediates for the isomerization.

Corad et al. postulated two types of sites active for double bond isomerization of 2,3-dimethyl-1-butene at 353 K.³⁷⁾ The catalyst deactivates during the reaction. The hydrogen transfer during the isomerization changes from predominantly intramolecular to intermolecular during the deactivation. The sites of the first type predominate on the fresh catalyst, but they are blocked by self-poisoning during the reaction. The sites of the second type are responsible for stable activity. They specified the active site of the second type to be made up by a basic oxygen ion, an incompletely coordinated Al ion and a hydroxyl group. A cyclic allylic carbanion-like species was proposed as an intermediate for the intermolecular isomerization.

Although basic sites appear to be responsible for alkene isomerization over Al_2O_3 , CO_2 does not poison the isomerization, while CO_2 strongly poisons the H-D exchange reactions such as $C_4H_8-D_2$ and $C_6H_6-C_6D_6$.^{38,39)} Different poisoning effects by CO_2 on the isomerization and exchange reactions indicate that the isomerization and the exchange reactions occur independently, though the exact structures of these sites are not clear.

C. H-D exchange

Alumina exhibits particularly high activity for the H-D exchange of CH₄ with D₂, CD₄ and surface OD groups. Larson and Hall reported that the mixing of isotopes between CH₄ and CD₄ took place at a readily measurable rate at room temperature with an activation energy of 23.8 kJ mol⁻¹.⁴⁰⁾ The H-D exchange of CD₄-H₂ occurred at about the same rate as CD₄-CH₄ equilibration. The H₂-D₂ equilibration was much faster (virtually instantaneous at 195 K). The mixing of CH₄ with D₂ proceeds about 1.8 times faster than the rate of mixing of CD₄ with H₂. It was inferred that the rate-determining step in the mixing of CD₄ with CH₄ is the breaking of C-D bonds.

Alumina is also active for exchange of D₂ with alkenes and cyclic alkenes. At temperatures below 373 K, only those H atoms which were initially vinyl, or which could become vinyl by isomerization of alkene underwent exchange. As methylenecyclopentane isomerizes to 1-methylcyclopentene, only 6 of 10 H atoms undergo exchange with D₂. 3-Methylcyclopentene does not isomerize, and only 2 H atoms undergo exchange.^{41,42)} Hydrogen atoms in benzene also exchange with D₂ at room temperature over alumina.³⁹⁾ Utilizing the high ability of alumina for exchange with D₂ without considerable hydrogenation, Larson et al. prepared perdeuterio alkenes and cyclopropane in the temperature range 300–483 K.⁴³⁾

All the H-D exchange reactions are poisoned by CO₂. This is in contrast to the alkene isomerization which CO₂ does not poison, as described in the previous section. Rosynek et al. reported CO₂ poisoning effects on 1-butene isomerization and C₄H₈-D₂ exchange.⁴⁴⁾ They postulated that the exposed Al³⁺ ions are responsible for the exchange. CO₂ is adsorbed on an exposed Al³⁺ ion to give an IR band at 1780 cm⁻¹, which was assigned by Parkyns to the linear CO₂ adsorbed on Al³⁺. Later, they favored a bicarbonate on an exposed Al³⁺ ion showing a band at 1480 cm⁻¹ as the CO₂ species that blocked the exchange sites.³⁸⁾

D. Reaction of 2-methyl-3-butyn-2-ol (MBOH)

Lauron-Pernot et al. carried out the reaction of MBOH over alumina at 453 K.⁴⁵⁾ The products were sensitive to the amount of Na₂O contained as an impurity. Among aluminas examined, the alumina containing the smallest amount of Na₂O at 250 ppm yielded 3-methylbut-3-ene-2-one (MIPK) as the main product, indicating the amphoteric properties of alumina. The alumina containing larger amounts of Na₂O at 2700 ppm, on the other hand, yielded acetylene and acetone indicating that basic properties predominate.

References

1. A. F. Wells, *Structural Inorganic Chemistry*, Clarendon Press, Oxford (1975).
2. T. Sato, *Thermochim. Acta*, **88**, 69 (1985).
3. E. V. Kul'ko, A. S. Ivanova, G. S. Litvak, G. N. Kryukova, S. V. T. Tsybulya, *Kinet. Catal.*, **45**, 714 (2004).
4. D. S. MacIver, H. H. Tobin, R. T. Barth, *J. Catal.*, **2**, 485 (1963).
5. T. Ono, Y. Ohguchi, O. Togari, *Stud. Surf. Sci. Catal.*, **16**, 631 (1983).
6. S. Inoue, S. Asaoka, M. Nakamura, *Catal. Survey Jpn.*, **2**, 87 (1998).

7. J. A. Wang, X. Bokhimi, O. Novara, T. Lopez, F. Tzompantzi, R. Gomez, J. Navarrete, M. E. Llanos, E. Lopez-Salinas, *J. Mol. Catal. A: Chemical*, **137**, 239 (1999).
8. F. Vaudry, S. Khodabandeh, M. E. Davis, *Chem. Mater.*, **8**, 1451 (1996).
9. C. Marquez-Alvarez, N. Zilkova, J. Perez-Pariente, J. Cejka, *Catal. Rev.*, **50**, 222 (2008).
10. C. Morterra, G. Magnacca, *Catal. Today*, **27**, 497 (1996).
11. J. B. Peri, *J. Phys. Chem.*, **69**, 211 (1965).
12. J. B. Peri, *J. Phys. Chem.*, **69**, 220 (1965).
13. A. A. Tsyganenko, V. N. Filimonov, *Spectrosc. Lett.*, **5**, 477 (1972).
14. A. A. Tsyganenko, V. N. Filimonov, *J. Mol. Struct.*, **19**, 579 (1973).
15. H. Knözinger, P. Ratnasamy, *Catal. Rev. Sci. Eng.*, **17**, 31 (1978).
16. G. Busca, V. Lorenzelli, V. S. Escribano, *Chem. Mater.*, **4**, 595 (1992).
17. G. Busca, V. Lorenzelli, V. S. Escribano, R. Gvidetti, *J. Catal.*, **131**, 167 (1991).
18. M. Digne, P. Sautet, R. Raybaud, P. Euzen, H. Toulbout, *J. Catal.*, **211**, 1 (2002).
19. M. Digne, P. Sautet, R. Raybaud, P. Euzen, H. Toulbout, *J. Catal.*, **216**, 54 (2004).
20. X. Krokidis, P. Raybaud, A. -E. Gobichon, B. Rebours, P. Euzen, H. Toulhoat, *J. Phys. Chem. B*, **105**, 5121 (2001).
21. H. Vigué, P. Quintard, T. Merle-Mejean, V. Lorenzelli, *J. Eur. Ceram. Soc.*, **18**, 305 (1998).
22. S. J. Gregg, J. D. F. Ramsay, *J. Phys. Chem.*, **73**, 1243 (1969).
23. C. Morterra, A. Zecchina, S. Coluccia, A. Chiorino, *J. Chem. Soc. Faraday Trans. I*, **73**, 1544 (1977).
24. Y. Amenomiya, Y. Morikawa, G. Pleizer, *J. Catal.*, **46**, 431 (1977).
25. N. D. Parkyn, *J. Chem. Soc. A*, **1969**, 410.
26. N. D. Parkyn, *J. Phys. Chem.*, **75**, 526 (1971).
27. H. Knözinger, *Adv. Catal.*, **25**, 184 (1976).
28. J. Baltusaitis, J. H. Jensen, V. H. Grassian, *J. Phys. Chem. B*, **110**, 12005 (2006).
29. F. F. Roca, A. Nohl, L. de Mourgues, Y. Trambouze, *C. R. Acad. Sci. Ser.*, **C266**, 1123 (1968).
30. H. Knözinger, H. Buehl, K. Kochloefl, *J. Catal.*, **24**, 57 (1972).
31. H. Knözinger, A. Scheglila, *J. Catal.*, **17**, 252 (1970).
32. M. Kraus, in: *Handbook of Heterogeneous Catalysis* (ed. G. Ertl, H. Knözinger, J. Weitkamp) Wiley-CCH (1997) p.1051.
33. J. W. Hightower, W. K. Hall, *J. Phys. Chem.*, **71**, 1014 (1963).
34. H. R. Gerberich, W. K. Hall, *J. Catal.*, **5**, 99 (1966).
35. J. B. Peri, *J. Phys. Chem.*, **69**, 231 (1965).
36. Gy. Gati, H. Knözinger, *Stud. Surf. Sci. Catal.*, **7**, 819 (1973).
37. A. Corado, A. Kiss, H. Knözinger, H.-D. Mueller, *J. Catal.*, **37**, 68 (1975).
38. M. P. Rosynek, J. W. Hightower, *Stud. Surf. Sci. Catal.*, **7**, 851 (1973).
39. P. C. Saunders, J. W. Hightower, *J. Phys. Chem.*, **74**, 4323 (1970).
40. J. G. Larson, W. K. Hall, *J. Phys. Chem.*, **69**, 3080 (1965).
41. J. W. Hightower, W. K. Hall, *Trans. Faraday Soc.*, **66**, 477 (1970).
42. J. W. Hightower, W. K. Hall, *J. Catal.*, **13**, 161 (1969).
43. J. G. Larson, J. W. Hightower, W. K. Hall, *J. Org. Chem.*, **31**, 1225 (1966).
44. M. P. Rosynek, W. D. Smith, J. W. Hightower, *J. Catal.*, **23**, 204 (1971).
45. H. Lauron-Pernot, F. Luck, J. M. Popa, *Appl. Catal.*, **78**, 213 (1991).

3.7 Mixed Oxides

Mixed oxides are combinations of two kinds of metal oxides. Among mixed oxides which show basic properties, those containing alkali metal oxides and the Al-Mg oxides obtained by calcination of hydrotalcite are widely studied. These mixed oxides are described in sections 3.8 and 4.1, respectively, and not included here.

Regarding mixed oxides that show basic properties, at least one of the component oxides possesses basic properties. No basic mixed oxide in which neither component oxide shows basic properties has been discovered. In most cases, the basicity of one component oxide is modified to some extent by the addition of the

second component oxide. Remarkable enhancement of the basic properties by mixing two oxides has not been observed. This is different from acidic mixed oxides for which marked enhancement of acidic properties is observed by mixing. Although a marked change in basic property has not been observed, marked changes in the activity and selectivity have been observed for certain reactions.

Mixed oxides are prepared by different methods such as coprecipitation, sol-gel method, kneading method, impregnation, fast combustion method, molten mixture method and others. The coprecipitation method is most commonly employed. To a mixed aqueous solution containing two metal salts, alkaline solution is added to increase pH to precipitate two metal components at the same time. The resulting precipitate is washed with water and calcined at an elevated temperature to obtain a mixed oxide. In some mixed solutions, the component forms sol and gel when alkaline solution is added. For example, as ammonia was added to a mixed aqueous solution of $\text{Ce}(\text{NO}_3)_3 \cdot 6\text{H}_2\text{O}$ and $\text{La}(\text{NO}_3)_3 \cdot 6\text{H}_2\text{O}$ to pH 9, a gel of the mixed hydroxides was obtained.¹⁾ The gel was filtered and washed, dried at 383 K and calcined at 873 K to obtain $\text{CeO}_2\text{-La}_2\text{O}_3$. Preparation from a mixture of metal alkoxides in alcoholic solution is also a sol-gel method. The kneading method is employed for the mixed oxides whose components precipitate at quite different pHs. This method was employed for preparation of MgO-TiO_2 . A mixture of MgO and TiO_2 was kneaded with a small amount of water for 2 h, followed by calcination at 573–973 K in air.²⁾ The impregnation method is a convenient method to prepare mixed oxides if the salt of the second component metal is decomposed to oxide by heating in air. This method is called “doping” in many cases. The fast combustion method was employed for preparation of $\text{Ce}_x\text{Zr}_{1-x}\text{O}_2$.³⁾ A solution containing $(\text{NH}_4)_2\text{Ce}(\text{NO}_3)_6$ and $\text{ZrO}(\text{NO}_3)_2$ was ignited at 623 K using carbonylhydrazide as a fuel to obtain fine powders of $\text{Ce}_x\text{Zr}_{1-x}\text{O}_2$. The molten mixture method is an amorphous citrate process⁴⁾ and was employed for the preparation of $\text{CeO}_2\text{-Fe}_2\text{O}_3$,⁵⁾ $\text{CeO}_2\text{-ZnO}$ ⁶⁾ and $\text{CeO}_2\text{-MgO}$.⁷⁾ For $\text{CeO}_2\text{-MgO}$, a mixture containing $\text{Ce}(\text{NO}_3)_3 \cdot 6\text{H}_2\text{O}$, $\text{Mg}(\text{NO}_3)_2 \cdot 6\text{H}_2\text{O}$ and citric acid monohydrate was heated at 343 K to melt. Then the molten mixture was evacuated in a rotary evaporator at 343 K to be gradually solidified and expanded. The resulting solid was finally calcined at 823 K in air.

3.7.1 Mixed Oxides Containing MgO

Ueda et al. added several metal ions to MgO and measured basicity by TPD of adsorbed CO_2 .⁸⁾ Addition of metal ions whose ionic radii are slightly larger than that of Mg^{2+} brought about an increase in the basicity, while addition of metal ions smaller than Mg^{2+} was not effective in enhancing basicity (Fig. 3.7.1). Thus, addition of Ni^{2+} and Cu^{2+} increased the basicity. Addition of metal ions far larger than Mg^{2+} such as Mn^{2+} and Cd^{2+} resulted in a small effect. Enhancement of basicity is ascribed to the distortion of the lattice surrounding the metal ions added. The distortion results in the expansion of the Mg-O bond and localization of electrons on the O atom. Ions that are too large cannot be incorporated into the lattice, and are thus ineffective in enhancement of basicity. The catalytic activities of MgO 's

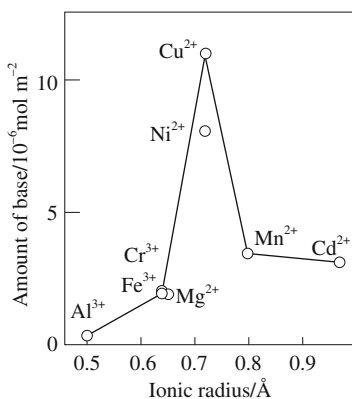


Fig.3.7.1 Relation between the amount of surface basic sites of metal ion-containing MgO and the ionic radius of added metal ion. Reprinted with permission from W. Ueda, T. Yokoyama, Y. Moro-oka, T. Ikawa, *Chem. Lett.*, **1985**, 1059, Fig. 1.

loaded with metal cations for dehydrogenation of 2-propanol correlate well with the basicities.

Noller et al. prepared MgO- Al_2O_3 and MgO- SiO_2 mixed oxides of different compositions, and examined their basic character by O_{1s} and Mg_{2p} binding energies in XPS, O-H stretching frequency shift caused by adsorption of acetone in IR and catalytic activities for 1-butanol decomposition and diacetone alcohol decomposition.⁹⁾ They concluded that the basic strength found with the mixed oxides is always in between the limits found for the components. In other words, the basic strength of mixed oxides is well expressed by Sanderson's intermediate electronegativity.

Tanabe et al. prepared MgO- TiO_2 mixed oxides of different compositions.²⁾ The maximum number of basic sites at $H_2 = 15.0$ was observed for the mixed oxide MgO : $TiO_2 = 9 : 1$ in wt%. Considering an increase in surface area by mixing, it cannot be said that basic sites are generated by mixing of two oxides. With further increase in TiO_2 fraction, basic sites decreased while acidic sites increased. At the composition MgO : $TiO_2 = 1 : 1$, the catalytic activity for alkylation of phenol with methanol showed the maximum. The MgO- TiO_2 1 : 1 mixed oxide possesses both acidic sites and basic sites though the number of these sites is not large. It was suggested that the reaction proceeds by an acid-base bifunctional mechanism.

Increase in the basicity by mixing MgO with TiO_2 and with ZrO_2 was reported by Aramendia et al.¹⁰⁾ The basicity was estimated by TPD of CO_2 , and catalytic activity was examined for 2-methyl-3-butyn-2-ol (MBOH) test reaction, decomposition of 2-propanol, double bond isomerization of allylbenzene, and aldol condensation of acetone. The basic site density was in the order MgO- $TiO_2 > MgO-ZrO_2 > ZrO_2 > MgO$. All catalysts gave the products characteristic of base-catalyzed reactions except for MBOH reaction on ZrO_2 showing amphoteric character.

The appearance of strong basic sites on MgO- La_2O_3 mixed oxide was reported.^{11,12)} The mixed oxide was prepared by coprecipitation from aqueous

solution of Mg and La nitrates, KOH and K_2CO_3 being used to adjust the pH of the mother liquid to 10. The resulting mixed oxide contained 5.4% K, and had a surface area of $37.6\text{ m}^2\text{g}^{-1}$ after calcination at 923K. The heat of adsorption of CO_2 exceeded 140 kJ mol^{-1} , which is higher than 120 and 100 kJ mol^{-1} observed for KF/Al_2O_3 and rehydrated hydrotalcite, respectively. The $MgO-La_2O_3$ mixed oxide showed high activities for transesterification between diethyl carbonate and alcohols, and Michael addition of the compounds having active methylene groups with a variety of unsaturated carbonyl compounds. The activities of the $MgO-La_2O_3$ mixed oxide were higher than those of hydrotalcite and KF/Al_2O_3 . The high activity in the Michael addition of nitromethane ($pK_a = 17.2$) with *trans*-chalcone indicates that the mixed oxide possesses basic sites stronger than $H_- = 17.2$.

Ortho-selective alkylation of phenol with methanol proceeds effectively over the $MgO-CeO_2$ mixed oxide in the temperature range 723–823 K.⁷⁾ Sato et al. prepared MgO catalysts combined with various metal oxides for the alkylation of phenol and found that only $MgO-CeO_2$ exhibited efficient catalytic activity without decay. Strong basic sites on MgO were eliminated by the addition of CeO_2 and weak basic sites which desorb CO_2 below 423 K in TPD were relevant to the reaction. The number of weak basic sites was maximized at the CeO_2 content of 11.2 mol%. They postulated that the active $MgO-CeO_2$ catalyst consists of the interstitial solid solution of fluorite-type $Mg_xCe_{1-x/2}O_2$ dispersed in the MgO matrix.

3.7.2 Mixed Oxides Containing CeO_2

Cerium oxide is a weakly basic oxide. Combination of CeO_2 with other metal oxides modifies the acidic and basic properties of the metal oxides. The basic properties have been studied for the metal oxides La_2O_3 , ZrO_2 and ZnO with which CeO_2 is combined.

Although both CeO_2 and La_2O_3 are known to produce 1-alkene in the dehydration of 2-alkanols, the selectivity further increased by combining the two oxides.^{1,13)} The selectivity to 4-methyl-1-pentene against 4-methyl-2-pentene in the dehydration of 4-methyl-2-pentanol was maximized for the $CeO_2-La_2O_3$ mixed oxide containing 20–60 atom% of La. It was assumed that well-balanced numbers of weak acidic sites and strong basic sites made possible efficient dehydration by E1cB mechanism.

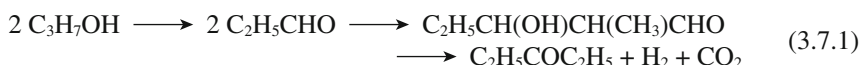
The combination of CeO_2 with ZrO_2 gives similar results to those of CeO_2 with La_2O_3 in both generation of acidic and basic sites and catalytic activity for 4-methyl-2-pentanol dehydration.^{14,15)} The mixed oxide containing 75 mol% CeO_2 showed maximum selectivity to 4-methyl-1-pentene due to increased numbers of strong basic sites and weak acidic sites to result in a well-balanced number of these sites.

ZrO_2 is active for transfer hydrogenation with 2-propanol (Meerwein-Ponndorf-Verley reduction) as described in section 3.3. The mixed oxide CeO_2-ZrO_2 shows higher activity and selectivity than pure ZrO_2 for transfer hydrogenation of cyclohexanone to cyclohexanol with 2-propanol.³⁾ The mixed oxide of the composition $Ce_{0.2}Zr_{0.8}O_2$ showed a selectivity higher than 98% at a conversion of

53% at 575 K. The activity was the highest for the $\text{Ce}_{0.4}\text{Zr}_{0.6}\text{O}_2$. The high activity and selectivity was postulated to be due to the reduction of the acidic property of ZrO_2 by combination with CeO_2 to form moderate acid-base pair sites.

ZnO is active for dehydrogenation of cyclohexanol and transfer hydrogenation of cyclohexanone with 2-propanol.⁶⁾ The activities for both reactions increased on combination with CeO_2 . Combination with CeO_2 reduced the strong basicity and enhanced acidity of ZnO , resulting in an increase in the activities for the two reactions.

CeO_2 is active for the formation of 3-pentanone from 1-propanol at a reaction temperature of 723 K. Kamimura et al. reported that the addition of Fe_2O_3 to CeO_2 enhanced the catalytic ability of CeO_2 .⁵⁾ The reaction started with dehydrogenation to propanal which underwent aldol addition to 3-hydroxy-2-methylpentanal, followed by decomposition into 3-pentanone. Instead of CO expected from stoichiometry, CO_2 was formed in the final products. The excess O may originate from impurity in the carrier gas or water produced by dehydration of 3-hydroxy-2-methylpentanal.



The basicity and the activity increased on addition of 20~30 mol% Fe to CeO_2 . Although Kamimura et al. mentioned the importance of redox properties in addition to acid-base properties, they stated that the addition of Fe_2O_3 to CeO_2 enhanced the ability of dehydrogenation of 1-propanol to propanal without losing the ability for the dimerization of propanal (aldol addition).

3.7.3 Mixed Oxides Containing Al_2O_3

Basicity of Al_2O_3 is enhanced by addition of alkali metals and alkali metal oxides, as described in section 3.9. Addition of alkaline earth oxides and rare earth oxides to Al_2O_3 also enhances the basicity of the resulting mixed oxides. Horiuchi et al. added a series of alkali metal oxides, alkaline earth oxides and rare earth oxides to Al_2O_3 in $4 \mu\text{mol m}^{-2}$, and measured the heat of adsorption of CO_2 by gas chromatography in the column temperature range 600 to 900 K.¹⁶⁾ While the heat of adsorption was 80 kJ mol^{-1} for Al_2O_3 , the heats of adsorption were ca. 160 kJ mol^{-1} for the Al_2O_3 's loaded with BaO, and SrO, and ca. 140 kJ mol^{-1} for the Al_2O_3 's loaded with CaO, MgO, La_2O_3 , Nd_2O_3 , and Pr_2O_3 .

Introduction of TiO_2 and ZrO_2 to Al_2O_3 decreases the basicity of Al_2O_3 . Lahousse et al. prepared $\text{TiO}_2\text{-Al}_2\text{O}_3$ ¹⁷⁾ and $\text{ZrO}_2\text{-Al}_2\text{O}_3$ ¹⁸⁾ with different compositions, and carried out the hydrolysis of COS and 2-propanol decomposition over these catalysts. The activity for COS hydrolysis was directly connected to the number of OH groups involved in the formation of hydrogencarbonate species when adsorbing CO_2 , which was confirmed by Bachelier et al.¹⁹⁾ The activities of the TiO_2 and ZrO_2 for COS hydrolysis decreased on addition of Al_2O_3 . The number of OH groups sufficiently basic to interact with CO_2 was minimal for $\text{TiO}_2\text{-Al}_2\text{O}_3$ containing 30% Al_2O_3 . The activity for 2-propanol dehydration was maximized

for $\text{TiO}_2\text{-Al}_2\text{O}_3$ containing 70% Al_2O_3 . For $\text{ZrO}_2\text{-Al}_2\text{O}_3$, the activity of ZrO_2 for COS hydrolysis decreased with the Al_2O_3 content, but the activity for 2-propanol dehydration increased with the Al_2O_3 content. The increase in the dehydration activity for both mixed oxides is due to an increase in the acidity by mixing two oxides.

References

1. M. G. Cutrufello, I. Ferino, R. Monaci, E. Rombi, G. Colon, J. A. Navio, *Phys. Chem. Chem. Phys.*, **2**, 2928 (2001).
2. K. Tanabe, H. Hattori, T. Sumiyoshi, K. Tamaru, T. Kondo, *J. Catal.*, **53**, 1 (1978).
3. G. R. Rao, H. R. Sahu, B. G. Mishra, *React. Kinet. Catal. Lett.*, **78**, 151 (2003).
4. C. Marcilly, P. Courty, B. Delmon, *J. Am. Ceram. Soc.*, **53**, 56 (1970).
5. Y. Kamimura, S. Sato, R. Takahashi, T. Sodesawa, T. Akashi, *Appl. Catal. A*, **252**, 399 (2003).
6. B. G. Mishra, G. R. Rao, *J. Mol. Catal. A*, **243**, 204 (2006).
7. S. Sato, K. Koizumi, F. Nozaki, *J. Catal.*, **178**, 264 (1998).
8. W. Ueda, T. Yokoyama, Y. Moro-oka, T. Ikawa, *Chem. Lett.*, **14**, 1059 (1985).
9. H. Noller, J. A. Lercher, H. Vinek, *Mater. Chem. Phys.*, **18**, 577 (1988).
10. M. A. Aramendia, V. Borau, C. Jimenez, A. Marinas, J. M. Marinas, J. R. Ruiz, F. J. Urbano, *J. Mol. Catal. A*, **218**, 81 (2004).
11. B. Veldurthy, F. Figueras, *Chem. Commun.*, **2004**, 734.
12. B. Veldurthy, J. M. Clacens, F. Figueras, *Adv. Synth. Chem.*, **347**, 767 (2005).
13. G. Colon, J. A. Navio, R. Monaci, I. Ferino, *Phys. Chem. Chem. Phys.*, **2**, 4453 (2000).
14. M. G. Cutrufello, I. Ferino, V. Solinas, A. Primavera, A. Trovarelli, A. Auroux, C. Picciau, *Phys. Chem. Chem. Phys.*, **1**, 3369 (1999).
15. V. Solinas, E. Rombi, I. Ferino, M. G. Cutrufello, G. Colon, J. A. Navio, *J. Mol. Catal. A*, **204-205**, 629 (2003).
16. T. Horiuchi, H. Hidaka, T. Fukui, Y. Kubo, M. Horio, K. Suzuki, T. Mori, *Appl. Catal. A*, **167**, 195 (1998).
17. C. Lahousse, F. Mauge, J. Bachelier, J.-C. Lavalley, *J. Chem. Faraday Trans.*, **91**, 2907 (1995).
18. C. Lahousse, A. Aboulayt, F. Mauge, J. Bachelier, J.-C. Lavalley, *J. Mol. Catal.*, **84**, 283 (1993).
19. J. Bachelier, K. Aboulayt, J. C. Lavalley, O. Legendre, F. Luck, *Catal. Today*, **17**, 55 (1993).

3.8 Metal Oxides Loaded with Alkali Metal Compounds

Because of the chemical nature of the alkali metal compounds, the materials modified by alkali metal compounds exhibit basic properties in many cases. Modification of the surface properties by loading alkali metal compounds results from various reasons, and it is often difficult to find the precise explanation for the activity enhancement in each case.

1) Alkali metal ions poison or neutralize acidic sites and reduce the rates of the reactions catalyzed by acid sites.

2) Alkali metal ions located either in the bulk or on the surface modify the electron density of the surface oxygen ions.

3) Alkali metal compounds are transformed by the appropriate pretreatment (calcination, heat treatment) into basic compounds such as alkali metal oxides which show basic properties.

4) Alkali metal compounds react with the support material to develop completely new compounds (or catalytically active sites).

Among the materials modified by alkali metal compounds, Al_2O_3 and MgO have been studied most extensively for their basic and catalytic properties. The

catalytic properties of alkali metal compound-loaded catalysts vary with the type of alkali metal compound. In this section, Al_2O_3 , MgO , SiO_2 , TiO_2 , and ZrO_2 loaded with alkali metal compounds, KF- and CsF-loaded Al_2O_3 , and KNH_2 -loaded Al_2O_3 are described.

3.8.1 Alkali Metal Compounds-loaded Al_2O_3

Alumina possesses both acidic and basic properties. Adding alkali compounds to Al_2O_3 enhances the basic properties and weakens the acidic properties. This was evidenced by microcalorimetric measurements of CO_2 and NH_3 adsorption on $\text{K}_2\text{O}/\text{Al}_2\text{O}_3$.^{1,2)} These changes caused by the addition of alkali compounds are reflected on the catalytic activities. Dehydration of 2-propanol, a representative reaction catalyzed by Al_2O_3 , was inhibited by the addition of alkali compounds.³⁻⁵⁾ Although the basic properties were enhanced, dehydrogenation of 2-propanol did not proceed over alkali compounds-loaded Al_2O_3 .

Increase in the heat of adsorption of CO_2 by the addition of alkali compounds to Al_2O_3 was observed as shown in Fig. 3.8.1.⁶⁾ Strong basic sites were generated by addition of K^+ ion to $\gamma\text{-Al}_2\text{O}_3$ followed by calcination at 873 K. The heat of adsorption was 170 kJ mol^{-1} for K^+ ion-loaded $\gamma\text{-Al}_2\text{O}_3$ while it was 100 kJ mol^{-1} for pure $\gamma\text{-Al}_2\text{O}_3$.

Several OH bands are observable for Al_2O_3 . Addition of Na^+ ion causes a complex change in the intensity of the OH bands. Paukshtis et al. observed that the band at 3803 cm^{-1} decreased moderately upon introduction of Na^+ .⁷⁾ The band at 3780 cm^{-1} decreased markedly with increasing Na^+ concentration, whereas the band at 3756 cm^{-1} increased. The proton affinity of the OH group was estimated from the band shift caused by the interaction with chloroform. As a result of hydrogen bond formation with chloroform, the band at 3756 cm^{-1} shifted to the lower frequency region by $20\text{--}25 \text{ cm}^{-1}$, which corresponds to the proton affinity of

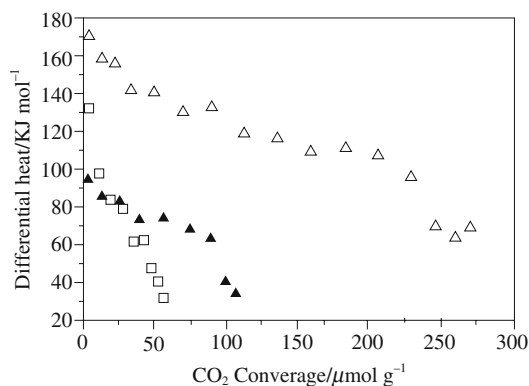


Fig. 3.8.1 Differential heat vs. adsorbate coverage for adsorption of CO_2 at 323 K on $\gamma\text{-Al}_2\text{O}_3$ (□), and on 6% $\text{K}_2\text{O}/\gamma\text{-Al}_2\text{O}_3$ calcined at 873 K (△) and 1273 K (▲). Reprinted with permission from H. Zou, X. Ge, J. Shen, *Thermochimica Acta*, **397**, 81 (2003) Fig. 3.

1540–1570 kJ mol^{-1} . The portion of acidic OH groups showing bands at 3735–3670 cm^{-1} decreased by Na^+ addition. Similar behavior of OH bands was reported by Srinivasan et al.⁸⁾ The highest frequency band of 3770 cm^{-1} of Al_2O_3 disappeared and a band appeared at 3750 cm^{-1} on addition of Na^+ .

SO_2 is a stronger acid than CO_2 and, accordingly, preadsorption of SO_2 on Al_2O_3 blocks the subsequent adsorption of CO_2 , indicating that both probes SO_2 and CO_2 are adsorbed on common sites.⁹⁾ SO_2 is adsorbed on the basic sites of Al_2O_3 and 3% Na^+ ion-loaded Al_2O_3 mostly in the form of sulfite ($-\text{Al}-\text{O}-\text{SO}_2$) as characterized by an IR band near 1060 cm^{-1} . The band position of the sulfite species is the same for both Al_2O_3 and Na^+ ion-loaded Al_2O_3 , but band intensity was stronger for the $\text{Na}^+/\text{Al}_2\text{O}_3$. The strength of adsorption and the quantity of adsorbed SO_2 were greater for $\text{Na}^+/\text{Al}_2\text{O}_3$, indicating the greater basicity of the Na^+ ion-loaded Al_2O_3 . The reactivity of the adsorbed sulfite toward H_2S , which is important for the Claus reaction, was lower on Na^+ ion-loaded Al_2O_3 than on Al_2O_3 . This is due to the stronger adsorption of SO_2 on Na^+ ion-loaded Al_2O_3 ; strongly adsorbed SO_2 is more stable, and therefore less reactive. In addition to the sulfite, hydrogensulfite species SO_3H^- or HOSO_2^- was suggested. Adsorption of SO_2 on the OH groups was also stronger on Na^+ ion-loaded Al_2O_3 than on Al_2O_3 .¹⁰⁾

Remarkable increase in the catalytic activities of alkali metal compounds-loaded Al_2O_3 was observed for the double bond isomerization of alkenes. Yamaguchi et al. impregnated Al_2O_3 with different amounts of KNO_3 followed by decomposition of the salts at elevated temperatures, and measured the catalytic activity for double bond migration of *cis*-2-butene and 3-methyl-1-butene.¹¹⁾ The maximum activity for the *cis*-2-butene isomerization was obtained for the Al_2O_3 loaded with $12 \times 10^{18} \text{ K}^+$ ions m^{-2} and decomposed at 773 K. The activity was higher than that of MgO ; the reaction proceeded at 273 K (with 2.5 mg of catalyst) in a closed recirculation reactor. Use of K_2CO_3 instead of KNO_3 resulted in the same activity. Cs^+ ion-loaded Al_2O_3 exhibited even much higher activity than K^+ ion-loaded Al_2O_3 for the double bond isomerization of 3-methyl-1-butene. A marked increase in activity for double bond isomerization by loading alkali ions was observed only for Al_2O_3 . The other metal oxides such as SiO_2 and TiO_2 did not become active by alkali ion loading under the same reaction conditions.

Yamaguchi et al. proposed the generation of strong basic sites on Al_2O_3 by loading alkali or alkaline earth salts followed by heat treatment at a high temperature.^{12,13)} During heat treatment after addition of the salts, decomposition of the salts occurred in two steps. An example is shown in Fig. 3.8.2 for the KNO_3 -loaded Al_2O_3 prepared by grinding Al_2O_3 with KNO_3 (13 K cation per $\text{nm}^{-2} \text{ Al}_2\text{O}_3$) with a small amount of water to form a paste followed by drying at 383 K. The sample was then subjected to TPD measurement monitoring the decomposition process. Two TPD peaks appeared. The low temperature peak was composed mostly of NO_2 caused by the decomposition of dissociated free NO_3^- ions, while the high temperature peak was composed of NO and O_2 caused by the decomposition of the agglomerated phase of KNO_3 . Similar two-step decomposition was observed for the Al_2O_3 's impregnated with alkali carbonates, and alkali and alka-

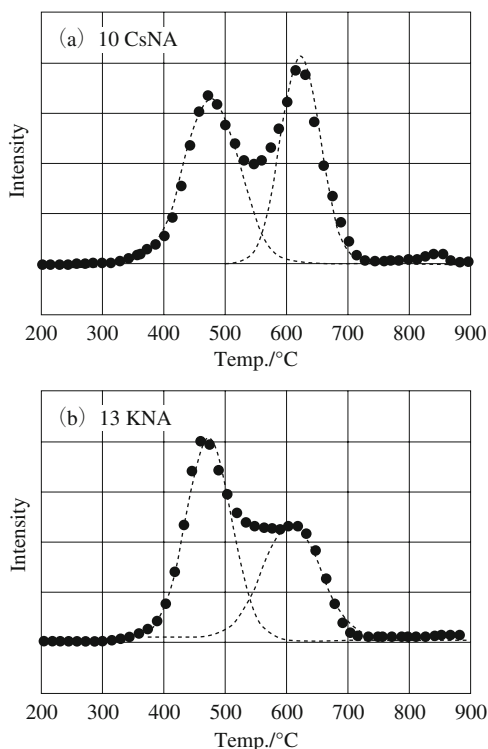
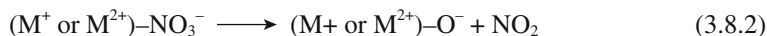
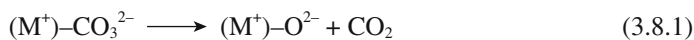
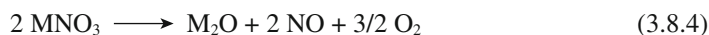


Fig. 3.8.2 TPD profiles and deconvolution for (a) Al_2O_3 mounted with 10 cations of $\text{CsNO}_3 \text{ nm}^{-2}$ and (b) Al_2O_3 mounted with 13 cations of $\text{KNO}_3 \text{ nm}^{-2}$. Reprinted with permission from T. Yamaguchi, M. Ookawa, *Catal. Today*, **116**, 191 (2006) Fig. 2.

line earth nitrates. The authors proposed that the strong basic sites were generated by the decomposition of the dissociated free anions forming O^{2-} or O^- anions which act as strong basic sites.



The decomposition of the agglomerated phase does not produce O^{2-} or O^- , but only metal oxides. These are not so strong as the O^{2-} or O^- anions.



3.8.2 Alkali Metal Compound-loaded Alkaline Earth Oxides

In 1985, it was reported that Li-promoted MgO exhibited activity for the oxidative

coupling of methane to produce ethane and ethene in good selectivity in the presence of oxygen.¹⁴⁾ Ito et al. prepared the Li-promoted MgO by adding MgO and Li₂CO₃ to deionized water and evaporating the water, while stirring, until only a thick paste remained. The paste was dried at 313 K for more than 5 h and calcined at 738 K. The Li/MgO was examined by ESR spectroscopy. The signal assigned to [Li⁺O⁻] centers was observed at $g_p = 2.054$. They proposed the mechanism for the [Li⁺O⁻] formation which is analogous to that described by Abraham and co-workers.¹⁵⁻¹⁸⁾ For every two Li⁺ ions leaving the carbonate phase, only one Mg²⁺ enters to form MgCO₃. From stoichiometric considerations, this excess of cations in the MgO matrix suggests the formation of oxygen vacancies which may exist on the surface. Gaseous oxygen molecules immediately react with the vacancies at high temperature, resulting in O²⁻ ions and holes. The [Li⁺O⁻] centers are produced by these holes being trapped at O²⁻ ions which are adjacent to Li⁺ ions.

This process is expressed as follows.



where \square denotes an oxygen vacancy. The [Li⁺O⁻] centers act as active sites for the formation of methyl radicals from methane.

Following the report by Ito and Lunsford, many studies have been performed on the catalytic activities of alkali metal compound-loaded MgO. Most of the studies focused on the oxidative coupling of methane. Application of the alkali metal ion-promoted MgO to base-catalyzed reactions appeared later.

Normally, alkali compounds such as alkali carbonate are loaded on the surface by an impregnation method then calcined at a high temperature. In most cases, loading alkali ions on MgO results in a considerable decrease in surface area. Nevertheless, the catalytic activities for a number of base-catalyzed reactions are enhanced. The degree of the promotive effects depends on the type of alkali compound and the type of reaction.

For 1-butene isomerization, an increase in the activity by loading alkali metal ions on MgO was reported.¹⁹⁾ Among Li⁺, K⁺ and Na⁺, Li⁺ was the most effective in enhancing the activity. However, too much loading caused a decrease in the activity. As compared to unmodified MgO, the Li₂O/MgO of 1 wt% Li showed activity about three times higher, while the Li₂O/MgO of 10 wt% Li showed one third at a reaction temperature of 273 K.

For decomposition of 2-propanol, loading alkali metal cations changes not only the activity but the selectivity as well. Loading all Li⁺, Na⁺, K⁺ and Cs⁺ cations on MgO increased the decomposition rate, but the enhancing effects were different for dehydrogenation and dehydration.²⁰⁾ Loading Li⁺ greatly enhanced the dehydrogenation activity, but loading Na⁺ and Cs⁺ enhanced the dehydration activity. It was interpreted that loading Cs⁺ generates very strong basic sites which promote dehydration, while loading Li⁺ generates basic sites of medium strength which promote dehydrogenation. For decomposition of 2-butanol, however, the selectivity for dehydrogenation as well as the decomposition activity increased upon loading Cs⁺ cations on MgO.²¹⁾

Aldol condensation is also promoted by loading alkali ions on MgO. The

effective alkali metal cations are different depending on the reaction. For the vapor-phase condensation of acetone to finally form isophorone at 573 K, Li^+ was most effective among Li^+ , Na^+ , K^+ and Cs^+ .²²⁾ Isophorone was formed by subsequent aldol condensation to phorone via mesityl oxide (MO), followed by intramolecular Michael addition of phorone. For the aldol condensation of citral with acetone to pseudoionone, however, Li^+ -loaded MgO was not so active as compared to Na^+ -loaded MgO, though the Li^+ -loaded MgO was more active than pure MgO.²³⁾

Oxidative coupling of methane and oxidative methylation of toluene over MgO was greatly enhanced by loading two kinds of alkali compounds²⁴⁾. The high basicity of the bi-alkali-promoted MgO was deduced to the high enrichment of the surface with alkali atoms as observed by XPS study. The enrichment was much higher in the bi-alkali-promoted system than in the respective mono-alkali-promoted system.

It was observed in many cases as described above that Li^+ ion is most effective for enhancing the basic properties of MgO. Kanno and Kobayashi measured TPD and IR of CO_2 adsorbed on MgO loaded with alkali metal cations.²⁵⁾ They also observed that Li^+ ion was most effective in enhancing the basic properties of MgO. The TPD peak appeared at the highest temperature of 673 K for Li^+ /MgO. In IR spectra of adsorbed CO_2 , the largest difference was observed for Li^+ /MgO in IR band position between symmetric vibration and asymmetric vibration of the bidentate carbonate. They suggested that similarity in the diameter between Mg^{2+} (0.066 nm) and Li^+ (0.068 nm) makes it easier to substitute Mg^{2+} by Li^+ , which results in the generation of strong basic sites.

Although the surface area of alkali ion-loaded MgO is normally small, Li^+ ion-loaded MgO with high surface area was prepared by the sol-gel method.²⁶⁾ A methanol solution containing $\text{Mg}(\text{OCH}_3)_2$ and LiNO_3 was mixed with water solution in methanol at room temperature and allowed to stand for 24 h for gelation. After drying at 323 K in a vacuum for 7 h, the gel was calcined at 773 K in air for 1 h. The resulting gel containing 1 wt% Li had a surface area of $190 \text{ m}^2 \text{ g}^{-1}$, which was not significantly smaller than the surface area of pure MgO $250 \text{ m}^2 \text{ g}^{-1}$. On calcination at 973 K, the surface area decreased to $60 \text{ m}^2 \text{ g}^{-1}$, but it was still higher than the surface area of the Li^+ -impregnated MgO $10 \text{ m}^2 \text{ g}^{-1}$.

Loading alkali metal compounds on CaO also enhances basic properties.

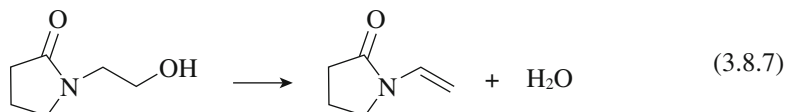
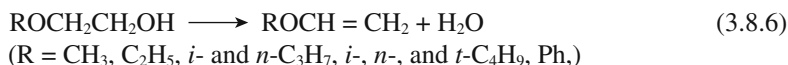
3.8.3 Alkali Metal Compound-loaded SiO_2 and Other Supports

A. Alkali metal compound-loaded SiO_2

Bal et al. prepared alkali-loaded SiO_2 and measured IR of adsorbed CO_2 and catalytic activities for 2-propanol decomposition and methylation of phenol with methanol.²⁷⁾ The catalysts were prepared by impregnation of SiO_2 with the alkali metal acetates or hydroxides followed by calcination at 773 K. Enhancement of basic properties by alkali loading was confirmed by IR measurements of adsorbed CO_2 . The adsorbed CO_2 transformed into a more stable bidentate carbonate species with increasing basicity of the alkali oxides loaded on SiO_2 . The activities increased with increasing basicity of the alkali metal (Li to Cs) in both 2-propanol

decomposition and methylation of phenol with methanol. In the decomposition of 2-propanol, dehydrogenation to acetone proceeded preferentially, and in the methylation, *O*-alkylation to produce anisole took place selectively. They applied the series of alkali-loaded SiO₂ to *O*-alkylation of 2-naphthol,²⁸⁾ dihydroxybenzenes²⁹⁾ with methanol, as well as *O*-alkylation of phenol with methanol, ethanol, propanol and butanol.³⁰⁾ The order of activity followed the basicity for all the *O*-alkylations: Li₂O/SiO₂ < Na₂O/SiO₂ < K₂O/SiO₂ < Cs₂O/SiO₂.

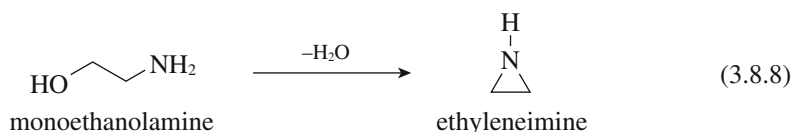
Cs₂O-loaded SiO₂ is being used in two industrial processes in the production of vinyl ether from glycol ether (eq. 3.8.6) and *N*-vinyl-2-pyrrolidone from *N*-(2-hydroxyethyl)-2-pyrrolidone (eq. 3.8.7). Both reactions are intramolecular dehydration.



For the intramolecular dehydration of 2-ethoxyethanol to ethyl vinyl ether, the SiO₂ loaded with Cs₂O in the Cs/Si atomic ratio of 0.03 showed a maximum conversion of 95.5% with a selectivity of 80% at a reaction temperature of 693 K.³¹⁾ A higher selectivity of 84.2% was obtained with the catalyst loaded with Cs₂O in the Cs/Si atomic ratio of 0.005. High activities and selectivities were observed for the other 2-alkoxyethanols such as ethoxy-, isopropoxy-, *n*-propoxy-, isobutoxy-, *t*-butoxy-, and phenoxyethanols. The high activity and selectivity were attributed to the existence of the acid and base pair sites whose acid and base strengths were lower than $H_0 = +6.8$ and $H_- = +9.4$, respectively.

For the intramolecular dehydration of *N*-(2-hydroxyethyl)-2-pyrrolidone to *N*-vinyl-2-pyrrolidone, the SiO₂'s loaded with a small amount of alkali metal oxides exhibited pronounced catalytic performance in the temperature range 633–673 K.³²⁾ Similar to the case of dehydration of 2-ethoxyethanol to ethyl vinyl ether, loading a small amount of alkali metal oxides generated weak acid-weak base pair sites on SiO₂ surface, which acted as active sites for the intramolecular dehydration.

Adjustment of acid-base pair sites by loading alkali metal cations together with phosphorus on SiO₂ produces an active catalyst for the production of ethyleneimine by intramolecular dehydration of monoethanolamine. The SiO₂ loaded with Cs and P in the atomic ratio Si/Cs/P = 1/0.1/0.08 gave a selectivity of 78.1% at a conversion of 70.1% at 643 K. The vapor phase process has been industrialized



for the production of ethyleneimine used for a raw material of pharmaceuticals and amino resins.³³⁾

Kelly et al. reported that Na₂O-loaded SiO₂ showed a high activity for vapor-phase aldol condensation of aldehydes (*n*-butanal and *n*-hexanal) in the temperature range 623–723 K. By combination of Na₂O-loaded SiO₂ with hydrogenation catalysts such as Pd and CuO/ZnO, saturated aldehyde and alcohols were produced in one step.^{34,35)}

Zhu's group attempted to generate strong basic sites on SiO₂ by loading KNO₃ followed by decomposition of the supported KNO₃ in the presence of methanol (redox strategy). Decomposition temperature was significantly lower in the presence of methanol. Low temperature decomposition of KNO₃ avoids the reaction of K compound with SiO₂ and generates strong basic sites of H_- of 22.5.³⁶⁾ The redox strategy could be successfully applied to other systems such as TiO₂³⁶⁾ and zeolite Y.³⁷⁾ They also prepared strong basic sites on mesoporous silica SBA-15 by coating with MgO on which KNO₃ was supported. MgO layer on SiO₂ passivated silanol groups.³⁸⁾ Mesoporous structure was retained after heat treatment at high temperature because KNO₃ did not react with SiO₂ to collapse the structure. The resulting material possessed strong basic sites of H_- of 27.0. This method was applied to zeolite Y.³⁹⁾

B. Alkali metal compound-loaded TiO₂

Zaroma et al. prepared alkali metal ion-loaded TiO₂ catalysts by sol-gel method in which titanium *n*-butoxide aqueous solution was added drop wise to a refluxed mixed solution of water, ethanol, alkaline chloride, and nitric acid at pH 3, followed by drying and calcining at 673 K.^{40–42)} The basic strengths of the catalysts measured by TPD of CO₂ were in the order Li⁺/TiO₂ < TiO₂ < Rb⁺/TiO₂ < Na⁺/TiO₂ < K⁺/TiO₂ < Cs⁺/TiO₂ after calcination at 673 K. On calcination at 873 K, the basic strength of Rb⁺/TiO₂ became between that of K⁺/TiO₂ and Cs⁺/TiO₂. The catalytic activities of the alkali ion-loaded TiO₂ for the condensation of acetone to mesityl oxide and isomesityl oxide at 573 K increased with an increase in the strength of basic sites. The catalysts possessing basic sites stronger than Li⁺/TiO₂ promoted further condensation to mesitylene.

C. Alkali metal compound-loaded ZrO₂

4-Methylpentan-2-ol undergoes dehydration and dehydrogenation over ZrO₂. The selectivities to 4-methyl-1-pentene, 4-methyl-2-pentene and 4-methylpentan-2-one depend on the preparation conditions. In particular, doping of Na⁺ on ZrO₂ greatly affects the selectivity. The ZrO₂ on which Na⁺ was loaded by immersion in aqueous NaOH or impregnation with aqueous NaOH showed a high selectivity to 4-methyl-1-pentene against 4-methyl-2-pentene.⁴³⁾ On the ZrO₂ immersed in aqueous NaOH and calcined at 673 K, 4-methylpentan-2-one was mainly yielded, the ratio of 1-alkene to 2-alkene being quite high in alkene products. Strong basic sites generated by Na⁺ loading abstract β-H (methyl H) to form a carbanionic species (an enolate ion), which can undergo cleavage of either α-H-C bond to produce ketone or C-OH bond to produce 1-alkene.

The ZrO_2 catalyst on which KNO_3 is mounted and decomposed at 873 K shows a high activity for *cis*-2-butene isomerization at 273 K. The reaction does not occur at all on pure ZrO_2 at 273 K. Generation of basic sites stronger than H_{27} was observed for the ZrO_2 on which 15% KNO_3 was mounted and decomposed at 873 K.⁴⁴⁾ In 2-propanol decomposition, dehydrogenation to form acetone increased and dehydration to form propene decreased with the amount of KNO_3 loaded.

D. Alkali metal compound-loaded carbon

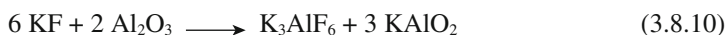
Wang et al. prepared alkali-loaded carbon catalysts by impregnation of activated carbon with an aqueous solution of alkali salts followed by heating under an N_2 stream at 773 K.⁴⁵⁾ The catalysts prepared using $NaNO_3$, KNO_3 , CH_3COONa and $NaHCO_3$ showed high activities for the formation of propionitrile from acetonitrile and methanol at 673 K. The most active catalyst was prepared by using $NaHCO_3$, the selectivity being more than 80% at a conversion of 70% at a reaction temperature of 753 K. The catalysts prepared using the salts that need a high temperature to decompose such as $CsNO_3$, Na_2SO_4 , Na_2HPO_4 and $NaCl$ showed low activities. The extent of the decomposition of the salts is not sufficient for these catalysts of low activity. Impregnation with $NaHCO_3$ is effective only for activated carbon. High activities were not observed for other supports such as CaO , MgO , TiO_2 , SiO_2 and Al_2O_3 .

3.8.4 KF/Al_2O_3 and CsF/Al_2O_3

KF/Al_2O_3 was developed by researchers engaged in synthetic organic chemistry and is now listed among the commercially available chemical reagents. Later, CsF/Al_2O_3 was found to show higher catalytic activity than KF/Al_2O_3 for certain types of base-catalyzed reactions.

A. Characterization

The basic strength of KF/Al_2O_3 was measured by Hammett indicator method to be in the range 12–15 in H_- scale.⁴⁶⁾ The mechanism of basic site appearance is controversial. It is established that the following reactions occur during the preparation of KF/Al_2O_3 .



Ando et al. reported that there are three basic species or mechanisms of appearance of the basicity of KF/Al_2O_3 ^{47–49)}: (1) the presence of active fluoride, (2) the presence of $[Al-O^-]$ ion which generates OH^- when water is added and (3) the cooperation of F^- and $[Al-OH]$.

The above mechanisms were proposed for the appearance of basic sites on KF/Al_2O_3 which had not been pretreated at a high temperature around 623 K. ^{19}F MAS NMR studies of the pretreated KF/Al_2O_3 suggested that the state of F show-

ing a peak at $-135 \text{ ppm}^{50,51}$) or a peak at -150 ppm is relevant to the catalytic activities.⁵¹⁾

Figueras et al. studied ^{19}F NMR of $\text{KF}/\alpha\text{-Al}_2\text{O}_3$ and $\text{KF}/\gamma\text{-Al}_2\text{O}_3$ with different loadings of KF .⁵³⁾ The peaks ascribed to liquid-like F^- , KF , and K_3AlF_6 were identified by ^{19}F NMR. With $\text{KF}/\alpha\text{-Al}_2\text{O}_3$, all three species were observed. With $\text{KF}/\gamma\text{-Al}_2\text{O}_3$, no peaks ascribed to liquid-like F^- and KF were observed; nearly all KF reacted with $\gamma\text{-Al}_2\text{O}_3$ when $\gamma\text{-Al}_2\text{O}_3$ was impregnated with KF aqueous solution. KF species appeared by decomposition of K_3AlF_6 at higher temperatures for $\text{KF}/\gamma\text{-Al}_2\text{O}_3$. Considering that $\text{KF}/\alpha\text{-Al}_2\text{O}_3$ exhibits catalytic activity without pretreatment and that $\text{KF}/\gamma\text{-Al}_2\text{O}_3$ shows significant activity only after activation at high temperature as reported,⁵³⁾ the authors concluded that KF reproduced on Al_2O_3 is the catalytically active phase of $\text{KF}/\text{Al}_2\text{O}_3$ catalysts.

Calorimetric measurement for CO_2 adsorption indicates that $\text{KF}/\alpha\text{-Al}_2\text{O}_3$ is a stronger base than $\text{KF}/\gamma\text{-Al}_2\text{O}_3$. Higher catalytic activity of $\text{KF}/\alpha\text{-Al}_2\text{O}_3$ than that of $\text{KF}/\gamma\text{-Al}_2\text{O}_3$ was observed for a number of base-catalyzed reactions; isophorone isomerization,⁵⁴⁾ Michael addition of 2-cyclohexen-1-one to nitroalkanes,⁵³⁾ transesterification of diethyl carbonate with alcohols to unsymmetrical carbonates.^{55,56)}

The state of F is also different on $\alpha\text{-Al}_2\text{O}_3$ and on $\gamma\text{-Al}_2\text{O}_3$. ^{19}F MAS NMR

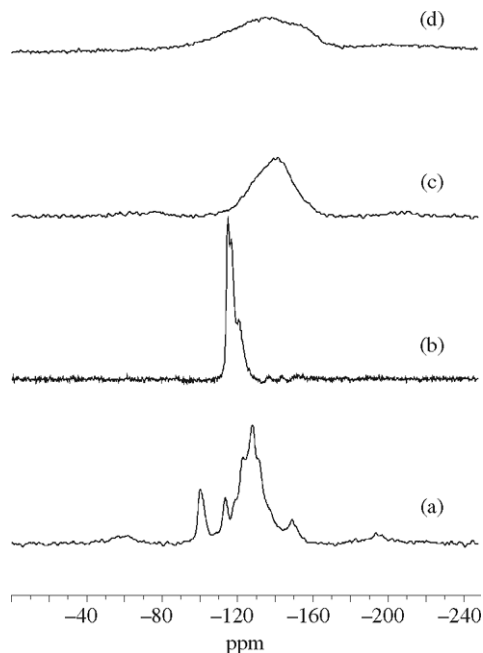


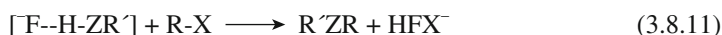
Fig. 3.8.3 ^{19}F -MAS NMR spectra of (a) $\text{CsF}/\alpha\text{-Al}_2\text{O}_3$ stored at ambient condition, (b) $\text{CsF}/\alpha\text{-Al}_2\text{O}_3$ after vacuum treatment at 723 K , (c) $\text{CsF}/\gamma\text{-Al}_2\text{O}_3$ stored at ambient conditions and (d) after vacuum treatment at 723 K .

Reprinted with permission from J.-M. Clacens, D. Genuit, B. Veldurthy, G. Bergeret, L. Delmotte, A. Garcia-Ruiz, F. Figueras, *Appl. Catal. B*, **53**, 95 (2004) Fig. 3.

spectra of CsF/ α -Al₂O₃ and CsF/ γ -Al₂O₃ either kept in air or dried in a vacuum at 723 K are shown in Fig. 3.8.3.⁵⁷⁾ CsF/ γ -Al₂O₃ measured in air gives a single broad line at -128 to 142 ppm which could be assigned to Cs₃AlF₆. This line was not displaced by heat treatment. CsF/ α -Al₂O₃ showed a more complex spectrum with at least three species. A line at -100 ppm, which disappeared upon evacuation at 723 K, was attributed to a hydrated fluoride, for instance, CsF·2H₂O. A line at -115 ppm, which grew in intensity upon dehydration and could be assigned to the intact CsF species, and a line at -128 ppm was attributed to Cs₃AlF₆.

B. Catalytic properties

KF is known to act as a base in a wide variety of organic reactions.⁵⁸⁾ A typical reaction that KF promotes is the hydrogen-bond-assisted reaction shown in eq. 3.8.11.⁵⁹⁾



The idea originates from the strong hydrogen bond between the F⁻ anion and a protic compound HZR' as a result of the large electron density of the small F⁻. The electron density (nucleophilicity of Z) is enhanced, and various types of nucleophilic substitution can be promoted in the presence of KF.

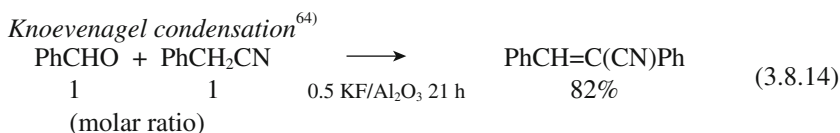
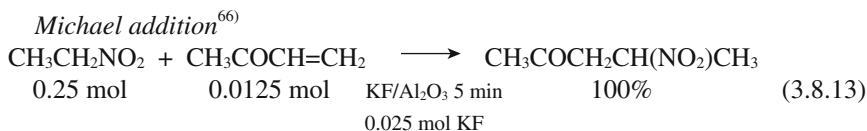
Ando and Yamawaki first found that KF supported on Celite was an efficient reagent for the alkylation of various protic compounds.⁶⁰⁾ Later, they found KF/Al₂O₃ to be the most efficient reagent for alkylation.⁶¹⁾ An example is shown in eq. 3.8.12.

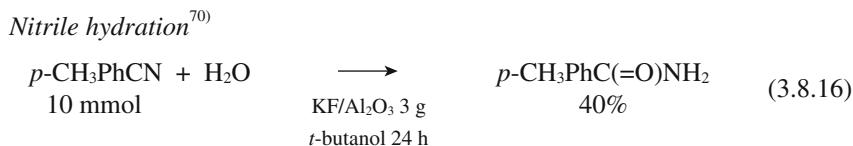
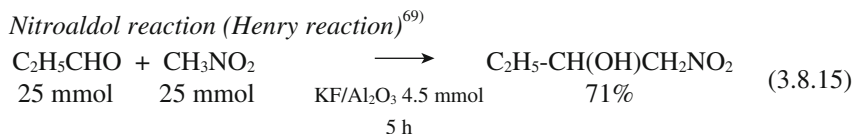


This reaction is not a catalytic reaction; KF/Al₂O₃ acts as a reagent.

The other reactions which are promoted in the presence of KF/Al₂O₃ include the Wittig reaction,⁶²⁾ Wittig-Honor reaction,^{62,63)} Danzens condensation^{63,64)} and alkene-, acetylene-forming elimination.⁶⁴⁾ In these reactions too, KF/Al₂O₃ acts as a reagent.

KF/Al₂O₃ acts also as a catalyst for a wide variety of base-catalyzed reactions such as Michael addition,⁶⁴⁻⁶⁷⁾ Knoevenagel condensation,^{62-64,66,68)} nitroaldol reaction (Henry reaction),⁶⁹⁾ nitrile hydration,⁷⁰⁾ and elimination.⁶⁴⁾ Selected examples of these reactions are shown below. All the reactions were carried out at room temperature.





For these reactions, $\text{KF/Al}_2\text{O}_3$ was used without any pretreatment or after heated at 473 K to dry. It was revealed later that the activity of $\text{KF/Al}_2\text{O}_3$ varies greatly with the pretreatment temperature under a vacuum. As shown in Fig. 3.8.4, all the activities for the isomerization of 1-pentene,⁷¹⁾ the isomerization of 2,3-dimethyl-1-butene,⁷¹⁾ the Tishchenko reaction of benzaldehyde,⁵¹⁾ and the disproportionation of trimethylsilylacetylene⁵⁰⁾ changed markedly with the pretreatment temperature. The activity for the Michael addition of nitromethane to butene-2-one, however, did not change much with the pretreatment temperature.⁷¹⁾ The strong dependency of the activity on the pretreatment temperature indicates that new active sites are generated by outgassing at about 623 K in addition to the active sites present without pretreatment as done in usual practice.

$\text{CsF/Al}_2\text{O}_3$ also acts as an efficient catalyst for base-catalyzed reactions such as Michael addition and transesterification.⁷²⁾ The catalytic activity is higher when CsF is supported on $\alpha\text{-Al}_2\text{O}_3$ than on $\gamma\text{-Al}_2\text{O}_3$. $\text{CsF}/\alpha\text{-Al}_2\text{O}_3$ is more active than $\text{KF}/\alpha\text{-Al}_2\text{O}_3$ for Michael addition of nitroalkanes to cyclohexen-1-one at 323 K.

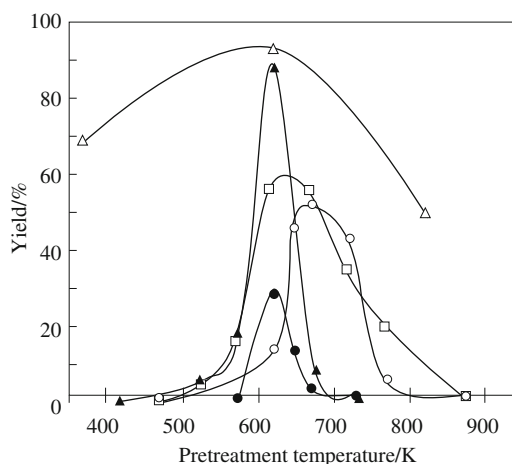


Fig. 3.8.4 Variations in the activities of $\text{KF/Al}_2\text{O}_3$ for (△) Michael addition of nitromethane to butene-2-one, (▲) 1-pentene isomerization, (□) disproportionation of trimethylsilylacetylene, (○) self-condensation of benzaldehyde, (●) 2,3-dimethyl-1-butene isomerization as a function of pretreatment temperature.

The conversions of the Michael addition of nitroethane to cyclohexen-1-one in 50 min were about 90, 60, 10 and 10% for CsF/ α -Al₂O₃, KF/ α -Al₂O₃, KF/ γ -Al₂O₃, and CsF/ γ -Al₂O₃, respectively. For the transesterification of diethyl carbonate by 1-phenylethanol at 403 K, α -Al₂O₃-supported CsF and KF are more active as compared to γ -Al₂O₃-supported CsF and KF.⁵⁶⁾ A quantitative yield was achieved in 0.45 h over CsF/ α -Al₂O₃, and in 5 h over KF/ α -Al₂O₃, while 57% and 36% yields were obtained for CsF/ γ -Al₂O₃ in 12 h and KF/ γ -Al₂O₃ in 12 h, respectively.

The first order rate constants of the transesterification of diethyl carbonate by 1-phenylethanol are plotted against the number of strong basic sites adsorbing CO₂ with an enthalpy > 120 kJ mol⁻¹ for various solid base catalysts (Fig. 3.8.5).⁵⁵⁾ A rough correlation appears between the number of the basic sites and the rate, but CsF/ α -Al₂O₃ falls well away from the line. The specificity of CsF/ α -Al₂O₃ was explained by a large Pauling radius of Cs (0.169 nm) as compared with K (0.133 nm). Because of the large radius of Cs⁺ ion, the alkoxide anion formed by proton abstraction from alcohol is weakly coordinated to the surface Cs⁺ cation, and more negatively charged. The alkoxides conjugated with Cs⁺ are believed to constitute “naked anions” exhibiting enhanced nucleophilicity. Therefore, it is believed that the Cs-alkoxides constitute weakly coordinated species that enhance nucleophilicity to a degree that affects the rate of nucleophilic attack on diethyl carbonate, resulting in a high rate.

KF/Al₂O₃ is used as a base which is generally required for Miyaura-Suzuki coupling reactions. Kabalka et al. used KF/Al₂O₃-supported Pd⁰ for the coupling reaction of iodobenzene and arylboronic acid to form 4-methylbiphenyl in a yield of 88–98% in 4 h at 373 K.⁷³⁾ The use of KF/Al₂O₃ as a support of Pd for Miyaura-Suzuki coupling reactions has been reported for several other reactions.^{74,75)}

Pd(0)/bis-phosphine complex catalyzes amination of halopyridine in the pres-

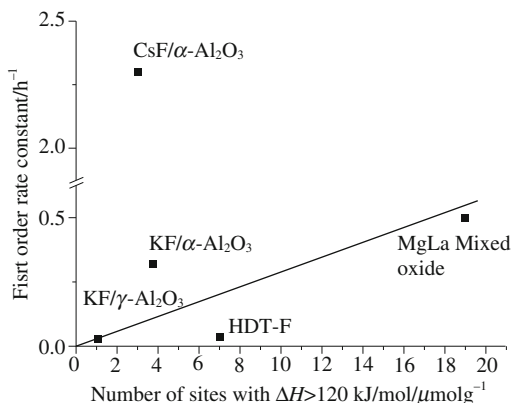


Fig. 3.8.5 Correlation between the reaction rate constant and the number of strong basic sites, adsorbing CO₂ with an enthalpy > 120 kJ mol⁻¹. Reprinted with permission from B. Veldurthy, J.-M. Clacens, F. Figueras, *J. Catal.*, **229**, 237 (2005) Fig. 5.

ence of strong bases such as sodium *t*-butoxide. Instead of a strong base, KF/Al₂O₃ can be used. Amination of various halopyridines with amines takes place at 350–373 K over Pd-phosphine supported on KF/Al₂O₃.⁷⁶⁾

3.8.5 KNH₂/Al₂O₃

KNH₂/Al₂O₃ is also a unique solid base catalyst in the sense that basic sites are not oxygen atoms or ions on the surface, and exhibits high activity particularly in double bond migration of unsaturated compounds.^{77,78)} The catalyst was found in the course of investigation of the supported metal catalysts prepared by impregnation with ammoniacal solution of alkali metals. Among the catalysts prepared from the ammoniacal solutions, K(NH₃)/Al₂O₃ and Na(NH₃)/Al₂O₃ prepared by impregnation of alumina with ammoniacal solution of K and Na, respectively, showed extraordinary high activity for a base-catalyzed reaction when pretreated in the temperature range 400–600 K.⁷⁹⁾ The catalysts could promote 1-pentene isomerization even at 201 K. This activity is far higher than that of the Na/Al₂O₃ prepared by the vapor deposition of Na metal on Al₂O₃. Based on the studies of the active species in K(NH₃)/Al₂O₃ by IR spectroscopy and TPD, it was revealed that the active species in K(NH₃)/Al₂O₃ is KNH₂ on Al₂O₃. This finding was confirmed by the very high activity of the KNH₂/Al₂O₃ prepared by direct loading of KNH₂ on Al₂O₃ as described below.

Alumina and a small amount of Fe₂O₃ (a catalyst for converting K into KNH₂ in liquid ammonia) are heated in the reactor under a vacuum at 773 K for 3 h. A piece of potassium metal is then put into the reactor under nitrogen. After evacuation, ammonia is liquefied into the reactor to dissolve the metal. Blue color due to solvated electrons disappears in about 10 min, indicating the formation of KNH₂. After 1 h, the reactor is warmed to room temperature to remove most of the ammonia and then heated at 573 K for 1 h under a vacuum.

The catalytic activity varies with KNH₂ loading as well as heat-treatment temperature. Fig. 3.8.6 shows effect of the loaded amount of K on the catalytic activity for isomerization of 2,3-dimethyl-1-butene at 201 K.⁷⁷⁾ The activity was negligible up to a loading of 3 wt%, which is almost equal to the amount of OH groups on the surface, indicating that the OH groups on the Al₂O₃ surface react with KNH₂ and that the resulting K compounds are inactive. The activity increased as the loading exceeded 3 wt% and reached maximum at 8–10 wt% loading. Fig. 3.8.7 shows the variation in the activity of KNH₂/Al₂O₃ for 2,3-dimethyl-1-butene isomerization at 201 K as a function of the evacuation temperature. The catalytic activity strongly depends on the heating temperature and gives the maximum at about 573 K. At 673 K, the activity declines sharply. Although KNH₂ supported on alumina has been proposed as a base catalyst, the catalyst was used after drying at a low temperature of 338 K.⁸⁰⁾ However, high temperature treatment at about 573 K is indispensable for KNH₂/Al₂O₃ to show the potential activities for various base-catalyzed reactions.⁷⁹⁾

The NH₂ groups in KNH₂/Al₂O₃ undergo H exchange with H₂, CH₄, C₂H₆, and 3-methylbut-1-ene. The H exchange of 3-methyl-1-butene is involved in the double

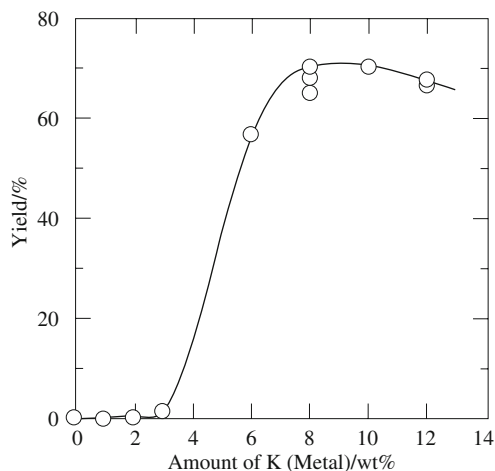


Fig. 3.8.6 Dependence of loaded amount of K on the catalytic activity of $\text{KNH}_2/\text{Al}_2\text{O}_3$ for the isomerization of dimethyl-1-butene (24 mmol) at 201 K. Reaction time; 10 min. Catalyst; 63 mg. Reprinted with permission from Y. Ono, T. Baba, *Catal. Today*, **38**, 321 (1997) Fig. 2.

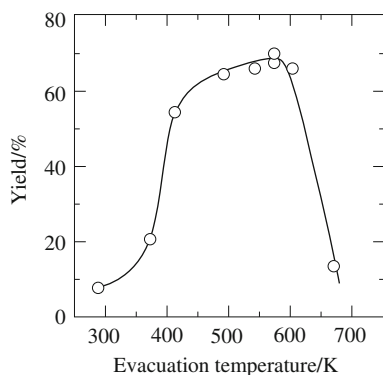


Fig. 3.8.7 Influence of the evacuation temperature on the catalytic activity of $\text{KNH}_2/\text{Al}_2\text{O}_3$ for the isomerization of 2,3-dimethyl-1-butene (24 mmol) at 201 K. Reaction time; 10 min. Catalyst; 63 mg. K-loading; 8 wt% as K. Reprinted with permission from Y. Ono, T. Baba, *Catal. Today*, **38**, 321 (1997) Fig. 3.

bond migration. Hydrogen atoms in 3-methyl-1-butene are incorporated into the NH_2 groups of the catalyst during the double bond migration.

The H exchange ability of the NH_2 , together with the fact that the activity declines by decomposition of the NH_2 groups to N_2 and H_2 above 600 K, indicates that the N atoms in NH_2 groups act as basic sites. The N atoms abstract an H^+ from the reactants to form anionic intermediates. This is dissimilar to most of the other solid base catalysts in which O atoms act as the basic sites.

$\text{KNH}_2/\text{Al}_2\text{O}_3$ shows catalytic activities also for the double bond isomerization of alkenes,⁷⁹⁾ the double bond isomerization of unsaturated amines to enamines,⁸¹⁾

the dimerization of phenylacetylene,⁸²⁾ the disproportionation of trimethylsilylacetylene,⁸³⁾ and the reaction of diethylsilane with toluene to diethylbenzylsilane.⁸⁴⁾

References

1. J. Shen, R. D. Cortright, Y. Chen, J. A. Dumesic, *J. Phys. Chem.*, **98**, 9067 (1994).
2. H. Zou, X. Ge, J. Shen, *Thermochemica Acta*, **397**, 81 (2003).
3. S. Srinivasan, C. R. Narayanan, A. K. Datye, *Appl. Catal. A*, **132**, 289 (1995).
4. P. Berteau, S. Ceckiewicz, B. Delmon, *Appl. Catal.*, **31**, 361 (1987).
5. P. Berteau, M.-A. Kellens, B. Delmon, *J. Chem. Soc. Faraday Trans.*, **87**, 1425 (1991).
6. H. Zou, X. Ge, J. Shen, *Thermochemica Acta*, **397**, 81 (2003).
7. E. A. Paukshtis, P. I. Soltanov, E. N. Yurchenko, K. Jiratova, *Coll. Czech. Chem. Commun.*, **47**, 2044 (1982).
8. S. Srinivasan, C. R. Narayanan, A. K. Datye, *Appl. Catal. A: General*, **132**, 289 (1995).
9. J. C. Lavalley, A. Janin, J. Preud'homme, *React. Kinet. Catal. Lett.*, **18**, 85 (1981).
10. A. B. Mohammed Saad, O. Saur, Y. Wang, C. P. Tripp, B. A. Morrow, J. C. Lavalley, *J. Phys. Chem.*, **99**, 4620 (1995).
11. T. Yamaguchi, Y. Wang, M. Komatsu, M. Ookawa, *Catal. Surv. from Jpn.*, **5**, 81 (2002).
12. T. Yamaguchi, M. Ookawa, *Catal. Today*, **116**, 191 (2006).
13. T. Yamaguchi, J.-H. Zhu, Y. Wang, M. Komatsu, M. Ookawa, *Chem. Lett.*, **26**, 989 (1997).
14. T. Ito, J. H. Lunsford, *Nature*, **314**, 721 (1985); T. Ito, J.-X. Wang, C.-H. Lin, J. H. Lunsford, *J. Am. Chem. Soc.*, **107**, 5062 (1985).
15. M. M. Abraham, Y. Chen, L. A. Boatner, R. W. Reynolds, *Phys. Rev. Lett.*, **37**, 849 (1976).
16. Y. Chen, H. T. Tohver, J. Narayan, M. M. Abraham, *Phys. Rev. B*, **16**, 5535 (1977).
17. J. B. Lacy, M. M. Abraham, O. J. L. Boldu, Y. Chen, J. Narayan, H. T. Tohver, *Phys. Rev. B*, **18**, 4136 (1978).
18. D. N. Olson, V. M. Orera, Y. Chen, M. M. Abraham, *Phys. Rev. B*, **21**, 1258 (1980).
19. T. Matsuda, Y. Sasaki, H. Miura, K. Sugiyama, *Bull. Chem. Soc. Jpn.*, **58**, 1041 (1985).
20. U. K. Diez, C. R. Apesteguia, J. I. Di Cosimo, *Catal. Today*, **63**, 53 (2000).
21. T. Thomasson, O. S. Tyagi, H. Knözinger, *Appl. Catal. A*, **181**, 181 (1999).
22. J. I. Di Cosimo, V. K. Ciez, C. R. Apesteguia, *Appl. Catal. A*, **137**, 149 (1996).
23. E. L. Jablonski, I. M. J. Vilella, S. C. Marina, S. R. deMignel, O. A. Salza, *Catal. Commun.*, **7**, 18 (2006).
24. A. Z. Khan, E. Ruchenstein, *J. Catal.*, **143**, 1 (1993).
25. T. Kanno, M. Kobayashi, *Bull. Chem. Soc. Jpn.*, **66**, 3806 (1993).
26. C. Trionfetti, I. V. Barich, K. Seshan, L. Lefferts, *Topics Catal.*, **39**, 191 (2006).
27. R. Bal, B. B. Tope, T. K. Das, S. G. Hegde, S. Sivasanker, *J. Catal.*, **204**, 358 (2001).
28. R. Bal, K. Chauhari, S. Sivasanker, *Catal. Lett.*, **70**, 75 (2000).
29. R. Bal, B. B. Tope, S. Sivasanker, *J. Mol. Catal. A*, **181**, 161 (2002).
30. R. Bal, S. Sivasanker, *Appl. Catal. A*, **246**, 373 (2003).
31. Y. Shimasaki, K. Ariyoshi, H. Kambe, H. Yano, S. Ugamura, *J. Mol. Catal. A*, **256**, 37 (2006).
32. Y. Shimasaki, H. Yano, K. Ariyoshi, H. Kambe, *J. Mol. Catal. A*, **239**, 125 (2005).
33. M. Ueshima, Y. Shimasaki, K. Ariyoshi, H. Yano, H. Tsuneki, *Proc. 10th Intern. Congr. Catal. Budapest, 1992*, p. 2447, Elsevier (1993).
34. F. King, G. J. Kelly, *Catal. Today*, **73**, 75 (2002).
35. G. J. Kelly, F. King, M. Kett, *Green Chem.*, **4**, 392 (2002).
36. L. B. Sun, F. N. Gu, Y. Chun, J. Yang, Y. Wang, J. H. Zhu, *J. Phys. Chem. C*, **112**, 4978 (2008).
37. L. B. Sun, Y. Chun, F. N. Gu, M. B. Yue, Q. Yu, Y. Wang, J. H. Zhu, *Mater. Lett.*, **61**, 2130 (2007).
38. Z. Y. Wu, Q. Jiang, Y. M. Wang, H. J. Wang, L. B. Sun, L. Y. Shi, J. H. Xu, Y. Wang, Y. Chu, J. H. Zhu, *Chem. Mater.*, **18**, 4600 (2006).
39. L. B. Sun, F. N. Gu, Y. Chun, J. H. Kou, J. Yang, Y. Wang, J. H. Zhu, Z. G. Zou, *Micropor. Mesopor. Mater.*, **116**, 498 (2008).
40. M. Zamora, T. Lopez, R. Gomez, M. Asomoza, R. Melendrez, *Appl. Surf. Sci.*, **252**, 828 (2005).
41. M. Zamora, T. Lopez, R. Gomez, M. Asomoza, R. Melendrez, *Catal. Today*, **107-108**, 289 (2005).
42. M. Zamora, T. Lopez, M. Asomoza, R. Melendrez, R. Gomez, *Catal. Today*, **116**, 234 (2006).
43. A. Auroux, P. Artizzu, I. Ferino, V. Solinas, G. Leofanti, M. Padovan, G. Messina, R. Mansani, *J. Chem. Soc. Faraday Trans.*, **91**, 3263 (1995).

44. Y. Wang, W. Y. Huang, Y. Chun, J. R. Xia, J. H. Zhu, *Chem. Mater.*, **13**, 670 (2001).
45. F. Wang, T. Tsai, W. Lin, *Catal. Lett.*, **73**, 215 (2001).
46. L. M. Weinstock, J. M. Stevenson, S. A. Tomellini, S.-H. Pan, T. Utne, R. B. Jobson, D. F. Reinhold, *Tetrahedron Lett.*, **27**, 3845 (1986).
47. T. Ando, J. H. Clark, D. G. Cork, T. Hanafusa, J. Ichihara, T. Kimura, *Tetrahedron Lett.*, **28**, 1421 (1987).
48. T. Ando, *Stud. Surf. Sci. Catal.*, **90**, 9 (1994).
49. T. Ando, S. J. Brown, J. H. Clark, D. G. Clark, T. Hanafusa, J. Ichihara, J. Miller, M. S. Robertson, *J. Chem. Soc. Perkin Trans. 2*, **1986**, 1133.
50. T. Baba, A. Kato, H. Takahashi, F. Toriyama, H. Handa, Y. Ono, H. Sugisawa, *J. Catal.*, **176**, 488 (1998).
51. H. Handa, T. Baba, H. Sugisawa, Y. Ono, *J. Mol. Catal.*, **134**, 171 (1998).
52. H. Kabashima, H. Tsuji, S. Nakata, Y. Tanaka, H. Hattori, *Appl. Catal. A*, **194-195**, 227 (2000).
53. J.-M. Clacens, D. Genuit, L. Delmotte, A. Garcia-Ruiz, G. Bergeret, R. Montiel, J. Lopez, F. Figueras, *J. Catal.*, **221**, 483 (2004).
54. F. Figueras, J. Lopez, J. Sanchez-Valente, T. T. H. Vu, J.-M. Clacens, J. Palomeque, *J. Catal.*, **211**, 144 (2002).
55. B. Veldurthy, J.-M. Clacens, F. Figueras, *J. Catal.*, **229**, 237 (2005).
56. B. Veldurthy, J.-M. Clacens, F. Figueras, *Eur. J. Org. Chem.*, **18**, 1972 (2005).
57. J.-M. Clacens, D. Genuit, B. Veldurthy, G. Bergeret, L. Delmotte, A. Garcia-Ruiz, F. Figueras, *Appl. Catal. B*, **53**, 95 (2004).
58. J. H. Clark, *Chem. Rev.*, **80**, 429 (1980).
59. J. H. Clark, J. M. Miller, *J. Am. Chem. Soc.*, **99**, 498 (1977).
60. T. Ando, J. Yamawaki, *Chem. Lett.*, **8**, 45 (1979).
61. J. Yamawaki, T. Ando, *Chem. Lett.*, **8**, 755 (1979).
62. F. Texier-Boullet, D. Villemin, M. Ricard, H. Moison, A. Foucaud, *Tetrahedron*, **1985**, 41.
63. D. Villemin, *Chem. Ind. (London)*, **1985**, 166.
64. J. Yamawaki, T. Kawata, T. Ando, T. Hanafusa, *Bull. Chem. Soc. Jpn.*, **56**, 1885 (1983).
65. P. Laszlo, P. Pennetreau, *Tetrahedron Lett.*, **26**, 2645 (1985).
66. D. Villemin, *J. Chem. Soc., Chem. Commun.*, **1983**, 1092.
67. J. H. Clark, D. G. Cork, M. S. Robertson, *Chem. Lett.*, **12**, 1145 (1983).
68. D. Villemin, M. Ricard, *Tetrahedron Lett.*, **25**, 1059 (1984).
69. J.-M. Melot, F. Texier-Boullet, A. Foucaud, *Tetrahedron Lett.*, **27**, 493 (1986).
70. C. G. Rao, *Synth. Comm.*, **12**, 177 (1982).
71. T. Tsuji, H. Kabashima, H. Kita, H. Hattori, *React. Kinet. Catal. Lett.*, **56**, 363 (1995).
72. J.-M. Clacens, D. Genuit, B. Veldurthy, G. Bergeret, L. Delmotte, A. Garcia-Ruiz, F. Figueras, *Appl. Catal. B*, **53**, 95 (2004).
73. G. W. Kabalka, R. M. Pagni, C. M. Hair, *Org. Lett.*, **1**, 1423 (1999).
74. D. Villemin, F. Caillot, *Tetrahedron Lett.*, **42**, 637 (2001).
75. B. Basu, P. Das, M. H. Bhuiyan, S. Jha, *Tetrahedron Lett.*, **44**, 3817 (2003).
76. B. Basu, S. Jha, N. K. Mridha, M. H. Bhuiyan, *Tetrahedron Lett.*, **43**, 7967 (2002).
77. Y. Ono, T. Baba, *Catal. Today*, **38**, 321 (1997).
78. B. Bouri, J. A. Dadeh, P. Pumpf, C. R. Hebd, *Seances Acad. Sci. Ser. C*, **267**, 167 (1968).
79. T. Baba, H. Hatada, Y. Ono, *J. Chem. Soc. Faraday Trans.*, **90**, 187 (1994).
80. A. J. Hubert, *J. Chem. Soc. (C)*, **1968**, 975.
81. H. Handa, T. Baba, H. Yamada, T. Takahashi, Y. Ono, *Catal. Lett.*, **44**, 119 (1997).
82. T. Baba, A. Kato, H. Handa, Y. Ono, *Catal. Lett.*, **47**, 77 (1997).
83. T. Baba, A. Kato, H. Takahashi, F. Toriyama, H. Handa, Y. Ono, *J. Catal.*, **176**, 488 (1998).
84. T. Baba, A. Kato, H. Yuasha, F. Toriyama, H. Handa, Y. Ono, *Catal. Today*, **44**, 271 (1998).

3.9 Metal Oxides and Carbon Materials Loaded with Alkali Metals

Addition of alkali metals to certain types of metal oxides results in the formation of strong basic sites. In 1955, Pines reported that Al_2O_3 became highly active for double bond migration of alkenes when modified with Na metal.¹⁾ This is one of

the earlier papers on solid base catalysts. Following Pines, there have been a considerable number of papers describing alkali metal addition to various types of metal oxides and carbons. The metal oxides to which alkali metals were added include Al_2O_3 , SiO_2 , MgO , CaO and zeolites. Carbon materials in different forms were also used for modification by the metals. In all cases, enhancement or generation of basic sites were observed. Enhancement or generation of basic sites is more effective by alkali metal than by alkali metal cation. The mechanisms for forming basic sites by addition of alkali metals and alkali metal cations vary.

Alkali metal-modified zeolites are described in section 4.2.3.

3.9.1 Preparation of Alkali Metal-modified Catalysts

Modification of metal oxides and carbons with alkali metals is performed in several different ways. Three methods are frequently employed. The first method is to expose the metal oxides to alkali metal vapor. Predried metal oxide or carbon and alkali metal are placed together in a vessel and heated to slightly above the melting point of the alkali metal to generate alkali metal vapor. The metal oxide or carbon is exposed to the vapor of alkali metal. The second method is also exposure of the metal oxide to alkali metal vapor, but the vapor is produced by the decomposition of alkali azide above the decomposition temperature of the alkali azide in a vacuum. Alkali azides decompose to yield alkali metal vapor and nitrogen. The third method is to impregnate the metal oxide with alcoholic solutions of alkali azide followed by the controlled decomposition of the azide in a vacuum or flowing inert gas. One other method is impregnation with the ammoniacal solution of an alkali metal.

There are many variations of the above three methods for addition of alkali metals. As one specific way to prepare a strong solid base, $\text{Na}/\text{NaOH}/\text{Al}_2\text{O}_3$ is described below as an example.²⁾ To 30 g of calcined $\gamma\text{-Al}_2\text{O}_3$ 5 g of NaOH was added in portions at 583–593 K with stirring under a flowing N_2 flow to remove water vapor generated. The stirring was continued for 3 h to give a white solid. Then 1.2 g of Na metal was added, and the reaction mixture was stirred for 1 h at the same temperature to finally yield a pale blue solid.

It should be noted that the states of alkali metals are not necessarily metallic on the surface of the metal oxide support. In most cases, the alkali metals added change to the ionic state.

3.9.2 State of Alkali Metal

In the literature published in 1950's, the alkali metals added on the supports were supposed to be in a metallic state. The catalytic reactions were well interpreted by a catalysis by alkali metals. Later, spectroscopic measurements revealed that the alkali metals were transformed to the ionic state.

The MgO modified with Na metal gave an ESR signal with a g value of 2.004 assigned to an F^+ center which was formed by electron trapped in an oxygen vacancy.³⁾ The electron is released from Na metal which turns to Na^+ ion. The ESR signal intensity increased with the added Na metal to reach maximum.

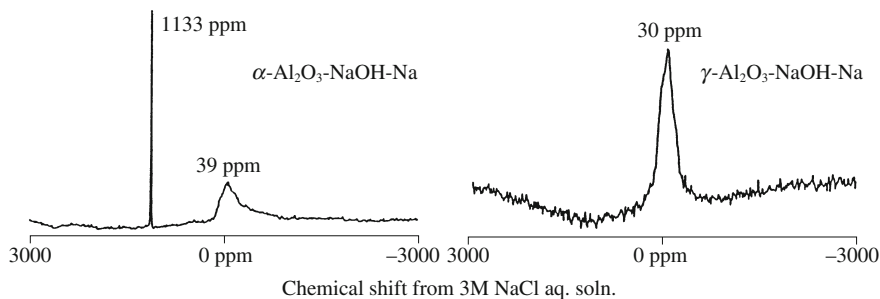


Fig. 3.9.1 ^{23}Na MAS NMR spectra of $\alpha\text{-Al}_2\text{O}_3\text{-NaOH-Na}$ (left) and $\gamma\text{-Al}_2\text{O}_3\text{-NaOH-Na}$ (right). Reprinted with permission from G. Suzukamo, M. Fukao, T. Hibi, K. Tanaka, M. Minobe, *Stud. Surf. Sci. Catal.*, **108**, 649 (1997) Fig. 2.

Further increase in the amount of Na metal added to MgO resulted in a decrease in the signal intensity. The F^+ center traps one more electron to form a diamagnetic F center, which is the oxygen vacancy trapping two electrons. Strong basic sites generated by the addition of Na metal to MgO are proposed to be O^{2-} ions adjacent to $\text{Mg}^{2+}\text{-[e]}$ (F^+ center) or $\text{Mg}^{2+}\text{-[ee]}$ (F center) as will be shown later.

The state of Na in $\text{Na/NaOH/Al}_2\text{O}_3$ prepared by addition of NaOH and Na metal to α - and $\gamma\text{-Al}_2\text{O}_3$ was examined by ^{23}Na MAS NMR.⁴⁾ The $\text{Na/NaOH/}\alpha\text{-Al}_2\text{O}_3$, which is inactive for base-catalyzed reactions, shows a peak of metallic Na at $\delta = 1133$ ppm, while the $\text{Na/NaOH/}\gamma\text{-Al}_2\text{O}_3$ shows only one peak at $\delta = 30$ ppm, which is assigned to the Na^+ ion. Even when Na metal was added, all Na species were ionized on the surface of $\text{Na/NaOH/}\gamma\text{-Al}_2\text{O}_3$ (Fig. 3.9.1).

3.9.3 Strength of Basic Sites

The strength of basic sites generated by modification with alkali metals was estimated by indicator method, TPD of CO_2 , XPS of O_{1s} , and catalytic performance in base-catalyzed reactions.

Kijenski and Malinowski measured the strength of basic sites of MgO, MgO loaded with NaOH (NaOH/MgO), and MgO loaded with Na metal (Na/MgO).⁵⁾ The maximum strength of the basic sites of each sample was $27 < H_- < 33$ for MgO and NaOH/MgO and $H_- > 35$ for Na/MgO ; all MgO samples were pretreated at 823 K in Ar. Loading alkali metals is more effective in enhancing the basic strength. Gorzawski and Hölderich prepared $\text{Na/NaOH/Al}_2\text{O}_3$ and Na/NaOH/MgO and measured the basic strength by indicator method. While the basic strength of both of Al_2O_3 and MgO was $9.3 < H_- < 15$, that of $\text{Na/NaOH/Al}_2\text{O}_3$ and Na/NaOH/MgO was $35 < H_- < 37$.⁶⁾

TPD of CO_2 showed that Na metal-loaded Al_2O_3 possessed stronger basic sites than Na^+ ion-loaded Al_2O_3 . More strong basic sites appeared on the sample prepared by loading Na metal on Na^+ ion-loaded Al_2O_3 . TPD of CO_2 is shown in Fig. 3.9.2 for these three samples.⁷⁾

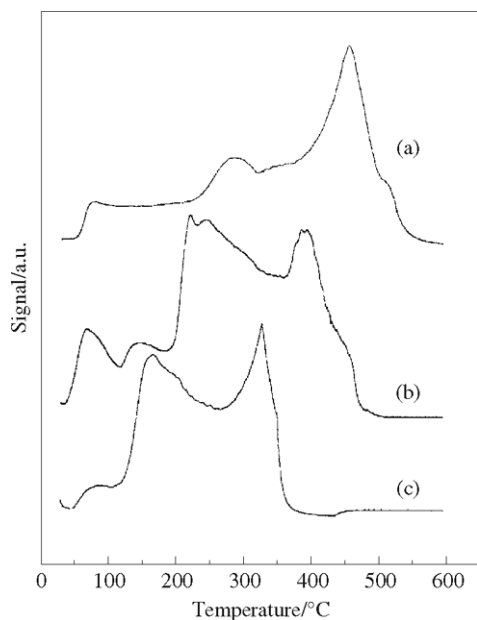


Fig 3.9.2 TPD analysis of CO_2 for (a) $\text{Na}/\text{NaOH}/\gamma\text{-Al}_2\text{O}_3$, (b) $\text{Na}/\gamma\text{-Al}_2\text{O}_3$ and $\text{NaOH}/\gamma\text{-Al}_2\text{O}_3$. Reprinted with permission from H.-J. Kim, B.-S. Kang, M.-J. Kim, Y. M. Park, D.-K. Kim, J.-S. Lee, K.-Y. Lee, *Catal. Today*, **93–95**, 315 (2004) Fig. 4.

XPS of O_{1s} binding energy also supported the above order of the three alkali-modified Al_2O_3 samples.⁷⁾ The XPS peaks shifted to lower binding energies in the order Al_2O_3 , $\text{NaOH}/\text{Al}_2\text{O}_3$, $\text{Na}/\text{Al}_2\text{O}_3$ and $\text{Na}/\text{NaOH}/\text{Al}_2\text{O}_3$, indicating that the

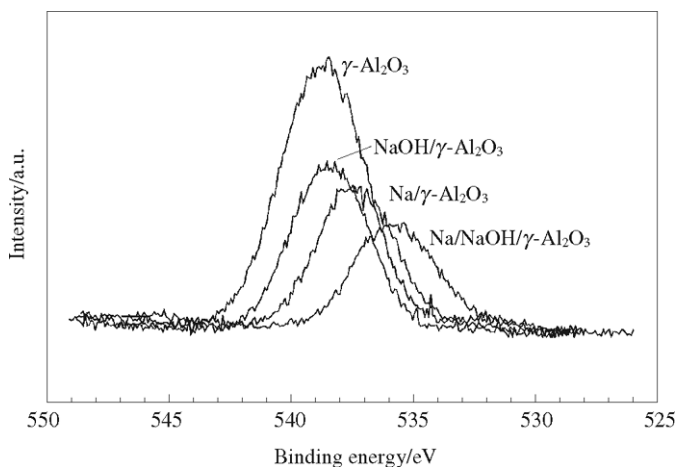


Fig. 3.9.3 XPS analysis of O_{1s} orbital. Reprinted with permission from H.-J. Kim, B.-S. Kang, M.-J. Kim, Y. M. Park, D.-K. Kim, J.-S. Lee, K.-Y. Lee, *Catal. Today*, **93–95**, 315 (2004) Fig. 3.

basic strength increased in the same order (Fig. 3.9.3). The same change in O_{1s} binding energy was reported by Suzukamo et al.⁴⁾

Enhancement of basic sites of MgO by alkali metal loading was evidenced by TPD of CO_2 .⁸⁾

3.9.4 Model of Basic Sites

A model has been proposed by Matsuhashi et al. for the generation of strongly basic sites on addition of alkali metals to MgO, as shown in Fig. 3.9.4 on the basis of ESR measurements as described in section 3.9.2.³⁾ When an alkali metal is adsorbed on the surface, it releases an electron to form the alkali cation. The electron released from the alkali metal is trapped in a single oxygen vacancy on the subsurface to form an electron (F^+ center) or paired electrons (F center). The three O^{2-} ions existing on the (111) microplane neighboring the F^+ center or F center are the strong basic sites.

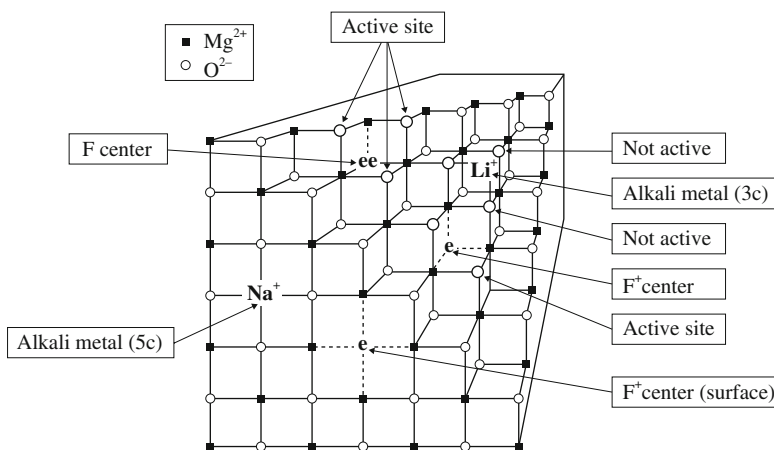
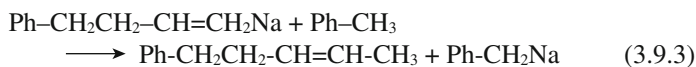
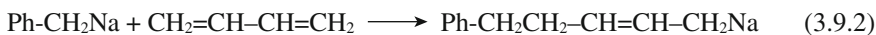
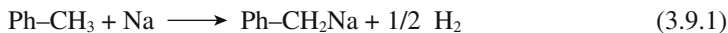


Fig. 3.9.4 Model structure of superbasic sites on alkali metal-loaded MgO. Reprinted with permission from H. Matsuhashi, M. Oikawa, K. Arata, *Langmuir*, **16**, 8201 (1997) Fig. 7.

3.9.5 Catalytic Properties

A. Alkali metal-modified MgO and CaO

The effect of alkali metal on alkaline earth oxide was examined long ago for the Na/CaO system in the addition of butadiene to alkylaromatic hydrocarbons.⁹⁾ For the addition of butadiene to toluene, Na and K metals added to CaO afforded 5-phenyl-2-pentene at 364–366 K. Side-chain alkylation occurred. It was proposed that the reaction was initiated by the metalation of toluene with Na metal to form benzylna which underwent 1,4-addition to butadiene followed by trans-metalation. In the proposed mechanism, the active component is Na metal on the surface of CaO, and participation of basic sites was not considered.



The idea that the alkali metal added to the metal oxide is directly involved in the reaction was proposed in early papers, but it became more common to consider the basic sites generated by the addition of alkali metals as active sites for the reactions occurring on the alkali metal-modified metal oxides. Participation of the basic sites generated by modification with Na metal was suggested for the decomposition of methyl formate to CO and H₂ at 473 K,¹⁰⁾ and for the formation of pentenes and heptenes from a mixture containing equal amounts of propene and ethylene over K metal-modified MgO at 483 K.¹¹⁾ The high activity of Na metal-modified MgO for double bond isomerization of 3-methyl-1-butene was also considered to be due to the strong basic sites (lattice O²⁻) existing on the (111) microplane neighboring the F⁺ or F centers which are formed by modification of MgO with Na metal.¹²⁾

Kijenski and Malinowski reported that MgO modified with Na vapor showed high activity for double bond isomerization of 1-pentene and 1-hexene at 298 K. They supposed two mechanisms: a ion-type mechanism involving basic sites and a radical-type mechanism involving one electron donor site.¹³⁾

Kijenski et al. studied side-chain alkylation of aromatics such as toluene, ethylbenzene, cumene and xylene with ethylene and propene.¹⁴⁾ Based on ESR measurement of the adsorbed states of the reactants as well as catalyst poisoning by the radical trap TEMPO (2,2,6,6-tetramethylpiperidine-1-oxyl) they proposed the active sites to be F⁺ centers formed by the modification of MgO with K metal and not to be basic sites.

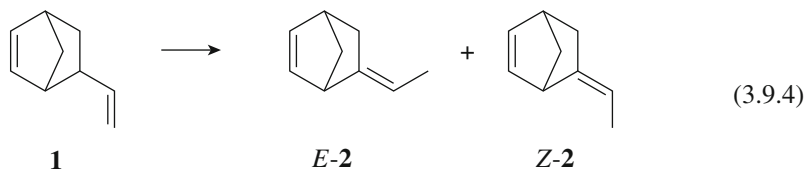
B. Alkali metal-loaded Al₂O₃

In 1955, Pines et al. reported that Na metal loaded on Al₂O₃ exhibited high activities for double bond isomerization of 1-butene and 1-decene, and dehydrogenation of limonene to *p*-cymene.¹⁾ It was suggested that the reaction proceeded via carbanions as reaction intermediates. This paper triggered the study of solid base catalysts. Pines et al. successively reported high activities of Na metal-modified Al₂O₃ for 1-pentene isomerization¹⁵⁾ and side-chain alkylation of alkyl aromatics such as toluene, cumene, xylene and indane with ethylene.¹⁶⁾ High activity of alkali metal-modified Al₂O₃ for double bond isomerization of 1-butene was demonstrated by O'Grady et al.^{17,18)} The reaction proceeded even at 213 K.

Alkali metal-modified Al₂O₃ was used as the catalyst for other reactions such as hydrogenation of ethylene, H₂-D₂ exchange,¹⁹⁾ and hydrogenation of conjugated dienes to monoolefins. Until the 1970's alkali metals dispersed on Al₂O₃ were considered to be the active sites for the reactions.

Suzukamo et al. prepared a strong basic catalyst Na/NaOH/Al₂O₃ as described

in section 3.9.1. The catalyst is effective for the isomerization of 5-vinylbicyclo[2.2.1]hept-2-ene **1** to 5-ethylidenebicyclo[2.2.1]hept-2-ene **2**, which is an important third comonomer of ethene-propene synthetic rubber, and actually used in the industrial process. The reaction proceeds completely even at 243 K.^{2,4,21)}



Na/NaOH/Al₂O₃ exhibits high activity also for the double bond isomerization of 4-methyl-1-pentene, 2,3-dimethyl-1-butene to 2,3-dimethyl-2-butene, and safrol to isosafrol.

In addition, Na/NaOH/Al₂O₃ is an effective catalyst for the side-chain alkylation of alkylbenzenes such as cumene, toluene and ethylbenzene with olefins such as ethylene and propylene. For these side-chain alkylation reactions, K/KOH/Al₂O₃ is much more active than the Na/NaOH/Al₂O₃. Alkylation of cumene with ethylene proceeded at 313 K.

Although Na metal is added to NaOH/Al₂O₃, the state of Na in Na/NaOH/Al₂O₃ is not metallic but ionic, which was confirmed by ²³Na MAS NMR as described in section 2.8. The binding energy of O_{1s} observed by XPS was lower for K/KOH/Al₂O₃ than for Na/NaOH/Al₂O₃, suggesting that the surface O is more electron-rich for the former than the latter, corresponding to the activities for the side-chain alkylation. Accordingly, it is plausible that the active sites on Na/NaOH/Al₂O₃ are the basic surface O atoms created by the addition of NaOH and Na metal to Al₂O₃.

Seki et al. prepared Na metal-modified mesoporous Al₂O₃ by impregnation with NaN₃ followed by decomposition, and measured its catalytic activities for double bond migration of 2,3-dimethyl-1-butene to 2,3-dimethyl-2-butene and α -pinene to β -pinene²²⁾. A high activity was obtained for the former reaction due to generation of strong basic sites, and a high selectivity was observed for the latter reaction due to suppression of acidic sites.

C. Alkali metal-loaded carbon

Foley's group prepared a Cs metal-modified nanoporous carbon catalyst by exposure of the carbogenic molecular sieves with a pore-size distribution centered around 0.5 nm and surface area of about 1000 m² g⁻¹ to Cs metal vapor.²³⁾ The resulting materials showed high activity for 1-butene isomerization at 273 K and side-chain alkylation of toluene with propene at 423 K.²⁴⁾ A high *cis* to *trans* ratio of 9 in the 1-butene isomerization was indicative of an allylic carbanion intermediate. A high *iso* to normal ratio of butylbenzene in the side chain alkylation also indicated an anionic rather than free-radical mechanism.²⁵⁾ For the benzene coupling to biphenyl in the temperature range 423–623 K, anion radicals of benzene were suggested to be the intermediates.²⁶⁾

The same catalyst enhanced the catalytic activity for aldol condensation of acetone to isophorone when the catalyst was oxidized by exposure to air.²⁷⁾ Crystalline form of CsOH formed. The resulting catalyst was much more active than the carbogenic molecular sieves impregnated with CsOH solution.

References

1. H. Pines, J. A. Vesely, V. N. Ipatieff, *J. Am. Chem. Soc.*, **77**, 347 (1955).
2. G. Suzukamo, M. Fukao, M. Minobe, *Chem. Lett.*, **16**, 585 (1987).
3. H. Matsuhashi, M. Oikawa, K. Arata, *Langmuir*, **16**, 8201 (2000).
4. G. Suzukamo, M. Fukao, T. Hibi, K. Tanaka, M. Minobe, *Stud. Surf. Sci. Catal.*, **108**, 649 (1997).
5. J. Kijeński, S. Malinowski, *J. Chem. Soc. Faraday Trans. 1*, **74**, 250 (1978).
6. H. Gorzawski, W. F. Hoelderich, *J. Mol. Catal. A*, **144**, 181 (1999).
7. H.-J. Kim, B.-S. Kang, M.-J. Kim, Y. M. Park, D.-K. Kim, J.-S. Lee, K.-Y. Lee, *Catal. Today*, **93-95**, 315 (2004).
8. T. Kanno, M. Kobayashi, *Bull. Chem. Soc. Jpn.*, **66**, 3806 (1993).
9. G. G. Eberhardt, H. Peterson, *J. Org. Chem.*, **30**, 82 (1965).
10. T. Ushikubo, H. Hattori, K. Tanabe, *Chem. Lett.*, **13**, 649 (1984).
11. N. Sun, K. Klabunde, *J. Catal.*, **185**, 506 (1999).
12. H. Matsuhashi, K. Arata, *J. Phy. Chem.*, **99**, 11178 (1995).
13. J. Kijeński, S. Malinowski, *React. Kinet. Catal. Lett.*, **3**, 343 (1975).
14. J. Kijeński, P. Radomski, E. Fedoryńska, *J. Catal.*, **203**, 407 (2001).
15. W. O. Haag, H. Pines, *J. Am. Chem. Soc.*, **82**, 387 (1960).
16. H. Pines, J. A. Vesely, V. N. Ipatief, *J. Am. Chem. Soc.*, **77**, 554 (1955).
17. T. M. O'Grady, R. M. Alm, M. C. Hoff, *Preprints, Meeting, Am. Chem. Soc. (Pet. Div.), 136th, Atlantic City, New Jersey*, 4 (1959) B65, Cited in [18].
18. H. Pines, W. M. Stalick, in: *Base-Catalyzed Reactions of Hydrocarbons and Related Compounds*, Chap.2, p.25, Academic Press (1977).
19. S. E. Voltz, *J. Phys. Chem.*, **61**, 756 (1957).
20. A. J. Hubert, *J. Chem. Soc. C*, **1967**, 2149.
21. G. Suzukamo, M. Fukao, T. Hibi, K. Tanaka, K. Chikaishi, in: *Acid-Base Catalysis*, (ed. K. Tanabe, H. Hattori, T. Yamaguchi, T. Tanaka), p.405, Kodansha-VCH (1989).
22. T. Seki, S. Ikeda, M. Onaka, *Micropor. Mesopor. Mater.*, **96**, 121 (2006).
23. H. C. Foley, *Micropor. Mater.*, **4**, 407 (1995).
24. M. G. Stevens, H. C. Foley, *Chem. Commun.*, **1997**, 519.
25. M. G. Steven, M. R. Anderson, H. C. Foley, *Chem. Commun.*, **1999**, 413.
26. M. G. Stevens, K. M. Sellers, S. Subramoney, H. C. Foley, *Chem. Commun.*, **1998**, 2679.
27. M. G. Stevens, D. Chen, H. C. Foley, *Chem. Commun.*, **1999**, 275.

4.

Preparation and Catalytic Properties of Solid Base Catalysts — II. Specific Materials for Solid Bases

4.1 Hydrotalcite and Mixed Oxides Derived from Hydrotalcite

Hydrotalcite and related materials are very important catalysts and catalyst precursors. The synthesis, structure and catalytic application of hydrotalcite have been reviewed by several authors.¹⁻³⁾ The catalytic aspects of hydrotalcite have also been reviewed.^{4,5)}

4.1.1 Structure of Hydrotalcite

Hydrotalcite is a natural mineral with the approximate formula $\text{Mg}_6\text{Al}_2(\text{OH})_{16}\text{CO}_3 \cdot 4\text{H}_2\text{O}$. The structure of hydrotalcite consists of positively charged, brucite-like hydroxide layers with negatively charged interlayers. In brucite, the magnesium cation is octahedrally surrounded by hydroxyl groups; the resulting octahedral share edges to form infinite sheets. In hydrotalcite, some of the magnesium ions in the brucite layer are isomorphously replaced by Al^{3+} ions. In natural hydrotalcite, CO_3^{2-} ions exist in the interlayers.

The composition of hydrotalcite can be modified in various ways. The composition of $\text{Mg}/(\text{Mg} + \text{Al})$ ratio, x , is changeable. Thus, the composition can be expressed as $[\text{Mg}_{1-x}\text{Al}_x(\text{OH})_2]^{x+}[\text{CO}_3^{2-}]_{x/2} \cdot n\text{H}_2\text{O}$. The value of x can be varied from about 0.1 to 0.34.^{6,7)} The materials are often called layered double hydroxide. By synthesis, Mg can be isomorphously replaced by Zn, Fe, Co, Ni, Cu, while Al can be replaced by Cr, Fe, In.

The interlayer anion, CO_3^{2-} , can be replaced by a wide variety of anions, as described below. The layer spacings depend on the nature of the interlayer anions and the state of hydrostatic attraction between the layers and interlayer anions. The modified hydrotalcite materials are often called hydrotalcite-like materials.

A layered double hydroxide, $[\text{Al}_2\text{Li}(\text{OH})_6]_2\text{CO}_3$ is also used as a source of Al_2O_3 - Li_2O mixed oxide, which exhibits catalytic activities for various base-catalyzed reactions.^{8,9)}

As for the base catalysts, Mg, Al-containing hydrotalcite with CO_3^{2-} ions are most often used as starting materials. The description in this section deals with these materials unless otherwise noted.

4.1.2 Synthesis of Hydrotalcite

The various ways to prepare hydrotalcite-like materials has been reviewed.^{2,10)} The most common way is coprecipitation followed by hydrothermal treatment. A homogeneous precipitation method using urea hydrolysis is also proposed to give well-defined particles of controlled sizes.¹¹⁻¹⁶⁾ The production of hydrotalcite in a continuous mode (in-line dispersion-precipitation method) was demonstrated by Abelló et al.¹⁷⁾ Preparation by sol-gel method is also a very useful method.¹⁸⁻²¹⁾ Comparative study of coprecipitation method, urea method, and sol-gel method on the morphology, crystal size and catalytic activity for aldol condensation of acetone was reported by Greenwell et al.¹⁶⁾ Typical examples of the preparation methods are given below.

A. Coprecipitation method²²⁾

Aqueous solutions containing 0.3 mol of $\text{MgCl}_2 \cdot 6\text{H}_2\text{O}$, 0.1 mol of $\text{AlCl}_3 \cdot 6\text{H}_2\text{O}$, 0.8 mol of NaOH and 0.02 mol of Na_2CO_3 were slowly mixed under vigorous stirring, maintaining the pH between 8 and 10, at 343 ± 5 K. The precipitate formed was aged in the mother liquor at this temperature for 15 h under stirring, and was then washed several times until the solution was free of chloride ions. The products were dried at 313 K. They contain both Cl^- and CO_3^{2-} as charge compensating ions.

The exchange of Cl^- anions was performed by contacting the hydrotalcite with a solution of Na_2CO_3 ; 2 g of the dried sample was dispersed in a 1.5×10^{-3} M solution of Na_2CO_3 and stirred at 343 K for 2 h. After filtration, the solids were washed and dried at 313 K. In order to achieve a higher degree of exchange, a successive exchange was carried out.

Aging or hydrothermal treatment is often performed to improve the crystallinity.^{2,23)} The time required for aging can greatly be shortened by microwave irradiation.²⁴⁻²⁶⁾ Microwave irradiation also modifies the textural properties, giving larger surface area.²⁶⁾

To obtain better solid base catalysts, the exchange of Cl^- ions in the precipitate with CO_3^{2-} is essential since the Cl^- ions in the calcined samples markedly reduce the adsorption amount of CO_2 and the catalytic activity for base-catalyzed reactions.^{18,22,27)} The effect of Cl^- ions in the mixed oxides is also evidenced by the adsorption capacity and heat of adsorption of CO_2 .²⁸⁾ The catalytic activity of rehydrated hydrotalcite is also retarded by the presence of Cl^- in the starting hydrotalcite.¹⁸⁾ Thus metal nitrates are often used instead of chlorides.

B. Sol-gel method¹⁸⁾

A 0.15 mol sample of magnesium ethoxide is dissolved by acid hydrolysis with HCl or HNO_3 in ethanol; the solution is refluxed at 353 K under constant stirring. A second solution, containing a suitable amount of aluminum acetylacetonate in a 1 : 1 mixture of acetone/ethanol in order to obtain $\text{Mg}^{2+}/\text{Al}^{3+}$ ratios in the range of 3 - 6, is slowly added, and the pH is adjusted at about 10 with NH_4OH . Water in molar amounts equal to the Mg^{2+} content is then slowly added. The solution is

refluxed at 353 K up to 17 h until gel formation. The gel is stirred into a 10^{-1} M Na_2CO_3 aqueous solution to exchange Cl^- ions coming from HCl. The samples are repeatedly washed in deionized water and then dried overnight at 353 K.

4.1.3 Thermal Decomposition of Hydrotalcite

The thermal decomposition of hydrotalcite has been studied extensively. Below 473 K, only interstitial water is lost. Though XRD shows that the layer structure is retained by dehydration,²⁷ ^{27}Al MAS NMR indicates that a certain amount of tetrahedrally coordinated Al appears at this temperature. Around 500 K, dehydroxylation of brucite layers starts. Between 523 K and 673 K, both carbon dioxide and more water by the dehydroxylation are lost. On calcination at 623 K to 973 K, the periclase (MgO) structure is formed, probably containing Al in solid solution²⁹ (Fig. 4.1.1). On calcination at 1273 K, XRD shows the presence of MgAl_2O_4 together with periclase, and the MgAl_2O_4 structure cannot be reconstructed into hydrotalcite structure by rehydration.

SEM analysis of the periclase phase shows retention of the original morphology of hydrotalcite, indicating that during the thermal decomposition steam and carbon dioxide escape through holes in the surface.³⁰

^{27}Al MAS NMR shows that as-synthesized hydrotalcite shows a single resonance (+10 ppm) due to octahedral aluminum. After the sample is heated to 723 K, a shoulder develops at +75 ppm due to tetrahedral aluminum, in addition to octahedrally coordinated aluminium in periclase.³⁰⁻³²

XPS shows that Mg/Al ratio at the surface of the calcined material is less than the bulk composition, indicating that the Al is not randomly distributed but concentrated near the surface.³³ These findings indicate that magnesium aluminate-type species are located at the outer surface of periclase-type $\text{MgO-Al}_2\text{O}_3$ solid solution. Therefore, the effect of the surface phase cannot be neglected in the surface properties of the calcined hydrotalcite.

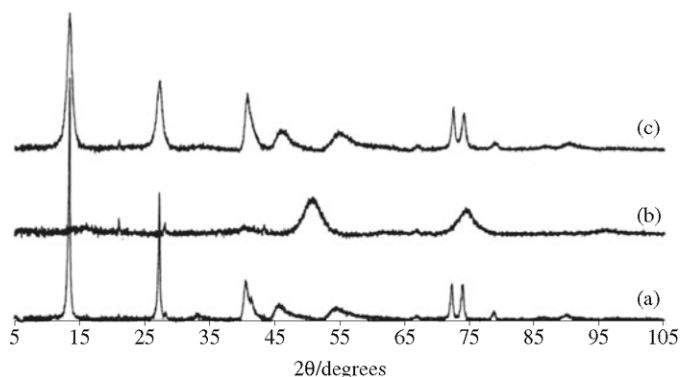


Fig. 4.1.1 XRD patterns of (a) as-synthesized hydrotalcite, (b) hydrotalcite calcined at 723 K and (c) hydrotalcite rehydrated in water.

Reprinted with permission from F. Winter, A. Jos van Dillen, K. P. de Jong, *J. Mol. Catal., A*, **219**, 273 (2004) p.275 Fig.2.

The surface area increases by calcination from $\sim 50 \text{ m}^2\text{g}^{-1}$ of as-synthesized hydrotalcite. The surface area shows maximum at the calcination temperature of 723–773 K ($200\text{--}270 \text{ m}^2\text{g}^{-1}$). The mixed oxides derived from hydrotalcite by sol-gel method exhibits 10–25% higher surface area than that by the coprecipitation method.¹⁹⁾

4.1.4 Rehydration of Calcined Hydrotalcite

Although hydrotalcite is converted to the periclase structure by calcination, this reaction is reversible, provided that the upper temperature does not exceed 773–873 K.^{29,30,34)}

XRD shows that hydration of the calcined product results in the reconstruction of the original structure²⁹⁾(Fig. 4.1.1). This phenomenon is known as the memory effect. When the calcined sample is rehydrated by exposure to atmosphere or liquid water, ²⁷Al NMR spectrum shows only the signal due to octahedral aluminum, indicating also that the original structure is restored.³²⁾

Rehydration can be carried out either by exposing calcined hydrotalcite in nitrogen saturated with water vapor or by immersing calcined hydrotalcite in decarbonated water. The rate of rehydration depends on the calcination temperature of the original hydrotalcite and the temperature of rehydration.³⁵⁾ The hydrotalcite reconstructed contains OH⁻ ions in the interlayers. When rehydration is carried out in air or non-decarbonated water, CO₃²⁻ ions are incorporated in the interlayers.

Various anions can be incorporated by utilizing the memory effect.³⁶⁾ When calcined hydrotalcite is rehydrated in aqueous solution containing anions, the original hydrotalcite structure is reconstructed and the corresponding anions are incorporated in the interlayers. By this method large anions such as *p*-toluenesulfonate and polyoxometalate (V₁₀O₂₈)⁶⁻ or (Mo₇O₂₄)⁶⁻ can be incorporated.

4.1.5 Introduction of Anions into Interlayers

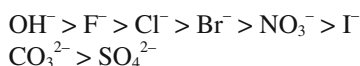
Anions can be introduced into interlayers mainly by four methods: (a) synthesis, (b) anion exchange, (c) reconstruction (memory effect) and (d) chemical reaction.

(a) By synthesis

Anions can be introduced into interlayers through the synthesis step by using compounds having the desired anions. The anions introduced by this method include CO₃²⁻, Cl⁻, NO₃⁻, ClO₄⁻, ⁻OCO(CH₂)₁₂COO⁻, terephthalate, alkoxides. When hydrotalcite with anions other than CO₃²⁻ is prepared, exposure to air must be avoided and decarbonated water has to be used in all the synthetic procedures, since CO₂ is easily incorporated as carbonate from the atmosphere.

(b) By ion exchange

Hydrotalcite or its analogues are anion exchangers. The order of stability for anions is approximately as follows.³⁷⁾



Multiply charged anions are much more stable than monovalent anions. Complex anions such as $\text{Fe}(\text{CN})_6^{3-}$, $\text{Fe}(\text{CN})_6^{4-}$, $\text{Co}(\text{CN})_6^{3-}$, NiCl_4^{2-} , polyoxometalate ions and alkylbenzenesulfonate ions can also be introduced by the anion exchange method.

tBuO^- ions can be incorporated by exchanging NO_3^- ions in the layers with 0.1 M solution of potassium *t*-butoxide in THF.^{38,39)} The material is a very active catalyst for base-catalyzed reactions, as described below.

(c) Under reconstruction conditions

Various anions can be incorporated in the interlayers of hydrotalcite structure by using the memory effect. The most important application with respect to base catalysis is the incorporation of OH^- ions from pure water. F^- ions can also be incorporated from an aqueous solution of KF .⁴⁰⁾ The strongly basic ions, tBuO^- and isopropylamide ions, can also be introduced by the addition of calcined hydrotalcite to a solution of $\text{KO}^\text{t} \text{Bu}$ and lithium diisopropylamide, respectively, in THF.^{41,42)} L-Proline anion can be incorporated into the interlayers by using the memory effect.^{43,44)}

(d) By chemical reactions

Exchange of halide ions in the interlayers of hydrotalcite materials can be achieved by the reaction with alkyl halide. I^- (or Br^-) ions in $\text{Zn}_2\text{Cr}(\text{OH})_6\text{I}\cdot 2\text{H}_2\text{O}$ (or $\text{Zn}_2\text{Cr}(\text{OH})_6\text{Br}\cdot 2\text{H}_2\text{O}$) can be substituted with Br^- (or I^-) ions by the reaction with alkyl bromides (or iodide) in liquid phase (363 K) and in vapor phase (423 K).⁴⁵⁾ Fig. 4.1.2 shows the reaction of $\text{Mg}_6\text{Al}_2(\text{OH})_{16}\text{Cl}_2$ and alkyl halides.⁴⁶⁾ The reaction was carried out using 1 g of hydrotalcite ($\text{Cl}^- = 3.3 \text{ mmol}$) and 33 mmol of alkyl halide in toluene at 353 K. In the case of benzyl bromide, 92% of Cl^- ions was replaced by Br^- ions in 30 min. The rate of the substitution depends on the alkyl groups. The order is isobutyl < isopropyl < butyl \approx propyl \ll benzyl. The

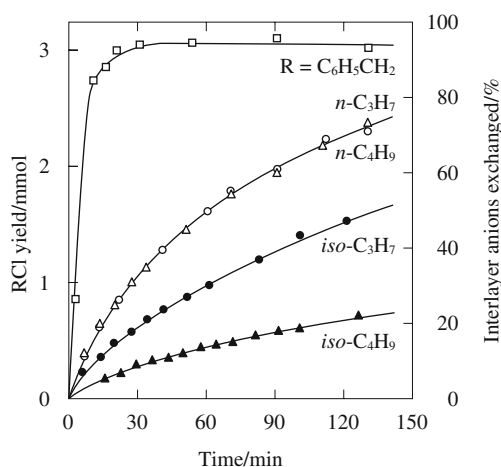
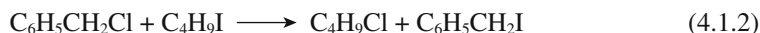


Fig. 4.1.2 Time course of the reaction of Cl^- containing hydrotalcite with alkyl bromide. Conditions: hydrotalcite 1 g ($\text{Cl}^- = 3.3 \text{ mol}$), alkyl bromide 33 mmol in toluene, 353 K. Reprinted with permission from T. Matsui, E. L. Salinas, E. Suzuki, Y. Ono, *Trans. Mater. Res. Soc. Jpn.*, **15A**, 145 (1994).

rate is also solvent dependent: DMSO > DMF > toluene. These orders are in general agreement with the reaction rates of alkyl halide in nucleophilic substitution reactions. Since benzyl bromide cannot penetrate into the interlayers, the reaction can occur only at the edges of the layers. The dependence of the rate on the alkyl groups shows that the rate-determining step is the chemical reaction at the edges, but not the diffusion of anions in the interlayers. Using these phenomena, hydrotalcite containing halide ions can be used as catalysts for halide substitution reactions.^{47,48)}



Substitution of CN^- ions in hydrotalcite with benzyl chloride proceeds to form benzyl cyanide.⁴⁹⁾ Chloride ligands of $[\text{NiCl}_4]^{2-}$ in interlayers are also completely removed by the reaction with $\text{C}_4\text{H}_9\text{Br}$ to form interstitial $[\text{NiBr}_4]^{2-}$ and $\text{C}_4\text{H}_9\text{Cl}$ in DMF.⁵⁰⁾

4.1.6 Application of Hydrotalcite-derived Materials to Base Catalysis

Hydrotalcite is used extensively as the basic catalyst for many organic reactions. The base catalysts derived from hydrotalcite can be divided into two categories. In the first group, the catalysts retain the hydrotalcite layer structure, though the interlayer anion is changeable. In the second category, the catalysts are mixed oxides, which are obtained by calcination of materials with the hydrotalcite structure.

A. Catalysis by as-synthesized hydrotalcite

For many reactions, the as-synthesized form of hydrotalcite is not catalytically active and the mixed oxides derived from hydrotalcite are much more active than the as-synthesized form. But for certain reactions, high activities of as-synthesized hydrotalcite are observed.

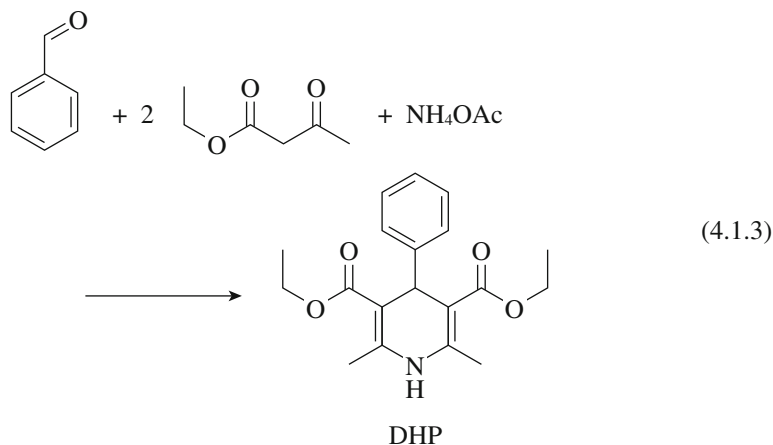
Constantino and Pinnavaia studied the reaction of 2-methyl-3-butyn-2-ol (MBOH) over hydrotalcite, $[\text{Mg}_{2.34}\text{Al}(\text{OH})_{6.68}](\text{CO}_3)_{0.5} \cdot 2.6\text{H}_2\text{O}$, heat-treated at various temperatures in a He flow for 2 h.⁵¹⁾ The results are shown in Table 2.5.8. In every case, the reaction products are acetone and acetylene. This indicates the basic nature of the catalysts [see section 2.5.4]. At 423 K, all of the hydrotalcite-derived catalysts exhibited high MBOH conversion. However, the reaction at 353 K clearly shows that hydrotalcite activated below the structural decomposition temperature (≤ 523 K) is an order of magnitude more active than the metal oxides generated at 723 K. The removal of water from the interlayer has a large effect on the catalytic activity. The results indicate that the nature of the basic sites of the dehydrated hydrotalcite and those on the mixed oxide derived from hydrotalcite are quite different.

A Ni-Al hydrotalcite-like compound was prepared by a urea hydrolysis method and its catalytic activity for Knoevenagel condensation studied.¹⁴⁾ When dried at 423 K, the material had the composition of $[\text{Ni}_{0.73}\text{Al}_{0.27}(\text{OH})_2](\text{CO}_3)_{0.135}$. Aliphatic and aromatic aldehydes react with ethyl cyanoacetate or malononitrile without solvent at 333 K. However, the material is not active for the condensation of benzaldehyde with dimethyl malonate ($\text{p}K_a = 13$). The base strength of the material by the indicator method was estimated to be $H_- = 11-11.8$. These results show that the base strength of the as-synthesized Ni, Al-hydrotalcite is weaker than the mixed oxide obtained by calcination of Mg-Al hydrotalcite.

As-synthesized hydrotalcite is active for Michael addition of 2-methylcyclohexane-1,3-dione, 2-acetylcyclopentanone, and 2-acetylcyclohexanone to methyl vinyl ketone.³¹⁾ The catalytic activity depends on the Mg/Al ratio of the materials. Calcined materials are also effective for these addition reactions. For Michael addition with less acidic donors, however, neither as-synthesized nor calcined hydrotalcites are active.⁵²⁾ The activity develops only after the calcined hydrotalcite is rehydrated.

Kishore and Kantam found that as-synthesized hydrotalcite materials are very efficient catalysts for isomerization of some alkenes, namely, safrole to isosafrole, eugenol to isoeugenol and estragole to anethole [see 6.1.5]⁵³⁻⁵⁵⁾. The as-synthesized materials are far more active than the mixed oxides. The active sites are considered to be the OH groups on the edges or the outer surface of hydrotalcite.

As-synthesized hydrotalcite is useful for the synthesis of Hantzsch dihydropyridine (DHP) by the condensation of benzaldehyde, ethyl acetate and ammonium acetate at room temperature.⁵⁶⁾



Hydrotalcite with Mg/Al = 2 gave a yield of 61% in 6.5 h using acetonitrile as solvent. Besides benzaldehyde, furfural and 2-methylpropanal are also converted into dihydropyridines. Calcined hydrotalcite did not show significant conversion, indicating the necessity of structural hydroxyl groups.

As-synthesized hydrotalcite is also effective for the epoxidation of alkenes and sulfoxidation of thioethers with hydrogen peroxide [see section 5.12].

B. Catalysis by mixed oxides derived from hydrotalcite

In 1971, Miyata et al. showed the effects of calcination of hydrotalcite on its surface area, structure, acid and base properties.³⁷⁾ As described above, calcination of hydrotalcite at 500 to 800 K gives the oxide with the periclase structure. The surface area and the amount of basic sites show maximum values at around 773 K.

Earlier works on base catalysis over mixed oxides derived from hydrotalcites include the polymerization of propylene oxide⁵⁷⁾ and propiolactone,⁵⁸⁾ aldol condensation of acetone⁵⁹⁾ and aldol condensation between acetone and formaldehyde.⁶⁰⁾ Later, the reactions were extended to a variety of base-catalyzed reactions such as Knoevenagel condensation, aldol condensation, Michael addition, epoxidation of alkenes, transfer hydrogenation, transesterification and alkylation of phenol and aniline. Most of the reactions are described in Chapter 5.

Calcination of hydrotalcite-type materials is one of the standard methods for preparing mixed oxides because of their high surface area and chemical homogeneity, though the presence of other species such as magnesian aluminate on the surface must not be neglected.

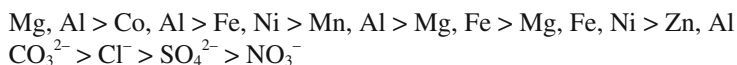
The base strength of hydrotalcite calcined at 723 K was estimated to be $18.0 > H_- \geq 17.2$ by an indicator method.⁵⁸⁾ On the other hand, Shaper et al. reported the base strength to be between 17.2 and 26.5 for the sample with Mg/Al ratio of 5 obtained by calcination at 773 K to 873 K.⁷⁾ Corma et al. estimated the base strength of calcined hydrotalcite by carrying out the condensation of benzaldehyde and molecules having activated methylene groups with different pK_a values in the presence of $MgO-Al_2O_3$ and concluded that this material shows basic sites with H_- value up to 16.5.⁶¹⁾ However, most of the basic sites show H_- values in the range 10.7–13.3, the base strength being higher than that of Cs^+ -exchanged X-zeolite or Cs^+ -exchanged sepiolite.⁶¹⁾

The TPD profiles of CO_2 on MgO , Al_2O_3 , and $MgO-Al_2O_3$ mixed oxides samples prepared by calcination of hydrotalcite with varying Mg/Al ratio was studied by Diez et al.⁶²⁾ The surfaces of MgO and the mixed oxides are not uniform and contain several types of adsorbed CO_2 . The TPD profiles are deconvoluted into three desorption peaks: a low temperature peak (L-peak) at 370 - 400 K, a middle temperature peak (M-peak) at 460 K and a high temperature peak (H-peak) at 550 K (Fig. 2.3.3, Table 2.3.1). The M-peak and H-peak are dominant on MgO and Mg_yAlO_x samples with $y \geq 1$. In Al rich samples ($y < 1$), the relative contributions of the M- and H-temperature peaks decrease with increasing Al content. Pure Al_2O_3 and $Mg_{0.11}AlO_x$ samples showed no contribution of the high-temperature peak in their TPD profiles. They also studied the IR spectrum of adsorbed CO_2 and observed bands due to several CO_2 species on the surface (Fig. 2.4.3). From the thermal stability of each band, they attributed L-, M-, and H-peaks to hydrogen-carbonate formed on basic OH groups, bidentate carbonates on metal-oxygen pairs and unidentate carbonates on low coordination oxygen anions, respectively.

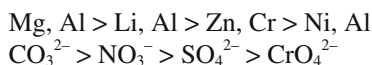
The mixed oxides also have acidic sites. An infrared study of adsorbed pyridine shows that acidity is entirely due to Lewis acid sites (the surface Mg^{2+} and Al^{3+} ions), and no Brønsted acid sites exist.³¹⁾ The acid strength is rather weak. Most pyridine desorbs by heating at 473 K, except for an Al rich sample ($x = 0.6$).

The catalytic activities of the mixed oxides prepared from a variety of hydrotalcite-like compounds have been tested. The activity is the highest for MgO-Al₂O₃ in most cases. The anions in the precursor hydrotalcite also influence the activity.

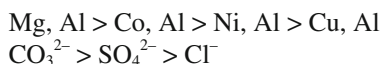
For Oppenauer oxidation of cyclohexanol with benzophenone,⁶³⁾



For vapor-phase aldol condensation of acetone and formaldehyde,⁶⁰⁾



For reductive dehydration of propiophenone with 2-propanol,⁶⁴⁾



For MgO-Al₂O₃, the basic character and catalytic activity depend on the Mg/Al ratio. The number of basic sites as determined by a titration method has the maximum value at Mg/Al = 3 ($x = 0.25$). The basicity also depends on the calcination temperature and the maximum value was obtained at a calcination temperature of ca. 773 K. The catalytic activity of the methanolysis of soybean oil showed maximum value when hydrotalcite with Mg/Al = 3 was calcined at 773 K.⁶⁵⁾ For alkylation of phenol with methanol, the highest activity was also observed at Mg/Al = 3.⁶⁾ In the isomerization of 1-pentene at 573 K, the sample with Mg/Al = 5 is more active than those with the ratio of 3 and 10.⁷⁾ For the transfer hydrogenation of phenylacetophenone with 2-propanol, the activity decreases in the order Mg/Al = 5 > 4 > 3.⁶⁴⁾ The activities of the mixed oxides are higher than that of MgO.

The structure of hydrocalmite is very similar to that of hydrotalcite, except that Ca and Al octahedral are accommodated in an orderly manner in the layers. Calcination of synthetic hydrocalmite [Ca₂Al(OH)₆]NO₃·mH₂O at 573, 773, and 873 K gives an amorphous pattern, CaO structure, and Ca₁₂Al₁₄O₃₃, respectively, their surface area being 116, 180 and 184 m²g⁻¹, respectively. Temperature programmed desorption of CO₂ shows that strong basic sites develop by calcination at higher temperatures. The material obtained by calcination at 973 K shows very high activity for the isomerization of 1-butene at 473 K.⁶⁶⁾

C. Catalysis by rehydrated hydrotalcite

As described above, hydrotalcite gives MgO-Al₂O₃ mixed oxide with periclase structure when calcined at 673 K to 773 K. The mixed oxide thus prepared recovers the materials with hydrotalcite (layered) structure when rehydrated. Rehydration occurs even under ambient conditions. In this case, CO₃²⁻ ions are incorporated in the interlayers by adsorbing carbon dioxide from the air. When rehydration is

performed without exposure to air, rehydrated materials contain OH^- ions in the interlayers. The structure is called the mexielite structure after the mineral having the composition $\text{Mg}_6\text{Al}_2(\text{OH})_{16}(\text{OH})_2 \cdot 4\text{H}_2\text{O}$. By rehydration, the surface area of materials usually decreases significantly.

In 1998, Figueras and coworkers reported that rehydrated hydrotalcite was a much more active catalyst for base catalyzed reactions such as aldol condensation, Knoevenagel reaction and cyanoethylation of alcohols.^{67,68)} The best performance for aldol condensation of benzaldehyde and acetone was obtained when hydrotalcite was calcined at 723 K and rehydrated under flowing nitrogen saturated with water for 7 h. The material thus obtained was over four times more active than the $\text{MgO-Al}_2\text{O}_3$ obtained by calcination.⁶⁸⁾ The number of basic sites and their strength as determined by calorimetry for CO_2 adsorption, however, showed lower basicity of the surface after rehydration. This indicates the difference in nature of the active sites, the active sites after rehydration being OH^- .⁶⁸⁾

The catalytic activity depends on the “water content” of the rehydrated catalysts. The maximum catalytic activity is usually observed when 30–40 wt% water is added to the calcined materials in aldol condensation reactions.^{69–71)}

Roelofs et al. also confirmed that rehydrated hydrotalcite is about six times more active than calcined hydrotalcite for the condensation of citral and acetone.⁷²⁾ The adsorption of CO_2 at 273 K is only 5% the amount of Al^{3+} (or the expected amount of OH^-). They suggested that only the OH^- ions located at the edges of hydrotalcite platelets are available and highly active for the condensation. Similar conclusions were also reached in the self-condensation of acetone.^{73,74)}

Abelló et al. studied the conditions of rehydration and their effects on the morphology and catalytic activity of the rehydrated materials: (1) rehydration in liquid phase leads to a much larger surface area ($200\text{--}400\text{ m}^2\text{g}^{-1}$) and much higher catalytic activity than that in gas phase ($15\text{ m}^2\text{g}^{-1}$), (2) in liquid phase rehydration, stirring speed shows a profound effect on the surface area of the rehydrated materials, (3) ultrasound irradiation is also useful for obtaining the high surface area material ($440\text{ m}^2\text{g}^{-1}$), (4) the higher surface area is the result of the exfoliation and formation of defects in the lamellar structure during rehydration, (5) the rates of the base catalyzed reactions, namely, the condensation of citral with acetone or methyl ethyl ketone and the epoxidation of styrene with hydrogen peroxide, are higher with the rehydrated samples with higher surface area.^{75,76)} The effectiveness of ultrasound during reconstruction was confirmed by the enhanced catalytic activity in the epoxidation of styrene with hydrogen peroxide.⁷⁷⁾ The high catalytic performance was attributed to the formation of defects in the lamellar structure of the small hydrotalcite particles.

Greenwell et al. prepared hydrotalcite by three different methods: coprecipitation, urea hydrolysis and sol-gel method.¹⁶⁾ Greater activity for aldol condensation was observed for the rehydrated hydrotalcite materials prepared by urea hydrolysis. These samples exhibited large crystallites with higher aspect ratios and improved crystallinity compared to coprecipitated or sol-gel samples. From these results, the authors suggest that it is less likely that basic sites are situated only at crystalline edges. Essentially the same results have been reported by Lei et al.⁷⁸⁾

Many more examples showing that rehydrated hydrotalcite exhibits higher activity than calcined hydrotalcite are found in the literature. Such reactions include Michaels addition⁵²⁾ and oxidation of benzothiophene with hydrogen peroxide.⁷⁹⁾ On the other hand, the mixed oxide was more active in the conversion of triglyceride transesterification with methanol.⁸⁰⁾

D. Catalysis by hydrotalcite with $t\text{BuO}^-$, F^- and diisopropylamide anions t -Butoxy ions can be incorporated in the interlayer by ion exchange method with potassium t -butoxide in THF.³⁸⁾ The material is very active for a variety of aldol condensation reactions (section 5.2) in liquid phase. In the aldol condensation of benzaldehyde and acetone, about 90% conversion was obtained over rehydrated hydrotalcite in 3 h, while the aldol product was obtained with a 95% yield in 15 min at 273 K in the presence of $t\text{BuO}^-$ -containing material.³⁸⁾ As shown in Table 4.1.1, the material is more active for the cyanoethylation reaction between acrylonitrile and methanol than rehydrated hydrotalcite, which is far much more active than the mixed oxide (calcined hydrotalcite).⁸¹⁾ $t\text{BuO}^-$ ions can also be introduced by the memory effect. For the Wittig-Hornor reaction, the catalysts prepared by the memory effect is superior to the one prepared by the ion-exchange method.⁸²⁾

High catalytic activity of $t\text{BuO}^-$ ion-incorporated hydrotalcite is also demonstrated in the epoxidation of alkenes,⁸³⁾ transesterification,⁸⁴⁾ Henry reaction,⁸⁵⁾ Michael addition³⁹⁾ and Knoevenagel condensation.³⁹⁾

Choudary et al. also prepared hydrotalcite containing F^- by using the memory effect.⁴⁰⁾ The material thus obtained showed very high activities for Knoevenagel condensation and Michael addition reactions. The activity is much higher than $\text{KF}/\text{Al}_2\text{O}_3$ for both types of reactions. The Knoevenagel condensation between benzaldehyde and malononitrile gave 100% yield of the product in 15 min at room temperature.

Table 4.1.1 Cyanoethylation reaction between acrylonitrile with methanol using various base catalysts^{a)}

Catalyst	Time/min	Conversion/% ^{b)}	Specific activity/mmol $\text{g}^{-1} \text{h}^{-1}$ ^{d)}
Hydrotalcite (uncalcined)	120	2.5	0.5
Hydrotalcite (calcined)	120	20	4.0
Hydrotalcite (rehydrated)	45	99.8	58.2
Hydrotalcite with $t\text{BuO}^-$	40	92 ^{c)}	110.4
MgO	120	98.7	19.7
CaO	120	94.7	18.9
BaO	120	78.2	15.6
$\gamma\text{-Al}_2\text{O}_3$	120	0	0
$\text{KF}/\text{Al}_2\text{O}_3$	120	52.3	10.5
$\text{KOH}/\text{Al}_2\text{O}_3$	120	85.3	17.1

^{a)} Reaction temperature, 323 K, catalyst 0.100 g ^{b)} Conversion was calculated by the decrease in acrylonitrile ^{c)} 0.05 g catalyst, isolated yield ^{d)} mmol of 3-methoxypropanitrile obtained per gram of catalyst per hour

Reprinted with permission from B. M. Choudary, M. Lakshmi Kantam, B. Kavita, *Green Chem.*, **289** (1999) Table 2, p.291.

Diisopropylamide anions were intercalated by ion exchange of NO_3^- ions of as-synthesized hydrocalcite or by using the memory effect from calcined hydrocalcite with lithium isopropylamide in THF.⁴²⁾ The materials thus prepared are active for a variety of base catalyzed reactions: aldol, Knoevenagel, nitroaldol, Michael, transesterification and epoxidation reactions.

References

1. W. T. Reiche, CHEMTECH, Jan. p.58 (1986).
2. F. Cavani, T. Trifirò, *Catal. Today*, **11**, 173 (1991).
3. A. Vaccari, *Catal. Today*, **41**, 53 (1998).
4. B. F. Sels, D. E. De Vos, P. A. Jacobs, *Catal. Rev.*, **43**, 443 (2001).
5. D. Ticht, B. Coq, *CATTECH*, **7**, 206 (2003).
6. S. Velu, C. S. Swamy, *Appl. Catal.*, **119**, 241 (1994).
7. H. Schaper J. J. Berg-Slot, W. H. J. Storr, *Appl. Catal.*, **54**, 79 (1989).
8. A. Corma, S. B. A. Hamid, S. Iborra, A. Veltý, *J. Catal.*, **234**, 340 (2005).
9. J. L. Schumaker, A. A. Tackett, E. Santillan-Jimenez, M. Crocker, *Catal. Lett.*, **115**, 56 (2007).
10. W. T. Reichle, *Solid State Ionics*, **22**, 135 (1986).
11. M. Ogawa, H. Kaiho, *Langmuir*, **16**, 4240 (2002).
12. M. Adachi-Paganno, C. Forano, J.-P. Besse, *J. Mater. Chem.*, **13**, 1988 (2003).
13. U. Constantino, F. Marmottini, M. Nocchetti, R. Vivani, *Eur. J. Inorg. Chem.*, 1439 (1998).
14. U. Constantino, M. Curini, F. Montanari, M. Nocchetti, O. Rosati, *J. Mol. Catal., A*, **195**, 245 (2003).
15. P. Yang, J. Yu, Z. Wang, Q. Liu, T. Wu, *React. Kinet. Catal. Lett.*, **83**, 275 (2004).
16. H. C. Greenwell, P. J. Hollman, W. Jones, B. V. Velasco, *Catal. Today*, **114**, 397 (2006).
17. S. Abelló, J. Pérez-Ramírez, *Adv. Mater.*, **18**, 2436 (2006).
18. F. Prinetto, G. Ghiotti, R. Durand, D. Ticht, *J. Phys. Chem. B*, **104**, 11117 (2000).
19. F. Prinetto, G. Ghiotti, P. Grafin, D. Ticht, *Micropor. Mesopor. Mater.*, **39**, 229 (2000).
20. M. Bolognini, F. Cavani, D. Scagliarini, C. Flego, C. Perego, M. Saba, *Micropor. Mesopor. Mater.*, **66**, 77 (2003).
21. J. S. Valente, M. Cantú, J. G. H. Cortez, R. Montiel, X. Bokhimi, E. López-Salinas, *J. Phys. Chem.*, **111**, 642 (2007).
22. D. Ticht, M. H. Lhouty, A. Guida, B. H. Chiche, F. Figueras, A. Auroux, D. Bartalini, E. Garrone, *J. Catal.*, **151**, 50 (1995).
23. F. Kovanda, D. Kolouslek, Z. Cilová, V. Hulinský, *Appl. Clay Sci.*, **28**, 101 (2005).
24. S. Miyata, *Clay Minerals*, **28**, 50 (1980).
25. S. Kannan, R.V. Jarsa, *J. Mater. Chem.*, **10**, 2311 (2000).
26. P. Benito, F. M. Labajos, J. Rocha, V. Rives, *Micropor. Mesopor. Mater.*, **94**, 148 (2006).
27. D. Ticht, M. N. Bennani, F. Figueras, J. R. Ruiz, *Langmuir*, **14**, 2086 (1988).
28. E. Dumitri, V. Hulea, C. Chelaru, C. Catrinescu, D. Ticht, R. Durand, *Appl. Catal.*, **178**, 145 (1999).
29. F. Winter, A. Jos van Dillen, K. P. de Jong, *J. Mol. Catal. A*, **219**, 273 (2004).
30. W. T. Reiche, *J. Catal.*, **101**, 352 (1986).
31. H. A. Prescott, Z.-J. Li, A. Trunschke, J. Deutsch, H. Lieske, A. Auroux, *J. Catal.*, **234**, 119 (2005).
32. J. Rocha, M. de Arco, V. Rives, M. A. Ulíbarri, *J. Mater. Chem.*, **9**, 2499 (1999).
33. A. I. Mckenzie, C. T. Fishel, R. J. Davis, *J. Catal.*, **138**, 547 (1992).
34. S. Miyata, T. Kumura, H. Hattori, K. Tanabe, *Nippon Kagaku Zasshi*, **92**, 514 (1971) (in Japanese).
35. J. Pérez-Ramírez, S. Abelló, N. M. van der Perez, *Chem. Eur. J.*, **13**, 870 (2007).
36. T. Sato, T. Wakabayashi, M. Shimada, *Ind. Eng. Chem. Prod. Res. Dev.* **25**, 89 (1986).
37. S. Miyata, *Clays Clay Miner.*, **31**, 305 (1983).
38. B. M. Choudary, M. L. Kantam, B. Kavita, Ch. V. Reddy, K. Koteswara Rao, F. Figueras, *Tetrahedron Lett.*, **39**, 3555 (1988).
39. B. M. Choudary, M. L. Kantam, B. Kavita, Ch. V. Reddy, F. Figueras, *Tetrahedron*, **56**, 9357 (2000).
40. B. M. Choudary, M. L. Kantam, Y. Neeraja, K. Koteswara Rao, F. Figueras, L. Delmotte, *Green Chem.*, **3**, 257 (2001).

41. B. M. Choudary, M. L. Kantam, C. Reddy, V. Reddy, B. Bharathi, F. Figueras, *J. Catal.*, **218**, 191 (2003).
42. M. L. Kantam, A. Ravindra, Ch. V. Reddy, B. Sreedhar, B. M. Choudary, *Adv. Synth. Catal.*, **348**, 569 (2006).
43. Z. An, W. Zhang, H. Shi, J. He, *J. Catal.*, **241**, 319 (2006).
44. S. Vijaikumar, A. Dhakshinamoorthy, K. Pitchumani, *Appl. Catal., A*, **340**, 25 (2008).
45. K. Martin, T. J. Pinnavaia, *J. Am. Chem. Soc.*, **108**, 541 (1986).
46. T. Matsui, E. L. Salinas, E. Suzuki, Y. Ono, *Trans. Mater. Res. Soc. Jpn*, **15A**, 145 (1994).
47. E. Suzuki, M. Okamoto, Y. Ono, *Chem. Lett.*, **9**, 1483 (1989).
48. E. Suzuki, M. Okamoto, Y. Ono, *J. Mol. Catal.*, **61**, 283 (1990).
49. E. Suzuki, A. Inoue, Y. Ono, *Chem. Lett.*, **18**, 1291 (1998).
50. E. Lopez-Salinas, N. Tomita, T. Matsui, E. Suzuki, Y. Ono, *J. Mol. Catal.*, **81**, 397 (1993).
51. V. R. Constantino, T. J. Pinnavaia, *Catal. Lett.*, **23**, 361 (1994).
52. B. M. Choudary, M. L. Kantam, C. R. V. Reddy, K. K. Rao, F. Figueras, *J. Mol. Catal., A*, **146**, 279 (1999).
53. D. Kishore, S. Kannan, *J. Mol. Catal., A*, **223**, 225 (2004).
54. D. Kishore, S. Kannan, *Appl. Catal., A*, **270**, 227 (2004).
55. D. Kishore, S. Kannan, *J. Mol. Catal., A*, **244**, 83 (2006).
56. C. A. Antonyraj, S. Kannan, *Appl. Catal.*, **A338**, 121 (2008).
57. S. Kohjiya, T. Sato, T. Nakayama, S. Yamashita, *Makromol. Chem. Rapid Commun.*, **2**, 231 (1981).
58. T. Nakatsuka, H. Kawasaki, S. Yamashita, S. Kohjiya, *Bull. Chem. Soc. Jpn.*, **52**, 2449 (1979).
59. W. T. Reiche, *J. Catal.*, **94**, 547 (1985).
60. E. Suzuki, Y. Ono, *Bull. Chem. Soc. Jpn.*, **61**, 1008 (1988).
61. A. Corma, V. Fornés, R. M. Martín-Aranda, F. Rey, *J. Catal.*, **134**, 58 (1992).
62. V. K. Diez, C. R. Apestegula, J. I. Di Cosimo, *J. Catal.*, **215**, 230 (2003).
63. T. Raja, T. M. Jyoshi, K. Sreekumar, M. B. Talawar, J. Santhanalakshmi, B. S. Rao, *Bull. Chem. Soc. Jpn.*, **72**, 2117 (1999).
64. T. M. Joshi, T. Raja, K. Sreekumar, M. B. Talawar, B. S. Rao, *J. Mol. Catal.*, **157**, 193 (2000).
65. W. Xie, H. Peng, L. Chen, *J. Catal.*, **246**, 24 (2006).
66. E. López-Salinas, M. E. L. Serrano, A. C. Jácome, I. S. Secora, *J. Porous Mater.*, **2**, 291 (1996).
67. M. L. Kantam, B. M. Choudary, Ch. V. Reddy, K. Koteswara Rao, F. Figueras, *Chem. Commun.*, 1033 (1998).
68. K. Koteswara Rao, M. Gravelle, J. Sanchez Valente, F. Figueras, *J. Catal.*, **173**, 115 (1998).
69. M. J. Climent, A. Corma, S. Iborra, A. Velty, *Catal. Lett.*, **79**, 157 (2002).
70. M. J. Climent, A. Corma, S. Iborra, A. Velty, *Green Chem.*, **4**, 474 (2002).
71. M. J. Climent, A. Corma, S. Iborra, A. Velty, *J. Catal.*, **221**, 474 (2004).
72. J. C. A. A. Roelofs, A. J. van Dillen, K. P. de Jong, *Catal. Today*, **60**, 297 (2000).
73. J. C. A. Roelofs, D. J. Lensveld, A. J. van Dillen, K. P. de Jong, *J. Catal.*, **203**, 184 (2001).
74. F. Winter, X. Xie, B. P. C. Hereijgers, J. H. Bitter, A. Jos van Dillen, M. M. Muhler, K. P. de Jong, *J. Phys. Chem., B*, **110**, 9211 (2006).
75. S. Abelló, F. Medina, D. Ticht, J. Pérez-Ramirez, J. C. Groen, J. E. Sueiras, P. Salagre, Y. Cesteros, *Chem. Eur. J.*, **11**, 728 (2005).
76. S. Abelló, F. Medina, D. Ticht, J. Pérez-Ramirez, Y. Cesteros, P. Salagre, J. E. Sueiras, *Chem. Commun.*, **2005**, 1453.
77. R. J. Chimentão, S. Abelló, F. Medina, J. Llorca, J. E. Sueiras, Y. Cesteros, P. Salagre, *J. Catal.*, **252**, 249 (2007).
78. X. Lei, F. Zhang, L. Yang, X. Guo, Y. Tian, S. Fu, F. Li, D. G. Evans, X. Duan, *AIChE J.*, **53**, 932 (2007).
79. J. Polomeque, J.-M. Clacens, F. Figueras, *J. Catal.*, **211**, 103 (2002).
80. Y. Liu, E. Lotero, J. G. Goodwin jr., X. Mo, *Appl. Catal., A*, **331**, 138 (2007).
81. B. M. Choudary, M. L. Kantam, B. Kavita, *Green Chem.*, 289 (1999).
82. B. M. Choudary, M. L. Kantam, C. Reddy, V. Reddy, B. Bharathi, F. Figueras, *J. Catal.*, **218**, 191 (2003).
83. B. M. Choudary, M. L. Kantam, Ch. V. Reddy, *Synlett*, 1203 (1998).
84. B. M. Choudary, M. L. Kantam, Ch. V. Reddy, S. Aranganthan, P. Lakshmi Santhi, F. Figueras, *J. Mol. Catal.*, **159**, 411 (2000).
85. B. M. Choudary, M. L. Kantam, B. Kavita, *J. Mol. Catal., A*, **169**, 193 (2001).

4.2 Zeolites

Alkali cation-exchanged zeolites are weak bases, and the zeolites to which alkali cations are added in excess of the ion exchange capacity (alkali metal oxide-loaded zeolites) are stronger bases. Addition of alkali metals to zeolites results in a further increase in basicity as compared to alkali metal oxide-loaded zeolites. The catalytic properties of these zeolites containing alkali metals in different forms have been reviewed by several researchers.¹⁻⁷⁾ Characterization of zeolite basicity by IR and MAS NMR using probe molecules has been reviewed by Sánchez-Sánchez and Blasco.⁸⁾

4.2.1 Alkali Cation-exchanged Zeolites

It was discovered some time ago that the faujasites (X and Y type zeolites) exchanged with alkali cations such as Cs⁺ and Rb⁺ catalyze the side-chain alkylation of toluene with methanol or formaldehyde to yield styrene and ethylbenzene, X-zeolites being more efficient than Y-zeolites.^{9,10)} In general, base catalysts lead to side-chain alkylation while acid catalysts bring about ring alkylation. Occurrence of the side-chain alkylation of toluene indicates that alkali cation-exchanged zeolites possess basic sites. Since then, alkali cation-exchanged zeolites, in particular faujasite type zeolites, have been extensively studied for their basic and catalytic properties.

In addition to zeolites, alkali ion-exchanged titanosilicates are included in this section.

A. Generation of basic properties

It is generally observed that the catalytic activities of alkali cation-exchanged zeolites increase with an increase in both the atomic number of the alkali metal and the Al/Si ratio of the zeolite framework. These general tendencies were interpreted by Barthomeuf¹¹⁻¹⁴⁾ in terms of the negative charge of the framework oxygen (O) which is calculated based on the Sanderson's electronegativity equalization principle.¹⁵⁾

Sanderson's electronegativity equalization principle was introduced to the field of zeolites by Mortier¹⁶⁾ for the first time. The intermediate electronegativity S_{int} of a given material reflects the mean electronegativity reached by all the atoms as a result of electron transfer during the formation of the compound. For a compound $P_pQ_qR_r$, the intermediate electronegativity S_{int} is given by

$$S_{\text{int}} = \{(S_P)^p(S_Q)^q(S_R)^r\}^{1/(p+q+r)} \quad (4.2.1)$$

where S_j denotes the electronegativity of atom j .

The mean charge (δ_j) on an atom j is calculated by

$$\delta_j = (S_{\text{int}} - S_j)/2.08 (S_O)^{1/2} \quad (4.2.2)$$

which gives the mean charge of the O atom δ_O with $S_j = 5.21$ for O.

$$\delta_o = (S_{\text{int}} - 5.21)/4.75 \quad (4.2.3)$$

The charges of negative oxygen for a series of alkali cation-exchanged zeolites are in negative values, and in the order $\text{Li} < \text{Na} < \text{K} < \text{Rb} < \text{Cs}$. The basicity, therefore, follows the order $\text{Li} < \text{Na} < \text{K} < \text{Rb} < \text{Cs}$. For a given alkali cation-exchanged zeolite, the oxygen charge increases with the Al to Si ratio in the zeolite framework; a higher Al/Si ratio renders the zeolite more basic.

In calculating the oxygen charge, no effect of the structure is considered, so the calculated oxygen charge is the averaged oxygen charge of the framework. Nevertheless the calculated oxygen charge based on the electronegativity is an useful method in estimating the basicity of alkali cation-exchanged zeolites. Barthomeuf reported that the oxygen charges of alkali cation-exchanged zeolites calculated based on Sanderson's S_{int} correlated well with the N-H vibration wavenumber of adsorbed pyrrole,¹⁴ as shown in Fig. 2.4.4. The wavenumber of N-H vibration shifted to a lower frequency with the basic strength of the oxygen of framework of zeolite on which pyrrole was adsorbed through the H of NH group in pyrrole. The correlation between the wavenumber shift and oxygen charge, however, holds within zeolites of similar structure.

The IR and XPS studies performed by Kaliaguine's group¹⁷⁻²⁰ confirmed the general trends which were observed by Barthomeuf. The model for pyrrole chemisorbed on a basic site is shown in Fig. 4.2.1. In the IR study of adsorbed pyrrole, they observed two bands for the zeolites containing two kinds of cations. For example, NaCsX zeolites showed the bands at 3175 and 3280 cm^{-1} . Since the latter band corresponded to the $\nu(\text{NH})$ band of pyrrole in NaX zeolites, this band was ascribed to pyrrole molecules interacting with oxygen ions adjacent to Na^+ ions. The 3175 cm^{-1} band was assigned to pyrrole adsorbed on oxygen ions adjacent to Cs^+ ions. They also observed a band at 3375 cm^{-1} , which was assigned to the $\nu(\text{NH})$ band of pyrrole situated on oxygen ions without any adjacent metal cations. These findings suggest that the basic properties in zeolites are mainly determined by the local environment rather than the zeolite structure. A detailed analysis of the infrared bands of pyrrole adsorbed on faujasites and EMT zeolite revealed the location of oxygen anions with which pyrrole molecules interact in each zeolite.^{21,22}

In the XPS study of pyrrole adsorbed on X- and Y-zeolites, two kinds of N_{1s}

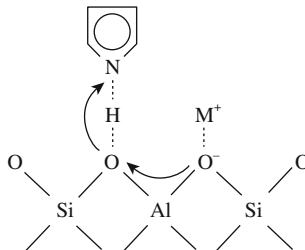


Fig. 4.2.1 Model for pyrrole chemisorbed on basic site of alkali ion-exchanged zeolite

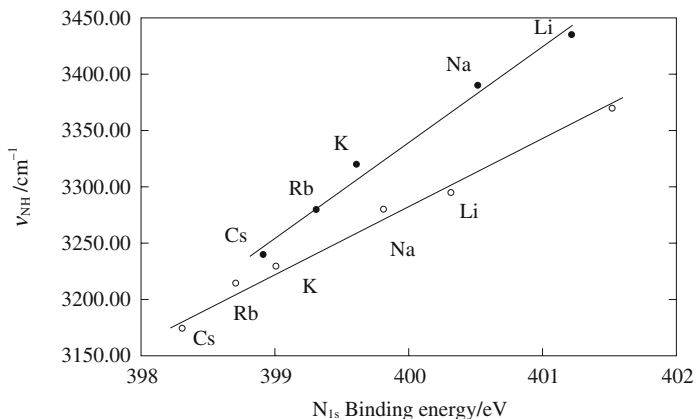


Fig. 4.2.2 Relationship Between N_{1s} binding energies and NH stretching vibration frequencies of chemisorbed pyrrole on X zeolites and Y zeolites. Reprinted with permission from M. Huang, A. Adnot, S. Kaliaguine, *J. Catal.*, **137**, 322 (1992) Fig. 3.

peaks of chemisorbed pyrrole were observed.^{16,18,19)} One (399.0–400.0 eV) was assigned to pyrrole molecules on the oxygen atoms adjacent to metal cations, while the other at 401.5 eV was assigned to those on the oxygen atoms with no adjacent cations in the case of X-zeolite. The binding energy of the former species decreased in the order $Li > Na > K > Rb > Cs$. When the samples have two kinds of cations in the supercages, two peaks are observed. Similar results were also obtained in the case of Y-zeolites. These results are in good conformity with the results of IR spectroscopy. Fig. 4.2.2 shows that the shifts of binding energy in XPS are well correlated with the shifts of NH stretching frequency in IR spectra.¹⁸⁾ A small peak at 401.5 eV was also observed for all the X-zeolites and assigned to weakly adsorbed pyrrole without any neighboring cations, corresponding to the 3375 cm^{-1} N-H band in their IR spectra.

Pyrrole adsorbed on alkali cation-exchanged X- and Y-zeolites was also studied by ^1H MAS NMR.²³⁾ The ^1H MAS NMR of adsorbed pyrrole shows three peaks with relative intensity 1 : 2 : 2 corresponding to the three types of protons in the molecule (Fig. 4.2.3). The less intense peak is due to the N-H group, whereas the other two are from the four C-H protons in the five-membered heterocycle; the two C-H groups in the α position and the two in the β position give rise to the intermediate and high field resonance, respectively. The N-H peak of liquid pyrrole appears at δ 7.1 and shifts to a higher frequency when it is adsorbed on the zeolites. The chemical shifts indicate that the basic strength of the zeolites increases in the order $LiY < NaY < KY < LiX < CsY < NaX < KX$. It was also shown by ^7Li and ^{23}Na MAS NMR spectra of Li, Na-Y with adsorbed pyrrole that the molecules interact with metal cations through its aromatic ring as well as with framework oxygen atoms through the N-H group. They studied the adsorption of pyrrole on alkali cation-exchanged X, and Y-zeolites with IR, MAS NMR, XRD

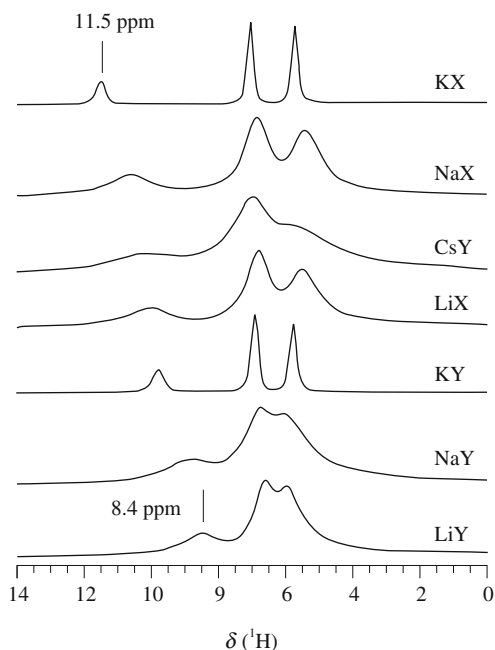


Fig. 4.2.3 ^1H -MAS NMR spectra of pyrrole adsorbed on zeolites. Reprinted with permission from M. Sanchez-Sanchez, T. Blasco, *Chem. Commun.*, **2000**, 491 Fig. 1.

techniques in more detail and concluded that the adsorption state of pyrrole was influenced by the kind and location of cations and also by the Al distribution in the framework.²⁴⁾

XPS studies of the framework of zeolites give information about basicity. The XPS binding energy (BE) for oxygen reflects the electron charge of the framework oxygen. As O_{1s} BE decreases, the ability of electron pair donation becomes stronger.

Okamoto et al. studied the effects of the type of ion-exchanged cation and the Al/Si ratio of the framework on the BE of framework O in X and Y type zeolites.²⁵⁾ Fig. 4.2.4 shows the BE of the O_{1s} as a function of the electronegativity (Pauling's electronegativity χ) of the ion-exchanged cation. With increasing electronegativity of the exchangeable cation, the O_{1s} BE decreased. For the same alkali cation, the O_{1s} BE was lower for the X zeolite than for the Y zeolite. The BE of the O_{1s} was also affected by the Al/Si ratio. The BE of the O_{1s} decreased linearly with the Al/Si ratio in the framework (Fig. 4.2.5). The framework oxygen basicity increased as the electronegativity of the ion-exchanged cation decreased, and also as the Al/Si ratio increased.

Barr measured BE of O_{1s} for NaA, NaX, NaY, Na-mordenite and Na-ZSM5.²⁶⁾ The Al/Si ratio decreased going from NaA to Na-ZSM5. It was shown that the BE of O_{1s} decreased with a decrease in the oxygen charge calculated from Sanderson's electronegativity, indicating that the basic strength is enhanced as the Al/Si ratio

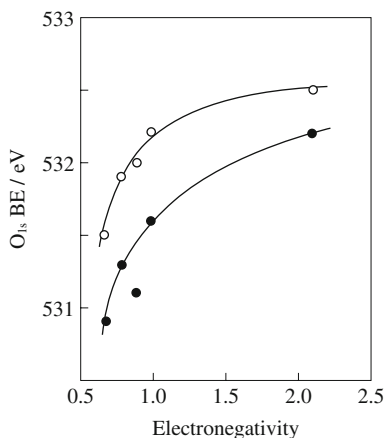


Fig. 4.2.4 Dependencies of the O_{1s} binding energy for the X and Y zeolites on the electronegativity of cations (●) X and (○) Y. Reprinted with permission from Y. Okamoto, M. Ogawa, A. Maezawa, T. Imanaka, *J. Catal.*, **112**, 427 (1988) Fig. 3.

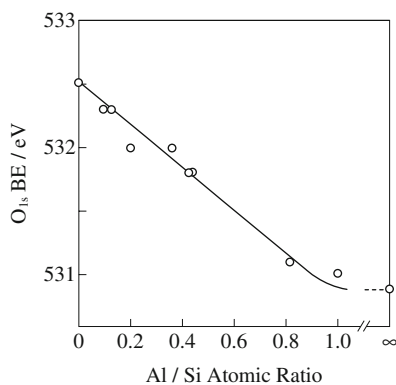


Fig. 4.2.5 Correlation between the binding energy of the O_{1s} band and the Al/Si atomic ratio. Reprinted with permission from Y. Okamoto, M. Ogawa, A. Maezawa, T. Imanaka, *J. Catal.*, **112**, 427 (1988) Fig. 1.

increases for the same exchanged cation. Decrease in the BE of O_{1s} with the Al/Si ratio was also observed by Gruenert et al.²⁷⁾

B. Catalytic properties

The characteristic features of the catalysis by alkali cation-exchanged zeolites arise from weak basicity and narrow pore structure. The alkali cation-exchanged zeolites possess weak basic sites compared with alkaline earth oxides and zeolites containing alkali compounds in excess of the ion-exchanged capacity. Accordingly, preadsorbed H_2O and CO_2 are desorbed by pretreatment at a relatively low temperature, and the catalysts can be used for the reactions producing H_2O or CO_2 as a product at a temperature at which H_2O and CO_2 are desorbed. Although the

basic sites are weak, the strength can be controlled by selecting the appropriate type of alkali cation. This merit makes it possible to use the ion-exchanged zeolites as versatile solid base catalysts. The narrow pore structure brings about shape selectivity but presents difficulties in the diffusion of the reactants and products. The diffusion problems become more serious when the catalysts are used in liquid phase reactions.

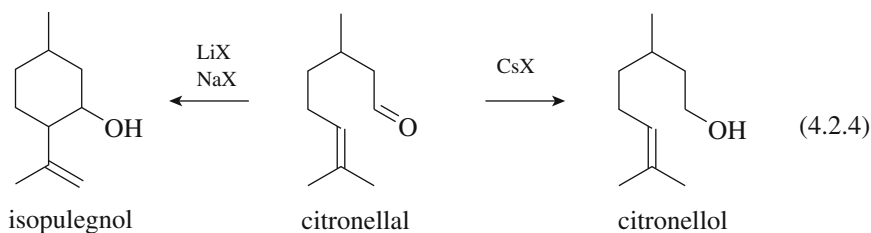
The selectivity for 2-propanol dehydration/dehydrogenation varies with the kinds of alkali cation and zeolite. Yashima et al. reported the activities and selectivity for 2-propanol dehydration/dehydrogenation over a series of alkali cation-exchanged zeolite X and Y.²⁸⁾ For zeolites X and Y exchanged with Li^+ and Na^+ , dehydration proceeded dominantly, while for zeolites exchanged with K^+ , Rb^+ and Cs^+ , dehydrogenation became appreciable, though selectivity to dehydration exceeded that to dehydrogenation at 698 K. Dehydrogenation to acetone increased as the exchanged cations changed from K^+ , Rb^+ , to Cs^+ except for CsX. The dehydration was suppressed by the introduction of pyridine, while the dehydrogenation was suppressed by the introduction of phenol. They interpreted the increase in the dehydrogenation selectivity as a result of basic site generation for K^+ , Rb^+ , and Cs^+ -exchanged zeolites X and Y.²⁸⁾ Philippou et al. reported that dehydrogenation to acetone was dominant for KX and CsX, while dehydration was dominant for NaX at 723 K.²⁹⁾ They concluded that K^+ and Cs^+ ions are more effective for the generation of basic sites than Na^+ ion as ion-exchanged cations of zeolite X.

The effects of the framework element are also strong. Concepcion-Heydorn et al. reported that the composition of the framework (X vs. Y, Ge in place of Si) appeared to have a stronger influence on the basicity than the charge balancing cations.³⁰⁾ They prepared four alkali cation-exchanged zeolites, a CsY zeolite with an intact faujasite structure and an exchange degree of nearly 100% prepared by solid-state ion exchange, a CsNaY obtained from CsY through exchange with aqueous NaCl solution, a CsNaX obtained from NaX and CsCl solution, and a Na(Ge)X with Si replaced by Ge. They measured the conversion of 2-propanol as a test reaction for basicity, and IR of adsorbed CO_2 . Na(Ge)X was the only sample to form monodentate carbonates upon CO_2 adsorption, and to produce acetone much more than propene. It was concluded the order of basicity to be Na(Ge)X > CsNaX > CsNaY ~ NaY. Both Na(Ge)X and CsNaX underwent structural change during preparation or catalytic reaction. They suggested that the basicity arises not from the ion-exchanged zeolite but from trace impurities formed during preparation such as extra-framework Al and Ge species.

The effects of the introduction of Ge into the framework were also reported by Corma et al. in Knoevenagel condensation.³¹⁾ The activity was enhanced because of basicity enhancement by the introduction of Ge.

Meerwein-Ponndorf-Verley (M-P-V) reduction of aldehydes with 2-propanol to yield corresponding 1-alcohol proceeds over Na^+ ion-exchanged X zeolite at 373 K and 453 K.³²⁾ Although the authors did not mention the relation between the activity and basicity of the catalyst, they suggested that the initial step of the reaction is abstraction of proton from 2-propanol by the framework O adjacent to Na^+ cation, the O acting as a base toward 2-propanol.

In the reaction of citronellal with 2-propanol, different products were obtained depending on the exchangeable alkali cations. Citronellal can be converted either to citronellol by M-P-V reduction or to isopulegol by ring closure. Over CsX, citronellol was produced with 92% selectivity at 77% conversion, while over NaX, 86% isopulegol and 14% citronellol were produced at 87% conversion.³²⁾ The selectivity difference between NaX and CsX was attributed to the steric hindrance caused by the large Cs⁺ ion preventing the cyclic compound from being formed. However, the selectivity difference may be caused by a small change in the acid-base relationship with the type of ion-exchanged alkali cation, as pointed out by Hölderich.³³⁾ The CsX is more basic than NaX and LiX, resulting in the selective formation of citronellol over CsX.



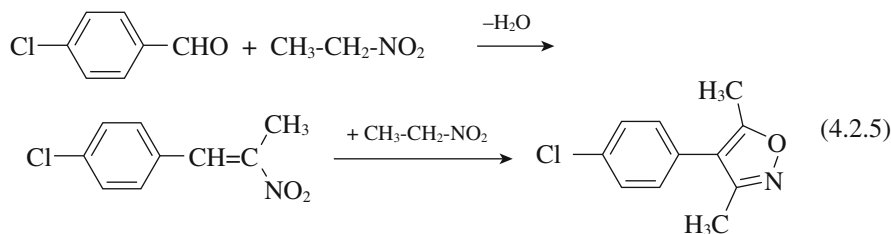
Corma et al. measured the activities of ion-exchanged zeolite X and Y for Knoevenagel condensation of benzaldehydes with esters and compared the basicities of zeolites with those of pyridine and piperidine³⁴⁾ (see section 2.5.5). The activities for the condensation of benzaldehyde with ethyl cyanoacetate in the temperature range 383–413 K were in the following order: all Y's < LiX < pyridine ($pK_b = 8.8$) < NaX < KX < CsX < piperidine ($pK_b = 11.12$). The rate was influenced by the pK_a of the reactant. The rate decreased with an increase in the pK_a value of the ester, the reactivities were in the order; ethyl cyanoacetate ($pK_a < 9$) > ethyl acetoacetate ($pK_a = 10.7$) > ethyl malonate ($pK_a = 13.3$). They concluded that most of the basic sites of alkali cation-exchanged X- and Y-zeolites possess basic sites in the range $H_- < 10.3$, and a few sites $H_- < 13$ for Cs-X.

The activity of NaX for Knoevenagel condensation of benzaldehyde derivatives with activated methylenic compounds is enhanced by the substitution of framework Si by Ge.³⁴⁾ The high activity of Ge-substituted zeolite indicates stronger basic properties. Generation of stronger basic properties of Ge-substituted zeolite could not be interpreted by the average Sanderson's electronegativity (3.28 and 3.25 for Ge and Si faujasites, respectively). Corma et al. concluded that the higher basicity of Ge zeolite is due to the difference in the T-O-T bond angle; unit cell sizes are 25.57 Å and 24.95 Å for Ge substituted NaX and NaX, respectively.

Nitroaldol condensation of aromatic aldehydes with nitroalkanes affording nitroalkenes is catalyzed by alkali cation-exchanged X and Y zeolites at 413 K.³⁵⁾ The activity increased with increase in both the Al content in the framework and the radius of the counter cation: the activity increased from Li to Cs and from Y to X zeolites. The presence of an electron acceptor group on the aromatic ring of benzaldehyde increased the yield. The role of basic sites is the abstraction of an

H^+ from nitroalkane to form nitroalkanide anion which attacks carbonyl carbon of the aldehyde.

In the reaction of aldehyde with nitroalkane, the produced nitroalkene has the possibility to undergo Michael addition to the reactant aldehyde to afford a bulky cyclic compound, isoxazole. The Michael addition producing the bulky product is suppressed in zeolite due to the shape selectivity of the zeolites.



A similar minimization of Michael addition by shape selectivity of alkali cation-exchanged zeolites was reported in the Knoevenagel condensation of benzaldehyde with ethyl cyanoacetate.³⁶⁾

Huang and Kaliaguine examined the activities and selectivities of Na^+ cation-exchanged zeolites A, X, Y, L, mordenite and ZSM-5 for a diagnostic reaction of 2-methyl-3-buten-2-ol (MBOH).³⁷⁾ For zeolites A, X, Y, L and mordenite, the main products were acetone and acetylene, indicating the basic nature of these zeolites. For ZSM-5, on the other hand, the main products were 3-methyl-3-buten-1-yne and 3-methyl-2-butenal, indicating the acid nature of the zeolite. The yields of acetone and acetylene increased in the order mordenite < L < Y < X < A, which is the same order as the negative charges of the framework O calculated from Sanderson's electronegativity equalization method. The acid-catalyzed reaction occurring over Na-ZSM-5 is interpreted by a larger positive charge on Na^+ cation in ZSM-5 than in L-, Y-, X- and A-zeolites.

C. Alkali cation-exchanged titanosilicate EST-10

ETS-10, a crystalline titanosilicate, is a zeotype material which contains a three-dimensional 12-ring pore system, and has an ideal chemical formula of $\text{M}_{2/n}\text{Si}_5\text{TiO}_{13}$, where M represents a cation with a charge of $+n$, and is ion-exchangeable. ETS-10 containing alkali cations exhibited catalytic activities for base-catalyzed reactions such as dehydration of *t*-butyl alcohol,³⁸⁾ dehydrogenation of 2-propanol,³⁹⁾ aldol condensation of acetone,⁴⁰⁾ and Knoevenagel condensation.⁴¹⁾

Philippou et al. reported dehydration of *t*-butyl alcohol, dehydrogenation/dehydration of 2-propanol and aldol condensation of acetone over ETS-10.³⁸⁻⁴⁰⁾ Dehydration of *t*-butyl alcohol proceeds in the temperature range 373–573 K over ETS-10.^{39,40)} The reaction is a base-catalyzed dehydration and highly selective for isobutene formation as compared to an acid-catalyzed dehydration over $\text{SiO}_2\text{-Al}_2\text{O}_3$ catalyst where considerable amounts of C_4 to C_9 hydrocarbons are formed. In 2-propanol reaction at 623 K, dehydrogenation to form acetone is predominant

over ETS-10.³⁹⁾ Cs ion-exchanged ETS-10 resulted in a small decrease in the activity but an increase in the selectivity to acetone in comparison with as-synthesized ETS-10. Cs₂O-impregnated ETS-10 showed an activity similar to as-synthesized ETS-10, but higher selectivity to acetone. Based on the activity and selectivity, basicity of as-synthesized ETS-10 was estimated to be comparable to that of Cs₂O-impregnated Cs-X.

Goa et al. studied the catalytic properties of alkali cation-exchanged ETS-10 for Knoevenagel reactions of benzaldehyde with ethyl cyanoacetate, and acetone with malononitrile, and correlated the basic strength of the catalyst, accessibility of the substrates to basic sites and reactivity of carbonyl compounds with the catalytic activity.⁴¹⁾ The order of the basic strength estimated by N-H stretching vibration frequency of adsorbed pyrrole was Cs-ETS-10 > Cs-Y > [Na,K]-ETS-10 > Na-Y. The activities for the reaction of benzaldehyde with ethyl cyanoacetate at 323 K were in the order Li-ETS-10 > [Na, K]-ETS-10 > Rb-ETS-10 > Cs-ETS-10, which accords with the micropore size, indicating that this rather facile reaction is controlled by diffusion. For the reaction of acetone with malononitrile, the activity of alkali-exchange ETS-10 at 313 K increased in the order Li-ETS-10 < [Na, K]-ETS-10 < K-ETS-10 < Rb-ETS-10 < Cs-ETS-10. In this case, the reaction rate is controlled by the surface reaction, and thus plausibly reflects the basic strength of the catalyst.

4.2.2 Alkali Metal Oxide-loaded Zeolites

Basicity is enhanced by loading zeolites with alkali ions in excess of the ion-exchange capacity. Hathaway and Davis prepared catalysts by impregnation of Cs⁺ and Na⁺ ion-exchanged X and Y zeolites with a cesium acetate aqueous solution followed by thermal decomposition of the cesium acetate in an He stream into oxide at 773 K.⁴²⁻⁴⁴⁾ Tsuji et al. prepared similar catalysts by impregnation of the Na⁺ ion-exchanged X and Y zeolites with cesium acetate followed by calcination at 673 K in an O₂ stream and outgassed at 673 K.⁴⁵⁾ Regardless of the differences in the preparation procedures, the resulting zeolites show much higher activities for a wide variety of base-catalyzed reactions as compared to Cs⁺ ion-exchanged zeolites. This results from the formation of strong basic sites in the cavities for alkali metal oxide-loaded zeolites.

A. Location and state of loaded alkali metal compounds

The location and state of alkali compounds in excess of the ion-exchange capacity were studied by ¹³³Cs MAS NMR and TPD of O₂ and CO₂ for Cs⁺ ion-loaded X and Y zeolites by Kim et al.⁴⁶⁾ and Yagi et al.⁴⁷⁾

Kim et al. measured ¹³³Cs MAS NMR of zeolite X containing Cs acetate in excess of the ion-exchange capacity.⁴⁵⁾ For the fully hydrated sample, two resonance peaks appeared at 47 and -31 ppm, which were assigned to the ion-exchanged Cs⁺ and the occluded Cs₂O (or hydrated versions thereof), respectively.

Yagi et al. also measured ¹³³Cs MAS NMR for zeolite X containing different amounts of Cs⁺ ions in excess of ion-exchange capacity.⁴⁷⁾ The samples were cal-

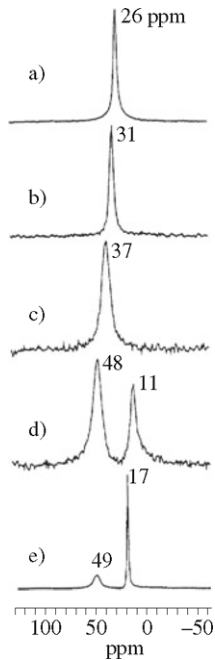


Fig. 4.2.6 ^{133}Cs MAS NMR spectra of zeolites X containing different amounts of Cs. (a) Cs^+ ion-exchanged zeolite X, (b) $\text{Cs}1.1\text{-X}$, (c) $\text{Cs}2.9\text{-X}$, (d) $\text{Cs}5.1\text{-X}$, (e) $\text{Cs}9.8\text{-X}$. All samples were calcined in oxygen at 673 K and hydrated in the water vapor of saturated aqueous ammonium chloride for more than 24 h. The number expressed after Cs denotes the number of excess Cs atoms per supercage.

Reprinted with permission from F. Yagi, N. Kanuka, H. Tsuji, H. Kita, H. Hattori, *Microporous Mater.*, **9**, 229 (1987) Fig. 2.

cined at 673 K in oxygen and hydrated at room temperature for more than one day. The spectra are shown in Fig. 4.2.6. The peak position and shape are dependent on the amount of Cs^+ ions. For the sample in which all Cs^+ ions were in exchangeable sites ($< 7.8 \text{ Cs}^+$ per supercage), only one ^{133}Cs resonance peak was observed at 26 ppm. As the Cs content increased, the peak shifted to a lower field, and when the Cs amount exceeded 2.9 Cs atoms per supercage, the peak split into two. The resonance peak at the higher field (11–17 ppm) was ascribed to the Cs^+ located on the outer surface of the zeolite. It was concluded that Cs^+ ions added to X zeolite in excess of the ion-exchange capacity are located in the intracrystalline cavities if the amount of the Cs^+ ions is less than 2.9 Cs atoms per supercage. At a loading of Cs^+ ions higher than 2.9 Cs atoms per supercage, the excess of Cs^+ ions are located on the outer surface of the zeolite crystallites. ^{23}Na MAS NMR was affected by the presence of Cs^+ ion up to 2.9 Cs atoms per supercage, but was not affected much if the content of Cs^+ ions exceeded 2.9 Cs atoms per supercage. This confirmed the location of the Cs^+ ions as described above, because Na^+ ions left unexchanged in the X zeolite should be located at the hexagonal prism sites far distant from the outer surface and would not be affected much by the Cs^+ ions present on the outer surface.

Hunger et al. measured ^{133}Cs MAS NMR for Y zeolite ion-exchanged with Cs^+ ion followed by impregnation with CsOH and subsequent calcination at 673 K.⁴⁸⁾ In addition to four peaks assigned to Cs^+ ion at ion-exchangeable positions, a broad peak centered at ca. -30 ppm, which was assigned to oxidic species of Cs, was observed. The peak position for bulk Cs_2O was 236 ppm. They stated that this significant difference in the chemical shift between the bulk phase compounds and the Cs_2O in the zeolite indicated that the latter species do not exist in the form of large clusters and hint of a high dispersion of the oxidic guest compound at the zeolite host.

The state of Cs is difficult to identify by ^{133}Cs MAS NMR because the samples must be hydrated to obtain clear resonance peaks. Accordingly, any form of cesium oxides or hydroxide becomes Cs^+ ions on hydration. The state of Cs in a dried condition was identified by TPD of CO_2 and O_2 .

Kim et al. measured TPD of CO_2 for the same sample as they measured ^{133}Cs MAS NMR as described above. TPD of CO_2 gave two peaks at 523 and 623 K. Referring to TPD of CO_2 from bulk Cs_2O , they assigned these two peaks to CO_2 from small particles of Cs_2O occluded in the intracrystalline cavities.⁴⁶⁾

Yagi et al. proposed from the results of TPD of $^{18}\text{O}_2$ that the form of Cs is small Cs_2O particles in the intracrystalline cavities.⁴⁹⁾ When $^{18}\text{O}_2$ was adsorbed on the dried X zeolite containing Cs^+ ions in excess of ion-exchange capacity, the desorbed oxygen molecules in TPD were composed mainly of $^{16}\text{O}_2$ and $^{18}\text{O}_2$, the content of $^{16}\text{O}^{18}\text{O}$ being small. This indicates that a pair of oxygen atoms in the Cs-containing zeolite is exchanged with an oxygen molecule. The retention of the molecular identity of oxygen during the exchange suggests the existence of the Cs_2O particles in the zeolite cavities. On adsorption of O_2 , part of the surface layers of the Cs_2O particles converts into the structure similar to those of per- and superoxides (Cs_2O_2 , Cs_2O_3 and Cs_2O_4) in which Cs^+ ions form bonds with negatively charged oxygen pairs O_2^{2-} and O_2^- . When the peroxide and superoxides convert into Cs_2O , the paired oxygen atoms can leave the peroxide and superoxide without breaking the bond between the two oxygen atoms, resulting in the retention of molecular identity. Following desorption of pairs of O atoms, the oxygen deficient peroxide and superoxide convert to Cs_2O by rearrangement of Cs and O. Accordingly, the Cs atoms exist in the zeolite cavities in the form of Cs_2O when the zeolite is calcined and evacuated at 673 K.

It should be noted that cesium oxide exists in different forms depending on the environment. Cesium superoxide (CsO_2), cesium peroxide (Cs_2O_2), cesium oxide (Cs_2O), cesium suboxide (Cs_7O), cesium metal and any combination thereof can be formed under a particular oxygen environment. Accordingly, the state of cesium occluded in zeolites should change depending on the oxygen environment or pretreatment condition. This is reasonably expressed by CsO_x -loaded zeolite for the zeolite containing cesium in excess of the ion-exchange capacity.

B. Strength of basic sites

Enhancement of basic strength by loading alkali metal oxides on X-zeolite in excess of the ion exchange capacity was demonstrated by TPD plots of CO_2 , as shown in

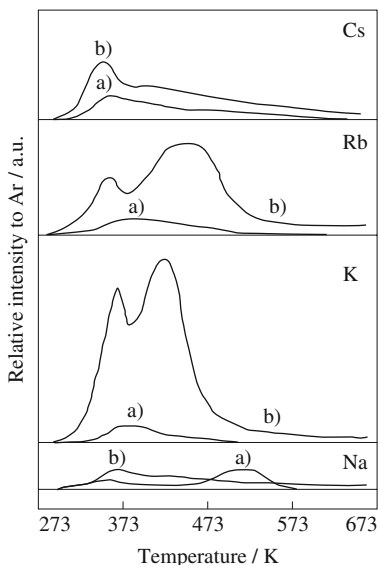


Fig. 4.2.7 TPD plots of CO_2 adsorbed on alkali metal ion-exchanged (a) and alkali metal ion-loaded zeolites (b). Reprinted with permission from F. Yagi, H. Tsuji, H. Hattori, *Microporous Mater.*, **9**, 237 (1997) Fig. 9.

Fig. 4.2.7.⁵⁰⁾ The peak areas are larger for the alkali metal oxide-loaded zeolites (b) than for the ion-exchanged zeolites (a). In particular, desorption of CO_2 continues up to 673 K for alkali metal oxide-loaded zeolites.

Calorimetric measurements of heat of adsorption of CO_2 showed the initial heat of adsorption of CO_2 on Cs_2O -loaded NaX to be $\sim 180 \text{ kJ mol}^{-1}$, which was much higher than $< 80 \text{ kJ mol}^{-1}$ for ion-exchanged NaX.⁵¹⁾ Similar results are presented in ref. 52.

The state of strongly adsorbed CO_2 is controversial. Unidentate carbonate and hydrogencarbonate have been proposed. Dorskocil and Davis reported that basic sites created by loading CsO_x onto K^+ ion-exchanged X zeolite strongly adsorbed CO_2 in the form of unidentate carbonate.⁵²⁾ On outgassing at 673 K, CO_2 was completely eliminated from K^+ ion-exchanged zeolite X, but retained on CsO_x -loaded KX. The retained CO_2 on the CsO_x -loaded KX was measured by IR and identified to be unidentate carbonate.⁵³⁾ On the other hand, Yagi et al. reported that CO_2 was adsorbed in the form of bidentate carbonate on the strong basic sites relevant to 1-butene isomerization.⁵⁰⁾

The basic strength of CsO_x -loaded zeolites was also studied by ^{13}C MAS NMR of adsorbed methyl iodide (see section 2.4.8).⁵⁴⁾

C. Catalytic properties

Generation of stronger base sites on alkali metal oxide-loaded zeolites as compared to those on alkali cation-exchanged zeolites is reflected clearly in the cata-

lytic activity for 1-butene isomerization. Kim et al. reported that 1-butene isomerization on the Cs₂O-loaded zeolites proceeded at 423 K with a flow type reactor, while no reaction took place on the ion-exchanged zeolite.⁴⁶⁾ Yagi et al. also reported that 1-butene isomerization proceeded even at 273 K with a closed recirculation reactor over alkali metal oxide-loaded zeolites, while no reaction took place over ion-exchanged zeolites at 273 K.⁵⁰⁾ Among the alkali metal ion-loaded zeolite, CsO_x-loaded X exhibited the highest activity.

The active sites for 1-butene isomerization are strong and retain CO₂ up to 573 K in the form of bidentate carbonate giving IR bands at 1570 and 1380 cm⁻¹. Once the active sites are poisoned by CO₂, the activity begins to recover by outgassing at 573 K, and the original activity is completely restored by outgassing at 673 K.⁵⁰⁾

The active sites were also poisoned by O₂.⁴⁹⁾ Although the adsorbed O₂ was completely desorbed by outgassing at 523 K, the activity was not restored until the outgassing temperature was raised to 673 K. On adsorption of O₂ on CsO_x-loaded KX, the surface layers of the Cs₂O particles change into per- and superoxide layers. On desorption of O₂ at 523 K from the per- and superoxide layers, oxygen-deficient per- and superoxide layers form. These are not active for 1-butene isomerization. To convert the oxygen-deficient per- and superoxide layers into Cs₂O particles, heating at 673 K is required.

Li and Davis also reported the enhanced activity of alkali metal oxide-loaded zeolites for 1-butene isomerization at 373 K.⁵⁵⁾ Initial turnover frequency based on the excess Cs atoms followed the order CsO_x/CsX > CsO_x/KX > KO_x/KX. Selective poisoning by CO₂ indicated that only about 5% of the sites for CO₂ adsorption at 373 K was active for 1-butene isomerization. Zhu et al. reported that KNO₃/KL showed activity for *cis*-2-butene isomerization at 273 K when pretreated at 773 K in a vacuum, though none of NaY, NaX, KL, KNO₃/NaY and KF/NaX showed any activity at 273 K.⁵⁶⁾ This is in coincidence with the results reported.^{57,58)}

For decomposition of 2-propanol, activity enhancement by loading CsO_x on NaX was observed. Daskocil and Mankidy prepared NaO_x-loaded NaX zeolites with different loadings of NaO_x.⁵²⁾ The rate of acetone formation was proportional to the NaO_x loading up to 3 NaO_x per supercage. The selectivity to acetone exceeded 90% over NaO_x-loaded NaX, while it was only 24% over NaX at 513 K. The propene formation rate was reduced by loading of CsO_x on NaX up to 2 NaO_x per supercage; this resulted from neutralization of acidic sites present on the NaX by loading of CsO_x. The increase in the dehydrogenation rate for NaO_x-loaded zeolite was ascribed to the formation of strong basic sites. This was confirmed by calorimetric measurement of heat of adsorption of CO₂ as described above.

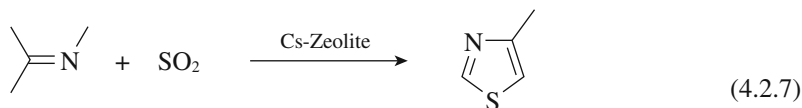
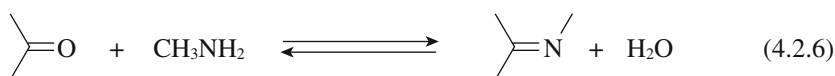
The catalytic activity for the dehydrogenation of 2-propanol increased an order of magnitude by loading CsO_x onto CsY. The activity of Cs₂O-loaded CsNaY was as high as that of MgO on a surface area basis. Due to the high surface area of the zeolite, the activity of Cs₂O-loaded CsNaY became five times greater than that of MgO on a weight basis.³⁾

Knoevenagel reaction of benzaldehyde and ethyl cyanoacetate was promoted by the loading of alkali metal oxides onto zeolites. The optimum loading is differ-

ent for X zeolite than for Y zeolite. The activity increases with a loading of CsO_x on CsNaX up to 16 Cs atoms per unit cell (2 Cs atoms per supercage), while loading of about 7 Cs atoms per unit cell gives the maximum activity for CsO_x -loaded CsNaY .^{59,60)} Rymasa et al. also reported that for the Knoevenagel condensation of benzaldehyde and malononitrile, alkali-impregnated catalysts were more active than ion-exchanged catalysts for X, Y and β -zeolites, CsO_x being the most effective among the alkali metal oxides in promoting the activity.⁶¹⁾

For the diagnostic reaction of the decomposition of 2-methyl-3-butyn-2-ol (MBOH), the activity of alkali metal oxide-loaded zeolites for the formation of acetone and acetylene increased with a decrease in the electronegativity of the over-loaded alkali metal cations, and CsO_x -loaded CsX showed the highest activity. For CsO_x -loaded NaX, the optimum loading was 1.46 mmol cesium acetate/g zeolite X (3.4Cs/supercage), which showed the highest amount of basic sites measured by TPD of CO_2 .⁶²⁾

The formation of 4-methylthiazole from acetone, methylamine and SO_2 is catalyzed by alkali metal oxide-loaded zeolites at 723–773 K in vapor phase. This reaction was studied for a commercial process.



4-methyl thiazole

The zeolites ZSM-5 and β were used for their hydrothermal stability. The activities follow the order $\text{CsO}_x > \text{RbO}_x \gg \text{KO}_x$. When NaO_x was loaded, the activity dropped. Among the source of Cs salts, cesium sulfate was the most suitable.^{3,63)}

Mesoporous materials such as MCM-41 and MCM-48 become active for base-catalyzed reactions of Knoevenagel condensation and Michael addition when loaded with alkali metal oxides. Kloestra and Bekkum reported that MCM-41 containing intraporous CsO_x particles showed a high regioselectivity in the Michael addition of diethyl malonate to neopentyl glycol diacrylate at 293 K, and the Michael addition of chalcone to diethyl malonate at 423 K.^{64,65)} For both reactions, CsO_x -loaded MCM-41 showed high activities due to the generation of strong basic sites by loading intraporous CsO_x evidenced by CO_2 TPD. In the former Michael addition, regioselectivity was observed; the mono-adduct was selectively formed over $\text{CsO}_x/\text{MCM-41}$, while the bis-adduct was selectively formed over bulk Cs_2O catalyst.

Ernst et al. also reported on the influence of ion-exchange with Cs^+ cation and impregnation with cesium acetate on the catalytic activity of MCM-41 and MCM-48 for the Knoevenagel condensation of benzaldehyde with malononitrile or ethyl cyanoacetate.⁶⁶⁾ While the parent mesoporous materials exhibited only a low

activity, an ion-exchange with Cs^+ ions led to a considerable increase in activity. Higher activity was obtained for the catalyst impregnated with cesium acetate in addition to the exchanged Cs^+ ions followed by calcination at 723 K, though the structure was destroyed to some extent. They did not state that the high activities resulted from an increase in the strength of basic sites, but it seems apparent that the high activities are due to the generation of strong basic sites.

High activities of MCM-41 catalysts modified with CsO_x and KO_x were reported for the cyclization of acetonylacetone to methylcyclopentanone and dimethylfuran.^{67,68)} It is known that the ratio methylcyclopentanone/dimethylfuran is a criterion of the acidic-basic character of the catalysts; a high value of the ratio is obtained for basic catalysts (see section 2.5.7).^{69,70)} CsO_x - and KO_x -loaded MCM-41 yielded exclusively methylcyclopentanone, indicating their basic character.

4.2.3 Alkali Metal-loaded Zeolites

Addition of alkali metals to zeolites is performed mainly by two methods: direct exposure of the zeolites to the vapor of alkali metals, and impregnation of the zeolites with alcoholic solution of alkali metal azides followed by decomposition of the azides at a high temperature.

In zeolite cavities, alkali metal azides are stabilized and require higher temperatures to decompose to give metallic alkalis as compared to pure alkali metal azides. The LiN_3 and NaN_3 in the cavities of NaY decompose at 660 K and 633 K, higher than the decomposition temperatures for pure azides by 155 K and 10 K, respectively. The CsN_3 in NaY cavities decomposes in two steps at 718 K and 813 K. This is higher than the decomposition temperature of 687 K for pure CsN_3 .⁷¹⁾

A. State of loaded alkali metal

The state of alkali metals loaded on zeolites varies with the preparation procedure. Martens et al. reported that three kinds of clusters were formed upon thermal activation of the Y zeolite impregnated with methanolic solution of sodium azide: (1) large extra lattice particle (Na_x^0) characterized by a broad ESR line at $g = 2.078$, (2) intracrystalline neutral cluster (Na_y^0) giving a sharp line at $g = 2.003$ and (3) ionic clusters (Na_4^{3+}) located in the sodalite cages of the zeolite, showing a 13-line hyperfine ESR signal.⁷²⁾ The distribution of the three types of clusters depended primarily on the heating rate for decomposition of the azide. Fast heating (25 K min^{-1}) resulted in ionic clusters while slower heating (1 K min^{-1}) gave primarily neutral metal clusters.

Although ionic and neutral alkali metal clusters were detected, the clusters were not necessarily the active sites for base-catalyzed reactions. Martens et al. measured the catalytic activities of the alkali metal-loaded zeolites for 1-butene isomerization, and claimed that 1-butene isomerization activity is due to the presence of neutral intracrystalline sodium clusters.⁷³⁾ However, they also described in a later paper that basic active sites were basic framework oxygen anions in the neighborhood of intracrystalline neutral sodium clusters.⁷⁴⁾

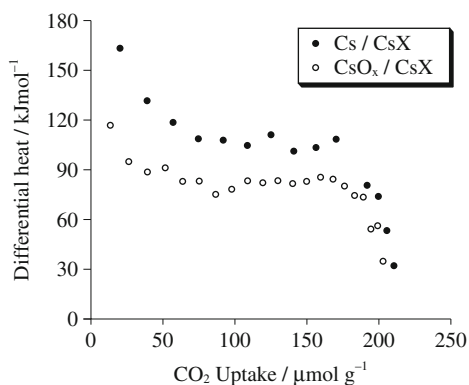


Fig. 4.2.8 Differential heats of adsorption as a function of CO₂ uptake for Cs/CsX (20 occluded Cs atoms per unit cell) and CsO_x/CsX (16 occluded Cs atoms per unit cell). Reprinted with permission from S. V. Bordawekar, R. J. Davis, *J. Catal.*, **189**, 79 (2000) Fig. 5.

B. Strength of basic sites

Enhancement of the strength of basic sites by alkali metal loading is evidenced by measuring heat of adsorption of CO₂. Fig. 4.2.8 shows examples of the differential heat of adsorption of CO₂ on CsO_x-loaded CsX and Cs metal-loaded CsX (Cs content: ca. 3.6 mmol g⁻¹) measured by microcalorimetry.⁷⁵⁾ The initial heat of adsorption was about 180 kJ mol⁻¹ for Cs metal-loaded CsX, while it was about 120 kJ mol⁻¹ for both CsO_x-loaded CsX and ion-exchanged CsX (not shown). Addition of alkali metal is more efficient than addition of alkali metal oxide in the formation of strong basic sites.

Doskoil and Mankidy reported similar results using CO₂ calorimetry for the samples containing different amounts of Na species on NaX.⁵²⁾ Na metal-loaded NaX showed stronger basic sites than NaO_x-loaded NaX. Increasing the loading Na metal resulted in an increase in the number of CO₂ adsorption sites, but did not significantly increase the highest strength of basic sites. For the sample containing 1.8 mmol g⁻¹ Na metal, the initial heat of adsorption of about 185 kJ mol⁻¹ decreased to a plateau in the range of 140–160 kJ mol⁻¹ for the CO₂ uptake 0.05–0.25 mmol⁻¹. For the sample containing 0.6 mmol g⁻¹ Na metal, initial heat of adsorption of about 185 kJ mol⁻¹ decreased continuously with CO₂ uptake to ca. 60 kJ mol⁻¹, an energy corresponding to CO₂ physisorption at room temperature, at about 0.12 mmol⁻¹ of CO₂ uptake.

C. Catalytic properties

Zeolites on which alkali metals are loaded show significant catalytic activity for several reactions for which alkali cation-exchanged or alkali metal oxide-loaded zeolites show no activity. Marten et al. formed metallic sodium particles in zeolites by decomposition of occluded sodium azide.^{72,73)} The catalyst Na/NaY showed high activity for isomerization of *n*-butenes at 325 K and for hydrogenation of *cis*-2-butene and acetylene at ca. 350 K, but no activity for hydrogenation of

benzene. The side-chain alkylation of toluene with ethylene proceeded over Na metal- and Cs metal-loaded zeolites (NaX, CsX, NaY, CsY) at 523 K, while the reaction did not proceed over alkali metal oxide-loaded zeolites under the same reaction conditions.^{72,76)} The same observation was reported for the side-chain alkenylation of *o*-xylene with 1,3-butadiene to form 5-*o*-tolyl-2-pentene.⁵³⁾ CsO_x-loaded CsX did not show any activity for the reaction, while the zeolites to which Na, K, or Cs metal was added from azides showed considerable activity at 416–418 K, though alkali metals leached out of the catalyst to some extent.

For the Michael addition of ethyl acrylate to acetone at 363 K, Na metal-loaded NaX showed better performance than CsO_x/CsX, Na/NaOH/ γ -Al₂O₃ and CsO_x/ γ -Al₂O₃, while NaX and CsX showed no activity.⁷⁶⁾ The order of the activity followed the order of basic strength: CsO_x/ γ -Al₂O₃ ($H_{-} > 37$) > Na/NaOH/ γ -Al₂O₃ ($37 > H_{-} > 35$) > CsO_x/CsX ($18.4 > H_{-} > 17.2$) \gg NaX ($9.3 > H_{-}$). Although the basic strength of Na metal-loaded NaX could not be measured by the indicator method because the catalyst is purple, the highest activity suggested the strongest basic sites for Na metal-loaded NaX.

Doskocil and Mankidy prepared zeolite NaX containing Na metal and NaO_x at loadings of 0.25, 1 and 3 Na species per cage by thermal decomposition of impregnated NaN₃ and sodium acetate, respectively, and examined the activity for 2-propanol dehydrogenation.⁵²⁾ Loadings of 0.25, 1 and 3 Na per supercage correspond to 0.15, 0.60 and 1.8 mmol g⁻¹, respectively. Basicity was measured by microcalorimetry of CO₂. Increasing the loading of Na metal or NaO_x resulted in an increase in the number of CO₂ adsorption sites, but did not significantly increase the highest strength of the basic sites. They measured the rates of dehydrogenation and dehydration at 513 K as a function of Na metal loading (Fig. 4.2.9). The dehydrogenation of 2-propanol increased linearly with the amount of

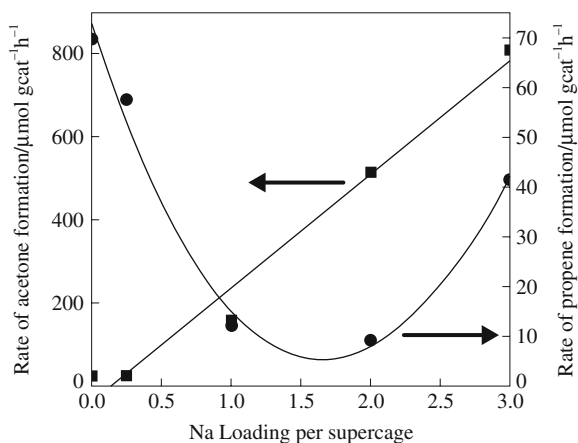


Fig. 4.2.9 Effect of increased loading of NaO_x on the rate of acetone and propene formation over Na/NaX catalysts
Reprinted with permission from E. J. Doskocil, P. J. Mankidy, *Appl. Catal. A*, **252**, 119 (2003) Fig. 6.

Na metal loaded. The rate of dehydration, however, initially decreased with the amount of loaded Na metal, attained a minimum at about 1.5 Na per supercage, and increased again with further increase in the amount of loaded Na metal. The same tendency was observed for NaO_x-loaded NaX. The Na metal-loaded NaX was more active than NaO_x-loaded NaX at the same loaded amount of Na species.

Reaction of 2-methyl-3-butyn-2-ol (MBOH) was examined over Na metal-loaded on different types of zeolite and Al₂O₃. Acetone was formed over all the catalysts, indicating base-catalyzed decomposition. The activity varied with the type of zeolite on which NaN₃ was impregnated and decomposed. The order of the activities was NaX > NaY > NaL > Naβ > Al₂O₃.⁷⁷⁾

References

1. D. Barthomeuf, A. Mallmann, *Stud. Surf. Sci.*, **37**, 365 (1988).
2. D. Barthomeuf, *Catal. Rev. -Sci. Eng.*, **38**, 521 (1996).
3. C. B. Dartt, M. E. Davis, *Catal. Today*, **19**, 151 (1994).
4. Y. Ono, *Catal. Today*, **38**, 321 (1997).
5. J. Weitkamp, M. Hunger, U. Ryma, *Micropor. Mesopor. Mater.*, **48**, 255 (2001).
6. R. J. Davis, *J. Catal.*, **216**, 396 (2003).
7. J. Weitkamp, M. Hunger, *Stud. Surf. Sci. Catal.*, **168**, 787 (2007).
8. M. Sánchez-Sánchez, T. Blasco, *Catal. Today*, **143**, 293 (2009).
9. Y. N. Sidorenko, P. N. Galich, V. S. Gutryra, V. G. Illin, I. E. Neimark, *Dokl. Akad. Nauk SSSR*, **175**, 177 (1967).
10. T. Yashima, K. Sato, T. Hayashi, N. Hara, *J. Catal.*, **26**, 303 (1972).
11. D. Barthomeuf, *J. Phys. Chem.*, **88**, 42 (1984).
12. D. Barthomeuf, *Mater. Chem. Phys.*, **18**, 553 (1988).
13. D. Barthomeuf, in *Catalysis and Adsorption by Zeolites*, (eds. G. Oehlmann et al.), Elsevier Science Publisher B. V. Amsterdam, 1991, p. 157.
14. D. Barthomeuf, in: *Acidity and Basicity of Solids; Theory, Assessment and Utility*, (eds. J. Fraissard, L. Petrakis) NATO ASI ser. C, Vol. 444, p. 181, Kluwer Academic Publishers, 1994.
15. R. T. Sanderson, *J. Am. Chem. Soc.*, **105**, 2259 (1983).
16. W. J. Mortier, *J. Catal.*, **55**, 138 (1978).
17. M. Huang, S. Kaliaguine, *J. Phys. Chem.*, **88**, 751 (1992).
18. M. Huang, A. Adnot, S. Kaliaguine, *J. Catal.*, **137**, 322 (1992).
19. M. Huang, S. Kaliaguine, *J. Chem. Soc. Faraday Trans.*, **88**, 751 (1992).
20. M. Huang, A. Adnot, S. Kaliaguine, *J. Am. Chem. Soc.*, **114**, 10005 (1992).
21. D. Murphy, P. Massiani, R. Franck, D. Barthomeuf, *Stud. Surf. Sci. Catal.*, **105**, 639 (1997).
22. D. Murphy, P. Massiani, R. Franck, D. Barthomeuf, *J. Phys. Chem.*, **100**, 6731 (1996).
23. M. Sánchez-Sánchez, T. Blasco, *Chem. Commun.*, 491 (2000).
24. M. Sánchez-Sánchez, T. Blasco, *J. Am. Chem. Soc.*, **124**, 3443 (2002).
25. Y. Okamoto, M. Ogawa, A. Maezawa, T. Imanaka, *J. Catal.*, **112**, 427 (1988).
26. T. L. Barr, *Zeolite*, **10**, 760 (1990).
27. W. Grünert, M. Muhler, K.-P. Schröder, J. Sauer, R. Schlögl, *J. Phys. Chem.*, **98**, 10920 (1994).
28. T. Yashima, H. Suzuki, N. Hara, *J. Catal.*, **33**, 486 (1974).
29. A. Philippou, J. Rocha, M. W. Anderson, *Catal. Lett.*, **57**, 151 (1999).
30. P. Concepción-Heydorn, C. Jia, D. Herein, N. Pfaender, H. G. Karge, F. C. Jentoft, *J. Mol. Catal. A*, **162**, 227 (2000).
31. A. Corma, R. M. Martín-Aranda, F. Sanchez, *J. Catal.*, **126**, 192 (1990).
32. J. Shabtai, R. Lazar, E. Biron, *J. Mol. Catal.*, **27**, 35 (1984).
33. W. F. Hölderich, in: *Acid-Base Catalysis* (eds. K. Tanabe, H. Hattori, T. Yamaguchi, T. Tanaka) Kodansha, Tokyo, 1988, pp.1-20.
34. A. Corma, V. Fornes, R. M. Martín-Aranda, H. Garcia, J. Primo, *Appl. Catal.*, **59**, 237 (1990).
35. R. Ballini, F. Bigi, E. Gogni, R. Maggi, G. Sartori, *J. Catal.*, **191**, 348 (2000).
36. A. Corma, R. M. Martín-Aranda, *J. Catal.*, **130**, 130 (1991).
37. M. Huang, S. Kaliaguine, *Stud. Surf. Sci. Catal.*, **78**, 559 (1993).

38. A. Philippou, M. Naderi, J. Rocha, M. W. Anderson, *Catal. Lett.*, **53**, 221 (1998).
39. A. Philippou, J. Rocha, M. W. Anderson, *Catal. Lett.*, **57**, 151 (1999).
40. A. Philippou, M. W. Anderson, *J. Catal.*, **189**, 395 (2000).
41. Y. Goa, P. Wu, T. Tatsumi, *J. Catal.*, **224**, 107 (2004).
42. P. E. Hathaway, M. E. Davis, *J. Catal.*, **116**, 263 (1989).
43. P. E. Hathaway, M. E. Davis, *J. Catal.*, **116**, 279 (1989).
44. P. E. Hathaway, M. E. Davis, *J. Catal.*, **119**, 497 (1989).
45. H. Tsuji, F. Yagi, H. Hattori, *Chem. Lett.*, **20**, 1881 (1991).
46. J. C. Kim, H.-X. Li, C.-Y. Chen, M. E. Davis, *Micropor. Mater.*, **2**, 413 (1994).
47. F. Yagi, N. Kanuka, H. Tsuji, S. Nakata, H. Kita, H. Hattori, *Micropor. Mater.*, **9**, 229 (1997).
48. M. Hunger, U. Schek, J. Weitkamp, *J. Mol. Catal. A*, **134**, 97 (1998).
49. F. Yagi, H. Hattori, *Micropor. Mater.*, **9**, 247 (1997).
50. F. Yagi, H. Tsuji, H. Hattori, *Micropor. Mater.*, **9**, 237 (1997).
51. S. V. Bordawekar, R. Davis, *J. Catal.*, **189**, 79 (2000).
52. E. J. Doskocil, P. J. Mankidy, *Appl. Catal. A*, **252**, 119 (2003).
53. E. J. Doskocil, R. J. Davis, *J. Catal.*, **188**, 353 (1999).
54. M. Hunger, U. Schenk, B. Burger, J. Weitkamp, *J. Mol. Catal. A*, **134**, 97 (1998).
55. J. Li, R. J. Davis, *Appl. Catal. A*, **239**, 59 (2003).
56. J. Zhu, Y. Chun, Y. Wang, Q. Xu, *Catal. Today*, **51**, 103 (1999).
57. M. Laspéras, H. Cambon, D. Brunel, I. Rodriguez, G. Geneste, *Micropor. Mater.*, **1**, 343 (1993).
58. M. Laspéras, H. Cambon, D. Brunel, I. Rodriguez, P. Geneste, *Micropor. Mater.*, **7**, 61 (1996).
59. I. Rodriguez, H. Cambon, D. Brunel, M. Laspéras, P. Geneste, *Stud. Surf. Sci. Catal.*, **78**, 623 (1993).
60. I. Rodriguez, H. Cambon, D. Brunel, M. Laspéras, *J. Mol. Catal. A*, **130**, 195 (1998).
61. U. Ryma, M. Hunger, H. Knözinger, J. Weitkamp, *Stud. Surf. Sci. Catal.*, **125**, 197 (1999).
62. U. Meyer, W. F. Hölderich, *J. Mol. Catal. A*, **142**, 213 (1999).
63. US Pat. 5231187, assigned to Merck & Co., Inc. (1993) Cited in ref. 3.
64. K. R. Koelstra, H. van Bekkum, *J. Chem. Soc. Chem. Commun.*, **1995**, 1005.
65. K. R. Koelstra, H. van Bekkum, *Stud. Surf. Sci. Catal.*, **105**, 431 (1997).
66. S. Ernst, T. Bongers, C. Casel, S. Munsch, *Stud. Surf. Sci. Catal.*, **125**, 367 (1999).
67. M. Ziolek, A. Michalska, J. Kujawa, A. Lewandowska, *Stud. Surf. Sci. Catal.*, **141**, 411 (2002).
68. A. Michalska, M. Daturi, J. Saussey, I. Noeak, M. Ziolek, *Micropor. Mesopor. Mater.*, **90**, 362 (2006).
69. R.M. Dessau, *Zeolites*, **10**, 205 (1990).
70. J. J. Alcaraz, B. J. Arena, R. D. Gillespie, J. S. Holmgren, *Catal. Today*, **43**, 89 (1998).
71. A. Beres, I. Hannus, I. Kiricsi, *J. Therm. Anal.*, **46**, 1301 (1996).
72. L. R. Martens, P. J. Grobet, W. J. M. Vermeiren, P. A. Jacobs, *Stud. Surf. Sci. Catal.*, **28**, 935 (1986).
73. L. R. M. Martens, P. J. Grobet, P. A. Jacob, *Nature*, **315**, 568 (1985).
74. L. R. M. Martens, W. J. Vermeiren, D. R. Huybrechts, P. J. Grobet, P. A. Jacobs, *Proc. 9th Intern. Congr. Catal. Calgary*, 1988, Vol. 1, 420.
75. S. V. Bordawekar, R. J. Davis, *J. Catal.*, **189**, 79 (2000).
76. U. Meyer, H. Gorzawski, W. F. Hölderich, *Catal. Lett.*, **59**, 201 (1999).
77. L. Martins, W. Hölderich, D. Cardoso, *J. Catal.*, **258**, 14 (2008).

4.3 Metal Phosphates

4.3.1 Metal Phosphates

Basic properties of alkali and alkaline earth phosphates were determined by indicator method.¹⁾ The results are shown in Table 4.3.1. Among the phosphates studied, K_3PO_4 shows the highest base strength. $Ca_3(PO_4)_2$ and Na_3PO_4 have weak basic sites. The catalytic activities of the phosphates for retro-aldol reaction of diacetone alcohol are in good agreement with the base strength.

Calcium phosphate, $Ca_3(PO_4)_2$, is highly selective for the methylation of phenol to *o*-cresol and 2,6-dimethylphenol.²⁾ At 733 K, the selectivity for *ortho*-

Table 4.3.1 Basic strength of alkali and alkaline earth metal phosphates

Original metal phosphate	Calcination temp./K	Basic strength (H_-) ^{a)}			
		7.1	9.3	15.0	17.2
Li ₃ PO ₄	295 – 673	–	–	–	–
Na ₃ PO ₄ ·12H ₂ O	295 – 973	+	+	–	–
Na ₂ HPO ₄ ·12H ₂ O	295 – 333	–	–	–	–
	423 – 773	+	+	–	–
NaH ₂ PO ₄ ·2H ₂ O	295 – 673	–	–	–	–
Na ₄ P ₂ O ₇ ·10H ₂ O	295 – 773	–	–	–	–
K ₃ PO ₄	295 – 1073	+	+	+	+
K ₃ HPO ₄	295 – 773	+	–	–	–
KH ₂ PO ₄	295 – 673	–	–	–	–
Ca ₄ (PO ₄) ₂	295 – 873	+	+	–	–
Ca(H ₃ PO ₄) ₂ ·H ₂ O	295 – 673	–	–	–	–

^{a)} + or – denotes yes or no.

Reprinted with permission from A. Tada, *Bull. Chem. Soc. Jpn.*, **48**, 1391 (1975) p.1391, Table 1.

alkylation was 68.2% at a phenol conversion of 77.7%. The selectivity based on methanol is also very high (93%), only a small amount of methanol being decomposed. Ca₃(PO₄)₂ has basic sites with $H_- \geq 7.1$. No basic sites are observed on CaHPO₄, Ca(H₂PO₄)₂ and BPO₄, and these phosphates show low activity and selectivity for *ortho*-alkylation.

Potassium phosphate, K₃PO₄, is highly active for cyanosilylation of 2-octanone with cyanotrimethylsilane.³⁾ On the other hand, acidic phosphates, Ca(HPO₄) and Ni₃PO₄ showed hardly any activities.

In the alkylation of toluene with methanol, K₃PO₄/activated carbon and Ca₃(PO₄)₂ gave ethylbenzene selectively at 773 K.⁴⁾

The synthetic diphosphate, Na₂CaP₂O₇, is an active catalyst for base-catalyzed reactions such as Knoevenagel condensation and Michael addition.⁵⁻⁷⁾ The Knoevenagel condensation of aldehydes and active methylene proceeds in methanol or ethanol in the presence of Na₂CaP₂O₇ at room temperature.⁵⁾ The activity is enhanced when water is added, leading to quantitative yields in a few minutes.

The potassium exchanged layered hydrogen zirconium phosphate, Zr(KPO₄)₂, is an efficient catalyst for Michael addition of β -dicarbonyl compounds⁸⁾ and the Knoevenagel condensation of aldehydes and active methylene compounds⁹⁾ in solvent-free conditions. Zr(KPO₄)₂ was prepared by exfoliation of layered hydrogen phosphate by intercalation of propylamine followed by ion-exchange with K⁺, the surface area being 15.5 m²g⁻¹. It is suggested that the surface $\equiv\text{P}-\text{O}^-$ group acts as a strong Brønsted base.⁹⁾

4.3.2 Hydroxyapatite, Fluoroapatite

Preparation techniques and characterization of hydroxyapatite (Ca₁₀(PO₄)₆(OH)₂, HAP) have been reviewed.¹⁰⁾

Acid-base properties of hydroxyapatite, $\text{Ca}_{10-x}(\text{HPO}_4)_x(\text{PO}_4)_{6-x}\text{OH}_{2-x}$, depend on its composition.^{11,12)} Hydroxyapatites vary from the stoichiometric composition, (HAP, $x = 0$), to the calcium-deficient nonstoichiometric form (NHAP, up to $x = 1$), without any fundamental change in the crystal lattice.¹³⁾ For moderate change in the Ca/P ratio, calcium deficiencies are compensated by protons. A stoichiometric preparation is basic, while NHAP is acidic because of protons.

Dehydration of alcohols over hydroxyapatite was studied in detail by Kibby and Hall.¹¹⁾ HAP catalyzed both dehydration and dehydrogenation of alcohols, while a NHAP ($x = 1$) is acidic and active only for dehydration.^{11,13)} The dehydration was much faster over NHAP than over HAP. From the evidence, the dehydration was concluded to proceed via an "E1-like mechanism" on acidic sites. On the other hand, the dehydrogenation was concluded to proceed through negatively-charged transition state. Hydrogen transfer reaction from alcohols to ketones proceeds much faster over HAP than over NHAP. Both dehydrogenation of alcohols and the hydrogen transfer reactions plausibly proceed on the same sites and involve the same reaction intermediate species.¹⁴⁾

In the reaction of ethanol, dehydration is predominant over the NHAP ($x = 0.46$), while 1-butanol due to Guerbet reaction was a main product with HAP. ($x = 0-0.1$).¹²⁾

The effect of high temperature treatment of hydroxyapatite under vacuum on the catalytic activity for 1-butene isomerization was reported by Imizu et al.¹⁵⁾ The HPA evacuated at 573 K showed no activity. When HAP was evacuated at 973 K, the isomerization proceeded with a large *cis/trans* ratio of produced 2-butene even at 273 K. The catalytic activity was completely retarded by adsorption of CO_2 . The reaction of the mixture of *cis*-2-butene- d_6 and *cis*-2-butene- d_8 showed that the isomerization occurred through intramolecular hydrogen shift. These results indicate that strongly basic sites develop upon high-temperature evacuation of HPA.

Hydroxyapatite (HAP) is very active for cyanosilylation of various carbonyl compounds.³⁾ For example, the reaction of benzophenone with cyanotrimethylsilane in toluene at 273 K gave the addition product in 98% yield at 273 K in 0.3 h. The reaction was completely retarded upon addition of CCl_3COOH , indicating the basic character of hydroxyapatite (see Fig. 2.3.1). The hydrosilylation of various carbonyl compounds with triethoxysilane proceeds over hydroxyapatite at 363 K (section 6.4.3).¹⁶⁾

Synthetic hydroxyapatite is an efficient catalyst for the Michael addition of mercaptanes to chalcone derivatives with high yields¹⁷⁾ (section 5.5.2), and also for epoxidation of alkenes.¹⁸⁾

The hydration of nitriles such as benzonitrile proceeds over NaNO_3 -modified hydroxyapatite and natural phosphate in the absence of organic solvents.¹⁹⁾ The corresponding amides were obtained efficiently and selectively in good yields.

Hydroxyapatite and fluoroapatite, $\text{Ca}_{10}(\text{PO}_4)_6\text{F}_2$, is an effective catalyst for the Knoevenagel condensation without a solvent.²⁰⁻²²⁾ The activities are enhanced by water, benzyltriethylammonium chloride (BTEAC) or both. The hydroxyapatite and fluoroapatite activated with water and BTEAC are excellent catalysts for the Knoevenagel condensation, leading to excellent yields in a few minutes.

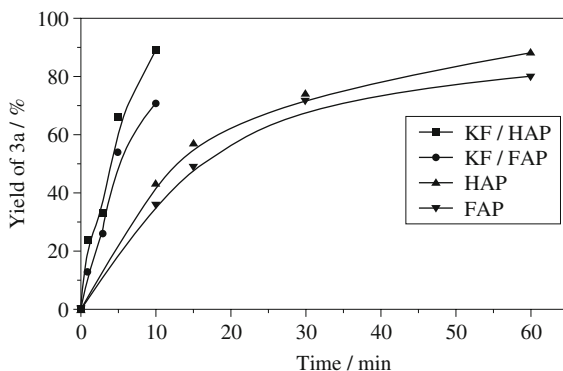


Fig. 4.3.1 Kinetic of the alkene synthesis from benzaldehyde and malononitrile in the presence of FAP, HAP, KF/FAP, KF/HAP at room temperature. Reaction conditions: benzaldehyde: 1.5 mmol, malononitrile: 1.5 mmol, catalyst: 0.1 g, solvent: methanol 1 ml. Reprinted with permission from A. Smahi, A. Solhy, H. Elbadaoui, A. Amouki, A. Tikad, M. Maizi, S. Sebti, *Appl. Catal., A*, **250**, 151 (2003) p. 157, Fig. 8.

Loading of KF on hydroxyapatite and fluoroapatite also shows the positive effect on the rate of the Knoevenagel condensation.²³⁾ Fig. 4.3.1 shows the kinetic curves of the reaction between benzaldehyde and malononitrile in the presence of hydroxyapatite (HAP), fluoroapatite (FAP), KF/hydroxyapatite and KF/fluoroapatite. The activity increases in the order FAP < HAP < KF/HAP < KF/HAP.

4.3.3 Natural Phosphate

Sebti and coworkers studied extensively the catalytic use of a natural phosphate for a variety of base-catalyzed reactions such as Knoevenagel condensation and Michael addition.^{24–28)} The natural phosphate comes from an extracted ore in the region of Khouriga (Morocco) and the structure is similar to that of fluoroapatite. The activity is greatly enhanced by doping KF or by loading NaNO_3 (or LiNO_3) followed by calcination.

References

1. A. Tada, *Bull. Chem. Soc. Jpn.*, **48**, 1391 (1975).
2. F. Nozaki, I. Kimura, *Bull. Chem. Soc. Jpn.*, **50**, 614 (1977).
3. K. Higuchi, M. Onaka, Y. Izumi, *Bull. Chem. Soc. Jpn.*, **66**, 2016 (1993).
4. T. Sodezawa, I. Kimura, F. Nozaki, *Bull. Chem. Soc. Jpn.*, **52**, 2431 (1979).
5. J. Bennazha, M. Zahouily, S. Sebti, A. Boukhari, E. M. Holt, *Catal. Commun.*, **2**, 101 (2001).
6. M. Zahouily, M. Salah, J. Bennazha, A. Rayadh, S. Sebti, *Tetrahedron Lett.*, **44**, 3255 (2003).
7. M. Zahouily, Y. Abrouki, A. Rayadh, *Tetrahedron Lett.*, **43**, 7729 (2002).
8. U. Constantino, F. Marmottini, M. Curini, O. Rosati, *Catal. Lett.*, **22**, 333 (1993).
9. M. Curini, F. Epifano, M. C. Marcotullio, O. Rosati, A. Tsadjout, *Synth. Commun.*, **32**, 355 (2002).
10. T. S. B. Narasraju, D. E. Phebe, *J. Mater. Sci.*, **31**, 1 (1996).
11. C. L. Kibby, W. K. Hall, *J. Catal.*, **29**, 144 (1973).
12. T. Tsuchida, J. Kubo, T. Yoshioka, S. Sakuma, T. Takeguchi, W. Ueda, *J. Catal.*, **259**, 183 (2008).

13. J. A. S. Bett, L. G. Christner, W. K. Hall, *J. Am. Chem. Soc.*, **89**, 5535 (1967).
14. C. L. Kibby, W. K. Hall, *J. Catal.*, **31**, 65 (1973).
15. Y. Imizu, M. Kadoya, H. Abe, *Catal. Lett.*, 415 (1982).
16. M. Onaka, K. Higuchi, H. Nanami, Y. Izumi, *Bull. Chem. Soc. Jpn.*, **66**, 2638 (1993).
17. M. Zahouily, Y. Abrouki, A. Rayadh, S. Sebti, *Catal. Commun.*, **4**, 521 (2003).
18. U. R. Pillai, E. Sahle-Demessie, *Appl. Catal., A*, **261**, 69 (2004).
19. F. Bazi, H. El Badaui, S. Tamani, S. Sokori, A. Solhy, D. J. Macquarrie, S. Sebti, *Appl. Catal., A*, **301**, 211 (2006).
20. S. Sebti, R. Tahir, R. Nazih, A. Saber. S. Boulaajaj, *Appl. Catal., A*, **228**, 155 (2002).
21. S. Sebti, N. Nasih, R. Tahir, L. Salhi, A. Saber, *Appl. Catal., A*, **197**, L187 (2000).
22. M. Zahouily, M. Salah, B. Bahlaouan, B. Mounir, A. Rayadh, S. Sebti, *Catal. Lett.*, **96**, 57 (2004).
23. A. Smahi, A. Solhy, H. El Badaoui, A. Amoukal, A. Tikad, M. Maïzi, S. Sebti, *Appl. Catal., A*, **250**, 151 (2003).
24. S. Sebti, A. Saber, A. Rhihil, R. Nazih, R. Tahir, *Appl. Catal., A*, **206**, 217 (2001).
25. S. Sebti, A. Solhy, R. Tahir, S. Abdelatif, S. Boulaajaj, J. A. Mayoral, J. I. Garcia, J. M. Fraile, A. Kossir, H. Oumimoun, *J. Catal.*, **213**, 1 (2003).
26. S. Sebti, A. Solhy, A. Smahi, A. Kossir, H. Oumimoun, *Catal. Commun.*, **3**, 335 (2002).
27. S. Sebti, A. Smahi, A. Solhy, *Tetrahedron Lett.*, **43**, 1813 (2002).
28. Y. Abouki, M. Zahouly, A. Rayadh, B. Bahlaouan, S. Sebti, *Tetrahedron Lett.*, **43**, 8951 (2002).

4.4 Metal Oxynitrides

Certain metal oxides exhibit basic properties when O atoms are partly substituted by N atoms and show catalytic activities for base-catalyzed reactions. These metal oxides include silica, aluminum phosphate, aluminum vanadate, zirconium phosphate and silica alumina in either amorphous or crystalline form.

Base catalysis by oxynitride was first reported by Lednor and de Rooter for silicon oxynitride.¹⁾ Soon after, aluminum phosphate, aluminum vanadate and zirconium phosphate were nitrated and the resulting oxynitrides were examined for their catalytic activities for base-catalyzed reactions. The nitridation was performed also on the ordered microporous and mesoporous materials. The resulting oxynitrides keep their porous properties and thus show characteristic catalytic properties arising from the pore structure.

4.4.1 Preparation

The most common way to prepare metal oxynitrides is to utilize the reaction of metal oxides with NH_3 at high temperature. For silicon oxynitride, SiO_2 was heated in a flowing NH_3 at 1373 K.²⁾ The degree of nitridation depends on the crystallinity; amorphous forms of SiO_2 give rise to higher bulk nitrogen contents than the crystalline ones when nitrated at the same temperature.¹⁾ Starting from Aerosil silica, the nitrated material had a composition corresponding to $\text{Si}_2\text{N}_2\text{O}$, i.e., 28 wt% N with a surface area of $150 \text{ m}^2\text{g}^{-1}$ after NH_3 treatment at 1373 K for 24 h. For aluminum phosphate oxynitride, aluminum phosphate (AlPO_4) was treated with flowing NH_3 up to 1073 K. The degree of nitridation is dependent on the temperature and time. Different N-related species are formed by treatment with NH_3 , which is dependent on the treatment temperature. The surface area did not change much on nitridation.³⁾

Table 4.4.1 Temperature for nitridation of different metal oxides

Metal oxide precursor	NH ₃ Treatment temperature/K	Metal oxynitride
Aluminum phosphate (AlPO)	1023–1073	AlPON
Aluminum gallium phosphate (AlGaPO)	1023	AlGaPON
Zirconium phosphate (ZrPO)	823–1073	ZrPON
Aluminum vanadate (VAIO)	873–1073	VAIPON
Silica (SiO ₂), SBA-15	1073–1323	
AlPO ₄ -5	1073–1148	
NaY	1123	
ZSM-5	1323–1373	

The proper temperature for nitridation depends on the type of metal oxide. In Table 4.4.1 are summarized the temperatures at which metal oxides were treated with NH₃ for metal oxynitrides. The oxides containing P (or V) can be nitrated much easier than the oxides composed of Si and Al without P (or V).

Two methods have been reported for the preparation of oxynitrides other than NH₃ treatment. One is liquid phase synthesis.⁴⁾ Silicon oxynitride was prepared as follows. A solution of SiCl₄ in a mixture of benzene and cyclohexane is allowed to react with liquid ammonia. Silicon diimide and ammonium chloride precipitate. The latter is washed out with liquid ammonia and the residue is then heated in a flowing gaseous ammonia at 1273 K for 5 h to give an amorphous product composed of Si 57%, N 25% and O 23%. The oxygen in the product probably arises from insufficient exclusion of air in manipulating the very moisture-sensitive SiCl₄ and air-sensitive silicon diimide.

Direct nitridation with N₂ was reported by Kapoor and Inagaki.⁵⁾ They started with a periodic ethane-bridged mesoporous silica having ≡Si-CH₂-CH₂-Si≡ units with hexagonal symmetry. The precursor was heated above 973 K under N₂ to form a mesoporous silicon oxynitride. The resulting material contained C, which could be removed by calcination in air. The mesoporous structure was retained up to a nitridation and calcination temperature of 1273 K.

Mesoporous structure of MCM-48 and MCM-41 is retained after nitridation at a high temperature. Xia and Mokaya prepared Na free MCM-48 and calcined at 823 K in air for 6 h followed by nitridation with NH₃ at 1173 K. Upon nitridation, *d* spacing, pore volume and pore size were reduced to a considerable extent, but surface area increased by ca. 7%. It should be noted that when MCM-48 was subjected to heat treatment at 1127 K in air for the same duration as for the nitridation (i.e., 20 h), it was virtually destroyed; surface area and pore volume were reduced to 62 m²g⁻¹ and 0.07 cm³g⁻¹, respectively. This implies that an NH₃ atmosphere is an important factor in maintaining structural ordering during nitridation.^{6,7)}

Crystalline structures of ZSM-5, NaY and AlPO₄-5 are retained after nitridation with NH₃ up to 1323 K for ZSM-5 and 1173 K for NaY and AlPO₄-5.^{8,9)}

4.4.2 Nitridation Mechanisms

The mechanisms of the reaction forming silicon oxynitride by high temperature treatment of SiO_2 with NH_3 were examined by Chino and Okubo.¹⁰⁾ Mesoporous silica SBA-15 was used as a starting SiO_2 .¹⁰⁾ IR of O-H and N-H stretching region and ^{29}Si MAS NMR were employed for tracing the structural change. It was revealed that in the temperature range 873–973 K, only NH_2 groups formed and in the range 973–1073 K, Si-NH-Si groups formed in addition to NH_2 groups. Above 1173 K, the NH_2 groups were mostly eliminated and the NH groups were predominant. ^{29}Si MAS NMR can distinguish among different components of Si: SiO_4 , $\text{SiO}_3(\text{OH})$, SiNO_3 , SiN_2O_2 , SiN_3O and SiN_4 . The fraction of these components varied with the nitridation temperature, as shown in Fig. 4.4.1.

Chino and Okubo proposed based on the IR and ^{29}Si MAS NMR observation that the nitridation progresses by the following equations as the temperature of NH_3 treatment is raised.

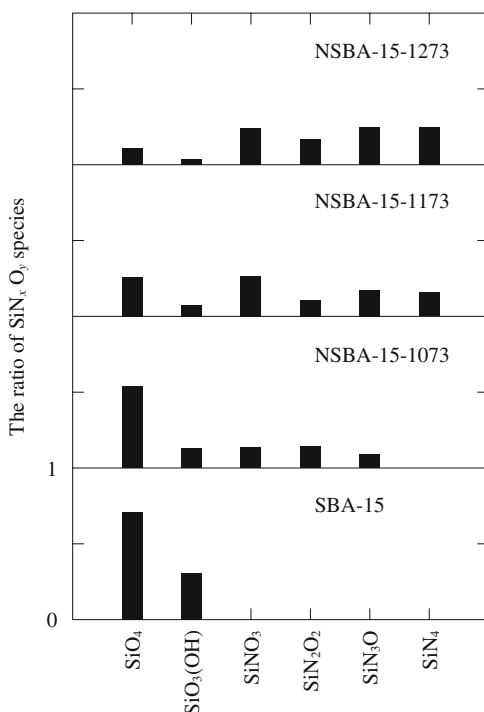
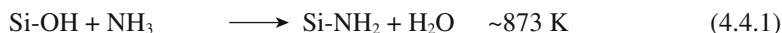
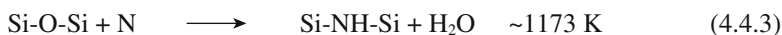
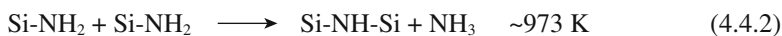


Fig. 4.4.1 Distribution of SiN_xO_y components ($x = 0-4$, $y = (4-x)$) on SBA-15 and nitrated SBA-15 (NSBA-15) samples. These results were obtained from ^{29}Si MAS NMR data. Reprinted with permission from N. Chino, T. Okubo, *Micropor. Mesopor. Mater.*, **87**, 15 (2005) Fig. 5.



Similar results were reported by Wang and Liu.¹¹⁾

The nitrated aluminophosphate known as AIPON is the most extensively studied for its catalytic activities. Nitridation of aluminophosphate with NH_3 is negligible below 923 K and phosphorus begins to be eliminated as PH_3 above 1073 K.¹²⁾

Benitez et al. measured XPS of the AIPON.¹²⁾ They observed that the binding energy (BE) of Al_{2p} did not shift on nitridation, but that of P_{2p} and N_{1s} shifted to lower values, indicating that N was preferentially bonded to P. The presence of a band at 1563 cm^{-1} is indicative of the $-\text{PNH}_2$ groups as chain termination in the AIPON framework.

Blasco et al. measured ^{31}P , ^{27}Al MAS NMR and IR spectra for AIPON treated with NH_3 at 1073–1123 K and 1273 K.¹³⁾ They observed IR bands at 1550 cm^{-1} and 3480 cm^{-1} which were assigned to bending vibration and stretching vibration, respectively, of P-NH₂ groups. The P-NH₂ groups are formed by the reaction



By the NH_3 treatment at 1273 K, an aluminophosphate trydimite phase appeared with $\text{PO}_{4-x}\text{N}_x$ entities. Although IR spectra showed a band 3370 cm^{-1} assigned to $-\text{NH}-$ stretching vibration, no NMR spectra showing the presence of Al-NH-P were obtained.

Benitez et al. studied the nitridation process for AIPON by XPS and IR (DRIFTS) for varying degree of nitridation.¹⁴⁾ The degree of nitridation can be controlled by the NH_3 treatment temperature and duration. At a low nitridation degree, the N_{1s} peak in XPS appeared at 398.9 eV assigned to $-\text{NH}_2$. At a higher degree of nitridation, the N_{1s} peak at 398.9 eV did not increase, but the other N_{1s} peak at 397.5 eV assigned to structural nitrogen ($>\text{N}-$, $=\text{N}-$, or $-\text{NH}-$) continuously increased with nitridation degree. In IR (DRIFTS) bands at 980 and 760 cm^{-1} , assigned to ν_{as} and ν_{a} of P-O-P bonds, respectively, appeared at a low nitridation degree. These bands became weaker and the band at 910 cm^{-1} assigned to ν_{as} of P-N-P or P-NH-P bonds was intensified. As the nitridation degree progressed, the band at 1560 cm^{-1} assigned to $-\text{NH}_2$ associated with P grew and the bands at 3785 and 3670 cm^{-1} assigned to Al-OH and P-OH, respectively, decreased and the band at 3350 cm^{-1} assigned to structural N-H stretching grew. It was proposed that nitridation starts at the surface of AlPO_4 by breaking P-O bonds and generating terminal P-NH₂. Once surface P-NH₂ saturation is achieved (above 3.6 wt% N), bulk nitridation occurs.

As described above, N is bonded to P and not to Al. This is due to the enhanced strength of P-N and Al-O bonds with respect to P-O and Al-N.¹⁴⁾

Nitridation of aluminovanadate occurs to form oxynitride (VAIPON) when treated with NH_3 at high temperature. In XPS, BE of $\text{V}_{2p\ 3/2}$ shifted to a lower

value by NH_3 treatment in the range 673–873 K, while BE of Al_{2p} remained constant in the temperature range 500–1273 K, indicating that nitridation begins between 673 and 873 K and affects only the V environment.¹⁵⁾

In the treatment of zirconophosphate with NH_3 , the nitridation takes place in the temperature range 823–1073 K to form oxynitride phase (ZrPON).¹⁶⁾ In the initial stage of nitridation, hydrogenated surface species such as NH_4^+ , NH_3 , $-\text{NH}_2$ and $-\text{NH}-$ are formed. The $-\text{NH}_2$ species are present preferentially in the coordination sphere of P.¹⁷⁾ As the nitridation proceeds, the nitride anions, N^{3-} form accordingly. Above 1073 K, the reduction of phosphorus P^{V} to P^{III} occurs, resulting in the formation of phosphine volatile species. When heated under an NH_3 flow up to 1573 K, the phosphorus is completely removed and ZrO_2 and $\text{Zr}_7\text{N}_4\text{O}_8$ phases appear.¹⁸⁾

4.4.3 Characterization of Basic Sites

The basic sites on metal oxynitrides are weak and their strength cannot be clearly estimated by TPD of CO_2 . For some oxynitrides, the strength of basic sites has been measured by calorimetry of SO_2 adsorption and IR of adsorbed CDCl_3 and compared with those of other metal oxides.

Differential heats of adsorption of SO_2 are 130–160 kJ mol^{-1} ¹⁷⁾ and ~ 140 kJ mol^{-1} ¹⁹⁾ for ZrPON and AlGaPON , respectively. These values are lower than 194 kJ mol^{-1} for Al_2O_3 and 215 kJ mol^{-1} for MgO , but higher than 60 kJ mol^{-1} for SiO_2 .

The IR absorption band due to C-D stretching vibration of adsorbed CDCl_3 reflects the strength of basic sites. The CDCl_3 adsorbed on VAION and AlGaPON show the bands at 2250 and 2249 cm^{-1} , respectively. In references, when CDCl_3 is adsorbed on SiO_2 , Al_2O_3 , CsNaY and MgO , the bands appear at 2265, 2253, 2243 and 2230 cm^{-1} , respectively. The basic sites on the oxynitrides are stronger than those on SiO_2 , weaker than those on CsNaY and MgO , and comparable to those on Al_2O_3 .

The strength of basic sites of AIPONs was estimated to be 10.7–11.2 in the H_- scale. Massion et al. compared the catalytic activity of AIPON with homogeneous bases of different $\text{p}K_a$.²⁰⁾ They used different reactants with different $\text{p}K_a$. The Knoevenagel condensations of benzaldehyde with malononitrile ($\text{p}K_a = 9$) and with ethyl cyanoacetate ($\text{p}K_a = 9$) proceeded, but not with diethyl malonate ($\text{p}K_a = 13$). The Knoevenagel condensations of benzaldehyde with malononitrile and with ethyl cyanoacetate were catalyzed neither by pyridine ($\text{p}K_a = 5.25$) nor by morpholine ($\text{p}K_a = 8.33$), but catalyzed by pyrrolidine ($\text{p}K_a = 11.25$) whose activity was comparable to that of AIPON. Taking into account of the results of Corma et al.^{21,22)} that the Knoevenagel condensations were catalyzed by basic oxides with $H_- < 10.7$, the series of AIPON catalysts containing different amounts of N possess basic sites in the range 10.7–11.2 in H_- scale.

4.4.4 Catalytic Properties

The catalytic properties of metal oxynitrides have been most commonly examined

for Knoevenagel condensations, in particular, the Knoevenagel condensation of benzaldehyde with malononitrile.



Over some metal oxynitrides, dehydration and dehydrogenation of alcohols, alkylation of toluene and 1-butene isomerization were examined.

The first oxynitride used for catalytic reaction was silicon oxynitride (SiON) by Lednor and de Ruiter in Knoevenagel condensations of benzaldehyde with ethyl cyanoacetate and with malonitrile at a reaction temperature of 323 K.²⁾ The SiON was obtained by treatment of SiO₂ with NH₃ at 1373 K and possessed a surface area of 185 m²g⁻¹ with a composition of 28 wt% N.²³⁾ The SiON functions as a solid base catalyst due to the presence of nitrogen on the surface; silica is inactive for the Knoevenagel condensation. Although the SiON functions as a solid base catalyst for the Knoevenagel condensation, it is inactive toward double bond isomerization of 1-butene even at 673 K.⁴⁾

Inaki et al. prepared mesoporous silicon oxynitride by treatment of mesoporous silica FSM-16 with NH₃ at different temperatures, 473 K and 923 K.²⁴⁾ The catalytic activity for the Knoevenagel condensation of benzaldehyde with ethyl cyanoacetate at 323 K was higher for the catalyst treated at 473 K than for that treated at 923 K when compared on the unit amount of N contained in the catalyst. The treatment with NH₃ at 473 K produced a pair of Si-NH₂ and Si-OH, while the treatment at 923 K produced an isolated Si-NH₂ (OH). They concluded that the pair of Si-NH₂ and Si-OH acts more efficiently as an active site for the Knoevenagel condensation.

Mesoporous silicon oxynitride was also prepared from MCM-48 by treatment with NH₃ at 1173 K and showed the activity for the Knoevenagel condensation of benzaldehyde with malononitrile at 333 K.²⁵⁾ The active sites are suggested to be surface NH_x species.

SBA-15 nitrified with NH₃ at 1273 K retains its mesoporous structure and shows catalytic activity for the Knoevenagel condensation of benzaldehyde with malononitrile at 303 K.²⁶⁾ The activity of the mesoporous silicon oxynitride exhibits much higher activity than an amorphous silicon oxynitride and crystallized nitrogen-containing microporous molecular sieves (AlPO₄-5 and ZSM-5).

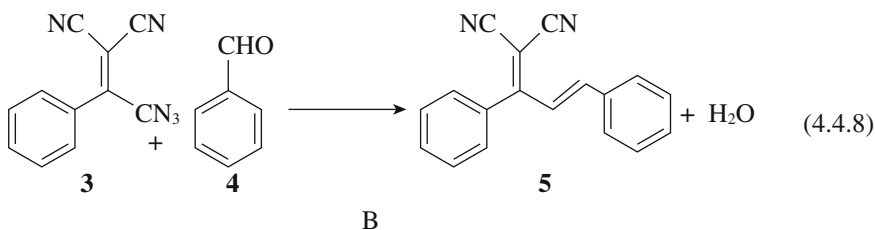
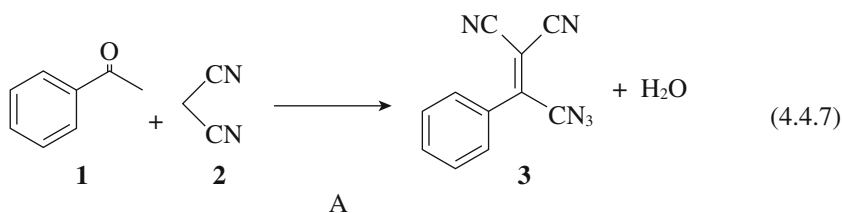
The catalytic activity of AIPON was reported by Grange et al.³⁾ They prepared AIPON by treatment of aluminumphosphate (AlPO) with NH₃ at 1023–1073 K and examined its catalytic activity for the Knoevenagel condensation of benzaldehyde with malononitrile at 323 K. The AIPON containing N 20% was more active than MgO (commercial MgO catalyst). The activity increased with an increase of N content in the range 2.6–22.0 wt%, while the P-O stretching frequency observed by IR decreased with the N content. Although the basic sites were not identified, it was proposed that the decrease in the P-O stretching frequency reflects the basicity of AIPONs.¹²⁾

Climont et al. measured the rates of Knoevenagel condensation of benzaldehyde with each of ethylcyanoacetate, malononitrile and diethyl malonate at 333 K over AIPON catalysts with different N contents.²⁷⁾ All the rates increased

with N content, but the dependency of the rate on the N content was different for different reactants. With malononitrile, the rate increased linearly with the N content, but with ethyl cyanoacetate and diethyl malonate, the rates increased exponentially with the N content. The ratio of the groups (-NH- / -NH₂) formed during nitrification increased with N content; the proportion of the stronger basic sites (-NH-) increased with N content. It was suggested that the -NH- groups and -NH₂ groups are equally active for the Knoevenagel condensation with malononitrile, but the -NH- groups are more effective than the -NH₂ groups for the reactions with diethyl malonate and with ethyl cyanomalonate.

One characteristic feature of AIPON as compared with MgO and hydrotalcite is its high selectivity for Knoevenagel condensation of benzaldehyde with diethyl malonate. For example, the Knoevenagel condensation product has the possibility to undergo Michael addition to diethyl malonate. While the Michael addition proceeded over MgO or hydrotalcite, the Michael addition did not proceed over AIPON. The basic strength of AIPON is sufficient for Knoevenagel condensation, but not sufficient for the Michael addition.

Due to the mild strength of basic sites on AIPON, 1,1-dicyano-2,4-diphenyl-1,3-butadiene (**5**) is effectively produced from acetophenone, malononitrile and benzaldehyde in one pot.²⁸⁾ The first step is the Knoevenagel condensation of acetophenone (**1**) with malononitrile (**2**) to yield α -methylbenzylidenemalononitrile (**3**). The second step is the condensation of **3** with benzaldehyde (**4**) to yield the target product **5**, but needs a higher temperature as compared to the first step. One pot reaction was carried out by the reaction between **1** and **2** first at 373 K in the presence of AIPON until the yield of **3** was 90% and then benzaldehyde was added and the temperature was raised to 423 K. In 6 h, the product **5** was obtained in 76% yield. MgO and hydrotalcite yielded several by-products to a considerable degree.



Both 2-butanol and 1-butanol undergo dehydration over AIPON. 2-Butanol is much more reactive than 1-butanol because basicity is higher for 2-butanol. 2-Butanol undergoes dehydration over AIPON at 473 K to form 1-butene, *trans*-2-

butene and *cis*-2-butene in the ratio, ca. 20, 41 and 39%, respectively. No dehydrogenation to methyl ethyl ketone takes place. The product distribution is typical of E1 mechanism. 1-Butanol undergoes dehydration at a considerably higher temperature of 548 K to form 1-butene (29%), *trans*-2-butene (7%), *cis*-2-butene (7%) and dibutyl ether (57%). No dehydrogenation to butyraldehyde takes place. These results suggest that 2-butanol undergoes dehydration by the E1 mechanism even on weak acid sites and 1-butanol by the E2 mechanism with co-operation of acidic and basic sites. Also, there are no strong basic sites which allow significant dehydration through the E1cB mechanism or dehydrogenation.²⁹⁾

ZrPON is also active for the Knoevenagel condensation of benzaldehyde with malononitrile at 323 K. The activity increased with the N content up to 19%, but not linearly. The activity was low when the N content was less than 5.4% and markedly increased as the N content exceeded 5.4% up to 19%. The NH_x species was almost saturated at 5.4% N content from the result of the point of zero charge (PZC). It was assumed that neither the $-\text{NH}_2$ nor the $-\text{NH}-$ group contributes to the catalytic activity for the Knoevenagel condensation. The active sites are assumed to be either nitride N^{3-} or non-bridging or double bonded O atoms appearing when divalent O atoms are replaced by trivalent N atoms.^{16,18)}

Aluminovanadate oxynitride (VAION) showed activity for the Knoevenagel condensation of benzaldehyde with malononitrile at 323 K. The selectivity was 100% for the Knoevenagel condensation product benzylidene malononitrile. The Michael addition, which would involve the reaction of another malonate carbanion with the double bond of the benzylidene malononitrile, did not proceed. The activity was proportional to the amount of NH_4^+ present on the surface, as measured by IR. The active site for the reaction was proposed to be the O of an OH group whose negative charge is increased by interaction with NH_3 . The active site can be described as $\text{V}-\text{O}^- \text{H}_4\text{N}$. The model proposed for the basic site is shown in Fig. 4.4.2. An H^+ is abstracted from malononitrile by the O^- to form a carbanion which is stabilized by NH_4^+ . Benzaldehyde is also activated by acidic site (NH_4^+), which makes the benzaldehyde more reactive toward the carbanion. An acid-base concerted mechanism was proposed.³⁰⁾

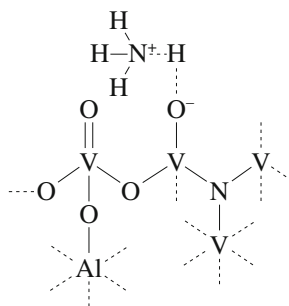


Fig. 4.4.2 Model proposed for the basic site in aluminovanadate oxynitride.

Reprinted with permission from H. Wiame, C. Cellier, P. Grange, *J. Catal.*, **190**, 406 (2000) Scheme 3.

1-Butanol undergoes dehydrogenation over VAION, which is in contrast to the other oxynitride catalysts like VAIPON and AlGaPON, which favor dehydration.³¹⁾ The reaction takes place in the temperature range 423–523 K and the selectivity for butyraldehyde is high (up to 75%).

Delsarte et al. showed that AlGaPON was active for the Knoevenagel condensation of benzaldehyde with malononitrile at 323 K.^{19,32)} The activity decreased as the catalyst was treated with He flow at a high temperature. They proposed that unstable N species are relevant to the reaction. Such N species are surface -NH₂ groups and/or the surface O atoms whose negative charge is increased by NH₃ adsorption.

2-Butanol undergoes dehydration over AlGaPON at 473 K.³³⁾ The activity decreases with N content. The selectivity for butene isomers is similar to those obtained with AlPO₄ and SiO₂-Al₂O₃ and indicates operation of the E₁ mechanism. In the reaction of 1-butanol at 548 K, intermolecular dehydration to form dibutyl ether is the main reaction, similar to the case of AlPON. Dehydrogenation to butanol takes place over AlGaPON to a small extent. This is different from the case of AlPON in which no butanol is formed.

Zeolites and related microporous materials such as AlPO₄-5, SAPO-11 and ZSM-5 were nitrated and the catalytic activity of the resulting materials measured for the Knoevenagel condensation of benzaldehyde with malononitrile.

Crystalline microporous material AlPO₄-5 become active for the Knoevenagel condensation at 353 K when nitrated with NH₃ above 1073 K. The activity is maximized at the NH₃ treatment temperature of 1148 K. The activity is lower than AlPON prepared from amorphous AlPO₄.

Zeolite NaY becomes active for the Knoevenagel condensation when nitrated above 1073 K. The activity increases markedly when the nitrating temperature is raised from 1073 K to 1123 K. The activity of nitrated NaY is higher than that of nitrated NaX.⁹⁾

Xiong et al. nitrated SAPO-11 doped with 2 wt% Ru at a low temperature of 673 K and examined for the Knoevenagel condensation activity at 323 K.³⁴⁾ The active sites were assumed to be AlN₄, AlN₂O₂ and PN₄ groups together with the terminal -NH₂ group. Without Ru, the activity was scarcely observed for the SAPO-11 nitrated in the range 673–1073 K. The surface area decreased markedly when SAPO-11 was nitrated at 1073 K.

Zhang et al. prepared nitrated ZSM-5 with a bimodal pore structure by calcination in air at 1273 K followed by NH₃ treatment at 1323 K or 1373 K.³⁵⁾ The resulting materials showed activities for the Knoevenagel condensation at 323 K. The activity was higher for the sample treated at 1323 K. The sample treated at 1373 K lost some crystalline structure. On the sample treated at 1323 K, alkylation of toluene with methanol took place at the ring position, but no side-chain alkylation occurred. The basic sites generated by NH₃ treatment are not strong enough to promote side-chain alkylation at 773 K, but the remaining acidic sites promote alkylation at the ring position at 723 K.

References

1. P. W. Lednor, R. de Ruiter, *J. Chem. Soc. Chem. Commun.*, **1989**, 320.
2. P. W. Lednor, R. de Ruiter, *J. Chem. Soc. Chem. Commun.*, **1991**, 1625.
3. P. Grange, P. Bastians, R. Conanec, R. Marchand, Y. Laurent, *Appl. Catal. A*, **114**, L191 (1994).
4. P. W. Lednor, *Catal. Today*, **15**, 243 (1992).
5. M. P. Kapoor, S. Inagaki, *Chem. Lett.* **32**, 94 (2003).
6. Y. Xia, R. Mokaya, *Angew. Chem. Int. Ed.* **42**, 2639 (2003).
7. Y. Xia, R. Mokaya, *J. Mater. Chem.* **14**, 2507 (2004).
8. C. Zhang, Z. Xu, K. Wan, Q. Liu, *Appl. Catal. A*, **258**, 55 (2004).
9. S. Ernst, M. Hartmann, S. Sauerbeck, T. Bongers, *Appl. Catal. A*, **200**, 117 (2000).
10. N. Chino, T. Okubo, *Micropor. Mesopor. Mater.* **87**, 15 (2005).
11. J. Wang, Q. Liu, *Micropor. Mesopor. Mater.*, **83**, 225 (2005).
12. J. J. Benítez, J. A. Odriozola, R. Marchand, Y. Laurent, P. Grange, *J. Chem. Soc. Faraday Trans.* **91**, 4477 (1995).
13. T. Blasco, A. Corma, L. Fernández, V. Fornés, R. Guil-López, *Phys. Chem. Chem. Phys.* **1**, 4493 (1999).
14. J. J. Benítez, A. Díaz, Y. Laurent, J. A. Odriozola, *J. Mater. Chem.* **8**, 687 (1998).
15. H. Wiame, L. Bois, P. Lharidon, Y. Laurent, P. Grange, *Solid State Ionics*, 101-103, 755 (1997).
16. N. Fripiat, P. Grange, *Chem. Commun.*, 1409 (1996).
17. N. Fripiat, R. Conanec, A. Auroux, Y. Laurent, P. Grange, *J. Catal.* **167**, 543 (1997).
18. N. Fripiat, V. Parvulescu, V. I. Parvulescu, P. Grange, *Appl. Catal. A*, **181**, 331 (1999).
19. S. Delsarte, A. Auroux, P. Grange, *Phys. Chem. Chem. Phys.* **2**, 2821 (2000).
20. A. Massion, J. A. Odriozola, Ph. Bastians, R. Conanec, R. Marchand, Y. Laurent, P. Grange, *Appl. Catal. A*, **137**, 9 (1996).
21. A. Corma, V. Fornés, R. M. Martín-Aranda, F. Rey, *J. Catal.*, **134**, 58 (1992).
22. M. J. Climent, A. Corma, V. Fornés, A. Frau, R. Guil-López, S. Iborra, J. Primo, *J. Catal.* **163**, 392 (1996).
23. P. W. Lednor, R. de Ruiter, *J. Chem. Soc. Chem. Commun.*, **1989**, 320.
24. Y. Inaki, Y. Kajita, H. Yoshida, K. Ito, T. Hattori, *Chem. Commun.*, **2001**, 2358.
25. Y. Xia, R. Mokaya, *Angew. Chem. Int. Ed.* **42**, 2639 (2003).
26. K. Wan, Q. Liu, C. Zhang, J. Wang, *Bull. Chem. Soc. Jpn.* **77**, 1409 (2004).
27. M. J. Climent, A. Corma, A. Frau, V. Fornés, R. Guil, S. Iborra, J. Primo, *J. Catal.*, **163**, 392 (1996).
28. M. J. Climent, A. Corma, R. Guil-Lopez, S. Lborra, *Catal. Lett.* **74**, 161 (2001).
29. S. Delsarte, P. Grange, *Appl. Catal. A*, **259**, 269 (2004).
30. H. Wiame, C. Cellier, P. Grange, *J. Catal.*, **190**, 406 (2000).
31. H. Wiame, L. Bois, P. L. Lharidon, Y. Laurent, P. Grange, *J. Eur. Ceram. Soc.* **17**, 2017 (1997).
32. S. Delsarte, P. Grange, *Stud. Surf. Sci. Catal.* **130**, 3237 (2000).
33. S. Delsarte, M. Florea, F. Maugé, P. Grange, *Catal. Today*, **116**, 216 (2006).
34. J. Xiong, Y. Ding, H. Zhu, L. Yan, X. Liu, L. Liu, *J. Phys. Chem. B*, **107**, 1366 (2003).
35. C. Zhang, Z. Xu, K. Wan, Q. Liu, *Appl. Catal. A*, **258**, 55 (2004).

4.5 Anion Exchange Resins

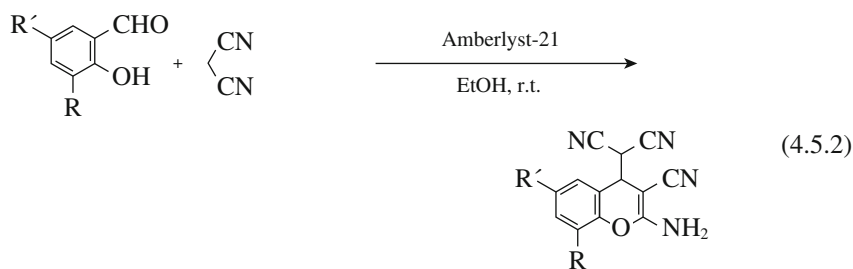
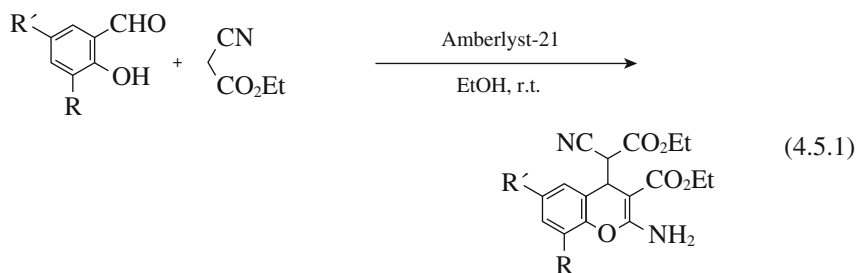
Typical ion exchange resins are based on cross-linked polystyrene. The required active groups are introduced after polymerization. Anion exchange resins are classified into strong or weak bases types, depending on whether the functional group is a quaternary ammonium ($-NR_3^+$) or an amino group ($-NR_2$). Two structural types of resins are used. With gel type resins, catalytic groups in a resin particle are entirely inaccessible to reactant molecules in the absence of strongly polar compounds such as water, which swell the resin network and allow the access of reactant molecules between polymer strands to the possible interior. Therefore, in nonaqueous or nonpolar systems, these resins have a negligible pore structure and show little activity. The macroreticular resins are much more useful for reactions involving weakly polar reactants. The catalytic activity is affected by the extent of

cross-linking and water content. The disadvantages of the anion exchange resins are low resistance to temperature and abrasion.

The various reactions are catalyzed by anion exchange resins. The aldol addition of acetone to diacetone alcohol is catalyzed by strongly basic anion exchange resin IRA-900 in the hydroxide form. Addition of water to the reaction system increased the catalyst life time and selectivity toward diacetone alcohol.¹⁾

For Knoevenagel condensation, weakly basic resins (amine form) are more effective than strongly basic ones (ammonium form), while, for aldol condensation and cyanoethylation of alcohols with acrylonitrile, strongly basic resins are more effective.²⁾ High water content and low thermal stability of anion exchange resins limit their usage. The catalytic activity is markedly influenced by the water content. Weakly acidic resins are effective as catalysts for Knoevenagel condensation even though one of the reactants is an acid as exemplified by the condensation of cyanoacetic acid with aldehydes or cyclohexanone.³⁾ Furthermore, the salts of the amine resins, such as benzoate, phenylacetate, etc, are more effective catalysts than the free amine resins.

Weakly basic resin Amberlyst A-21 is a good catalyst for the synthesis of substituted 4H-chromens from *o*-hydroxybenzaldehydes and ethyl cyanoacetate, or malononitrile at room temperature.⁴⁾ The catalyst was recycled up to eight times with only a slight decrease in the conversion (97–86%) in the reaction of salicylaldehyde and malononitrile (section 5.4.2).



Amberlyst 21 catalyzes the synthesis of β -alkanols by nitroaldol reaction from a wide variety of starting materials. No dehydrated products were formed.⁵⁾

Amberlyst 27, a macroreticular anionic resin with $[-\text{N}(\text{CH}_3)_3^+]$ as the functional group, is an efficient catalyst for the Michael reaction of nitroalkanes with a variety of electrophilic alkenes, even those substituted at β -position.⁶⁾ The

Michael reaction between methyl 1-oxoindan-2-carboxylate and methyl vinyl ketone in toluene was achieved in a flow reactor.⁷⁾

Carbonylation of methanol with carbon monoxide gives methyl formate in the presence of strong bases such as sodium methoxide. The reaction was studied by Girolamo and coworkers using various types of anion exchange resins.⁸⁻¹⁰⁾



Characteristics of the basic ion exchange resins used and catalytic results are shown in Tables 4.5.1 and 4.5.2, respectively. Each resin was carefully activated to assure the complete exchange of the Cl^- ions with OH^- ions and subsequently with CH_3O^- groups. The strongly basic resins Amberlyst A 26 and IRA 900 displayed higher activities than sodium methoxide, the industrial catalyst, in turnover frequency basis. The lower activity of Amberlyst A 27 compared with Amberlyst A 26 was attributed to its fragility. The low activity of Amberlite 416, functionalized with ethanolamine groups, was related to the lower basic strength of its functional groups. Though deactivation was observed, the activity of Amberlyst A 26 was restored simply through caustic washing. The catalyst is stable even at 343 K.

Table 4.5.1 Characteristics of anion exchange resins

Resins	Morphology	Functional group ^{a)}	Moisture/%	Exchange capacity/ mmol g ⁻¹	Maximum operating temperature/K
Amberlyst 26	Macroporous	I	61	4.4	333
Amberlyst 27	Macroporous	I	45	2.6	333
IRA 900	Macroporous	I	59	3.7	333
IRA 400	Gel	I	46	4.4	333
IRA 416	Gel	II	50	3.8	308

^{a)} Functional group: I = $-\text{CH}_2\text{N}(\text{CH}_3)_3^+ \text{OCH}_3^-$, II = $-\text{CH}_2\text{N}(\text{CH}_3)_2(\text{CH}_2\text{CH}_2\text{OH})^+ \text{OCH}_3^-$

Reprinted with permission from C. Carlini, M. Di Girolamo, M. Marchionna, A. M. Raspolli Galletti, G. Sbrana, *Stud. Surf. Sci. Catal.*, **119**, 491 (1998) p.492, Table 1.

Table 4.5.2 Methanol carbonylation with basic catalysts^{a)}

Catalyst	Conversion/%	TOF/h ⁻¹
EtONa	32	22.4
MeONBu ₄	15	10.5
Amberlyst A26	40	28.0
Amberlyst A27	29	20.3
IRA 900	34	23.8
IRA 400	40	28.0
IRA 416	19	13.3

^{a)} Reaction conditions: MeOH: 1.25 mmol; CO: 5 MPa, 333 K, Catalyst: 3.57 meq. Time: 5 h, Turnover after 3 h

Reprinted with permission from C. Carlini, M. Di Girolamo, M. Marchionna, A.M. Raspolli Galletti, G. Sbrana, *Stud. Surf. Sci. Catal.*, **119**, 491 (1998) p.493, Table 2.

Table 4.5.3 Hexanol carbonylation with basic catalysts^{a)}

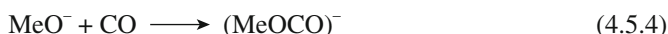
Catalyst	Conversion/%		TOF/h ⁻¹
	3 h	5 h	
Amgerlyst A26	68	85	79.3
Amgerlyst A27	16	27	18.6
IRA 900	47	61	54.8
IRA 400	84	89	98.0
IRA 416	12	20	14.0

^{a)} Reaction conditions: hexanol: 1 mol; CO: 5 MPa, 333 K, Catalyst: 2.85 meq. Turnover after 3 h

Reprinted with permission from C. Carlini, M. Di Girolamo, M. Marchionna, A. M. Raspolli Galletti, G. Sbrana, *Stud. Surf. Sci. Catal.*, **119**, 491 (1998) p.495, Table 4.

Unexpected high thermal stability was explained by the presence of -OMe instead of -OH counter anions under reaction conditions.

The reaction mechanism is considered to be as follows.



The strongly basic resins are also effective for carbonylation of ethanol and hexanol to the corresponding alkyl formates.⁹⁾ The result for carbonylation of hexanol is shown in Table 4.5.3.

Thermally stable anion exchange resin was developed by Mitsubishi Chemical Corporation. This resin has $-(\text{CH}_2)_4\text{N}(\text{CH}_3)_3^+$ groups attached to the benzene ring of polystyrene structure instead of conventional $-\text{CH}_2\text{N}(\text{CH}_3)_3^+$ groups, its maximum operating temperature being 373 K.¹¹⁾ Aika et al. used this resin for carbonylation of methanol.¹²⁾ The extent of methanol carbonylation reached 80% of the equilibrium in 5 min and the equilibrium was attained in 40 min at 373–393 K. Then they tried direct methanol synthesis from CO and H₂ in the presence of hydrogenation catalyst (Raney Cu) together with the resin, since the hydrogenation of methyl formate gives methanol.



After 4 h, 72% of CO was converted to produce 33 mmol of methanol and 6.9 mmol of methyl formate at 393 K. This method provides a mild synthetic way for methanol production.

The transesterification of ethylene carbonate with methanol was studied in a flow reactor with a variety of anionic resins with tertiary amines and quaternary ammonium ions.¹³⁾ Amberlite IRA-68, having dimethylamino functionality bonded to acrylic-divinylbenzene polymer, gave 23.8% dimethyl carbonate and ethylene glycol. Estimated selectivities are 98 and > 99 mol%, respectively. Similar results are realized with Amberlyst A-21, where dimethylamino functionality is bonded to a macroporous resin. Amberlyst IRA-68 maintains activity over 1000 h. No loss

in performance occurred and the physical appearance, color and the composition of the resin indicated no major deterioration.¹³⁾ The reaction was also studied in a slurry reactor with anion exchange resins with diethylamino- and trimethylammonium functionality.^{14,15)}

When weakly acidic cation exchange resin in -COOH form (Amberlite IRC-50) is partially exchanged with $\text{H}_2\text{N}(\text{CH}_2)_n\text{N}(\text{CH}_3)_2^+ \text{OH}^-$ ($n = 2-5$), the resin becomes an efficient catalyst for Knoevenagel condensation.¹⁶⁾ The catalytic activity depends on the value of n and the extent of neutralization. The reaction is believed to proceed by the cooperative action of an acidic component (-COOH) and an ammonium group fixed by (-COO⁻).

References

1. G. G. Podrebarac, F. T. T. Ng, G. L. Rempel, *Chem. Eng. Sci.*, **52**, (1997).
2. M. J. Astle, J. A. Zaslowsky, *Ind. Eng. Chem.*, **44**, 2867 (1952).
3. M. J. Astle, W. C. Gergel, *J. Org. Chem.*, **21**, 493 (1956).
4. J. S. Yadav, B. V. Subbareddy, M. J. Gupta, I. Prathap, S. K. Pandey, *Catal. Commun.*, **8**, 2208 (2007).
5. R. Ballini, G. Bosica, P. Forconi, *Tetrahedron*, **52**, 1677 (1996).
6. R. Ballini, P. Marziali, A. Mozzicafreddo, *J. Org. Chem.*, **61**, 3209 (1996).
7. F. Bonfils, I. Cazaux, P. Hodge, C. Caze, *Org. Bioorg. Chem.*, **4**, 493 (2006).
8. M. Di Girolamo, M. Lami, M. Marchionna, D. Sanfilippo, M. Andreoni, A. M. Raspoli Galletti, G. Sbrana, *Catal. Lett.*, **38**, 127 (1996).
9. C. Carlini, M. Di Girolamo, M. Marchionna, A. M. Raspoli Galletti, G. Sbrana, *Stud. Surf. Sci. Catal.*, **119**, 491 (1998).
10. M. Di Girolamo, M. Marchionna, *J. Mol. Catal.*, **177**, 33 (2001).
11. M. Yasutomi, H. Kubota, *Stud. Surf. Sci. Catal.*, **145**, 555 (2003).
12. K. Aika, H. Kobayashi, K. Harada, K. Imazu, *Chem. Lett.*, **33**, 1252 (2004).
13. J. F. Knifton, R. G. Duranleau, *J. Mol. Catal.*, **67**, 389 (1991).
14. S. M. Dhuri, V. V. Mahajani, *J. Chem. Technol. Biotechnol.*, **81**, 62 (2006).
15. M. Cao, Y. Meng, Y. Lu, *React. Kinet. Catal. Lett.*, **88**, 251 (2006).
16. T. Saito, H. Goto, K. Honda, T. Fujii, *Tetrahedron Lett.*, **49**, 7535 (1992).

4.6 Amines and Ammonium Ions Tethered to Solid Surfaces

Since amines and alkyl ammonium ions are common catalysts for base-catalyzed reactions, immobilization of these basic moieties has been studied extensively. Various types of amino and ammonium groups are tethered to silica materials as shown in Fig. 4.6.1. The preparation of these organic-inorganic hybrid catalysts has been reviewed.^{1,2)}

4.6.1 Loading of Basic Functional Groups to High Surface-area Silica Materials

A. Grafting method (post synthesis)

The most common method for tethering of amino and ammonium groups to solid surfaces is the reaction of hydroxyl groups of silica with silane coupling agent with having these functional groups. The method is often called the grafting method or post-synthesis method.

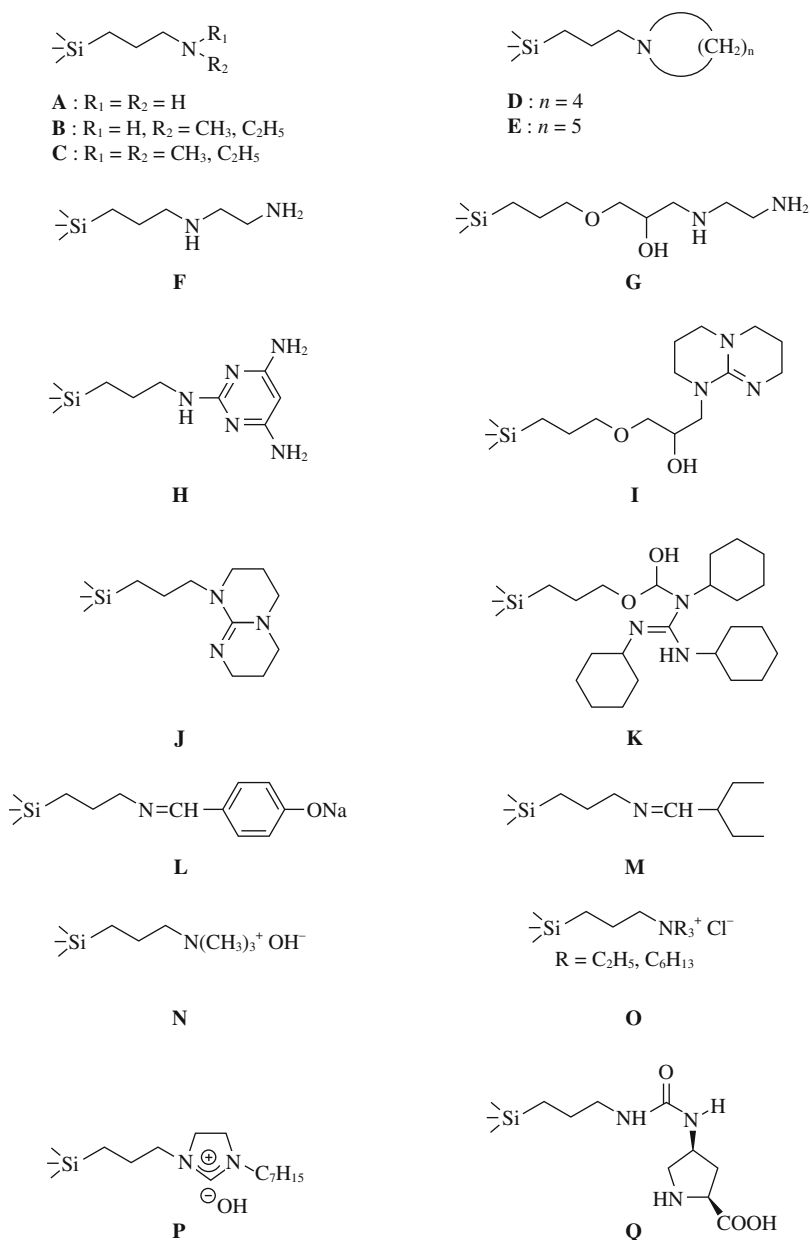


Fig. 4.6.1 Amino- and ammonium groups tethered to silica materials.

Angeletti et al. prepared aminopropyl (**A**) and *N,N*-dimethylaminopropyl (**C**) groups immobilized on silica gel by using trimethoxy(3-aminopropyl)silane and 3-(*N,N*-dimethylamino)propyltrimethoxysilane, respectively, as coupling agents, and their high catalytic activities for a variety of Knoevenagel condensation.^{3,4} Silica with aminopropyl groups (**A**) was more active than the one with *N,N*-dimethylaminopropyl (**C**) groups. The authors proposed a mechanism, where the amino group abstracts a proton from the active methylene compound and the remaining silanol groups activate the carbonyl compounds and promotes the dehydration of aldol.

Since the discovery of the MCM-41 types of mesoporous materials, grafting of amino groups on their surfaces is attempted to use the advantage of their high surface area. Brunel and coworkers introduced amino-groups (**A**) on the surface of MCM-41 and showed that the materials had high activity for Knoevenagel condensation.^{5,6} They also prepared MCM-41 tethered with piperidino groups (**E**). In this case, MCM-41 is first reacted with 3-chloro- or 3-iodo-propyltrialkoxysilane followed by nucleophilic displacement of the halogen atom by piperidine. The MCM-41 bearing piperidino groups (**E**) is less active than that with aminopropyl groups (**A**) for Knoevenagel condensation. The authors proposed a reaction mechanism in which primary amino groups play an essential role (Fig. 4.6.2). The formation of benzaldimine groups (1645 cm^{-1}) and their reaction with ethyl cyanoacetate were confirmed by attenuated total reflection infrared spectroscopy⁷.

Mhoe et al. prepared the *N,N*-dimethyl-3-aminopropyl (**C**)-derived amorphous silica and MCM-41 by a post synthesis method.⁸ A higher amount of amino groups could be introduced on MCM-41 (2.2 mmol g^{-1}) than on amorphous silica (0.85 mmol), and the former showed higher activity than the latter for Michael addition.⁸

1,5,7-Triazabicyclo[4,4,0]dec-5-ene (TBD) is a strong base which has a pK_a value of 25. Subba Rao et al. introduced TBD moieties by a two-step procedure⁹ (Fig. 4.6.3). MCM-41-TBD(**I**) is very active for Michael addition, which requires stronger bases than Knoevenagel condensation. The material is also active for the epoxidation of alkenes with hydrogen peroxide⁹ and transesterification of β -ketoesters.¹⁰

Derrien et al. also introduced TBD moieties (**J**).¹¹ The procedures include the introduction of chloropropyl groups by the reaction of surface hydroxyl groups with chloropropyltrimethoxysilane (CPS) followed by elimination of the residual hydroxyl groups by the reaction with hexamethyldisilazane (HMDZ), and the reaction of chloropropyl groups with TBD, as shown in Fig. 4.6.4.¹¹ The removal of the hydroxyl groups is expected to avoid their interaction with the imine-type N atoms of TBD moieties.¹¹ The end-capped catalyst was much higher activity than the catalyst with OH groups in the transesterification of ethyl propionate with butanol. The basic strength of TBD-anchored silica (**J**) was estimated as $H_- = \sim 15$.¹²

1,2,3-Tricyclohexylguanidine (TCG, **K**) can be anchored on MCM-41 in a manner similar to that of Subba Rao et al. and used for aldol condensation between benzaldehyde and acetone.¹³ An 89% yield of the condensation product was

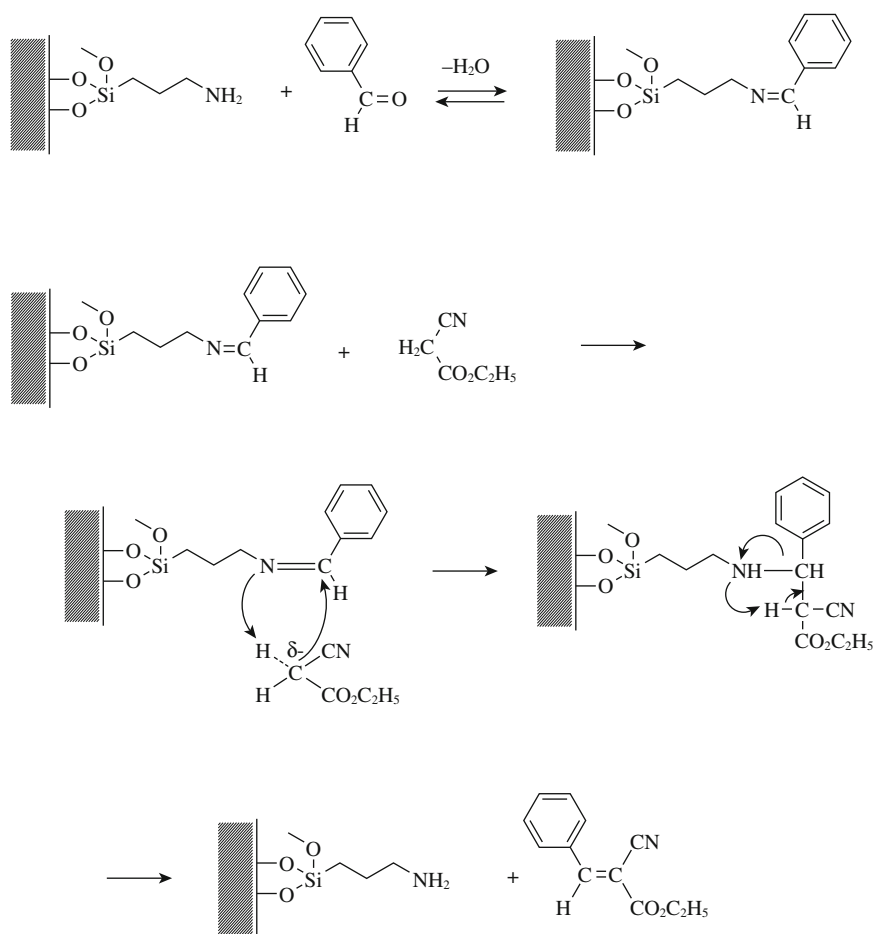


Fig. 4.6.2 Mechanism of Knoevenagel condensation over MCM-41 tethered with aminopropyl groups. Rprinted with permission from M. Laspéras, T. Llorett, L. Chavez, I. Rodriguez, A. Cauvel, D. Brunel, *Stud. Surf. Sci. Catal.*, **108**, 75 (1997) p.80 Scheme 3.

obtained in the reaction in methanol at 298 K; 8–10% of TCG leached out during the reaction.

Tetraalkylammonium moieties (N) were introduced on MCM-41.^{14,15)} The preparation involves the reaction of 3-trimethoxysilylpropyl(trimethyl)ammonium chloride with hydroxyl groups on dehydrated MCM-41, followed by the ion exchange of chloride ions with OH⁻ in a methanolic solution of N(CH₃)₄OH. The material showed high activities for Knoevenagel condensation, Michael addition and aldol condensation.

Udayakumar et al. introduced tetraalkylammonium moieties by the reaction of chloropropylated MCM-41 with trialkylamines and tested the prepared materials (O) for the reaction of allyl glycidyl ether with carbon dioxide.¹⁶⁾

Yamguchi et al. prepared an *N*-octyldihydroimidazolium hydroxide fragment

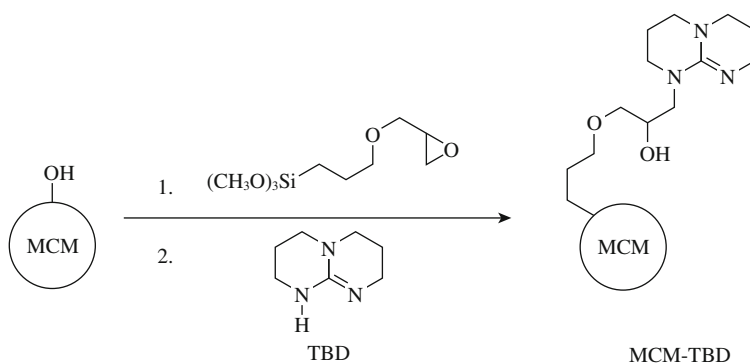


Fig 4.6.3 Immobilization of 1,5,7-triazabicyclo [4,4,0] dec-5-ene (TBD) in MCM-41. Reprinted with permission from Y. V. Subba Rao, D. E. DeVos, P. A. Jacobs, *Angew. Chem. Int. Ed. Engl.*, **36**, 2061 (1997) p.2662, Scheme 1.

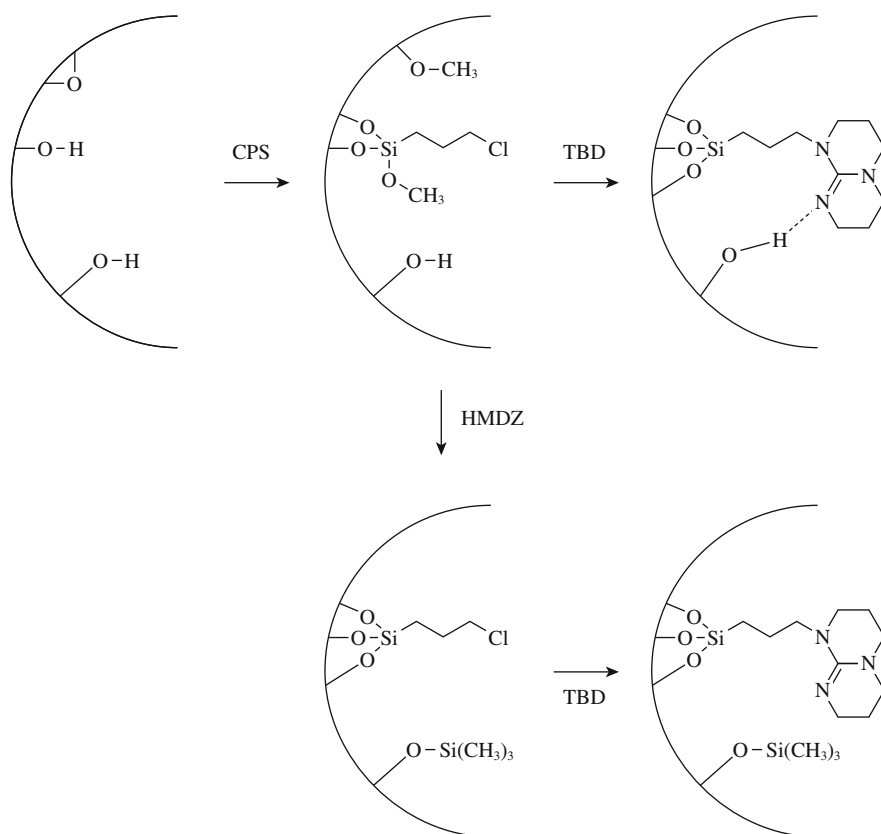


Fig. 4.6.4 Immobilization of 1,5,7-triazabicyclo [4,4,0] dec-5-ene (TBD) in mesoporous silica. Reprinted with permission from A. Derrien, G. Renard, D. Brunel, *Stud. Surf. Sci. Catal.*, **117**, 445 (1998) p.445, Scheme 1.

(P) onto silica gel by a post-modification method.¹⁷⁾ The catalyst was active for the cyanosilylation of carbonyl compounds with trimethylsilyl cyanide and the epoxidation of electron-deficient alkenes with hydrogen peroxide.

L-Proline (Q) grafted to MCM-41 gives high enantioselectivity in the aldol reactions of hydroxyacetone and different aldehydes.¹⁸⁾ The rate is greatly enhanced by microwave irradiation. Thus the reaction of hydroxyacetone with cyclohexylaldehyde gave 90% conversion to give the aldol product with e.e >99% in 10 min under microwave irradiation.

X-type zeolites grafted with aminopropyl groups (A) are active for Claisen-Schmidt condensation between benzaldehyde and acetophenone under ultrasonic irradiation.¹⁹⁾

B. Direct method

The second method for preparing silica materials bearing amino groups uses trialkoxysilanes with amino groups as one of the starting substances in the synthesis step of amorphous or ordered mesoporous silica. The method is called the direct or co-condensation method.

Macquarrie prepared HMS (hexagonal mesoporous silica) with aminopropyl groups (A) using tetraethoxysilane and trimethoxy(3-aminopropyl)silane. Mesoporous materials with high surface area (600–750 m² g⁻¹) were obtained and a higher amount of amino-groups (2.5 mmol g⁻¹) could be loaded.^{20,21)} The materials thus obtained were active for Knoevenagel condensation.²¹⁾ Besides aminopropyl groups (A), *N*-methylaminopropyl (B), *N,N*-dimethylaminopropyl (C), and *N*-(2-aminoethyl)aminopropyl (F) groups were also introduced to HMS by the direct method.²²⁾ Introduction of various amino-groups to MCM-41 by the direct method is also possible.^{23–27)}

SBA-15 with A, B or F groups synthesized by a sol-gel method has a well-ordered structure and has been tested for Knoevenagel condensation, Michael addition and flavanone synthesis.^{28–31)}

Ethylenediamine attached silica (G) was prepared by DeOliveira and Prado.³²⁾ Teteramethoxysilane and 3-glycididoxypopyltrimethoxysilane were co-condensed using a neutral *n*-decylamine as a template. The glycididoxo ring was opened by the reaction with ethylenediamine. The material had a surface area of 796 m² g⁻¹ and a mesoporous structure with pore diameter of approximately 50 nm. The material thus prepared had a high catalytic activity for Michael addition of nitromethane to cyclopentenone.

Magnesium organo-silicate (MOS) with a talc-like structure was synthesized by sol-gel method and the applicability of amine (A)- and diamine (F)-functionalized MOS was tested as catalysts for aldol condensation reactions including the synthesis of jasminaldehyde by condensation of 1-heptanal with benzaldehyde.^{33,34)} Although the catalysts had small surface area (2–3 m² g⁻¹), they were active for a variety of aldol condensation.

Crystalline metal-organic frameworks (MOFs) having amino-groups in the structure shows catalytic activities for the Knoevenagel condensation.^{35,36)} For example, MOFs based on 2-aminoterephthalic acid are highly active and stable for

the Knoevenagel condensation of benzaldehyde and ethyl acetoacetate.³⁶⁾ The amino groups in IRMOF-3³⁷⁾ are more active than aniline. The reaction mechanism involving benzaldimine intermediates is proposed based on DRIFTS.

4.6.2 Catalysis Using Basic Functional Groups Tethered to Silica Materials

Lin et al. prepared five types of amines anchored on MCM-41; aminopropyl (**A**), 1-piperidinopropyl (**D**), 1-pyrrolidinylpropyl (**E**), 1-pyridiminopropyl (**H**) and TBD-propyl (**J**) groups.³⁸⁾ The materials were tested for the synthesis of mono-glycerides from glycidol and lauric acid. The reactivity order was TBD > 1-piperidino > 1-pyrrolidinyl > pyrimidyl > amino. The activity order correlates approximately with the basic strength of the organic bases except for the catalyst with pyrrolidinyl groups. This was considered to be due to the high chloride content found on this catalyst.

Zhang et al. introduced four types of functional groups, namely, **A**, **F**, **H**, and **J** on silica by a grafting method under microwave irradiation.³⁹⁾ The amount of **A** loaded under microwave irradiation (2.00 mmol g⁻¹) is much larger than that prepared without irradiation (1.13 mmol g⁻¹). The basic strength of the four materials was measured by an indicator method. As shown in Table 4.6.1, TBD/SiO₂ (**J**) has the highest strength of $H_{-} \sim 15.0$, while **A** and **F** only have a basicity of $H_{-} \sim 9.3$ and $9.3 < H_{-} < -15.0$, respectively. Among the four modified silica materials, **H** has the weakest basicity of $H_{-} < 7.2$. Thus, the basic strength of the samples is in the order **J** > **F** > **A** > **H**. They also studied the catalytic activities of the four materials for the reaction of propylene oxide with methanol. For this reaction, the materials **A**, **F**, and **J** showed high propylene oxide conversion (> 94%), but with different isomer selectivity (Table 4.6.1). The lower isomer selectivity of TBD-SiO₂ (**J**) was attributed to the large molecular framework of TBD.

When MCM-41 was modified with primary (**A**), secondary (**B**) and tertiary

Table 4.6.1 Base strength of amine-grafted silica and results for the synthesis of 1-methoxy-2-propanol from propylene oxide and methanol

Catalyst	pK _a value of indicators			Reaction results	
	7.2	9.3	15.0	Conversion/%	Isomer selectivity/%
None				27.3	72.3
Porous silica				35.7	68.3
H /SiO ₂	-	-	-	89.0	68.6
A /SiO ₂	+	±	-	94.1	82.8
F /SiO ₂	+	+	-	100.0	84.1
J /SiO ₂	+	+	±	94.5	73.7

(+) color changes clearly; (-) color does not change; (±) color changes unclearly. Reaction conditions: 403 K, catalyst: 1.5 g, reaction time 10 h. Isomer selectivity = 1-methoxy-2-propanol/total propylene glycol methyl ester.

Reprinted with permission from X. Zhang, W. Zhang, J. Li, N. Zhao, W. Wei, Y. Sun, *Catal. Commun.*, **8**, 2007, 437, p.440, Table 3.

amino (**C**) groups by a post synthesis method, the order of catalytic activities of amine moieties for the reactions of benzaldehyde and nitromethane or nitroethane was primary > secondary > tertiary.⁴⁰⁾ The authors explained the higher activity of primary amine (**A**) by the mechanism which involves the formation of anchored imine, similar to the mechanism shown in Fig. 4.6.2 proposed by Laspéras et al. for Knoevenagel condensation.⁵⁾ Actually, when the catalyst was treated with benzaldehyde, a new IR peak appeared at 1636 cm^{-1} due to C-N stretching. On the other hand, for the Michael addition of nitromethane to 2-cyclohexen-1-one, the secondary amine moiety was most efficient.

Amine-functionalized silica materials were tested for nitroaldol and Michael reactions.⁴¹⁾ For nitroaldol reaction of benzaldehyde with nitromethane, the silica grafted with a primary amine was the most effective for nitroaldol reaction. This was again ascribed to the formation of the imine-type intermediates in the case of primary amine. On the other hand, for Michael reaction, the primary amine gave an extremely poor yield compared to secondary or tertiary amines. In this case, the basic strength of the amine is a decisive factor for the catalysis.

Hagiwara et al. prepared silica gel having aminopropyl (**A**), *N*-methylaminopropyl (**B**), and *N,N*-diethylaminopropyl (**C**) groups and tested for transesterification of β -ketoesters⁴²⁾ and aldol condensation of decanal.⁴³⁾ The silica gel having *N,N*-diethylaminopropyl groups was the most active for the transesterification while silica gel having *N*-methylaminopropyl groups was the most active for aldol condensation.

The effect of the preparation methods of aminopropylated silica was also studied.⁴⁴⁾ Four aminopropylsilicas were prepared by different synthetic procedures, i.e., the grafting method (amorphous silica, MCM-41) and the sol-gel method (MCM-41, amorphous silica), and tested for the nitroaldol condensation between nitromethane and benzaldehyde and the Michael addition of nitromethane to 2-cyclohexen-1-one. For both reactions, the catalysts prepared by the grafting method showed much higher activity than those prepared by the sol-gel method. The results were attributed to the difference in the accessibility of the reactants to the aminopropyl groups.

Silica-supported imines such as **L** and **M** were prepared and tested for Knoevenagel condensation and Michael addition.⁴⁵⁾ These imine-loaded catalysts outperform aminopropylated silica catalysts for the Knoevenagel reaction.

The pore structure of amine-grafted mesoporous silica is an important factor especially in liquid-phase reactions. Suzuki et al. prepared mesoporous silica with similar particle sizes but different pore sizes (0–2.66 nm) and introduced aminopropyl groups (**A**) on the surfaces by a grafting method.⁴⁶⁾ The optimum pore sizes on the catalytic activities for nitroaldol reactions between substituted benzaldehydes and nitromethane depended on the type and number of the substituent groups on the reactants.

Das et al. prepared MCM-41 with expanded pores (up to 20 nm).⁴⁷⁾ The expansion of pores was performed by using long chain *N,N*-dimethylalkylamines. The material was then grafted with various amino (or ammonium) groups and measured for activity for Knoevenagel condensation. Even after aminopropyl

groups are grafted to the material (pore diameter = 11 nm), the pore diameter was still as large as 8.2 nm. The activities of the materials with the expanded pores are higher than that with ordinary pore sizes (3 nm) for Knoevenagel condensation, probably because of enhanced diffusion of the reactants and/or products in the pores. Large-pore mesoporous silica (3.8–6.8 nm) was synthesized and functionalized with aminopropyl groups.⁴⁸⁾ The distinct effect of pore size on the activity and selectivity was observed in the reaction of benzaldehyde and 2'-hydroxyacetophenone (flavanone synthesis).

Suzuki et al. prepared monodispersed silica functionalized with amino-groups by the direct method.⁴⁹⁾ They succeeded in preparing the functionalized silica with different particle diameter with the same mesopore size, and used these materials for nitroaldol reactions of 4-methoxybenzaldehyde with nitromethane and estimated the catalytic effectiveness factor, which varied between 0.80 and 0.82. On the other hand, the material prepared by the grafting method showed a value of 0.62. Sujandi prepared amino-functionalized SBA-15 type mesoporous silica having unique hexagonal platelet morphologies with short channels (100–300 nm) by a direct method³¹⁾. This material showed much higher activity than the ordinary SBA-15 to which the amino groups are tethered either by direct or grafting method for base-catalyzed reactions, i.e., Knoevenagel condensation, nitroaldol reaction and Claisen-Schmidt condensation. No serious diffusion or mass transfer limits was observed.

4.6.3 Acid-Base Bifunctional Catalysis

The effect of hydroxyl groups near anchored amino groups is controversial. While hydroxyl groups are proposed to be involved in the catalytic cycles of Knoevenagel³⁾ and nitroaldol condensations,⁵⁰⁾ works by Brunel and coworkers showed that the removal of the OH groups by the reaction with hexamethyldisilazane improved the catalytic activities for monoglyceride synthesis and transesterification.^{6,11)} Macquarrie prepared HMS with phenyl groups in addition to propylamino groups by a deirect method.⁵¹⁾ This material was far more active than HMS without phenyl groups for Knoevenagel condensation reactions. The rate enhancement was ascribed to the change in the polarity of the HMS surface. The enhancement effect of the second groups was also observed in the nitroaldol reactions over MCM-41 with methyl groups in addition to aminopropyl groups.⁵²⁾ Here, the catalysts were prepared by a grafting method.

The effect of the environment of the amino groups, "outer-sphere effect" was proposed by Bass et al.^{53,54)} They prepared three kinds of modified silica catalysts with aminopropyl groups: (I) silica with OH groups, (II) silica of which OH groups are replaced by $\text{OSi}(\text{CH}_2)_3\text{CH}_3$ groups, (III) silica of which OH groups were replaced by $\text{-OSi}(\text{CH}_2)_3\text{CN}$. In the Knoevenagel condensation of 3-nitrobenzaldehyde and malononitrile, catalyst I is far more effective than catalysts II and III, indicating the acid (-OH) and base (-NH₂) bifunctionality of the catalysis. Catalyst III is more active than II. In addition, for the Michael addition of malononitrile to β -nitrostyrene, catalyst III is also much more active than II. The higher

activities of III over II in these reactions were attributed to the “dielectric outer sphere effect.” The high dielectric environment of the amino groups in III facilitates ion-pair formation and charge separation in the transition state in the deprotonation step of malononitrile.

For nitroaldol reaction between 4-nitrobenzaldehyde and nitromethane, the activity and product selectivity depended greatly on the catalyst, and two types of mechanisms were proposed, an imine mechanism (Fig 4.6.5) and an ion-pair mechanism (Fig. 4.6.6). In the imine mechanism, both imine formation and imine protonation steps to form iminium ions are promoted by acid (-OH) and base (-NH₂) bifunctionality. This mechanism is operative in the case of catalyst I. In the case of catalysts II and III, the ion-pair mechanism is assumed to be operative. The reaction product is expected to reflect the difference in the reaction mechanism; the α,β -unsaturated product is formed via the imine mechanism and the β -nitro alcohol via the ion-pair mechanism. For nitroaldol reaction between 4-nitrobenzaldehyde and nitromethane, the product ratios, α,β -unsaturated product and β -nitroalcohol, were 80 : 20, 40 : 60, and 1 : 99 for catalysts, I, II, and III. The catalytic activity of III is ~50 times higher than II. This was again attributed to the dielectric environment effect.

Zeidan and Davis prepared mesoporous silica materials having both aminopropyl groups and acidic functional groups by one-pot synthesis.^{55,56)} The acidic functional groups are sulfonic, phosphoric and carbonic acids. The catalysts were tested for aldol condensation of *p*-nitrobenzaldehyde and acetone. As shown in Table 4.6.2, materials with only aminopropyl groups gave a conversion of 33%. The materials with only an acidic functionality were totally inactive. When the materials have both acidic and basic functionalities, high activities for the reaction were attained. The results indicate the importance of the synergetic effects of acidic and basic sites.

Motokuma et al. prepared SiO₂-Al₂O₃ grafted with amino- or diethylamino-groups (SA-NR₂).⁵⁷⁾ The catalyst was very active for cyano-ethoxycarbonylation (section 5.8.4), the Michael addition and nitroaldol reaction. The activity of SA-NR₂ was much higher than SiO₂ grafted with the same groups. The high activity of SA-NR₂ was attributed to the higher acidity of the OH groups on SiO₂-Al₂O₃ compared with those on SiO₂. The authors proposes a bifunctional mechanism which involves the basic (-NEt₂) and acidic (OH) groups as active centers.

The catalytic activity of mesoporous silica carrying tertiary amine for the conjugate addition of acetylacetone to nitrostyrene is greatly enhanced by coloaded thiourea residue.⁵⁸⁾



The yield of the adduct was 43% over silica loaded with dimethylamino groups, while it was 80% when the amino group and thiourea residue were coloaded.

Strivastava et al. prepared SBA-15 having an adenine moiety (P) and attempted

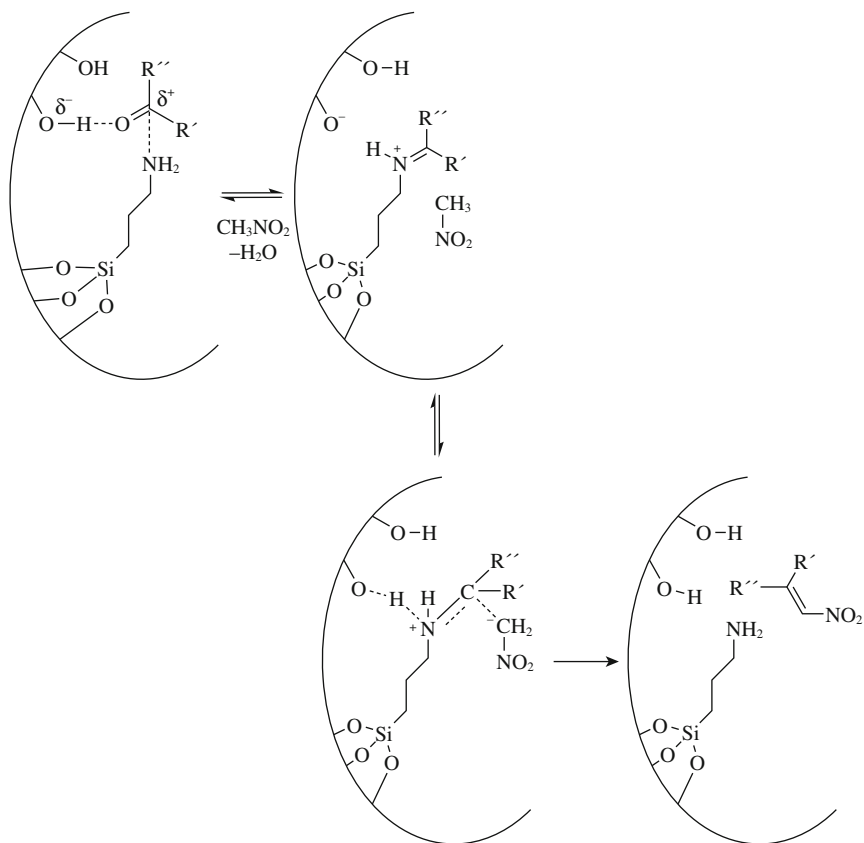


Fig. 4.6.5 Imine catalytic mechanism for the production of the dehydrated product for the nitroaldol reaction.
Reprinted with permission from J. D. Bass, A. Andrew, J. Pascail, A. Katz, *J. Amer. Chem. Soc.*, **128**, 3737 (2006) p.3743, Scheme 5.

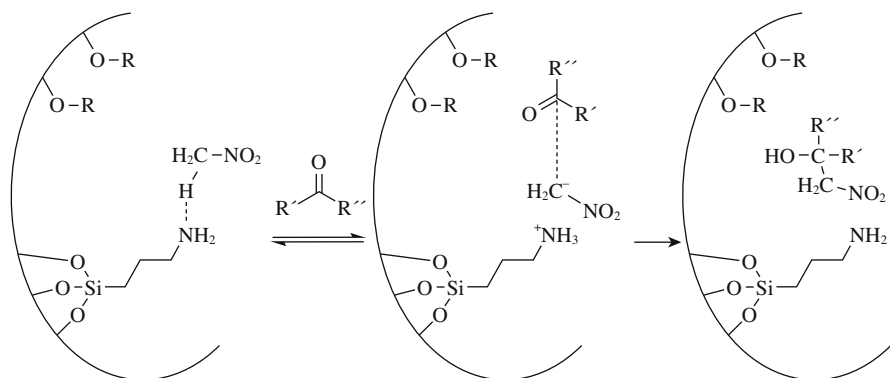


Fig. 4.6.6 Ion-pair mechanism for the production of β -nitro-alcohol product in the nitroaldol reaction.
Reprinted with permission from J. D. Bass, A. Andrew, J. Pascail, A. Katz, *J. Amer. Chem. Soc.*, **128**, 3737 (2006) p.3743, Scheme 6.

Table 4.6.2 Acid-base catalysis in aldol catalysis

Entry	Catalyst (10 mol%)	A/%	B/%	Conv. / % ^{a)}
1	SBA-15 + SBA-15	45	17	62
2	SBA-15	8	8	16
3	SBA-15	25	8	33
4	SBA-15-A/SBA-15-B ^{b)}	30	14	44
5	SBA-15	0	0	0
6	+	0	0	0
7		3	5	8
8		3	1	4

^{a)} Total conversion. Yields determined through ¹H NMR spectroscopic analysis with THF as the internal standard. ^{b)} 1 : 1 mixture of sulfonic acid functionalized SBA-15 (SBA-15-A) and amine-functionalized SBA-15 (SBA-15-B).

Reprinted with permission from R. K. Zeidan, M. E. Davis, *J. Catal.*, **247**, 379 (2007) p.382, Table 1.

the addition of carbon dioxide to epichlorohydrin.^{59,60)} The conversion of the epoxide was 80.5% with selectivity to cyclic carbonate of 75%. By incorporating Ti or Al in the SBA-15 framework, both the conversion and selectivity were improved. The conversion and selectivity were 91.9% and 89.1%, respectively, over Ti-SBA-15 tethered with adenine, and they were 98.1% and 89.1%, over Al-SBA-tethered with adenine. The enhancement was attributed to the cooperative effect of amine moieties and Lewis acid sites (Ti, Al) on the surfaces.

4.6.4 Catalysis by Occluded Structure Directing Agent

Kubota found that as-synthesized ordered mesoporous materials containing alkylammonium cations in the pores were effective catalysts for base-catalyzed reactions such as Knoevenagel condensation, Michael addition and aldol condensation.^{61,62)} Thus, MCM-41 synthesized using hexadecyltrimethylammonium cation as a structure directing agent works as a catalyst for Knoevenagel condensation of benzaldehyde with cyanoacetate. The yield of the condensation product was 82%

after 1 h reaction at 393 K. The material is also active for Michael reaction of chalcone with dimethyl malonate.

Three-dimensional layered silicate PLS-1 contains tetramethylammonium hydroxide (TMAOH) in the interlayers. The material is active for Knoevenagel condensation of benzaldehyde and cyanoacetate and nitroaldol reaction of nitro-methane and aldehydes.⁶³ The active species is considered to be TMAOH. The activity of the recycled materials decreased because of the leaching of TMAOH.

References

1. M. H. Valkenberg, W. F. Hölderich, *Catal. Rev.*, **44**, 321 (2002).
2. A. P. Wight, M. E. Davis, *Chem. Rev.*, **102**, 3589 (2002).
3. E. Angeletti, C. Canepa, G. Martinetti, F. Venurello, *Tetrahedron Lett.*, **29**, 2261 (1988).
4. E. Angeletti, C. Canepa, G. Martinetti, F. Venurello, *J. Chem. Soc., Perkin Trans., I*, **1989**, 105.
5. M. Laspéras, T. Llorett, L. Chaves, I. Rodriguez, A. Cauvel, D. Brunel, *Stud. Surf. Sci. Catal.*, **108**, 75 (1998).
6. A. Cauvel, G. Renard, D. Brunel, *J. Org. Chem.*, **62**, 749 (1997).
7. R. Wirz, D. Ferri, A. Baiker, *Langmuir*, **22**, 3698 (2006).
8. J. E. Mhoe, J. H. Clark, D. J. Macquarrie, *Synlett*, 625 (1998).
9. Y. V. Subba Rao, D. E. De Vos, P. A. Jacobs, *Angew. Chem. Int. Ed. Engl.*, **36**, 2661 (1997).
10. M. L. Kantam, P. Srekanth, *Catal. Lett.*, **77**, 241 (2001).
11. A. Derrien, G. Renard, D. Brunel, *Stud. Surf. Sci. Catal.*, **117**, 445 (1998).
12. X. Zhang, Y. Zhang, Y. Yang, Q. Wei, X. Zhang, *React. Kinet. Catal. Lett.*, **94**, 385 (2008).
13. R. Sercheli, A. L. B. Ferreira, M. C. Guerreiro, R. M. Vargas, R. A. Sheldon, U. Schuchardt, *Tetrahedron Lett.*, **38**, 1325 (1997).
14. I. Rodriguez, S. Ibbora, A. Corma, F. Rey, J. L. Jordá, *Chem. Commun.*, **1999**, 593.
15. I. Rodriguez, S. Ibbora, A. Corma, *Appl. Catal., A*, **194/195**, 241 (2000).
16. S. Udayakumar, S.-W. Park, D.-W. Park, B.-S. Choi, *Catal. Commun.*, **9**, 1563 (2006).
17. K. Yamaguchi, T. Imago, Y. Ogasawara, J. Kasai, M. Kotani, N. Mizuno, *Adv. Synth. Catal.*, **348**, 1516 (2006).
18. F. Caldelón, R. Fernández, F. Sánchez, A. Fernández-Mayoralas, *Adv. Synth. Catal.*, **347**, 1395 (2005).
19. E. Perozo-Rondón, R. M. Martín-Aranda, B. Casal, C. J. Durán-Valle, W. N. Lau, X. F. Zhang, K. L. Yeung, *Catal. Today*, **114**, 183 (2006).
20. D. J. Macquarrie, *Chem. Commun.*, **1996**, 1961.
21. D. J. Macquarrie, *Chem. Commun.*, **1997**, 1781.
22. D. J. Macquarrie, D. M. Jackson, J. E. G. Mdoe, J. H. Clark, *New. J. Chem.*, **23**, 539 (1999).
23. C. E. Fowler, S. L. Burkett, S. Mann, *Chem. Commun.*, **1997**, 1797.
24. C. Venekatesan, A. P. Singh, *Catal. Lett.*, **80**, 7 (2002).
25. S. Huh, J. W. Wiench, J.-C. Yoo, M. Pruski, V. S.-Y. Lin, *Chem. Mater.*, **15**, 4247 (2003).
26. T. Yokoi, H. Yoshitake, T. Tatsumi, *J. Mater. Chem.*, **14**, 951 (2004).
27. T. Yokoi, H. Yoshitake, T. Yamada, Y. Kubota, T. Tatsumi, *J. Mater. Chem.*, **16**, 1125 (2006).
28. X. Wang, K. S. K. Lin, J. C. C. Chan, S. Cheng, *J. Phys. Chem., B*, **109**, 1763 (2005).
29. X. Wang, Y.-H. Tseng, J. C. C. Chan, S. Cheng, *Micropor. Mesopor. Mater.*, **85**, 241 (2005).
30. X. Wang, J. C. C. Chan, Y.-H. Tseng, S. Cheng, *Micropor. Mesopor. Mater.*, **95**, 57 (2006).
31. a) Sujandi, S.-E. Park, D.-S. Han, S.-C. Han, M.-J. Jin, T. Osuna, *Chem. Commun.*, **2006**, 4131; b) Sujandi, E. A. Prasetyanto, S.-E. Park, *Appl. Catal., A*, **350**, 244 (2008).
32. E. DeOliveira, A. G. S. Prado, *J. Mol. Catal., A*, **271**, 63 (2007).
33. S. K. Sharma, H. A. Patel, R. V. Jarsa, *J. Mol. Catal., A*, **280**, 61 (2008).
34. H. Patel, S. Sharma, R. V. Jarsa, *J. Mol. Catal., A*, **286**, 31 (2008).
35. Y. K. Hwang, D.-Y. Hong, J.-S. Chang, S. H. Jung, Y.-K. Seo, J. Kim, A. Vimont, M. Daturi, C. Serre, G. Férey, *Angew. Chem. Int. Ed.*, **47**, 4144 (2008).
36. J. Gascon, U. Aktay, M. D. Hernandez-Alonso, G. P. M. van Klink, F. Kaptejin, *J. Catal.*, **261**, 75 (2009).
37. M. Eddaoudi, J. Kim, N. Rosi, D. Vodak, J. Wachter, M. O'Keefe, O. M. Yaghi, *Science*, **295**, 469 (2002).

38. X. Lin, G. K. Chuah, S. Jaenicke, *J. Mol. Catal., A*, **150**, 287 (1999).
39. K. Zhang, W. Zhang, J. Li, N. Zhao, W. Wei, Y. Sun, *Catal. Commun.*, **8**, 437 (2007).
40. G. Demicheli, R. Maggi, A. Mazzacani, P. Righi, G. Sartori, F. Biggi, *Tetrahedron Lett.*, **42**, 2401 (2001).
41. L. Solidi, W. Ferstl, S. Loebbecke, R. Maggi, C. Malmassari, G. Sartori, S. Yada, *J. Catal.*, **238**, 289 (2008).
42. H. Hagiwara, A. Koseki, K. Isobe, K. Shimizu, T. Hoshi, T. Suzuki, *Synlett*, **2004**, 2188.
43. H. Hagiwara, J. Hamaya, T. Hoshi, C. Yokoyama, *Tetrahedron Lett.*, **46**, 393 (2005).
44. D. J. Macquarrie, R. Maggi, A. Mazzacani, G. Sartori, R. Sartorio, *Appl. Catal., A*, **246**, 183 (2003).
45. K. A. Utting, D. J. Macquarrie, *New J. Chem.*, **24**, 591 (2000).
46. T. M. Suzuki, M. Yamamoto, K. Fukumoto, Y. Akimoto, K. Yano, *J. Catal.*, **251**, 249 (2007).
47. D. D. Das, P. J. E. Harlick, A. Soyari, *Catal. Commun.*, **8**, 829 (2007).
48. J. Huang, G. Tian, H. Wang, L. Xu, Q. Kan, *J. Mol. Catal.*, **271**, 300 (2007).
49. T. M. Suzuki, T. Nakamura, K. Fukumoto, M. Yamamoto, Y. Akimoto, K. Yano, *J. Mol. Catal. A*, **280**, 224 (2007).
50. K. K. Sharma, T. Asefa, *Angew. Chem. Int. Ed.*, **46**, 2879 (2007).
51. D. J. Macquarrie, *Green Chem.*, **1**, 195 (1999).
52. A. Anan, K. K. Sharma, T. Asefa, *J. Mol. Catal., A*, **288**, 1 (2008).
53. J. D. Bass, S. L. Anderson, A. Katz, *Angew. Chem. Int. Ed.*, **42**, 5219 (2003).
54. J. D. Bass, A. Andrew, J. Pascail, A. Katz, *J. Am. Chem. Soc.*, **128**, 3737 (2006).
55. R. K. Zeidan, S.-J. Hwang, M. E. Davis, *Angew. Chem. Int. Ed.*, **45**, 6332 (2006).
56. R. K. Zeidan, M. E. Davis, *J. Catal.*, **247**, 379 (2007).
57. K. Motokuma, M. Tomita, M. Tada, Y. Iwasawa, *Chem. Eur. J.*, **14**, 4017 (2008).
58. A. Puglisi, R. Annunziata, M. Benaglia, F. Cozzi, A. Gervasini, V. Bertacche, M. C. Sala, *Adv. Synth. Catal.*, **351**, 219 (2009).
59. R. Srivastava, D. Srinivas, P. Ratnasamy, *J. Catal.*, **233**, 1 (2005).
60. R. Srivastava, D. Srinivas, P. Ratnasamy, *Micropor. Mesopor. Mater.*, **90**, 314 (2006).
61. Y. Kubota, Y. Nishizaki, H. Ikeya, J. Nagaya, Y. Sugi, *Stud. Surf. Sci. Catal.*, **141**, 553 (2002).
62. Y. Kubota, H. Ikeya, Y. Sugi, T. Yamada, T. Tatsumi, *J. Mol. Catal., A*, **249**, 181 (2006).
63. K. Komura, T. Kawamura, Y. Sugi, *Catal. Commun.*, **8**, 644 (2007).

5.

Reactions Catalyzed by Solid Bases

5.1 Isomerization of Alkenes and Alkynes

5.1.1 Isomerization of Alkenes

In 1958, Pines and Haag reported that when sodium dispersed on powdered alumina (8 wt%) was used as a catalyst, double bond isomerization of 1-butene proceeded at 310 K.¹⁾ The ratio of *cis/trans* was much greater than that of the thermodynamic equilibrium mixture. In contrast to the well-known acid-catalyzed isomerization proceeding through carbenium ions, no rearrangements of the carbon skeleton were observed in the base-catalyzed reactions, indicating the anionic nature of the intermediate. This was the first report on solid base catalysis.

Tanabe et al. showed that CaO treated in air did not catalyze the isomerization of 1-butene at 473 K, while CaO treated under vacuum above 673 K catalyzed the isomerization even at 303 K.²⁾ Hattori et al. showed that MgO became active for double bond migration of 1-butene when pretreated above 673 K (see. Fig. 3.1.3) at which temperature the oxide surfaces begin to be exposed by removal of H₂O and CO₂, and the basic sites were generated.³⁾ The activity of MgO was so high that the reaction proceeded even at 223 K. These discoveries were the initiation of alkaline earth oxides as solid base catalysts.

The reaction mechanism of double bond migration of 1-butene over solid bases is shown in Fig. 2.5.2 (section 2.5.2). The reaction is initiated by the abstraction of an allylic proton by a basic site to form the *cis* and *trans* forms of the allyl anion. The *cis*-2-butene is predominantly formed at the initial stage of the reaction. A high *cis/trans* ratio is characteristic of base-catalyzed double bond isomerization. This is caused by the higher stability of the *cis*-allylic anion over the *trans*-2-allylic anion.^{4,5)}

Intermediacy of the π -allyl species was confirmed by the infrared spectroscopy of adsorbed butenes during isomerization over ZnO.^{6,7)} The analysis of the band shift indicates that the π -allyl species have a carbanion character. Two types of the π -allyl species, *trans* and *cis* forms, were distinguished in the spectra.

When a dose of *cis*-2-butene was added to a zinc oxide sample, only the *cis*- π -allyl species was observed besides the π -bonded butenes. No *trans*- π -allyl species was observed even when equilibrium was approached. In the adsorption of *trans*-2-butene, the *trans*- π -allyl species was observed in the beginning, but the intensity of this species decreased with time and finally only *cis*- π -allyl was

observed. In the case of 1-butene, only the *cis*- π -allyl was observed, the *trans*-form being not observed during the reaction. The product ratio, *cis/trans*, was 10.5. These results indicate the much higher stability of the *cis*-form than the *trans*-form on the surface. The interconversion between the π -allyl species was proposed to occur via a dynamic $\sigma \rightarrow \pi$ equilibrium.

The formation of the π -allyl species from propene on ZnO was also confirmed by infrared spectroscopy. The chemisorbed species from $\text{CH}_3\text{-CH=CD}_2$ and $\text{CD}_3\text{-CH=CH}_2$ gave essentially identical spectra except that the former yielded an OH fragment on adsorption, and the latter an OD fragment.⁸⁾

Various catalysts are reported for the isomerization of butenes, as shown in Table 2.5.4 (section 2.5.2). Since the $\text{p}K_{\text{a}}$ values of alkenes are rather high, only strong solid bases are useful if the π -allyl anions are not stabilized by the attached groups. Table 5.1.1 compares the catalytic activities of strong bases for the iso-

Table 5.1.1 The catalytic activities of solid base catalysts for the isomerization of 2,3-dimethylbut-1-ene to 2,3-dimethylbut-2-ene at 313 K for 20 h^{a)}

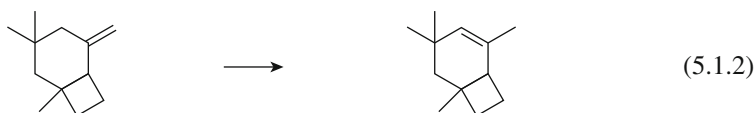
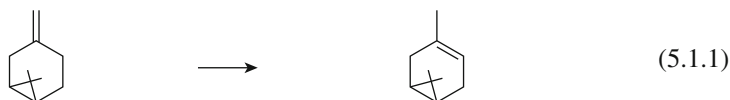
Catalyst	Pretreatment		Conversion/%
	Temperature/K	Time/h	
Metals supported from liq. NH_3 ^{b),c)}			
$\text{KNH}_2/\text{Al}_2\text{O}_3(2.6)$	573	1	91.3
$\text{K}(\text{NH}_3)/\text{Al}_2\text{O}_3(2.0)$	423	1	89.4
$\text{Na}(\text{NH}_3)/\text{Al}_2\text{O}_3(3.5)$	423	1	89.3
$\text{Eu}(\text{NH}_3)/\text{Al}_2\text{O}_3(0.5)$	523	1	83.4
$\text{Yb}(\text{NH}_3)/\text{Al}_2\text{O}_3(0.5)$	473	1	29.4
$\text{Eu}(\text{NH}_3)/\text{Al}_2\text{O}_3(0.5)$	423	1	2.3
$\text{Yb}(\text{NH}_3)/\text{Al}_2\text{O}_3(0.5)$	473	1	1.0
Alkali metals/ Al_2O_3			
$\text{KNO}_3/\text{Al}_2\text{O}_3(5.0)$	873	3	90.7
$\text{KOH}/\text{Al}_2\text{O}_3(5.0)$	673	3	86.0
$\text{KF}/\text{Al}_2\text{O}_3(5.0)$	623	3	25.6
Metal oxides			
CaO	1073	3	89.8
MgO	873	3	84.9
SrO	1023	3	1.6
BaO	1073	3	0.4
Sm_2O_3	773	3	1.2
Eu_2O_3	923	3	1.0
Yb_2O_3	923	3	0.9
Al_2O_3	773	3	3.9
Mixed oxides ^{d)}			
4 CaO, Al_2O_3	1073	1	11.9
4 MgO, Al_2O_3	773	4	1.3
Zeolites			
KY	773	3	<0.1

^{a)} Conditions: catalyst = 0.25 g, 2,3-dimethylbut-1-ene = 3 mL (24 mmol). ^{b)} Number in parentheses: supported amount in mmol g^{-1} . ^{c)} $\text{KNH}_2/\text{Al}_2\text{O}_3$ prepared by loading KNH_2 on Al_2O_3 from ammoniacal solution of KNH_2 , $\text{M}(\text{NH}_3)$ ($\text{M} = \text{K, Na, Eu}$ and Yb) prepared by impregnation from the metal dissolved in liquid ammonia. ^{d)} Prepared from hydrotalcite structure.

Reprinted with permission from H. Handa, T. Baba, Y. Ono, *Catal. Lett.*, **59**, 195 (1999) p.197, Table 1

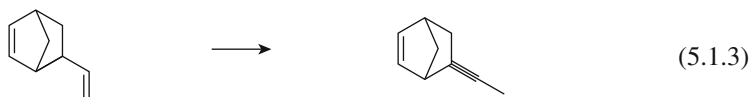
merization of 2,3-dimethyl-1-butene to 2,3-dimethyl-2-butene.⁹⁾ The reaction proceeds even at 201 K over most active catalysts.⁹⁾

Alkenes with exo-double bonds such as β -pinene are quantitatively converted into the isomers over alkaline earth oxides.^{10,11)}



The isomerization of β -pinene [eq. (5.1.1)] was also studied by various solid superbases. Na/NaOH/Al₂O₃ and Cs_xO/Al₂O₃ showed the highest activity, the reaction at room temperature giving 98% conversion in 30 min at a reactant/catalyst ratio of 30.¹²⁾ The catalysts were deactivated and the activity could not be regained under the applied conditions of regeneration.

The isomerization of 5-vinylbicyclo[2,2,1]-2-heptene to 5-ethylidenebicyclo[2,2,1]-2-heptene, a compound used for vulcanization purposes, proceeds completely even at 243 K.^{13, 14)}

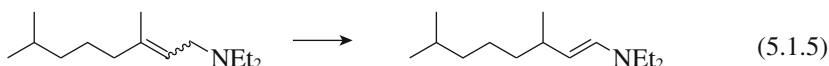


KNH₂/Al₂O₃ is also active, and the conversion of the reactant (21 mmol) reached 98% in 10 min at 273 K in the presence of 63 mg of the catalyst.¹⁵⁾ Alkaline earth oxides (CaO, MgO) are also effective for the isomerization when properly activated.^{16, 17)}

Allylamines are isomerized to enamines. 1-*N*-pyrrolidino-2-propene to 1-*N*-pyrrolidino-1-propene over alkaline earth oxides proceeds at 313 K.¹⁸⁾

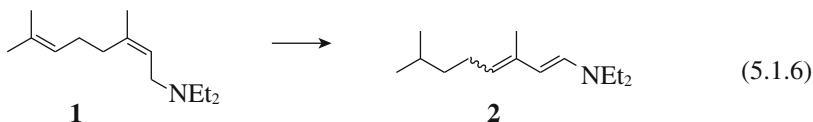


N,N-Dimethyl-3,7-dimethyloct-2-enylamine gives the corresponding enamine with a 100% *E* configuration in the presence of KNH₂/Al₂O₃ at 353 K.¹⁹⁾



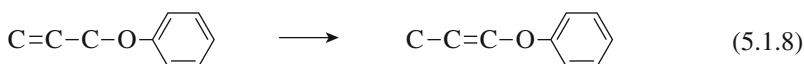
The isomerization of *N,N*-dimethyl-3,7-dimethylocta-2(*Z*),6-dienylamine **1**, proceeds over KNH₂/Al₂O₃ at 313 K to afford exclusively *N,N*-diethyl-3,7-dimethylocta-1,3-dienylamine **2**.¹⁹⁾ The ratio of *E/Z* of the double bond at the

3-position in the product is almost 1 : 1. The double bond at the 1-position is 100% *E*.



Passing an ethyl acetate-hexane solution of **2** through a column of silicagel yielded quantitatively 3,7-dimethyl-2-octene-1-al. The *E/Z* ratio of the aldehyde was 12 : 1. This shows that the selective isomerization of **1** to **2** offers a convenient route to monoterpene aldehyde, since the reactant is easily prepared by the dimeric addition of isoprene to the dialkylamine in the presence of a base catalyst.

The isomerization of propenyl ethers over a variety of metal oxides was reported by Matsushashi and Hattori.²⁰⁾ Among the metal oxides studied, CaO exhibited the highest activity, and La₂O₃, SrO and MgO also showed high activities. The reaction temperatures required to initiate the reactions are different for each reactant.

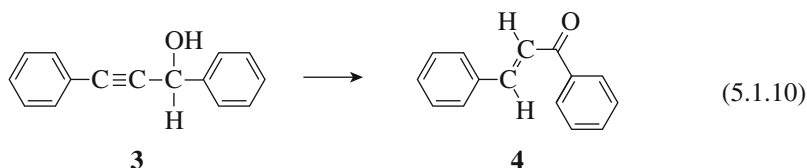


The isomerization of alkenyl aromatics of perfumery interest is described in 6.1.5 (a).

5.1.2 Isomerization of Alkynes

Alkynes are easily isomerized in the presence of KNH₂/Al₂O₃.²¹⁾ Thus, 1-hexyne is isomerized exclusively to 2-hexyne in a 92% yield in dioxane at 333 K in 20 h. CaO, prepared by evacuating CaCO₃ at 998 K also catalyzed the isomerization of 1-hexyne. The yields of 2-hexyne and 3-hexyne were 79% and 13%, respectively at 313 K in 20 h.²¹⁾

The isomerization of substituted 2-propynyl alcohols to α,β -unsaturated ketones proceeds over solid bases.²²⁾ Thus, in the reaction of **3** with Cs₂CO₃/Al₂O₃ for 20 h in dioxane, **4** was obtained in a 97% yield.



References

1. H. Pines, O. Haag, *J. Org. Chem.*, **23**, 328 (1958).
2. K. Tanabe, N. Yoshii, *Chem. Commun.*, **1971**, 494.
3. H. Hattori, N. Yoshii, K. Tanabe, *Proc. 5th intern. Congr. Catal.*, Miami Beach (1972) p.233.
4. S. Bank, A. Schriesheim, C. A. Rowe, Jr., *J. Am. Chem. Soc.*, **87**, 3244 (1965).
5. S. Bank, *J. Am. Chem. Soc.*, **87**, 3245 (1965).
6. A. L. Dent, R. J. Kokes, *J. Phys. Chem.*, **78**, 487 (1971).
7. C. C. Chang, W. C. Conner, R. J. Kokes, *J. Phys. Chem.*, **77**, 1957 (1973).
8. A. L. Dent, R. J. Kokes, *J. Amer. Chem. Soc.*, **92**, 1092 (1970), *ibid.* **92**, 6709 (1970).
9. H. Handa, Y. Fu, T. Baba, Y. Ono, *Catal. Lett.*, **59**, 195 (1999).
10. R. Onishi, K. Tanabe, *Chem. Lett.*, **3**, 207 (1974).
11. H. Hattori, K. Tanabe, K. Hayano, H. Shirahama, T. Matsumoto, *Chem. Lett.*, **8**, 133 (1979).
12. H. Garzawski, W. F. Hoelderich, *J. Mol. Catal., A*, **144**, 181 (1999).
13. G. Suzukamo, M. Fukao, T. Hibi, K. Tanabe, K. Chikaishi, in : *Acid-Base Catalysis*, (eds. K. Kozo, H. Hattori, T. Yamaguchi, T. Tanaka) Kodansha, Tokyo, and VCH Weinheim, 1989, p. 405.
14. G. Suzukamo, M. Fukao, M. Minobe, *Chem. Lett.*, **16**, 585 (1987).
15. T. Baba, H. Handa, Y. Ono, *J. Chem. Soc., Faraday Trans.*, **90**, 187 (1994).
16. T. Baba, T. Endo, H. Handa, Y. Ono, *Appl. Catal.*, **A97**, L19 (1997).
17. H. Kabashima, H. Tsuji, H. Hattori, *React. Kinet. Catal. Lett.*, **58**, 255 (1999).
18. A. Hattori, H. Hattori, *J. Catal.*, **65**, 246 (1980).
19. H. Handa, T. Baba, H. Yamada, T. Takahashi, Y. Ono, *Catal. Lett.*, **44**, 77 (1997).
20. H. Matsuhashi, H. Hattori, *J. Catal.*, **85**, 457 (1984).
21. Y. Ono, *Specialist Periodical Series (Catalysis, vol.15)*, p. 1, Royal Society of Chemistry (2000).
22. T. Baba, H. Kizuka, H. Handa, Y. Ono, *Appl. Catal.*, **A194/195**, 203 (2000).

5.2 Aldol Addition and Aldol Condensation

Aldol addition and aldol condensation are very useful for C-C bond formation. These reactions are catalyzed by an acid or base. In the presence of a base, the aldol addition occurs by nucleophilic addition of the enolate ion of an aldehyde or ketone to the carbonyl group of another molecule to form β -hydroxyaldehyde or ketone (aldol addition).

The β -hydroxyaldehyde or ketone formed in aldol addition can be easily dehydrated to yield α,β -unsaturated ketone under the reaction conditions (aldol condensation).

Aldol addition of acetone to diacetone alcohol is often used for the characterization of solid base catalysts (see section 2.5.6).

5.2.1 Condensation of Propanal and Butanal

The aldol addition of butanal in the presence of metal oxides was studied by Tanabe and coworkers.^{1, 2)} Alkaline earth oxides showed high activities, while La_2O_3 and ZrO_2 showed low activities at 273 K. The order of activity per unit surface area is $\text{SrO} > \text{CaO} > \text{MgO} \gg \text{La}_2\text{O}_3, > \text{ZrO}_2$.¹⁾ Alumina also showed activity, but it was lower than that of MgO and CaO .²⁾ The products are not only simple dimerization products but contain a large amount of trimers (trimeric glycol ester), which are the products of the Tishchenko-type cross-esterification of the aldol dimer with butanal (Fig. 5.2.1). In the case of MgO , the products consist of 2-ethyl-3-hydroxyhexanal (81.7%), 2-ethylhexenal (2.8%), the trimer (16.3%) and a small

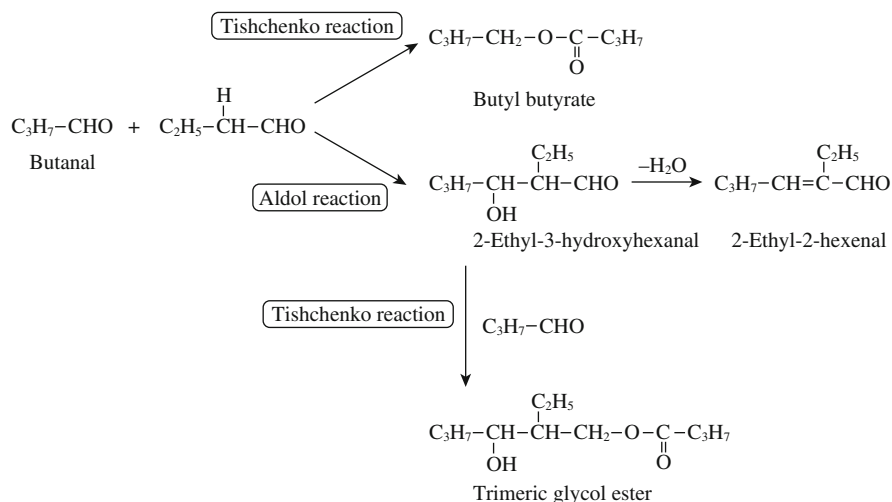


Fig. 5.2.1 Reaction scheme for self-condensation of butanal over solid base catalysts. Reprinted with permission from H. Tsuji, F. Yagi, H. Hattori, H. Kita, *J. Catal.*, **148**, 759 (1994) p.766, Fig 4.

amount of butyl butyrate and butanol. In the case of CaO, the trimer accounts for 56.9% of the products. Butyl butyrate is the Tishchenko reaction product of butanal. The authors suggest that aldol addition proceeds on basic sites and Tishchenko reactions require both acidic and basic sites. Actually, when alumina was loaded with an alkali metal oxide, the activity was greatly enhanced.²⁾ The selectivity for the aldol addition product also greatly increased to >92%, while the trimer yield was diminished to below 3%.

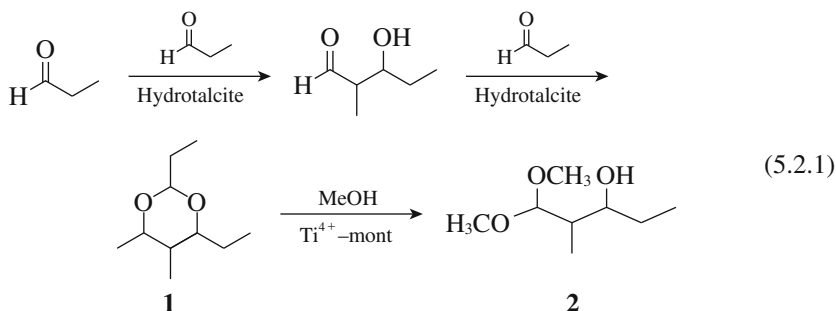
Self-aldol condensation of unmodified aldehydes such as decanal to the corresponding enals is catalyzed by *N*-methylaminopropyl groups tethered to silica gel under supercritical carbon dioxide.³⁾

Aldol condensation of propanal to 2-methylpentenal was studied in liquid phase in the presence of alkali ion-exchanged zeolites, alumina, KOH-loaded alumina and MgO-Al₂O₃ mixed oxides derived from hydrotalcite.⁴⁾ The maximum conversion (97%) of propanal with 99% selectivity for 2-methylpentenal was obtained in 10 h using MgO-Al₂O₃ mixed oxide (Mg/Al = 3.5). The catalyst could be recycled six times without significant loss in conversion or selectivity.

Magnesium organo-silicate (MOS) with a talc-like structure was synthesized by the sol-gel method and the applicability of amine- and diamine-functionalized MOS as catalysts for a variety of self- and cross aldol condensation was tested.⁵⁾ Although the catalysts had a small surface area (2–3 m² g⁻¹), they were active for the aldol condensation. In the case of propanal, the conversion of propanal reached 86% with 95% selectivity for 2-methylpentenal in DMSO over amine-functionalized MOS in 10 h at 373 K.

The reaction of propanal in the presence of rehydrated hydrotalcite gives hemiacetal **1**.⁶⁾ Though the hemiacetal is not stable for analyses using gas-

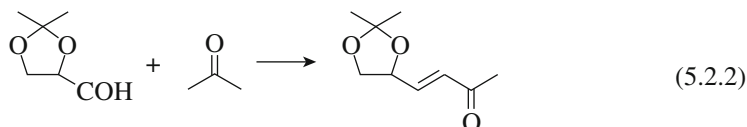
chromatography, it can be converted into 1,1-dimethoxy-2-methyl-3-pentanol **2** in methanol in the presence of solid acid catalyst, Ti^{4+} -exchanged montmollironite.



An 89% yield of **2** was obtained by the reaction in water at room temperature for 1 h. Acetaldehyde also gives the corresponding dimethoxyacetal in 85% yield in 2 h. As the hydrophilic hydrotalcite existed in the aqueous phase, water insoluble butanal resulted in a low yield (9%). Addition of a cationic surfactant, dodecyltrimethylammonium bromide, however, could accelerate the aldol reaction of butanal to give a 90% yield of the corresponding products within 2 h. The same catalyst is also effective for cross aldol reaction of aliphatic aldehydes with ketones when excess ketones is used to avoid self-aldolization of the aldehyde. Acetone reacted with isovaleraldehyde to give 4-hydroxy-6-methyl-2-heptanone in 78% yield in 10 h.

5.2.2 Condensation of Glyceraldehyde Acetonide with Acetone

Durbey et al. showed that ordered mesoporous MgO is an effective catalyst for Knoevenagel condensation, Michael addition and aldol condensation.⁷⁾ They also showed that mesoporous MgO catalyzed the aldol condensation reaction of glyceraldehyde acetonide with acetone, a very useful reaction to synthesize α,β -unsaturated compounds.⁷⁾

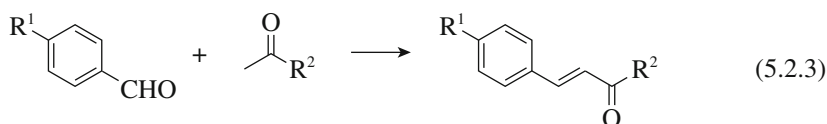


The reaction was carried out with the acetone/glyceraldehyde acetonide ratio of 30 without solvent at 373 K. The conversion of glyceraldehyde acetonide was 85% with 82.5% selectivity for the desired product in 24 h reaction. Mesoporous MgO was more active and selective than $\text{MgO-Al}_2\text{O}_3$ mixed oxide derived from hydrotalcite.⁷⁾

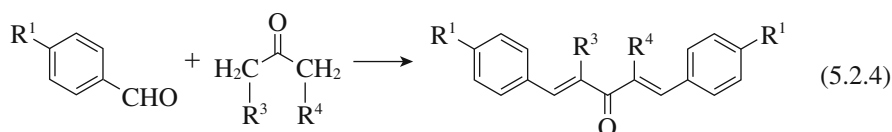
5.2.3 Claisen-Schmidt Condensation

Claisen-Schmidt condensation (aldol condensation between aromatic aldehyde and aliphatic carbonyl compound) are catalyzed by a variety of solid bases.

Barium hydroxide was reported to be effective catalysts for Claisen-Schmidt condensation of substituted benzaldehyde and methyl alkyl ketone.⁸⁾



The catalyst was prepared by partial dehydration of commercial Ba(OH)₂·8H₂O by heating in air at 473 K.⁸⁾ Aldehyde (0.04 mol) and ketone (0.08 mol) are mixed with 96% ethanol (20 mL), the catalyst (1 g) is added, and the mixture is refluxed for 1 h. The results are shown in Table 5.2.1. Distyryl ketones can be also prepared in good yields.⁸⁾



The condensation of benzaldehyde with acetone and methyl ethyl ketone proceeds in liquid phase in the presence of alumina.⁹⁾ The reaction of substituted benzaldehyde and acetone gives the Hammett reaction constant ($\rho = 1.43$). The reaction of benzaldehyde with methyl ethyl ketone affords 1-phenyl-1-penten-3-one and 4-phenyl-3-methyl-3-butene-2-one, the former being predominant. These results indicate that the active centers are basic sites on Al₂O₃.

MgO is active for Claisen-Schmidt condensation. Usually, MgO (100) facet is the most stable and the sole surface generated by wet chemical methods. Zhu et al.

Table 5.2.1 Claisen-Schmidt reactions [eq. 5.2.3] in the presence of Ba(OH)₂

R ¹	R ²	Yield ^{b)} /%	R ¹	R ²	Yield/%
H	CH ₃	89–93	Cl	<i>n</i> -C ₄ H ₉	83–87
H	<i>n</i> -C ₃ H ₇	79–83	Cl	<i>iso</i> -C ₃ H ₇	85–89
H	<i>iso</i> -C ₃ H ₇	92–95	Cl	<i>n</i> -C ₅ H ₁₁	90–93
H	<i>t</i> -C ₄ H ₉	93–96	NO ₂	C ₆ H ₅	94–97 ^{c)}
H	C ₆ H ₅	94–98	NO ₂	<i>t</i> -C ₄ H ₉	24–25 ^{c),d)}
OCH ₃	<i>n</i> -C ₃ H ₇	79–84	CH ₃	<i>iso</i> -C ₃ H ₇	99–100
OCH ₃	<i>n</i> -C ₅ H ₁₁	81–85	CH ₃	<i>iso</i> -C ₄ H ₉	70–71
OCH ₃	<i>iso</i> -C ₃ H ₇	81–85	CH ₃	<i>n</i> -C ₃ H ₇	99–100
OCH ₃	<i>iso</i> -C ₅ H ₁₀	86–89	CH ₃	<i>n</i> -C ₄ H ₉	54–55
Cl	<i>n</i> -C ₃ H ₇	83–85			

^{a)} Reaction conditions: see text

^{b)} Recrystallized or distilled product

^{c)} Reaction time: 1 h

^{d)} Product polymerized in presence of catalyst

Reprinted with permission from J. V. Siniesterra, A. Garcia-Raso, J. A. Cabello, J. M. Marinas, *Synthesis*, **1984**, 502 p. 503, Table 1.

prepared a MgO nanosheet that possess the (111) lattice plane as the main surface and compared the catalytic activity of this material for Claisen-Schmidt condensation of benzaldehyde with acetophenone with those of MgO crystallites prepared by different methods.¹⁰⁾ The order of the catalytic activity decreased in the order Mg(111) nanosheet \gg aerogel-prepared MgO > conventionally prepared MgO > commercial MgO. Mg(111) surface was much more active than high-surface-area MgO prepared by aerogel method. The reaction was completed within 5 min at 383 K.

MgO-Al₂O₃ mixed oxides which are prepared by calcinations of hydrotalcite are active for Claisen-Schmidt reactions.^{11,12)} Furthermore, hydrotalcite, which is reconstructed from the oxides by rehydration shows much higher activities for the Claisen-Schmidt reactions between acetone and substituted benzaldehydes.^{13,14)} The condensation reactions proceeded to the dehydrated products at 333 K.¹³⁾ When the reaction was carried out at 273 K, the reaction of benzaldehyde and acetone selectively provided aldol instead of the dehydrated products.¹⁵⁾ Under the same reaction conditions, the mixed oxides (calcined hydrotalcites) showed very little activity. It is noteworthy that the amount of CO₂ adsorbed and the heat of adsorption of CO₂ suggests a higher basicity of the mixed oxides compared with the rehydrated hydrotalcite. This shows that OH⁻ ions in the interlayer are much more effective than surface oxygen anions on the mixed oxide for the reaction. The reaction was first order with respect to acetone and reciprocally first order with respect to benzaldehyde.

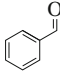
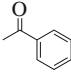
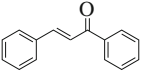
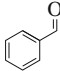
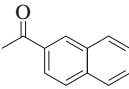
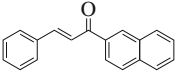
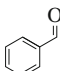
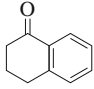
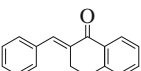
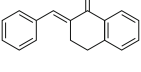
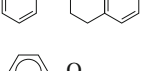
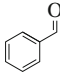
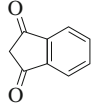
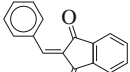
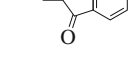
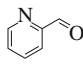
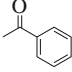
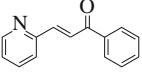
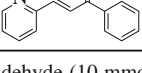
The higher activities of rehydrated hydrotalcites over the mixed oxides were also observed in the Claisen-Schmidt condensation of benzaldehyde and acetophenone.¹⁶⁾ In this case, rehydration was done by simply adding the optimum amount of water (35 wt%) to the calcined hydrotalcite. Various types of chalcone derivatives were synthesized with rehydrated hydrotalcite (Table 5.2.2).

When *t*-butoxide ions are introduced by ion exchange into the interlayers of hydrotalcite, very basic catalysts are formed. This catalyst shows very high activities for the reactions of substituted benzaldehydes with acetone.¹⁷⁾ The reactions proceed efficiently at 273 K and give high conversions in 15 min. Aldol products are obtained selectively.

Choudary et al. reported the reactions of various aldehydes with acetone over a diamino-functionalized MCM-41 at 323 K. The products were a mixture of aldol adduct and the dehydrated product, the ratio being dependent on the aldehyde.¹⁸⁾ The reaction of 4-nitrobenzaldehyde and acetone proceeds in the presence of amine-functionalized mesoporous silica.^{19,20)} Among the immobilized amines, secondary amine showed the highest activity.^{19,20)} Particularly high activity was shown by FSM-16 with *N*-methylaminopropyl groups, the yields of the aldol adduct and its dehydration product being 86% and 7%, respectively, at 303 K.¹⁹⁾

Amino-grafted X-zeolite shows a high activity for the condensation of benzaldehyde and acetophenone under ultrasound irradiation.²¹⁾ A 99% yield of chalcone was obtained at 323 K in 3 h under ultrasound irradiation. Similarly, 4'-hydroxy-2,4-dichlorochalcone and 4'-carboxy-2,4-dichlorochalcone were obtained in 45% and 65% yields, respectively, in 5 h under ultrasound irradiation.

Table 5.2.2 Synthesis of chalcone derivatives using rehydrated hydrotalcite (HTc)

Entry	Aldehyde	Alkyl aryl ketone	Chalcone derivative	T/K	Yield/%	Selectivity/%
1				333	87 (2 h)	99
2				333	68 (2 h)	99
3				333	26 (7 h)	99
				373	60 (7 h)	99
				393	88 (7 h)	99
4				298 ^{b)}	95 (7 h)	99
				333 ^{b)}	93 (1 h)	99
5				333	45 (7 h)	99
				373	75 (4 h)	99

^{a)} Reaction conditions: ketone (10 mmol); aldehyde (10 mmol), using HTc(0.025), (10 wt%) with 35 wt% of water (HTc-A (0.25) sample). Reactions were carried out in the absence of solvent except for entry 4.

^{b)} 10 mL of CH₂Cl₂ as a solvent.

Reprinted with permission from M. J. Climent, A. Corma, S. Iborra, A. Verty, *J. Catal.*, **221**, 474 (2004) p.479, Table 3.

Without irradiation, the yields of these compounds were around 20% and 35%, respectively.

Chitosan is a polysaccharide and obtained by removing most of acetyl groups from chitin. Because of the presence of amino groups, it can be used as a solid base catalyst. Aldol reactions between aromatic aldehydes and acetone were studied in the presence of chitosan in DMSO²²⁾. The aromatic aldehydes, having an electron-withdrawing substituents such as *p*-nitrobenzaldehyde, gave the corresponding aldol products in high yields with good selectivities.²²⁾

5.2.4 Mukaiyama Aldol Reactions

Mukaiyama aldol reactions of silylenol ether and aldehyde are promoted by 1,5,7-triazabicyclo[4,4,0]-5-decene (TBD)-tethered to SBA-15.²³⁾

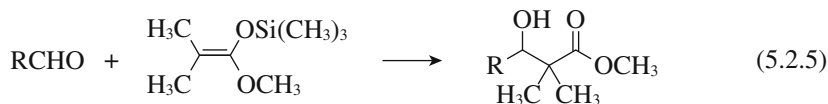
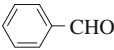

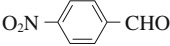
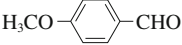
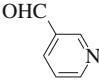

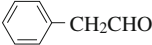
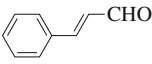


Table 5.2.3 shows the experimental results for Mukaiyama reactions of several

Table 5.2.3 Aldol condensation of 1-methoxy-2-methyl-1-trimethylsilylpropene with a variety of aldehydes [eq. (5.2.5)] in the presence of TBD tethered to SBA-15

Entry no.	Aldehyde	Yield/%
1		70
2		81
3		58
4		57
5		47
6		62 (12) ^{a)}
7		60 (10) ^{a)}
8		85

Reaction conditions: 1-methoxy-2-methyl-1-trimethylsilyloxypropene (6 mmol), aldehyde (3 mmol), catalysts (0.3 mmol), reaction temperature (383 K), run time (12 h).

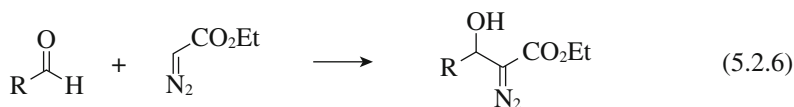
^{a)} Values in parentheses represent the percentage yield of self-condensed product.

Reprinted with permission from R. Srivastava, *J. Mol. Catal., A*, **264**, 149 (2007) p. 151, Table 2.

aldehydes with 1-methoxy-2-methyl-1-trimethylsilyloxypropene at room temperature.

5.2.5 Reactions of Aldehydes and Imines with Ethyl Diazoacetate

The direct aldol-type reaction of ethyl diazoacetate and various aldehydes affords the corresponding α -diazo- β -hydroxy esters in the presence of high-surface-area MgO.²⁴⁾



A variety of different aromatic aldehydes containing electron-withdrawing or donating groups were subjected to this reaction, as shown in Table 5.2.4. DMSO was found to be the best solvent. Excellent yields were also obtained for heterocyclic aldehydes such as 2-, 3-, 4-pyridylaldehydes, 2-furfurylaldehyde and 2-thiophenylaldehyde.

The same type of reaction also proceeds over MgO-La₂O₃ mixed oxide.²⁵⁾ In this case, the reaction proceeds in water, though the rate is slower.

Table 5.2.4 Aldol-type reaction of various aldehydes and ethyl diazoacetate [eq. (5.2.6)] using MgO

Entry	Substrate (R)	Time/h	Yield ^{b)} /%
1	C ₆ H ₅	2	78
2	4-Cl-C ₆ H ₄	1	92
3	4-CN-C ₆ H ₄	1	98, 93 ^{c)}
4	4-CF ₃ -C ₆ H ₄	0.5	98
5	4-F-C ₆ H ₄	2	83
6	4-NO ₂ -C ₆ H ₄	2	65
7	2-Cl-C ₆ H ₄	2	81
8	2-NO ₂ -C ₆ H ₄	2	93
9	3-NO ₂ -C ₆ H ₄	2	93
10	4-Br-C ₆ H ₄	2	72
11	4-OMe-C ₆ H ₄	6	50
12	4-CH ₃ -C ₆ H ₄	6	92
13	2-Naphthyl	3	83
14	Cyclohexyl	6	91
15	6-Bromo piperonyl	3	80

^a NAP-MgO (50 mg), aldehyde (0.5 mmol), EDA (0.55 mmol), DMSO (2 mL), r.t.

^b Isolated yield.

^c Yield after third cycle.

Reprinted with permission from M. L. Kantam, L. Chakrapani, T. Ramani, *Tetrahedron Lett.*, **48**, 6121 (2007) p. 6122, Table 1.

5.2.6 Vapor Phase Aldol Condensation

Aldol condensation can be performed in the vapor phase. Since the reaction temperature inevitably becomes high, control of the side reactions are key for high performance. The balance of acidity and basicity is very important.

Aldol reaction of acetone in liquid phase gives diacetone alcohol as described above. However, if the reaction is conducted in gas phase at higher temperatures, diacetone alcohol dehydrates rapidly to yield mesityl oxide, which in turn undergoes reactions leading to phorones and other carbonyl compounds. For example, the reaction of acetone over MgO at 573 K gave isomesityl oxide, mesityl oxide and isophorone.²⁶⁾ The selectivity for the three compounds was 18%, 67% and 15%, respectively, at a conversion of 24%. The activity was enhanced by loading alkali and alkaline earth ions on MgO and correlated with the number of basic sites (irreversibly adsorbed CO₂).

MgO-Al₂O₃ oxides (calcined hydrotalcite) are used as catalysts for vapor-phase reaction of formaldehyde and acetone to form methyl vinyl ketone (MVK).²⁷⁾ An MVK yield of 20% was obtained with the selectivity of 95% and 20% based on acetone and formaldehyde, respectively, at 673 K.



Aldol condensation of formaldehyde and acetaldehyde to form acrylaldehyde (2-propenal) was studied by Ai.²⁸⁾



Among the binary oxides, MgO-SiO₂, Li₂O-SiO₂, Na₂O-SiO₂ and ZnO-SiO₂ showed the highest yield. The yield of acrylaldehyde was 96% at a temperature between 553 K and 613 K. The feed was composed of acetaldehyde/formaldehyde/methanol/water/N₂ with rates of 13/26/5.6/71/350 mmol h⁻¹, respectively. Ai also noted that several phosphate catalysts showed good performance.²⁹⁾ The weakly basic sites are suggested to be responsible for the catalysis.

The same reaction was studied using MgO-Al₂O₃ mixed oxides derived from hydrotalcite-like materials.³⁰⁾ The oxide containing Mg and Al or Co and Al showed high selectivity (80%) for acrylaldehyde. In the proposed mechanism, the basic sites of certain strength activate the acetaldehyde by the abstraction of an H atom at the α-position, while the acidic sites of weak strength activate formaldehyde by an increase in the electrophilicity of the carbon atom.

Synthesis of methyl methacrylate by aldol condensation of formaldehyde and methyl propionate over zeolite catalysts was reported.³¹⁾ A 74.1% selectivity for methyl methacrylate based on methyl propionate at a methyl propionate conversion of 13.8% was obtained over KOH-loaded KY under the reaction conditions of a methyl methacrylate/ formaldehyde ratio of 3.4 and at 633 K.

The reaction of formaldehyde and propionic acid formed methacrylic acid over a series of alkali ion-doped silica.^{32,33)} Activity and selectivity increased in the order Li < Na < K < Cs.³²⁾ The characterization suggested that both acid and base sites are needed to catalyze the reaction.³³⁾ Cs-loaded SiO₂ gave 100% selectivity at 14.7% conversion of propionic acid in the feed of a propionic acid : formaldehyde ratio of 3 : 2 at 598 K.³³⁾

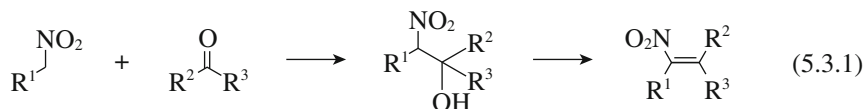
References

1. G. Zhang, H. Hattori, K. Tanabe, *Bull. Chem. Soc. Jpn.*, **62**, 2070 (1989).
2. H. Tsuji, F. Yagi, H. Hattori, H. Kita, *J. Catal.*, **148**, 759 (1994).
3. H. Hagiwara, J. Hamaya, T. Hoshi, C. Yokoyama, *Tetrahedron Lett.*, **46**, 393 (2005).
4. S. K. Sharma, P. A. Parikh, R. V. Jarsa, *J. Mol. Catal., A*, **278**, 135 (2007).
5. H. A. Patel, S. K. Sharma, R. V. Jarsa, *J. Mol. Catal., A*, **286**, 31 (2008).
6. K. Ebitani, K. Motokuma, K. Mori, T. Mizugaki, K. Kaneda, *J. Org. Chem.*, **71**, 5440 (2006).
7. A. Dubey, B. G. Mishra, D. Sachdev, *Appl. Catal., A*, **338**, 20 (2008).
8. J. V. Sinisterra, A. Garcia-Raso, J. A. Cabello, J. M. Marinas, *Synthesis*, **1984**, 502.
9. L. Nondek, J. Málek, *Coll. Czech. Chem. Commun.*, **45**, 1812 (1980).
10. K. Zhu, J. Hu, C. Kübel, R. Richards, *Angew. Chem. Int. Ed.*, **45**, 7277 (2006).
11. A. Guida, M. H. Lhouty, D. Ticht, F. Figueras, P. Geneste, *Appl. Catal., A*, **164**, 251 (1997).
12. M. J. Climent, A. Corma, S. Iborra, J. Primo, *J. Catal.*, **151**, 60 (1995).
13. M. L. Kantam, B. M. Choudary, Ch. V. Reddy, K. K. Rao, F. Figueras, *Chem. Commun.*, **1998**, 1033.
14. M. Campanati, S. Franceschini, O. Piccolo, A. Vaccari, A. Zicmanis, *Catal. Commun.*, **5**, 145 (2004).
15. K. K. Rao, M. Gravelle, J. S. Valene, F. Figueras, *J. Catal.*, **173**, 115 (1998).
16. M. J. Climent, A. Corma, S. Iborra, A. Verty, *J. Catal.*, **221**, 474 (2004).
17. R. M. Choudary, M. L. Kantam, B. Kavita, Ch. V. Reddy, K. Kolerwara, F. Figueras, *Tetrahedron Lett.*, **39**, 3535 (1998).
18. R. M. Choudary, M. L. Kantam, P. Streerkanth, T. Bandopadhyay, F. Figueras, A. Tuel, *J. Mol. Catal., A*, **142**, 361 (1999).

19. Y. Kubota, K. Goto, S. Miyata, Y. Goto, Y. Fukushima, Y. Sugi, *Chem. Lett.*, **32**, 234 (2003).
20. Y. Xie, K. K. Sharma, A. Anan, G. Wang, A. V. Biradar, T. Asefa, *J. Catal.*, **265**, 131 (2009).
21. E. Perozo-Rondón, R. M. Martín-Aranda, B. Casal, C. J. Durán-Valle, W. N. Lau, X. F. Zhang, K. L. Yeung, *Catal. Today*, **114**, 183 (2006).
22. E. R. Reddy, K. Rajgopal, C. U. Maheswari, M. L. Kantam, *New J. Chem.*, **30**, 1549 (2006).
23. R. Srivastava, *J. Mol. Catal.*, **264**, 146 (2007).
24. M. L. Kantam, L. Chakrapani, T. Ramani, *Tetrahedron Lett.*, **48**, 6121 (2007).
25. M. Lashmi Kantam, V. Balasubramanyam, K. B. Shiva Kumar, G. T. Venkanna, F. Figueras, *Adv. Synth. Catal.*, **349**, 1887 (2007).
26. J. L. Di Cosimo, V. K. Díez, C. R. Apesteguía, *Appl. Catal., A*, **137**, 149 (1996).
27. E. Suzuki, Y. Ono, *Bull. Chem. Soc. Jpn.*, **41**, 1008 (1988).
28. M. Ai, *Bull. Chem. Soc. Jpn.*, **64**, 1342 (1991).
29. M. Ai, *Bull. Chem. Soc. Jpn.*, **64**, 1346 (1991).
30. E. Dumitriu, V. Hulea, C. Chelaru, C. Catrinescu, D. Ticht, R. Durand, *Appl. Catal., A*, **178**, 145 (1999).
31. P. T. Wierchowski, L. W. Zatorski, *Catal. Lett.*, **9**, 411 (1991).
32. O. H. Baily, R. A. Montag, J. S. Yao, *Appl. Catal.*, **88**, 163 (1992).
33. J. Tai, R. J. Davis, *Catal. Today*, **123**, 43 (2007).

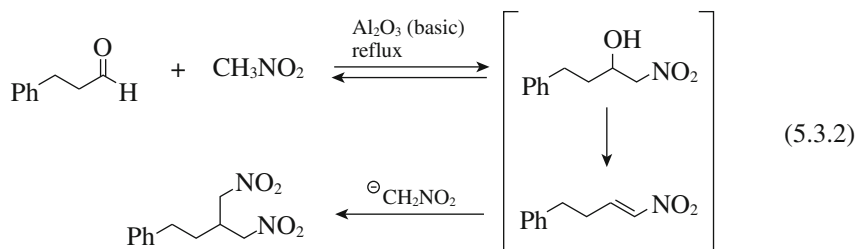
5.3 Nitroaldol Reactions (Henry Reaction)

The nitroaldol reaction, or Henry reaction, is an aldol type reaction between a nitro compound and a carbonyl compound. The primary aldol products may be dehydrated to the corresponding nitroalkenes.



Rosini et al. reported that 2-nitroalkanols were effectively synthesized from nitroalkanes and aldehydes on an alumina surface without solvent.¹⁾ In this case, the reactants were completely adsorbed on alumina and the products were extracted after 24–36 h with dichloromethane. Therefore, a large amount of alumina was required for the syntheses. Nitroaldol reactions proceed more efficiently when KF/Al₂O₃ is used as a catalyst.²⁾

When the reaction of aldehydes and nitromethane was carried out with excess nitromethane in the presence of basic alumina at refluxing temperature, 1,3-dinitroalkane was obtained in good yields (60–78%).³⁾ The reaction proceeds as follows.



Ballini et al. showed that Amberlyst 21 (an anion exchange resin with alkyl-

amine function) is a far better catalyst than alumina or $\text{KF}/\text{Al}_2\text{O}_3$ for various combinations of nitroalkanes with aliphatic and aromatic aldehydes for the nitroaldol reaction.⁴⁾ No dehydrated products were formed.

Akutsu et al. investigated the nitroaldol reaction of a variety of combinations of carbonyl- and nitro-compounds over various solid base catalysts.⁵⁾ Among the catalysts examined, MgO , CaO , $\text{Ba}(\text{OH})_2$, $\text{KOH}/\text{Al}_2\text{O}_3$, $\text{KF}/\text{Al}_2\text{O}_3$, $\text{MgO}-\text{Al}_2\text{O}_3$ and MgCO_3 exhibited high activity for nitroaldol reaction of nitromethane with propionaldehyde, the activities being in this order. Over these catalysts, the yields exceeded 20% at a reaction temperature of 313 K and a reaction time of 1 h, 1-nitro-2-butanol being the main product. $\text{Mg}(\text{OH})_2$, $\gamma\text{-Al}_2\text{O}_3$, SrO_2 , $\text{Ca}(\text{OH})_2$, BaCO_3 , SrCO_3 , BaO and La_2O_3 exhibited moderate activities; the yields were in the range 20 - 2%. CaCO_3 , ZrO_2 and ZnO scarcely showed any activity. They concluded that strong basic sites are not required for the reaction because the abstraction of a proton from a nitro compound is easy.

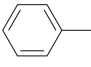
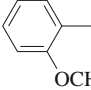
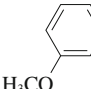
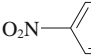
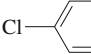
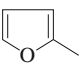
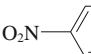
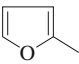
The reactivity of the nitro compounds over MgO were nitroethane > nitromethane > 2-nitropropane, and those of carbonyl compounds were propanal > isobutyraldehyde > pivalaldehyde > acetone > benzaldehyde > methyl propionate. The reactivities of the carbonyl compounds were attributed to the steric hindrance around the carbonyl carbon. For the reactivities of the nitro compounds, three factors were taken into consideration: ease of formation of the carbanion from nitroalkane, reactivity of the carbanion, and steric hindrance of the negatively charged C in the carbanion. A stable carbanion is more easily formed than an unstable carbanion, while an unstable carbanion may be more reactive than a stable carbanion in the nucleophilic addition to the adsorbed carbonyl compound. The higher reactivity of the unstable carbanion may be the reason why nitroethane reacted faster than nitromethane with propanal. 2-Nitropropane, however, reacted most slowly among the nitro compounds examined. The tertiary carbanion formed from 2-nitropropane is sterically hindered at the central C, and, accordingly, reacted slowly with the adsorbed propanol.

The nitroaldol reaction of nitromethane with propanal over MgO was scarcely poisoned by CO_2 and H_2O ; nitromethane is so acidic that it was able to be adsorbed on the catalyst on which CO_2 or H_2O was preadsorbed, as observed by IR study of co-adsorption of nitromethane, CO_2 , and H_2O .

Nitroaldol reactions of aromatic aldehydes and nitromethane/nitroethane in the presence of silica or mesoporous silica containing aminopropyl groups as catalysts have been reported by Sartori and coworkers.⁶⁾ The amino group was introduced by a sol-gel method. The products were nitrostyrenes, formed by dehydration of primary addition products. The activity depended on the loading amount of the amino group, the highest yield being obtained at the amino group content of 5-6 mmol g^{-1} . In the reaction of benzaldehyde and nitromethane, the yield of (*E*)-nitrostyrene yield reached 95% with selectivity of 97% in 2 h at 363 K. Amorphous silica grafted with aminopropyl groups by a post synthesis method are also active for various Henry reactions to afford nitroaldols at room temperature.⁷⁾

When MCM-41 was modified with amino groups by a post synthesis method, the order of catalytic activities of amine moieties for the reactions of benzaldehyde

Table 5.3.1 Synthesis of nitroaldols by the reaction of aldehydes (R^1CHO) and nitroalkenes ($R^2CH_2NO_2$) catalyzed by rehydrated and $tBuO^-$ hydrotalcite

R^1	R^2	Rehydrated hydrotalcite ^{a)}		Hydrotalcite with $tBuO^-$ ions ^{b)}	
		Time/min	Yield ^{c)} /%	Time/min	Yield ^{c)} /%
	H	30	95 ^{d)}	15	98
	H	60	98	30	96
	H	90	98	60	63
	H	30	100	30	92
	H	60	95	60	95
$CH_3CH_2^-$	H	60	100	30	92
$(CH_3)_2CH_2^-$	H			40	94
	H	60	92	30	73
$CH_3CH_2^-$	CH_3			120	92
$(CH_3)_2CH_2^-$	CH_3			120	96
	CH_3			90	93
	CH_3			120	82

^{c)} Determined by 1H NMR.^{d)} isolated yield.

and nitromethane or nitroethane was primary > secondary > tertiary.⁸⁾ The product is almost exclusively (*E*)-nitrostyrene. The higher activity of the primary amine (propylamine) moieties was explained by the mechanism which involves the formation of anchored imine (section 4.6.2). In fact, when the catalyst was treated with benzaldehyde, a new IR peak appeared at 1636 cm^{-1} due to C-N stretching. In contrast, Aman et al. reported that the selectivity to nitroalcohol or nitroalkene depends on the amino groups in the reaction of *p*-nitrobenzaldehyde and nitromethane; nitroalkene was the main product over MCM-41 anchored to propyl-amino groups, while nitroalkene was the predominant product over MCM-41 anchored to methylaminopropyl- or diethylaminopropyl groups.⁹⁾

Sujandi et al. prepared short-channeled aminopropylated SBA-15 by a direct method. This material showed greatly improved catalytic activity for nitroaldol

Table 5.3.2 1,3-Dinitroalkane synthesis from various aldehydes and nitromethane^{a)}

Entry	Aldehyde	t/h	Conversion/% ^{b)}	Yield/% ^{b)}
1	X = H	8	>99	93
2	X = Me	5	99	93
3	X = OMe	5	99	91
4	X = OH	5	>99	91
5	X = Cl	8	98	83 (8) ^{c)}
6	X = NO ₂	8	95	48 (36) ^{c)}
7		5	97	89
8		5	99	88
9		5	99	89
10		8	94	80

^{a)} Reaction conditions: aldehyde (1 mmol), nitromethane (2 mL), SA-NH₂, NEt₃ (0.1 g, NH₂: 0.044 mmol, NEt₃: 0.036 mmol), 373 K. ^{b)} Determined by ¹H NMR spectroscopy, based on aldehyde.

^{c)} Yield of nitroalcohol.

Reprinted with permission from K. Motokuma, M. Tada, Y. Iwasawa, *Angew. Chem., Int. Ed.*, **47**, 9230. p. 9232, Table 3.

reactions over typical fibrous SBA-15 catalyst with long channels. In this case the products were α,β -unsaturated alkenes.¹⁰⁾

The modification of OH groups in the propylamino-modified silica affects the product distribution of the reaction between 4-nitrobenzaldehyde and nitromethane.¹¹⁾ When the OH groups exist, the product is mainly α,β -unsaturated product. On the other hand, when the OH groups are replaced by OSi(CH₂)₃CN, the product is β -nitro alcohol. The authors proposed a change in the reaction mechanism due to the modification (section 4.6.3).

Mesoporous silica which contains diamino functions [Si-O-(CH₂)₃-NH-(CH₂)₂-NH₂] is also active for nitroaldol reactions.¹²⁾ Reactions were carried out using toluene as a solvent at 323 K. When nitromethane was used as the nucleophile, all the substrates except *p*-nitrobenzaldehyde and propanal afforded

nitroalkenes exclusively, while with nitroethane all the substrates gave only dehydrated products.

MgO-Al₂O₃ mixed oxides (calcined hydrotalcite) are also effective for the Henry reactions.¹³⁾ Both aliphatic and aromatic aldehydes can be employed for affording the corresponding nitroalkanols in high yields. The reactions were performed in THF under refluxing conditions. In the case of nitroaldols derived from 4-nitrobenzaldehyde, 2-chlorobenzaldehyde and 2-chloroquinoline-3-carboxaldehyde, exclusive formation of the *threo* isomer was obtained.

2-Nitroalkanols are selectively synthesized in the presence of rehydrated hydrotalcite,¹⁴⁾ and hydrotalcite containing *t*-butoxy ions in the interlayers (Mg-Al-O^{*t*}Bu⁻).¹⁵⁾ The results over rehydrated hydrotalcite and Mg-Al-^{*t*}BuO⁻ are given in Table 5.3.1,^{14,15)} which shows the high yields in short reaction time. Hydrotalcite to which diisopropylamide was introduced by using memory effect is also active for the nitroaldol reaction.¹⁶⁾

Cs-exchanged X-zeolite also shows activity for the formation of nitroalkenes.¹⁷⁾

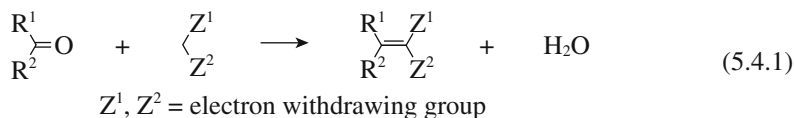
A silica-alumina modified with two types of amines (primary and tertiary) is highly active for the production of 1,3-dinitroalkanes from various aldehydes and nitromethane at 373 K, as shown in Table 5.3.2.¹⁸⁾ In contrast to alumina catalyst³⁾, a stoichiometric amount of nitromethane was used. A silica-alumina modified with single amines shows almost no significant activity for this reaction.¹⁸⁾

References

1. G. Rosini, R. Ballini, P. Sorrenti, *Synthesis*, **1983**, 1014.
2. J.-M. Mélot, F. Texier-Boullet, A. Foucaud, *Tetrahedron Lett.*, **27**, 493 (1986).
3. R. Ballini, G. Bosica, D. Fiorini, A. Palmieri, *Synthesis*, **2004**, 1938.
4. R. Ballini, G. Bosica, F. Forconi, *Tetrahedron*, **52**, 1677 (1996).
5. K. Akutsu, H. Kabashima, T. Seki, H. Hattori, *Appl. Catal., A*, **247**, 65 (2003).
6. G. Sartori, F. Bigi, R. Maggi, R. Sastorio, M. J. Macquarrie, L. Storaro, S. Coluccia, G. Marta, *J. Catal.*, **222**, 410 (2004).
7. R. Ballini, G. Bosica, D. Livi, A. Palmieri, R. Maggi, G. Sartori, *Tetrahedron Lett.*, **44**, 2271 (2003).
8. G. Demicheli, R. Maggi, A. Mazzacani, P. Righi, G. Sartori, F. Bigi, *Tetrahedron Lett.*, **42**, 2401 (2001).
9. A. Anan, R. Vathyam, K. K. Sharma, T. Asefa, *Catal. Lett.*, **126**, 142 (2008).
10. Sujandi, E. A. Prasetyanto, S.-E. Park, *Appl. Catal., A*, **350**, 244 (2008).
11. J. D. Bass-I, A. Solovyov, A. J. Andrew, J. Pascal, A. Katz, *J. Am. Chem. Soc.*, **128**, 3737 (2006).
12. M. L. Kantam, P. Sreekanth, *Catal. Lett.*, **57**, 227 (1999).
13. V. J. Bulbule, V. H. Deshpands, S. Velu, A. Sudalai, S. Sivasankar, V. T. Sathe, *Tetrahedron*, **55**, 9325 (1990).
14. B. M. Choudary, M. L. Kantam, Ch. Venkat Reddy, K. Koteswara Rao, F. Figueras, *Green Chem.*, **1**, 187 (1999).
15. B. M. Choudary, M. L. Kantam, B. Kavita, *J. Mol. Catal., A*, **169**, 193 (2001).
16. M. L. Kantam, A. Ravindra, Ch. V. Reddy, B. Sreedhar, M. Choudary, *Adv. Synth. Catal.*, **348**, 569 (2006).
17. R. Ballini, F. Bigi, E. Gogni, R. Maggi, G. Sartori, *J. Catal.*, **191**, 348 (2000).
18. K. Motokuma, M. Tada, Y. Iwasawa, *Angew. Chem. Int. Ed.*, **47**, 9230 (2008).

5.4 Knoevenagel Condensation

The Knoevenagel condensation is a very useful reaction in organic synthesis. It allows the preparation of molecules containing a double bond conjugated with a carbonyl function by the condensation of a molecule with a carbonyl group and another with an activated methylene group. The condensation is classically catalyzed by bases in the liquid phase system.



The Knoevenagel condensation reactions are very often used as a test reaction for characterizing the basic properties of solid bases. This aspect of the Knoevenagel condensation is described in section 2.5.5. The Knoevenagel condensation of benzaldehyde and ethyl cyanoacetate or malonitrile is often used as favored test reactions. The results of the two reactions in the literature are summarized in Table 5.4.1.

5.4.1 Catalysts

Knoevenagel condensation has been studied with a number of solid base catalysts.

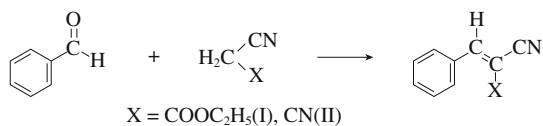
High-surface-area MgO is very effective for the Knoevenagel condensation.³⁾ The results of the condensation of various aldehydes with ethyl cyanoacetate and malonitrile are shown in Table 5.4.2. The catalyst was reusable. Although the reactions of benzaldehyde with malonitrile and ethyl cyanoacetate gave high yields, no reactions occurred with 2,4-pentandione, ethyl acetate, nitromethane, or dimethyl malonate.

Oxynitrides also show activities for the Knoevenagel condensations. Lednor et al. prepared silicon oxynitride and proved that the material has basic sites by Knoevenagel condensation.⁵⁾ AIPONs and their families also show activity for the condensation.^{6,28)} Nitrided MCM-48, which has a surface area of 1487 m² g⁻¹ gave an alkene yield of 96% in the reaction of benzaldehyde and malonitrile at 333 K.⁷⁾

A Ni-Al-hydrotalcite-like compound, [Ni_{0.73}Al_{0.27}(OH)₂](CO₃)_{0.135}, is found to be active for the Knoevenagel condensations between various aldehydes with ethyl cyanoacetate or malonitrile when dehydrated at 423 K, where the material still has the layered structure.⁸⁾ The reaction of benzaldehyde with malonitrile occurs much faster than that with ethyl cyanoacetate (Table 5.4.1). A 97% yield of the corresponding alkene was obtained in 30 min at 333 K. However, the material was inactive for the reactions with dimethyl malonate (pK_a = 13). The indicator method showed that the material has basic sites with *H*₊ value of 11-11.8.

Kantam et al. reported that Knoevenagel condensations involving various aromatic carbonyl compounds and aliphatic ketones with malonitrile and cyanoacetate proceeded very smoothly with rehydrated hydrotalcite as catalyst in quantitative yields.⁹⁾ The rehydrated hydrotalcite has OH⁻ ions in the interlayers. The

Table 5.4.1 The Knoevenagel condensation of benzaldehyde with ethyl cyanoacetate (I) and malononitrile (II)



Catalyst	Amount of each reactant solvent ^{a)}	Temp. /K ^{b)}	Ethyl cyanoacetate		Malononitrile		Ref.
			Time/ min	Yield/ %	Time/ min	Yield/ %	
Al ₂ O ₃ , 3 g	10 mmol	r.t.	3	100	3	96	1
MgO, 4 g	10 mmol	293	30	94	5	94	2
MgO, 0.05 g	2 mmol, DMF	r.t.	30	97	30	100	3
CsX, 22 mg g	9.4 mmol	438	120	~ 37			4
Silicon oxynitride, 0.2 g	4 mmol, toluene	333	240	85	240	90	5
AlPON, 5 wt%	10 mmol	333	60	36	15	77	6
Nitrided MCM-48, 0.05 g	10 mmol, toluene	333			180	96	7
Ni ⁻ Al hydrotalcite dried at 423 K, 50 mg	1 mmol	333	24 h	35%	30	97	8
Rehydrated hydrotalcite, 50 mg	2 mmol, toluene	r.t.	120	50	60	100	9
F ⁻ -Hydrotalcite, 35 mg	1 mmol	333 for I r.t. for II	120	92	15	100	10
^t BuO ⁻ -Hydrotalcite, 50 mg	2 mmol, DMF	r.t.	20	98	10	99	11
KF/Al ₂ O ₃	Aldehyde/II = 1/20	r.t.			180	86	12
CH ₃ COOK/Al ₂ O ₃ Calcined at 773 K	9 mmol	413	300	80.3			13
Na ₂ CaP ₂ O ₇ , 0.416 g	1.5 mmol ethanol-water (94 : 6)	r.t.	20	85	7	94	14
Zr(KPO ₄) ₂ , 50 mg	1 mmol	373 for I, 333 for II	180	88	12	92	15
Hydroxyapatite, 0.1 g	1.5 mmol methanol	r.t.	120	23	15	57	16
KF/hydroxyapatite, 0.1 g	1.5 mmol methanol	r.t.	120	64	15	91	16
Fluoroapatite, 1.25 g	1.5 mmol	r.t.	90	45	90	95	17
NaNO ₃ /fluoroapatite, 1.25 g	1.5 mmol	r.t.	15	94	7	94	17
Natural phosphate, 0.1 g (micronized)	1.5 mmol methanol	r.t.	20	89	5	93	18

(continued)

Catalyst	Amount of each reactant solvent ^{a)}	Temp. /K ^{b)}	Ethyl cyanoacetate		Malononitrile		Ref.
			Time/ min	Yield/ %	Time/ min	Yield/ %	
NaNO ₃ /natural phosphate, 0.1 g	1.5 mmol methanol	r.t.	60	94	1	96	19
Propylamino-silica, 0.25 g	20 mmol, decane	refluxing	240	99			20
Propylamino-MCM-41, 45 mg	120 mmol cyclohexane	355	30	>99			21
Propylamino-MCM-48, 0.5 g	10 mmol, toluene	288	60	98			22
Diamino-functionalized-MCM-41, 20 mg	2 mmol, toluene	323	15	100	15	99	23
TBD-MCM-41, 5 mg	1 mmol	r.t.	60-120	54	60-120	95	24
-(CH ₂) ₃ N(CH ₃) ₃ ⁺ OH ⁻ grafted to MCM-41, 80 mg	Aldehyde: 10 mmol I : 8 mmol	333	30	95			25
Anion exchange resin with -NH ₂ and -COOH	2.0 mmol benzene	r.t.	300	87	300	92	26
MgF, 0.10 g	5.2 mmol, ethanol	r.t.	240	96	150	100	27

^{a)} No solvent was used if not cited. ^{b)} r.t. : room temperature.

reactions proceed smoothly in toluene at room temperature with the exception of the reactions of ethyl cyanoacetate with cinnamaldehyde and cyclohexanone. However, when DMF was used as the solvent, cinnamaldehyde and cyclohexanone condensed with ethyl cyanoacetate to afford the corresponding products. Rehydrated hydrotalcite is very effective for Knoevenagel condensation even in the presence of water.²⁸⁾ Table 5.4.3 shows that a variety of combinations of nitriles and ketones gives high yields of products in H₂O-DMF.²⁹⁾

The hydrotalcite to which F⁻, ^tBuO⁻, or [(CH₃)₂CH]₂N⁻ ions are introduced in the interlayers by ion exchange are very active for a variety of Knoevenagel condensation reactions.^{10,11,30)} The reaction of benzaldehyde with malononitrile gave a 99% yield in 10 min in the presence of ^tBuO⁻-hydrotalcite.¹¹⁾

It has been reported that phosphate compounds and natural phosphate are very efficient catalysts for Knoevenagel condensations. The reaction of benzaldehyde with malononitrile in EtOH-water (94 : 6) gave a 94% yield of the corresponding alkene in 7 min at room temperature in the presence of Na₂CaP₂O₇.¹⁴⁾ Layered zirconium phosphate, Zr(KPO₄)₂,¹⁵⁾ hydroxyapatite,¹⁶⁾ fluoroapatite,^{16,17)} KF/hydroxyapatite,¹⁶⁾ NaNO₃/fluoroapatite¹⁷⁾ and natural phosphate^{18,19)} are also good catalysts for the Knoevenagel condensation.

Modified silica and mesoporous materials have also been tested as catalysts for Knoevenagel condensation. Silica with aminopropyl groups are active catalysts for the Knoevenagel reactions.^{20,31,32)} Various ketones and aldehydes react smoothly with ethyl cyanoacetate in the presence of aminopropylated silica. Only

Table 5.4.2 Knoevenagel condensation of aldehydes with ethyl cyanoacetate and malononitrile over MgO

$$\begin{array}{c} \text{R} \\ \text{H} \end{array} \text{C}=\text{O} + \begin{array}{c} \text{R}' \\ \text{CN} \end{array} \longrightarrow \begin{array}{c} \text{R} \\ \text{H} \end{array} \text{C}=\text{C} \begin{array}{c} \text{CN} \\ \text{R}' \end{array} + \text{H}_2\text{O}$$

R	R'	Solvent	Time/min	Conversion/%	Selectivity/%
Phenyl	CN	DMF	5	94	100
			30	100	
Phenyl	CO ₂ Et	DMF	30	97	100
2-Furyl	CN	DMF	30	100	100
2-Furyl	CO ₂ Et	DMF	30	99.9	100
2-Methyl-butyl	CN	DMF	60	99	100
2-Methyl-butyl	CO ₂ Et	DMF	60	80	100
Butyl	CN	DMF	30	88	100
Butyl	CO ₂ Et	DMF	30	76	100
<i>c</i> -C ₅ H ₁₀	CN	DMF	60	97	100
<i>c</i> -C ₅ H ₁₀	CO ₂ Et	DMF	60	23	100
Cinnamyl	CN	DMF			
Cinnamyl	CO ₂ Et	DMF	60	50	57

Reaction conditions: benzaldehyde (2 mmol), ethylcyanoacetate or malononitrile (2 mmol), MgO (0.05 g) in DMF (2 mL), room temperature

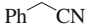
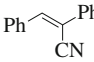
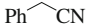
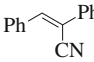
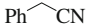
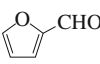
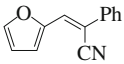
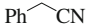
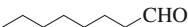
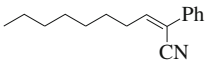
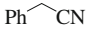
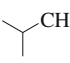
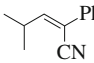
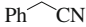
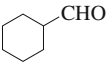
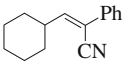
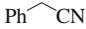
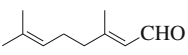
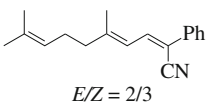
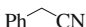
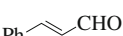
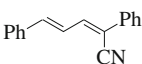
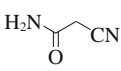
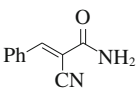
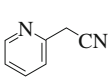
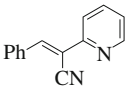
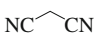
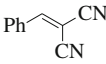
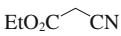
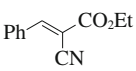
Reprinted with permission from C. Xu, J. K. Bartley, D. I. Enache, D. W. Knight, G. J. Hutchings, *Synthesis*, **2005**, 3468, p. 3473, Table 6.

sterically hindered ketones, benzophenone and methyl *t*-butyl ketone failed to give good yields. The rates of the reaction were further enhanced by removing water formed during the reaction. Nonpolar solvents such as cyclohexane, hexane and toluene were better than polar solvents such as 1,3-dichlorobenzene and chlorobenzene.²⁰⁾ The reactions can be performed in water.³²⁾ CsX grafted with aminopropyl-group shows a higher activity for the condensation of benzaldehyde with ethyl cyanoacetate or diethyl malonate than aminopropylated MCM-41. This material is also active for the reaction of benzaldehyde with diethyl acetoacetate.³³⁾

Mesoporous materials which are tethered with amino or ammonium groups are found to be active catalysts for the Knoevenagel condensation. Aminopropylated MCM-41 is 20–30% more active than aminopropylated silica.³⁴⁾ The turnover frequency of the primary and tertiary amine sites for the condensation of benzaldehyde and ethyl cyanoacetate were 0.34 and 0.06 min⁻¹, respectively.³⁵⁾ This difference has been explained by two different mechanisms during the base catalysis. Catalysis by tertiary amine is relevant to classical base activation of the methylene group of ethyl cyanoacetate. On the other hand, the primary amino group can activate the carbonyl group by imine formation followed by nucleophilic attack of the activated ethyl cyanoacetate, as shown in Fig. 4.6.2.³⁵⁾

Kubota et al. prepared a large variety of amine-immobilized microporous and mesoporous silicates and examined their catalytic activities for Knoevenagel condensation of benzaldehyde and ethyl cyanoacetate.³⁶⁾ Microporous materials generally showed high activities; mesoporous materials such as MCM-41 and SBA-15 with aminopropyl groups have high activities as well. Secondary amino groups

Table 5.4.3 Knoevenagel condensation of nitriles with various carbonyl compounds

Entry	Donor	Acceptor	Product	Time/h	Yield/% ^{b)}
1		Ph-CHO		1	96(81)
2 ^{c)}		Ph-CHO		1	9
3				1	quant (96)
4 ^{d)}				10	quant(80)
5				24	90(86)
6				24	77(70)
7 ^{d)}		 <i>E/Z = 2/3</i>	 <i>E/Z = 2/3</i>	3	78(70)
8 ^{d),e)}				4	76(70)
9		Ph-CHO		1	97(93)
10		Ph-CHO		1	96(95)
11 ^{f),g)}		Ph-CHO		1	96(91)
12 ^{f)}		Ph-CHO		10	94(90)

^{a)} Reaction conditions: donor (3 mmol), acceptor (6 mmol), water (0.3 mL), DMF (2 mL), dehydrated hydrotalcite (0.15 g), 80°C.

^{b)} Determined by GC using an internal standard method. Values in parentheses are isolated yields.

^{c)} Diethylamine (4 mmol) was used as a catalyst.

^{d)} 1,4-Dioxane (2 mL) was used as a cosolvent.

^{e)} At 40°C, donor (1 mmol), acceptor (3 mmol).

^{f)} Donor (10 mmol), acceptor (10 mmol), water (1 mL), 60°C.

^{g)} The corresponding coupling product was obtained in 82% yield in the absence of the reconstructed hydrotalcite catalyst.

Reprinted with permission from K. Ebitani, K. Motokuma, K. Mori, T. Mizugaki, K. Kaneda, *J. Org. Chem.*, **71**, 5440 (2006) p. 5444, Table 3.

showed lower activity than a primary amino group (aminopropyl group). No activity was observed when tertiary amino groups were grafted.

MCM-41 with expanded pore diameter, when grafted with aminopropyl groups, shows higher activity for Knoevenagel condensation than ordinary MCM-41 with aminopropyl groups. The higher activity is ascribed to the higher diffusion rate in the expanded pores.²¹⁾ MCM-48 modified with aminopropyl groups shows a very high activity for condensation of benzaldehyde with ethyl cyanoacetate.²²⁾ The conversion of 97% was obtained in 1 h at 288 K. Amine-functionalized SBA-15 with short channels shows much higher activity for the Knoevenagel condensation than the typical SBA-15 catalyst having long channels.³⁷⁾ This is due to the easy diffusion and rapid mass transfer in short channeled material.

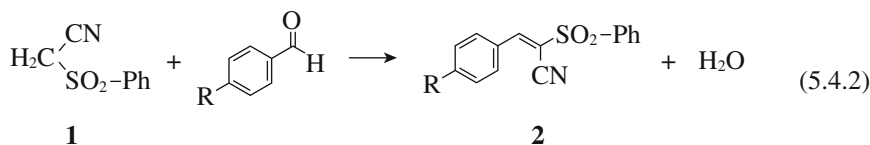
MCM-41 bearing diamino groups, $-\text{Si}(\text{CH}_2)_3\text{-NHCH}_2\text{CH}_2\text{NH}_2$, show high activities for Knoevenagel condensations in toluene at 323 K.²³⁾ DMF shows the favorable solvent effect for the condensation of cinnamaldehyde with ethyl cyanoacetate. The turnover frequency of this catalyst is much higher than MCM-41 bearing aminopropyl groups. A high activity of SBA-15 with diamino groups for Knoevenagel condensation was also reported by Wang et al.³⁸⁾

Rodriguez et al. showed that MCM-41 bearing a quaternary ammonium group $\text{Si}(\text{CH}_2)_3\text{N}(\text{CH}_3)_3^+ \text{OH}^-$ was an active catalyst for the condensation of benzaldehyde and ethyl cyanoacetate.²⁵⁾ The polarity of the solvent strongly affected the rate of the reaction. The order of the activity was $\text{EtOH} > \text{CH}_3\text{CN} > \text{HCCl}_3 > \text{CCl}_4$. The reaction was, however, catalyzed in the absence of any solvent.

Chitosan, a natural polyamine, act as an active catalyst for Knoevenagel condensations of various aromatic carbonyl compounds with malononitrile, ethyl cyanoacetate and diethyl malonate in DMSO at room temperature.³⁹⁾

5.4.2 Catalytic Reactions

α -Phenylsulfonylcinnamnitrite **1** and derivatives were obtained by condensation of phenylsulfonylacetonitrile **2** with benzaldehyde and 4-substituted benzaldehyde using MgO, MgO-Al₂O₃ (calcinated hydrotalcite) and AIPONs. AIPONs were the most active.⁴⁰⁾

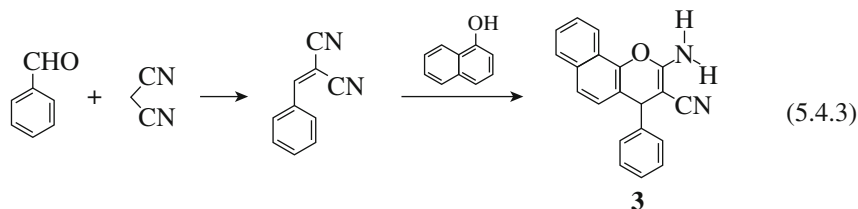


The yields of **2** were 95%, 98%, 88% and 80% for R = H, NO₂, CH₃ and OCH₃, respectively, in 1 h at 373 K. The presence of electron donor groups in the aromatic ring decreases the reaction rate, while the presence of electron acceptor groups increases the reaction rate. The rate of the reaction between **1** and benzaldehyde was proportional to the nitrogen content of AIPONs.

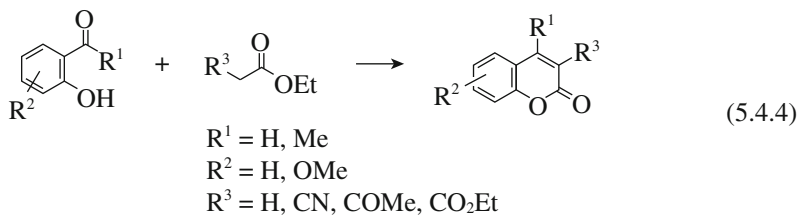
The condensation of **1** and benzaldehyde was completed within 1 h achieving 100% selectivity to α -phenylsulfonylcinnamnitrite in the presence of tetra-

alkylammonium hydroxide anchored on MCM-41.²⁵⁾ $\text{Na}_2\text{CaP}_2\text{O}_7$ is also active for the reaction.⁴¹⁾ Synthesis of **2** ($\text{R} = \text{H}, \text{NO}_2, \text{CH}_3, \text{OCH}_3$ and Cl) was also reported to proceed over fluoroapatite doped with sodium nitrate.⁴²⁾ The reaction rate was enhanced in the presence of benzyltriethylammonium chloride.

Substituted 2-aminochromenes **3** are obtained in excellent yield (96%) and selectivity (98%) simply by mixing benzaldehyde, malononitrile and α -naphthol in water in the presence of basic alumina.⁴³⁾ The catalysts can be reused four times without significant loss of activity. A variety of aromatic aldehydes having functionalities such as NO_2 , OCH_3 and Cl also gave good yields and selectivity.

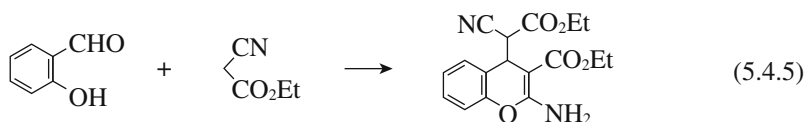


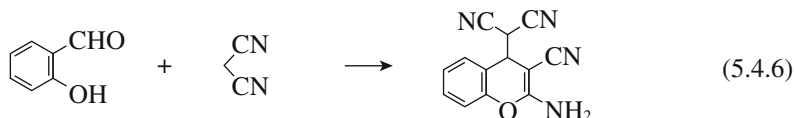
Knoevenagel condensation of various phenols with 2-substituted ethyl acetate gives the coumarins in good yields in refluxing toluene for ca. 4 h in the presence of 10% (w/w) $\text{MgO-Al}_2\text{O}_3$ ($\text{Mg/Al} = 3$) obtained by calcination of hydrotalcite.⁴⁴⁾



The order of the reactivity of the reagents is ethyl cyanoacetate > diethyl malonate > ethyl acetoacetate > ethyl acetate. 3-Cyanocoumarin was obtained in 93% isolated yield and 3-cyano-8-methoxycoumarin was obtained in 85% yield.

Weakly basic resin, Amberlyst A-21, is a good catalyst for the synthesis of substituted 4*H*-chromene derivatives from *o*-hydroxybenzaldehyde and ethyl cyanoacetate or malononitrile in ethanol at room temperature.⁴⁵⁾ Thus, the reactions of salicylaldehyde with ethyl cyanoacetate and malononitrile gave the corresponding products in 85% and 70% yields, respectively, in 4 h. The recovered catalyst was recycled in five subsequent runs with no decay in activity. Various substituted salicylaldehydes also reacts with ethyl cyanoacetate and malononitrile to afford good yields of substituted 4*H*-chromenes. $\text{Zr}(\text{KPO}_4)_2$ is also active for this reaction.⁴⁴⁾





The reaction scheme involving double addition of active methylene compounds is proposed for this 4*H*-chromenes synthesis (Fig. 5.4.1).

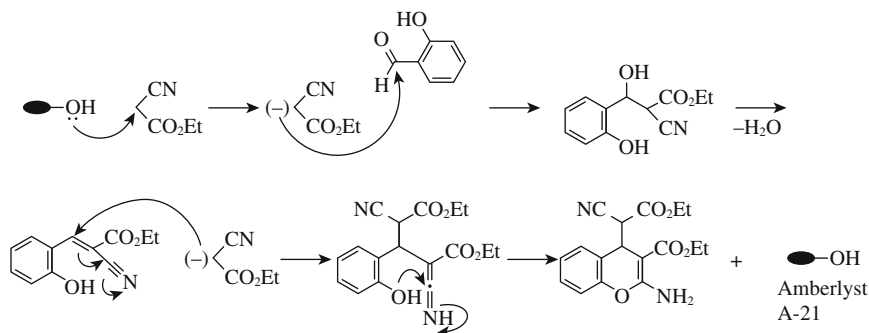
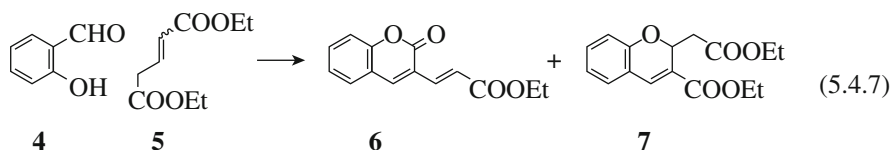
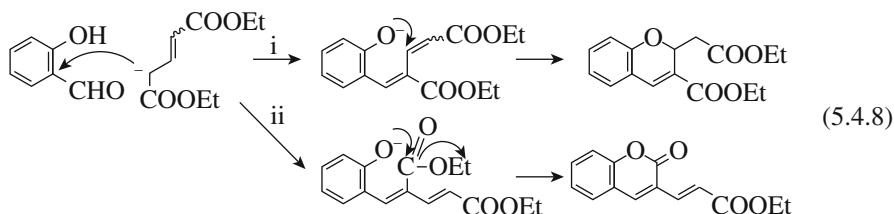


Fig. 5.4.1 Mechanism of 4*H*-chromene synthesis over anion exchange resin. Reprinted with permission from J. S. Yadav, B. V. Subba Reddy, M. K. Gupta, I. Prathaps, S. K. Pandey, *Catal. Commun.*, **8**, 2208 (2007) p. 2210, Scheme 3.

The condensation of salicylaldehyde **4** and diethyl glutaconate **5** over MCM-41 with OH^- gives chromarin-3-acrylate **6** and chromene derivatives **7**.²⁵⁾



When the reaction was carried out at 383 K without solvent, high conversion (90%) and high selectivity for chromene **7** was achieved within 6 h. The rest of the product is chromarine **6**. The following mechanism involves the Knoevenagel condensation at the first stage, followed by intramolecular Michael addition.



Intramolecular Knoevenagel condensation of aldehyde and ester are reported in high temperature reactions. When benzoate ester of 3-hydroxy-3-methyl-2-butanone **8a** was heated with CsF at 573 K for 5 min under a nitrogen atmosphere,

23. B. M. Choudary, M. Lakshmi Kantam, P. Sreekanth, T. Bandopadhyay, F. Figueras, T. Tuel, *J. Mol. Catal., A*, **142**, 361 (1999).
24. Y. V. Subba Rao, D. E. De Vos, P. A. Jacobs, *Angew. Chem. Int. Ed. Engl.*, **30**, 2661 (1997).
25. I. Rodríguez, S. Iborra, F. Rey, A. Corma, *Appl. Catal., A*, **194/195**, 241 (2000).
26. T. Saito, H. Goto, K. Honda, T. Fuji, *Tetrahedron Lett.*, **33**, 7535 (1992).
27. R. M. Kumbhare, M. Sridhar, *Catal. Commun.*, **9**, 403 (2008).
28. P. Grange, Ph. Bastians, R. Conanec, R. Marchand, Y. Laurant, L. M. Ganda, M. Montes, J. Fernandes, J. A. Odriozola, *Appl. Catal.*, **91**, 389 (1994).
29. K. Ebitani, K. Motokuma, K. Mori, T. Mizugaki, K. Kaneda, *J. Org. Chem.*, **71**, 5440 (2006).
30. M. L. Kantam, A. Ravindra, Ch. V. Reddy, B. Sreedhar, H. M. Choudary, *Adv. Synth. Catal.*, **348**, 569 (2006).
31. E. Angretti, C. Canepa, G. Martinetti, P. Venterello, *J. Chem. Soc., Perkin Trans.*, **1**, 105 (1989).
32. K. Isobe, T. Hoshi, T. Suzuki, H. Hagiwara, *Mol. Diversity*, **9**, 315 (2005).
33. X. Zhang, E. S. M. Lai, R. Martin-Aranda, K. L. Yeung, *Appl. Catal., A*, **261**, 109 (2004).
34. D. J. Macquarrie, D. E. Jackson, *Chem. Commun.*, **1997**, 1781.
35. D. Brunel, *Micropor. Mesopor. Mater.*, **27**, 329 (1999).
36. Y. Kubota, Y. Nishizaki, H. Ikeya, M. Saeki, T. Hida, S. Kawazu, M. Yoshida, H. Fuji, Y. Sugi, *Micropor. Mesopor. Mater.*, **70**, 135 (2004).
37. Sujandi, E. A. Prasetyanto, S. -E. Park, *Appl. Catal., A*, **350**, 244 (2008).
38. X. Wang, J. C. C. Chan, Y. -H. Tseng, S. Cheng, *Micropor. Mesopor. Mater.*, **95**, 57 (200).
39. K. R. Reddy, K. Rajgopal, C. U. Maheswari, M. L. Kantam, *New J. Chem.*, **30**, 1549 (2006).
40. M. J. Climent, A. Corma, R. Guil-Lopez, S. Iborra, J. Primo, *Catal. Lett.*, **59**, 33 (1999).
41. M. Zahouily, M. Salah, J. Bennazha, A. Rayadh, S. Sebtí, *Tetrahedron Lett.*, **44**, 3255 (2003).
42. M. Zahouily, M. Salah, B. Bahlaouan, A. Rayadh, S. Sebtí, *Catal. Lett.*, **96**, 57 (2004).
43. R. Maggi, R. Ballani, G. Sartori, R. Sartorio, *Tetrahedron Lett.*, **45**, 2297 (2004).
44. A. Ramani, B. M. Chanda, S. Velu, S. Sivasanker, *Green Chem.*, **1**, 163 (1999).
45. J. S. Yadav, B. V. Subba Reddy, M. K. Gupta, I. Prathaps, S. K. Pandey, *Catal. Commun.*, **8**, 2208 (2007).
46. D. Villemin, P. Jefferès, M. Hachémi, *Tetrahedron Lett.*, **38**, 537 (1997).
47. D. Villemin, M. Hachemi, *React. Kinet. Catal. Lett.*, **72**, 3 (2001).

5.5 Michael Addition (Conjugated Addition)

The Michael addition or Michael reaction is originally defined as the addition of an enolate of a ketone or aldehyde to an α,β -unsaturated carbonyl compound at the β carbon. The definition is now extended to include the nucleophilic addition of a doubly stabilized carbon nucleophile to an α,β -unsaturated carbonyl compound. The Michael addition is very useful as a C-C bond-forming reaction in synthetic chemistry. Typically, the reaction involves a nucleophilic addition of carbanions to α,β -unsaturated carbonyl compounds. A base is used to form the carbanions by abstracting a proton from the activated methylene precursor. In addition to its synthetic utility, the Michael addition is often employed as a useful test reaction for studying the catalytic ability of solid bases.

5.5.1 Addition of Active Methylene Compounds to α,β -Unsaturated Carbonyl Compounds

The catalytic results for three typical Michael addition reactions are summarized in Tables 5.5.1–5.5.3.

A catalyst, which is obtained by heating $\text{Ba}(\text{OH})_2 \cdot 8\text{H}_2\text{O}$ at 473 K for 3 h, is active for Michael reactions of chalcones with active methylene compounds such as ethyl malonate at room or refluxing temperature.¹⁶⁾

Al_2O_3 was used for the Michael addition of nitroalkanes and α,β -unsaturated carbonyl compounds.²¹⁻²³⁾ The Michael reaction of β -dicarbonyl compounds such as ethyl cyanoacetate and diethyl malonate with methyl vinyl ketone, acrolein or methyl acrylate proceeds efficiently on Al_2O_3 without any solvent.²³⁾

High surface MgO was reported to be a highly effective catalyst for the Michael addition.¹⁷⁾ The catalyst was prepared by calcination of $(\text{MgCO}_3)_4\text{Mg}(\text{OH})_2$ at 723 K for 2 h. The main results are given in Table 5.5.4. The reaction depends strongly on the solvent used, the order of the yield being hexane > toluene > EtOAc \approx MeCN \gg DMSO \gg MeOH, CHCl_3 . In chloroform or methanol, MgO is inactive. The catalyst can be reused. Microcrystalline MgO is effective for asymmetric Michael addition in the presence of an appropriate chiral auxiliary compound.²⁴⁾

Prescott et al. prepared a series of magnesium oxide fluorides $(\text{Mg}(\text{OH})_{2-x}\text{F}_x)$ of high surface area by a sol-gel method and tested them as catalysts for Michael additions.²⁵⁾ The sample prepared with F/Mg = 1/6 exhibited a catalytic activity similar to MgO- Al_2O_3 mixed oxide prepared from hydrotalcite in the Michael addition of 2-methylcyclohexane-1,3-dione to methyl vinyl ketone.

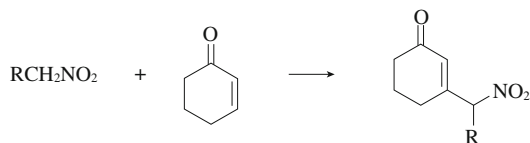
KF/ Al_2O_3 and CsF/ Al_2O_3 were also effective for the Michael addition.^{1-3,26)} In the reaction of nitroethane (0.05 mol) and phenyl 2-phenylethenyl ketone in the presence of KF/ Al_2O_3 (molar ratio 1 : 20 : 0.2) for 3.5 h at room temperature, the yield of the Michael addition product was 74%.²⁴⁾ Bergbreiter and Lalonde applied KF/basic Al_2O_3 for Michael addition between nitroalkanes and α,β -unsaturated carbonyl compounds.³⁾

Kabashima et al. studied the catalytic activities of solid bases such as KF/

Table 5.5.1 Michael addition (I)
 $\text{RCH}_2\text{NO}_2(\text{I}) + \text{CH}_3\text{COCH}=\text{CH}_2(\text{II}) \longrightarrow \text{CH}_3\text{COCH}_2\text{CHR}(\text{NO}_2)$

Catalyst	Weight	R	I/mmol	II/mmol	Temp. /K	Time/min	Yield /%	Ref.
KF/ Al_2O_3	2.5 g	CH_3	250	12.5	r.t.	1-3	100	1
	50 mg	CH_3	50	2.5	r.t.	45	75.5	2
	5 g	CH_3		12	r.t.	120	100	3
Amberlyst 27	8-10 g	CH_3	50	50	273	240	76	4
<i>N,N</i> -Dimethylamino-propyl-HMS	0.5 g	H	25 mL	20 mmol	reflux	240	80	5
		CH_3				72	94	
<i>N,N</i> -Diethylamino-propyl-silica	0.42 g	CH_3	4.2	2.1	r.t.	180	75	6
Rehydrated hydrotalcite	0.2 g	H	2	2	r.t.	90	100	7
KF/ Al_2O_3 pretreated at 623 K	10 mg	H	8	2	273	30	93.0	8
KOH/ Al_2O_3	10 mg	H	8	2	273	30	49.0	8
MgO	0.1 g	H	8 L	2	323	120	1.5	8
CaO	0.1 g	H	8	2	323	120	0.9%	8
Al_2O_3	0.1 g	H	8	2	323	120	0.9%	8
Zr(KPO_4) ₂	0.5 mmol	CH_3	1	1	293	180	69	9
KF/Natural phosphate	2	CH_3	6	6	r.t.	120	55	10

Table 5.5.2 Michael addition (2)



Catalyst	Weight	R	I/mmol	III/mmol	Temp./K	Time/min	Yield/%	Ref.
KF/Al ₂ O ₃	3 g	CH ₃		5	r.t.	120	100	3
CsF/ α -Al ₂ O ₃	0.1	CH ₃		1 : 1	323	45	~90	11
Aminopropylated silica	72 mg	H	3 mL	2.5	363	240	95	12
	72 mg	CH ₃	3 mL	2.5	363	240	92	
Diaminopropyl-silica	0.5 g	H	25 mL	20 mmol	reflux	240	90	5
		CH ₃				90	88	
Amberlyst 27	8–10 g		50	50	r.t.	1200	93	4
F ⁻ -hydrotalcite	0.1 g	CH ₃	1	1	r.t.	120	95	13
^t BuO ⁻ -hydrotalcite	0.1 g	CH ₃	2	2	r.t.	30	98	14
KF/ γ -Al ₂ O ₃ Pretreated at 623 K	0.1 g	H	12	4	323	30	99.8	8
KOH/Al ₂ O ₃ Pretreated at 823 K	0.1 g	H	12	4	323	30	93.0	8
MgO	0.1 g	H	12	4	323	30	20.5	8
CaO	0.1 g	H	12	4	323	30	5.4	8
Al ₂ O ₃	0.1 g	H	12	4	323	30	6.9	8
SrO	0.1 g	H	12	4	323	30	1.4	8
BaO	0.1 g	H	12	4	323	30	0.7	8
La ₂ O ₃	0.1 g	H	12	4	323	30	0	8
MgO-La ₂ O ₃	0.1 g	H	2.2	2	r.t.	15	98	15

Table 5.5.3 Michael addition (3)



Catalyst	Weight	V/mmol	VI/mmol	Temp./K	Time/h	Yield/%	Ref.
Ba(OH) ₂ ·0.8H ₂ O	0.05 g	25	25	r.t.	8 h	95%	16
MgO	0.2 g	2	2	r.t.	2	93	17
Cs-MCM-41	(1.8 %)	20	26	423	0.5	79	18
Rehydrated hydrotalcite	0.2 g	2	2	r.t.	6	96	7
F ⁻ -hydrotalcite	0.1 g	1	1	r.t.	2	95	13
^t BuO ⁻ -hydrotalcite	0.1 g	2	2	r.t.	2	95	14
[(CH ₃) ₂ CH] ₂ N ⁻ -hydrotalcite	0.05 g	2	2	333	7	98	19
Aminopropylated MCM-41	0.1 g	1.375	1.25	353	24	87	20
Aminopropylated SBA-15	0.1 g	1.375	1.25	353	24	84	20
Aminopropylated Faujasite	0.1 g	1.375	1.25	353	24	87	20
Mg-La oxide	0.1 g	2.2	2	r.t.	5.5	98%	15

Table 5.5.4 Michael additions catalyzed by high surface area MgO

Run	Acceptor	Donor	Time/h	Yield/%
1	Chalcone	Diethyl malonate	2	93
2	Chalcone	Ethyl cyanoacetate	2	88
3	Chalcone	Malononitrile	1.5	88
4	2-Cyclohexen-1-one	Dimethyl malonate	1	93
5	Methyl crotonate	<i>p</i> -Toluenethiol	0.5	100
6	4-Phenyl-3-buten-2-one	Malononitrile	1	13

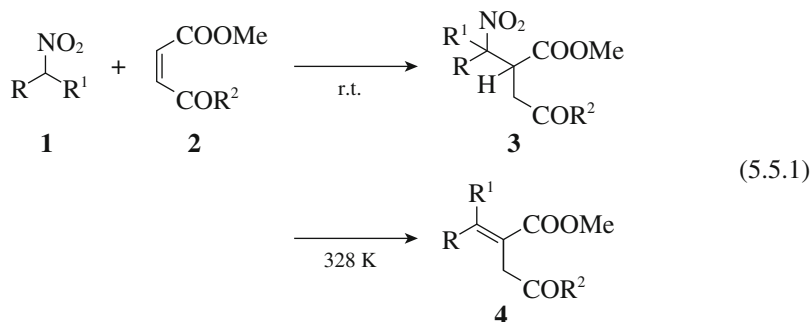
Reaction conditions: acceptor (2 mmol), donor (2 mmol), MgO (0.2 g) in toluene (2 mL), (acetonitrile for run 5).

Reprinted with permission from C. Xu, J. K. Bartley, D. I. Enache, D. W. Knight, G. Hutchings, *Synthesis*, 3468 (2005) p. 3470, Table 1.

Al₂O₃, KOH/Al₂O₃, alkaline earth oxides and La₂O₃ for the Michael addition of nitromethane to α,β -substituted carbonyl compounds (methyl crotonate, butene-2-one, 2-cyclohexen-1-one and crotonaldehyde).⁸⁾ KF/Al₂O₃ and KOH/Al₂O₃ were pretreated under vacuum at 623 K and 873 K, respectively. For all Michael additions of nitromethane, KF/Al₂O₃ and KOH/Al₂O₃ exhibited high activities, while MgO and CaO exhibited no activity for methyl crotonate and butene-2-one, but low activities for 2-cyclohexen-2-one and crotonaldehyde. For the Michael addition of nitromethane to α,β -unsaturated carbonyl compounds, the order of reactivity on these catalysts was methyl crotonate < buten-2-one < 2-cyclohexen-1-one < crotonaldehyde. This order is in agreement with the order of the charge in the β -position except for methyl crotonate, which is the least reactive. SrO, BaO and La₂O₃ exhibited practically no activity for all Michael additions examined.

KF supported on α -Al₂O₃ is more active than KF on γ -Al₂O₃ in the Michael addition of nitroethane to 2-cyclohexen-1-one.¹¹⁾ Furthermore, CsF/ α -Al₂O₃ is more active than CsF/ γ -Al₂O₃.¹¹⁾

The conjugated addition of nitroalkanes **1** to electron-poor alkenes with two electron-withdrawing groups **2** in the α - and β -positions, proceeds in the presence of KF/basic-Al₂O₃ catalysts.²⁷⁾ The product is temperature-dependent. At room temperature, the Michael addition occurs to result in the formation of a compound with a C-C single bond. At 328 K, the product is a compound having of a C=C double bond **4** by the elimination of HNO₂ from the intermediate product **3**.



For example, the reaction of methyl 4-nitrobutanoate ($R = \text{MeOCO}(\text{CH}_2)_2-$, $R^1 = \text{H}$) and dimethyl maleate ($R^2 = \text{OMe}$) gave the corresponding addition product **3** in an 80% yield at room temperature in 7 h. At 328 K, the product was obtained in a 78% yield in 7 h.

Na-forms of zeolite Y and Beta are reported to be efficient catalysts for the Michael addition of several 1,3-dicarbonyl compounds as donors with methyl vinyl ketone, acrolein and methyl acrylate as acceptors without any solvent.²⁷⁾

MgO-La₂O₃ mixed oxide (Mg/La = 4.26) is very active for the Michael addition of various combinations of Michael donors and acceptors.¹⁵⁾ The best solvent for the reaction is dimethylformamide, but good yields were also obtained using toluene as solvent. Nitroethane reacts with chalcone to give 98% yield in 2 h. The high reactivity of nitroethane ($\text{p}K_{\text{a}} = 17.2$) in the presence of MgO-La₂O₃ indicates the high basic strength of the mixed oxide.

Rehydrated hydrotalcite, which contains OH⁻ groups in the interlayers, is found to be highly active for the Michael addition of methyl vinyl ketone, methyl acrylate, simple and substituted chalcones by donors such as nitroalkane, malononitrile, diphenyl malonate, cyanoacetamide and thiols.⁶⁾ The addition products are obtained in quantitative yields under mild conditions. Rehydrated hydrotalcite gave Michael products in the reactions of phenylacetone with enones, e.g., 2-cyclohexen-1-one, 3-nonen-2-one, benzalacetone and cinnamitrile in water-1,4-dioxane at 353 K.²⁹⁾

Hydrotalcite containing F⁻, ^tBuO⁻ or [(CH₃)₂CH]₂N⁻ ions are also highly active for Michael addition reactions of a variety of combinations of donors and acceptors.^{13,14,19)} The results for Michael addition over ^tBuO-hydrotalcite are shown in Table 5.5.5.¹⁴⁾

Anion exchange resins have been shown to be effective for a variety of Michael addition, but a rather large amount of the catalyst is required.⁴⁾

Amine-functionalized silica materials are active for the Michael addition. Mdoe et al. prepared the amorphous silica (AMS) and HMS (hexagonal mesoporous silica) functionalized with *N,N*-dimethyl-3-aminopropyl groups.⁵⁾ The former was prepared by anchoring *N,N*-dimethyl-3-aminopropyl groups on AMS by post synthesis while the latter was prepared by a templated sol-gel method by starting from tetraethoxysilane and *N,N*-dimethyl-3-aminopropyltrimethoxysilane. The catalytic activities of the two catalysts were compared for the Michael addition between nitroalkanes and methyl vinyl ketone or 2-cyclohexen-1-one. Both catalysts were active, the latter being more active. A 90% yield of Michael adduct (isolated yield 86%) was obtained from nitromethane and 2-cyclohexen-1-one in 4 h. Macquarrie et al. prepared aminopropylsilicas, prepared following different synthetic modifications, by the grafting method and by the sol-gel method.¹²⁾ The catalytic activities of the catalysts were compared for the nitroaldol and the Michael addition reactions. In contrast to the results by Mdoe et al.,⁵⁾ the catalysts prepared by the grafting method were far more active than the catalysts prepared by the sol-gel method. The difference in the activities of the two groups was ascribed to the accessibility of the reagents to the amino groups. For the reaction of nitromethane and 2-cyclohexen-1-one, a Michael adduct yield of 97% was

Table 5.5.5 Micheal addition catalyzed by ^tBuO-hydratalcite

Entry	Acceptor	Donor ^{a)}	Time/h	Product	Isolated yield(%)
a		NM	0.16		93
b		NE	0.5		98
c		NM	0.75		96
d		DMM	0.83		94
e		DEM	0.5		98
f		DEM	2		95
g		DMM	1		90
h		DMM	1		96
i		DMM	1.3		95
j		DMM	1		92
k		EAA	0.16		86
l		EAA	0.33		90

Reaction conditions: acceptor: 2 mmol, donor: 20 mmol, solvent: methanol 10 mL, catalyst: 0.1 g.

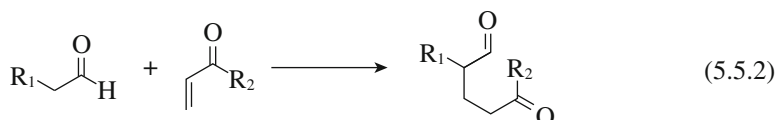
^{a)} DMM: dimethyl malonate, NM: nitrimethane, NE: nitroethane, DEM: diethyl malonate, EAA: ethyl acetoacetate

Reprinted with permission from B. M. Choudary, M. L. Kantam, B. Kavita, Ch. Venkat Reddy, F. Figueras, *Tetrahedron*, **56**, 9357 (2000) p. 9358, Table 1.

obtained with selectivity of 99% in 20 h. Aminopropylated silica is also effective for the Michael addition of nitroalkanes and conjugated alkenes.⁷⁾

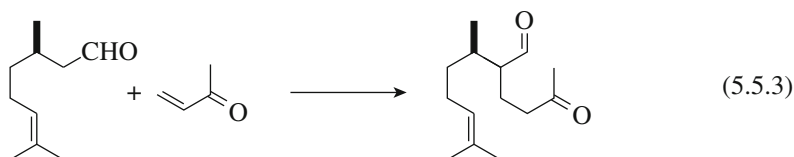
Ethylenediamine attached to mesoporous silica was very active for the Michael addition of 2-cyclopenten-1-one and nitromethane.³⁰⁾ A nitromethylcyclopentanone yield of as high as 98% was attained in 30 min of reaction.

Direct 1,4-addition of unmodified aldehydes to vinylketones is catalyzed by mesoporous silica (FSM-16) functionalized with *N*-methyl-3-aminopropyl groups.³¹⁾



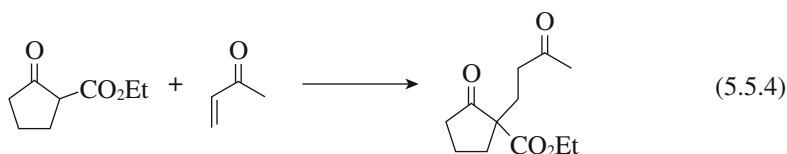
Thus, butanal, hexanal, octanal and decanal react with methyl vinyl ketone or ethyl vinyl ketone. The reaction of heptanal (1 mmol) with ethyl vinyl ketone (1.5 mmol) in toluene (5 mL) in the presence of FSM-16 functionalized with *N*-methyl-3-aminopropyl groups (1 mol%) under nitrogen gave a 93% yield of the addition product at reflux temperature. MgO and hydrotalcite have no activity for the reactions.

The same catalyst works as a catalyst for the addition reaction of citronellal and methyl vinyl ketone in ionic liquid.³²⁾



The reaction was carried out at 353 K in [bmin]PF₆ for 4 h, the yield of 5-ketoaldehyde being 62% (bmin = 1-butyl-3-methyl-imidazolium).

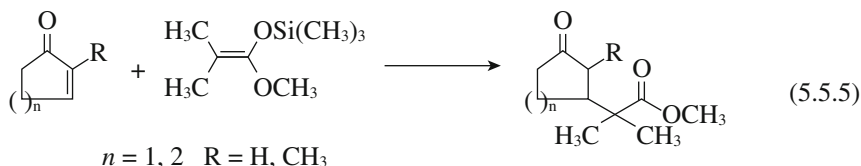
Amine-grafted amorphous silica was reported to be very effective for Michael addition under microwave irradiation. *N,N*-dimethylpropylated silica was most effective.³³⁾ For example, the reaction between ethyl 2-oxocyclopentanecarboxylate and methyl vinyl ketone give a 92% isolated yield of the Michael adduct in 10 min.



Subba Rao et al. immobilized 1,5,7-triazabicyclo[4,4,0]dec-5-ene (TBD) on the surface of MCM-41.³⁴⁾ This material, MCM-TBD, was found to be very effective for the Michael addition. Excellent selectivity was obtained for the reactions

of typical Michael donors and enones in a short reaction time, e.g., from ethyl cyanoacetate and cyclopentanone, the 1,4-adduct being obtained in 52% yield and 100% selectivity.

Srivastava prepared SBA-15 grafted with TBD and applied it to Michael reactions. Cyclopentenones and cyclohexenones react smoothly with 1-methoxy-2-methyl-1-trimethylsiloxypropene to afford the Michael adducts in yields of 70 - 78% without solvent at 383 K in 12 h.³⁵⁾



Quarternary carbon is synthesized by reacting 2-acetylcyclopentanone with activated terminal alkenes such as acrylonitrile in the presence of the TBD-grafted SBA-15 (Table 5.5.6).³⁵⁾

The catalytic activity of MCM-41 grafted with tetralkylammonium hydroxide for the Michael addition was also reported.³⁶⁾ For example, the reaction (5.5.4) gives 85% yield of the Michael adduct with 100% selectivity within 1 h at room temperature.

Kubota found that as-synthesized ordered mesoporous materials containing alkylammonium cations in the pores were effective catalysts for base-catalyzed reactions.²⁰⁾ Thus, MCM-41 synthesized by using hexadecyltrimethylammonium cation as a structure directing agent was an active catalyst for the Michael addition of chalcone with dimethyl malonate.

Zr(KPO₄)₂, which was obtained by exfoliation of layered hydrogen phosphate followed by ion-exchange with potassium cations, was an efficient catalyst for the Michael addition of β -dicarboxyl compounds in mild conditions, as shown in Table 5.5.7.⁹⁾

Table 5.5.6 SBA-15 grafted with TBD catalyzed Michael reaction of 2-acetylcyclopentanone with alkenes

Entry no.	R	Time/h	Yield/%
1	CN	12	70
2	COOCH ₃	8	87
3	COOC ₂ H ₅	8	88
4	COOC ₆ H ₅	8	92

Reaction conditions: 2-acetylcyclopentanone (3 mmol), alkenes (6 mmol), catalysts (0.3 mmol), reaction temperature (383 K).

Reprinted with permission from R. Srivastava, *J. Mol. Catal., A*, **264**, 146 (2007) p. 151, Table 6.

Table 5.5.7 Michael addition catalyzed by $Zr(KPO_4)_2$

Acceptor	Donor	Adduct	Time	Yield/%
Methyl vinyl ketone	Acetylacetone		30 min	85
Methyl vinyl ketone	Ethyl benzoylacetate		1 h	95
Methyl vinyl ketone	Dimethyl malonate		3 h	95
Methyl vinyl ketone	Nitroethane		3 h	69 ^a
2-Cyclohexen-1-one	Acetylacetone		10 h	92
Crotonaldehyde	Ethyl acetoacetate		1 h	89
Acrolein	Ethyl benzoylacetate		30 min	98

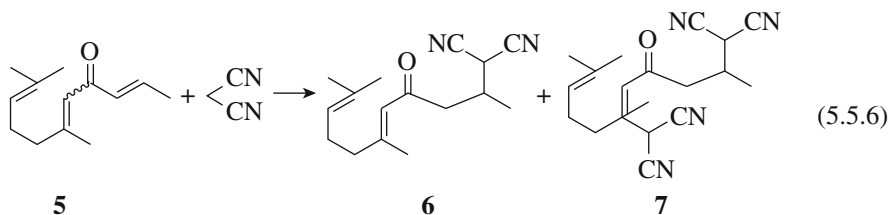
Reaction conditions: Donor 1 mmol, Acceptor 1 mmol, Catalyst 0.5 mmol, 333 K

^a) Reaction temperature: 298 K

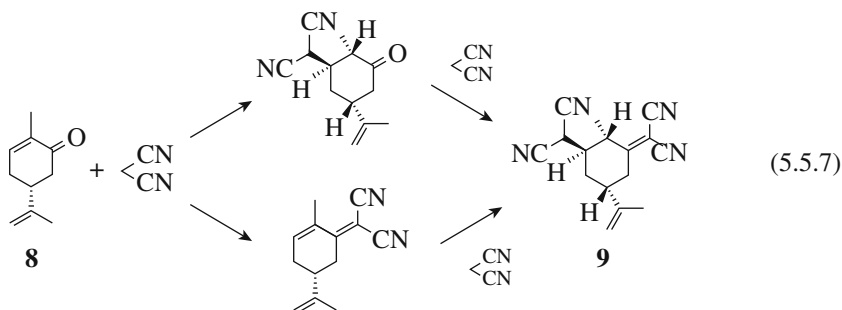
Reprinted with permission from U. Constantino, F. Marmottini, M. Curini, O. Rosati, *Catal. Lett.* **22**, 333 (1993) p. 335, Table 1.

The Michael addition of acetone to ethyl acrylate to form 5-oxohexanoic acid ethyl ester was studied using strong solid bases $Na/NaOH/Al_2O_3$, Cs_xO/Al_2O_3 , Na/NaX and Cs_xO/CsX in the liquid phase.³⁷⁾ Na/NaX was the most active; at a temperature of 363 K and a catalyst loading of 0.05 mol ester/g-catalyst, a selectivity of 57% was obtained at a conversion of 84%. The main by-product was 5-oxononandiacid dimethyl ester formed by the double Michael addition of acrylic ester and 5-oxohexanoic acid ethyl ester.

The terpenoids with α,β -unsaturated carbonyl group react with malononitrile in the presence of Cs/Cs -beta prepared by impregnation of Cs -beta with aqueous cesium formate followed by calcinations at 773 K.³⁸⁾ The reaction of φ -damascone **5** (*cis* + *trans* isomer mixture 1 : 1) with malononitrile yielded compounds **6** (62% yield) and **7** (9%).

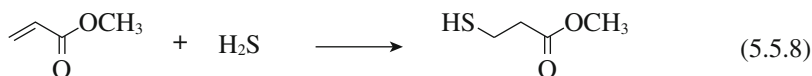


The reaction of carvone **8** with malononitrile formed compound **9** in 53% yield. Compound **9** is the product of the tandem Michael-Knoevenagel (or Knoevenagel-Michael) reactions.



5.5.2 Michael Addition of H_2S and Thiols

The Michael-type addition of H_2S to methyl acrylate to yield methyl 3-mercapto-propionate (MMP) over various solid base catalysts was studied at 413 K.^{39,40)}



The sequence of activity is as follows: alkali/alkaline earth-doped MgO > MgO > $\text{MgO-Al}_2\text{O}_3$ > γ -alumina > alkali cation-exchanged zeolites > rehydrated hydro-talcite. Na-doped MgO shows the highest initial activity. The selectivity for MMP was 78% at 40% conversion, the main by-product being 3,3'-thiomercapto-diporopinate formed by the reaction of MMP with H_2S . The activity order is well correlated with the basic strength as determined by the heat of adsorption of CO_2 . From kinetic and infrared spectroscopic studies, the reaction is shown to proceed between HS^- and physically adsorbed methyl acrylate, though strong chemisorption of methyl acrylate also occurs on the surface, as shown in Fig. 5.5.1.

Synthetic hydroxyapatite is found to be a very efficient catalyst for the Michael addition of mercaptans to chalcone derivatives.⁴¹⁾

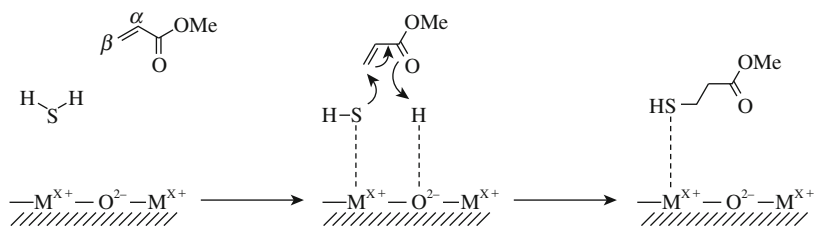
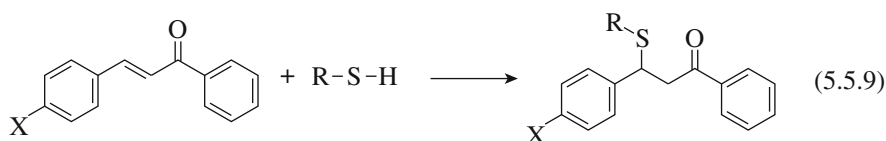


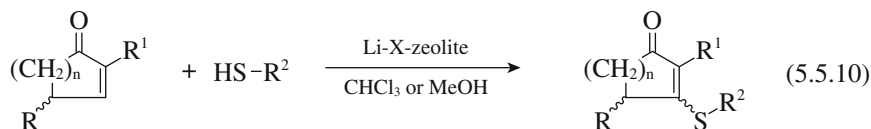
Fig. 5.5.1 Reaction mechanism for the base-catalyzed addition of H_2S to methyl acrylate
Reprinted with permission from E. Breysee, F. Fajula, A. Finiels, G. Frémy, J. Lamotte, F. Maugé, J. -C. Lavalley, C. Moreau, *J. Catal.*, **233**, 288 (2005) p. 289, Scheme 1.



High yields are obtained within a few minutes and under mild conditions. For example, in the reaction of thiophenol and chalcone, when ethanol or methanol is used as the solvent, the addition products are formed in 91% and 93% yields, respectively, in 5 min. On the other hand, no products are formed when hexane, pentanol or 2-propanol is used. The results of the reactions of various combinations of chalcone derivatives and thiols are shown in Table 5.5.8

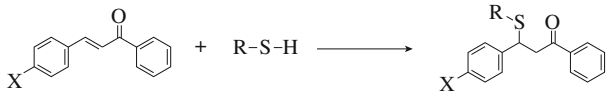
Michael addition of benzenethiol to 2-cyclopenten-1-one and 2-cyclohexen-1-one is catalyzed by alkali ion-exchanged zeolites.⁴²⁾ The activity order is, in general, in accordance with the basicity of the zeolites. The best results were obtained with NaY, KY and X-zeolites. However, in the presence of more basic zeolites such as CsX, a side reaction occurs in which the significant amount of thiols is oxidized to disulfide.

The Michael addition of a variety of substituted thiols to cyclic enones proceeds in the presence of LiX zeolite.⁴³⁾ For example, the reaction of 2-cyclohexen-1-one with 4-chlorobenzenethiol gives the Michael adduct in 82% yield at 273 K.



Similarly, the reaction of enone **10** and substituted thiol **11** results in the formation of 13-thiaprostandins **12** (60-80% yield). Ketone functionality in the thiaprostandins can be reduced with sodium borohydride to yield the corresponding hydroxyderivatives **13** in almost quantitative yield.

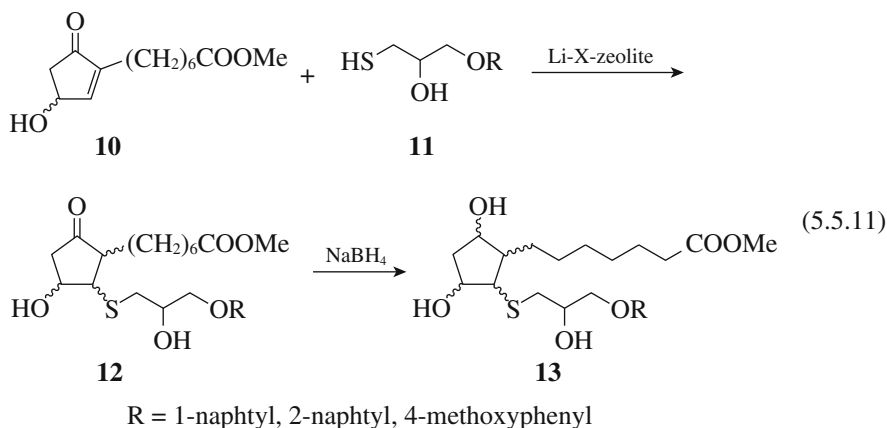
Table 5.5.8 Michael addition of chalcone with thiol using hydroxyapatite as catalyst



X	R	Time/min	Yield/%
H	C ₆ H ₅	5	93
H	2-NH ₂ -C ₆ H ₄	3	96
H	EtCO ₂ CH ₂	5	82
<i>p</i> -Cl	C ₆ H ₅	5	95
<i>p</i> -Cl	2-NH ₂ -C ₆ H ₄	2	96
<i>p</i> -Cl	EtCO ₂ CH ₂	5	84
<i>m</i> -NO ₂	C ₆ H ₅	5	93
<i>m</i> -NO ₂	2-NH ₂ -C ₆ H ₄	2	92
<i>m</i> -NO ₂	EtCO ₂ CH ₂	5	87
<i>p</i> -NO ₂	C ₆ H ₅	3	94
<i>p</i> -NO ₂	2-NH ₂ -C ₆ H ₄	1	91
<i>p</i> -NO ₂	EtCO ₂ CH ₂	5	91
<i>p</i> -OMe	C ₆ H ₅	60	90
<i>p</i> -OMe	2-NH ₂ -C ₆ H ₄	4	94
<i>p</i> -OMe	EtCO ₂ CH ₂	60	52
<i>p</i> -Me	C ₆ H ₅	20	91
<i>p</i> -Me	2-NH ₂ -C ₆ H ₄	3	92
<i>p</i> -Me	EtCO ₂ CH ₂	60	68

Reaction conditions: chalcone 1 mmol, thiol 1 mmol, methanol 1.5 mL, Catalyst 0.1 g, room temperature.

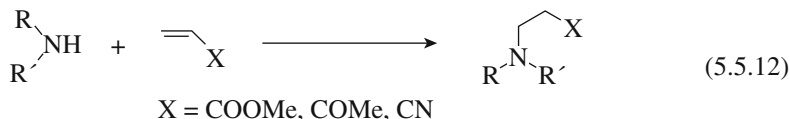
Reprinted with permission from M. Zahouily, Y. Arouki, B. Bahlouan, A. Rayadh, S. Sebti, *Catal. Commun.*, **4**, 521 (2003) p.523 Table 1.



The reaction of *p*-toluenethiol with methyl crotonate or methyl vinyl ketone gives the high yield of the corresponding addition products in the presence of MgO¹⁵⁾ and rehydrated hydrotalcite.⁶⁾ Addition of ethyl thioglycidate to methyl vinyl ketone or acrolein proceeds in the presence of zeolites.²⁶⁾

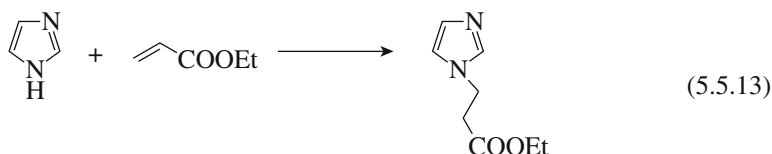
5.5.3 Addition of Amines to α,β -Unsaturated Compounds

Aza-Michael addition of amines to α,β -unsaturated compounds proceeds in the presence of hydrotalcite at room temperature.⁴⁴⁾



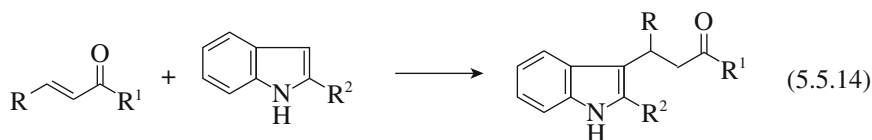
Mg-Al hydrotalcites containing NO_3^- , OH^- , F^- , O^tBu^- ions, MgO-Al₂O₃ mixed oxides and MgO are active catalysts to give 52-90% of the products in the reaction of dibutylamine and methyl acrylate. Cu-Al hydroxide (Cu/Al = 3) is more active. Various cyclic, acyclic and aliphatic amines including morpholine underwent 1,4-addition with a range of α,β -unsaturated compounds to afford the corresponding aza-Michael adducts, as shown in Table 5.5.9. However, there is no reaction when aromatic amines such as aniline are treated with methyl acrylate.

Imidazole can be condensed with ethyl acrylate in the presence of Li^+ - and Cs^+ -containing montmorillonite (Cs^+ -M) as catalysts under microwave or ultrasound activation.^{45,46)}



Under microwave irradiation, the greater the basicity and the irradiation time and power of microwave irradiation, the higher were the conversions.⁴⁵⁾ The yield of *N*-substituted product was 75% in the presence of Cs^+ -M with 100% selectivity at 850W in 5-min irradiation at 348 K. In the case of ultrasound activation, a conversion of about 97% was reached with 100% selectivity in the presence of Cs^+ -M at 323 K.⁴⁶⁾

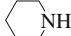
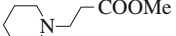
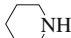
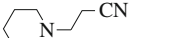

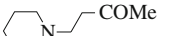
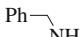
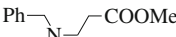
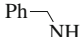
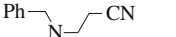
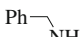
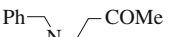

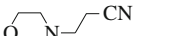

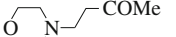
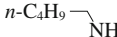
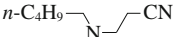
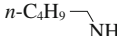
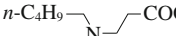

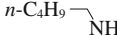
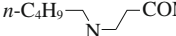

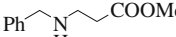
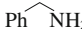
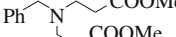
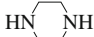
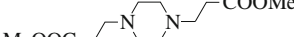
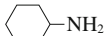

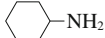
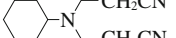
Indoles react with α,β -unsaturated ketones to afford indonyl ketones in the presence of nanocrystalline titanium dioxide.⁴⁷⁾



Thus, as shown in Table 5.5.10, the reaction of enone and indole in the presence of TiO₂ (10 mol%) in dichloromethane at room temperature gives the 3-substituted indole in excellent yield in 6 h.

Conjugated addition of indoles to nitroalkenes proceeds over basic alumina in solvent-free conditions at 333 K.⁴⁸⁾

Table 5.5.9 Aza-Michael reaction with Cu-Al hydrotalcite^a

Amine	Acceptor	Time/h	Product	Yield/% ^b
	$\text{CH}_2=\text{CHCOOMe}$	3.0		90
	$\text{CH}_2=\text{CHCN}$	3.5		88
	$\text{CH}_2=\text{CHCOMe}$	4.0		84
	$\text{CH}_2=\text{CHCOOMe}$	5.0		75
	$\text{CH}_2=\text{CHCN}$	5.5		80
	$\text{CH}_2=\text{CHCOMe}$	5.0		75
	$\text{CH}_2=\text{CHCN}$	4.0		86
	$\text{CH}_2=\text{CHCOMe}$	2.5		80
	$\text{CH}_2=\text{CHCN}$	5.0		88
	$\text{CH}_2=\text{CHCOOMe}$	3.0		90
	$\text{CH}_2=\text{CHCOMe}$	3.0		89 ^c
	$\text{CH}_2=\text{CHCOMe}$	5.0		88
	$\text{CH}_2=\text{CHCOOMe}$	5.5		78 ^d
	$\text{CH}_2=\text{CHCOOMe}$	5.5		80 ^e
	$\text{CH}_2=\text{CHCOOMe}$	5.0		90 ^e
	$\text{CH}_2=\text{CHCN}$	5.0		70 ^d
	$\text{CH}_2=\text{CHCN}$	5.0		70 ^e

^a Reaction conditions: amine 1.0 mmol, acceptor 1.2 mmol, methanol 5 mL room temperature

^b Isolated yield after silica gel chromatography

^c Isolated yield after fourth cycle

^d Five to nine percent of bis-adduct was formed

^e 2.4 equivalents of acceptor used

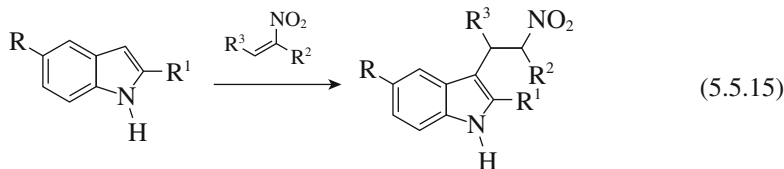
Reprinted with permission from M. L. Kantam, B. Neelima, V. Reddy, *J. Mol. Catal., A*, **241**, 147 (2005) p.149, Table 2.

Table 5.5.10 TiO₂-catalyzed Michael addition of α,β -unsaturated ketones with indole and 2-methylindole

Entry	Enone	Indole	Product	Yield ^{b)} /%
1				75, 71 ^{c)} , 68 ^{d)}
2				82
3				83
4				81
5				92
6				81
7				88
8				85
9				93
10				92 ^{a)}

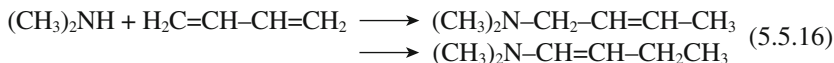
^{a)} Reaction conditions: all the reactions were carried out in anhydrous dichloromethane at room temperature, employing 10 mol% nano TiO₂, reaction time: 6 h. ^{b)} Isolated yields. ^{c)} Yields after fifth cycle. ^{d)} Reaction was done using bottle-grade DCM. ^{e)} Reaction time: 3 h.

Reprinted with permission from M. L. Kantam, S. Laha, J. Yadav, B. M. Choudary, B. Sreedhar, *Adv. Synth. Catal.*, **348**, 867 (2006) p.869, Table 2.



5.5.4 Addition of Amines to Butadiene

Kakuno and Hattori studied the addition of amines to conjugated dienes to yield unsaturated amines over basic metal oxides, MgO, CaO, SrO, La₂O₃, ThO₂ and ZrO₂.⁴⁹⁾ Diethylamine, ethylamine, piperidine, aniline and triethylamine were used. Among the catalysts studied, CaO is most active, while ThO₂ and ZrO₂ are inactive. The reactivity of amines is in the order dimethylamine > ethylamine > piperidine ≫ aniline, triethylamine. In the addition of dimethylamine with butadiene over CaO, the primary products consist of mainly, *N,N*-dimethyl-2-butenylamine which resulted from 1,4-addition of a dimethylamino group and an H to the diene. As the reaction proceeds, the 1,4-addition product undergoes double bond migration to the enamine, *N,N*-dimethyl-1-butenylamine.



In the case of SrO, the enamine is the almost exclusive product. Over La₂O₃, *N,N*-dimethyl-2-butenylamine is the sole product, the isomerization to enamine not being observed.

5.5.5 Cyanoethylation of Alcohols

Acrylonitriles react with compounds containing an active hydrogen to form β-alkoxynitriles, which are in turn converted to carboxylic acids by hydrolysis and to amine by reduction. Cyanoethylation of alcohols is a widely used reaction for the synthesis of drug intermediates and organic chemicals of industrial interest.



The reactions are catalyzed by homogeneous bases such as alkali hydroxide. Use of anion exchange resins as heterogeneous catalysts has been reported. The reaction of acetonitrile with diols (ethylene glycol, diethylene glycol, 1,4-butanediol and 1,5-pentanediol) gives a yield of 80-95% with use of an anion exchange resin in its hydroxide form at 323 K in 20 h.⁵⁰⁾



Kabashima and Hattori studied the cyanoethylation of alcohols with acetonitrile over various types of solid bases.⁵¹⁾ In the case of methanol, all the alkaline earth oxides exhibited very high catalytic activities at 323 K. Alkaline earth hydroxides also show high activity. The activities of KF/Al₂O₃ and KOH/Al₂O₃

Table 5.5.11 Cyanoethylation of alcohols with acrylonitrile catalyzed by $t\text{BuO}^-$ -hydrotalcite

Alcohol or thiol	Time/h	Product	Yield ^{a)/b)} %
MeOH	0.6		92 ^b
EtOH	1.5		96 ^b
	4.0		90 ^b
Ph-CH ₂ OH	1.5		100
	2.0		100
	4.0		87
	2.5		89
	2.0		80
	3.0		100
	2.0		98
	0.5		90
	0.6		100
	1.5		90
Me-[CH ₂] ₁₁ -SH	0.5		94

Reaction conditions: alcohol or thiol (4 mmol), acrylonitrile 4 mmol, solvent CH₂Cl₂, catalyst 50 mg, room temperature

^{a)} Yields based on ¹H NMR, ^{b)} Isolated yield

Reprinted with permission from B. M. Choudary, M. L. Kantam, B. Kelvita, *Green Chem.*, **1**, 289 (1999) p.290 Table 1.

were comparable with those of alkaline earth hydroxides. The alkaline carbonates, however, exhibited no or very low activity. La₂O₃ showed low activity, while Al₂O₃, ZrO₂ and ZnO were inactive. The order of reactivities of alcohols varied with the type of catalyst. With alkaline earth oxides, La₂O₃, KF/Al₂O₃ and KOH/Al₂O₃, the reactivity of alcohols increased in the order, methanol < ethanol < 2-propanol, while for magnesium hydroxide and calcium hydroxide, the reactivity order was the opposite. 2-Methyl-2-propanol showed very low or no reactivity

toward acrylonitrile over all of the catalysts studied. The authors discussed the reactivity orders in terms of the acidity of alcohols and the basic strength of the catalysts. The activities of the catalysts were scarcely affected by the exposure of the catalysts to air. This was interpreted as the result of stronger adsorption of alcohols in comparison with those of CO₂ and H₂O.

Hydrotalcite materials show high activity for cyanoethylation of alcohols with acrylonitrile. An as-synthesized hydrotalcite showed very low activity, while the oxide obtained by the decomposition of the material at 723 K under nitrogen showed increased activity. The activity is further increased by the rehydration of the oxide in wet nitrogen. The rehydrated hydrotalcite gave 99.8% conversion of acetonitrile in methanol at 323 K in 45 min.⁵²⁾ The catalyst was reusable and air stable. The activity is seemingly higher than that of MgO treated at 1073 K under vacuum. The catalyst was also active for ethanol, 2-propanol and butanol. The selectivity for the corresponding alkoxypropionitrile was 100%, except for 2-propanol, in which case the selectivity for β -isopropoxypropionitrile was 80%.

The catalytic activity of hydrotalcite further increased by introducing *t*-butoxide ions (^tBuO⁻) in the interlayers.⁵³⁾ The catalyst is highly active for the addition of alcohols and thiols to acetonitrile, as shown in Table 5.5.11. The selectivity for 3-alkoxypropionitriles and 3-alkylmercaptopypropionitriles is quantitative. The high activity of ^tBuO⁻ containing hydrotalcite is due to the high basicity of this ion and the easier formation of alkoxy anions from alcohols.

5.5.6 Addition of Alcohol to Vinyl Ketones and Vinyl Sulfones

The catalytic activities of different types of solid bases for the addition of methanol to 3-buten-2-one at 273 K were studied by Kabashima et al.⁵⁴⁾



In every case, the selectivity for the addition product exceeded 99%. All alkaline earth oxides exhibited high activity. The yields obtained with MgO, CaO and SrO exceeded 92% in 10 min. Even with BaO, which has a small surface area of 2 m² g⁻¹, the yield reached 73%. Sr(OH)₂·8H₂O and Ba(OH)₂·8H₂O also exhibited high activity, the yields being 75% and 70%, respectively. Mg(OH)₂ and Ca(OH)₂ also showed good activity, much lower than that of Sr(OH)₂·8H₂O and Ba(OH)₂·8H₂O. All alkaline earth carbonates showed very little activity. La₂O₃, ZrO₂, ZnO and Al₂O₃ showed very low activity. KF/Al₂O₃ and KOH/Al₂O₃ exhibited high activity, the yields being comparable to those observed for BaO, Sr(OH)₂·8H₂O and Ba(OH)₂·8H₂O.

The MgO catalyst was prepared by *in-situ* decomposition of Mg(OH)₂ under vacuum. The catalytic activity of MgO was maximum when the decomposition temperature was 673 K. At this temperature, the decomposition of Mg(OH)₂ to MgO was incomplete and a large amount of OH⁻ groups remained on the surface. Since Mg(OH)₂ itself showed some activity, the authors concluded that the surface OH⁻ groups act as the active sites.

29. K. Ebitani, K. Motokuma, K. Mori, T. Mizugaki, K. Kaneda, *J. Org. Chem.*, **71**, 5440 (2006).
30. E. DeOliveira, A. G. S. Prado, *J. Mol. Catal.*, **271**, 63 (2007).
31. K. Shimizu, H. Suzuki, E. Hayashi, T. Kodama, Y. Tsuchiya, H. Hagiwara, Y. Kitayama, *Chem. Commun.*, 1068 (2002).
32. H. Hagiwara, T. Sayuri, T. Okabe, T. Hoshi, T. Suzuki, H. Suzuki, K. Shimizu, Y. Kitayama, *Green Chem.*, **4**, 461 (2002).
33. H. Hagiwara, S. Inotsume, M. Fukushima, T. Hoshi, T. Suzuki, *Chem. Lett.*, **35**, 926 (2006).
34. Y. V. Subba Rao, D. E. De Vos, P. A. Jacobs, *Angew. Chem. Int. Ed. Engl.*, **30**, 2661 (1997).
35. R. Srivastava, *J. Mol. Catal., A*, **264**, 146 (2007).
36. I. Rodriguea, S. Iborra, A. Corma, *Appl. Catal., A*, **194/195**, 241 (2000).
37. U. Meyer, H. Gorzawski, W. F. Hölderich, *Catal. Lett.*, **59**, 201 (1999).
38. K. P. Volcho, S. Yu. Kurbakova, D. V. Korzhagina, E. V. Suslov, N. F. Salkhudinov, A. V. Toktarev, G. V. Echevskii, V. A. Barkhash, *J. Mol. Catal., A*, **195**, 263 (2003).
39. E. Breysse, F. Fajula, A. Finiels, G. Frémy, J. Lamotte, F. Maugé, J. -C. Lavalley, C. Moreau, *J. Mol. Catal., A*, **198**, 185 (2003).
40. E. Breysse, F. Faula, G. Frémy, D. Ticht, C. Moreau, *J. Catal.*, **211**, 288 (2005).
41. M. Zahouily, Y. Arouki, B. Bahlouan, A. Rayadh, S. Sebti, *Catal. Commun.*, **4**, 521 (2003).
42. M. Kummarraja, K. Pitchumani, *J. Mol. Catal., A*, **256**, 138 (2006).
43. P. D. Shinde, V. A. Mahajan, H. B. Borate, V. H. Tillu, R. Bal, A. Chandwadkar, R. D. Wakharkar, *J. Mol. Catal., A*, **216**, 115 (2004).
44. M. L. Kantam, B. Neelima, V. Reddy, *J. Mol. Catal., A*, **241**, 147 (2005).
45. R. M. Martín-Aranda, M. A. Vicenete-Rodríguez, J. M. López-Pestana, A. J. López-Peinado, A. Jerez, J. de D. López-González, M. A. Banares-Munoz, *J. Mol. Catal.*, **124**, 115 (1997).
46. R. M. Martín-Aranda, E. Ortega-Cantero, M. L. Rojas-Cervantes, M. A. Vincente-Rodríguez, M. A. Banares-Munoz, *Catal. Lett.*, **84**, 204 (2002).
47. M. L. Kantam, S. Laha, J. Yadav, B. M. Choudary, B. Sreedhar, *Adv. Synth. Catal.*, **348**, 867 (2006).
48. R. Ballini, R. R. Clemente, A. Palmieri, *Adv. Synth. Catal.*, **348**, 191 (2006).
49. Y. Kakuno, H. Hattori, *J. Catal.*, **85**, 509 (1984).
50. C. S. H. Chen, *J. Org. Chem.*, **27**, 1920 (1962).
51. H. Kabashima, H. Hattori, *Appl. Catal., A*, L33 (1997); *Catal. Today*, **44**, 277 (1998).
52. P. S. Kumbbar, J. Sanchez-Valente, F. Figueras, *Chem. Commun.*, **1998**, 1091.
53. B. M. Choudary, M. L. Kantam, B. Kelvita, *Green Chem.*, **1**, 289 (1999).
54. H. Kabashima, T. Katou, H. Hattori, *Appl. Catal., A*, **214**, 121 (2001).
55. R. Giovannini, M. Petrini, *Chem. Commun.*, **1997**, 1829.

5.6 Tishchenko Reactions

The Tishchenko reaction is the catalytic dimerization of aldehydes giving the corresponding esters. The first successful reaction was accomplished by Claisen using sodium alkoxide as the catalyst.¹⁾



Tishchenko used aluminum alkoxides as catalysts and succeeded in promoting the Tishchenko reaction of both non-enolizable and enolizable aldehydes.²⁾ Recently several organometallic compounds have also been described and found to be very selective.³⁾

With solid base catalysts, Tanabe and Sato reported the Tishchenko reaction of benzaldehyde over alkaline earth oxides.⁴⁾ The reaction proceeded at 423 K, and the order of catalytic activity per unit surface is $\text{BeO} \ll \text{MgO} < \text{CaO} \ll \text{SrO} \ll \text{BaO}$. The catalytic activity was well correlated with the number of basic sites determined by a titration method. The activity decreased with the addition of benzoic acid and was almost entirely lost by the addition of phenol or pyridine.

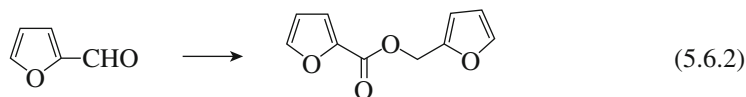
Infrared spectra of adsorbed benzaldehyde showed the existence of the metal benzyolate and benzoate on the surface. The authors proposed the reaction mechanism to be as shown in Fig. 5.6.1. The first step is the adsorption of benzaldehyde onto the basic (O^{2-}) and metal cations, resulting in the formation of the intermediates, (I) and (II), respectively. In the next step, hydride ion is transferred from (I) to (II) to form III and the active species (IV) for the ester formation. The active species (IV) attacks the carbon atom of an aldehyde to form the intermediate (V). Then the intermediate (V) draws another aldehyde onto a metal cation, followed by hydride ion transfer to a product ester and regenerates the active species (IV). The first order kinetics indicates that the rate-determining step is the nucleophilic addition of the active species (IV) to the carbonyl carbon atom of an aldehyde. The catalysts that Tanabe and Saito used were calcined in air, and the reactions were carried out at 423 K. Later, it was revealed that the Tishchenko reaction proceeds at a much lower temperature of 353 K over alkaline earth oxides pretreated under vacuum.⁵⁾

The reactivities of aldehydes were examined by carrying out a mixed-Tishchenko reaction in which an equal amount of two different aldehydes was allowed to react over a series of alkaline earth oxides.^{5,6)} Four types of esters were formed by two self-Tishchenko reactions and two cross-Tishchenko reactions. Based on the product distribution as well as quantum chemical calculation, it was concluded that the reaction proceeds faster for the aldehyde that has more positively charged and sterically less hindered carbonyl carbon atom of aldehyde with the active species (IV in Fig. 5.6.1) having a less hindered oxygen atom.

KF and KNH_2 supported on $\gamma-Al_2O_3$ exhibit high activities for the Tishchenko reaction of benzaldehyde.⁷⁾ The catalytic activity greatly depends on the evacuation temperature of the KF/Al_2O_3 under vacuum^{7,8)} (Section. 3.9.4). Over the KF/Al_2O_3 evacuated at 673 K, the conversion reached 94% and 99% in 3 h and 20 h, respectively, at 323 K.⁷⁾

Tsuji and Hattori revealed that oxides surface trade oxygen atoms with benzaldehyde during the Tishchenko reaction over MgO and CaO with ^{18}O -labelled surfaces and that the lattice oxygen extensively incorporated into the product, benzyl benzoate.⁹⁾ The authors proposed that incorporation of the lattice oxygen is due to the formation of a bidentate intermediate (Fig 5.6.2). The amount of surface oxygen incorporated into the product was estimated to be $500 \mu mol g^{-1}$ in the case of MgO.

Among aldehydes, fulfural is an aldehyde which undergoes the Tishchenko reaction with difficulty. Over CaO and SrO, the Tishchenko reaction of fulfural proceeds at 353 K.¹⁰⁾



A 93% yield of the ester was obtained at 353 K in 6 h in the presence of SrO with almost 100% selectivity. The SrO catalysts was prepared by pretreatment of

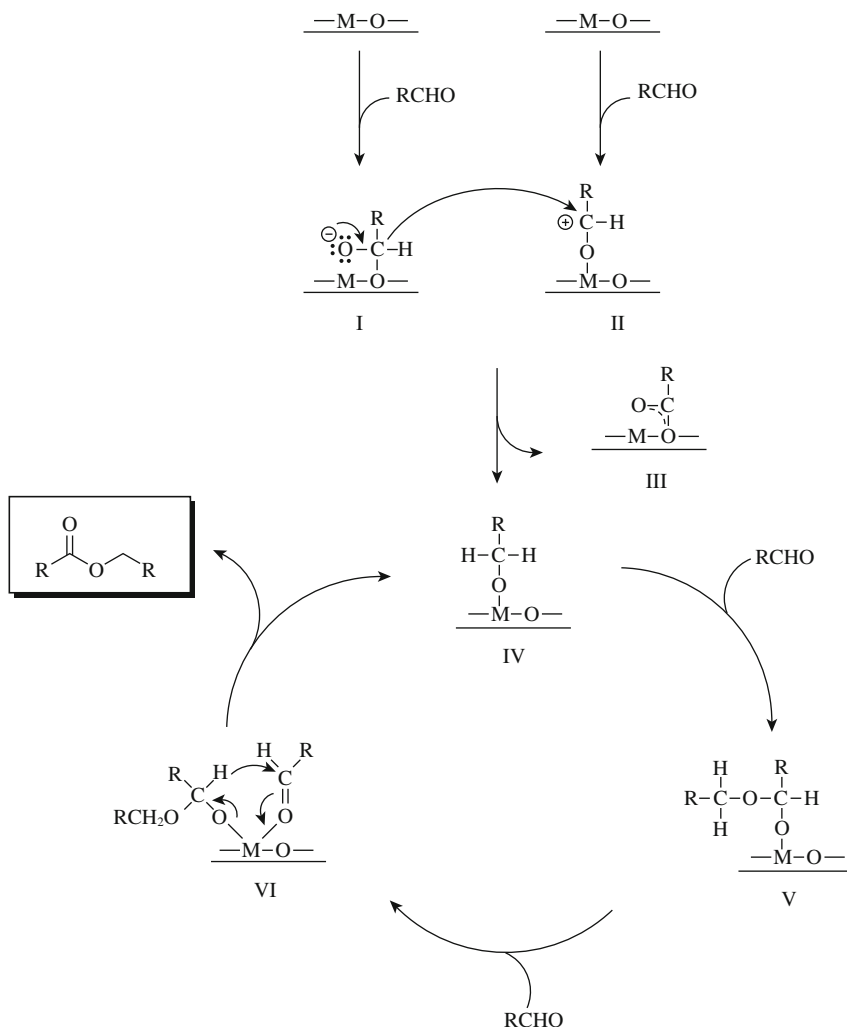


Fig. 5.6.1 Reaction mechanism of Tishchenko reaction over MgO and CaO proposed by Tanabe and Saito.⁴⁾ Scheme reprinted with permission from T. Seki, H. Hattori, *Catal. Surv. Jan.*, **7**, 145 (2003) p.149, Scheme 2.

SrCO_3 in a vacuum at 1273 K. For this reaction, MgO and BaO were not active. La_2O_3 , ZrO_2 , ZnO , Al_2O_3 , $\text{KF}/\text{Al}_2\text{O}_3$, $\text{KOH}/\text{Al}_2\text{O}_3$ were all inactive. SrO is also active for the Tishchenko reaction of 3-furaldehyde.⁶⁾

The intramolecular Tishchenko reaction of *o*-phthaldehyde to form phthalide is also catalyzed by solid bases.^{11,12)}

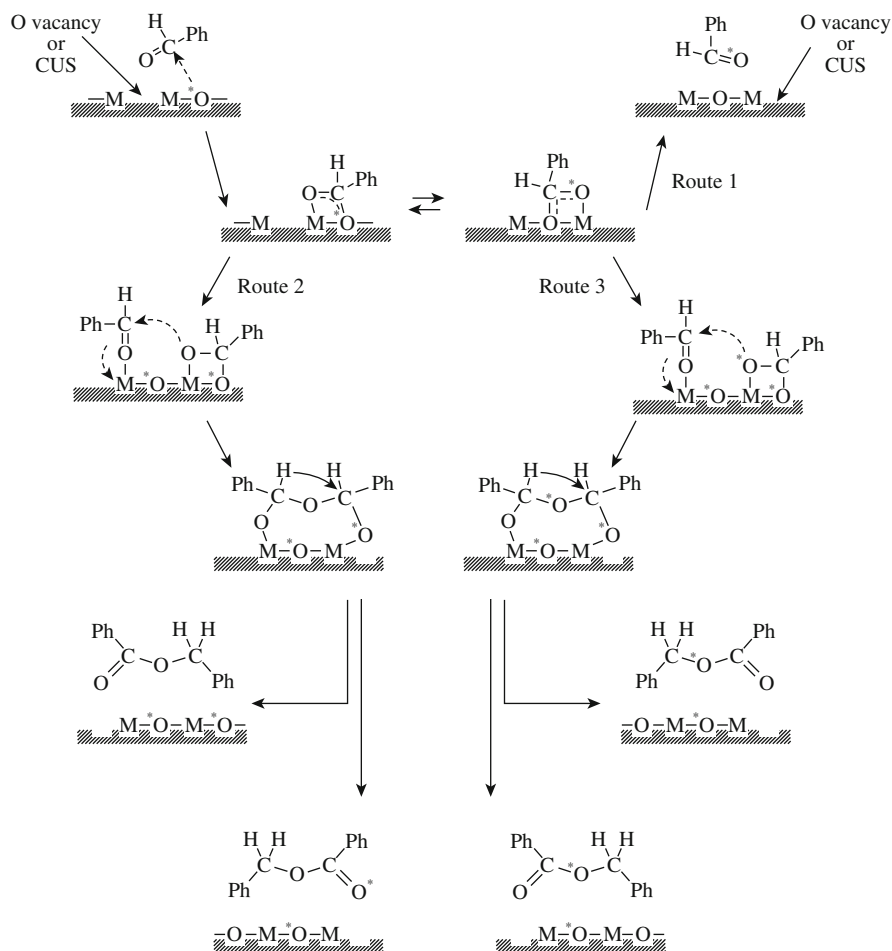
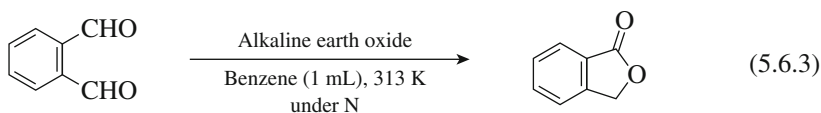


Fig. 5.6.2 Reaction mechanism of Tishchenko reaction over alkaline earth oxides proposed by Tsuji and Hattori.⁹⁾ Reprinted with permission from H. Tsuji, H. Hattori, *ChemPhysChem.*, **5**, 733 (2004), p.735, Fig. 2



MgO, CaO and SrO are active, but BaO is inactive. The quantitative yield of phthalide is obtained in 15 min at 313 K in the presence of CaO. Al₂O₃ is also active, though less active than CaO. KF/Al₂O₃ and KOH//Al₂O₃ are moderately active. MgO-Al₂O₃ mixed oxide (prepared by calcinations of hydrotalcite), La₂O₃, ZrO₂ and ZnO are inactive. The intramolecular Tishchenko reaction of

2,3-naphthalenedicarbaldehyde also proceeds in the presence of CaO or Al₂O₃. A 94% yield of the lactone is obtained at 333 K in 2 h.

References

1. L. Claisen, *Ber.* **20**, 646 (1887).
2. W. Tischtschenko, *J. Russ. Phys. Chem.*, **38**, 355 (1906).
3. T. Seki, T. Nakajo, M. Onaka, *Chem. Lett.*, **35**, 824 (2005).
4. K. Tanabe, K. Saito, *J. Catal.*, **35**, 247 (1974).
5. T. Seki, H. Kabashima, K. Akutsu, H. Tachikawa, H. Hattori, *J. Catal.*, **204**, 393 (2001).
6. T. Seki, H. Hattori, *Catal. Surv. Jpn.*, **7**, 145 (2003).
7. H. Handa, T. Baba, H. Sugisawa, Y. Ono, *J. Mol. Catal., A*, **134**, 171 (1998).
8. H. Kabashima, H. Tsuji, S. Nakata, Y. Tanaka, H. Hattori, *Appl. Catal., A*, **194/195**, 227 (2000).
9. H. Tsuji, H. Hattori, *ChemPhysChem.*, **5**, 733 (2004).
10. T. Seki, K. Akutsu, H. Hattori, *Chem. Commun.*, **2001**, 1000.
11. T. Seki, H. Hattori, *Chem. Commun.*, **2001**, 2510.
12. T. Seki, H. Tachikawa, T. Yamada, H. Hattori, *J. Catal.*, **217**, 117 (2003).

5.7 Alkylation Reactions

5.7.1 Alkylation of Phenols

A. Ring alkylation of phenol with methanol

A number of works have been reported on the alkylation of phenol with methanol over metal oxides and zeolites as catalysts. Generally, alkylation over acidic oxides such as SiO₂-Al₂O₃ gives mainly a mixture of three isomers of cresols and anisole. On the other hand, basic oxides such as MgO favor alkylation at *ortho* positions. The reaction is industrially important since the reaction product, 2,6-xyleneol, is a monomer for good heat-resisting resin.

Mixed oxides containing Fe₂O₃ are selective catalysts for *ortho*-alkylation of phenol.^{1,2)} Table 5.7.1 shows the activities and the selectivities for *ortho*-alkylation at 623 K over the mixed oxides where the composition of oxides is M/Fe ratio of 2, M standing for the second metal.¹⁾ As shown in Table 5.7.1, phenol is selectively methylated at the *ortho* position, except for NiO-Fe₂O₃. The mixed oxides, ZnO-Fe₂O₃ catalysts are also active for *ortho*-alkylation of phenol with ethanol, 1-propanol and 2-propanol.³⁾

Calcium phosphate, Ca₃(PO₄)₂, is a selective catalyst for *ortho*-alkylation of phenol with methanol.⁴⁾ The selectivity for *ortho*-alkylation products (*o*-cresol + 2,6-dimethylphenol) was 88% at phenol conversion of 77.7% at 773 K. Selectivity of methylation based on methanol (93%) was much higher than those found in the alkylation by Fe₂O₃-containing mixed oxides.

TiO₂ is very selective for *ortho*-alkylation.^{5,6)} The selectivity for *ortho*-alkylation (*o*-cresol + 2,6-dimethylphenol) was 88% at the conversion of 78% at 733 K. Strong Lewis acid and weak Lewis base pairs were proposed to be the active sites for the alkylation.

Tanabe and Nishizaki⁷⁾ studied the infrared spectra of phenol adsorbed on MgO and SiO₂-Al₂O₃. Phenol molecules are dissociatively adsorbed on both catalysts to form surface phenoxide. However, the ratio of the intensity of the band at

Table 5.7.1 Reaction products from phenol and methanol over MO-Fe₂O₃

M of M-Fe ₂ O ₃	Cu	Mg	Ca	Ba	Zn	Mn	Co	Ni ^a
Phenol converted, mol %	95.3	8.8	68.7	82.5	88.4	24.0	63.9	67.5
Selectivity, % ^b								
<i>o</i> -Cresol	41.0	75.3	79.3	64.3	43.5	83.9	82.6	53.2
2,6-Xylenol	59.0	24.7	20.3	35.6	56.5	13.1	17.3	18.6
Methanol converted, mol %	42.3	5.1	23.1	28.7	66.5	2.2	23.8	98.3
Selectivity, % ^c								
Methylation	31.5	22.1	41.9	38.7	21.0	100	32.5	6.6
Gasification	68.5	77.9	58.0	61.3	79.0	—	67.5	93.3

^{a)} Selectivity for benzene, toluene, xylene and carbonization are 12.4, 5.0, 1.0, and 9.8, respectively.

^{b)} Given by (moles of *o*-cresol or 2,6-xylenol per moles of phenol converted).

^{c)} Given by (moles of methyl group in products or gaseous products per moles of methanol converted).

Reaction conditions: 623 K; phenol + methanol = 63 kPa; phenol/methanol = 1/10; contact time 1.6 s. Reprinted with permission from T. Kotanigawa, M. Yamamoto, K. Shimokawa, Y. Yoshida, *Bull. Chem. Soc. Jpn.*, **44**, 1962 (1971) p. 1962, Table 1.

1496 cm⁻¹ to that around 1600 cm⁻¹ was quite different in the two catalysts, though both bands are due to the in-plane skeletal vibration of the benzene ring. With MgO, the ratio was the same as that of phenol in the liquid phase, while it was quite different from the liquid phenol with SiO₂-Al₂O₃. From these observations, they suggested that the selectivity difference in the two catalysts is caused by the adsorbed state of phenol (Fig. 5.7.1). On the acidic catalysts, the interaction of the aromatic ring of the phenoxide and the surface is strong and the aromatic ring of the phenoxide lies close to the surface. This facilitates the ring alkylation at *meta* and *para* positions in addition to *O*-alkylation. On the other hand, the interaction of the phenoxide and the surface is weak on the basic oxide, and the aromatic ring of the phenoxide is in more or less an upright position. This inhibits alkylation at positions other than the *ortho* position.

The reaction scheme for the formation of *ortho*-alkylation depends on the catalysts used. Velu and Swamy proposed the intermediacy of anisole in the case of MgO-Al₂O₃, since anisole was the main product at low contact times and the anisole selectivity decreased and 2-methylanisole and 2,6-dimethylphenol increased at the later stage.⁸⁾ Actually, the reaction of anisole with methanol gave *o*-cresol, 2,6-dimethylphenol together with 2-methylanisole. Thus, the authors proposed that path A in Fig. 5.7.2 is predominant in the alkylation over MgO-Al₂O₃. They also reported that Path B (direct methylation of the benzene ring) is predominant over CuO-Al₂O₃, MgO-Fe₂O₃ and MgO-Cr₂O₃ catalysts.^{9,10)}

Kotanigawa et al. concluded that *o*-cresol is formed by the direct methylation of phenol in the case of ZnO-Fe₂O₃ catalyst, since no reaction was observed between anisole and methanol on this catalyst.¹¹⁾

2,3,6-Trimethylphenol is an industrial starting material for synthetic vitamin E. The alkylation of *m*-cresol with methanol over MgO in the vapor phase gave a *m*-cresol conversion of 95–100% and 2,3,6-trimethylphenol selectivity of 80–90% at 20–30 bar at 773 K.¹²⁾

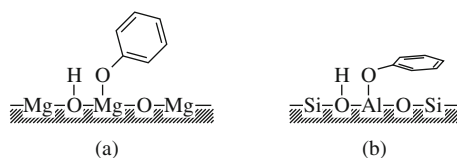


Fig. 5.7.1 Adsorbed state of phenol on (a) MgO and (b) SiO₂-Al₂O₃.

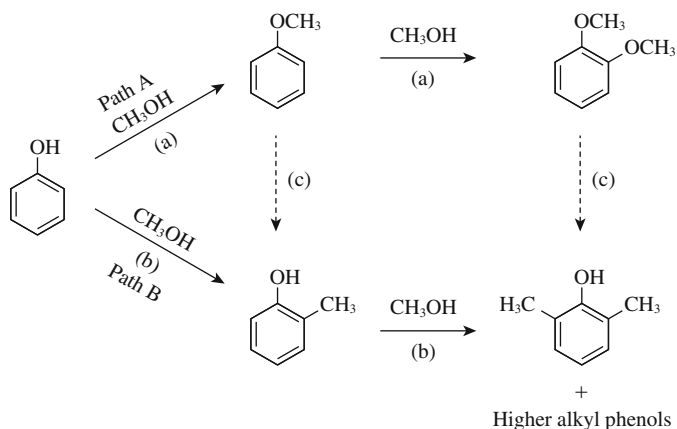


Fig. 5.7.2 Reaction scheme for alkylation of phenol. Reprinted with permission from S. Velu and C. S. Swamy, *Appl. Catal., A*, **145**, 141 (1996) p. 151, Scheme.

B. *O*-Alkylation of phenol with methanol

Alkali cation-loaded X-zeolite catalyses *O*-alkylation of phenol derivatives with methanol.¹³ The catalytic activity of alkali cation-exchanged zeolites in the *O*-alkylation increases as the basicity of zeolites increases. In the reaction of phenol with methanol, anisole was the sole product at 543 K. However, rapid deactivation was found. *O*-Alkylation of phenol with methanol also proceeds over alkali-loaded silica.¹⁴ Activities of the catalysts increase with metal loading and with basicity of the metal oxides (Cs₂O/SiO₂ > K₂O/SiO₂ > Na₂O/SiO₂ > Li₂O/SiO₂). Very high conversion (~90%) and 100% *O*-methylation selectivity were obtained over Cs₂O/SiO₂. The *O*-alkylation also proceeds with ethanol, 1-propanol and 1-butanol. Conversion decreases with increase in the carbon chain of the alkylating agent.

C. *O*-Alkylation of phenol with dimethyl carbonate

Tundo et al. studied the reaction of phenol with dimethyl carbonate (DMC) under gas-liquid phase transfer conditions.¹⁵ The catalyst was K₂CO₃ coated with 5 wt% PEG 6000. A very high conversion of phenol to anisole was observed at 453 K. Fu and Ono reported that the alkylation of phenol with DMC proceeded in the gas phase over alkali cation-exchanged X-zeolites.¹⁶ Fig. 5.7.3 shows the change in

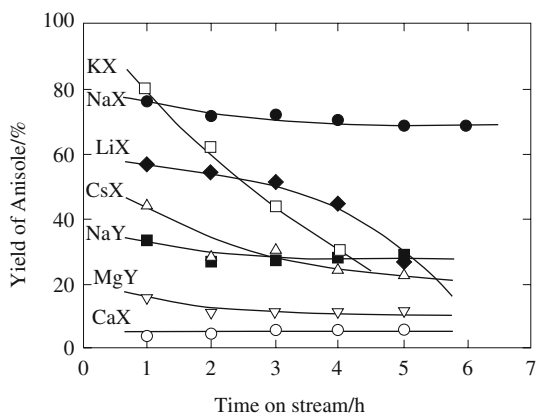


Fig. 5.7.3 Change in anisole yield with time on stream in the methylation of phenol with dimethyl carbonate (DMC) over various zeolites.

Reaction conditions, 553 K, phenol pressure: 24.7 kPa, DMC/phenol molar ratio = 1, $W/F = 12.0 \text{ g h mol}^{-1}$.

Reprinted with permission from Z.-H. Fu, Y. Ono, *Catal. Lett.*, **21**, 43 (1993) p. 45, Fig. 1.

the conversion of phenol with time on stream at 553 K. Alkali cation-exchanged zeolites show high catalytic activities for anisole formation, while the zeolites containing alkaline earth cations (CaX, MgY) give low yields of anisole, indicating that the basicity is essential for the *O*-methylation of phenol. The selectivities for anisole were 93% and 94% over NaX and KX, respectively. Among alkali cation-exchanged zeolites, only NaX gives high and stable activity. In the cases of KX and CsX, the activity decays quickly with time on stream.

Liquid-phase *O*-methylation of phenol with DMC over basic zeolites in a batch reactor was reported by Romero.¹⁷⁾ The catalyst was as-synthesized KNaX, which contains alkaline hydroxides. Phenol conversion and selectivity toward anisole were 100% and 85%, respectively, at 438 K with a DMC/phenol molar ratio of 2.

Wu et al. prepared fluorine-modified mesoporous MgO-Al₂O₃-mixed oxides, which were prepared by calcination of F⁻ containing hydrotalcite.¹⁸⁾ The XRD revealed that the materials contained a MgF₂ phase in addition to MgO phase characteristic of calcined hydrotalcite. The materials showed high activities and selectivity in the liquid-phase *O*-methylation of phenol with DMC. They were more effective than unmodified mixed oxide. The phenol conversion was proportional to the amount of the moderate and strong basic sites as determined by temperature-programmed desorption of carbon dioxide. The 100% selectivity for anisole at 99.3% phenol conversion was attained at 473 K.

D. Alkylation of phenol with propanols

Vapor phase alkylation of phenol with 1-propanol and 2-propanol was studied in a fixed-bed reactor over MgO-Al₂O₃ mixed oxide prepared by calcining hydrotalcite.¹⁹⁾ The oxide (Mg/Al = 3) showed a phenol conversion of ca. 80% in the

alkylation with 1-propanol at 623 K. Both *O*- and *C*-alkylation took place without any skeletal isomerization of the propyl moiety. On the other hand, with 2-propanol, *C*-alkylation occurred exclusively. Isomorphous substitution of Mg^{2+} by Cu^{2+} in the starting hydrocalcite framework resulted in a higher selectivity for 2-propylphenol and 2-isopropylphenol in the reaction of 1-propanol and 2-propanol, respectively.

Ortho-selective alkylation of phenol with 1-propanol over $\text{CeO}_2\text{-MgO}$ was reported.²⁰⁾ The $\text{CeO}_2\text{-MgO}$ (CeO_2 11.2%) showed a high selectivity (85%) for 2-propylphenol at a phenol conversion of 23%.

E. Alkylation of dihydroxybenzenes with methanol

Catechol (1,2-dihydroxybenzene) is methylated with methanol over Al_2O_3 in the temperature range of 533–583 K.²¹⁾ The main products were 3-methyl-1,2-benzenediol and 2-methoxyphenol. The overall selectivity for these two products was 80–90%.

Hydroquinone (1,4-dihydroxybenzene) is selectively *O*-alkylated with methanol into 4-methoxyphenol and 1,4-dimethoxybenzene in liquid phase in the presence of CsX .¹³⁾ By the reaction of hydroquinone with excess methanol at 523 K for 2 h, 100% selectivity for monomethylation was obtained at a conversion of 19.7%. The reaction at 563 K for 2 h gave 97.9% conversion of hydroquinone with selectivities of 70% and 28% for mono- and di-methylated products, respectively.

Bal et al. studied vapor-phase *O*-alkylation of dihydroxybenzenes with metal over alkali-loaded silica catalysts.²²⁾ The results are shown in Table 5.7.2. The alkali metals were loaded (1.5 mmol g^{-1}) onto the silica by an impregnation procedure using an aqueous solution of metal hydroxide/acetate. The materials were dried at 373 K and calcined at 773 K. The activity is in the order $\text{Li}_2\text{O/SiO}_2 < \text{Na}_2\text{O/SiO}_2 < \text{K}_2\text{O/SiO}_2 < \text{Cs}_2\text{O/SiO}_2$. The selectivity for the *O*-methylated products is very high over all the catalysts and increases in the same order as the activity, selectivity being 100% in the case of $\text{Cs}_2\text{O/SiO}_2$. The reactivity of dihydroxybenzenes matches the acidity of the reactants: 1,2-dihydrobenzene $<$ 1,4-dihydroxybenzene $<$ 1,3-dihydroxybenzene.

F. Alkylation of dihydroxybenzenes with dimethyl carbonate

Fu et al. studied the alkylation of catechol with dimethyl carbonate (DMC) with alumina and alumina loaded with alkaline compounds.²³⁻²⁶⁾ Dimethyl carbonate is a much more efficient methylating agent than methanol for catechol. Over alumina, the main product was guaiacol (2-methoxyphenol). The selectivity for guaiacol is about 70% and 3-methylcatechol is formed with 20% selectivity. Cofeeding of carbon dioxide greatly reduced the activity, indicating that basic sites are involved in the methylation.

Loading of alkaline compounds on alumina greatly enhances the activity and changes the selectivity in the alkylation. Fig. 5.7.4 shows the change in the conversion of catechol and yield of the products in the reaction over Al_2O_3 , which was loaded with KNO_3 and calcined at 673 K. It is clearly seen that guaiacol and cate-

Table 5.7.2 Catalytic activities of alkali-loaded silica for methylation of dihydroxybenzenes (Reaction conditions: 673 K, substrate/methanol = 1/5)

Catalyst	Catechol		Resorcinol		Hydroquinone		<i>p</i> -Methoxy phenol				
	Conversion	Selectivity ^{a)} (mono)	Selectivity ^{b)} (di)	Conversion	Selectivity ^{c)} (mono)	Selectivity ^{d)} (di)	Conversion	Selectivity ^{e)} (mono)	Selectivity ^{f)} (di)	Conversion	Selectivity ^{f)} (di)
Li(1.5)SiO ₂	5.2	75.1	15.7	30.9	36.9	44.3	27.1	59.1	14.0	49.7	100
Na(1.5)SiO ₂	10.3	71.3	22.5	45.3	33.8	52.1	44.2	47.7	31.0	63.8	100
K(1.5)SiO ₂	17.3	63.3	31.5	65.7	22.6	64.7	49.1	45.8	41.0	75.8	100
Cs(1.5)SiO ₂	57.2	47.0	53.0	87.4	10.7	89.3	87.9	24.8	75.2	96.4	100

^{a)} 2-Methoxy phenol.

^{b)} 1,2-Dimethoxy benzene.

^{c)} 3-Methoxy phenol.

^{d)} 1,2-Dimethoxy benzene.

^{e)} 4-Methoxy phenol.

^{f)} 1,4-Dimethoxy benzene.

Reprinted with permission from R. Bal, B. B. Tope, S. Sivasankar, *J. Mol. Catal.*, **181**, 161 (2002) p.163, Table 1.

chol carbonate are the intermediate products and that they are converted into veratrole (*o*-dimethoxybenzene) by further methylation, as shown in the scheme in Fig. 5.7.5. No *C*-methylated products are formed over Al_2O_3 loaded with alkaline compounds.

The relative rates of the four steps of the reactions in Scheme in Fig. 5.7.5 depend on the catalyst, DMC/catechol ratio and reaction conditions. $\text{LiOH}/\text{Al}_2\text{O}_3$ gives the highest selectivity (84%) for guaiacol at 100% conversion of catechol at 583 K. Over $\text{CeOH}/\text{Al}_2\text{O}_3$, catechol carbonate can be obtained at 50% selectivity at 88% conversion of catechol at 583 K. $\text{KNO}_3/\text{Al}_2\text{O}_3$ shows much higher activity than Al_2O_3 loaded with alkali hydroxide and gives easily veratrole at the same temperature (Fig. 5.7.4).

Methylation of catechol with DMC was studied over $\text{MgO}-\text{Al}_2\text{O}_3$ (calcined hydrotalcite) in the temperature range of 523–623 K.²⁷⁾ Guaiacol and veratrole

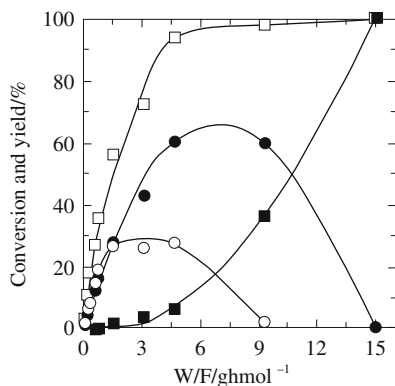


Fig. 5.7.4 Effect of contact time (W/F) on the yields of products in the reaction of catechol with dimethyl carbonate over $\text{KNO}_3/\text{Al}_2\text{O}_3$. Catechol conversion (\square), yields of guaiacol (\bullet), catechol carbonate (\circ), and veratrole (\blacksquare)
 Reaction conditions: 583 K, catechol = 10 kPa, catechol/methanol = 1/4
 Reprinted with permission from Y. Fu, T. Baba, Y. Ono, *Appl. Catal., A*, **176**, 201 (1999), p. 203, Fig. 2.

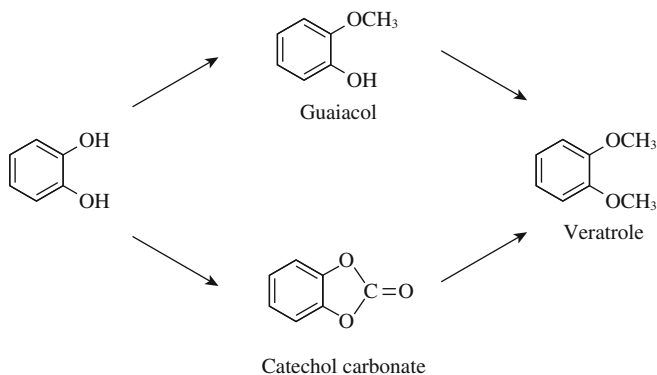


Fig. 5.7.5 Reaction scheme of the reaction of catechol with dimethyl carbonate.

were obtained as the major products, along with small amounts of catechol carbonate and *C*-alkylated products. At 573 K, the overall *O*-selectivity was 96.1% with a guaiacol selectivity of 84%. MgO was less active than the mixed oxides, while Al₂O₃ gave appreciable amounts of *C*-alkylated products.

Vijayraj and Gopinath studied the alkylation of three dihydrobenzene isomers with DMC.²⁸⁾ K⁺ (5 wt%)-doped MgO gave the best results. In the reaction of catechol with DMC at 583 K, K⁺/MgO showed 100% conversion of catechol with stable activity, the main product being guaiacol (ca. 70%) and veratrole (97%) with a DMC/catechol ratio of 2 and 4, respectively. In the reaction of hydroquinone with DMC (hydroquinone/DMC ratio of 2) at 583 K, 4-methoxyphenol was obtained with high selectivity (94%) at a hydroquinone conversion of 83%. By increasing the DMC/hydroquinone ratio, the conversion increased to 100%; the selectivity for 4-methoxyphenol decreased to 70%, 1,4-dimethoxybenzene being obtained with 30% selectivity. In the alkylation of resorcinol with DMC (DMC/resorcinol = 2) at 583 K, 3-methoxyphenol and 1,3-dimethoxybenzene were obtained with selectivity of 83% and 11%, respectively, at a resorcinol conversion of 82%.

G. *O*-Methylation of 2-naphthol with methanol

O-Methylation of 2-naphthol was studied in the vapor phase over alkali-loaded silica and Cs-loaded MCM-41.²⁹⁾ Both SiO₂ and MCM-41 had low *C*-alkylation activities. The introduction of alkali ions considerably increased 2-naphthol conversion with 2-methoxynaphthalene being the major product. The activity of the catalysts increased in the order Cs > K > Na > Li. Very high conversion (~99%) of 2-naphthol together with high selectivity (>95%) for 2-methoxynaphthalene were obtained over Cs-loaded fumed silica and MCM-41.

5.7.2 Side-chain Alkylation of Alkyl Aromatics

While alkylation of alkylaromatics with alkenes or alcohols occurs at the aromatic ring over acid catalysts, alkylation of the alkyl group proceeds over basic catalysts.

A. Alkylation of toluene with methanol

Sodorenko et al. reported that the alkylation of toluene with methanol over alkali cation-exchanged zeolites gave a mixture of xylenes, styrene and ethylbenzene at 678 and 728 K. In particular, KX and RbX gave predominantly styrene and ethylbenzene.³⁰⁾ Yashima et al. studied the reaction in more detail.³¹⁾ Over LiX or LiY zeolite, xylenes were the sole products, while over Na⁺, K⁺, Rb⁺ and Cs⁺-exchanged zeolites, styrene and ethylbenzene were produced selectively. The activity for side-chain alkylation has a tendency to be greater with X-type zeolites than the corresponding Y-type zeolites, and also depends on the size of the alkali cations, that is, Na⁺ < K⁺ < Rb⁺, Cs⁺. These trends were also found in the alkylation of toluene with formaldehyde. Addition of hydrogen chloride promoted the ring alkylation and inhibited the side-chain alkylation. On the other hand, addition of aniline to the feed inhibited xylene formation over LiY, but promoted the side-

chain alkylation over KX and RbY. From these findings, Yashima et al. stressed the importance of basic sites in side-chain alkylation over zeolites. The basicity of KX and KY was confirmed by the color change of adsorbed indicators, cresol red and thymolphthalein. They proposed a mechanism where, in the first stage, methanol is converted into formaldehyde, followed by aldol-type condensation of formaldehyde and toluene to form styrene. Ethylbenzene is produced by hydrogenation of styrene as well as direct hydrocondensation of toluene with methanol.



Actually, formaldehyde is better alkylating agent than methanol in the side-chain alkylation of toluene, styrene being the major alkylation product. For both steps (5.7.2) and (5.7.4), benzyl anion, $\text{C}_6\text{H}_5\text{CH}_2^-$, is a plausible intermediate. Therefore, the basic sites should be involved in the dehydrogenation of methanol (5.7.1) and the activation of toluene (5.7.2) and (5.7.4).

Addition of certain inorganic compounds such as phosphoric acid or boric acid to the ion-exchange solution improved the selectivity for the side-chain alkylation.³²⁾ The borate-promoted CsX zeolite was the most favorable and gave a selectivity of >50% for styrene + ethylbenzene on methanol base. High selectivity of CsX is suggested to be due to the adsorption of a toluene molecule between two (or more) large cations in an overcrowded supercage of X-zeolite in such a way that (1) an electrostatic potential at the molecule is higher than one would normally expect; (2) only the methyl group is exposed for alkylation; (3) because of the strong interaction of the cations with aromatic molecules, the protons of the methyl group become more acidic and susceptible to attack. It is also suggested that incorporation of borate in the supercage slowed the decomposition of formaldehyde, a real alkylating agent. A favorable effect of boron addition to CsX was also confirmed by Wieland et al., who suggested that the primary effect of boron addition was to reduce the decomposition of intermediate formaldehyde to carbon monoxide without inhibiting the sites active for alkylation by poisoning some of the strongly basic sites.³³⁾ They also found that CsL is a unique catalyst for side-chain alkylation of toluene.³⁴⁾ The yield at 760 K over CsL was similar to that over boron-promoted CsY at 683 K, but the former catalyst was not accompanied by a substantial production of CO. Formaldehyde formed is mostly recovered.

Itoh et al. indicated from quantum chemical calculation that, though the presence of basic sites is indispensable for side-chain alkylation, specific configurations of acidic sites and basic sites promote the alkylation.³⁵⁾ Actually, RbX with a small amount of Li^+ ions showed higher activity than RbX for side-chain alkylation of *p*-xylene.^{36,37)} It was shown that Li,Rb-X has slightly stronger acid sites

than RbX. Incorporation of Li^+ ions also suppressed the decomposition of the formaldehyde intermediate.³⁷⁾

Several other means for enhancing the catalytic activity for side-chain alkylation have been reported. Deposition of Cu or Ag metal on CsX or boron-promoted CsX enhances the activity under hydrogen, but the product is solely ethylbenzene. The metals are assumed to enhance the dehydrogenation of methanol to formaldehyde.³⁸⁾ Selectivity for side-chain alkylation increased when alkali hydroxide instead of alkali salts was used for ion exchange.³⁹⁾ High selectivity for ethylbenzene was achieved in the KX or CsX containing excess alkali hydroxide. The activity and selectivity for styrene increased with the use of binary zeolite catalysts such as KX-KZSM-5.⁴⁰⁾

In connection with side-chain alkylation of toluene, the adsorption and transformation of toluene, methanol, formaldehyde and a mixture of toluene and methanol/formaldehyde have been studied by a variety of spectroscopic techniques. Unland studied the adsorption of methanol at 673 K by infrared spectroscopy.⁴¹⁾ On NaX, formation of methoxide, carbonate ions and several forms of formate ions was observed. On KX, RbX and CsX, the formation of formate ions was indicated. King and Garces examined the infrared spectra during the reaction of toluene and methanol at 673 K.⁴²⁾ CsX, RbX and KX show formation of unidentate and bidentate formates on the surface during the reaction. LiX and NaX show no formate formation. The unidentate formate is suggested to be an intermediate for side-chain alkylation. Palomares et al. showed from infrared spectroscopy and temperature-programmed desorption of a mixture of toluene and methanol that the main adsorbed species was methanol with NaX, while it was toluene with CsX and RbX.⁴³⁾

Sefcik showed by ^{13}C NMR that toluene behaves as a freely tumbling molecule on NaX, but considerable inhibition to rotation is encountered on CsX.⁴⁴⁾ Hunger et al. showed a strong interaction of toluene with Cs^+ ions in CsY by ^{133}Cs MAS NMR, but ^{13}C MAS NMR gave no evidence for polarization of the methyl group of toluene adsorbed on CsY.⁴⁵⁾ ^{13}C MAS NMR revealed the formation of CO upon heating methanol at 673 K in the presence of CsY, indicating the formation of formaldehyde as an intermediate.

B. Alkylation of methylpyridines with methanol

Alkylation of methylpyridines with methanol over alkali cation-exchanged X- and Y-zeolites produces mainly the side-chain methylated products, ethylpyridines and vinylpyridines. The yields of ethylpyridine were highest over CsY at 723 K, while the yields of vinylpyridines were highest over CsX at 698 K.⁴⁶⁾

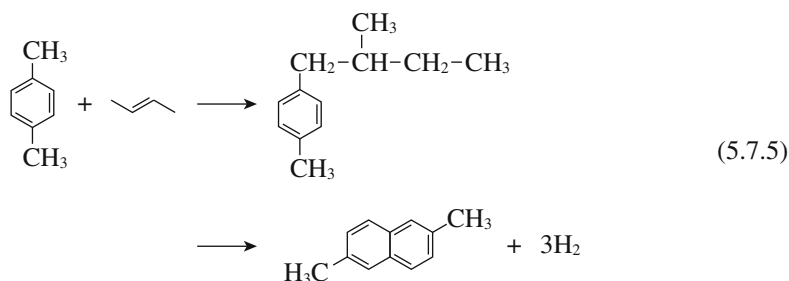
Side-chain alkylation of methylpyridines with formaldehyde proceeds very selectively over alkali cation-exchanged ZSM-5.⁴⁷⁻⁴⁹⁾ 2-Vinylpyridine and 4-vinylpyridine were obtained in 95.6% and 80.5% selectivity at a conversion of 80.4% and 94.8%, respectively, over K-ZSM-5 at 573 K.^{47,48)} The reaction of 2,6-lutidine with methanol over K-ZSM-5 gave 2-methylpyridine (54.8%) and 2,6-vinylpyridine (45.2%) at a conversion of 73.4% at 573 K.

C. Side-chain alkylation of alkylaromatics with alkenes

Strong solid base catalysts such as $\text{NaN}_3/\text{zeolite}^{50}$, $\text{Na}/\text{NaOH}/\text{Al}_2\text{O}_3^{51}$ (section 3.9) and $\text{Cs}/\text{carbon}^{52}$ catalyze the side-chain alkylation of alkylaromatics with alkenes such as ethylene and propene under mild conditions. Addition of butadiene to alkyl aromatics proceeds over K or Na on a CaO support.⁵³ For example, at about 380 K, the reaction of butadiene with toluene and *o*-xylene give 5-phenyl-2-pentene and 5-(*o*-tolyl)-2-pentene, respectively, where the latter is a precursor for 2,6-dimethylnaphthalene.

The reaction of butadiene and *o*-xylene has been commercialized using K/CaO or $\text{Na}/\text{K}_2\text{CO}_3$ at 413 K.⁵⁴ The selectivity based on butadiene is 65% and that based on *o*-xylene is approximately 93% at 30% conversion of *o*-xylene.

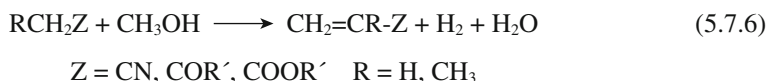
A synthetic route to 2,6-dimethylnaphthalene from *p*-xylene and 2-butene has been reported.^{55,56}



Alkylation of *p*-xylene with 2-butene was catalyzed by sodium or potassium supported on calcined hydrotalcite. The catalysts were prepared by impregnating the calcined hydrotalcite with the alkali metal dissolved in liquid ammonia. The reaction was carried out in a batch reactor at 453 K. The highest selectivity to 2-methyl-1-(*p*-tolyl)-butane was 81% based on 32% xylene conversion and 69% based on 91% butene conversion using a catalyst containing ca. 5 wt% sodium on calcined hydrotalcite.

5.7.3 Synthesis of α,β -Unsaturated Compounds from Activated Methylene Compounds and Methanol

The synthesis of α,β -unsaturated compounds can be accomplished by the reaction of methanol with an activated C-H containing compounds over metal oxides at elevated temperatures.



These types of C-C bond-forming reactions were extensively studied by Ueda and coworkers.⁵⁷⁻⁶¹ The catalysts used were MgO modified with metal ions such as Cr and Mn . Table 5.7.3 shows the results of the reaction of acetonitrile with

Table 5.7.3 Methylation of acetonitrile with methanol over MgO modified with metal ions^{a)}

Catalyst ^{b)}	Conversion/%	Selectivity/%		
		AN	PN	MAN
MgO	0.1	tr	tr	—
Al-MgO	2.5	tr	tr	—
Fe-MgO	11.2	73.2	11.6	tr
Cr-MgO	9.6	94.2	5.4	tr
Mn-MgO	9.1	96.4	2.7	0.9
Ni-MgO	5.5	2.8	33.5	tr
Cu-MgO	2.2	91.0	9.0	—

^{a)} 623 K, acetonitrile 1.3 kPa, methanol/acetonitrile = 10

^{b)} Metal ion loading: 3 wt%

AN: acrylonitrile, PN: propionitrile, MAN: methacrylonitrile

Reprinted with permission from H. Kurokawa, T. Kato, W. Ueda, Y. Morikawa, Y. Moro-oka, T. Ikawa, *J. Catal.*, **126**, 199 (1990) p.201, Table 1.

methanol.⁶⁰⁾ The reaction was carried out in a flow reactor with a methanol/acetonitrile molar ratio of 10 with 1.3 kPa of acetonitrile at 623 K. MgO has little activity. The activity developed when MgO was loaded with Cr or Mn ions (3 wt%). The main product was acrylonitrile with minor amounts of propionitrile and methacrylonitrile. Propionitrile is a hydrogenation product of acrylonitrile. Loading of Ni (1 wt%) together with Mn (2 wt%) facilitates the hydrogenation of acrylonitrile to propionitrile. Thus, at 12% conversion of acetonitrile, the main product is propionitrile (88.5% selectivity), the other products being acrylonitrile (6.7%) and methacrylonitrile (0.4%).

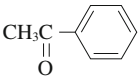
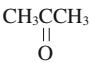
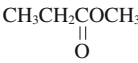
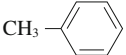
The reaction of propionitrile with methanol gives methacrylonitrile; isobutyronitrile and crotonitrile being the by-products.⁶⁰⁾ Isobutyronitrile is the hydrogenation product of methacrylonitrile and crotonitrile is the isomerization product of methacrylonitrile. The selectivity for methacrylonitrile was 97% at a propionitrile conversion of 31.5% over Mn-loaded MgO, as shown in Table 5.7.4.

Methyl methacrylate is formed from methyl propionate.⁵⁹⁾ The selectivity for methyl methacrylate was 65% at 16.7% conversion of methyl propionate over Mn-loaded MgO at 673 K. The by-products were methyl isobutyl ketone, diethyl ketone and ethyl isopropenyl ketone.

Methyl vinyl ketone is formed from acetone and methanol.⁵⁷⁾ The selectivity for methyl vinyl ketone was 55% at 12% conversion of acetone over Fe-loaded MgO. The by-products were methyl ethyl ketone, isopropyl alcohol and C₅-ketones.

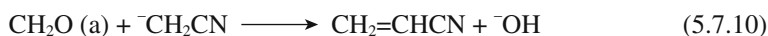
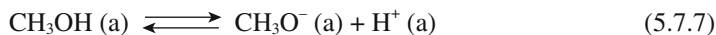
The rate of C-C bond formation is related to the acidity of the C-H bond from which hydrogen is abstracted. Table 5.7.4 shows the relation between the rates of the formation of α,β -unsaturated compounds at 625 K for six substrates over Cr/MgO and Fe/MgO and their pK_a values.⁶¹⁾ This suggests that the C-H bond cleavage is involved in the step, which affects the rate of the reaction. In the case of acetonitrile, it was shown that the kinetic isotope effect exists when CH₃OH is replaced by CD₃OH.⁶¹⁾ These results suggest that the cleavage of the C-H bonds

Table 5.7.4 The pK_a values of substrates and the reaction rates of methylation over Cr-MgO and Fe-MgO at 623 K

Reactant	pK _a ^b	Reaction rate/ $\mu\text{mol min}^{-1} \text{g-cat}^{-1}$	
		3 wt% Cr/MgO	3 wt% Fe/MgO
	19	8.2 ^c	34.9
	20	11.9	11.6
CH ₃ CN	25	3.8	4.5
CH ₃ CH ₂ CN	> 25	1.9	1.6
	> 25	0.1	–
	37	tr	tr

Reprinted with permission from H. Kurokawa, T. Kato, T. Kuwabara, W. Ueda, Y. Morikawa, Y. Moro-oka, T. Ikawa, *J. Catal.*, **126**, 208 (1990) p.210, Table 1.

of both the substrate and methanol are critical for the reaction. Kurokawa et al. propose a mechanism which is similar to the side-chain alkylation of toluene with methanol.⁶¹⁾



Methanol is dehydrogenated to formaldehyde on the surface and aldol type condensation occurs between adsorbed formaldehyde and the substrate. The cleavage of the C-H bond of the substrate occurs on the basic sites to form the anionic intermediate (⁻CH₂CN). Dehydrogenation of methanol to adsorbed formaldehyde involves both basic sites and Lewis acid sites (metal ions). The anionic intermediate reacts with adsorbed formaldehyde to form α,β -unsaturated product.

The reaction of acetonitrile with methanol on alkali cation-loaded MgO was reported.⁶²⁾ Among alkali metals, Na⁺-loaded MgO was most effective. In this case, the main product was propionitrile, the yield of acrylonitrile being low. When oxygen was fed with the reactants, acrylonitrile became the main product. The yield of acrylonitrile was 28.3% over K⁺/MgO at 673 K.

Alkylation of acetonitrile with methanol also proceeds over basic zeolites to

afford propionitrile and acrylonitrile.⁶³ The reaction over CsNaX loaded with CsOH with a CH₃OH/acetonitrile ratio of 10 at 623 K gave yields of propionitrile and acrylonitrile of 7.9% and 2.1%, respectively.

Activated carbon or carbon fibers promoted with Na⁺ ions are very active for the reaction of acetonitrile and methanol.^{64,65} The activity depends on the sodium compound used for ion exchange and the Na content of the catalyst. In the case of Na-loaded carbon fibers, the activity decays with time on stream, but the sulfur treatment of the activated carbon fibers can stabilize the exchanged Na and the catalyst decay can be reduced. The selectivity for propionitrile was about 90% at 60% acetonitrile conversion at a methanol/acetonitrile ratio of 10 at 753 K, the main by-product being 2-methylpropionitrile. The selectivity for propionitrile can be increased by lowering the conversion of acetonitrile.

5.7.4 Condensation of Alcohols (Guerbert Reaction)

The condensation of alcohols is the reaction that is used to increase the carbon number of alcohols and called the Guerbert reaction. In this reaction a primary or secondary alcohol reacts with itself or another alcohol to produce a higher alcohol.

Ueda et al. reported that methanol is condensed with other primary alcohols having a methyl or methylene group at the β -position.^{66,67}



MgO was most active for the reaction and yielded the higher alcohol in high selectivity (> 80%) (Table 5.7.5). At 653 K with feed ratio of N₂ : ethanol : methanol = 10 : 0.15 : 3, the conversion of ethanol was 50%. The products were propanol (35.7%), isobutyl alcohol (40.3%), acetaldehyde (8.0%), propanal (2.6%) and butanal (3.9%). In the reaction of methanol with propanol, butanol and isobutyl alcohol, the main products were isobutyl alcohol, 2-methylbutyl alcohol and 2,2-dimethylbutyl alcohol with selectivity of 82.5%, 78.5% and 86.0% at conversions of 48.3%, 60.2% and 50.2%, respectively. The authors suggested a mechanism in which the dehydrogenation of alcohols to aldehydes and cross aldol condensation between the aldehydes followed by rapid hydrogen transfer to the condensation product from methanol.

Table 5.7.5 Condensation of alcohols with methanol over MgO at 653 K

Reactant(C _n H _{2n+1} OH)	Conversion of C _n H _{2n+1} OH/%	Selectivity(%)to ^{a)}				
		C _{n-1} H _{2n-1} CHO	C _{n+1} H _{2n+3} OH	C _n H _{2n+1} CHO	C _{n+2} H _{2n+3} OH	C _{n+1} H _{2n+3} CHO
2 ethanol	50.3	8.0	35.7	2.6	40.3	3.9
3 1-propanol	48.3	6.7	82.5	7.3	—	—
4 1-butanol	60.2	6.1	78.5	8.2	—	—
5 1-pentanol	50.2	2.5	86.0	3.1	—	—

^{a)} Condensation products are 2-methyl form.

Reprinted with permission from W. Ueda, T. Ohshida, T. Kuwabara, Y. Morikawa, *Catal. Lett.*, **12**, 97 (1992) p.99, Table 1.

NaX zeolite loaded with Na_2CO_3 are also active for the reaction of methanol with primary alcohols, though NaX itself is inactive, indicating the necessity of the strong bases for the reactions.⁶⁸⁾

$\text{MgO-Al}_2\text{O}_3$ mixed oxides (calcined hydrotalcite) is not active for the reaction of methanol with propanol. On the other hand, $\text{CuO-MgO-Al}_2\text{O}_3$ mixed oxides prepared from hydrotalcite-like materials are active for the condensation.⁶⁹⁾ The selectivity for isobutyl alcohol is 79.3% at 100% conversion of propanol at 573 K. In this case, the copper component seemingly serves as hydrogenation/dehydrogenation catalyst. The aldol condensation between propanol and formaldehyde proceeds over the basic sites of the catalyst.

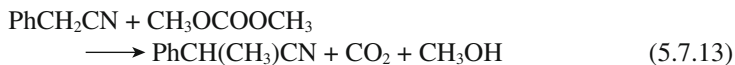
Yang and Meng reported that Rb^+ -impregnated LiX and NaX were active for the reaction of ethanol to butanol.⁷⁰⁾ Over LiX and NaX, no butanol was formed. At 693 K, selectivity for butanol was about 40% over Rb^+ -loaded LiX. When crotonaldehyde was added to the feed, the yield of 1-butanol fell to zero. From this fact, the authors concluded that crotonaldehyde, a condensation product of acetaldehyde, cannot be the intermediate for butanol. Instead, they proposed a mechanism in which one molecule of ethanol is activated at the C-H bond at the β -position and condenses with another molecule of ethanol by the elimination of one molecule of water.

Nodou and Coville carried out the reaction of ethanol over various metal oxides.⁷¹⁾ Only MgO was active for butanol formation. The selectivity for butanol was 33% at 56% conversion on ethanol at 723 K. From the results with addition of acetaldehyde or crotonaldehyde to the feed, they also denied the aldol condensation pathway and supported the mechanism proposed by Yang and Meng. The same authors reported the reaction of propanol over MgO.⁷²⁾ The main products were 2-methylpentanol and propanal. The selectivity for 2-methylpentanol was about 50% at the conversion of 30% at 723 K. In this case, the authors proposed a mechanism involving aldol condensation of propanal.

Nonstoichiometric hydroxyapatite was reported to be effective for the conversion of ethanol into butanol.⁷³⁾ Over hydroxyapatite with $\text{Ca/P} = 1.61$, 76.3% selectivity for butanol was obtained at an ethanol conversion of 14.7% at 573 K. Among the by-products, C_6 -alcohols were most predominant (8.6% selectivity). At 673 K, ethanol conversion increased to 57.4%, the selectivity for butanol, C_6 -alcohols and C_{10} -alcohols were 44.8%, 13.7%, and 4.1%, respectively. At the higher temperature of 763 K, ethanol gives gasoline with a RON of 99, comprised chiefly of hydrocarbons from C_6 to C_{10} as well as oxygenates.⁷⁴⁾ The gasoline synthesis involves the Guebert reaction, the Lebedev reaction, and dehydration and dehydrogenation of branched alcohols.

5.7.5 Alkylation of Nitriles (C-Alkylation)

In the alkylation of acetonitrile, Tundo and coworkers found that α -methylation of acetonitrile proceeded selectively using dimethyl carbonate (DMC) as an alkylating agent.^{75,76)}



Under the gas-liquid phase-transfer conditions at 453 K, by sending a mixture of DMC and phenylacetonitrile (PAN) or (*p*-isobutylphenyl)acetonitrile in a 1 : 4 molar ratio on a catalyst bed of 100 g, the corresponding 2-phenylpropionitrile was obtained with 90% selectivity at > 95% conversion. The catalyst was 5% PEG 6000 and 5% K₂CO₃ supported on Al₂O₃. The reaction also proceeds with K₂CO₃ in an autoclave.⁷⁵⁾ From kinetic studies, Tundo et al. proposed a mechanism involving the methoxycarbonylation as the first step of the reaction.⁷⁶⁾

Fu and Ono studied the gas-phase methylation of PAN with methanol and DMC over alkali cation-exchanged faujasites.⁷⁷⁾ In the case of alkylation with methanol, among X-type zeolites, the order of initial activity was CsX > RbX > NaX > LiX. The activity of CsX was higher than CsY. These orders of the activities are consistent with the order of base strength. These facts indicate that the methylation is promoted by the basic sites of faujasites. Stable activity of CsX was observed up to 633 K, but the activity decayed over 648 K with time on stream. A 27% yield of 2-phenylpropionitrile was obtained at 623 K. The conversion of PAN was much higher in the alkylation with DMC than with methanol. In the alkylation with DMC, the activities of stronger basic zeolites such as CsY and CsX decayed with time on stream. Stable activity was observed with NaY, plausibly because of weaker adsorption of CO₂, one of the products. Over NaY, a 72% yield of 2-phenylpropionitrile was obtained over NaY at 533 K.

Selective monomethylation of PAN with DMC can be achieved with 3-aminopropyl-functionalized MCM-41 in an autoclave.⁷⁸⁾ The catalyst was more active than alkali ion-exchanged MCM-41. A 92% selectivity for 2-phenylpropionitrile was obtained at 98.4% conversion of PAN in 10 h at 453 K.

A very efficient α -alkylation of nitriles with primary alcohols was reported with Ru- and Pd-loaded hydrotalcite.⁷⁹⁾ While Ru-loaded hydrotalcite gives high activity, the alkylation hardly occurs at all in the presence of hydrotalcite or RuCl₃. The synergy of basic sites and Ru species is considered to be the origin of the Ru-loaded hydrotalcite (section 6.6.2). The Ru-loaded hydrotalcite catalyst is also active for alkylation of carbonyl compounds. Thus acetophenone reacts with benzyl alcohol to afford 1,3-diphenyl-1-propanone.

5.7.6 *N*-Alkylation Reactions

A. Alkylation of aniline with methanol

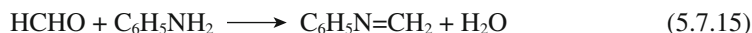
The gas-phase alkylation of aniline with methanol has been studied by many authors. In general, acidic catalysts give mainly *C*-alkylation products, while basic catalysts give mainly *N*-alkylation products.

The reaction of aniline with methanol or dimethyl ether over alumina was reported by Evans and Bourns.⁸⁰⁾ In both cases, the main alkylation product was *N,N*-dimethylaniline. At 560 K, a 95.5% yield of *N,N*-dimethylaniline was obtained in the alkylation with methanol at a methanol-to-aniline molar ratio of

10. The rest of the products was *N*-methylaniline. The reaction of aniline with dimethyl ether gave a 99% yield of *N,N*-dimethylaniline at an ether-to-aniline molar ratio of 5 at 548–573 K. Alkylation of aniline with methanol over γ -Al₂O₃ was also studied by Ko et al.⁸¹⁾ *N*-Methylation was a predominant reaction with a selectivity higher than 98% in the temperature range of 573–698 K. *N*-Methylaniline reacts faster than aniline. At 623 K, the selectivities for *N*-methylaniline and *N,N*-dimethylaniline were 64.2% and 35.7%, respectively, at an aniline conversion of 34.5%. The FT-IR study revealed that both aniline and methanol were adsorbed nondissociatively on the Lewis acid-base dual sites of γ -Al₂O₃.

Chen et al. studied the alkylation over ZSM-5 zeolites.⁸²⁾ The ratio of *N*-alkylation to *C*-alkylation depends on the acidic and basic properties of the zeolites. Thus the ratios over H-ZSM-5, Na-ZSM-5 and CsH-ZSM-5 were 3.06, 3.21 and 9.53, respectively, at 623 K. The ratio further increases to 20.41 over Cs₂O-loaded Na-ZSM-5. The alkylation over faujasite type zeolites exchanged with alkali cations was studied at 673 K by Su and Barthomeuf.⁸³⁾ The more basic zeolites (X and Y zeolites exchanged with K, Rb, Cs) favor the production of *N*-alkylates, while the more acidic zeolites (Li, Na) give rise to *C*-alkylation (*p*- and *o*-toluidine, 2,4- and 2,6-dimethylaniline and *N,N*-dimethyl-*p*-toluidine). The more basic zeolites display considerable aging probably because of anionic polymerization which poisons the active sites.

Ivanova et al. studied the alkylation over HY and CsNaY loaded with CsOH by ¹³C NMR. In the case of HY, methoxyl groups are the intermediates in *N*-alkylation.⁸⁴⁾ For both catalysts, *N*-methylaniline was a primary product. CsNa-Y loaded with CsOH gave higher selectivity and formaldehyde was suggested to be the intermediate in this case. The following scheme was proposed for *N*-methylation.



On CsOH/CsNaY, aniline conversion was 99% with a selectivity to *N*-methylaniline of 98.7% at 673 K.⁸⁵⁾

The alkylation of aniline with methanol over MgO-Al₂O₃ mixed oxide (calcined hydrotalcite) is unique, for *N*-methylaniline is a single product.⁸⁶⁾ The best results were obtained with a methanol/aniline ratio of 7 over the mixed oxide with Mg/Al = 4. The conversion of aniline was 68% at 678 K. The absence of dimethylated products was attributed to the steric effect of the N-atom site of *N*-methylaniline. Gasification of methanol was totally absent.

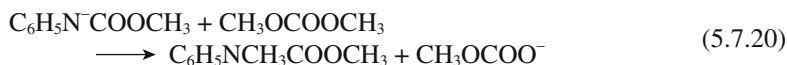
Various magnesium phosphates were studied as catalysts for the alkylation of aniline with methanol.⁸⁷⁾ The catalysts gave *N*-methylaniline and *N,N*-dimethylaniline only. At 623 K, magnesium pyrophosphate is about 68% selective for *N*-methylaniline with about 45% conversion.

B. *N*-Alkylation of anilines with alkyl carbonates

Tundo et al. reported that mono-*N*-alkylation of aniline proceeds selectively by using dimethyl carbonate (DMC) under gas-liquid phase transfer catalysts in a continuous flow process.⁸⁸⁾



The catalysts used were K_2CO_3 coated with 5 wt% of PEG 6000 or α -alumina coated with 5 wt% of K_2CO_3 and 5 wt% PEG 6000. At 453 K, the product yields were 40.8% $\text{C}_6\text{H}_5\text{NHCH}_3$, 1.6% $\text{C}_6\text{H}_5\text{N}(\text{CH}_3)_2$ and 3.3% $\text{C}_6\text{H}_5\text{NCH}_3\text{COOCH}_3$. The authors proposed the following mechanism with the intermediacy of a methoxy-carbonylated product.



Fu and Ono found that *N*-methylation of aniline with DMC selectively proceeded over alkali cation-exchanged faujasite in gas phase.⁸⁹⁾ The methylation with DMC occurs at a much lower temperature than that with methanol. The ratio of the products, *N*-methylaniline and *N,N*-dimethylaniline, depends on the catalyst used and the reaction conditions. Fig. 5.7.6 shows the change in the conversion of aniline and the yields of *N*-methylaniline and *N,N*-dimethylaniline as a function of contact time, W/F , where W and F stand for the weight of the catalyst and total flow rate (aniline + DMC + N_2), over KY with DMC/aniline ratio of 1.25 at 453 K. Under the reaction conditions, the selectivity for *N*-methylaniline was very high. At $W/F = 2.08 \text{ g h mol}^{-1}$, the selectivity for *N*-methylaniline was 93.5% at 99.6% conversion of aniline. On the other hand, the selectivity for *N,N*-dimethylaniline was 96% with a 100% conversion of aniline over NaX with a DMC/aniline ratio of 2.5 and $W/F = 5.92$ at 513 K. K-EMT is as selective as K-Y for the formation of *N*-methylaniline.⁹⁰⁾

The mono-*N*-alkylation of anilines including *p*-nitro-, *p*-cyano- and *o*-methoxy-aniline with DMC proceeded smoothly also in liquid phase in the presence of NaY at 393–423 K.⁹¹⁾ The formation of *N*-methylanilines takes place with a selectivity of 92–98%, at conversion of 72–93%. Alkylation of functionalized anilines such as aminophenols, aminobenzyl alcohols, aminobenzoic acids and aminobenzamides with DMC proceeds chemoselectively over NaY.⁹²⁾ The reaction proceeds with the exclusive formation of *N*-methylanilines without any concurrent *O*-methylation or *N/O*-methoxycarbonylation reactions. Besides DMC, various

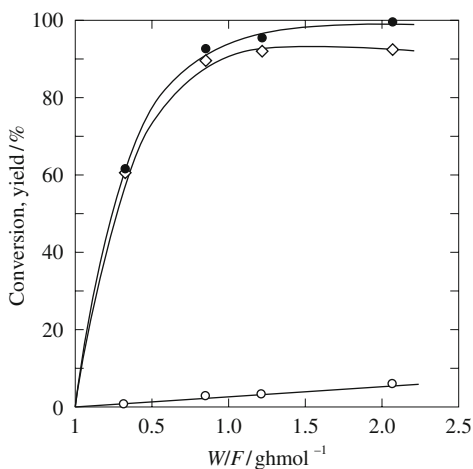


Fig. 5.7.6 Change in the conversion of aniline and the selectivity for *N*-methylaniline with contact time in the methylation of aniline with dimethyl carbonate over KY.

(●) aniline conversion, (◇) yield of *N*-methylaniline and (○) yield of *N,N*-dimethylaniline.

Reprinted from Z. Fu, Y. Ono, *Catal. Lett.*, **22**, 277 (1993) p.280, Fig.1.

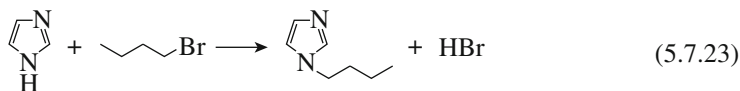
dialkylcarbonates (ROCOOR) are effective for selective mono-*N*-alkylation of anilines in the presence of NaY. Thus mono-*N*-alkylated products are obtained by alkylation of aniline with dialkylcarbonates with R = Et, benzyl and allyl, in 84–94% yields. *p*-Cl- and *p*-NO₂-aniline are also *N*-methylated.

C. *N*-Alkylation of amines with alkyl halides

N-Alkylation of amines by alkyl halides such as benzyl bromide and hexyl bromide proceeds selectively in acetonitrile in the presence of K⁺-loaded Al₂O₃ as a catalyst.⁹³⁾ The catalyst was prepared as follows: 26 g of KNO₃, and 74 g of Al₂O₃ were crushed in a mortar, then water, which can be adsorbed by Al₂O₃, was added. After grinding, the mixture was dried at 383 K for 1 h, then activated at 873 K for 3 h. For example, alkylation of piperidine with benzyl bromide and hexyl bromide gave the corresponding *N*-alkylation products in 85% and 90% yields, respectively, in 4 h at 303 K.

Alkylation of imidazole with alkyl halides in the presence of alkali cation-exchanged carbon gives selectively 1-alkylimidazole.^{94,95)} The activity depends on the cation exchanged, the order of activity being Na⁺ < K⁺ < Cs⁺. In every case, *N*-alkylation occurs exclusively. The conversion changes with alkyl halide, the order of reactivity is: 1-bromobutane > 2-bromobutane ≫ 1-bromohexane.

In the reaction of imidazole with butyl bromide, the yield of 1-butyylimidazole was 70–75% at 333 K. The product, HBr, possibly is adsorbed on the basic sites and reduces the catalytic activity, since the rate significantly decreases at high conversion levels.



The reaction was enhanced by ultrasound irradiation. Under ultrasound irradiation, the conversion reached 90% with 100% selectivity in 120 min at 313 K, while the conversion was 53.4% without ultrasound irradiation.

Cs⁺ ion-exchanged carbon is also active for *N*-alkylation of imidazole with 2-propynyl bromide.⁹⁶⁾ The imidazole conversion is 33% at 333 K in 60 min. The rate of the reaction is greatly enhanced by microwave irradiation. Under microwave irradiation of 300 W, the conversion reaches 83% with > 99% selectivity in 3 min. The alkylation of imidazole also proceeds with long-chain alkyl bromides (C_nH_{2n+1} Br, n = 9, 10, 12) over alkali-loaded carbons.⁹⁷⁾ The reactions are enhanced greatly by microwave irradiation.⁹⁷⁾

D. *N*-Alkylation of benzylamine with dimethyl carbonate

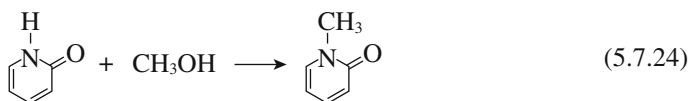
Benzylamine can be *N*-alkylated with dimethyl carbonate (DMC) or CH₃OCO(CH₂)₂O(CH₂)₂OCOCH₃ in the presence of alkali cation-exchanged Y-zeolites.⁹⁸⁾ Though *N*-methylation selectivity is high, the ratio of the products, *N*-methylbenzylamine and *N,N*-dimethylamine, depends on the conversion of aniline. In the alkylation with DMC in the presence of NaY for 22 h at 363 K, the conversion of aniline was 67%, the yields of *N*-methylbenzylamine and *N,N*-dimethylbenzylamine being 42% and 20%, respectively.

E. *N*-alkylation of heterocyclic compounds with alcohols

N-Alkylation of imidazole with methanol proceeds in the gas phase. MgO-Al₂O₃ mixed oxides (calcined hydrotalcite, Al/Mg = 2) are reported to be effective catalysts for alkylation of imidazole with methanol and ethanol.^{99,100)} The mixed oxide affords 97.4% selectivity for 1-methylimidazole at 93.0% conversion of imidazole at 613 K.¹⁰⁰⁾ It is proposed that methanol and imidazole are activated by the acidic and basic sites, respectively.^{99,100)}

Selective *N*-alkylation of imidazoles and pyrazoles with alcohols also proceeds in the gas phase with use of acidic zeolites as catalysts.¹⁰¹⁻¹⁰³⁾ Thus 100% yield of 1-methylimidazole and 1-methylpyrazole are obtained over H-Y in the reaction of methanol with imidazole (at 553 K) and pyrazole (at 573 K), respectively,

Vapor-phase reaction of pyridine-2-one with methanol over Al₂O₃ proceeds to selectively afford 1-methylpyridine-2-one.¹⁰⁴⁾ Thus 1-methylpyridine-2-one was obtained in 99% selectivity at 100% conversion of 2-pyridinone at 573 K.



5.7.7 *S*-Methylation of Thiols with Dimethyl Carbonate (*S*-Alkylation)

The reactions of dimethyl carbonate with *o*- and *p*-mercaptophenols and *o*- and *p*-mercaptobenzoic acids in the presence of NaY give chemoselectively *S*-methylated products.¹⁰⁵⁾ For example, the reaction of dimethyl carbonate with *o*-mercaptophenol for 13 h at 423 K gives 2-hydroxythioanisole in 94% yield, the rest of the product is the disulfide (6%).

References

1. T. Kotanigawa, M. Yamamoto, K. Shimokawa, Y. Yoshida, *Bull. Chem. Soc. Jpn.*, **44**, 1961 (1971).
2. H. Grabowska, J. Jabliński, W. Miśta, J. Wrzyszczyk, *Res. Chem. Intermed.*, **22**, 53 (1996).
3. T. Kotanigawa, K. Shimokawa, *Bull. Chem. Soc. Jpn.*, **47**, 1535 (1974).
4. F. Nozaki, I. Kimura, *Bull. Chem. Soc. Jpn.*, **50**, 614 (1977).
5. A. R. Gandhe, J. B. Fernandes, *Catal. Commun.*, **5**, 89 (2004).
6. A. R. Gandhe, J. B. Fernandes, S. Varma, N. M. Gupta, *J. Mol. Catal.*, **238**, 63 (2005).
7. K. Tanabe, T. Nishizaki, *Proc. 6th Intern. Congr. Catal.*, 1956, London, 1977, p. 863.
8. S. Velu, C. S. Swamy, *Appl. Catal.*, A, **119**, 241 (1994).
9. S. Velu, C. S. Swamy, *Appl. Catal.*, A, **145**, 141 (1996).
10. S. Velu, C. S. Swamy, *Appl. Catal.*, A, **162**, 81 (1997).
11. T. Kotanigawa, *Bull. Chem. Soc. Jpn.*, **47**, 950 (1974).
12. Durgakumari, G. Sreekanth, S. Narayanan, *Res. Chem. Intermed.*, **14**, 223 (1990).
13. S. C. Lee, S. W. Lee, K. S. Kim, T. J. Lee, D. H. Kim, J. C. Kim, *Catal. Today*, **44**, 253 (1998).
14. R. Bal, S. Sivasanker, *Appl. Catal.*, A, **246**, 373 (2003).
15. P. Tundo, F. Trotta, G. Moragin, F. Ligorati, *Ind. Eng. Chem. Res.*, **27**, 1565 (1988).
16. Z. Fu, Y. Ono, *Catal. Lett.*, **21**, 43 (1993).
17. M. D. Romero, G. Ovejero, A. Rodriguez, J. M. Gómez, I. Águeda, *Ind. Eng. Chem. Res.*, **43**, 8194 (2004).
18. G. Wu, X. Wang, B. Chen, J. Lin, N. Zhao, W. Wei, Y. Sun, *Appl. Catal.*, A, **329**, 106 (2007).
19. S. Velu, C. S. Swamy, *Catal. Lett.*, **40**, 265 (1996).
20. S. Sato, R. Takahashi, T. Sodezawa, K. Matsumoto, Y. Kamimura, *J. Catal.*, **184**, 180 (1999).
21. S. Porchet, S. Su, R. Doepper, A. Renken, *Chem. Eng. Technol.*, **17**, 108 (1994).
22. R. Bal, B. B. Tope, S. Sivasanker, *J. Mol. Catal.*, A, **181**, 161 (2002).
23. Y. Fu, T. Baba, Y. Ono, *Appl. Catal.*, A, **106**, 419 (1998).
24. Y. Fu, T. Baba, Y. Ono, *Appl. Catal.*, A, **106**, 425 (1998).
25. Y. Fu, T. Baba, Y. Ono, *Appl. Catal.*, A, **175**, 201 (1998).
26. Y. Fu, T. Baba, Y. Ono, *Appl. Catal.*, A, **178**, 219 (1998).
27. T. M. Joythi, T. Raja, M. B. Talawar, B. S. Rao, *Appl. Catal.*, A, **211**, 41 (2001).
28. M. Vijayaraj, C. S. Gopinath, *J. Catal.*, **243**, 376 (2006).
29. R. Bal, K. Chaudhari, S. Sivasanker, *Catal. Lett.*, **70**, 75 (2000).
30. Y. N. Sidorenko, P. N. Galich, V. S. Gutyrva, V. G. Ill'in, I. E. Niemark, *Dokl. Akad. Nauk SSR*, **173**, 132 (1967).
31. T. Yashima, K. Sato, T. Hayasaka, N. Hara, *J. Catal.*, **26**, 303 (1972).
32. M. L. Unland, G. E. Baker, in: *Catalysis in Organic Reactions* (W. R. Moser, ed.) Marcel Dekker, New York, Basel, 1981, p.51.
33. W. S. Wieland, R. J. Davis, J. M. Garces, *Catal. Today*, **28**, 443 (1996).
34. W. S. Wieland, R. J. Davis, J. M. Garces, *J. Catal.*, **173**, 490 (1998).
35. H. Itoh, A. Miyamoto, Y. Murakami, *J. Catal.*, **64**, 284 (1980).
36. H. Itoh, T. Hattori, K. Suzuki, A. Miyamoto, Y. Murakami, *J. Catal.*, **72**, 170 (1981).
37. H. Itoh, T. Hattori, K. Suzuki, Y. Murakami, *J. Catal.*, **79**, 21 (1983).
38. C. Lacroix, A. Deluzarche, A. Kiennemann, A. Bayer, *Zeolites*, **4**, 109 (1984).
39. J. Engelhardt, J. Sznyl, J. Valyon, *J. Catal.*, **107**, 296 (1987).
40. X. Wang, G. Wang, D. Shen, C. Fu, M. Wei, *Zeolites*, **11**, 254 (1991).
41. M. L. Unland, *J. Phys. Chem.*, **82**, 580 (1978).
42. S. T. King, J. M. Garces, *J. Catal.*, **104**, 59 (1987).

43. A. E. Palomerias, G. Eder-Mirth, J. A. Lercher, *J. Catal.*, **168**, 442 (1997).
44. M. D. Sefcik, *J. Am. Chem. Soc.*, **101**, 2164 (1979).
45. M. Hunger, U. Schenk, J. Weitkamp, *J. Mol. Catal., A*, **134**, 97 (1998).
46. H. Kashiwagi, S. Enomoto, *Chem. Pharm. Bull.*, 404 (1982).
47. G. Madhavi, S. J. Kulkarni, K.V.V.S.B.S.R. Murthy, V. Viewanathan, K. V. Raghavan, *J. Porous Mater.*, **14**, 433 (2007).
48. G. Madhavi, S. J. Kulkarni, K.V.V.S.B.S.R. Murthy, V. Viewanathan, K. V. Raghavan, *Appl. Catal., A*, **246**, 265 (2003).
49. G. Madhavi, S. J. Kulkarni, K. V. Raghavan, *J. Porous Mater.*, **14**, 379 (2007).
50. L. R. Martenes, W. J. Vermeiren, D. R. Huybrechts, P. J. Grobet, P. J. Jacobs, *Proc. 9th Int. Congr. Catal.*, 1988, Vol. 1, p. 420.
51. G. Suzukamo, M. Fukao, T. Hibi, K. Tanabe, K. Chikaishi, in: *Acid-Base Catalysis*, (K. Tanabe, H. Hattori, T. Yamaguchi, T. Tanaka, eds.) Kodansha Tokyo and VCH, Weinheim, 1989, p.405.
52. M. G. Stevens, M. R. Anderson, H. C. Forey, *Chem. Commun.*, **1999**, 413.
53. C. G. Eberhardt, H. Peterson, *J. Org. Chem.*, **30**, 82 (1965).
54. K. Tanabe, W. F. Hölderich, *Appl. Catal., A*, **161**, 399 (1999).
55. *Chemtech*, May, 23 (1997).
56. T. Matsumoto, S. Nishikawa, F. Kumata, US Patent 5 608 132 (1997).
57. W. Ueda, T. Yokoyama, Y. Moro-oka, T. Ikawa, *J. Chem. Soc., Chem. Commun.*, **1984**, 39.
58. W. Ueda, T. Yokoyama, Y. Moro-oka, T. Ikawa, *Ind. Eng. Chem. Res.*, **24**, 340 (1985).
59. W. Ueda, H. Kurokawa, Y. Moro-oka, T. Ikawa, *Chem. Lett.*, **14**, 819 (1985).
60. H. Kurokawa, T. Kato, W. Ueda, Y. Morikawa, Y. Moro-oka, T. Ikawa, *J. Catal.*, **126**, 199 (1990).
61. H. Kurokawa, T. Kato, T. Kuwabara, W. Ueda, Y. Morikawa, Y. Moro-oka, T. Ikawa, *J. Catal.*, **126**, 208 (1990).
62. J. M. Hur, H.-Y. Coh, H.-I. Lee, *Catal. Today*, **63**, 189 (2000).
63. T. Sooknot, J. Dwyer, *J. Mol. Catal., A*, **211**, 155 (2004).
64. F. Wang, T. Tsai, W.-B. Lin, *Catal. Lett.*, **73**, 215 (2001).
65. F. Wang, C. Hwang, *Appl. Catal., A*, **276**, 9 (2004).
66. W. Ueda, T. Kuwabara, T. Ohshida, Y. Morikawa, *J. Chem. Soc., Chem. Commun.*, **1990**, 1558.
67. W. Ueda, T. Ohshida, T. Kuwabara, Y. Morikawa, *Catal. Lett.*, **12**, 97 (1992).
68. K. Gotoh, S. Nakamura, T. Mori, Y. Morikawa, *Stud. Surf. Sci. Catal.*, **130**, 2669 (2000).
69. C. Carlini, M. Marchionna, M. Noviello, A. M. R. Galetti, G. Sbrana, F. Bassila, A. Vaccardi, *J. Mol. Catal., A*, **232**, 13 (2005).
70. C. Yang, Z. Meng, *J. Catal.*, **142**, 37 (1993).
71. A. S. Nodou, N. J. Coville, *J. Catal.*, **142**, 37 (1993).
72. A. S. Nodou, N. J. Coville, *Appl. Catal., A*, **275**, 103 (2004).
73. T. Tsuchida, S. Sakuma, T. Takeguchi, W. Ueda, *Ind. Eng. Chem. Res.*, **45**, 8634 (2006).
74. T. Tsuchida, T. Yoshioka, S. Sakuma, T. Takeguchi, W. Ueda, *Ind. Eng. Chem. Res.*, **47**, 1443 (2008).
75. P. Tundo, M. Selva, *ACS Symp. Ser.*, **626**, 81 (1996).
76. P. Tundo, M. Selva, A. Perosa, S. Memoli, *J. Org. Chem.*, **67**, 1071 (2002).
77. Z.-H. Fu, Y. Ono, *J. Catal.*, **145**, 166 (1994).
78. C. Venakatesan, A. P. Singh, *Catal. Lett.*, **80**, 7 (2002).
79. K. Motokura, N. Fujita, T. Mizugaki, K. Ebitani, K. Jitsukawa, K. Kaneda, *Chem. Eur. J.*, **12**, 8228 (2006).
80. T. H. Evans, A. N. Bourns, *Canad. J. Technol.*, **29**, 1 (1951).
81. A. -N. Ko, C. -L. Yang, W. -d. Zhu, H. -e. Lin, *Appl. Catal., A*, **134**, 53 (1996).
82. P. Y. Chen, H. C. Chen, H. Y. Chung, T. K. Chuang, *Stud. Surf. Sci. Catal.*, **28**, 739 (1986).
83. B. L. Su, D. Barthomeuf, *Appl. Catal., A*, **124**, 73 (1995).
84. I. I. Ivanova, E. B. Pomakhina, A. I. Rebrov, W. Wang, M. Hunger, J. Weitkamp, *Kinet. Catal.*, **44**, 701 (2003).
85. I. I. Ivanova, O. A. Ponomoreva, E. B. Pomakhina, E. E. Knyazeva, V. V. Yuschenko, M. Hunger, J. Weitkamp, *Stud. Surf. Sci. Catal.*, **142**, 659 (2002).
86. J. Santhanalakshmi, T. Raja, *Appl. Catal., A*, **147**, 69 (1996).
87. M. Ángeles, A. Aramendía, V. Borau, C. Jiménez, J. M. Marinas, F. J. Romero, *Appl. Catal., A*, **183**, 74 (1999).
88. F. Tundo, P. Tundo, G. Moraglio, *J. Org. Chem.*, **52**, 1500 (1987).
89. Z. Fu, Y. Ono, *Catal. Lett.*, **22**, 277 (1993).
90. P. R. Hari Prasad Rao, P. Massiani, D. Barthomeuf, *Catal. Lett.*, **31**, 115 (1995).
91. M. Selva, M. Bomben, P. Tundo, *J. Chem. Soc., Perkin Trans., 1*, **1997**, 1041.

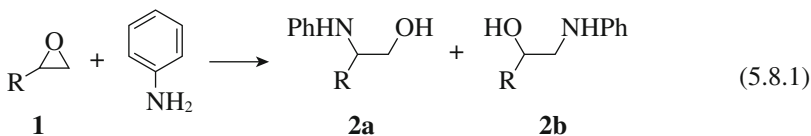
92. M. Selva, P. Tundo, A. Perosa, *J. Org. Chem.*, **68**, 7374 (2003).
93. M. B. Gawande, S. S. Deshpande, J. R. Satan, R. V. Jayaram, *Catal. Commun.*, **8**, 576 (2007).
94. J. M. López-Pestana, J. Díaz-Terán, M. J. Avila-Rey, M. L. Rojas-Cervantes, R. M. Martin-Aranda, *Micropor. Macropor. Mater.*, **67**, 87 (2004).
95. J. M. López-Pestana, M. J. Avila-Rey, R. M. Martin-Aranda, *Green Chem.*, **4**, 628 (2002).
96. V. Calvino-Casilda, A. J. López-Peinado, J. L. G. Fierro, R. M. Martin-Aranda, *Appl. Catal., A*, **240**, 287 (2000).
97. V. Calvino-Casilda, R. M. Martin-Aranda, A. J. López-Peinado, *Catal. Lett.*, **129**, 281 (2008).
98. M. Selva, P. Tundo, A. Perosa, *J. Org. Chem.*, **67**, 9238 (2002).
99. J. Santhanalakshmi, T. Rao, *Bull. Chem. Soc. Jpn.*, **70**, 2829 (1997).
100. H. Grabowska, M. Zawadzki, L. Syper, W. Mišta, *Appl. Catal., A*, **292**, 208 (2005).
101. Y. Ono, Y. Izawa, Z. Fu, *J. Chem. Soc., Chem. Commun.*, 9 (1995).
102. Y. Ono, Z. Fu, Y. Izawa, *Stud. Surf. Sci. Catal.*, **94**, 697 (1995).
103. Y. Ono, Y. Izawa, Z. Fu, *Catal. Lett.*, **47**, 251 (1997).
104. M. Okamoto, M. Tanaka, Y. Ono, *Catal. Lett.*, **46**, 123 (1997).
105. M. Selva, P. Tundo, *J. Org. Chem.*, **71**, 1464 (2006).

5.8 Addition Reactions

5.8.1 Addition to Epoxides

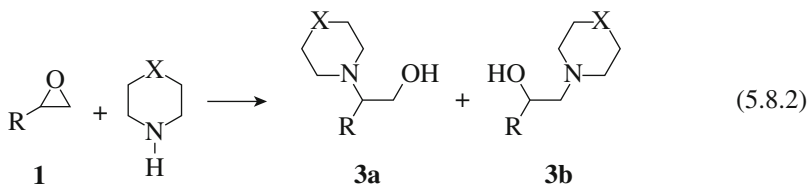
Nucleophilic ring opening of epoxides is very useful in organic synthesis because it gives 1,2-difunctional systems. Posner and Rogers reported that γ -alumina promotes selective opening of epoxides by alcohols or amine.¹⁾ In these cases, however, a relatively large amount of “catalysts” were used to promote the reactions.

The reactions of epoxides with amines were studied using a variety of zeolites.^{2,3)} Among the zeolites studied, NaY was the most effective and the addition products were obtained in high yields even at room temperature. The regioselectivity of the ring opening of unsymmetrical epoxides **1** with aniline depends on the substituents.

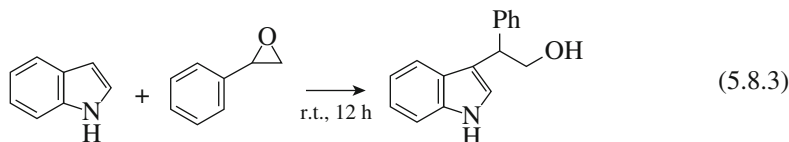


When R is alkyl (CH_3 , $n\text{-C}_4\text{H}_9$, $n\text{-C}_6\text{H}_{13}$), the product **2b** is predominant, but when R is phenyl, the predominant product is **2a**.

In the reaction of epoxides (R = $n\text{-C}_6\text{H}_{13}$, phenyl) with piperidine (X = N) or morpholine (X = O), the main products were **3b** for both substituents.³⁾

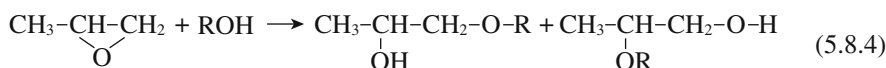


Alkylation of indoles with epoxides are catalyzed by nanocrystalline TiO_2 ($500 \text{ m}^2 \text{ g}^{-1}$) to afford 3-alkyl indole derivatives with good to high regioselectivity,⁴⁾ Thus treatment of indole with styrene oxide resulted in the formation of 2-(3-indolyl)-2-phenylethanol in 64% using 10 mol% nano TiO_2 .



CaO and MgO are effective for nucleophilic ring opening of epoxides with Me_3SiCN . The reactions are described in 6.4.2.

Hattori et al. studied the catalytic activities of a series of solid bases including alkaline earth oxides for ring opening of propylene oxide with alcohols at 323 K .⁵⁾



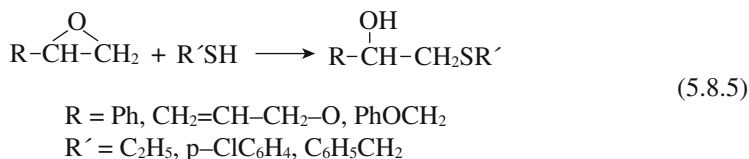
Alkaline earth oxides were effective, but $\text{KF/Al}_2\text{O}_3$ and alkaline earth hydroxides scarcely showed activity. Reactivities of alcohols with propylene oxide were in the order, methanol > ethanol > 2-propanol > 2-methyl-2-propyl alcohol (no reaction).

The reaction of propylene oxide with methanol over X- and Y-type zeolites ion-exchanged with alkali cations, CH_3NH_3^+ (Me_1N) and $(\text{CH}_3)_4\text{N}^+$ (Me_4N) ions were examined by Martins et al. at 413 K .⁶⁾ The order of conversion after 5 h was $\text{Me}_1\text{N-Y}$ (90.7%) \sim $\text{Me}_1\text{N-X}$ (90.6%) > CsX (72.3%) > NaX (67.5%) \sim $\text{Me}_4\text{N-X}$ (66.1%) > $\text{Me}_4\text{N-Y}$ (47.7%) > CsY (41.2%) > NaY (39.4%). The order of selectivity (ratio of 1-methoxy-2-propanol to 2-methoxy-1-propanol) was $\text{Me}_1\text{N-X}$ (11.0) > $\text{Me}_1\text{N-Y}$ (9.1) > CsX (8.1) > NaX (7.6) > $\text{Me}_4\text{N-X}$ (6.4) > $\text{Me}_4\text{N-Y}$ (3.4) \sim NaY (3.4) \sim CsY (3.2) > HY (0.9). It is known that the bond preferentially opens at the less hindered position, leading to mostly secondary alcohols in basic catalysis. Acid catalysts provide a mixture of secondary and primary alcohols. Thus these findings indicate that CH_3NH_3^+ -exchanged X- and Y-zeolites are highly basic catalysts.

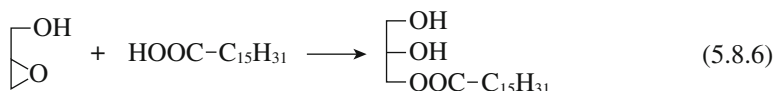
The reaction of propylene oxide with methanol occurred in the presence of four kinds of amines tethered to silica. The amines with moderate basic strength such as ethylene diamine moieties were the most active. A 100% conversion of propylene oxide with 84.1% isomer selectivity for 1-methoxy-2-propanol was obtained at 403 K .⁷⁾ The reaction of propylene oxide and methanol over MgO , CaO , Al_2O_3 and $\text{MgO-Al}_2\text{O}_3$ mixed oxide was also reported.^{8,9)}

CsF supported on Celite catalyzes the ring opening of epoxides with thiols in acetonitrile under mild conditions and affords the corresponding β -hydroxysulfides in excellent yields.¹⁰⁾ The reaction of epoxide (10 mmol) and thiol (10 mmol) with the catalyst (10 mmol) was carried out in acetonitrile under reflux condition. The

ring opening was regioselective with nucleophilic incorporation at the less hindered carbon atom of epoxides.

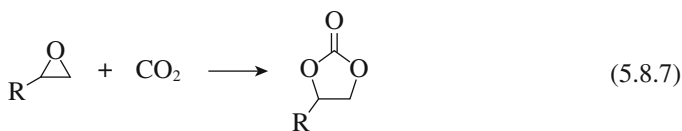


Ring opening of glycidol (oxirane-2-methanol) with fatty acids provide a route to monoglycerides, which are important food additives as emulsifiers and antimicrobial agents. Cauvel et al. found that MCM-41 grafted with 3-amino-propyl and 3-piperidinopropyl groups were active catalysts for the ring opening of glycidol with lauric acid (dodecanoic acid).¹¹⁾ The selectivity was improved by treating the catalyst with hexamethyldisilazane to block the residual OH groups of the surface. The gas chromatographic and isolated yields of lauric monoglyceride were >95% and 70%, respectively, in the presence of MCM-41 grafted with 3-piperidinopropyl groups at 393 K in 24 h.



Jaenicke and coworkers also prepared MCM-41 grafted with various types of amine functions and carried out the ring opening of glycidol with lauric acid.^{12,13)} The most active form was MCM-41 on which TBD (triazabicyclo[4,4,0]dec-5-ene) was immobilized.

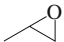
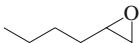
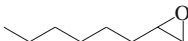
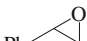
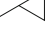
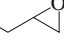
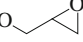
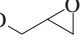
Cycloaddition of carbon dioxide to epoxides has been studied by many workers.



MgO is an active catalyst for the cycloaddition of carbon dioxide to styrene oxide under mild conditions.¹⁴⁾ Styrene oxide in DMF was reacted with CO₂ (20 kg cm⁻²) for 12 h at 408 K. The reaction of (*R*)-styrene oxide with carbon dioxide gives (*R*)-phenylethylene carbonate in 97% *ee* with retention of stereochemistry.

MgO-Al₂O₃ mixed oxides (calcined hydrotalcite) are very efficient catalysts for the cycloaddition.¹⁵⁾ By using MgO-Al₂O₃ oxide with Mg/Al ratio of 5 calcined at 673 K, various kinds of epoxides in DMF can be quantitatively converted into the corresponding cyclic carbonates, as shown in Table 5.8.1. The addition reaction proceeds retaining the stereochemistry of epoxides; the reactions of carbon dioxide with (*R*)- and (*S*)-benzyl glycidyl ethers give (*R*)- and (*S*)-4-(benzyloxymethyl)-1,3-dioxalane-2-one in 78% and 76% chemical yields with

Table 5.8.1 Cycloaddition of CO₂ to various epoxides catalyzed by MgO-Al₂O₃ mixed oxide^a

Entry	Substrate	Convsn/% ^b	Yield of carbonate/% ^b
1 ^{c)}		96	88
2 ^{c)}		100	89
3 ^{c)}		100	> 99
4 ^{d)}		92	90(91)
5 ^{e)}	Ph 	39	38
6	Ph 	100	94
7	MeO 	100	> 99
8 ^{d)}	PhO 	94	90(86)

^{a)} Reaction conditions: Mg-Al mixed oxide (Mg/Al = 5, calcined at 400°C) 0.5 g, epoxide 4 mmol, DMF 3mL CO₂ pressure 5 atm, 100°C, and 24 h. ^{b)} Yields of carbonates were determined by GLC analysis using internal standards, based on epoxides. Values in parentheses are isolated yields. In the case of the product isolation experiments, the reaction scale was twice as much as that of reaction conditions (a). ^{c)} 120°C. ^{d)} 15 h. ^{e)} A physical mixture of MgO and Al₂O₃ (Mg/Al = 5) was used in place of the above Mg-Al mixed oxide.

Reprinted with permission from K. Yamaguchi, K. Ebitani, T. Yoshida, H. Yoshida, K. Kaneda, *J. Am. Chem. Soc.*, **121**, 4526 (1999) p.4527, Table 1.

>99% *ee*, respectively.¹⁵⁾ Guanidine tethered to MCM-41 is also active for cycloaddition of CO₂ to various epoxides.¹⁶⁾

The reactions of ethylene oxide and propylene oxide (PO) with carbon dioxide to the corresponding alkene carbonates have been studied, since these reactions are important for the synthesis of dimethyl carbonate by the transesterification of the resulting alkene carbonates with methanol. The catalysts used for the synthesis of alkene carbonates are alkaline earth oxides,¹⁷⁾ smectite clays,¹⁸⁾ various zeolites,¹⁹⁾ KOH supported on NaA zeolite²⁰⁾ amino-functionalized silica²¹⁾ and anion exchange resins.²²⁾ A smectite clay containing Mg, Na and K showed high activity and selectivity for the reaction of PO with carbon dioxide into propylene carbonate (PC). A high selectivity of 94.3% for PC at a PO conversion of 85% was obtained in the reaction without solvent under 8 MPa of CO₂ at 423 K in 15 h.¹⁸⁾ TBD (1,5,7-triazabicyclo[4,4,0]-5-decene) anchored to silica also showed high activity for the same reaction, the PC conversion being 100% with 99.8% selectivity for PC under 1.5 MPa of CO₂ at 423 K in 15 h.²¹⁾

One-step synthesis of dimethyl carbonate from alkene oxide, carbon dioxide and methanol has been studied. (See section 5.11)

Strivastava et al. prepared SBA-15 tethered with an adenine moiety and found it to be an efficient catalyst for the addition of carbon dioxide to epoxy-compounds.^{23,24)} By incorporating Ti or Al in the SBA-15 framework, both conversion and selectivity were improved (Table 5.8.2). The conversion and selectivity

Table 5.8.2 Cyclic carbonate synthesis over adenine-modified SBA-15 materials

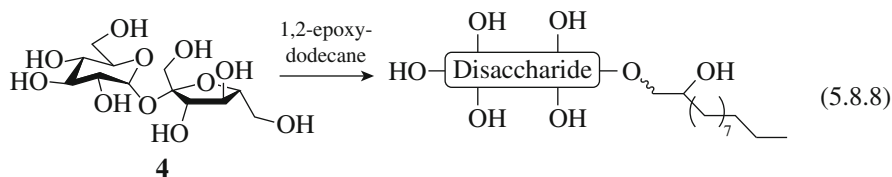
Catalyst	Epoxides	Time	Conversion/%	Selectivity/%
SBA-15	Epichlorohidrine	4	15.8	59.0
Ti-SBA-15	Epichlorohidrine	4	20.1	86.3
Al-SBA-15	Epichlorohidrine	4	22.1	92.2
SBA-15-adenine	Epichlorohidrine	4	80.5	75.0
Ti-SBA-15-adenine	Epichlorohidrine	4	93.9	89.1
Al-SBA-15-adenine	Epichlorohidrine	4	98.1	89.1
SBA-15-adenine	Styrene oxide	8	86.4	97.2
Ti-SBA-15-adenine	Styrene oxide	8	94.0	94.6
Al-SBA-15-adenine	Styrene oxide	8	98.4	97.9
Ti-SBA-15-adenine	Propylene oxide	6	89.2	91.7

Reaction conditions: catalyst 100 mg, epoxide (18 mmol), CO₂ (6.9 bar), temperature (393 K)

Reproduced with permission from R. Srivastava, D. Srinivas, P. Ratnasamy, *J. Catal.*, **233**, 1 (2005), Table 3 (p.10), *Microporous Mesoporous Mater.*, **90**, 314 (2006) Tables 3 & 4, p. 334.

ity were 91.9% and 89.1%, respectively, over Ti-SBA-15 tethered with adenine, and they were 98.1% and 89.1%, over Al-SBA tethered with adenine. The enhancement was attributed to the cooperative effect of amine moieties and Lewis acid sites (Ti, Al) on the surfaces.

Carbohydrates are a very important class of natural organic building blocks notably for the synthesis of non-ionic surfactants for detergents. The direct etherification of three disaccharide polyols, sucrose, trehalose and isomalt[®], with 1,2-epoxydodecane over various solid base catalysts was studied by Villandier et al.²⁵⁾ The best catalyst was an anion-exchange resin of polystyrene network having strong quaternary ammonium ions (-NMe₃⁺ OH⁻).



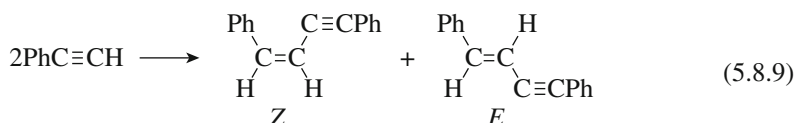
5.8.2 Nucleophilic Addition of Alkynes

Addition of alkynes such as phenylacetylene to double or triple bonds of various molecules occurs plausibly via formation of the alkynide ion, PhC⁻≡C⁻.

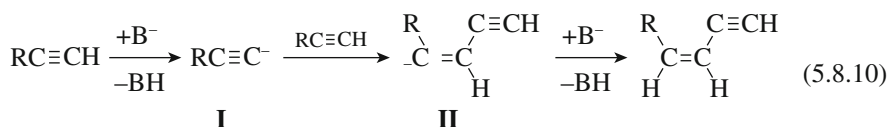
A. Dimerization of phenylacetylene

The base-catalyzed dimerization of phenyl acetylene was first described by Malkhasyan et al.²⁶⁾ They found that phenylacetylene reacts in the presence of metallic sodium in an aprotic polar solvent to give 1,3-diphenyl-1-buten-3-yne and diphenylbut-1,3-diyne. Later, Trofimov et al. further demonstrated that stirring of phenylacetylene with a KOH-DMSO suspension in a ball-mill at room temperature for 1 h gave a mixture of *E*- and *Z*-isomers of 1,4-diphenyl-1-buten-3-yne in a ratio of 6 : 1.²⁷⁾

Phenylacetylene dimerizes in the presence of a $\text{KNH}_2/\text{Al}_2\text{O}_3$ catalyst to afford (*Z*)- and (*E*)-1,4-diphenyl-1-buten-3-yne, the ratio of *Z* : *E* being 96 : 4, the yield being 97% in 20 h at 363 K.²⁸⁾



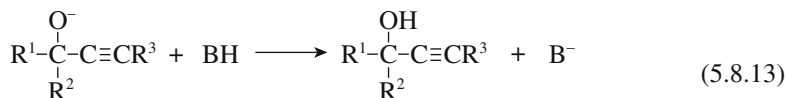
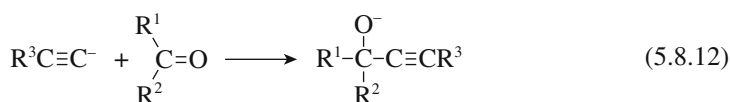
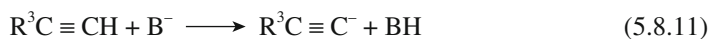
The dimerization proceeds through the formation of an alkynide-type intermediate and its addition to the triple bond of another molecule of phenylacetylene.



The predominance of head-to-head over head-to-tail dimerization is probably caused by the severe steric repulsion between the alkynide (**I**) and phenylacetylene in comparison with head-to-tail dimerization. The high stereoselectivity is also caused by the stability of the *Z*-type intermediate (**II**) over the corresponding *E*-type intermediate because of the steric repulsion between the bulky substituent and the solid surface in the latter case.

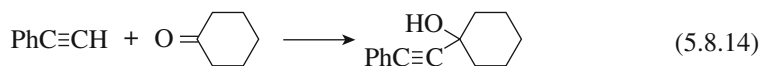
B. Addition of 1-alkyne to ketone or aldehyde

1-Alkynes such as $\text{PhC}\equiv\text{CH}$ react with ketones or aldehydes through the formation of alkynyl anions over solid bases, as shown in the following scheme.



$\text{R}^1 = \text{H}$ or alkyl, $\text{R}^2 = \text{alkyl}$

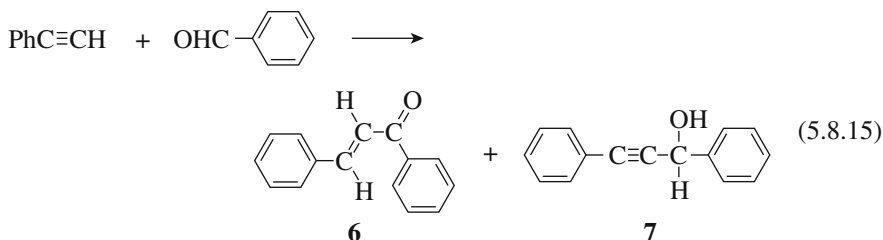
The reaction of phenylacetylene with cyclohexanone in the presence of $\text{KNH}_2/\text{Al}_2\text{O}_3$ in dioxane affords 1-phenylethynylcyclohexanol in 67% yield in 20 h at 363 K.²⁹⁾



Under this condition, the dimerization does not proceed at all, though it yields 1,4-diphenyl-1-buten-3-yne in the absence of cyclohexanone as described above.

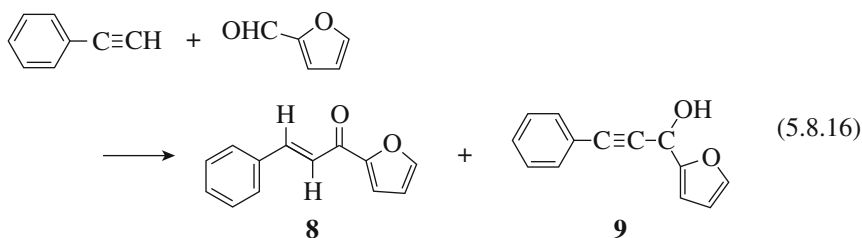
Table 5.8.3 lists the results of the reactions of various combinations of 1-alkyne and ketone in the presence of $\text{KNH}_2/\text{Al}_2\text{O}_3$.²⁹⁾ In every case, the condensation occurs to afford a corresponding alcohol, but in varying amounts. The selectivity for the alcohol based on cyclohexanone is generally higher than 95%.

The reaction of phenylacetylene with benzaldehyde in the presence of solid bases gives chalcone, **6** together with a small amount of **7**.²⁹⁾ When $\text{Cs}_2\text{CO}_3/\text{Al}_2\text{O}_3$ was pretreated at 673 K under vacuum and used as a catalyst, **6** was obtained in 65% yield in 20 h at 363 K in dioxane.



Chalcones are usually produced by the cross-aldol condensation of benzaldehyde and phenyl methylketone in the presence of a base such as KOH. The reaction (5.8.15) offers a new synthetic route for chalcones.

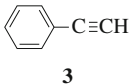
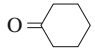
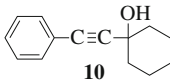
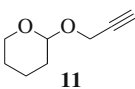
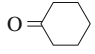
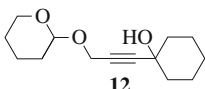
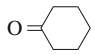
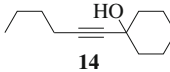
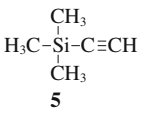
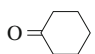
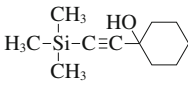
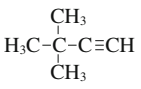
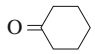
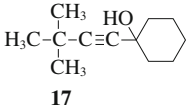
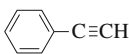
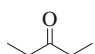
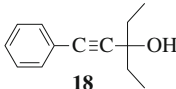
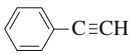
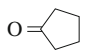
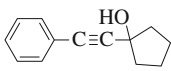
Phenylacetylene also reacts with 2-furyl aldehyde to yield an α,β -unsaturated ketone, **8** as the main product in the presence of $\text{Cs}_2\text{CO}_3/\text{Al}_2\text{O}_3$, α -alkynyl alcohol, **9** being the sole side product.²⁹⁾



The yields of **8** and **9** were 49% and 5%, respectively, when 5 mmol of phenylacetylene was used with an equimolar amount of 2-furyl aldehyde over 0.125 g of $\text{Cs}_2\text{CO}_3/\text{Al}_2\text{O}_3$ at 363 K in 20 h.

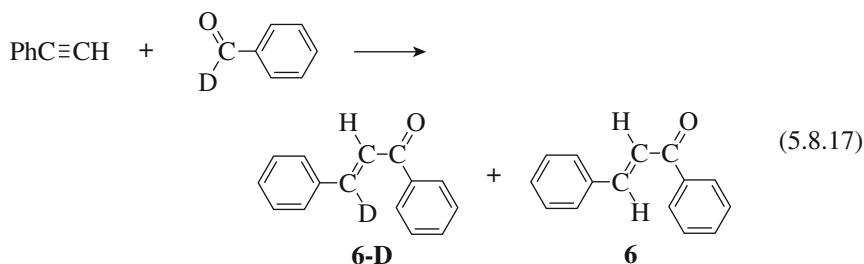
The reaction mechanism for the formation of **6** was investigated by using deuteriated benzaldehyde (PhCDO).²⁹⁾ Thus the reaction of phenylacetylene with deuteriated benzaldehyde was carried out at 343 K for 20 h using $\text{CsOH}/\text{Al}_2\text{O}_3$ as a catalyst. Deuteriated **6** (**6-D**) was the sole deuteriated product, no other products containing D atoms being found, though the ratio of **6-D** to **6** was 82/18 as determined by ^1H NMR.

Table 5.8.3 Reaction of 1-alkynes with ketones over $\text{KNH}_2/\text{Al}_2\text{O}_3$ ^{a)}

Acetylene/mmol	Ketone/mmol	Reduction temperature/K	Product	Yield/%
		363		87
		363		68
$\text{CH}(\text{CH}_2)_3\text{C}\equiv\text{CH}$ (13)		333		51
		318		27
		303		7
		363		36
		318		1

^{a)} $\text{KNH}_2/\text{Al}_2\text{O}_3 = 0.125 \text{ g (K} = 26 \text{ mmol/g-Al}_2\text{O}_3\text{)}$, solvent; dioxane (3 cm^3): reaction time: 20 h.

Reprinted with permission from T. Baba, K. Kizuka, H. Handa, Y. Ono, *Appl. Catal., A*, **194/195**, 203 (2000) p.208, Table 3.



This indicates that the scrambling of H and D atoms may occur on the surface of the catalyst. On the basis of this observation, the reaction scheme shown in Fig. 5.8.1 was proposed. A unique feature of the mechanism is the 1,3-shift of D- (H-) in the intermediate **III** to form **IV**. The fact that the main product is **6** indicates that the transformation of the anionic intermediate **III** to **IV** is much faster than the protonation of **III**.

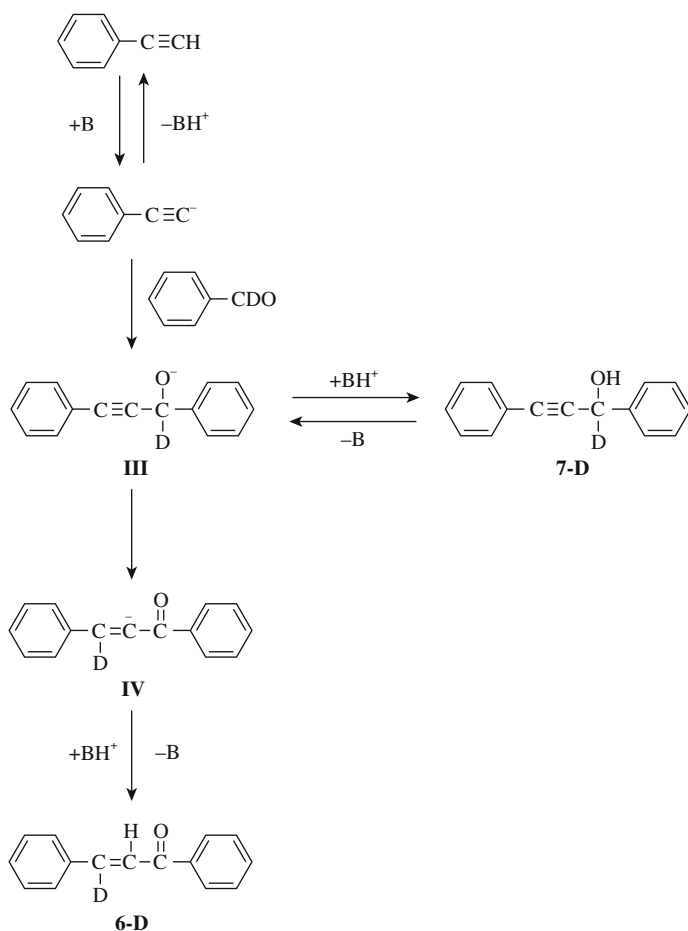
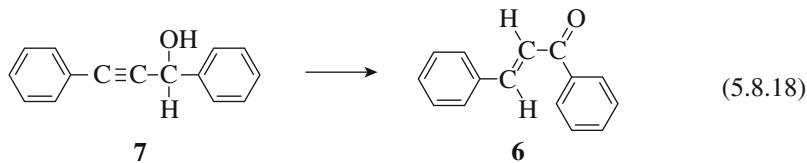


Fig. 5.8.1 Reaction scheme of the reaction between phenylacetylene and benzaldehyde. Reprinted with permission from T. Baba, H. Kizuka, H. Handa, Y. Ono, *Appl. Catal., A*, **194/195**, 203 (2000) p.210, Scheme 3.

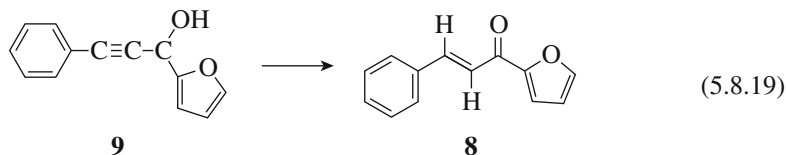
Obviously, alcohols are the products in the case of the reactions of 1-alkyne with ketones since the rearrangement of the anionic intermediates is not possible.

Figure 5.8.1 suggests that there is a possibility that **6** is prepared by the isomerization of **7** if the deprotonation of **7** and the protonation of **III** are reversible.



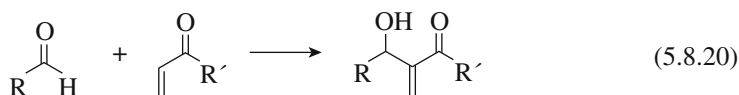
When the isomerization of **7** (1 mmol) was carried out over $\text{Cs}_2\text{CO}_3/\text{Al}_2\text{O}_3$ in dioxane (3 mL) at 303 K, **6** was obtained selectively. Thus the yield of **6** was 92%

and 98% in the reaction for 3 h and 20 h, respectively.²⁹⁾ The isomerization of alkyn-2-yl alcohol to α,β -unsaturated ketone has not been reported in any other cases. This novel rearrangement was observed also in the case of **9**.²⁹⁾ The yield of **8** was 98% in the reaction for 20 h at 363 K in the presence of $\text{Cs}_2\text{CO}_3/\text{Al}_2\text{O}_3$.

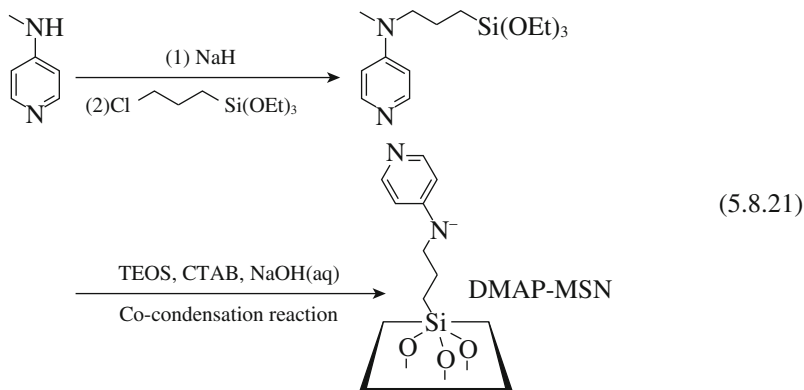


5.8.3 Baylis-Hillman Reaction

The Baylis-Hillman reaction is a C-C forming reaction of an aldehyde and an α,β -unsaturated electron-withdrawing group catalyzed by bases.

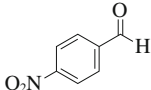
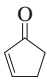
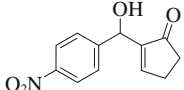
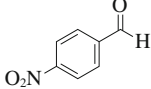
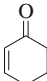
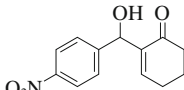
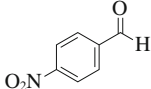
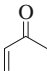
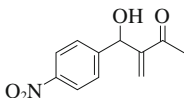
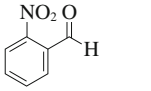
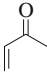
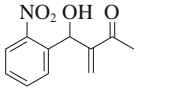
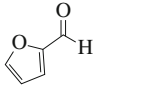
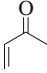
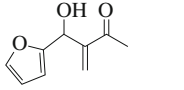
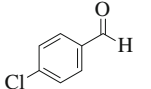
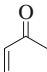
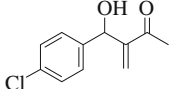
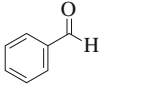
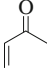
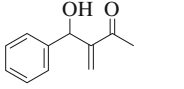
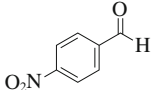
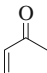
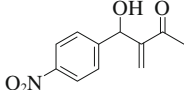
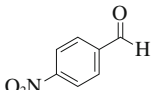
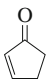
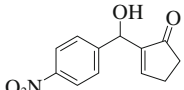


Chen et al. prepared mesoporous silica nanosphere (MSN) functionalized with dimethylaminopyridine (DMAP) moieties by a direct method.³⁰⁾ The catalyst contains $1.6 (\pm 0.15) \text{ mmol g}^{-1}$ of the organic groups.



As shown in Table 5.8.4, the catalyst thus prepared (DMAP-MSN) was an excellent catalyst for the Baylis-Hillman reaction of aryl aldehyde and various α,β -unsaturated ketones. In the reaction of 4-nitrobenzaldehyde and methyl vinyl ketone, the desired product was obtained quantitatively. The reactivity of α,β -unsaturated ketones follows the order, methyl vinyl ketone > cyclopentanone > cyclohexanone. The catalyst was much more active than 3-(dimethylamino)propyl-functionalized silica gel.

Table 5.8.4 Baylis-Hillman reaction catalyzed by DMAM-MSN

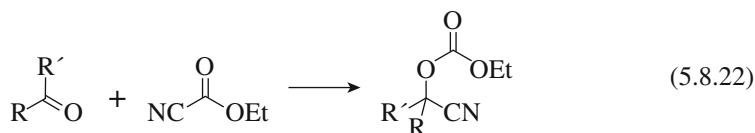
Entry	Aldehyde	Ketone	Catalyst	Product	Yield/% ^{b)}
1			DMAP-MSN		86
2			DMAP-MSN		49
3			DMAP-MSN		99
4			DMAP-MSN		49
5			DMAP-MSN		25
6 ^{c)}			DMAP-MSN		50
7 ^{c)}			DMAP-MSN		25
8			DMA-SiO ₂ ^{d)}		20
9			MCM-41		NR ^{e)}

^{a)} Reaction conditions: aldehyde (0.25 mmol), α,β -unsaturated ketone (0.5 mmol) and catalyst (50 mg, 30 mol%) in THF/H₂O = 1 : 3 (2 mL) at 323 K for 24 h. ^{b)} Isolated yield. ^{c)} Aldehyde/Ketone = 1 : 4 at 323 K for 3 d. ^{d)} 3-(dimethylaminopropyl)-functionalized silica gel. ^{e)} No reaction.

Reprinted with permission from H. -T. Chen, S. Huh, J. W. Wench, M. Pruski, V.Y. Lin, *J. Am. Chem. Soc.*, **127**, 13305 (2005) p.13309, Table 2.

5.8.4 Cyano-*O*-ethoxycarbonylation of Carbonyl Compounds

Cyano-*O*-ethoxylation of carbonyl compounds with ethyl cyanofornate proceeds in the presence of 3-diethylaminopropyl groups grafted to silica gel ($\text{NEt}_2\text{-SiO}_2$) in toluene at room temperature, as shown in Table 5.8.5.^{31,32} The cyanation products are obtained in excellent yield in every case.



The catalytic activity increased dramatically when 3-diethylamino-groups were tethered to a more acidic support, $\text{SiO}_2\text{-Al}_2\text{O}_3$, instead of silica gel. The authors proposed a synergetic action of acid (OH) and base (amine) centers on the surface.

The reaction of benzaldehyde with diethyl cyanophosphonate also proceeds in the presence of $\text{NEt}_2\text{-SiO}_2$.³¹⁾

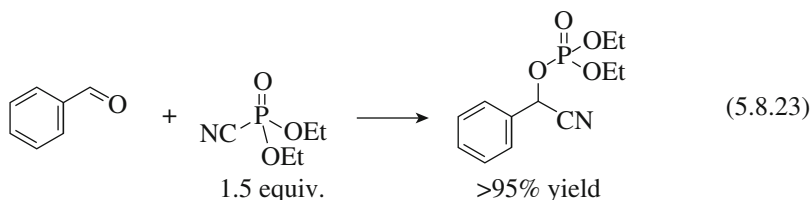
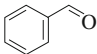
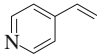
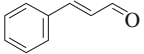

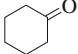


Table 5.8.5 Cyano-*O*-ethoxycarbonylation of ketones with ethyl cyanofornate over $\text{NEt}_2\text{-silica}$

Entry	Carbonyl compounds	Time/h	Conversion/% ^b	Yield/% ^b
1		1	> 99	98
2		1	> 99	87
3		5	> 99	96
4		3	94	94
5		48	92	86

^{a)} Carbonyl compounds (0.5 mmol), ethyl cyanofornate (0.6 mmol), $\text{SiO}_2\text{-NEt}_2$ (0.05 g, 0.035 mmol of amine), toluene (1 mL), room temp.

Reprinted with permission from K. Motokuma, N. Viswanadham, G. M. Dhar, Y. Iwasawa, *Catal. Today*, **141**, 19 (2009) p.22, Table. 2.

References

1. G. H. Posner, D. Z. Rogers, *J. Am. Chem. Soc.*, **99**, 8208, 8214 (1977).
2. M. Onaka, M. Kawai, Y. Izumi, *Chem. Lett.*, **14**, 779 (1985).
3. R. I. Kureshy, S. Singh, N. H. Khan, S. H. R. Abdi, E. Suresh, R. V. Jarsa, *J. Mol. Catal., A*, **264**, 162 (2007).
4. M. L. Kantam, S. Laha, J. Yadav, B. Sreedhar, *Tetrahedron Lett.*, **47**, 6213 (2005).
5. H. Hattori, M. Shima, H. Kabashima, *Stud. Surf. Sci. Catal.*, **130**, 3507 (2000).
6. L. Martins, W. Hölderich, D. Cardoso, *J. Catal.*, **258**, 14 (2008).
7. X. Zhang, W. Zhang, J. Li, N. Zhao, W. Wei, Y. Sun, *Catal. Commun.*, **8**, 437 (2007).
8. W. Zhang, H. Wang, W. Wei, Y. Sun, *J. Mol. Catal., A*, **231**, 83 (2005).
9. W. Zhang, H. Wang, Q. Li, Q. Dong, N. Zhao, W. Wei, Y. Sun, *Appl. Catal., A*, **294**, 188 (2005).
10. V. Polshettiwar, M. P. Kaushik, *Catal. Commun.*, **5**, 515 (2004).
11. A. Cauvel, G. Renard, D. Brunel, *J. Org. Chem.*, **62**, 749 (1997).
12. X. Lin, G. K. Chuah, S. Jaenecke, *J. Mol. Catal.*, **150**, 287 (1999).
13. S. Jaenecke, G. K. Chuah, X. H. Lin, X. C. Hu, *Micropor. Mesopor. Mater.*, **35/36**, 143 (2000).
14. T. Yano, H. Matsui, T. Koike, H. Ishiguro, H. Fujihara, M. Yoshihara, T. Maeshima, *Chem. Commun.*, **1997**, 1129.
15. K. Yamaguchi, K. Ebitani, T. Yoshida, H. Yoshida, K. Kaneda, *J. Am. Chem. Soc.*, **121**, 4526 (1999).
16. A. Barabarini, R. Magi, A. Mazzacani, G. Mori, G. Sartori, R. Sartorio, *Tetrahedron Lett.*, **64**, 2931 (2003).
17. B. M. Bhanage, S. Fujita, Y. Ikushima, M. Arai, *Appl. Catal., A*, **219**, 259 (2001).
18. S. Fujita, B. M. Bhanage, Y. Ikushima, M. Shirai, K. Torii, M. Arai, *Green Chem.*, **5**, 71 (2003).
19. E. J. Dosckocil, S. V. Bordawekar, B. G. Kaye, R. J. Davis, *J. Phys. Chem., B*, **103**, 6277 (1999).
20. Y. Li, X. Zhao, Y. Wang, *Appl. Catal., A*, **279**, 205 (2005).
21. X. Zhang, Y. Zhang, Y. Yang, Q. Wei, X. Zhang, *React. Kinet. Catal. Lett.*, **94**, 385 (2008).
22. M. Cao, Y. Meng, Y. Lu, *React. Kinet. Catal. Lett.*, **88**, 251 (2006).
23. R. Srivastava, D. Srinivas, P. Ratnasamy, *J. Catal.*, **233**, 1 (2005).
24. R. Srivastava, D. Srinivas, P. Ratnasamy, *Micropor. Mesopor. Mater.*, **90**, 314 (2006).
25. N. Villandier, I. Adam, F. Jérôme, J. Barrault, P. Pierre, A. Bonchu, J. Fitremann, Y. Queneau, *J. Mol. Catal., A*, **259**, 67 (2006).
26. A. Ts. Malkhasyan, Zh. I. Dzhandzhayan, G. T. Martiosyan, I. P. Beletskaya, *Zh. Org. Khim.*, **15**, 342 (1979).
27. B. A. Trofimov, L. N. Sobenina, O. V. Petrova, A. I. Mikhalaria, *Dokl. Akad. Nauk*, **328**, 29 (1993).
28. T. Baba, A. Kato, H. Handa, Y. Ono, *Catal. Lett.*, **50**, 83 (1998).
29. T. Baba, H. Kizuka, H. Handa, Y. Ono, *Appl. Catal., A*, **194/195**, 203 (2000).
30. H. -T. Chen, S. Huh, J. W. Wench, M. Pruski, V. Y. Lin, *J. Am. Chem. Soc.*, **127**, 13305 (2005).
31. K. Motokuma, N. Viswanadham, G. M. Dhar, Y. Iwasawa, *Catal. Today*, **141**, 19 (2009).
32. K. Motokuma, M. Tomita, M. Tada, Y. Iwasawa, *Chem. Eur. J.*, **14**, 4017 (2008).

5.9 Hydrogenation Reactions

5.9.1 Hydrogenation of Alkenes

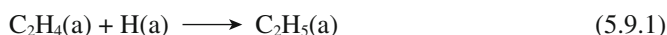
It was reported that Na and Li metal dispersed on alumina or silica are active for the hydrogenation of ethylene, propene even below room temperature.¹⁾

Hydrogenation of ethylene, propene and 1-butene over alkaline earth oxides was investigated. The catalytic activities depended on the evacuation temperature of the catalysts.²⁾ The oxides became active on evacuation above 873 K, and showed maximum activities at an evacuation temperature of around 1273 K. The catalytic activity at 523 K increased in the order MgO < CaO < BaO < SrO.

Minachev et al. studied the hydrogenation of ethylene over a series of rare earth oxides.³⁾ The catalytic activities depend on the temperature of pretreatment.

Among the oxides, the sesquioxides of Pr, La and Nd are the most active. La_2O_3 is active even at 157 K. The catalytic activity is well correlated with the basicity of the catalysts. Acidic oxides (CeO_2 , PrO_2 , TbO_2 , ZrO_2 and TiO_2) are not active. The acidic substances (NO_2 , CO_2) and water are catalytic poisons. Ethylene hydrogenation with D_2 over Dy_2O_3 gives only $\text{C}_2\text{H}_4\text{D}_2$ at 218 K, indicating that there is no H-D exchange between the hydrocarbon and deuterium.

Hydrogenation of ethylene over ZnO was studied by Kokes and coworkers. When the hydrogenation of ethylene is carried out with D_2 , the product is > 95% 1,2-dideuteroethane.⁵⁾ The simple addition of two D atoms across the double bond was also observed in hydrogenation of ethylene, propene and 3,3-dimethylbutene over ZrO_2 .⁵⁾ This is a big contrast to hydrogenation over metals, which gives a mixture of $\text{C}_2\text{H}_{6-x}\text{D}_x$. This indicates that step (5.9.1) in the hydrogenation is irreversible.



When the hydrogenation is carried out with a 1 : 1 mixture of H_2 and D_2 , the products are mainly C_2H_6 and $\text{C}_2\text{H}_4\text{D}_2$ at room temperature, indicating that the hydrogen added to form the ethane retains its molecular identity.⁶⁾

From adsorption, kinetic and tracer studies, Dent and Kokes indicated that there were two types of hydrogen adsorption on ZnO.^{7,8)} Type I is rapid and reversible. Type II is irreversible and occurs rapidly initially but slowly in the later stages. Type I hydrogen is responsible for the observed OH and ZnH bands in the infrared and the principal source for the hydrogenation of ethylene at room temperature. Type II does not participate in the hydrogenation at room temperature but modifies the catalyst and enhances its activity. They also studied the adsorption state of ethylene and the mixture of ethylene and H_2 (and D_2) by infrared spectroscopy.⁹⁾ Ethylene is π -bonded in the chemisorbed state and the C_2H_5 (and $\text{CH}_2\text{CH}_2\text{D}$) species is the intermediate of the hydrogenation. From these results, hydrogenation is believed to occur on a limited number of Zn-O pair sites capable of adsorbing hydrogen to form Zn-H and OH.

The reaction of C_3H_6 with D_2 exclusively gives $\text{CH}_3\text{CDCH}_2\text{D}$ over ZnO in the beginning of the reaction.¹⁰⁾ This suggests that the π -allyl species is not the reaction intermediate in hydrogenation, though it is observed by infrared spectroscopy.

5.9.2 Hydrogenation of Butadienes

The catalytic activity of alkaline earth oxides for hydrogenation of 1,3-butadiene is much higher than that for hydrogenation of simple alkenes such as ethylene, propene and butenes.¹¹⁾ Effective hydrogenation of simple alkenes requires reaction temperatures above 520 K, while hydrogenation of 1,3-butadiene proceeds readily even at 273 K. The time course of the hydrogenation over MgO is shown in Fig. 5.9.1. The product consists of butene isomers, *cis*-butene being the most predominant at the initial stage. Over CaO, SrO and BaO, the products are an

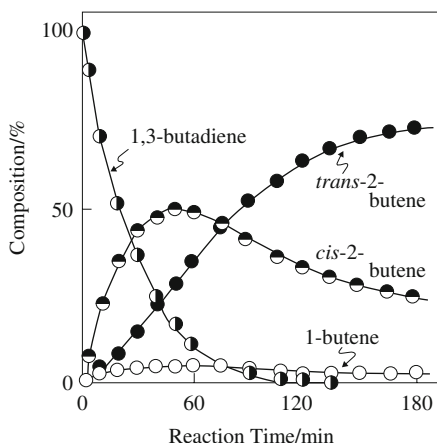


Fig. 5.9.1 Hydrogenation of 1,3-butadiene over MgO at 273 K. Reprinted with permission from Y. Tanaka, H. Hattori, K. Tanabe, *Chem. Lett.*, 37 (1976) p.38, Fig. 1.

equilibrium mixture of butenes. No butane is formed even after the disappearance of 1,3-butadiene. The high activity for 1,3-butadiene compared to that of simple alkenes indicates the intermediacy of the π -allyl carbanion species. Hydrogenation of 1,3-butadiene with D_2 over MgO pretreated at 1100 K gives predominantly *cis*-2-butene containing D atoms at the 1 and 4 positions at 273 K.¹²⁾ Furthermore, the product of the hydrogenation with a mixture of H_2 and D_2 is almost exclusively butenes- d_0 and d_2 , indicating that H_2 (or D_2) maintains its molecular identity, that is, both H (or D) atoms in H_2 (or D_2) are incorporated into one hydrogenated molecule. Under the same reaction conditions, no H_2 - D_2 exchange proceeds over MgO pretreated at 1100 K.

Hydrogenation of 1,3-butadiene also proceeds over ZrO_2 ,¹³⁻¹⁵⁾ ThO_2 ¹⁶⁾ and La_2O_3 .^{17,18)} In every case, the most predominant products of hydrogenation with D_2 are 2-butene- d_2 due to 1,4-addition of deuterium atoms. The molecular identity of H_2 (or D_2) is maintained. Butane is not formed in any case. In contrast to hydrogenation over MgO, hydrogenation over these oxides gives mainly *trans*-2-butene (Table 5.9.1).

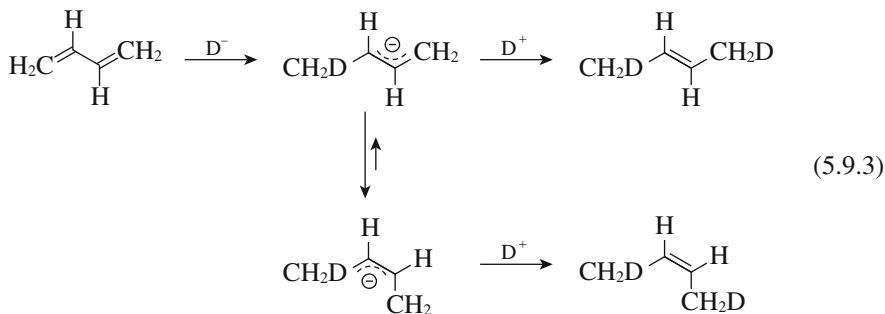
Table 5.9.1 Product distribution in hydrogenation of 1,3-butadiene and 2-methyl-1,3-butadiene

Catalyst	1,3-Butadiene			2-Methyl-1,3-butadiene			
	1-B	2-B	(<i>trans</i> : <i>cis</i>)	2-Me-1-B	3-Me-1-B	2-Me-2-B	(<i>E</i> : <i>Z</i>)
MgO	7	93	(18 : 82)	5.8	0.6	92.6	(60 : 40)
La_2O_3	2	98	(86 : 14)	7.8	0.5	91.6	(64 : 36)
ThO_2	8	92	(90 : 10)	13.3	1.0	85.7	(89 : 11)
ZrO_2	15	85	(94 : 6)	55	30	15	(89 : 11)
Equilibrium	3.2	96.8	(79 : 21)	10.9	6.2	88.9	

1-B: 1-butene, 2-B: 2-butene

Based on Y. Nakano, T. Yamaguchi, K. Tanabe, *J. Catal.*, **80**, 307 (1983) p.311, Table 1.

Hattori and coworkers proposed the mechanism of hydrogenation (or deuteration) shown below.¹²⁾



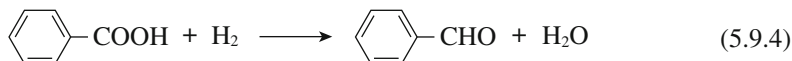
The deuterium molecules are dissociated to form D^+ and D^- on the surface. At first, D^- attacks 1,3-butadiene to form the allylic anion of the *trans* form. 1,3-Butadiene consists of 93% *s-trans* conformer and 7% *s-cis* conformer in gas phase. It is assumed the conformation in gas phase is retained in the allylic anion intermediates, which undergo either interconversion to form *cis*-allylic anions or addition of D^+ to form butenes. Since the electron density of allylic anion is the highest on the terminal carbon atom, positively charged D^+ selectively adds to the terminal carbon atom to complete 1,4-addition of D atoms to yield 2-butene. If the interconversion of the allylic anions is faster than the addition of D^+ ion (MgO), *cis*-2-butene- d_2 is obtained as the main product. On the other hand, if the addition is faster than the interconversion between the allylic anions, *trans*-2-butene- d_2 is obtained as the main product (ZrO_2 , ThO_2 , La_2O_3).

Hydrogenation of 2-methyl-1,3-butadiene with H_2 (or D_2) were also studied over MgO ,^{11,17)} ThO_2 ,^{15,17)} La_2O_3 ^{16,17)} and ZrO_2 .¹⁴⁾ The essential features of the hydrogenation is the same as that of 1,3-butadiene. The predominant products in this case are (*E*) and (*Z*) forms of 2-methyl-2-butene- d_2 . The ratios of the two predominant products are given in Table 5.9.1.

In the hydrogenation of 1,3-butadiene with D_2 over ZnO , addition of D atoms occurs only at the 1,2-positions.¹⁰⁾

5.9.3 Hydrogenation of Benzoic Acid

Hydrogenation of benzoic acid into benzaldehyde was commercialized by Mitsubishi Kasei Corp. (now Mitsubishi Chemical Corp.). The reaction is carried out at 350 - 400 under 0 - 3 kg cm^{-2} of hydrogen pressure.¹⁸⁾



Yokoyama et al. reported on the chemistry of the reaction.¹⁸⁾ Among the metal oxides tested, ZrO_2 showed excellent selectivity for benzaldehyde, but the activity was low. By modifying ZrO_2 with Pb^{2+} , In^{3+} , Cr^{3+} or Mn^{2+} , the activity was remarkably enhanced. The catalysts were useful for hydrogenation of various

Table 5.9.2 Hydrogenation of various carboxylic acids with Cr³⁺ modified ZrO₂ catalysts

Carboxylic acids or esters	Conversion of acid/%	Selectivity to aldehyde/%
Benzoic acid	98	96
α -Methylbenzoic acid	98	97
<i>m</i> -Phenoxybenzoic acid	97	96
Dimethyl terephthalate	64	73
<i>m</i> -Chlorobenzoic acid	82	77
Trimethylacetic acid	97	99
Methyl <i>n</i> -hexanonate	50	70
Cyclohexanecarboxylic acid	95	98
Methyl nicotinate	86	83
4-Methyl-5-carbomethoxythiazole	74	80
3-Furoic acid	62	52

Reprinted with permission from T. Yokoyama, T. Setoyama, N. Fujita, M. Nakajima, T. Maki, *Appl. Catal. A*, **88**, 149 (1992) p.155, Table 4.

carboxylic acids, as shown in Table 5.9.2. The bidentate carboxylate was observed upon adsorption of benzoic acid by infrared spectroscopy.¹⁹⁾ The carboxylate was stable up to 623 K and decomposed to benzene. It was reduced to benzaldehyde under hydrogen at 623 K. These results indicate that the carboxylate is the intermediate which is hydrogenated by the dissociatively adsorbed hydrogen. The existence of a combination of weakly acidic and weakly basic sites is essential for the reaction. Strongly acidic sites facilitate the decarboxylation, while strongly basic sites form the salt with benzoic acid and no further reaction occurs under the hydrogenation conditions.

Sakata et al. examined the catalytic performance of a series of metal oxides for the transformation of benzoic acid under hydrogen and found that ZrO₂ and ZnO are the most active and selective for benzaldehyde and proposed that one oxygen atom of benzoic acid is trapped by the oxygen vacancy on the surface.²⁰⁾ The oxygen atom trapped was hydrogenated with hydrogen to water to regenerate the oxygen vacancy.

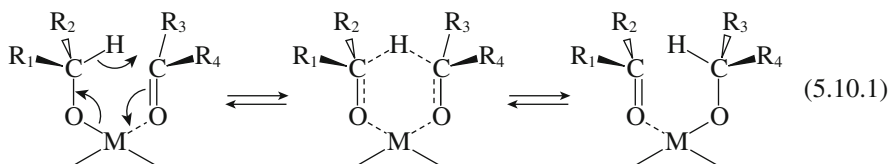
References

1. S. Voltz, *J. Phys. Chem.*, **61**, 4, 756 (1957).
2. H. Hattori, Y. Tanaka, K. Tanabe, *Chem. Lett.*, **4**, 659 (1975).
3. Kh. M. Minachev, Yu. S. Khodakov, V. S. Nakhshunov, *J. Catal.*, **49**, 207 (1977).
4. W. C. Conner, R. A. Innes, R. J. Kokes, *J. Am. Chem. Soc.*, **90**, 6858 (1968).
5. R. Bird, C. Kemball, H. F. Leach, *J. Chem. Soc., Faraday Trans. 1*, **83**, 3069 (1987).
6. W. C. Conner, R. J. Kokes, *J. Phys. Chem.*, **73**, 2436 (1989).
7. A. L. Dent, R. J. Kokes, *J. Phys. Chem.*, **73**, 3772 (1969).
8. A. L. Dent, R. J. Kokes, *J. Phys. Chem.*, **73**, 3781 (1969).
9. A. L. Dent, R. J. Kokes, *J. Phys. Chem.*, **74**, 3653 (1970).
10. S. Naito, T. Kondo, M. Ichikawa, K. Tamaru, *J. Phys. Chem.*, **76**, 2184 (1972).
11. Y. Tanaka, H. Hattori, K. Tanabe, *Chem. Lett.*, **5**, 37 (1976).
12. H. Hattori, Y. Tanaka, K. Tanabe, *J. Am. Chem. Soc.*, **98**, 4652 (1976).
13. T. Yamaguchi, J. W. Hightower, *J. Am. Chem. Soc.*, **99**, 4201 (1977).
14. Y. Nakano, T. Yamaguchi, K. Tanabe, *J. Catal.*, **80**, 307 (1983).
15. Y. Imizu, K. Tanabe, H. Hattori, *J. Catal.*, **56**, 303 (1979).

16. Y. Imizu, K. Saito, H. Hattori, *J. Catal.*, **76**, 65 (1982).
17. Y. Imizu, H. Hattori, K. Tanabe, *J. Chem. Soc., Chem. Commun.*, **1978**, 1091.
18. T. Yokoyama, T. Setoyama, N. Fujita, M. Nakajima, T. Maki, *Appl. Catal., A*, **88**, 149 (1992).
19. J. Kondo, N. Ding, K. Maruya, K. Domen, T. Yokoyama, N. Fujita, T. Maki, *Bull. Chem. Soc. Jpn.*, **66**, 3085 (1993).
20. Y. Sakata, C. A. van Tol Koutstaal, V. Ponec, *J. Catal.*, **169**, 13 (1997).

5.10 Transfer Hydrogenation Reactions (Meerwein-Ponndorf-Verley Reduction and Oppenauer Oxidation)

The Meerwein-Ponndorf-Verley (MPV) reduction of ketones or aldehydes with aluminum isopropoxide is a well known hydrogen transfer reaction whose mechanism involves a hydrogen transfer from the alkoxide to the carbonyl carbon of the ketone. The following cyclic intermediate is generally accepted.



When ketones are the desired products, the reaction is called the Oppenauer oxidation. The MPV reaction is suitable for the reduction of α,β -unsaturated carbonyl compounds, since the reduction is highly selective for the C=O double bond and leaves C=C untouched. The MPV reaction, however, requires an alkoxide excess of at least 100–200% and it is subsequently necessary to neutralize the residual alkoxide in the medium with a strong acid. Use of heterogeneous catalysts has been extensively explored. Heterogeneous catalysts can be classified into two types. One is the case in which metal cations such as Al^{3+} , Zr^{4+} and Sn^{4+} serve as Lewis acid sites. Metal cations are incorporated as part of the zeolite framework¹⁻³⁾ or supported in the form of a metal alkoxide.⁴⁾ In these cases, the reaction mechanisms similar to the classical alkoxide catalysts are proposed. The other is the case in which solid bases such as MgO or amphoteric oxides serve as catalysts. The involvement of both acid sites and basic sites are often proposed. A comprehensive review on MPV reduction has been published by Chuah et al.⁵⁾

5.10.1 Reaction Mechanism over Solid Base Catalysts

Niiyama and Echigoya studied the catalytic activities of MgO and MgO-SiO₂ mixed oxides for the vapor-phase transfer hydrogenation between acetone and alcohols.⁶⁾ The activities for the ethanol-acetone reaction at 473 K correlate well with the amount of the basic sites, while the activities for the 2-butanol-acetone reaction are correlated with neither the amount of basic sites nor that of acidic sites at 413 K. The authors concluded that the activation of ethanol with basic sites is

more important than the activation of ketone by acidic sites for the ethanol-acetone reaction, while both sites contribute equally to the butanol-acetone reaction. The MPV reaction between ethanol and acetone in vapor phase was investigated over various metal oxides having different acid-base properties by Ivanov et al.⁷⁾ Brønsted acid catalysts were not active towards the MPV reaction. The reaction proceeded on Lewis acid (Al_2O_3 modified with Cl) or base catalysts (MgO , ZrO_2). Over alumina, an amphoteric oxide, the MPV reaction proceeded with side reactions: dehydration and the condensation of acetone and acetaldehyde. Infrared spectroscopic study showed that ethanol is dissociatively adsorbed to form ethoxide species on MgO . Acetone forms various species on MgO , but it does not chemisorb on MgO when ethanol coexists. From these facts, the reaction mechanism over basic catalysts involving the reaction of acetone with dissociated alcohol was proposed.

Okamoto et al., reported hydrogen transfer between various alcohols and methyl ethyl ketone (MEK) over MgO .⁸⁾ The reactivity of alcohols depends on the delocalizability of the hydrogen attached to the α -carbon of the alcohol. The isotope effects of 1.39 and 0.96 ($k_{\text{H}}/k_{\text{D}}$) were observed for the methanol (CD_3OD)-MEK system and the ethanol ($\text{C}_2\text{H}_5\text{OD}$)-MEK system, respectively. These facts indicate that the rate-determining step is the hydrogen abstraction process from the α -carbon of the alcohol. Pyridine has no effect on the reaction, indicating that ketone is not adsorbed or activated by acidic sites. The authors propose a reaction mechanism involving the heterolytic dissociation of alcohol followed by the direct transfer of α -hydrogen (as H^-) of the alkoxide to an adsorbed ketone molecule, as shown in Fig. 5.10.1.

Kibby and Hall studied hydrogen transfer from 2-butanol to 3-pentanone over hydroxyapatite.⁹⁾ Tracer experiments revealed a very specific transfer of D from 2-butanol-2d to the product 3-pentanol-3d. The isotope effect was found for hydrogen transfer, ($k_{\text{H}}/k_{\text{D}}$) = 1.9. This also indicates that the rate-limiting step is the transfer of the α -hydrogen.

A linear Hammett correlation was observed for the reduction of substituted benzaldehyde by 2-propanol by Na^+ -doped Al_2O_3 at 573 K in the vapor phase.¹⁰⁾ The positive value of the slope ($\rho = +0.76$) indicates a mechanism involving a hydride transfer to the electron-deficient carbonyl carbon.

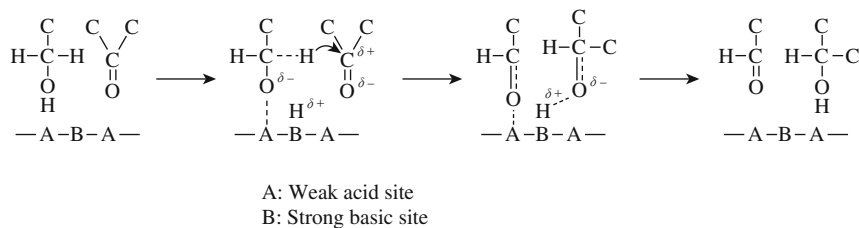


Fig. 5.10.1 Mechanism of hydrogen transfer between alcohol and ketone. Reprinted with permission from Y. Okamoto T. Imanaka, S. Terasaki, *Bull. Chem. Soc. Jpn.*, **45**, 3207 (1972) p. 3208 (Scheme).

5.10.2 Hydrogenation of Ketones with Alcohols

Posner et al. reported that 2-propanol on alumina reduces structurally diverse aldehydes at room temperature.¹¹⁾ α,β -Unsaturated aldehydes are selectively converted into allylic alcohols. A large amount of alumina was used compared to the reactants.

Ramana and Pillai reported that Al_2O_3 containing about 2.2 wt% of Na^+ was an effective catalyst for the reduction of a number of aliphatic and aromatic aldehydes and ketones by 2-propanol in vapor phase at 573 K.¹²⁾ On Al_2O_3 containing less Na^+ , considerable dehydration of 2-propanol took place. $\text{Na}^+/\text{Al}_2\text{O}_3$ is also effective for the reverse reaction, the oxidation of primary and secondary alcohols by ketones such as acetone and cyclohexanone at 573 K.

The reduction of a variety of ketones by 2-propanol over MgO in vapor phase was investigated by Kijenski et al.¹³⁾ In the reduction of methyl alkyl ketones of the general formula CH_3COR , where R = Et, Pr, ⁱPr, Bu, ⁱBu, ^tBu and pentyl, the selectivity for the corresponding alcohol was higher than 95% up to 523 K. Their yields were close to 70%, which practically corresponds to the equilibrium value. A series of long chain aliphatic ketones, $\text{CH}_3(\text{CH}_2)_n\text{CO}(\text{CH}_2)_n\text{CH}_3$, where $n = 4-7$ were hydrogenated with 2-propanol into corresponding alcohols over MgO at 573–723 K. The yields of the alcohols exceeded 50%.¹⁴⁾ Above 623 K, the consecutive dehydration of alcohols formed took place with moderate yields leading to internal alkenes. The yields of alkenes were greatly enhanced when the acidity was introduced by loading H_3PO_4 on MgO. Thus direct synthesis of C_{13} alkene from 7-tridecanone was realized with high yield (>90%) over $\text{H}_3\text{PO}_4/\text{MgO}$.

Cyclopentanone and cyclohexanone were also reduced to the corresponding alcohols. Their yields reached ca. 86.5%, which was very close to the equilibrium values.¹³⁾ Aryl alkyl ketones of general formula ArCOCH_3 , where Ar = $p\text{-C}_6\text{H}_4\text{Me}$, $p\text{-C}_6\text{H}_4\text{Et}$, $p\text{-C}_6\text{H}_4\text{Pr}$, $p\text{-C}_6\text{H}_4\text{OMe}$ and $p\text{-C}_6\text{H}_4\text{Cl}$, can be reduced to the corresponding alcohols with 2-propanol.^{13,15)} In the case of 4-isopropylacetophenone, the yield of the corresponding alcohol was ca. 63.3% at 473 K.¹³⁾ Above 573 K, the alcohols produced were dehydrated to the corresponding styrene. Maximum yields of styrenes reached values higher than 95% at 673 K in the case of *p*-methyl, *p*-ethyl and *p*-isopropyl acetophenone. The yields of styrenes increased by modifying MgO with H_2SO_4 or H_3PO_4 .¹⁶⁾ Acetophenone, 4-isopropylacetophenone, propiophenone and 5-nonanone were quantitatively transformed into the corresponding alkenes at 523–673 K.

Vapor-phase transfer hydrogenation of α -chloro ketone to α -chloroalcohol with 2-butanol was reported by Gotoh et al.¹⁷⁾ Thus 1,3-dichloro-2-propanone hydrogenated with 2-butanol over MgO at 423 K gave a 89.4% selectivity for 1,3-dichloro-2-propanol at 24.2% conversion, other products being 1-chloro-2-propanone (8.3%) and 1,1-dichloropropanone (2.2%). The selectivity for the alcohol drops to 68% at 80.0% conversion. ZrO_2 is also an effective catalyst for the reaction. Al_2O_3 and $\text{SiO}_2/\text{Al}_2\text{O}_3$ give much higher activity, but considerable dehydration of 2-butanol occurs.

Allylic alcohols are obtained by the gas-phase reaction of α,β -unsaturated

ketones with 2-propanol over MgO.¹⁸⁾ Thus the reaction of 4-hexen-3-one with 2-propanol gave α,β -unsaturated alcohol in a 71% yield at 523 K. No reduction of the carbon-carbon double bond occurred. The use of a vapor-phase flow system is essential to avoid the condensation reactions.

Vapor-phase reduction of methacrolein to methallyl alcohol with ethanol over modified MgO was reported.¹⁹⁾ The catalytic performance varies with the acidic and basic properties of the catalysts. Addition of SiO₂ and K₂O to MgO generates both weakly acidic and weakly basic sites. Over this catalyst, 88% selectivity at 69% conversion of methacrolein was attained over K-Si-Mg mixed oxide with an atomic ratio of Si/Mg = 0.1 and K/Mg = 0.01.

Aldehydes are hydrogenated by methanol or ethanol over MgO.²⁰⁾ In the case of propanal and benzaldehyde, the corresponding alcohols are the only the reaction products. In the case of acrolein, a mixture of propanal, 1-propanol and allyl alcohol is obtained at 643 K.

Mixed oxides prepared by calcinations of hydrotalcite are reported to be active for transfer hydrogenation of a variety of aldehydes and ketones in liquid phase. In the MPV reaction of 4-*t*-butylcyclohexanone with 2-propanol, 98% conversion was reached within 4 h with selectivity for alcohol greater than 95% (*trans* : *cis* ratio: 85 : 15) at 355 K.²¹⁾ The hydrotalcite having Mg : Al ratio of 3 : 1, calcined at 723 K was found to be the most active. The addition of a base (diisopropylamine) had only a small effect on the rate, but benzoic acid dramatically inhibited the reactions, indicating that the reactions are catalyzed by basic sites.²¹⁾ A variety of aldehydes and ketones can be hydrogenated with 2-propanol over MgO-Al₂O₃.²²⁾

MgO-Al₂O₃ was used for hydrogenation of citronellal, cinnamaldehyde (3-phenyl-2-propenal) and citral (3,7-dimethyl-2,6-octadienal). Unsaturated alcohols were obtained with high conversions and high selectivity at 355 K. High selectivity in the hydrogenation of citral to the corresponding alcohol (neral + geraniol) with 2-propanol under a refluxing condition over MgO-Al₂O₃ was also reported by Aramendía et al.²³⁾ Reduction of citral with 2-propanol also proceeds with high selectivity in the presence of hydrous zirconia.²⁴⁾ In this case, the OH groups of hydrous zirconia are considered to be the active sites.

The MPV reactions of various α,β -unsaturated aldehyde (3 mmol) and 2-propanol (60 mmol) proceed under a refluxing condition (355 K) in the presence of MgO-Al₂O₃ mixed oxide prepared by calcination of hydrotalcite precursors.²⁵⁾ The results are given in Table 5.10.1.

The mixed oxides can be used for vapor-phase MPV reactions.^{26,27)} For the MPV reaction of propiophenone at 523 K, Mg-Al mixed oxide is the most active among Mg-Al, Co-Al, Ni-Al and Cu-Al mixed oxides. The products are a mixture of 1-phenylpropyl alcohol and 2-methylstyrene, the ratio depending on the reaction temperature. Over MgO-Al₂O₃, propiophenone is completely converted into 2-methylstyrene. On MgO, the alcohol was formed predominantly in the temperature range 523–548 K.

The reduction of carbonyl compounds can be performed with hydrogen using supported metal catalysts such as Pt/C and Pd/C. However, carbonyl compounds

Table 5.10.1 Catalytic activity of MgO-Al₂O₃ for the transfer hydrogenation of α , β -unsaturated aldehydes with 2-propanol

Entry	Reductant	Product	Yield/% (h) ^{b)}	S/% ^{c)}	r_a ^{d)}
1			100 (9)	99	1.19
2			100 (9)	98	1.10
3			98 (10)	97	1.07
4			41 (10)	90	0.21
5			76 (10)	95	0.55
6			71 (10)	93	0.50

a) Reaction conditions: 3 mmol of aldehyde; 60 mmol of 2-propanol; $T = 355$ K; catalyst: 1 g.

b) Yield at time in parentheses.

c) Selectivity.

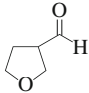
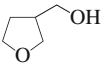
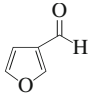
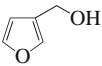
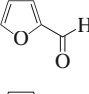
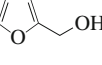
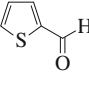
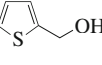
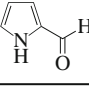
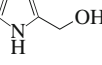
d) Catalytic activity in $\text{mmol h}^{-1} \text{g}_{\text{cat}}^{-1}$.

Reprinted with permission from M. A. Aramendia, V. Borau, C. Jiménez, J. M. Marinas, J. R. Ruiz, F. J. Urbano, *Appl. Catal., A*, **249**, 1 (2003) p.8, Table 5.

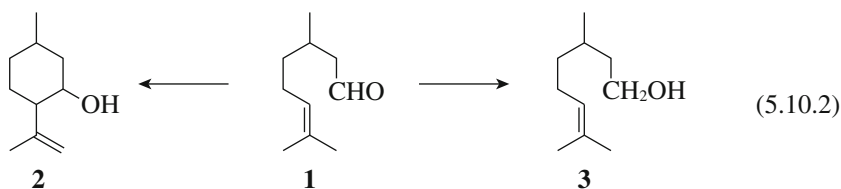
containing sulfur or nitrogen moieties cannot be reduced with metals as the metal is poisoned by the sulfur. Therefore, transfer hydrogenation is a useful means for the reduction of these compounds. Heterocyclic carbaldehydes can be hydrogenated with alcohols with MgO-Al₂O₃ mixed oxides. Vu et al. used a MgO-Al₂O₃ (Mg/Al = 2) for the hydrogenation of sulfur compound, thiophenecarbaldehyde, 5-bromothiophenecarbaldehyde and 4-methylthiobenzaldehyde.²⁸⁾ The three aldehydes were quantitatively reduced with 2-butanol into the corresponding alcohols in 3 h at 371 K. Various heterocyclic carbaldehydes were hydrogenated with 2-propanol in the presence of MgO-Al₂O₃ (Mg/Al = 2/0.84) and MgO-Al₂O₃-ZrO₂ (Mg/Al/Zr = 2.0/0.81/0.11).²⁹⁾ As shown in Table 5.10.2, the reactions provided conversions close to 90% with 100% selectivity in 24 h in all cases at 355 K. Regarding the heteroatom in the carbaldehyde, the reaction rate decreases in the following order thiophene > furane > pyrrole. Also the reaction proceeds faster with carbonyl substituents at position 2 than at 3.

Shabtai et al. studied the activities of zeolites for hydrogen transfer reactions using 2-propanol in a continuous flow reactor. *n*-Alkanals (C₅-C₁₂) are converted into alcohols at 453 K with high conversions and high selectivity (>95%) over NaX. Non-substituted and alkyl-substituted cycloalkanones having 4–15 membered rings were also investigated.³⁰⁾ The conversions depended on the position and size of the alkyl substituent. In the case of the reaction of citronellal **1**, two competing reactions, i.e., cyclization to isoplegol **2** and normal MPV reduction to citronellol **3**. The direction of the reaction is strongly dependent on the exchangeable cations. CsX yielded the MPV reduction product **3** with a selectivity of 92.3% at 423 K, while LiX, NaX and CaX preferentially produced the cyclic compound **2**.

Table 5.10.2 Transfer hydrogenation of heterocyclic carbaldehyde with 2-propanol over oxide catalysts

Substrate	Product	Conversion/%	
		MgO-Al ₂ O ₃	MgO-Al ₂ O ₃ -ZrO ₂
		69	90
		97	87
		99	95
		91	98
		89	100

Reaction conditions: carbonyl compounds: 3 mmol, 2-propanol: 60 mmol, catalyst: 1 g, 24 h, 353 K. Reprinted with permission from C. Jimenez-Sanchidrian, J. M. Hidargo, J. R. Ruiz, *Appl. Catal., A*, **303**, 23 (2006) p. 26, Table 3.

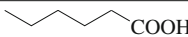
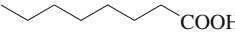
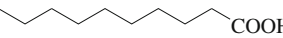
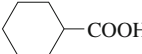
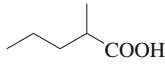
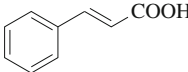
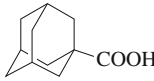
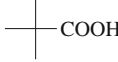
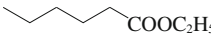
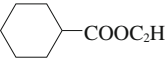
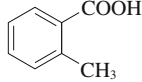
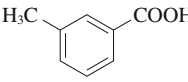
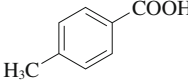


Hydrous zirconia is an excellent hydrogen transfer catalyst. Aldehydes and ketones are efficiently hydrogenated with 2-propanol under refluxing conditions.^{31,32} In the case of ketones, an α -substituted methyl group hinders the reaction. Thus cyclohexanone and 4-methylcyclohexanone were reduced faster than 2-methylcyclohexanone. The presence of a double bond conjugated to a carbonyl group serves to slow down the rate of some reactions. Only basic alcohols are effective for the transfer hydrogenation. The reduction of hexanal, benzaldehyde, cyclohexanone and acetophenone with 2-propanol-2*d* revealed the kinetic isotope effect of $(k_H/k_D) = 2.16\text{--}2.46$, indicating that the cleavage of C-H bond at the 2-position in 2-propanol is involved in the rate-limiting step. Cinnamaldehyde is selectively transformed into cinnamyl alcohol.³³ The aldehydes and ketones can be efficiently hydrogenated with 2-propanol also in the vapor phase.³⁴

Hydrated zirconia is also effective for the reduction of carboxylic acids and the esters with 2-propanol.³⁵⁾ The reactions were carried out with a flow reactor at 573 K. The corresponding alcohols were obtained in high yields, as shown in Table 5.10.3. The ester of the carboxylic acid was obtained as a by-product.

Dicarboxylic acid anhydride can be also reduced with 2-propanol over hydrous zirconia in vapor phase. For example, succinic anhydride gave γ -butyrolactone

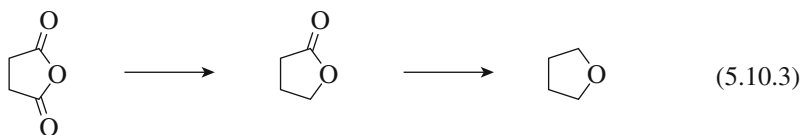
Table 5.10.3 Transfer hydrogenation of carboxylic acids with 2-propanol over hydrated zirconia

Reactant	Conversion/%	Selectivity/%	
		Alcohol	Ester
	100	81	tr.
	100	64	10
	100	34	19
	100	95	4
	100	84	tr.
	100	78	tr.
	89	53	2
	100	98	tr.
	100	80	—
	100	92	—
	43	0	67
	98	25	59
	100	31	33

Reaction conditions: ketone: carboxylic acid or ester: 0.2 mmol cm⁻³ in 2-propanol, feed rate: 5 cm³ h⁻¹, catalyst 2.0 g, temperature 573 K.

Reprinted with permission from K. Takahashi, M. Shibagaki, H. Kuno, H. Matsushita, *Chem. Lett.*, **18**, 1141 (1989) p.1142, Table 1.

(20% yield) and tetrahydrofuran (62% yield) at 553 K.³⁶⁾ γ -Butyrolactone is reduced to tetrahydrofuran under the same reaction conditions.



In the reduction of styrene oxide with ethanol and 2-propanol in the presence of MgO, 2-phenylethanol is obtained in 94.5% and 92.4% yields, respectively, free of isomeric 1-phenylethanol at 623 K.²⁰⁾

5.10.3 Reduction of Nitro-compounds and Nitriles with Alcohols

Nitro-compounds are hydrogenated into the corresponding amines with alcohols over MgO.³⁷⁾ In the reaction of nitrobenzene the order of reactivity for hydrogen donation of alcohols was methanol (91.4%) \approx 2-propanol (91.0%) > 2-butanol (54.4%) > 1-propanol (51.3%) > ethanol (47.3%) > 1-butanol (37.1%) > isobutyl alcohol (29.9%), where the numbers in parentheses are the yields of aniline at 723 K. In the reduction of β -nitrostyrene, a mixture of a total reduction product (β -phenylethylamine) and partial reduction products (β -phenylvinylamine and β -phenylnitroethane) are obtained. Nitroalkanes are also hydrogenated with alcohols. At 723 K, 1-nitropropane was hydrogenated with 2-propanol to yield 94.9% propylamine with almost 100% selectivity. At the same temperature, 1-nitrobutane was hydrogenated with 2-butanol to give butylamine in a 93.5% yield with 100% selectivity.

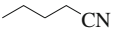
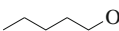
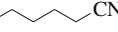
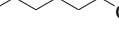
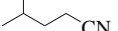
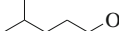
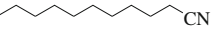
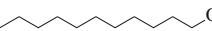
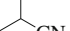
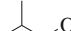


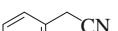
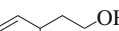
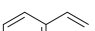
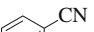
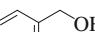
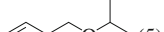
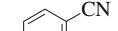
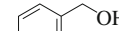
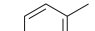
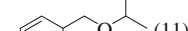
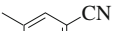
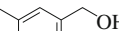
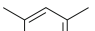
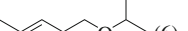
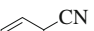
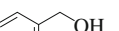
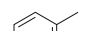

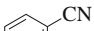
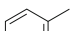
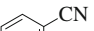
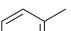
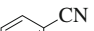
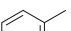
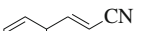
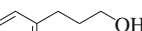



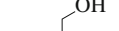


Nitriles are reduced with 2-propanol in vapor phase into the corresponding alcohols at 573 K over hydrous zirconia as shown in Table 5.10.4.³⁸⁾ The reduction of aliphatic nitriles proceeds efficiently to give the corresponding alcohols. Aromatic nitriles are also converted to the corresponding alcohols as main products. In the case of tolunitriles, isopropyl ethers of the produced alcohols and xylenes are also formed. The reduction of cyanopyridines gives mainly the corresponding picolines.

5.10.4 Oppenauer Oxidation

The dehydrogenation of 2-ethyl-1-hexanol to 2-ethylhexanal by hydrogen transfer with aliphatic aldehyde proceeds in gas phase over MgO.³⁹⁾ The reaction was done with acceptor/donor ratio of 3 at 673 K. As hydrogen acceptor, propanal was found to be the most effective in terms of activity and catalyst life-time.

MgO-Al₂O₃ mixed oxides (calcined hydrotalcite) were used for Oppenauer oxidation of various alcohols with benzophenone in toluene.⁴⁰⁾ Alcohols such as cyclohexanol, 1-hexanol, 2-hexanol, 2-methylcyclohexanol and borneol (*endo*-1,7,7-trimethylbicyclo[2,2,1]heptan-2-ol) were converted into the corresponding ketones at 383 K.

Table 5.10.4 Transfer hydrogenation of nitriles with 2-propanol over hydrated zirconia

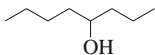
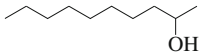
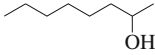
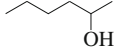
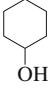
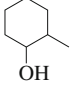
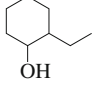
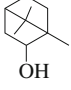
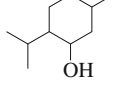
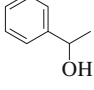
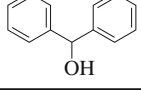
Nitrile	Conversion /%	Product (Selectivity/%)	
	98		(73)
	89		(78)
	92		(83)
	58		(52)
	98		(95)
	89		(90)
	100	 (29)	 (39)
	98	 (64)	 (5)
	83	 (54)	 (8)  (11)
	86	 (71)	 (2)  (6)
	79	 (58)	 (2)  (7)
	100		(39)
	100		(50)
	66		(30)
	100		(46)
	88		(88)
	100	 (43)	 (21)  (29)

Reaction conditions: 0.2 mmol cm^{-3} in 2-propanol, feed: $5 \text{ cm}^3 \text{ h}^{-1}$, catalyst: 2.0 g, temperature: 573 K
 Reprinted with permission from K. Takahashi, M. Shibagaki, H. Matsushita, *Chem. Lett.*, **19**, 311 (1990) p.313, Table 1.

Piperonal (1,3-benzodioxole-5-carbaldehyde, heriotropine) is widely used in fragrance and pharmaceutical preparations.⁴¹⁾ Piperonal can be synthesized from piperonyl alcohol by Oppenauer oxidation, using paraformaldehyde as the hydrogen acceptor with toluene as the solvent at 383 K. Calcined hydrotalcite gives 97% selectivity for piperonal with almost 100% conversion of piperonyl alcohol in 8 h. The catalyst can be regenerated by calcination at 823 K.

The Oppenauer oxidation of various secondary alcohols with acetone in ben-

Table 5.10.5 Oxidation of secondary alcohols with acetone over hydrated zirconia

Reactant	Time/h	Conv./%	Yield/%	k/s^{-1}
	8.0	100.0	100.0	3.33×10^{-5}
	8.0	100.0	91.9	6.39×10^{-5}
	4.0	100.0	99.6	8.89×10^{-5}
	1.5	100.0	87.4	2.31×10^{-4}
	1.5	68.7	48.1	—
	8.0	100.0	87.9	6.11×10^{-5}
	10.0	100.0	92.7	4.01×10^{-5}
	8.0	100.0	100.0	3.89×10^{-5}
	8.0	19.2	19.2	2.78×10^{-6}
	6.0	100.0	98.6	8.33×10^{-5}
	8.0	100.0	100.0	3.06×10^{-5}

Reaction conditions: alcohol; 0.25 mmol, acetone; 1.0 cm³, benzene; 9.0 cm³, temperature; 353 K.

Reprinted with permission from H. Kuno, K. Takahashi, M. Shibagaki, *Bull. Chem. Soc. Jpn.*, **63**, 1943 (1990) p. 1944, Table 1.

zene proceeds very efficiently in the presence of hydrous zirconia at 353 K.⁴²⁾ For example, borneol is converted into camphor in a 100% yield (Table 5.10.5).

In the oxidation of primary alcohols, acetone is not effective as a hydrogen acceptor. Instead, benzophenone can be used.⁴³⁾ The reaction can also be performed with a flow reaction system. With a flow reaction system, 1-octanol was oxidized with benzophenone to the corresponding aldehyde in a 74.1% yield at 473 K. The catalytic activity and selectivity are promoted by modifying hydrous zirconia with trimethylsilyl chloride.⁴⁴⁾ The modification inhibits the aldol condensation of the hydrogen acceptor and the aldehyde product by the acidic hydroxyl groups. Thus, 1-octanol can be oxidized with benzaldehyde to afford a 67% yield of the corresponding aldehyde in xylene under a reflux condition.

The Oppenauer oxidation of cinnamyl alcohol and geraniol in the presence of hydrous zirconia was reported by Liu et al.⁴⁵⁾ Furfural was found to be more efficient than benzaldehyde as the oxidant. Hydrous zirconia showed higher activity when about 1 wt% of Si was incorporated. The hydrated zirconia was most active when calcined at 523–573 K. Cinnamyl alcohol was oxidized with furfural in toluene to give cinnamaldehyde in a 92.4% yield with 100% selectivity in 24 h at 483 K (under reflux) in the presence of hydrated zirconia containing 1.2% Si. Using the same catalyst, geraniol gave citral in 93.8% selectivity at 85.3% conversion of geraniol in 24 h.

5.10.5 Reduction with Hydrocarbons

Hydrogen transfer reductions can be performed by using hydrocarbons such as cyclohexene or *n*-alkane over MgO.⁴⁶⁾ Cyclohexene oxide was reduced with cyclohexene to cyclohexanol (38% yield) at 673 K. Nitrobenzene was reduced with cyclohexene and decane to afford aniline in 56% and 57% yields, respectively, at 673 K.

Hydrogenation of 1,3-butadiene with 1,3-cyclohexadiene over metal oxides such as MgO, CeO₂ and ZrO₂ has been studied.⁴⁷⁻⁵⁰⁾ The rates of the transfer hydrogenation with 1,3-cyclohexadiene are higher by one or two orders of magnitude than those of hydrogenation with H₂. Over ZrO₂, the main product is 1-butene in the transfer hydrogenation, while it was 2-butenes in the hydrogenation with H₂.

References

1. E. J. Creighton, S. D. Ganeshie, R. S. Downing, H. van Bekkum, *J. Mol. Catal., A*, **115**, 457 (1967).
2. Y. Zhu, G. Chuah, S. Jaenicke, *J. Catal.*, **227**, 1 (2004).
3. A. Corma, M. E. Domine, S. Valencia, *J. Catal.*, **215**, 294 (2003).
4. Y. Zhu, S. Jaenicke, G. K. Chuah, *J. Catal.*, **218**, 396 (2003).
5. G. K. Chuah, S. Jaenicke, Y. Z. Zhu, S. H. Liu, *Curr. Org. Chem.*, **14**, 1639 (2006).
6. H. Niiyama, E. Echigoya, *Bull. Chem. Soc. Jpn.*, **45**, 939 (1972).
7. V. A. Ivanov, J. Bachelier, F. Audry, J. C. Lavalley, *J. Mol. Catal.*, **91**, 45 (1994).
8. Y. Okamoto, T. Imanaka, S. Terasaki, *Bull. Chem. Soc. Jpn.*, **45**, 3207 (1972).
9. C. L. Kibby, W. K. Hall, *J. Catal.*, **31**, 65 (1973).

10. N. Venkatasubramanian, D. V. Ramana, C. N. Pillai, *J. Catal.*, **51**, 40 (1978).
11. G. H. Posner, A. W. Rumquist, M. J. Chapdelaine, *J. Org. Chem.*, **42**, 1202 (1977).
12. D. V. Ramana, C. N. Pillai, *J. Canad. Chem.*, **47**, 3704 (1969).
13. J. Kijeński, M. Gliński, J. Czarecki, *J. Chem. Soc., Perkin Trans. 1*, **1991**, 1695.
14. M. Gliński, A. Gadomska, *React. Kinet. Catal. Lett.*, **65**, 121 (1998).
15. M. Gliński, *Appl. Catal., A*, **349**, 133 (2008).
16. J. Kijeński, M. Gliński, A. Quiroz, *Appl. Catal., A*, **150**, 77 (1997).
17. K. Gotoh, J. Kubo, W. Ueda, T. Mori, Y. Morikawa, *Chem. Lett.*, **32**, 1132 (2003).
18. J. Kasper, A. Trovarelli, M. Lenarda, M. Graziani, *Tetrahedron Lett.*, **30**, 2705 (1989).
19. M. Ueshima, Y. Shimazaki, *Catal. Lett.*, **15**, 405 (1992).
20. J. Kijeński, M. Gliński, J. Reinhercs, *Stud. Surf. Sci. Catal.*, **41**, 231 (1989).
21. P. S. Kumbher, J. Sanchez-Valente, J. Lopez, F. Figueras, *Chem. Commun.*, **1998**, 535.
22. J. R. Ruiz, C. Jiménez-sanchidrián, J. M. Hidalgo, J. M. Marinas, *J. Mol. Catal., A*, **246**, 190 (2006).
23. M. A. Aramendía, V. Borau, C. Jiménez, J. M. Marinas, J. R. Ruiz, F. J. Urbano, *Appl. Catal., A*, **206**, 95 (2001).
24. Y. Zhu, S. S. Liu, S. Jaenicke, G. Chuah, *Catal. Today*, **97**, 249 (2004).
25. M. A. Aramendía, V. Borau, C. Jiménez, J. M. Marinas, J. R. Ruiz, F. J. Urbano, *Appl. Catal., A*, **249**, 1 (2003).
26. T. M. Joshi, T. Raja, K. Sreekumar, M. B. Talawar, B. S. Rao, *Appl. Catal., A*, **157**, 193 (2001).
27. T. M. Joshi, T. Raja, B. S. Rao, *J. Mol. Catal.*, **168**, 187 (2001).
28. T.-T. Vu, R. S. Kumbher, F. Figueras, *Adv. Synth. Catal.*, **345**, 493 (2003).
29. C. Jiménez-Sanchidrián, J. M. Hidalgo, J. R. Ruiz, *Appl. Catal., A*, **303**, 23 (2006).
30. J. Shabtai, A. Lazer, E. Biron, *J. Mol. Catal.*, **27**, 35 (1984).
31. H. Matsushita, S. Ishiguro, H. Iichinose, *Chem. Lett.*, **14**, 731 (1985).
32. M. Shibagaki, K. Takahashi, H. Matsushita, *Bull. Chem. Soc. Jpn.*, **61**, 3283 (1988).
33. S. H. Liu, S. Jaenicke, G. K. Chah, *J. Catal.*, **206**, 321 (2002).
34. M. Shibagaki, K. Takahashi, H. Kubo, H. Kawakami, H. Matsushita, *Chem. Lett.*, **17**, 1633 (1988).
35. K. Takahashi, M. Shibagaki, H. Kuno, H. Matsushita, *Chem. Lett.*, **18**, 1141 (1989).
36. K. Takahashi, M. Shibagaki, H. Matsushita, *Bull. Chem. Soc. Jpn.*, **65**, 262 (1992).
37. J. Kijeński, M. Gliński, R. Wiśniewski, S. Murghani, *Stud. Surf. Sci. Catal.*, **59**, 169 (1991).
38. K. Takahashi, M. Shibagaki, H. Matsushita, *Chem. Lett.*, **19**, 311 (1990).
39. M. Gliński, J. Kijeński, J. Rusczyński, *React. Kinet. Catal. Lett.*, **54**, 1 (1995).
40. T. Raja, T. M. Jyoshi, K. Streeumar, M. B. Talawar, J. Santhanalakshmi, B. S. Rao, *Bull. Chem. Soc. Jpn.*, **72**, 2117 (1999).
41. V. Vorzatta, E. Capparella, R. Chiappino, D. Impalá, E. Poluzzi, A. Vaccardi, *Catal. Today*, **140**, 112 (2008).
42. H. Kuno, K. Takahashi, M. Shibagaki, *Bull. Chem. Soc. Jpn.*, **63**, 1943 (1990).
43. H. Kuno, M. Shibagaki, K. Takahashi, H. Matsushita, *Bull. Chem. Soc. Jpn.*, **64**, 312 (1991).
44. H. Kuno, M. Shibagaki, K. Takahashi, H. Matsushita, *Bull. Chem. Soc. Jpn.*, **66**, 1699 (1993).
45. S. H. Liu, G. K. Chuah, S. Jaenicke, *J. Mol. Catal., A*, **220**, 267 (2004).
46. M. Gliński, R. Wolski, *React. Kinet. Catal. Lett.*, **73**, 21 (2001).
47. T. Yamaguchi, J. W. Hightower, *J. Am. Chem. Soc.*, **99**, 4201 (1974).
48. T. Yamaguchi, H. Shima, *Chem. Lett.*, **8**, 899 (1979).
49. Y. Nakano, T. Yamaguchi, K. Tanabe, *J. Catal.*, **80**, 307 (1983).
50. H. Shima, T. Yamaguchi, *J. Catal.*, **90**, 160 (1984).

5.11 Esterification and Transesterification

5.11.1 Catalysts for Esterification and Transesterification

Esterification reactions are catalyzed by both acids and bases. For esterification, solid acids such as cation-exchange resins are mainly used. Solid bases are useful as catalyst for transesterification reactions.

Hydrous zirconia is very efficient catalyst for the esterification of a great

variety of combination of acids and alcohols in both liquid and vapor phase.¹⁾ Table 5.11.1 shows the results of the esterification in vapor phase.

The transesterification of ethyl acetate with methanol, 2-propanol and *t*-butyl alcohol was examined on a variety of solid bases by Hattori et al.²⁾ For transesterification of ethyl acetate with methanol and 2-propanol, high activity was observed for MgO, CaO, SrO, BaO, KF/Al₂O₃ and KOH/Al₂O₃. Alkaline earth carbonates, ZrO₂, ZnO and γ -alumina were inactive. La₂O₃ showed high activity for methanol but low activity for 2-propanol. For transesterification of ethyl acetate with *t*-butyl alcohol, alkaline earth oxides, KF/Al₂O₃ and KOH/Al₂O₃ showed activities one order of magnitude smaller than those with methanol over the same catalysts. For transesterification, the catalysts retained their activity even after exposure to air though a short induction time appeared. Stronger adsorption of alcohols over carbon dioxide was demonstrated by infrared spectroscopy.

Acylation of alcohols with acetic acid proceeds efficiently in the liquid phase over the microporous titanasilicate ETS-10.³⁾ Activity for acylation of primary alcohols depends on the exchanged cations and increases in the order Li < Na < K < Ba ~ H ~ Rb ~ Cs. Table 5.11.2 shows the results of acylation of alcohols with acetic acid over Na, K-ETS-10. Primary alcohols are more reactive than secondary alcohols. The catalyst shows good activity even after three cycles. ETS-10 is also active for the acylation of 2-phenylethanol with long chain acids (octanoic, nanoic and decanoic acid).

The transesterification of methyl benzoate and dimethyl terephthalate with ethylene glycol was investigated in the presence of basic zeolites.⁴⁾ An excess amount of ethylene glycol was used and liberated methanol was continuously removed. In the transesterification of methyl benzoate with ethylene glycol, the pure NaX resulted in a high conversion of the benzoate with a high selectivity for 2-hydroxyethyl benzoate. Loading of Na or Cs₂O on NaX and CsX, respectively, led to increased conversion. The conversion of the benzoate and the selectivity over Cs₂O/CsX were 83.7% and 92.2%, respectively. In the transesterification of dimethyl terephthalate and ethylene glycol at 453 K, NaX gave a very high conversion, the product being exclusively the monoester, 2-hydroxyethyl terephthalate. Over Cs₂O/CsX, the transesterification of dimethyl terephthalate and ethylene glycol led to the formation of bis (2-hydroxyethyl) terephthalate with a selectivity of 59% at a conversion of 94% at 453 K.

Transesterification of dimethyl malonate with various alcohols with amino-functionalized SBA-15 was reported.⁵⁾

β -Ketoesters are transesterified with a variety of alcohols over solid bases. The catalysts include TBD anchored on MCM-41,⁶⁾ amine-functionalized silica gel,^{7,8)} calcined hydrotalcite⁹⁾ and hydrotalcite with *t*-butoxide ions (Mg-Al-BuO⁻).¹⁰⁾

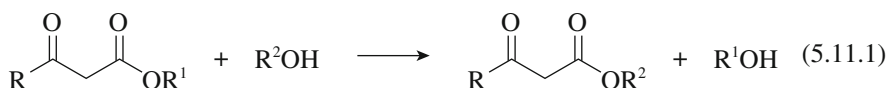
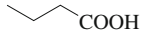
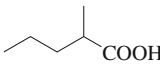
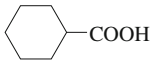
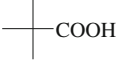
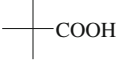
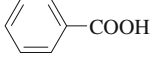
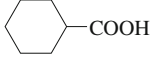

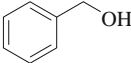
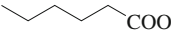
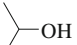

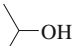
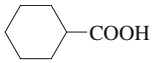
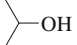
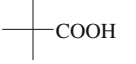
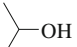
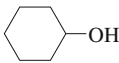
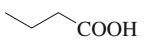
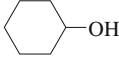
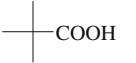
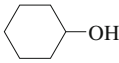
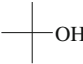


Table 5.11.1 Esterification in vapor phase over hydrous zirconium oxide^{a)}

Entry	Reactant	Temperature/°C	Conversion/%	Selectivity/%	
1		C ₂ H ₅ OH	200	100	100
2		C ₂ H ₅ OH	200	100	100
3		C ₂ H ₅ OH	215	100	91
4		C ₂ H ₅ OH	200	99	98
5		C ₂ H ₅ OH	250	100	60
6		C ₂ H ₅ OH	200	100	100
7			250	100	78
8 ^{b)}	CH ₃ COOH		150	37	100
9			215	100	87
10			200	96	97
11			215	80	94
12			200	31	100
13 ^{c)}	CH ₃ COOH		200	100	100
14 ^{c)}			200	34	98
15 ^{c)}			280	22	83
16	C ₂ H ₅ COOH		200	7	98

^{a)} Catalyst: 2.0 g; carboxylic acid: 0.1 mol dm⁻³ in alcohol; sample feed: 10 cm³ h⁻¹.

^{b)} Acetic acid: benzyl alcohol = 2.5 : 1; sample feed: 5 cm³ h⁻¹.

^{c)} Carboxylic acid: 0.1 mol dm⁻³; alcohol: 0.5 mol⁻³ in benzene.

Reprinted with permission from K. Takahashi, M. Shiragaki, H. Matsushita, *Bull. Chem. Soc. Jpn.*, **62**, 2353 (1989) p. 2354, Table 1.

Table 5.11.2 Acylation of various alcohols with acetic acid over Na, K-ETS-10

Nos.	Substrate	Conversion/%	Others ^{a)} /%	Acylation selectivity/% ^{b)}
1	Benzyl alcohol	97.2	1.2	98.7
2	2-Phenylethanol	97.8	0.8	99.2
3	1st recycle ^{c)}	96.2	0.9	99.0
4	2nd recycle ^{c)}	94.2	0.7	99.2
5	3rd recycle ^{c)}	91.3	0.8	99.1
6	2-Phenylethyl alcohol ^{d)}	31.1	1.2	97.3
7	Tetrahydrofurfuryl alcohol	98.0	0.9	99.1
8	1-Nonanol	91.5	0.1	99.8
9	1-Dodecanol	99.4	—	100
10	1-Dodecanol ^{d)}	29.3	0.1	99.8
11	β -Citronellol	99.5	9.0	90.9
12	Hexane-3-ol	87.2	4.3	95.1
13	Cyclohexanol	83.7	—	100
14	Cyclohexanol ^{d)}	23.7	0.2	99.1
15	Menthol	70.3	—	100

Reaction conditions: temperature = 120°C; substrate = 5 mmol; acetic acid = 4 mL; duration of run = 8 h.

^{a)} Mainly C-alkylated products.

^{b)} Selectivity = (mol% expected product/mol% conversion) \times 100.

^{c)} Catalyst recycled for acylation of 2-phenylethanol.

^{d)} Without catalyst.

Reprinted with permission from S. B. Waghmode, V. V. Thakur, A. Sudalai, S. Sivasanker, *Tetrahedron Lett.*, **42**, 3145 (2001) p. 3146, Table 2.

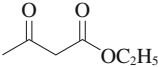
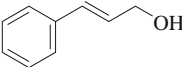
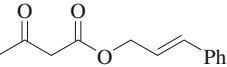
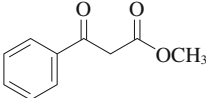
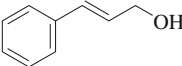
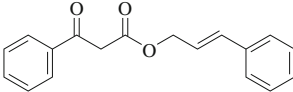
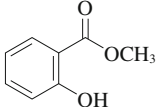
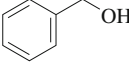
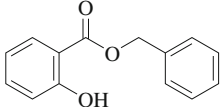
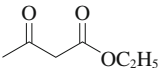

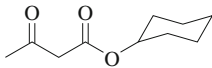
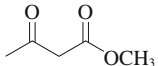
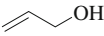
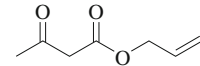
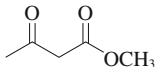
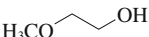
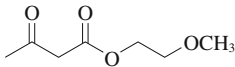
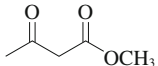
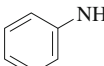
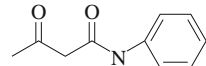
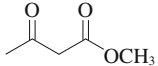

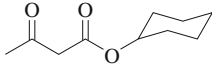
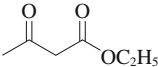
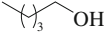
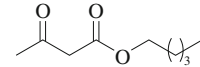
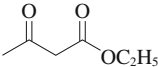
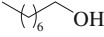
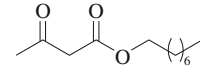
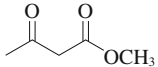
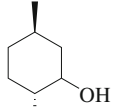
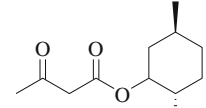
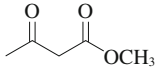
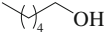
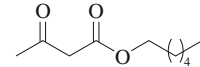
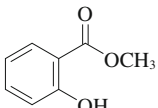
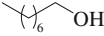
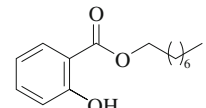
Table 5.11.3 shows the results with Mg-Al-^tBuO⁻.⁹⁾ In a typical run, 0.130 g (1 mmol) of ethyl acetoacetate, 0.134 g (1 mmol) of cinnamyl alcohol and 25 mg of catalyst in 10 mL dry toluene was stirred for 2 h at 363 K. Excellent yields were obtained with a variety of primary, secondary, unsaturated, allylic, cyclic and hindered alcohols.⁹⁾ The catalyst is also useful for normal esters (entries 3 and 13). The transamidation also affords an excellent yield (entry 7). The Mg-Al-^tBuO⁻ catalyst is more active than rehydrated hydrotalcite and calcined hydrotalcite. As-synthesized hydrotalcite has no activity.

Transesterification of β -ketoesters by *N, N*-diaminopropylated silica was reported by Hagiwara et al. For example, the reaction of methyl acetoacetate with menthol over this catalyst in refluxing xylene gave a 98% of the expected product in 7 h.⁷⁾ The transesterification of 2-carbomethoxypentanone with various alcohols also proceeds to give a very high yield.⁷⁾

Transesterification of α -haloesters can be performed by their reactions with aromatic or aliphatic alcohols under reflux in toluene using Dean-Stark apparatus in the presence of MgO-Al₂O₃ mixed oxide (calcined hydrotalcite) at 723 K.⁹⁾ The corresponding esters were obtained in good to excellent yields. For example, the reaction of methyl bromoacetate with benzyl alcohol gave benzyl bromoacetate in 88% yield in the presence of the mixed oxide in 2 h.⁹⁾

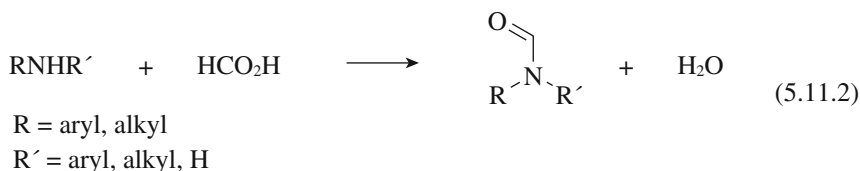
The reaction of amines with formic acid in the presence of ZnO under solvent-free conditions brings about highly efficient *N*-formylation to give the corresponding formamides in excellent yields under mild conditions.¹¹⁾

Table 5.11.3 Transesterification of β -ketoesters by hydrotalcite with $t\text{BuO}^-$ ions

Entry	Substrate (1)	Substrate (2)	Time /h	Product (3)	Yields (3) ^{a)}
1			2		74
2			2		90
3			3		98
4			2		97
5			1.5		95
6			1		96
7			2		95
8			2		98
9			3		97
10			2.5		97
11			2		90
12			2		98 (97) ^{b)}
13			2		92

^{a)} Isolated yields. ^{b)} Yield after 6th cycles.

Reprinted with permission from B. M. Choudary, M. L. Kantam, Ch. V. Reddy, S. Arangnatham, P. L. Santhi, F. Figueras, *J. Mol. Catal.*, **159**, 411 (2006) p. 413, Table 1.



The reaction of aniline (1 mmol) with formic acid (3 mmol) in the presence of ZnO (0.04 g) at 333 K gave *N*-methylformanilide in 99% yield in 10 min. The reaction is chemoselective.

5.11.2 Reactions of Alkyl Carbonates with Acids and Alcohols

Reactions of *o*- and *p*-hydroxybenzoic acids in dimethyl carbonate (DMC) in the presence of NaY chemoselectively give the methyl esters of the benzoic acids.¹²⁾ No *O*-alkylation occurs. Thus, the reaction of *o*-hydroxybenzoic acid for 15 h at 423 K gave the corresponding methyl ester in 93% isolated yield. Similarly, the reactions of mandelic acid and phenyllauric acid in DMC give the corresponding methyl ester selectively in the presence of NaY at 438 K.

Reaction of indoyl-3-acetic acid with DMC selectively affords the methyl ester (95-96% isolated yield) in the presence of NaX or KX at 433 K.¹³⁾ In the reaction at a higher temperature (453 K), both esterification and methoxycarbonylation occur to afford methyl (*N*-methoxycarbonyl)indoyl-3-acetate in 97-98% isolated yield). The reactions of indoyl-3-propanoic acid and indoyl-3-butanoic acid with DMC proceed in a similar manner.¹³⁾

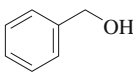
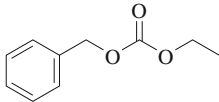
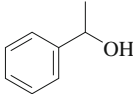
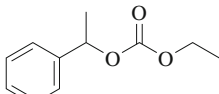
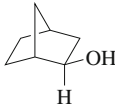
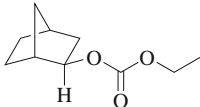
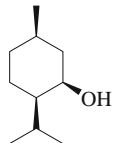
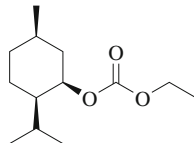
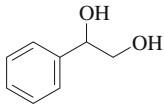
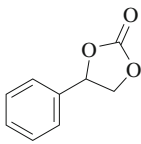
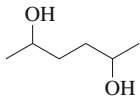
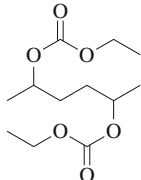
Diphenyl carbonate is a precursor for the production of aromatic polycarbonate. The reaction of phenol with dimethyl carbonate (DMC) over as-synthesized hydrotalcite was reported.¹⁴⁾ The hydrotalcite bearing NO₃⁻ in the interlayer is more active than the calcined hydrotalcite. A 14.7% yield of diphenyl carbonate and 11.6% yield of methyl phenyl carbonate based on DMC were obtained together with 5.6% of anisole at 433 to 453 K in 10 h. Gas-phase transesterification of DMC and phenol over TiO₂/SiO₂ has been reported.¹⁵⁾

When DMC and ethanol (1 : 4) was reacted in the presence of hydrotalcite having ^tBuO⁻ ions in the interlayers at 353 K gave 86.4% conversion of DMC in 7 h, the product selectivity being 70.8% and 25.9% for diethyl carbonate and ethyl methyl carbonate, respectively.¹⁶⁾

Dipropyl carbonate (DPC) is a more stable and safer electrolyte for lithium batteries than DMC or diethyl carbonate (DEC). Li et al. synthesized DPC from DMC and 1-propanol using KNO₃ supported on MCM-48.¹⁷⁾ The activity depended on the calcination temperature and loading amount of KNO₃. The highest DMC conversion and DPC selectivity were 99.9% and 93.4%, respectively.

Unsymmetrical alkyl carbonates can be synthesized from dialkyl carbonate and alcohols. The efficient synthesis of unsymmetrical carbonates from DEC and alcohols in the presence of CsF/ α -Al₂O₃ was reported.^{18,19)} Different unsymmetrical alkyl carbonates are synthesized in good yield and excellent selectivity, as shown in Table 5.11.4. Diols also react with DEC.

Table 5.11.4 Transesterification of diethyl carbonate with various alcohols over CsF/ α -Al₂O₃^{a)}

Alcohol ^{a)}	Product	Reaction time/min	Yield/% ^{b)}
		30	98
		20 30 ^{c)} 90 ^{d)} 720 ^{e)}	99 98 ^{c)} 82 ^{d)} 14 ^{e)}
		15	99
		40 45 ^{c)}	99 97 ^{c)}
		25	98
		45	98

^{a)} Reactions performed on 2 mmol alcohol with 33 mmol of diethyl carbonate and 0.1 g of catalyst without solvent in nitrogen atmosphere at 403 K.

^{b)} Isolated yields.

^{c)} Second cycle.

^{d)} Third cycle.

^{e)} Fourth cycle.

Reproduced with permission from J.-M. Clacens, D. Genuit, B. Veldurthy, G. Bergeret, L. Delmonte, A. Garcia-Ruiz, F. Figueras, *Appl. Catal., B*, **53**, 95 (2004) p.99, Table 4.

MgO-La₂O₃ mixed oxides,²⁰⁾ diisopropylamide-loaded hydrotalcite²¹⁾, high-surface area MgO²²⁾ and TBD tethered to MCM-41²³⁾ are also active for the transesterification of alkyl carbonates and alcohols.

Polycarbonate diols (PCDL) can be synthesized by the reaction of DMC and hexane-1,6-diol followed by vacuum evacuation in the presence of KF/Al₂O₃.²⁴⁾



A yield of PCDL up to 96% was obtained with the Mn of 1006.

Glycerol carbonate can be synthesized from glycerol and DMC in the presence of solid base catalysts such as CaO.²⁵⁾ CaO was most active when calcined at 1173 K. CaO, which was not calcined but simply dried at 383 K overnight, was also active and gave 100% conversion of glycerol with >95% selectivity at 368 K and DMC/glycerol molar ratio = 3.5 at the reaction time of 1.5 h.

5.11.3 Reaction of Alkyl Carbonates with Amines

Carbamates are synthesized from amines and alkyl carbonates. Vauthey et al. reported that the synthesis of carbamates by reaction of dimethyl carbonate with amines such as aniline, 1-phenylethylamine and octylamine in good to excellent yields in the presence of $\gamma\text{-Al}_2\text{O}_3$.²⁶⁾



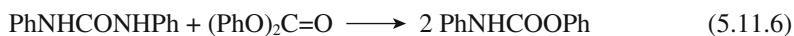
The reaction requires a large amount of catalyst.

The reaction of aliphatic amines with diethyl carbonate using TBD tethered to MCM-41 gives carbamates.²³⁾



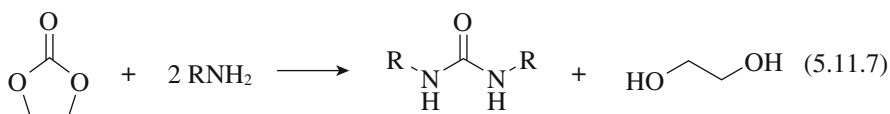
Products are obtained in high yield and very good selectivity, as shown in Table 5.11.5. *N*-Carbathoxyguanidium ion is proposed as an intermediate.

Reaction of *N,N*-diphenyl urea with diphenyl carbonate gives phenyl *N*-phenyl carbamate.²⁷⁾



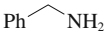
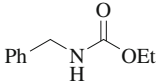
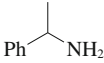
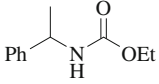
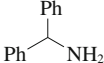
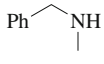
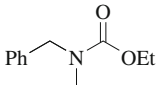
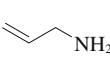
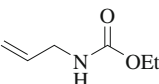
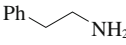
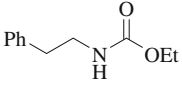
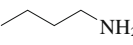
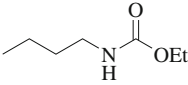
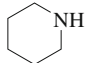
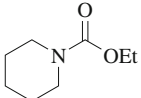
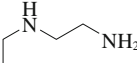
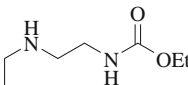
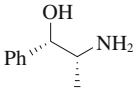
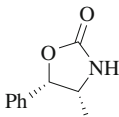
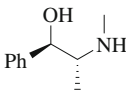
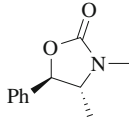
The reaction was catalyzed by solid bases such as hydrotalcite, Na-ZSM-5 and $\text{LiO}_2\text{-MgO}$ to afford the high yield of the carbamate (90–95%) at 423 K. Silica gel also showed high activity.

Reaction of amine and ethylene carbonate gives *N,N'*-substituted urea.



Reaction of ethylene carbonate with propylamine and butylamine at 373 K for 3 h in the presence of CaO gave the corresponding urea in 68% and 78% yields, respectively.²⁸⁾ Similarly, the reaction of ethylene carbonate with hexyl amine and benzyl amine gave the urea in 77% and 55% yields at 398 K and 423 K, respectively.

Table 5.11.5 Synthesis of carbamates from aliphatic amines and diethyl carbonate in the presence of TBD-MCM-41

Entry	Reagent	Product	Yield/%	Selectivity/%
a			98	99
b			16 52 ^{a)}	98 97
c		—	0	0
d			76	97
e			55	98
f			82	97
g			72	98
h			90	98
i			89	97
j			59 ^{a)}	86
k			72 ^{a)}	87

Reaction conditions: amine: 10 mmol, diethyl carbonate: 20 mL, TBD-MCM-41: 0.100 g, at reflux temperature, 15 h.

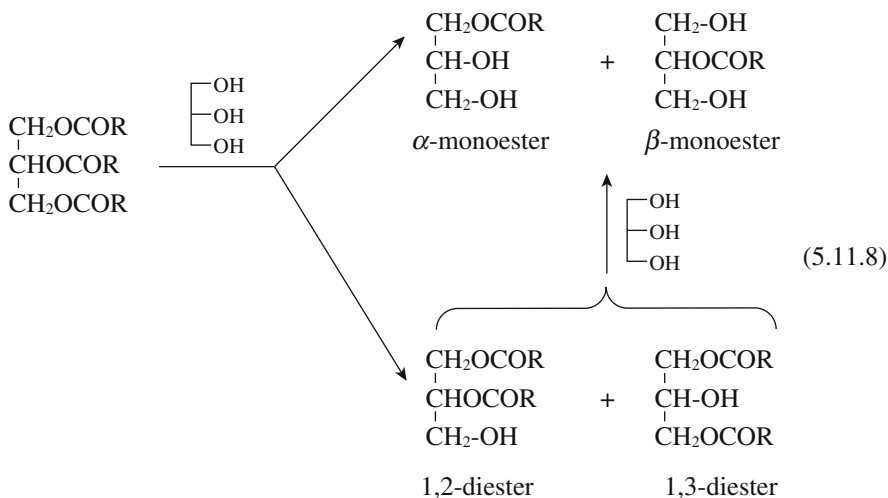
^{a)} TBD-MCM-41: 0.200 g, 24 h.

Reprinted with permission from S. Carloni, D. E. De Vos, P. A. Jacobs, R. Maggi, G. Sartori, R. Sartorio, *J. Catal.*, **205**, 199 (2002) p. 203, Table 1.

5.11.4 Synthesis of Monoglyceride

Edible and surface active monoesters and diesters of fatty acids and glycerol are the major emulsifiers used in food products as well as the pharmaceutical and cosmetic industries. The glycerolysis of fats and oils is one of the important methods for the preparation of mono- and diglycerides.

Corma et al. evaluated solid base catalysts, e.g., Cs-exchanged MCM-41, MgO and MgO-Al₂O₃ mixed oxides (calcined hydrotalcite), for the glycerolysis of triolein (trioleoyl glycerol) and rapeseed oil.²⁹⁾ The reaction paths can be expressed as follows.



They obtained the best results with MgO, while the MgO-Al₂O₃ mixed oxides also showed good activity for the glycerolysis of triolein. The conversion of triolein reached 97% after 5 h reaction at 513 K and monoglyceride selectivities of 73% were achieved. A large molar excess of glycerol (12 : 1) must be used because of the low solubility of glycerol in fat phase. The transesterification of rapeseed oil with glycerol also proceeded efficiently over MgO and the mixed oxides.

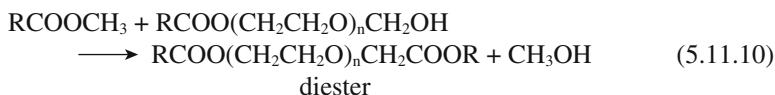
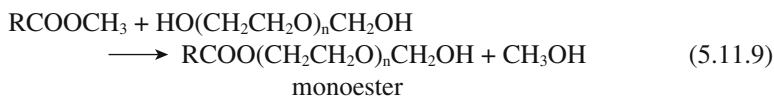
The catalytic activity of K₂CO₃/Al₂O₃, which has been heated at 823 K under vacuum, is also active for the transesterification of triolein with glycerol.³⁰⁾ The reaction with a glycerol/triolein molar ratio of 6 in 1,4-dioxane at 453 K for 5 h gave monooleins in 72% yield with 28% dioleins.

The transesterification of glycerol with fatty acid esters is another method for obtaining monoglycerides. Bancquart et al. studied the preparation of the monoglyceride and diglyceride by transesterification of glycerol with methyl stearate with basic metal oxides, MgO, CeO₂, La₂O₃ and ZnO.³¹⁾ MgO was the most active catalyst. The catalytic activity of the MgO was further increased by the addition of lithium.³²⁾ Corma et al. examined the activities and selectivity in transesterification of methyl stearate with glycerol by various solid base catalysts.³³⁾ All catalysts studied gave high conversions (>95%). The activity order was KF/Al₂O₃ >

$\text{Al}_2\text{O}_3\text{-Li}_2\text{O}$ (HT) > rehydrated hydrotalcite \approx MgO > $\text{MgO-Al}_2\text{O}_3$; here $\text{Al}_2\text{O}_3\text{-Li}_2\text{O}$ (HT) and $\text{MgO-Al}_2\text{O}_3$ (HT) are mixed oxides prepared by calcinations of hydrotalcite materials containing corresponding elements. The highest selectivity (80%) for the monoglyceride was obtained with rehydrated hydrotalcite.

5.11.5 Synthesis of Polyoxyglycol Esters

Fatty acid monoesters of polyethylene glycols are non-ionic surfactants having wide applications. The transesterification of methyl ester of fatty acids and various polyglycols of different molecular weights proceeds over solid base catalysts.³³⁾



MgO , calcined and rehydrated hydrotalcite, and $\text{Al}_2\text{O}_3\text{-Li}_2\text{O}$ mixed oxide obtained by calcination of the layered double hydroxide $[\text{Al}_2\text{Li}(\text{OH})_6]_2\text{CO}_3 \cdot n\text{H}_2\text{O}$, showed good performance. 90% conversion of methyl oleate (MeO) with 98% selectivity to the monoester was attained in the reaction with 4 : 1 ratio of PEG-600/MeO over $\text{Al}_2\text{O}_3\text{-Li}_2\text{O}$ at 493 K for 1 h.

References

1. K. Takahashi, M. Shiragaki, H. Matsushita, *Bull. Chem. Soc. Jpn.*, **62**, 2353 (1989).
2. H. Hattori, M. Shima, H. Kabashima, *Stud. Surf. Sci. Catal.*, **130**, 3507 (2000).
3. S. B. Waghmode, V. V. Thakur, A. Sudalai, S. Sivasanker, *Tetrahedron Lett.*, **42**, 3145 (2001).
4. S. Saravanamurgan, Sujandi, D.-S. Han, J.-B. Koo, S.-E. Park, *Catal. Commun.*, **9**, 158 (2008).
5. U. Meyer, W. F. Hölderich, *Appl. Catal., A*, **178**, 159 (1999).
6. M. L. Kantam, P. Sreekanth, *Catal. Lett.*, **77**, 241 (2001).
7. H. Hagiwara, A. Koseki, K. Isobe, K. Shimizu, T. Hoshi, T. Suzuli, *Synlett*, 2188 (2004).
8. G. Sathicq, L. Musante, G. Romanelli, G. Pasquale, J. Autimo, H. Thomas, P. Vázquez, *Catal. Today*, **133-135**, 455 (2008).
9. V. J. Bulbule, H. B. Borate, Y. S. Munot, Y. S. Munot, V. H. Deshpande, S. P. Sawargave, A. G. Gaiwad, *J. Mol. Catal., A*, **279**, 158 (2007).
10. B. M. Choudary, Ch. V. Reddy, S. Arangathan, *J. Mol. Catal., A*, **159**, 411 (2000).
11. M. Hosseini-Sarvari, H. Sharghi, *J. Org. Chem.*, **71**, 6652 (2006).
12. M. Selva, P. Tundo, *J. Org. Chem.*, **71**, 1664 (2006).
13. M. Selva, P. Tundo, D. Brunelli, A. Perosa, *Green Chem.*, **9**, 463 (2007).
14. M. Fuming, P. Zhi, L. Guangxing, *Org. Process Res. Dev.*, **8**, 372 (2003).
15. W. B. Kim, J. S. Lee, *J. Catal.*, **185**, 307 (1999).
16. F. Mei, E. Chen, G. Li, A. Zhang, *React. Kinet. Catal. Lett.*, **93**, 101 (2008).
17. Y. Li, Y. Zhang, B. Xue, Y. Guo, *J. Mol. Catal.*, **287**, 9 (2008).
18. J.-M. Clacens, D. Genuit, B. Veldurthy, G. Bergeret, L. Delmonte, A. Garcia-Ruiz, F. Figueras, *Appl. Catal., B*, **53**, 95 (2004).
19. B. Veldurthy, J.-M. Clacens, F. Figueras, *J. Catal.*, **229**, 237 (2005).
20. B. Veldurthy, F. Figueras, *Chem. Commun.*, **2004**, 734.

21. M. L. Kantam, A. Ravindra, Ch. V. Reddy, B. Sreedhar, B. M. Choudary, *Adv. Synth. Catal.*, **348**, 569 (2006).
22. M. L. Kantam, U. Pal, B. Sreedhar, B. M. Choudary, *Adv. Synth. Catal.*, **349**, 1671 (2007).
23. S. Carloni, D. E. De Vos, P. A. Jacobs, R. Maggi, G. Sartori, R. Sartorio, *J. Catal.*, **205**, 199 (2002).
24. Y. X. Feng, N. Yin, Q. F. Li, J. W. Wang, M. Q. Kang, X. K. Wang, *Catal. Lett.*, **121**, 97 (2008).
25. J. R. Ochoa-Gómez, O. Gómez-Jiménez-Aberasturi, B. Maestro-Madurga, A. Presquerra-Rodríguez, C. Ramírez-López, L. Lorenzo-Ibarreta, J. Torrecilla-Soria, M. Villarín-Velasco, *Appl. Catal., A*, **366**, 315 (2009).
26. I. Vauthey, F. Valot, C. Gozzi, F. Fache, M. Lemaire, *Tetrahedron Lett.*, **41**, 6347 (2000).
27. S. P. Gupte, A. B. Shivarkar, R. V. Chaudhari, *Chem. Commun.*, **2001**, 2620.
28. S. Fujita, B. Bhanage, M. Arai, *Chem. Lett.*, **33**, 742 (2004).
29. A. Corma, S. Iborra, S. Miquel, J. Primo, *J. Catal.*, **173**, 315 (1998).
30. T. Ebiura, T. Echizen, A. Ishikawa, K. Murai, T. Baba, *Appl. Catal., A*, **283**, 111 (2005).
31. S. Bancquart, C. Vanhove, Y. Pouilloux, J. Barrault, *Appl. Catal., A*, **218**, 1 (2001).
32. J. Barrault, Y. Pouilloux, J. M. Clacens, C. Vanhove, S. Bancquart, *Catal. Today.*, **75**, 171 (2002).
33. A. Corma, S. B. A. Hamid, S. Iborra, A. Velty, *J. Catal.*, **234**, 340 (2005).
34. M. J. Climent, A. Corma, S. B. A. Hamid, S. Iborra, M. Mifsud, *Green Chem.*, **8**, 524 (2005).

5.12 Liquid-phase Oxidation

Solid bases participate in liquid-phase oxidation in various ways. Oxidation with basic solids has been reviewed by Fraile et al. in 2000.¹⁾

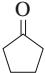
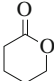
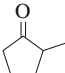
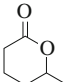
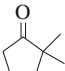
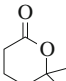
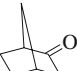
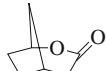
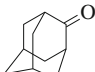
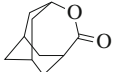
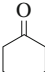
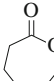
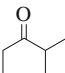
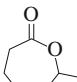
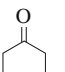
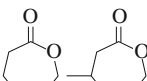
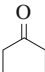
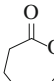
5.12.1 Oxidation with Molecular Oxygen

Weakly acidic hydrocarbons such as fluorine were oxidized by air in the presence of $\text{KF}/\text{Al}_2\text{O}_3$ at room temperature.²⁾ Thus fluorine and anthrone in acetonitrile were oxidized into fluorenone (92% conversion) and anthraquinone (100% conversion), respectively, in 16 h. A mechanism involving the abstraction of protons by basic catalysts was proposed.

Kaneda et al. found that Baeyer-Villiger oxidation of ketones with molecular oxygen and benzaldehyde proceeded in the presence of as-synthesized hydrotalcite.³⁻⁶⁾ The results of oxidation of cyclic ketones in the presence of hydrotalcite $[\text{Mg}_{10}\text{Al}_2(\text{OH})_{24}\text{CO}_3]$ and benzaldehyde are listed in Table 5.12.1. Acyclic ketones also undergo Baeyer-Villiger oxidation. For example *p*-methoxyacetophenone gives *p*-methoxyphenyl acetate in an almost quantitative yield.⁵⁾ The proposed mechanism for the oxidation with benzaldehyde and oxygen over hydrotalcite is shown in Fig. 5.12.1. Here benzaldehyde is oxidized with molecular oxygen to form perbenzoic acid. Hydrotalcite catalyze the oxygen transfer from perbenzoic acid to the ketone to form the Baeyer-Villiger product and benzoic acid. Actually, *m*-chloroperbenzoic acid can be used instead of benzaldehyde and oxygen.⁵⁾

Hydrotalcite-like materials containing Fe or Cu were reported to be more effective for Baeyer-Villiger oxidation.⁴⁾ Fe or Cu ions are considered to promote the oxidation step of benzaldehyde to perbenzoic acid.

Table 5.12.1 Baeyer-Villiger oxidation of acyclic ketones with molecular oxygen in the presence and absence of hydrotalcite

Substrate	Product	Reaction Time/h	Conversion, Yield/%	
			Mg ₁₀ Al ₂ (OH) ₂₄ CO ₃	No Catalyst
		5	94, 90(82)	45, 40
		5	96, 95	10, 8
		24	65, 61	trace
		3	100, 91(83) ^{a)}	26, 24
		5	100, quantitative(85)	43, 43
		5	82, 80	83, 80
		3	100, 93	77, 74
		5	56, 48	51, 47
		3	63, 53	50, 49

Reaction conditions: hydrotalcite 0.025 g, ketone 2 mmol, benzaldehyde 12 mmol, 1,2-dichloethane 20 mL, 313 K.

^{a)} 3-Oxabicyclo[3,2,1]octa-2-one as a regioisomer (6%) was detected in ¹H NMR.

Reprinted with permission from K. Kaneda, S. Ueno, *ACS Symp. Ser.*, **638**, 300 (1996) p.309, Table IV.

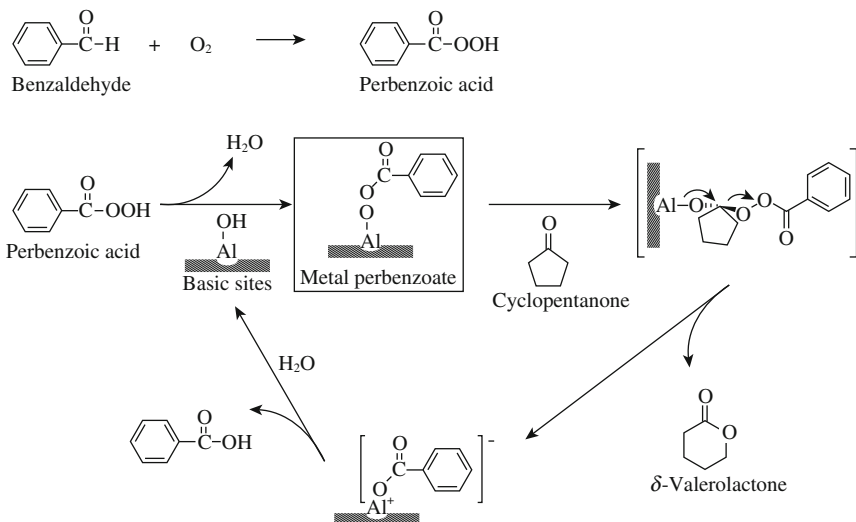


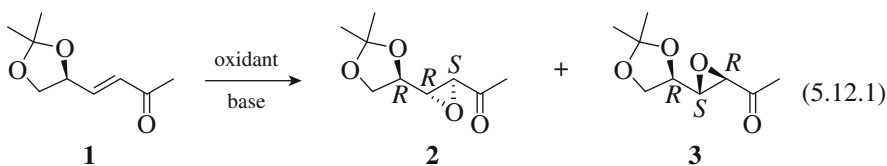
Fig. 5.12.1 Reaction scheme of Baeyer-Villiger oxidation of cyclopentanone with molecular oxygen and benzaldehyde in the presence of hydrotalcite.

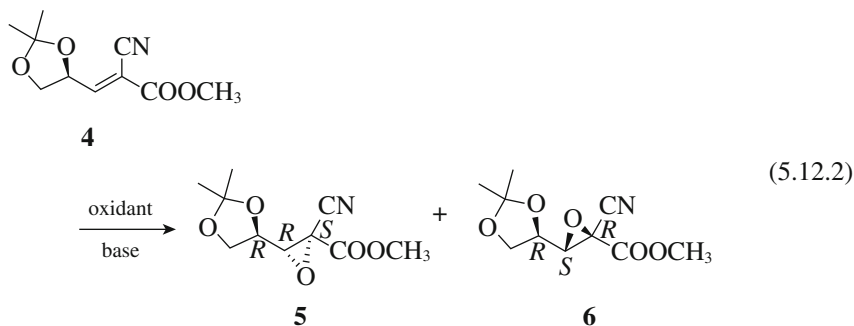
Reprinted with permission from S. Ueno, K. Ebitani, A. Ookubo, K. Kanda, *Appl. Surf. Sci.*, **121/122**, 366 (1997) p.369, Scheme 1.

5.12.2 Epoxidation of Alkenes with Alkylperoxide

Epoxidation of electron-deficient alkenes are oxidized with ^tBuOOH (TBHP) in the presence of KF/Al₂O₃.^{7,8)} Chalcone and dibenzalacetone are oxidized rapidly to the epoxy products, while 2-cyclohexen-1-one is oxidized at moderate rate in high yields of the epoxy product in acetonitrile at room temperature.⁷⁾ Isophorone is oxidized to give 96% yield of the corresponding epoxide in toluene.⁸⁾

Fraile et al. carried out the epoxidation of two chiral alkenes derived from *D*-glyceraldehyde, bearing different electron-withdrawing groups at room temperature.⁹⁾ TBHP-KF/Al₂O₃ was efficient and selective, leading to high diastereometric excess (de). Thus, TBHP-KF/Al₂O₃ gave 100% conversion of **1** and **4** in 24 h, with high diastereoselectivities, 40% de (**2** was the major product) and 50% de (**5** was the major product) and no detectable by-products. The oxidation of **1** and **4** with H₂O₂ by MgO-Al₂O₃ mixed oxide (calcined hydroalcite) gave lower selectivity for the epoxidation products.





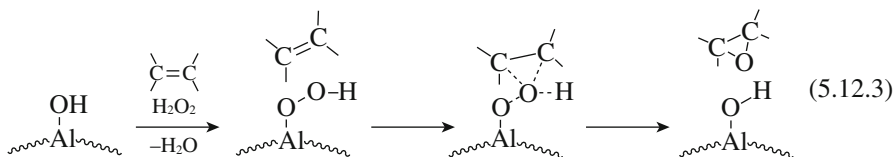
Rehydrated hydrotalcite is active for the epoxidation of 2-cyclohexen-1-one with t BuOOH.¹⁰⁾ An 87% yield of the epoxide was obtained in 6 h at room temperature.¹⁰⁾

Synthesis of chiral epoxyketones via Claisen-Schmidt condensation and asymmetric epoxidation reactions over MgO has been reported by Choudary et al. (section 6.5.1).¹¹⁾

5.12.3 Epoxidation of Alkenes with Hydrogen Peroxide

Alumina is an active, selective and cheap catalyst for the epoxidation of alkenes under nearly anhydrous conditions.¹²⁻¹⁶⁾ Low water content in the reaction medium is a prerequisite to avoid alumina-catalyzed decomposition of epoxides and hydrogen peroxide. Almost no activity was observed in the case of 60% hydrogen peroxide. The hydrogen peroxide can be used as a preformed anhydrous solution in ethyl acetate or by *in situ* drying of aqueous hydrogen peroxide by conducting the reaction under reflux with Dean-Stark water separation. Table 5.12.2 shows the epoxidation of a range of alkenes under Dean-Stark conditions. Lower yields of the epoxides from 1-methylcyclohexene and 2-methyl-2-heptene are due to evaporation and condensation of the reactant in the Dean-Stark trap.¹²⁾

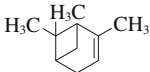
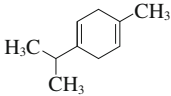
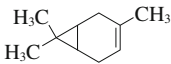
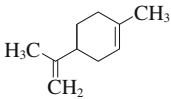
The following reaction scheme involving Al-OOH was proposed.



It is proposed that Al^{IV}-OH groups (Knözinger-Ratnasamy model, section 3.6.2) on alumina surface are responsible for the activation of hydrogen peroxide, giving AlOOH.¹⁷⁾

A MgO-Al₂O₃-mixed oxide (calcined hydrotalcite) at 723 K was found effective for epoxidation of electron deficient alkenes (α,β -unsaturated compounds) such as chalcone with aqueous H₂O₂.¹⁸⁾ As-synthesized hydrotalcite is also active

Table 5.12.2 Alumina catalyzed epoxidation of alkenes with aqueous H₂O₂ under Dean-Stark conditions

Alkene	Time/h	Yield/%
α -Pinene	4	69
		
γ -Terpinene	4	41 ^{b)}
	22	40 ^{c)}
3-Carene	3	87
		
Limonene	4	83 ^{d)}
		
1-Methylcyclohexene	4	42
1-Isopropylcyclohexene	4	79
1- <i>tert</i> -Butylcyclohexene	4	91
2-Methylocta-2,7-diene	3	80 ^{e)}
2-Methylocta-2,7-diene ^{f)}	3	79 ^{e)}
2-Methyl-2-heptene	2	58
Cyclooctene	8	90

^{a)} Reagents and conditions: 10 mmol alkene, 1 mmol dibutyl ether 0.50 g alumina (Aldrich, weakly acidic), 10 mL ethyl acetate 20 mmol 60% H₂O₂, reflux with a Dean-Stark trap under N₂. Analysis by GLC.

^{b)} Monoepoxides accompanied by 31% cymene.

^{c)} Diepoxide accompanied by 36% cymene.

^{d)} Sum of mono- and di-epoxides.

^{e)} Only 2,3-epoxide formed.

^{f)} 0.50 g of recovered alumina was used.

Reprinted with permission from M. C. A. Van Vliet, D. Mandelli, W. C. E. Arends, U. Schuchardt, R. A. Sheldon, *Green Chem.*, **3**, 243 (2001) p. 244, Table 3.

for the epoxidation of α,β -unsaturated ketones with H₂O₂.^{19,20)} The addition of a cationic surfactant such as dodecyltrimethylammonium bromide accelerates the epoxidation.

Hydrotalcite containing ^tBuO⁻ or [(CH₃)₂CH]₂N⁺ ions in the interlayers shows very high activity for epoxidation of electron-deficient alkenes with H₂O₂.^{21,22)} The

activity of these materials is much higher than that of as-synthesized and calcined hydrotalcite. The main results by hydrotalcite with $t\text{BuO}^-$ are given in Table 5.12.3.²¹⁾

Natural phosphate loaded with NaNO_3 is also very active for the epoxidation of α,β -unsaturated ketones with H_2O_2 .²³⁾

Unfunctionalized linear and cyclic alkenes such as 1-octene and cyclohexene are oxidized to the corresponding epoxides with 30% H_2O_2 in excellent yields in 24 h over hydrotalcite in the presence of nitriles at 333 K.²⁴⁾ The epoxidation involves two steps: (1) formation of peroxy-carboximidic acid by the reaction of a nitrile with H_2O_2 and (2) oxygen transfer from peroxy-carboximidic acid to alkene, as shown in Fig. 5.12.2.²⁵⁾ Hydrotalcite is considered to act as the base and promote the formation of OOH^- and the oxygen transfer step from peroxy-carboximidic acid to alkenes.

For the oxidation of cyclohexene with various nitriles, the yields of cyclohex-

Table 5.12.3 Epoxidation of electron-deficient alkenes with H_2O_2 catalyzed by hydrotalcite having $t\text{BuO}^-$ ions^{a)}

Substrate	Time/min	Product	Yield/% ^{b)}
	10		100 93 ^{c)}
	30		100
	45		53
	15		86
	10		88
	5 ^{d)}		90
	5		94

^{a)} Reaction conditions: 30% H_2O_2 (0.35 mL), 1 mmol of substrate and 0.03 g of catalyst in methanol, at room temperature

^{b)} Yields of epoxides determined by ^1H NMR

^{c)} Isolated yield

^{d)} Reaction conducted at 273 K using 0.005 g of catalyst

Reprinted with permission from B. M. Choudary, M. L. Kantam, Ch. V. Reddy, *Synlett*, 1203 (1998) p. 1203, Table 1.

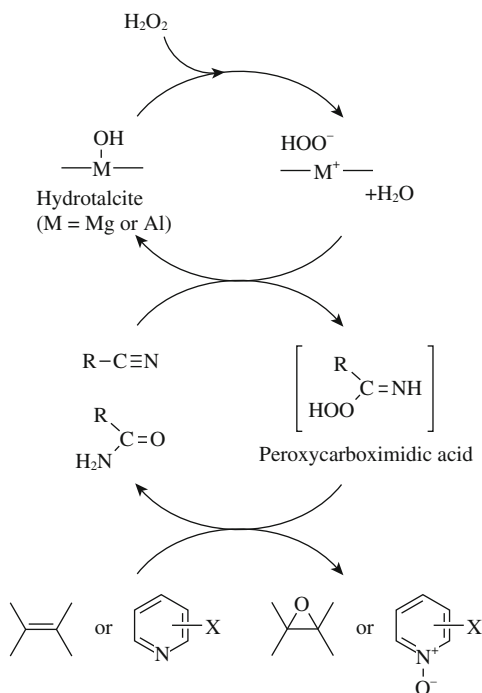


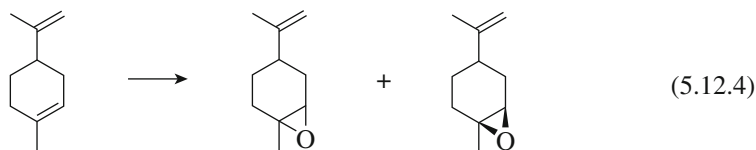
Fig 5.12.2 Reaction scheme of oxidation of alkenes and pyridines with molecular oxygen and benzonitrile (acetonitrile) in the presence of hydrotalcite. Reprinted with permission from K. Kaneda, K. Yamaguchi, K. Mori, T. Miyazaki, K. Ebitani, *Catal. Surv. Jpn.*, **5**, 31 (2000) p. 34, Scheme 2.

ene oxide are as follows: benzonitrile > acetonitrile > propionitrile.²⁴⁾ On the other hand, in the case of the epoxidation of styrene, acetonitrile is more effective than benzonitrile.²⁶⁾ Isobutyramide can be used instead of nitriles.²⁷⁾ The reaction rate noticeably increases with the use of an anionic surfactant such as sodium dodecylsulfate due to an increase in the interface between the organic (alkene, nitrile) and the aqueous (H_2O_2) phases.²⁴⁾

Calcined hydrotalcite is more effective than as-synthesized hydrotalcite in the epoxidation of styrene, plausibly because of the formation of reconstructed hydrotalcite by water in the system during the reaction.²⁶⁾ Actually, rehydrated hydrotalcite is also active for the epoxidation. Very high activity of rehydrated hydrotalcite with high surface area ($466 \text{ m}^2 \text{ g}^{-1}$) for epoxidation of styrene with H_2O_2 was reported. Total conversion of styrene was achieved in 30 min in the presence of acetonitrile and rehydrated hydrotalcite.²⁸⁾

The epoxidation of alkenes with H_2O_2 in the presence of acetonitrile over calcined hydrotalcite is greatly enhanced by microwave irradiation.²⁹⁾ For example, cyclohexene and 1-hexene give the corresponding epoxides in 100% yield in 1 and 3 min, respectively.

Limonene is oxidized to limonene epoxide with H_2O_2 and benzonitrile in the presence of calcined hydrotalcite.³⁰⁾



Use of 1,2- or 1,3-dicyanobenzene instead of benzonitrile much improved the conversion and selectivity. Thus 98% conversion of limonene with selectivity for limonene epoxide of 74% was obtained at 338 K in 24 h.

Hydrotalcite with diisopropylamide is also active for the epoxidation of unfunctionalized alkenes in the presence of benzonitrile.²²⁾

Hydrotalcite containing ^tBuO⁻ ions in the interlayers shows much higher activity for the epoxidation of unfunctionalized alkenes with H₂O₂ and benzonitrile²¹⁾ (Table 5.12.4). Thus styrene gave 100% yield of the styrene oxide in 10 min.

Table 5.12.4 Epoxidation of unfunctionalized alkenes with H₂O₂ catalyzed by hydrotalcite with ^tBuO⁻ ions^{a)}

Substrate	Time/min	Product	Yield/%
	10		100 90 ^{c)}
	30		90
	15		100
	30		76
	15		60
	30		80
	15		90
	15		90

^{a)} Reaction conditions: 30% H₂O₂ (2.4 mL), 4 mmol of substrate, 10.5 mmol of benzonitrile and 0.01 g of catalyst in methanol, at 333 K

^{b)} Yields of epoxides determined by ¹H NMR

^{c)} Isolated yield

Reprinted with permission from B. M. Choudary, M. L. Kantam, Ch. V. Reddy, *Synlett*, 1203 (1998) p.1204, Table 2.

Hydroxyapatites, prepared by a sonochemical method, is active for oxidation of a variety of alkenes and α,β -unsaturated ketones with H_2O_2 and acetonitrile.³¹⁾

5.12.4 Baeyer-Villiger Oxidation with Hydrogen Peroxide

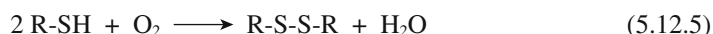
The Baeyer-Villiger oxidation of cyclohexanone with hydrogen peroxide (30% aqueous solution) and benzonitrile is achieved in the presence of mixed oxides derived by calcination of hydrotalcite-like compounds.³²⁾ $\text{MgO-Al}_2\text{O}_3$ and $\text{MgO-Al}_2\text{O}_3\text{-SnO}$ were found to be effective catalysts. A 83% yield of ϵ -caprolactam was obtained in the combination of $\text{MgO-Al}_2\text{O}_3\text{-SnO}$ mixed oxide in 6 h at 333 K.

Llamas et al. synthesized various magnesium hydroxides and magnesium oxides and used as catalysts for the Baeyer-Villiger oxidation of cyclohexanone with a mixture of 30% aqueous solution and benzonitrile as oxidants.³³⁾ Hydroxides are more active than their corresponding oxides. The magnesium hydroxide obtained by precipitation from the nitrate gave the highest activity. The addition of surfactant had a favorable effect on the reaction. A 100% yield of ϵ -caprolactam was obtained in the presence of sodium dodecylbenzenesulfonate in 1.5 h at 343 K.

The Baeyer-Villiger oxidation of cyclohexanone with 70% aqueous or anhydrous hydrogen peroxide is catalyzed by alumina.³⁴⁾ The reaction was carried out in ethyl acetate under azeotropic water removal at 363 K and a molar ratio cyclohexanone/oxidant of 1/4. Under these conditions, the conversion was 53% with a selectivity of 88% for ϵ -caprolactam.

5.12.5 Oxidation of Thiols, Thioethers and Pyridines

Liu and Tong reported that oxidation of thiols to disulfides with air easily proceeds in benzene at room temperature in the presence of basic alumina.³⁵⁾ Fifty gram of Al_2O_3 was used for 0.05 mol of a substrate.



Hydrotalcite, when dried, is active for air oxidation of a large variety of thiols (aromatic, aliphatic and alicyclic thiols) in hexane to afford the corresponding disulfides in excellent to quantitative yield at 303 K.³⁶⁾

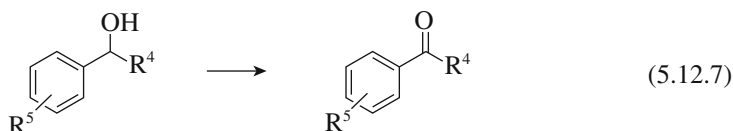
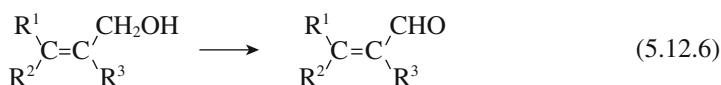
Thioethers are oxidized to sulfoxides with H_2O_2 and acetonitrile in the presence of hydrotalcite containing Ni^{2+} .³⁷⁾ The products are either the corresponding sulfoxide or sulfone, or both, the sulfoxide and sulfone formation being the consecutive steps. The thioethers are oxidized at different rates depending on the electron density of the sulfur atom, $(n\text{-C}_3\text{H}_7)_2\text{S} > \text{CH}_3\text{SPh} > \text{Rh}_2\text{S}$.

Dibenzothiophene is oxidized by H_2O_2 into the sulfone in the presence of rehydrated hydrotalcite with acetonitrile as a solvent at 333 K.³⁸⁾

5.12.6 Oxidation of Alcohols with Molecular Oxygen

Hydrotalcite containing Ru and Co ions such as $\text{Mg}_6\text{Al}_2\text{Ru}_{0.5}(\text{OH})_{16}\text{CO}_3$ is reported

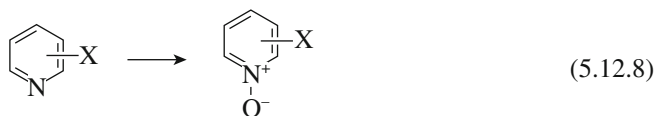
to be effective for oxidation of allylic and benzylic alcohols with molecular oxygen at 333 K.^{39,40)} A mechanism in which both basic hydroxyl groups and Ru ions are involved is proposed.³⁹⁾



5.12.7 Oxidation of Amines with Hydrogen Peroxide

Arylamines are oxidized to azoxybenzenes with H_2O_2 over titanasilicate ETS 10.⁴¹⁾ Aniline in methanol was transformed into azoxybenzene in greater than 97% yield in 6 h at 333 K.

Hydrotalcite [$\text{Mg}_{10}\text{Al}_2(\text{OH})_{24}\text{CO}_3$] is active for the oxidation of pyridines to the corresponding pyridine *N*-oxides by a combined oxidant of H_2O_2 and benzonitrile.⁴²⁾ The reaction mechanism is similar to that of alkene-oxidation as given in Fig. 5.12.2.



Hydrotalcite having $^t\text{BuO}^-$ ions is active for the oxidation of secondary and tertiary amines to nitrons (Table 5.12.5) and amine *N*-oxides, respectively, with 30% hydrogen peroxide in the presence of benzonitrile in methanol under a reflux condition.⁴³⁾

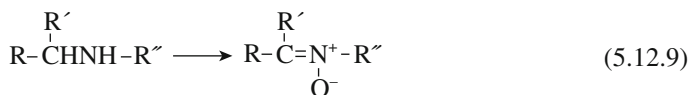


Table 5.12.5 Oxidation of secondary amines with H₂O₂ catalyzed by hydrotalcite having *t*-BuO⁻ ions

Sec-amine (a)	Nitron (b)	Time/h	Yield/% ^{a)}
		5	85
		5	88 (82) ^{b)}
		5	75
		5	95
		5	92
		5	92
		5	90
		3	72

^{a)} Isolated yield.^{b)} After fifth cycle.Reprinted with permission from B. M. Choudary, Ch. V. Reddy, B. V. Prakash, B. Bharahi, M. L. Kantam, *J. Mol. Catal., A*, **217**, 81 (2004) p.83, Table 2.

References

1. M. Fraile, J. I. Garcia, J. A. Mayoral, *Catal. Today*, **57**, 3 (2000).
2. D. Villemin and M. Ricard, *React. Kinet. Catal. Lett.*, **52**, 255 (1994).
3. K. Kaneda, S. Ueno, T. Imanaka, *J. Chem. Soc., Chem. Commun.*, **1994**, 797.
4. K. Kaneda, S. Ueno, T. Imanaka, *J. Mol. Catal., A*, **102**, 135 (1995).
5. K. Kaneda, S. Ueno, *ACS Symp. Ser.*, **638**, 300 (1996).
6. S. Ueno, K. Ebitani, A. Ookubo, K. Kaneda, *Appl. Surf. Sci.*, **121/122**, 366 (1997).
7. V. K. Yadav, K. K. Kapoor, *Tetrahedron*, **52**, 3659 (1996).
8. J. M. Fraile, J. I. García, J. A. Mayoral, F. Figueras, *Tetrahedron Lett.*, **37**, 5995 (1996).
9. J. M. Fraile, J. I. Garcia, D. Marco, J. A. Mayoral, *Appl. Catal., A*, **207**, 239 (2001).
10. J. Palomeque, J. Lopez, F. Figueras, *J. Catal.*, **211**, 150 (2002).
11. B. M. Choudary, M. L. Kantam, K. V. S. Ranganath, K. Mahendar, B. Sreedhar, *J. Am. Chem. Soc.*, **126**, 3396 (2004).

12. M. C. A. van Vliet, D. Mandelli, I. W. C. E. Arends, U. Schuchardt, R. A. Sheldon, *Green Chem.*, **3**, 243 (2001).
13. D. Mandelli, M. C. A. van Vliet, R. A. Sheldon, U. Schuchardt, *Appl. Catal., A*, **219**, 209 (2001).
14. R. Rinardi, J. Sepúlveda, U. Schuchardt, *Adv. Synth. Catal.*, **346**, 281 (2004).
15. R. Rinardi, U. Schuchardt, *J. Catal.*, **227**, 109 (2004).
16. R. Rinaldi, F. Y. Fujiwara, W. Hölderich, U. Schuchardt, *J. Catal.*, **244**, 92 (2006).
17. J. M. de S. e Silva, F. S. Vinhado, D. Mandelli, U. Schuchardt, R. Rinaldi, *J. Mol. Catal., A*, **252**, 186 (2006).
18. C. Cativiela, F. Figueras, J. M. Fraile, J. I. García, J. A. Mayoral, *Tetrahedron Lett.*, **36**, 4125 (1995).
19. K. Yamaguchi, K. Mori, T. Mizugaki, K. Ebitani, K. Kaneda, *J. Org. Chem.*, **65**, 6897 (2000).
20. T. Honma, M. Nakajo, T. Mizugaki, K. Ebitani, K. Kaneda, *Tetrahedron Lett.*, **43**, 6229 (2002).
21. B. M. Choudary, M. L. Kantam, Ch. V. Reddy, *Synlett*, **1998**, 1203.
22. M. L. Kantam, A. Ravindra, Ch. V. Reddy, B. Sreedhar, H. M. Choudary, *Adv. Synth. Catal.*, **348**, 569 (2006).
23. J. Fraile, J. García, J. A. Mayoral, S. Sebtí, R. Tahir, *Green Chem.*, **3**, 271 (2001).
24. S. Ueno, K. Yamaguchi, K. Ebitani, K. Kaneda, *Chem. Commun.*, **1998**, 295.
25. K. Kaneda, K. Yamaguchi, K. Mori, T. Mizugaki, K. Ebitani, *Catal. Surv. Jpn.*, **4**, 31 (2000).
26. I. Kirm, F. Medina, X. Rodríguez, Y. Cesteros, P. Salagre, J. Sueiras, *Appl. Catal., A*, **272**, 175 (2001).
27. K. Yamaguchi, K. Ebitani, K. Kaneda, *J. Org. Chem.*, **64**, 2966 (1999).
28. R. J. Chimentão, S. Abelló, F. Medina, J. E. Sueiras, Y. Cesteros, P. Salagre, *J. Catal.*, **252**, 249 (2007).
29. L. R. Pillai, E. Sahle-Demessie, R. S. Varama, *Tetrahedron Lett.*, **43**, 2909 (2002).
30. M. A. Aramendía, V. Borau, C. Jiménez, J. M. Luque, J. M. Marinas, J. R. Ruiz, F. J. Urbano, *Appl. Catal., A*, **216**, 257 (2001).
31. U. Pillai, E. Sahle-Demessie, *Appl. Catal., A*, **261**, 69 (2004).
32. C. Jiménez-Sanchidrián, J. M. Hidargo, R. Llamas, J. R. Ruiz, *J. Catal.*, **312**, 86 (2006).
33. R. Llamas, C. Jiménez-Sanchidrián, J. R. Ruiz, *Appl. Catal., B*, **72**, 18 (2007).
34. R. A. Steffen, S. Teixeira, J. Sepúlveda, R. Rinaldi, U. Schuchardt, *J. Mol. Catal., A*, **287**, 41 (2008).
35. K. -T. Liu, Y. -C. Tong, *Synthesis*, **1978**, 669.
36. M. Hirano, H. Minobe, S. Yakabe, T. Morimoto, *J. Chem. Res. (S)*, **1999**, 374.
37. E. Dmitriu, C. Guimon, A. Cordoneanu, S. Casenave, T. Hulea, C. Chelaru, H. Martinez, V. Hulea, *Catal. Rev.*, **66**, 539 (2001).
38. J. Palomeque, J. -M. Clacents, F. Figueras, *J. Catal.*, **211**, 103 (2002).
39. K. Kaneda, T. Yamashita, T. Matsushita, K. Ebitani, *J. Org. Chem.*, **63**, 1750 (1998).
40. T. Matsushita, K. Ebitani, K. Kaneda, *Chem. Commun.*, **1999**, 265.
41. S. B. Waghmode, S. M. Sabne, S. Sivasanker, *Green Chem.*, **3**, 285 (2001).
42. K. Yamaguchi, T. Mizugaki, K. Ebitani, K. Kaneda, *New J. Chem.*, **23**, 799 (1999).
43. B. M. Choudary, Ch. V. Reddy, B. V. Prakash, B. Bharahi, M. L. Kantam, *J. Mol. Catal., A*, **217**, 81 (2004).

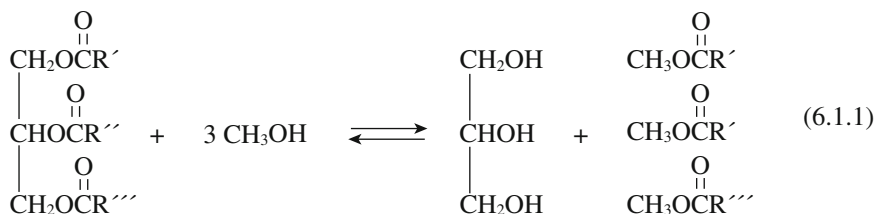
6.

Solid Base Catalysts for Specific Subjects

6.1 Solid Base Catalysts for Environmentally Benign Chemistry

6.1.1 Biodiesel Synthesis

Fatty acid methyl esters derived from vegetable oil are considered to be a potential diesel fuel extender known as biodiesel. Methyl esters of fatty acids are produced by transesterification of triglycerides with methanol in the presence of an acid or base catalyst.



Homogeneous base catalysts such as sodium hydroxide, sodium methoxide have been used as catalysts. For operational reasons, heterogeneous catalysts have been extensively explored.^{1,2)} The first plant using a heterogeneous catalyst was built in France.^{3,4)} In this continuous process, the catalyst consists of a mixed oxide of zinc and aluminum.⁴⁾ McNeff et al. described a continuous biodiesel production system (Mcgyan process).⁵⁾ The catalysts used were porous metal oxides (zirconia, titania and alumina). The reaction was performed at high pressure (ca. 2500 psi) and elevated temperatures (573–723 K). The titania-based catalyst maintained greater than 96% conversion over 4,000 min of continuous operation without loss in conversion rate using soybean oil as a feedstock. Furthermore, an 86–95% conversion was achieved for 25 kinds of lipid feedstocks including algae oil and beef tallow.

The transesterification of vegetable oil with methanol has been studied by many workers. The catalysts and main reaction conditions are listed in Table 6.1.1.

Suppes et al. reported the transesterification of soybean oil with methanol in the presence of a series of alkali cation-exchanged zeolites, NaX with occluded sodium oxide or sodium azide, and alkali cation-exchanged ETS-10.⁶⁾ The ETS-10 catalysts were more active than the X-zeolites catalysts and the increased activity

Table 6.1.1 Biodiesel synthesis with solid base catalysts

Catalyst	Methanol/ oil ratio*	Temp.	Time/h	Yield/%	Remarks	Reference
ETS-10	6	373 K	3	92		6
KNO ₃ /Al ₂ O ₃ calcined at 773 K	15	reflux	7	87		7
MgO-Al ₂ O ₃ (Mg/Al = 3.0)	15	reflux	9	67 (conv.)		8
MgO-Al ₂ O ₃ (Mg/Al = 4)	0.88 g/2.0 g	453 K	1	92		9
MgO-Al ₂ O ₃ (Mg/Al = 2.3)	30	393 K	8	93	can be regenerated by air calcination	10
MgO-Al ₂ O ₃ (Mg/Al = 3)	6 rapeseed oil	318 K	6	90.5		11
K ₂ O/MgO-Al ₂ O ₃	45	373 K	9	87	31% at second run	12
KF (15wt%)/ZnO calcined at 873 K	9	reflux	9	87		13
KF (20 wt%)/Al ₂ O ₃	4 soybean oil, rapeseed oil, sunflower oil	345 K	0.5	complete	under microwave irradiation stable up to 4 cycles	14
KI/Al ₂ O ₃ calcined at 773 K	15	reflux	8	96		15
Na/NaOH/Al ₂ O ₃	9	333 K	2	94		16
Li ₂ O-Al ₂ O ₃	15	reflux	2	94	minor deactivation small Li leaching	17
BaNO ₃ /ZnO calcined at 873 K	12	reflux	1	95.8	43.2% (second run). probable Ba leaching	18
LiNO ₃ /ZnO calcined at 873 K	12	338 K	3	96	stability was not satisfactory	19
K ₂ CO ₃ /Al ₂ O ₃ calcined at 873 K	25 sunflower oil	333 K	1	98.0	33.0% (2 nd run) 6.6% (3 rd run) K leaching	20
Eu ₂ O ₃ /Al ₂ O ₃	6	343 K	8	61.3	52.3% (5 th run)	21
MgO	55	403 K	7	83		22
MgO	4 sunflower oil	343 K	40 min	>98		23
MgO	36	533 K	10 min	complete	under supercritical methanol	24
LiNO ₃ /MgO calcined at 873 K	6	333 K	40 min	>95		25
CaO	27	Room temp.	24	>99	96% (4 th run) 74% (5 th run)	26
CaO	6.0 poultry oil	Room temp.	6.0	>99		26
CaO	12	338 K	3	>95		27
CaO	13 sunflower oil	333 K	1.5	94	Ca species leached into the liquid is also active.	28
CaO	500 mL/50 mL	reflux	2	90		29

(continued)

Catalyst	Methanol/ oil ratio*	Temp.	Time/h	Yield/%	Remarks	Reference
Li-doped CaO	12 karanja oil	338 K	8	94.9	oil contains 1.45% free fatty acid	30
CaO/SBA-15	12 sunflower oil	333 K	5	95		31
	12 castor oil	333 K	1	65		
Modified dolomite	15	333 K	3	99.9		32
ZnO-CaO (Zn/Ca = 4)	30 parm kernel oil	333 K	1	>99.4		33
CaO-La ₂ O ₃ (Ca/La = 3)	20	331 K	1	94.3		34
MgO-CaO	12 sunflower oil	333 K	3	92		35
CaO (16.5wt%)/ MgO	18 rapeseed oil	337,7 K	3.5	92	activity sustained up to 3 runs	36
SrO	12	338 K	0.5	> 94	activity sustained for 10 runs	37
ZnO-La ₂ O ₃ (La/Zn = 3)	36	473 K	1	> 95		38
Sr-loaded hydroxyapatite	9	343 K	5	85		39

*Soybean oil unless otherwise noted.

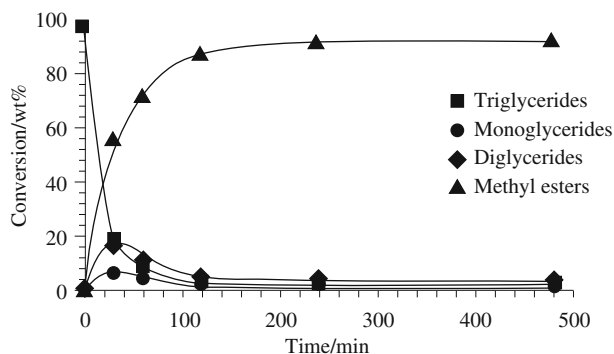


Fig. 6.1.1 Reaction Profiles of diesel oil and methanol over EST-10 at 373 K. Reprinted with permission from G. J. Suppes, M. A. Dasari, E. J. Dockocil, P. J. Mankidy, M. J. Goff, *Appl. Catal., A*, **257**, 213 (2004) p.272, Fig. 6.

was attributed to the higher basicity of ETS-10 and larger pores. The occlusion of sodium oxide and sodium azide in X-type zeolites enhanced the activity to a level similar to that of ETS-10. Fig. 6.1.1 shows the conversion profile of a mixture of soybean oil and methanol (1 : 6 molar ratio) in the presence of the as-synthesized ETS-10 catalyst at 373 K. A conversion to methyl ester of 92% was attained in 3 h and a monoglyceride concentration of 2% and diglyceride concentration of 4%.

The transesterification of poultry fat with MgO-Al₂O₃ mixed oxide prepared from hydrotalcite was also reported.¹⁰⁾ The rehydrated hydrotalcite was less active than the mixed oxide, indicating that the reaction has no specificity for interlayer OH⁻ ions.

Ebiura et al. studied the transesterification of triolein (trioleoyl glycerol, a model compound) with methanol in the presence of alumina-supported alkali metal salts heated under vacuum at 823 K.⁴⁰⁾ A K₂CO₃-loaded alumina showed the highest activity among the catalysts studied and gave a 94% yield of methyl oleate and a 89% yield of glycerol from triolein and methanol (molar ratio, 1: 24.8).

Leaching of the catalytically active species to the polar reactants is a very important factor. ETS-10 is also active for the transesterification of triacetin (triacetyl glycerol, a model compound) with methanol.⁴¹⁾ However, the reaction proceeds in the homogeneous phase where the active species is sodium methoxide formed by the reaction of methanol with Na⁺ ions in ETS-10. Transesterification of triacetin with methanol by ammonium-type anion exchange resin has been reported by Liu et al.⁴²⁾ Decomposition of the active component was not observed and the catalyst could be used repeatedly without significant activity loss.

K₂CO₃-loaded Al₂O₃ calcined at 873 K gave high activity for the transesterification of sunflower oil with methanol. However, because of severe leaching of K species into the reactant solution, the activity dropped largely in the second and third runs.¹⁹⁾ Similarly, CH₃COOK-loaded MgO-Al₂O₃ calcined at 873 K also showed high activity for the transesterification of palm oil and methanol. The activity, however, dropped significantly in the second run. Reloading of the K-compound was necessary to regain the activity.¹²⁾ Leaching of alkaline components from various alkali-doped metal oxides was observed and part of the activity was due to the leached species.²⁵⁾

CaO is also very active for the transesterification of sunflower oil and soybean oil and can be re-used without significant deactivation.^{27,28)} The activity is enhanced in the presence of a small amount of water (2.03%).²⁷⁾ CaO is slightly soluble in the reaction media and the contribution of the homogeneous reaction due to soluble species has been discussed,^{28,29,43,44)} The contribution of the homogeneous phase is much smaller than that arising from the heterogeneous sites, though the soluble substances are rather active.²⁸⁾ Kouzu et al. studied the transesterification of soybean oil with methanol under reflux conditions in the presence of CaO and found that CaO was converted into calcium diglyceroxide, Ca(C₃H₇O₃)₂, during the course of the reaction.^{44,45)} Calcium diglyceroxide prepared separately was active for the transesterification. This indicates that, though the active phase was CaO in the beginning, it changes to calcium diglyceroxide during the reaction. They also found that calcium diglyceroxide is more tolerant to air exposure than CaO and could be a better catalyst than CaO.

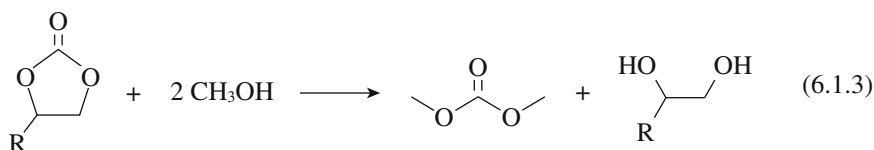
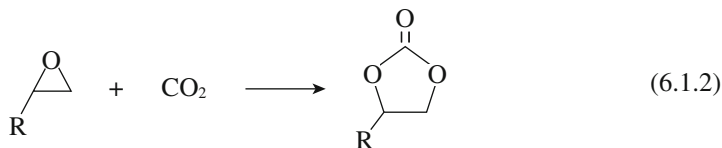
On the other hand, MgO and MgO-CaO mixed oxides are stable under reaction conditions.⁴⁶⁾

6.1.2 Synthesis of Dimethyl Carbonate

A. Synthesis of dimethyl carbonate from alkene carbonate and methanol
Dimethyl carbonate (DMC) is an important intermediate for polycarbonate resins as well as a useful carbonylation and methylation agent. Because of the negligible toxicity of DMC, it is a promising substitute for toxic and corrosive phosgene, dimethyl sulfate or methyl iodide.⁴⁷⁻⁴⁹ It also has potential use as a gasoline octane enhancer. Many examples of the alkylation and transesterification reactions of DMC are found in the sections 5.6 and 5.11. The reaction of DMC with amorphous silica provides tetraethoxysilane (section 6.4.4).

DMC has long been synthesized by reaction of methanol and phosgene. A tremendous amount of research has been pursued to establish environmentally compatible non-phosgene routes for the preparation of DMC. DMC production from methanol, carbon monoxide and oxygen has been industrialized using a Cu or Pd catalyst.

DMC can also be produced by the transesterification reaction between methanol and cyclic carbonates such as ethylene carbonate and propylene carbonate. These carbonates are obtained by the reaction of ethylene oxide or propylene oxide with carbon dioxide.



Both acids and bases catalyze the transesterification reaction (6.1.2), but base catalysts have been reported to be more effective.⁵⁰ However, homogeneous basic catalysts such as alkali alkoxides and trialkylamine give rise to the problem of product separation and catalyst reuse, and consequently, solid base catalysts have gained much attention. Therefore, extensive studies have been conducted on the transesterification using heterogeneous catalysts.

Tatsumi et al. reported that K⁺-exchanged TS-1 gave 68% conversion of ethylene carbonate (EC) with a yield of 57% of DMC in 3 h under refluxing conditions (methanol/EC = 4).⁵¹ Under the same reaction conditions, as-synthesized hydrotalcite with a Mg/Al ratio of 2.5 gave a 58% yield of DMC at 70% conversion of EC.⁵²

A 60.1% yield of DMC with selectivity of 73% was obtained from the reactants with a methanol/EC ratio of 8 in the presence of MgO by the reaction by a batch reactor at 423 K in 4 h.⁵³ The yield and selectivity increased to 66.1% and

100%, respectively, under CO₂ of 8 MPa. This suggests that CO₂ prevents the decomposition of EC to CO₂ and ethylene. The reaction of propylene carbonate (PC) with methanol gave 28.0% conversion with 100% selectivity for DMC and propan-1,2-diol in the presence of MgO and CO₂. CaO was also active and selective for the reaction. Bhanage et al. also showed that Mg-containing smectite was effective for the DMC synthesis from PC and methanol.⁵⁴⁾

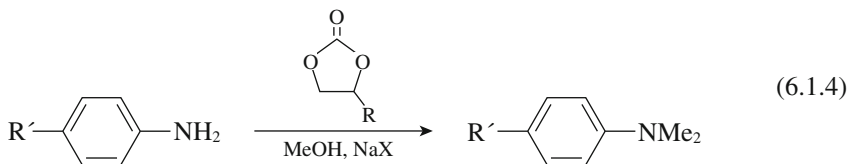
The catalytic activities of MgO-CeO₂ mixed oxides, for the reaction of EC and methanol were studied under a flow condition.^{55,56)} The activity depends on the composition of the mixed oxide, MgO-CeO₂ (CeO₂ = 24.4%) showing the highest activity.⁵⁵⁾ A DMC yield of 64% with selectivity of 95% was attained at 423 K.

The transesterification of ethylene carbonate with methanol (4 : 1) was studied in a flow reactor at 373 K with a variety of anionic resins with tertiary amines and quaternary ammonium ions.⁵⁰⁾ Amberlite IRA-68 having dimethylamino functionality bonded to acrylic-divinylbenzene polymer gave ethylene carbonate conversion of 58%, which is close to the equilibrium. Estimated selectivities are 98 and >99 mol%, respectively. Similar results are realized with Amberlyst A-21, where diaminomethyl functionality is bonded to a macroporous resin. Amberlite IRA-68 maintained activity over 1000 h.⁵⁰⁾ The reaction was also studied in a slurry reactor with anion exchange resins having diethylamino- or trimethylammonium hydroxide functionality.^{57,58)} The reaction was pseudo-first order with respect to EC and activation energy of 85.8 kJ mol⁻¹.⁵⁷⁾

Wei et al. found that CaO prepared by the decomposition of CaCO₃ at elevated temperatures to be a very effective catalyst for the synthesis of DMC from methanol and PC in a batch system.⁵⁹⁾ Equilibrium was reached in 30 min at 293 K. Since CaO thus prepared was ultrafine and difficult to filter from the products and reuse, they prepared a CaO-carbon composite (CaO/C), which was prepared by heating a composite of linear phenolic resin, hexamethylenetetramine and CaCO₃ (weight ratio 5 : 1 : 5) at 1173 K for 1 h in a N₂ atmosphere. The composite was active for the transesterification, though less active than CaO because of diffusion resistance. Equilibrium was reached in 45 min from methanol and PC (4 : 1) at 323 K (DMC yield 45%). CaO-ZrO₂ solid solutions (Ca 10–30 mol%) also show stable activity for the synthesis of DMC from PC and methanol.⁶⁰⁾ With use of a distillation reactor, a PC conversion of >95% was maintained even after 250 h.

Feng et al. used tertiary amino groups tethered to MCM-41 for the reaction of EC and methanol in a flow reactor.⁶¹⁾ The catalyst showed good activity at 393 K and excellent stability, no obvious loss of activity being observed for 110 h.

Since DMC is a good methylation agent for aromatic amines (section 5.7.6), *N*-methylation of aromatic amines can be performed from EC, methanol and aromatic amines with use of alkali cation-exchanged zeolites.⁶²⁾



NaX and KX are the most effective catalysts. Thus the reaction of aniline, EC and methanol (in excess) in the presence of NaX at 453 K for 16 h gave *N,N*-dimethylaniline in very high selectivity and yield (89%). Aromatic amines cannot be methylated with methanol, indicating that DMC formed from ethylene carbonate and methanol serves as an alkylation agent.

B. One-step synthesis of dimethyl carbonate from alkene oxide, CO₂ and methanol

Since MgO is also active for the reaction of ethylene oxide with CO₂ to form EC [eq. (6.1.2)], one-step synthesis of DMC from ethylene oxide, CO₂ and methanol was attempted. A high conversion of ethylene oxide (96.1%) was obtained in the presence of MgO at 423 K.⁵³⁾ The products consisted of DMC (28.0%), ethylene glycol (26.3%), EC (31.4%) and ethylene glycol monomethyl ether (36.7%). DMC was also obtained from propylene oxide, CO₂ and methanol under the same reaction conditions. The products were DMC (13.6%), propylene glycol (14.8%), PC (14.4%), 1-methoxy-2-propanol (21.6%) and 2-methoxy-1-propanol (29.9%).

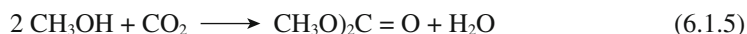
Chang et al. reported that KI/ZnO and KI + K₂CO₃/ZnO, when calcined at 773 K, are very active for one-step synthesis of DMC from ethylene oxide (or propylene oxide), methanol and supercritical CO₂.⁶³⁾ In the reaction of ethylene oxide and methanol and supercritical CO₂ (16.5 MPa) in the presence of KI (3 mmol g⁻¹) + K₂CO₃ (1 mmol g⁻¹)/ZnO at 423 K for 2 h, ethylene oxide conversion was 98.2%, the product yields being DMC (68.6%), ethylene glycol (71.9%) and EC (28.0%).

Jiang and Yang reported that MgO, which was loaded with KCl and K₂CO₃ and [30 wt%, K₂CO₃/KCl = 1 (wt/wt)] and calcined at 873 K, was highly active and selective for the one-step synthesis of DMC from propylene oxide, CO₂ and methanol.⁶⁴⁾ The products consist of DMC (46.2%), propylene glycol (50.1%), PC (1.23%) and methoxypropanols (2.47%) with 100% conversion of propylene oxide at 433 K. The high activity was attributed to high basic strength of the catalysts, $H_- > 27$.

Choline hydroxide, [(CH₃)₃NCH₂CH₂OH]⁺ OH⁻, supported on MgO is also active for the one-pot synthesis of DMC from propylene oxide, methanol and carbon dioxide.⁶⁵⁾ Under the conditions of 393 K, CO₂ pressure of 2.5 MPa, methanol/propylene oxide = 20, a propylene oxide conversion of 98% was achieved; the selectivity and yield of DMC were about 67% and 65% in 6 h.

C. Direct synthesis of dimethyl carbonate

Dimethyl carbonate can be synthesized directly from methanol and carbon dioxide with high selectivity using ZrO₂, CeO₂ and ZrO₂-CeO₂ mixed oxides as catalysts.⁶⁶⁻⁶⁹⁾



Over ZrO₂, 0.36 mmol of DMC was obtained under the reaction conditions of methanol : CO₂ = 192 mmol : 200 mmol with 0.5 g of the catalyst at 443 K.⁶⁶⁾ The catalytic activity was enhanced by loading H₃PO₄ on ZrO₂ followed by calcination

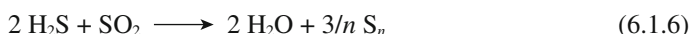
at 673 K.⁶⁷⁾ The amount of DMC formed over $\text{H}_3\text{PO}_4/\text{ZrO}_2$ ($\text{P}/\text{Zr} = 0.025$) was about four times larger than that on ZrO_2 at 423 K.⁶⁷⁾ Based on infrared spectroscopic studies, the authors suggest a mechanism which includes the surface methyl carbonate species formed by the reaction of CO_2 with methoxy species on ZrO_2 surface (section 3.2.3).⁶⁷⁾

CeO_2 is more active than ZrO_2 or $\text{H}_3\text{PO}_4/\text{ZrO}_2$.⁶⁸⁾ $\text{ZrO}_2\text{-CeO}_2$ mixed oxide showed far higher activity than CeO_2 .⁶⁹⁾ The mixed oxides ($\text{Ce}/\text{Zr} = 0.25$) calcined at 1273 K gave 0.88 and 1.1 mmol of DMC in 2 and 16 h at 383 K. The DMC amount formed increased further by increasing CO_2 pressure to 1.6 mmol.

The drawback of this direct synthesis is the low equilibrium limit for DMC production (about 1% at 443 K).⁶⁶⁾

6.1.3 Reaction of H_2S and SO_2

The Claus process has been used extensively for many years in the recovery of sulfur from acidic gases generated in refinery processes. In the Claus process, a portion of H_2S is first converted to SO_2 then the rest of the H_2S is oxidized by SO_2 .



Activated alumina is commonly used as the catalysts in this process. Zeolites have been studied as model catalysts. Zotin and Faro prepared several aluminas with different crystal structures (γ , η and χ) and controlled amounts of impurities (Na and sulfate).⁷⁰⁾ A linear correlation was found between the catalytic activity and basic sites density, which was determined as the amount of SO_2 chemisorption at 373 K, except for one with 3.9 wt% of Na.

To elucidate the mechanism of the reaction, spectroscopic studies on the adsorbed states of H_2S and SO_2 and their interactions on the surfaces have been widely conducted.

H_2S adsorption onto faujasite-type zeolite was monitored by combined IR and UV/VIS spectroscopy.^{71,72)} The first molecules adsorbed on NaX dissociate completely to form S^{2-} ions (250 nm) + OH (3635 cm^{-1}) on NaX.



A further dose of H_2S gives the dissociative adsorption of H_2S to form $\text{Na}^+(\text{SH}^-)$ (S-H: 2560 cm^{-1}) and OH (3650 and 3580 cm^{-1}). Some of the newly formed OH groups exhibit Brønsted acidity.



The extent of dissociative adsorption of H_2S depends on the Si/Al ratio of the faujasite zeolites.⁷¹⁾ Dissociative adsorption occurs only on aluminum-rich faujasites, while no dissociative adsorption occurs on Y-type zeolites ($\text{Si}/\text{Al} > 2.5$).

With respect to SO_2 adsorption on Al_2O_3 , SO_2 adsorption on basic O^{2-} sites gives rise to an absorption band near 1060 cm^{-1} , which is attributed to a sulfite type species in a unidentate fashion.⁷³⁾ This assignment was also supported by various works.⁷⁴⁻⁷⁶⁾ On the other hand, Karge et al. suggested a strong probability

that the IR bands were due to the formation of HSO_3^- species upon adsorption on Al_2O_3 as well as on zeolites.⁷⁸⁾

The species giving 1060 cm^{-1} band easily reacts with gaseous H_2S even at room temperature.^{77,78)} Raman spectroscopy showed new bands at 151, 220 and 480 cm^{-1} characteristic of S_8 species.⁷⁷⁾

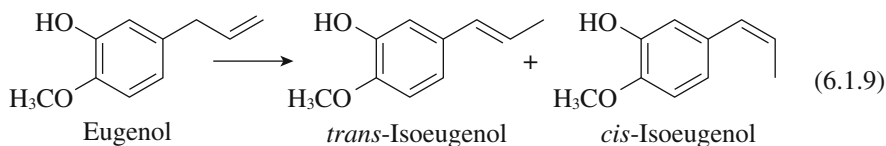
Karge et al. also studied the interaction of SO_2 and H_2S on faujasite-type zeolites by combined UV-VIS and IR spectroscopy.⁷²⁾ The interaction of preadsorbed SO_2 with H_2S leads to the formation of $\text{S}_2\text{O}_4^{2-}$, S_2^{2-} , $c\text{-S}_8$ and polymeric sulfur as intermediates and products. The same bands were observed when preadsorbed H_2S was exposed to SO_2 .

6.1.4 Environmentally Benign Synthesis of Fine Chemicals

Advantages of solid base catalysts in organic synthetic reactions have been described in the introduction (section 1.1). In this section some examples of the synthetic reactions over solid base catalysts are given. More examples are found in sections in Chapter 5 and other sections of this chapter.

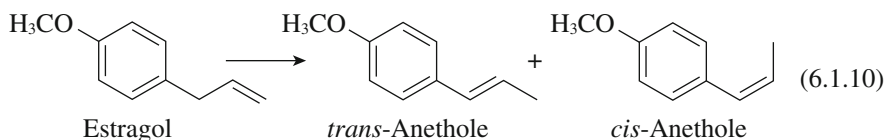
A. Synthesis of isoeugenol, anethole and isosafrole by isomerization reactions

Isoeugenol is used in pharmaceuticals and as a wide variety of blossom compositions in fragrances, and can be obtained by the isomerization of eugenol. The isomerization is in general carried out in a homogeneous medium using KOH in alcoholic solutions. Kishore and Kannan reported that the isomerization of eugenol to isoeugenol proceeded over as-synthesized hydrotalcite.^{79,80)}



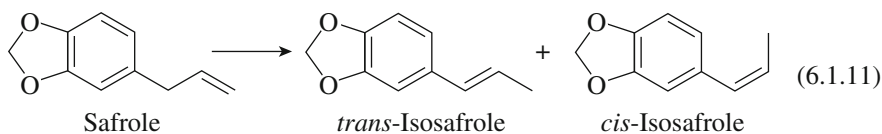
Among various hydrotalcite-like materials, MgAl and NiAl combinations offered high activity. The ternary hydrotalcite containing Mg, Ni and Al gave a still higher activity and 94% conversion with a *cis/trans* ratio of 16/84 at 473 K. The calcined hydrotalcites gave lower activity.

Anethole finds application in alcoholic beverages and in oral hygiene products and can be produced by the isomerization of estragole. The isomerization can be performed by aqueous alkali hydroxides. Kishore and Kannan reported that as-synthesized hydrotalcite-like materials with MgAl, NiAl and MgNiAl combinations were also active for the isomerization of estragole to anethole.⁸¹⁾ MgNiAl-hydrotalcite [(Mg + Ni)/Al = 4, Mg/Ni = 3] gave 99% conversion of estragole with a *cis/trans* ratio of 15/85 with a substrate : catalyst mass ratio of 10 : 1 in 6 h at 473 K. The activity was lost when the hydrotalcite was calcined.



In contrast with the work by Kishore and Kannan,⁸¹⁾ Srivastara et al. reported that this reaction was effectively catalyzed by MgO-Al₂O₃ mixed oxide prepared by calcination of hydrotalcite.⁸²⁾ It gave 98% conversion with 100% selectivity at 491 K (refluxing). Cs-exchanged X-type zeolite and KOH/Al₂O₃ are also active for this reaction.⁸²⁾

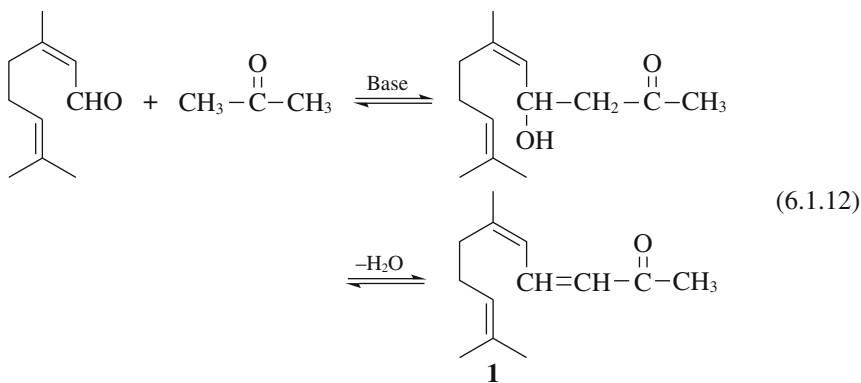
Isosafrole is used in fragrance industries and obtained by the isomerization of safrole. The catalysts used for the isomerization is KOH in alcoholic solutions or a transition metal complex. As-synthesized hydrotalcite is effective for the isomerization of safrole to isosafrole.^{79,83)} The conversion was >95% with a *cis/trans* ratio of ca. 1/9 at 473 K in 1 h.



The isomerization of safrole to isosafrole proceeds smoothly at 393 K over Na/NaOH/Al₂O₃.⁸⁴⁾

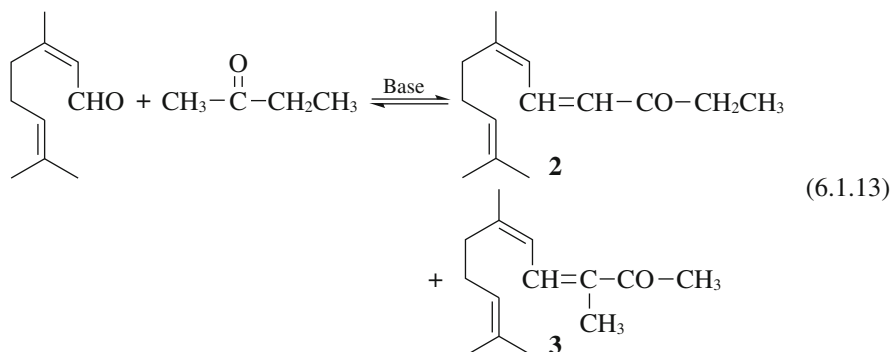
B. Synthesis of pseudoionones

Ionone and methylionones are important intermediates in flavors and fragrances. Ionones and methylionones are produced by acid-catalyzed ring closure of pseudoionone and methylpseudoionones, respectively. Pseudoionone **1** is synthesized by aldol condensation of citral with acetone. Pseudoionone is also an intermediate for the production of vitamin A.



The reaction of citral with methyl ethyl ketone gives methylpseudoionones. When the aldehyde group of citral reacts with the methyl group of methyl ethyl

ketone, *n*-methylpseudoionone **2** is obtained, whereas the reaction with the methylene group leads to the formation of isopseudoionone **3**.



Synthesis of pseudoionone (and methylpseudoionones) by condensation of citral and acetone (and methyl ethyl ketone) has been reported by several groups. The acetone/citral ratio and reaction temperature are key factors for the synthesis.

A very high yield of pseudoionone from citral and acetone in the presence of basic alumina under reflux for 4 h has been reported.⁸⁵⁾ A large amount of alumina was, however, used for the synthesis.

Na⁺-doped MgO shows the catalytic activity for citral condensation.⁸⁶⁾ The yield of pseudoionone reached 100% under the reaction conditions of an acetone/citral ratio of 25 and catalyst/citral weight ratio of 0.4 at 323 K.

The catalytic activity of MgO-Al₂O₃-mixed oxides (calcined hydrotalcite) was studied in detail by Noda-Pérez et al.⁸⁷⁾ The best catalytic activity and pseudoionone yield were obtained from the mixed oxide with Mg/Al = 4 derived from hydrotalcite aged at 333 K and calcined at 723 K. Using an acetone/citral molar ratio of 1 and 5 wt% of catalyst with respect to the weight of reaction mixture, about 60% yield of pseudoionone was obtained with selectivity of 60–80%.

Roelofs et al. studied the reaction over rehydrated hydrotalcite.^{88,89)} When the amount of citral was 1 wt% in acetone, both acetone self-condensation and citral-acetone condensation were observed. At 273 K, 65% citral was converted after 24 h. Selectivity for pseudoionone was 90%. When the citral concentration was increased to 10 wt% (acetone/citral ratio = 20), no reaction took place. Strong inhibition by citral was suggested. When the reaction of citral with methyl ethyl ketone was carried out at 293 K, a 76% yield of methylpseudoionones was obtained after 24 h.⁸⁹⁾

Climent et al. carried out the reaction in the presence of acid (HY and β zeolites), acid-base (amorphous aluminophosphate) and basic catalysts such as ALPON, MgO and calcined hydrotalcite.⁹⁰⁾ Only MgO and calcined hydrotalcite showed good activity, calcined hydrotalcite being more selective than MgO. The catalytic activity of the calcined hydrotalcite was improved by its rehydration (36% water). The inhibiting effect of citral was avoided by carrying out the reaction at higher temperatures. Thus, pseudoionone was obtained with high yield (98%) and high selectivity (99%) at low molar ratio (2.4) at 333 K in 1 h using 40

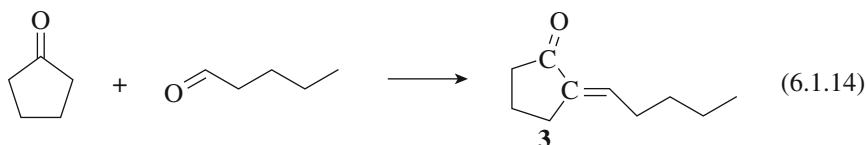
wt% of the catalyst with respect to citral. The same catalyst is also active for the condensation of citral and methyl ethyl ketone.⁹¹⁾ A 96% yield of methylpseudoionones was obtained with a *n*- and isomethylpseudoionone ratio of 2.3 at a ketone/citral ratio of 14 at 357 K.

The preparation method of rehydrated hydrotalcite strongly affects the performance. Hydrotalcite precipitated under sonication gives smaller crystal size and high surface area ($284 \text{ m}^2 \text{ g}^{-1}$).⁹²⁾ Rehydrated hydrotalcite obtained from this sample by sonication give 96% conversion with 99% selectivity under the conditions of acetone/citral = 2.8 in 15 min at 333 K.

Abelló et al. studied the effect of the method of rehydration on the catalytic activity.^{93,94)} Rehydration in liquid phase is much more effective than that in gas phase. In the liquid phase rehydration, the surface area and the catalytic activities of the rehydrated hydrotalcite depend greatly on the agitation speed and rehydration time. The surface area of the materials rehydrated in the liquid phase is as high as $400 \text{ m}^2 \text{ g}^{-1}$.⁹³⁾ The citral conversion was 99.9% with 100% selectivity for the sample rehydrated in liquid phase after 1 h of the reaction of citral and acetone (4.4 : 1) at 333 K. The rehydrated hydrotalcite, however, cannot be reused because of deactivation due to adsorbed organic molecules. The regeneration by calcination at 723 K followed by rehydration largely recovered the citral conversion.⁹⁴⁾

C. Synthesis of 2-pentylidene-cyclopentanone

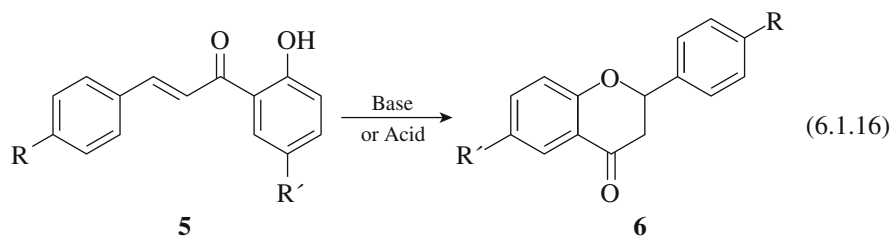
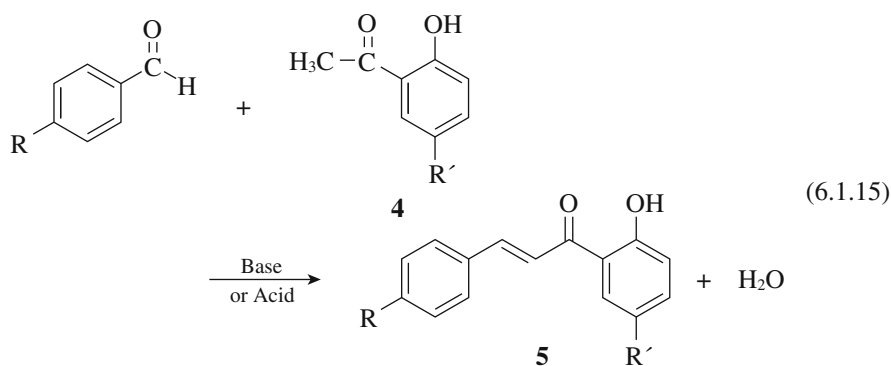
Aldol condensation of cyclopentanone with valeraldehyde gives 2-pentylidene-cyclopentanone, which is a precursor of perfume ingredient.



This reaction proceeds over various acidic and basic catalysts in a batch reactor at 403 K.⁹⁵⁾ Among the catalysts studied, ZrPON was most active. The conversion of valeraldehyde reached 94% in 2 h with 72% selectivity for the cross condensation product.

D. Synthesis of flavanone

Flavanone is a common intermediate compound for many fine chemical and pharmaceutical products. A common route to flavanone is the Claisen-Schmidt condensation of benzaldehyde and 2-hydroxyacetophenone **4** to form 2'-hydroxychalcone **5** and the subsequent isomerization of this intermediate to flavanone **6**.



Climent et al. studied this condensation reaction without any solvent in the presence of MgO-Al₂O₃ mixed oxides obtained by calcination of hydrotalcite (Mg/Al = 3).⁹⁶⁾ The isomerization of the chalcone to flavanone occurs under the reaction conditions. In the reaction of 2-hydroxyacetophenone and benzaldehyde (R = R' = H) at 423 K under air, the total conversion was 78%, the yield of the chalcone and flavanone being 50% and 28%, respectively. In the reaction in the presence of air, some of benzaldehyde was oxidized to benzoic acid. In the reaction under argon, the conversion reached 97% at 393 K after 22 h. The reactions with substituted starting materials (R = H, R' = OCH₃; R = NO₃, Cl, or OCH₃, R' = H) were also reported.

In the reaction with MgO as catalyst and DMSO as solvent, the yields of the chalcone and flavanone were 54% and 24%, respectively after 1.5 h of the reaction at 443 K.⁹⁷⁾ High surface-area MgO (590 m²g⁻¹) is very effective for the reaction.⁹⁸⁾ The yield of flavanone was 90% and 100% with total conversion of benzaldehyde when the reaction was carried out for 12 h in ethanol and DMSO, respectively.

Mesoporous silica functionalized with amino-groups⁹⁹⁻¹⁰¹⁾ is active for flavanone synthesis. The results of the reactions with various substitute groups in the presence of SBA-15 functionalized with aminopropyl groups under solvent-free conditions are summarized in Table 6.1.2.⁹⁹⁾

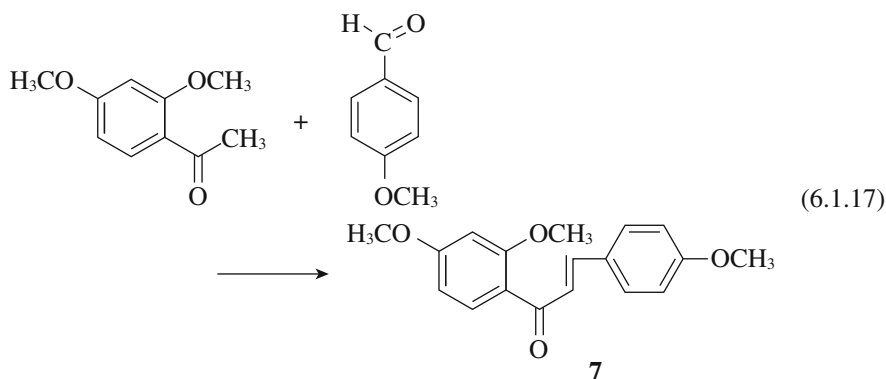
Vesidryl (2,4,4'-trimethoxychalcone) **7** is of pharmaceutical interest for its diuretic and choleric properties.

Table 6.1.2 Reaction between 2'-hydroxyacetophenone (10 mmol) and benzaldehyde (15 mmol) with various substituting groups over aminopropylated SBA-15

R	R'	Conversion of 4 /%	Selectivity to 5	Selectivity to 6
H	H	92	31	69
H	NO ₂	66	14	86
H	Cl	83	27	73
H	CH ₃ O	87	39	61
CH ₃ O	H	89	16	84
Cl	H	92	25	75
CH ₃ O	CH ₃ O	84	18	82

Reaction conditions: 413 K, 8 h

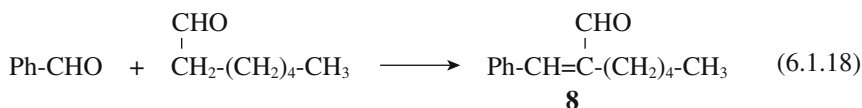
Reprinted with permission from X. Wang, S. Cheng, *Catal. Commun.*, **7**, 689 (2006) p. 693, Table 4.



The MgO-Al₂O₃ mixed oxide derived from hydroxide was active for this condensation. Vasidyl was obtained in a 85% yield in 20 h reaction in air at 443 K.⁹⁶⁾ Rehydrated hydrotalcite is more active for this condensation. A yield of 90% with 99% selectivity was obtained at 408 K in 4 h.¹⁰²⁾

E. Synthesis of jasminealdehyde (α -amylcinnamaldehyde)

Jasminealdehyde **8** is used in perfumery and flavoring. It is traditionally manufactured from benzaldehyde and heptanal.



Climent et al. studied the condensation with various catalysts such as acidic zeolites, Al-MCM-41 and amorphous aluminophosphates.¹⁰³⁾ Amorphous aluminum phosphate, which possesses weak acid sites and weak basic sites, showed the best activity. When this catalyst was exchanged with Na⁺ ions, the activity dropped. From these facts, the authors concluded that both acidic and basic sites

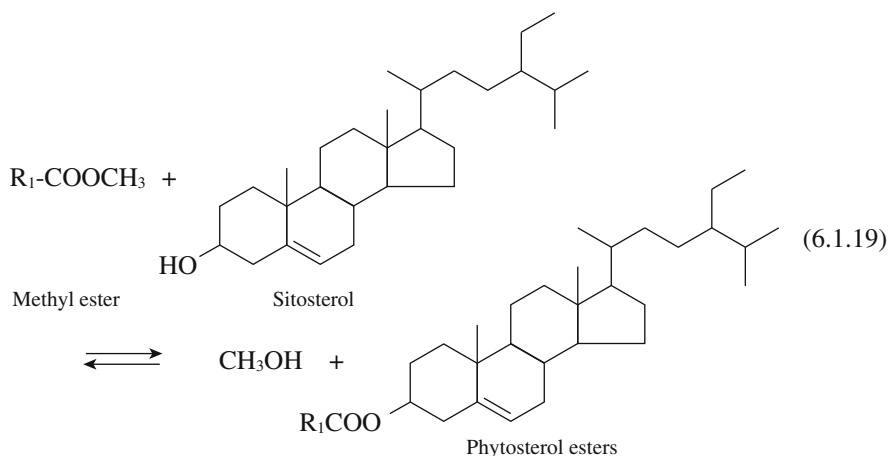
are required for the reaction; the role of weak acid sites is the activation of benzaldehyde by protonation of the carbonyl group followed by the attack of the enolate heptanal intermediate generated on the weak basic sites (Fig. 1.4.2). The total conversion of heptanal was attained in 1 h at 413 K at a reactant ratio of benzaldehyde/heptanal = 5. The selectivity for jasminealdehyde was about 80%, the rest being a self-condensation product of heptanal.

Magnesium organo-silicate (MOS) with a talc-like structure was active for the synthesis of jasminealdehyde.¹⁰⁴⁾ The conversion of heptanal was 99% with 80–82% selectivity for jasminealdehyde at 398 K in 8 h.

The synthesis of jasminealdehyde was also studied using MgO,¹⁰⁵⁾ MgO-loaded Al-MCM-41,¹⁰⁵⁾ as-synthesized and calcined hydrotalcite,^{106,107)} as well as KLaO₂/MCM-41.¹⁰⁸⁾

F. Synthesis of phytosterol esters

Phytosterol esters are useful in the food and cosmetics industries and can be prepared by esterification or transesterification reactions. The synthesis of phytosterol ester by the transesterification between β -sitosterol and methyl dodecanoate proceeds in the presence of solid bases such as MgO, ZnO and La₂O₃.^{109,110)}



In the presence of La₂O₃ prepared by the self-combustion method, phytosterol was obtained over 90% yield with 96% selectivity at 513 K in 3 h.¹⁰⁵⁾ The basic sites responsible for this reaction was concluded to be the unidentate carbonate species on the La₂O₃ surface. The presence of acid sites leads to a side reaction, the dehydration of sitosterol.

References

1. Z. Helwani, M. R. Othman, N. Aziz, J. Kim, W. J. M. Fernando, *Appl. Catal., B*, **363**, 1 (2009).
2. R. Jothiramalingen, M. K. Wang, *Ind. Eng. Chem. Res.*, **48**, 6162 (2009).
3. *Chem.Eng.*, October 2004, p.13.

4. L. Bournay, D. Casanave, B. Delfort, G. Hillion, J. A. Chodorge, *Catal. Today*, **106**, 190 (2005).
5. C. W. McNeff, L. C. McNeff, B. Yan, D. T. Nowlan, M. Rasmussen, A. E. Gyberg, B. J. Krohn, R. L. Fedie, T. R. Hoye, *Appl. Catal., A*, **341**, 39 (2008).
6. G. J. Suppes, M. A. Dasari, E. J. Dockocil, P. J. Mankidy, M. J. Goff, *Appl. Catal., A*, **257**, 213 (2004).
7. W. Xie, H. Peng, L. Chen, *Appl. Catal., A*, **300**, 67 (2006).
8. W. Xie, H. Peng, L. Chen, *J. Mol. Catal., A*, **246**, 24 (2006).
9. M. Di Serio, M. Ledda, M. Cezzolino, G. Minutillo, R. Tesser, S. Santacesaria, *Ind. Eng. Chem. Res.*, **45**, 3009 (2006).
10. Y. Liu, E. Lotero, J. G. Goodwin Jr., X. Mo, *Appl. Catal.*, **331**, 138 (2007).
11. H. -Y. Zeng, Z. Feng, X. Ding, Y. -q. Li, *Fuel*, **87**, 3071, (2008).
12. T. Tittabut, W. Trakarupruk, *Ind. Eng. Chem. Res.*, **47**, 2176 (2006).
13. W. Xie, X. Huang, *Catal. Lett.*, **107**, 53 (2006).
14. M. Verziu, M. Florea, S. Simon, V. Simon, P. Filip, V. I. Parvulescu, C. Hardacre, *J. Catal.*, **263**, 56 (2009).
15. W. Xie, H. Li, *Appl. Catal., A*, **255**, 1 (2006).
16. H. -J. Kim, B. -S. Kang, Y. M. Park, D. -K. Kim, J. -S. Lee, K. -Y. Lee, *Catal. Today*, **93-95**, 315 (2004).
17. J. L. Schumaker, C. Crofcheck, E. Santillan-Jimenez, M. Crocker, *Catal. Lett.*, **115**, 56 (2007).
18. W. Xie, Z. Yang, *Catal. Lett.*, **117**, 159 (2007).
19. W. Xie, Z. Yang, H. Chun, *Ind. Eng. Chem. Res.*, **46**, 7942 (2007).
20. D. Martín Alonso, R. Mariscal, R. Moreo-Tost, M. D. Zafra Poves, M. López Granados, *Catal. Commun.*, **8**, 2074 (2007).
21. X. Li, G. Lu, Y. Guo, Y. Guo, Y. Wang, Z. Zhang, X. Liu, Y. Wang, *Catal. Commun.*, **8**, 1969 (1972).
22. W. M. Antunes, C. Veloso, C. A. Henriques, *Catal. Today*, **133-135**, 548 (2006).
23. M. Verziu, B. Cojocar, J. Hu, R. Richards, C. Ciuculescu, P. Filip, V. I. Parvulescu, *Green Chem.*, **10**, 373 (2008).
24. L. Wang, J. Yang, *Fuel*, **86**, 328 (2007).
25. C. S. MacLeod, A. P. Harvey, A. F. Lee, K. Wilson, *Chem. Eng. J.*, **135**, 63 (2008).
26. C. Reddy, V. Reddy, R. Oshel, J. G. Verkade, *Energy Fuels*, **20**, 1310 (2006).
27. X. Liu, H. He, Y. Wang, S. Zhu, X. Piao, *Fuel*, **87**, 216 (2008).
28. M. L. Granados, M. D. Z. Povas, D. M. Alonso, R. Mariscal, F. C. Galisteo, R. Moreno-Tost, J. Santamaría, J. L. G. Fierro, *Appl. Catal., B*, **73**, 317 (2007).
29. M. Kouzu, T. Kasuno, M. Tajika, Y. Sugimoto, S. Yamanaka, J. Hidaka, *Fuel*, **87**, 2798 (2008).
30. L. C. Meher, M. G. Kulkarni, A. K. Dalal, S. N. Nalk, *Eur. J. Lipid Sci. Technol.*, **108**, 389 (2006).
31. M. C. G. Albuquerque, I. Jiménez-Urbistondo, J. Santamaría-González, J. M. Mérida-Robles, R. Moreno-Tost, E. Rododríguez-Catellón, A. Jiménez-López, D. C. S. Azevedo, C. L. Cavalcante Jr., P. Mareles-Torres, *Appl. Catal., A*, **334**, 35 (2008).
32. C. Ngamcharussrivichai, W. Wiwatnimit, S. Wangnoi, *J. Mol. Catal., A*, **276**, 24 (2007).
33. C. Ngamcharussrivichai, P. Totarat, K. Bunyakiat, *Appl. Catal., A*, **341**, 77 (2008).
34. S. Yan, M. Kim, S. O. Salley, K. Y. S. Ng, *Appl. Catal., A*, **360**, 163 (2009).
35. M. C. G. Albuquerque, J. Santamaría-González, J. M. Mérida-Robles, I. R. Moreno-Tost, E. Rododríguez-Catellón, A. Jiménez-López, D. C. S. Azevedo, C. L. Cavalcante Jr., P. Mareles-Torres, *Appl. Catal., A*, **347**, 152 (2008).
36. S. Yan, H. Lu, B. Liang, *Energy Fuels*, **22**, 646 (2005).
37. X. Lin, H. He, Y. Wang, S. Zhu, *Catal. Commun.*, **8**, 1107 (2007).
38. S. Yan, S. O. Salley, K. Y. S. Ng, *Appl. Catal., A*, **353**, 203 (2008).
39. C. Wei, H. Zhiliang, L. Yu, H. Qianjun, *Catal. Commun.*, **9**, 516 (2008).
40. T. Ebiura, T. Echizen, A. Ishikawa, K. Murai, T. Baba, *Appl. Catal., A*, **283**, 111 (2005).
41. D. E. López, J. G. Goodwin Jr., D. A. Bruce, E. Lotero, *Appl. Catal., A*, **295**, 97 (2005).
42. Y. Liu, E. Lotero, J. G. Goodwin Jr., Changqing Liu, *J. Catal.*, **246**, 428 (2007).
43. M. L. Granados, D. M. Alonso, I. Sádaba, R. Mariscal, P. Ocón, *Appl. Catal., B*, **89**, 265 (2009).
44. M. Kouzu, S. Yamanaka, J. Hidaka, M. Ysunomori, *Appl. Catal., A*, **355**, 94 (2009).
45. M. Kouzu, T. Kasuno, M. Tajika, S. Yamanaka, J. Hidaka, *Appl. Catal., A*, **334**, 357 (2008).
46. M. C. G. Albuquerque, D. C. S. Azevedo, C. L. Cavalcante Jr., J. Santamaría-González, J. M. Mérida-Robles, R. Moreno-Tost, E. Rodríguez-Castellón, A. Jiménez-López, P. Mareles-Torres, *J. Mol. Catal., A*, **300**, 19 (2009).
47. Y. Ono, *Pure Appl. Chem.*, **68**, 367 (1996).
48. Y. Ono, *Appl. Catal.*, **155**, 133 (1997).

49. P. Tundo, *Pure Appl. Chem.*, **73**, 1117 (2001).
50. J. F. Knifton, R. G. Duranleau, *J. Mol. Catal.*, **67**, 389 (1991).
51. T. Tatsumi, Y. Watanabe, K. A. Koyano, *Chem. Commun.*, **1996**, 2251.
52. Y. Watanabe, T. Tatsumi, *Micropor. Mesopor. Mater.*, **22**, 399 (1998).
53. B. M. Bhanage, S. Fujita, Y. Ikushima, M. Arai, *Appl. Catal., A*, **219**, 259 (2001).
54. B. M. Bhanage, S. Fujita, Y. He, Y. Ikushima, M. Shairai, K. Torii, M. Arai, *Catal. Lett.*, **83**, 137 (2002).
55. H. Abmanyu, C. S. Kim, B. S. Ahn, K. Y. Yoo, *Catal. Lett.*, **118**, 30 (2007).
56. H. Abimanyu, B. S. Ahn, C. S. Kim, K. S. Yoo, *Ind. Eng. Chem. Res.*, **45**, 7936 (2007).
57. S. M. Duri, V. V. Mahajani, *J. Chem. Technol. Biotechnol.*, **81**, 62 (2006).
58. M. Cao, Y. Meng, Y. Lu, *React. Kinet. Catal. Lett.*, **88**, 251 (2006).
59. T. Wei, M. Wang, W. Wei, Y. Sun, B. Zhong, *Green Chem.*, **5**, 343 (2003).
60. H. Wang, M. Wang, W. Zhang, N. Zhao, W. Wei, Y. Sun, *Catal. Today*, **115**, 107 (2006).
61. X. -J. Feng, X. -B. Lu, R. He, *Appl. Catal., A*, **272**, 347 (2004).
62. M. Selva, A. Perosa, M. Fabris, *Green Chem.*, **10**, 1068 (2008).
63. Y. Chang, T. Jiang, Z. Liu, W. Wu, L. Gao, J. Li, H. Gao, G. Zhao, J. Huag, *Appl. Catal., A*, **263**, 179 (2004).
64. Q. Jiang, Y. Yang, *Catal. Lett.*, **95**, 127 (2004).
65. C. De, B. Li, H. Lv, Y. Yu, Q. Cai, *Catal. Lett.*, **128**, 459 (2009).
66. K. Tomishige, T. Sakaibori, Y. Ikeda, K. Fujimoto, *Catal. Lett.*, **58**, 225 (1999).
67. Y. Ikeda, M. Asasullah, K. Fujimoto, K. Tomishige, *J. Phys. Chem., B*, **105**, 10653 (2001).
68. Y. Yoshida, Y. Arai, S. Kado, K. Kunimori, K. Tomishige, *Catal. Today*, **115**, 95 (2006).
69. K. Tomishige, Y. Furusawa, Y. Ikeda, M. A. Assadullah, K. Fujita, *Catal. Lett.*, **76**, 71 (2001).
70. J. L. Zotin, F. C. Faro, Jr., *Catal. Today*, **5**, 423 (1989).
71. H. G. Karge, L. Rasko, *J. Colloid Interface Sci.*, **64**, 522 (1978).
72. H. Karge, M. Łaniecki, M. Ziolek, *J. Catal.*, **109**, 252 (1988).
73. C. Chang, *J. Catal.*, **53**, 374 (1978).
74. M. Waqif, A. M. Saad, M. Bensitel, J. Bachelier, O. Saur, J. -C. Lavalley, *J. Chem. Soc., Faraday Trans.*, **88**, 2931 (1982).
75. A. Datta, R. C. Cavell, R. W. Tower, Z. M. George, *J. Phys. Chem.*, **89**, 443 (1988).
76. H. G. Karge, M. Ziolek, M. Łaniecki, *Zeolites*, **7**, 197 (1987).
77. A. B. Mohammed Saad, O. Saur, Y. Wang, C. P. Tripp, B. A. Morrow, J. C. Lavalley, *J. Phys. Chem.*, **99**, 4620 (1995).
78. H. G. Karge, M. Łaniecki, M. Ziolek, *Proc. 7th Int. Zeolite Conf. Tokyo, 1986*, p. 617, Kodansha, Tokyo and Elsevier, Amsterdam, 1986.
79. D. Kishore, S. Kannan, *Green Chem.*, **4**, 607 (2002).
80. D. Kishore, S. Kannan, *Appl. Catal., A*, **270**, 227 (2004).
81. D. Kishore, S. Kannan, *J. Mol. Catal., A*, **244**, 83 (2006).
82. V. K. Srivastava, H. C. Bajaj, R. V. Jasra, *Catal. Commun.*, **4**, 543 (2003).
83. D. Kishore, S. Kannan, *J. Mol. Catal., A*, **223**, 225 (2004).
84. G. Suzukamo, M. Fukao, T. Hibi, K. Tanabe, K. Chikaishi, in: *Acid-Base Catalysis* (K. Kozo, H. Hattori, T. Yamaguchi, T. Tanaka, eds.) Kodansha, Tokyo and VCH Weinheim, 1989, p. 405.
85. P. A. Vatakencherry, K. N. Pushpakumarian, *Chem. Ind.*, **1987**, 163.
86. E. L. Jablonski, I. M. J. Vilella, S. C. Maina, S. R. de Miguel, O. A. Scelza, *Catal. Commun.*, **7**, 18 (2005).
87. C. Noda Pérez, C. A. Pérez, C. A. Henriques, J. L. F. Monteiro, *Appl. Catal., A*, **272**, 229 (2004).
88. J. C. A. A. Roelofs, A. J. Dillen, K. P. de Jong, *Catal. Today*, **60**, 297 (2000).
89. J. C. A. A. Roelofs, A. J. van Dillen, K. P. de Jong, *Catal. Lett.*, **74**, 91 (2001).
90. M. J. Climent, A. Corma, S. Iborra, A. Verty, *Catal. Lett.*, **79**, 157 (2002).
91. M. J. Climent, A. Corma, S. Iborra, A. Verty, *Green Chem.*, **4**, 474 (2002).
92. M. J. Climent, A. Corma, S. Iborra, K. Epping, A. Velly, *J. Catal.*, **225**, 316 (2004).
93. S. Abelló, F. Medina, D. Ticht, J. Pérez-Ramírez, J. C. Groen, J. E. Sueiras, P. Salagre, Y. Cesteros, *Chem. Eur. J.*, **11**, 728 (2005).
94. S. Abelló, D. Vijaya-Shankar, J. Pérez-Ramírez, *Appl. Catal., A*, **342**, 119 (2007).
95. M. Hasni, G. Prado, J. Ruchaud, P. Grange, M. Devillers, S. Delsarte, *J. Mol. Catal., A*, **247**, 116 (2006).
96. M. J. Climent, A. Corma, S. Iborra, J. Primo, *J. Catal.*, **151**, 60 (1995).
97. M. T. Drexler, M. D. Amiridis, *Catal. Lett.*, **79**, 175 (2002).
98. B. M. Choudary, K. V. S. Ranganath, J. Yadav, M. Lakshmi Kantam, *Tetrahedron Lett.*, **46**, 1369 (2005).

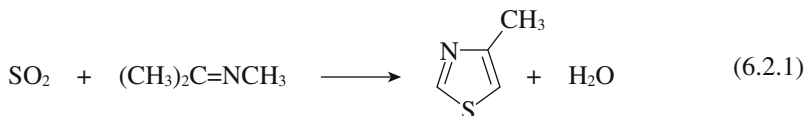
99. X. Wang, S. Cheng, *Catal. Commun.*, **7**, 689 (2006).
100. X. Wang, Y. -H. Tseng, J. C. C. Chan, S. Cheng, *Micropor. Mesopor. Mater.*, **85**, 241 (2005).
101. X. Wang, Y. -H. Tseng, J. C. C. Chen, S. Cheng, *J. Catal.*, **233**, 266 (2005).
102. M. J. Climent, A. Corma, S. Iborra, A. Verty, *J. Catal.*, **221**, 474 (2004).
103. M. J. Climent, A. Corma, H. Garcia, R. Guil-Lopez, S. Iborra, V. Fornés, *J. Catal.*, **197**, 385 (2001).
104. S. K. Sharma, H. A. Patel, R. V. Jarsa, *J. Mol. Catal., A*, **280**, 61 (2008).
105. J. -I. Yu, S. Y. Shiau, A. -N. Ko, *Catal. Lett.*, **17**, 165 (2001).
106. S. K. Sharma, P. A. Parikh, R. J. Jarsa, *J. Mol. Catal.*, **286**, 55 (2008).
107. J. -I. Yu, S. Y. Shiau, A. -N. Ko, *React. Kinet. Catal. Lett.*, **72**, 365 (2001).
108. S. Jaenicke, G. K. Chuah, X. H. Lin, X. C. Hu, *Micropor. Mesopor. Mater.*, **35/36**, 143 (2000).
109. Y. Pouilloux, G. Courtols, M. Boisseau, A. Piccirilli, J. Barrault, *Green Chem.*, **5**, 89 (2003).
110. S. Vallange, A. Beauchaud, J. Barrault, Z. Gabelica, M. Daturi, F. Can, *J. Catal.*, **251**, 113 (2007).

6.2 Synthesis and Ring Transformation of Heterocycles

6.2.1 Synthesis of Heterocycles

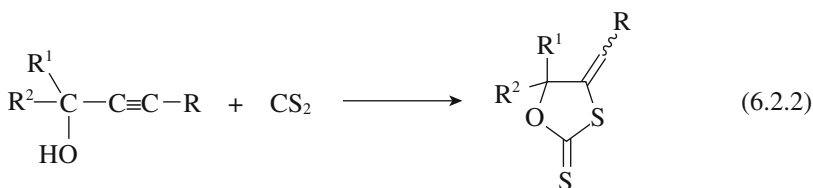
The vapor-phase reaction of α,β -unsaturated compounds with hydrogen disulfide gives thiophenes over K_2O -doped Al_2O_3 .¹⁾ For example, the reaction of crotonaldehyde with hydrogen sulfide at 673 K gave thiophene in 77% selectivity at a conversion of 35%.

The vapor phase reaction of imines with sulfur dioxide gives thiazoles at 723–773 K.²⁾ For example, the reaction of acetone methylimine with sulfur dioxide over soda lime with 1% ZrO_2 gives a 70% yield of 4-methylthiazole.



For the reaction of acetone methylimine with SO_2 , Cs-loaded ZSM-5 gives excellent performance, e.g., activity, selectivity and life time. The reaction is run at 700 K in the presence of water.³⁾

The reaction of α -alkynyl alcohols and carbon disulfide on KF/Al_2O_3 without solvent affords selectively 4-alkylidene-2-thione-1,3-oxathialones.⁴⁾ A mixture of α -alkynyl alcohol (10 mmol) and carbon disulfide (1 mL) was adsorbed on KF/Al_2O_3 (6 g). After 16 h at room temperature, the solid was extracted with CH_2Cl_2 . The experimental results are shown in Table 6.2.1.

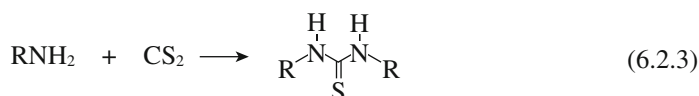


Amines react with carbon disulfide in the presence of $ZnO-Al_2O_3$ to afford N,N' -substituted thioureas.⁵⁾

Table 6.2.1 Condensation of α -alkynyl alcohol with carbon disulfide [eq. (6.2.2)] by adsorption on KF/Al₂O₃ at room temperature for 16 h

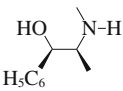
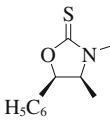
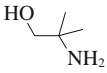
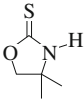
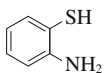
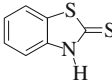
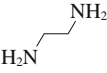
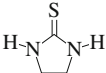
R ¹	R ²	R	Yield/%
CH ₃	C ₂ H ₅	H	70
H	(CH ₃) ₂ CH	CH ₃	57
CH ₃	CH ₃	H	94
CH ₃	CH ₃	CH ₃ C≡C	64
	C ₆ H ₁₀	H	60

Reprinted with permission from D. Villemin, A. Ben Alloum, *Synth. Commun.*, **22**, 1351 (1992) p.1353, Table.



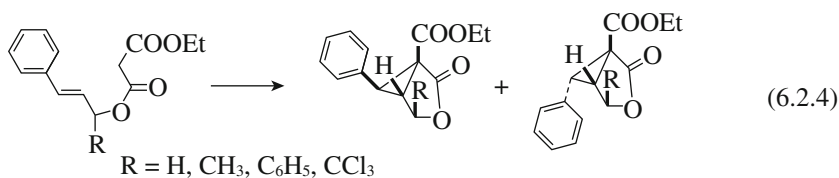
The reaction of aniline with carbon disulfide at 373 K gave the corresponding thiourea in a 83% yield in 2 h. When amine contains an additional nucleophilic group, heterocyclic thione is obtained in high yield, as shown in Table 6.2.2. The catalyst ZnO-Al₂O₃ is prepared by calcining the Zn-Al-hydrotalcite-like compound at 773 K. The XRD of the fresh catalyst shows the pattern of ZnO (zincite) as the unique crystalline phase. After the catalytic runs, a set of large peaks of ZnS (sphalerite) are superimposed over that of ZnO. Despite this, five cycles were repeated without apparent loss of catalytic activity.

Table 6.2.2 Reaction of amines bearing an additional nucleophile group with CS₂ over ZnO-Al₂O₃

Amine	Product	Yield[sel.]/%
		98 [98]
		92 [94]
		92 [99]
		100 [100]

Reprinted with permission from M. Ballabeni, R. Ballini, F. Bigi, R. Maggi, M. Parrini, G. Predieri, G. Sartori, *J. Org. Chem.*, **64**, 1029 (1999) p. 1030, Table 2.

As-synthesized hydrotalcite ($Mg/Al = 3$) is a suitable catalyst in the intramolecular cyclization reaction of malonic acid allylic esters into bicyclic cyclopropane carboxylic acid lactones.⁶⁾

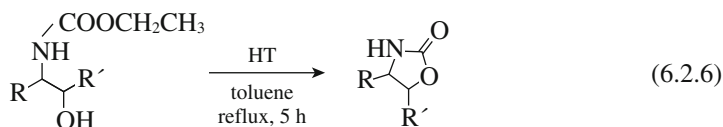


The reaction is carried out by adding dropwise ester (1 mmol) in toluene to a stirred mixture of hydrotalcite (0.5 g) and iodine (0.57 g) with a drop of TCMC (tricaprylmethyl ammonium chloride) in toluene (10 mL) at 393 K.

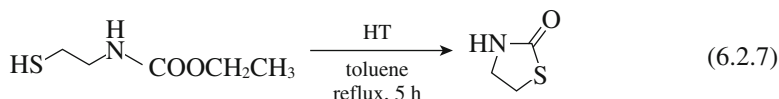
The same catalyst is also useful for the intermolecular cyclization reaction of 1,2-dibromoethane and dimethyl malonate into cyclopropane dicarboxylic acid ester in the presence of iodine and a phase transfer agent, TEBA (triethylbenzylammonium chloride).



Oxazolidine-2-ones can be synthesized by the cyclization of carbamates in the presence of rehydrated hydrotalcite.⁷⁾



For example, the reaction of (2-hydroxypropyl)-carbamic acid ester ($R = H, R' = CH_3$) in toluene gives the corresponding oxazolidine-2-one in 88% yield in 5 h at 383 K. Calcined hydrotalcite shows low catalytic activity (20% yield). Similarly, the synthesis of (2-mercaptoethyl)-carbamic acid ethyl ester gave 2-thiazolidinone in 50% yield under similar reaction conditions.



Nanocrystalline ZnO and (as synthesized) Zn, Al-hydrotalcite (as synthesized) are effective catalysts for the (2 + 3) cycloaddition of sodium azide with nitriles to afford 5-substituted 1H-tetrazoles in good yields.^{8,9)} Zn, Al-hydrotalcite (0.1 g) was added to a mixture of benzonitrile (2 mmol), sodium azide in DMF and stirred at 393 K. The results with a variety of structurally divergent benzonitriles are shown in Table 6.2.3.¹⁰⁾ 1,2- and 1,3-Dicyanobenzonitriles afforded mono-

Table 6.2.3 Synthesis of 5-substituted 1H-tetrazoles over as-synthesized Zn, Al-hydroxalcite^{a)}

Entry	Substrate	Temperature/°C	Time/h	Yield/% ^{b)}
1		393	12	84
2		393	12	86
3		393	12	81
4		403	24	79
5		403	12	82
6		403	24	69
7		403	5	91
8		403	5	86
9		403	24	78

^{a)} Reaction conditions: nitrile (2 mL), NaN₃ (3 mmol), Zn/Al hydroxalcite (0.1 g), DMF (5 mL).

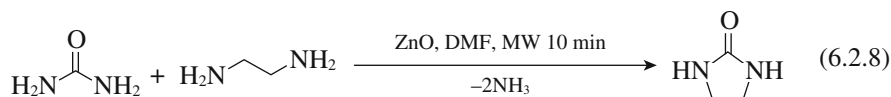
^{b)} Isolated yields.

Reprinted with permission from M. Lakshmi Kantam, K. B. Shiva Kumar, K. Phani Raja, *J. Mol. Catal., A*, **247**, 186 (2006) p.187, Table 2.

addition product. Heteroaromatic nitriles such as 2-pyridinecarbonitrile and cyano-pyrazine give the corresponding tetrazoles in shorter reaction times.

The facile synthesis of cyclic ureas from diamines and urea can be achieved in the presence of ZnO under microwave (MW) irradiation at 393 K.¹⁰⁾ Microwave-assisted coupling of urea with ethylenedimine was carried out in the presence of ZnO at 393 K, 100-150 W of MW power and reduced pressure of 71 kPa in DMF

for 10 min. The imidazoline-2-one was obtained in nearly quantitative yield.



Similarly, the reactions of 1,2-propanediamine, 1,3-propanediamine, and *o*-phenylenediamine with urea give 4-methylimidazoline-2-one, tetrahydro-2-pyrimidinone and dihydrobenzimidazole-2-one, respectively, in high yields. The reaction can be extended to aliphatic aminoalcohols under same conditions.¹¹⁾ The result is shown in Table 6.2.4. 2-Aminophenol also reacts with urea to afford 2-benzoxazolone in a 70% yield.

Seifi and Sheibani developed the three-component reaction of aryl aldehydes, malononitrile and α -hydroxy- or α -amino-activated C-H acids to afford the pyran annulated heterocycle systems.¹¹⁾ The authors confirmed that MgO was an effective catalyst for the following two reactions.

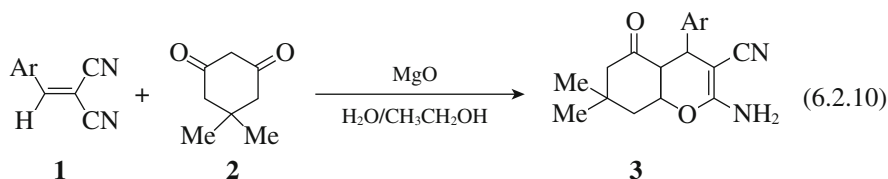
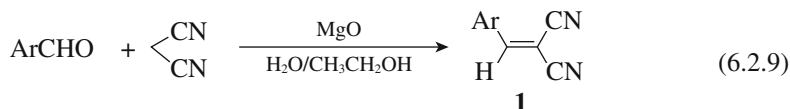
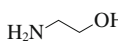
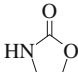
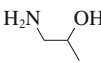
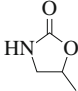
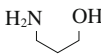
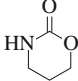


Table 6.2.4 The coupling reactions of aliphatic aminoalcohols and urea for the formation of cyclic urethanes^{a)}

Entry	Aminoalcohols	Product	Yield/% ^{b)}
1			100
2			98
3			90

^{a)} Condition urea 0.6 g (10 mmol), amino alcohols 10 mmol, DMF 1 g, ZnO 7.3 mol%, $T = 120^\circ\text{C}$, $P = 71$ kPa, $t = 10$ min, MW power = 150 W.

^{b)} Yields obtained from GC-MS.

Reprinted with permission from Y. J. Kim, R. S. Varma, *Tetrahedron Lett.*, **45**, 7205 (2004) p. 7207, Table 3.

The first reaction is the Knoevenagel reaction between benzaldehydes and malononitrile to afford benzylidenemalononitrile **1**, and the second reaction is the Michael addition of **1** with dimedone **2** to afford the heterocyclic compound **3**. Then the three-component reaction of benzaldehyde, malononitrile and dimedone was tested and the heterocyclic compound was obtained in high yield over MgO in refluxing ethanol-water solvent. Various three-component reactions can be achieved in a similar manner, as shown in Fig. 6.2.1. The products were obtained in 87–96% yields.

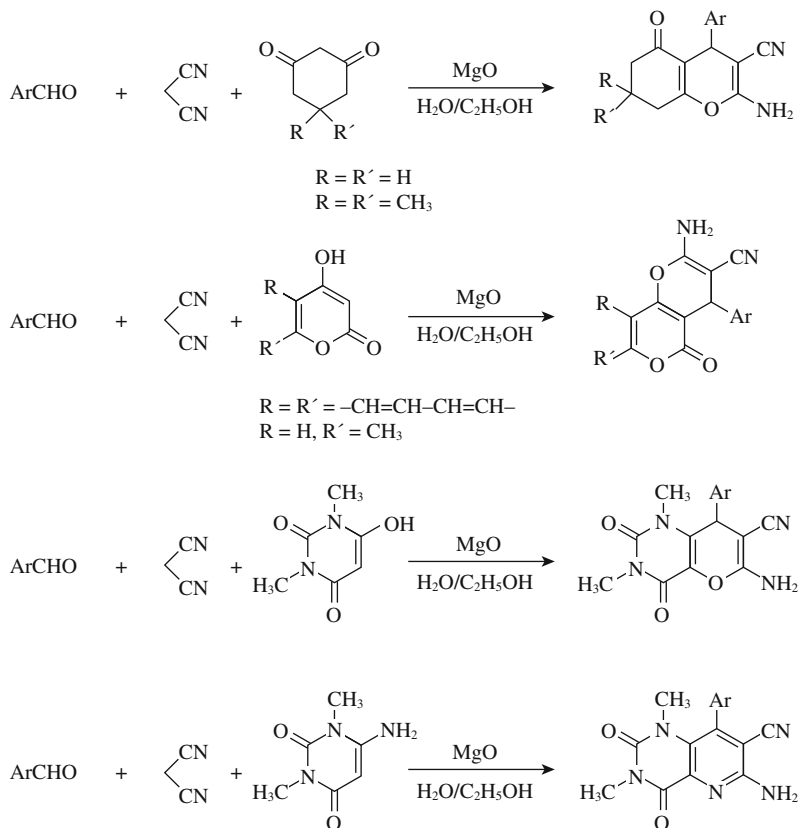


Fig 6.2.1 Three-component synthesis of heterocycles over MgO. Reprinted with permission from M. Seifi, H. Sheibani, *Catal. Lett.*, **126**, 275 (2008) p. 277, Scheme 1.

6.2.2 Ring transformation of Heterocycles

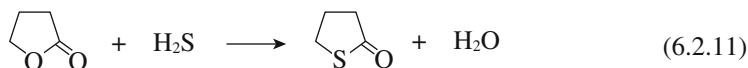
The vapor-phase reaction of γ -butyrolactone and hydrogen sulfide over zeolites to give γ -butyrothiolactone was reported by Venuto and Landis.¹²⁾

Table 6.2.5 Catalytic activities of zeolites for ring transformation of γ -butyrolactone to γ -butyrothiolactone[eg.(6.2.11)]

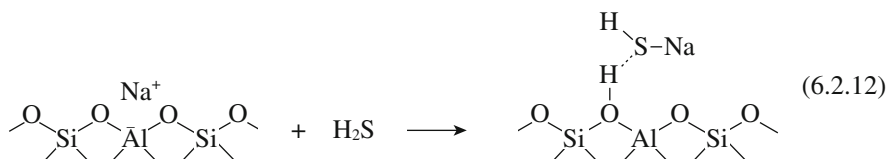
Catalyst	Exchanged/%	Conversion/%	Yield/%
LiY	58	27	26
NaY	-	52	51
KY	97	45	45
RbY	64	51	51
CsY	64	79	78
NaX	-	99	86
KL	-	23	22
HY	66	4	1
MgY	56	2	2

Reaction conditions: 603 K, $\text{H}_2\text{S}/\text{lactone} = 6$, $\text{W}/\text{F} = 6.26 \text{ g h mol}^{-1}$

Reprinted with permission from K. Hatada, Y. Takeyama, Y. Ono, *Bull. Chem. Soc. Jpn*, **51**, 448 (1978) p.448, Table 1.



The reaction was studied in more detail by Hatada et al.^{13,14} The catalytic activities of various forms of faujasites at 603 K are shown in Table 6.2.5 where the following features of the reaction are clearly seen. (i) Alkali cation-exchanged zeolites are much more active than acidic zeolites (HY, MgY). (ii) The catalytic activities of alkali cation-exchanged Y-zeolites increases in the order Li-Y < Na-Y < K-Y < Rb-Y < Cs-Y. By increasing the contact time, 99% yield with 100% selectivity can be attained over Cs-Y at 603 K. (iii) Na-X is more active than Na-Y. These features indicate that basic sites are responsible for the reaction. The activity was completely lost when hydrogen chloride was fed together with reactants. On the other hand, addition of pyridine to the feed enhanced the reaction rate. These results indicate that basic sites are responsible for the reaction. The enhancement of the activity by pyridine may be caused by enrichment of the electron density of the oxygen ions in the $(\text{AlO}_4)^-$ unit by the induced effect of pyridine adsorbed on the sites close to the basic sites. The dissociative adsorption of H_2S on the cation- $(\text{AlO}_4)^-$ pair is postulated.

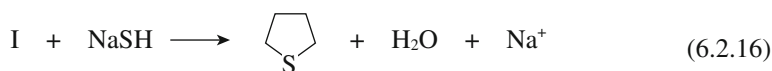
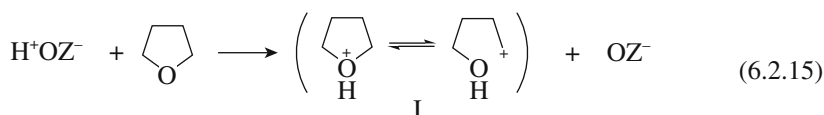
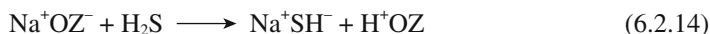


The rate of the reaction is expressed by the Langmuir-Hinshelwood mechanism where both reactants compete for the same active sites. This indicates that the lactone molecules also activated by $\text{Na}^+(\text{AlO}_4)^-$ pair in the zeolite cavities.

Ring transformation of tetrahydrofuran (THF) into tetrahydrothiophene proceeds also over alkali cation-exchanged zeolites.^{14,15}

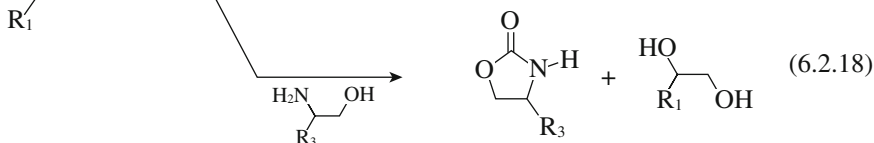
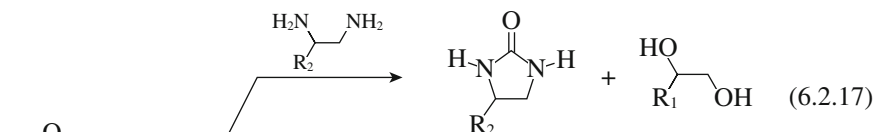


A 94% yield of tetrahydrothiophene was attained at 613 K. As in the case of γ -butyrolactone into γ -butyrothiolactone, acidic zeolites show very low activities. The catalytic activity is considerably suppressed by the addition of either hydrogen chloride or pyridine, indicating that both acidic and basic sites are required for the reaction. In the case of the synthesis of pyrrolidine by the reaction of THF with ammonia, H-Y is the most effective catalyst. This indicates that protons are essential for the activation of THF. Thus the following reaction scheme is postulated.



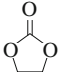
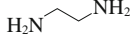
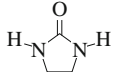
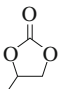
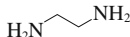
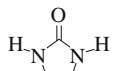
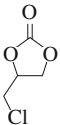
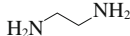
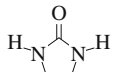
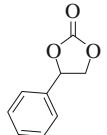
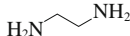
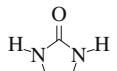
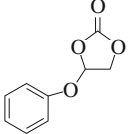
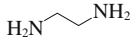
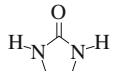
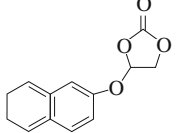
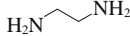
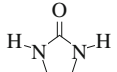
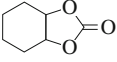
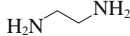
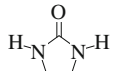
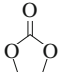
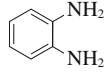
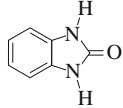
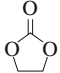
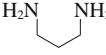
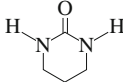
Here, Brønsted acid sites are generated by the dissociative adsorption of H_2S . The reaction rate is of 0.7 order with respect to H_2S and 0.2 order with respect to THF. This implies that the dissociative adsorption of H_2S is the rate-determining step of the reaction.

The synthesis of imidazolidinones and 2-oxazolidinones by transesterification of ethylene carbonate with 1,2-diamines and β -aminoalcohols, respectively, over solid bases was studied by Jagtap et al.¹⁶⁾



MgO was found to be the best catalyst with excellent recyclability. Both reactions proceed to give the products in excellent yields at 353 K within 6 h in ethanol. The results of the synthesis of 2-imidazolidines from ethylene carbonate and 1,2-diamines are given in Table 6.2.6.

Table 6.2.6 Synthesis of 2-imidazolidinones from 1,2-diamines and cyclic carbonates

Entry	Cyclic carbonates	Diamines	2-imidazolidinones	Yield/%
1				85
2				81
3				83
4				80
5				79
6				75
7				77
8				no reaction
9				82

Reaction conditions: cyclic carbonate, 10 mmol; 1,2-diamine, 10 mmol; ethanol, 5mL; temperature, 80°C; time, 6 h; MgO 15 wt%. Yields are based analysis. GC-MS (entries-1-7) m/z 86 (M^+), 58, 42 (entry-9) m/z 100(M^+), 71, 56, 40.

Reprinted with permission from S. R. Jagtap, Y. P. Patil, S. Fujita, M. Arai, B. M. Bhauage, *Appl. Catal., A*, **341**, 133 (2008) p. 137, Table 4.

References

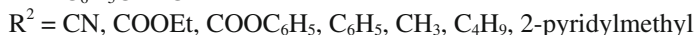
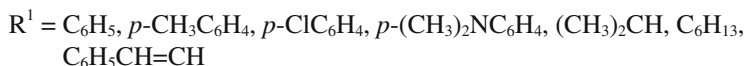
1. J. Barrault, M. Guisnet, J. Lucien, R. Maurel, *J. Chem. Res. (M)* 2634 (1978).
2. J. A. Amato, S. Karady, B. T. Phillips, L. M. Weistck, *Heterocycles*, **22**, 1947 (1984).
3. F. P. Gortsema, B. Beshty, J. J. Friedman, D. Matsumoto, J. J. Sharkey, G. Wildman, T. J. Blacklock, S. H. Pan, the work cited in M. E. Davis, *Acc. Chem. Res.*, **26**, 113 (1993).
4. D. Villemin, A. B. Alloum, *Synth. Commun.*, **22**, 1371 (1992).
5. M. Ballableni, R. Ballini, F. Bigi, R. Maggi, M. Parrini, G. Predieri, M. Sartori, *J. Org. Chem.*, **64**, 1029 (1999).
6. Z. Finta, Z. Hell, D. Balán, A. Cwik, S. Kennéy, F. Figueras, *J. Mol. Catal., A*, **161**, 149 (2000).
7. A. Cwik, A. Fuchs, Z. Hell, H. Böjtös, D. Halmi, P. Bombicz, *Org. Biomol. Chem.*, **3**, 967 (2005).
8. M. Lakshmi Kantam, K. B. Shiva Kumar, Ch. Sridhar, *Adv. Synth. Catal.*, **347**, 1212 (2005).
9. M. Lakshmi Kantam, K. B. Shiva Kumar, K. Phani Raja, *J. Mol. Catal., A*, **247**, 186 (2006).
10. Y. J. Kim, R. S. Varma, *Tetrahedron Lett.*, **45**, 7205 (2004).
11. M. Seifi, H. Sheibani, *Catal. Lett.*, **126**, 275 (2008).
12. P. B. Venuto, P. S. Landis, *Adv. Catal.*, **18**, 259 (1968).
13. K. Hatada, Y. Takeyama, Y. Ono, *Bull. Chem. Soc. Jpn.*, **51**, 448 (1978).
14. Y. Ono, *Heterocycles*, **16**, 1755 (1981).
15. Y. Ono, T. Mori, K. Hatada, *Acta Phys. Chem.*, **24**, 233 (1978).
16. S. R. Jagtap, Y. P. Patil, S. Fujita, M. Arai, B. M. Bhanage, *Appl. Catal., A*, **341**, 133 (2008).

6.3 Reactions of Phosphorus Compounds

6.3.1 Wittig Reactions

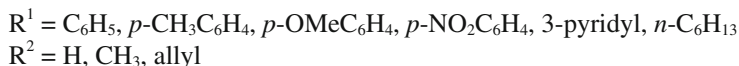
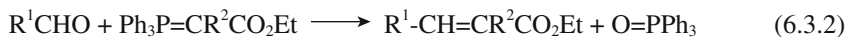
The Wittig reaction is one of the most important reactions for the synthesis of alkenes with unambiguous positioning of the double bond. The reaction involves interaction of phosphonium ylide with an aldehyde or ketone. The ylide is formed from a phosphonium salt in a solution of base such as BuLi and KOH. Usually, the base is required in a stoichiometric amount.

The reactions of benzaldehydes with phosphonium chloride proceeds in the presence of Al₂O₃,¹⁾ KF/Al₂O₃,¹⁾ MgO,²⁾ ZnO²⁾ or Ba(OH)₂.³⁾ The yield of alkenes is 47–87%, depending on the reaction system. The *E/Z* ratios of the products also depend on the system, being 8/92–60/40. Addition of a small amount water promotes the rate of the reactions.^{1,3)}



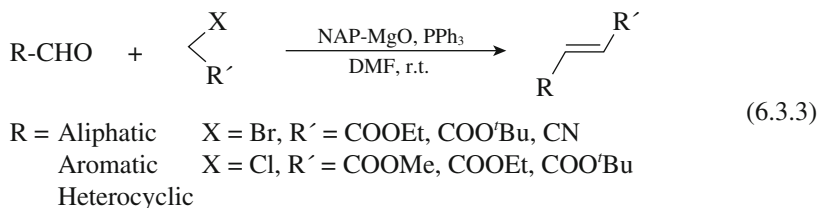
MgO-Al₂O₃ mixed oxide (calcined hydrotalcite at 773 K) is also effective.⁴⁾ The rate depends on the pK_a value of phosphonium salt. In the combinations of aldehydes (R¹ = C₆H₅, C₆H₁₃) with phosphonium salts (R² = COOEt, COOPh), the yields of alkenes are 100% in dioxane-water solvent at 333 K in the reaction time of 0.5–2.0 h. On the other hand, the reactions of the aldehydes (R¹ = C₆H₅, C₆H₁₃) with phosphonium salt with R² = C₄H₉, the yields were 15% and 20% after 6 h.

The reactions of aldehydes with phosphoranes also afford ethyl cinnamates in the presence of Al₂O₃ under solvent-free conditions.⁵⁾



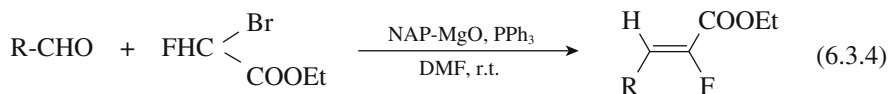
The reactions are *E*-selective, *E/Z* ratios being 80/20–100/0, depending on the reaction system. A fairly large amount of Al_2O_3 is used.

A one-pot Wittig reaction using nanocrystalline magnesium oxide was reported by Choudary et al.⁶⁾ The reaction of an aldehyde, α -haloester (or bromoacetonitrile) and triphenylphosphine in the presence of nanocrystalline MgO (NAP-MgO) afforded α,β -unsaturated esters (nitrile) in excellent yields with high *E*-stereoselectivity under mild conditions.



For example, the reaction of benzaldehyde, ethyl bromoacetate and triphenylphosphine in DMF gave the corresponding α,β -unsaturated ester in 96% yield with an *E/Z* ratio of 99/1 in 8 h at room temperature. The reaction of benzaldehyde with bromoacetonitrile gave phenylacetonitrile in 96% yield with an *E/Z* ratio of 50/50 in 14 h.

α -Fluoro- α,β -unsaturated esters can be prepared in a similar manner.



The reaction of benzaldehyde, ethyl bromofluoroacetate and triphenylphosphine gave the corresponding product in 56% yield with an *E/Z* ratio of 10:90 in 40 h.

The authors proposed the reaction scheme shown in Fig. 6.3.1 for the one-pot Wittig reaction. In this reaction scheme, MgO participates in the steps of the formation of the phosphonium ylide and the alkene formation. The intermediacy of the ylide species was confirmed by ^{31}P NMR.

6.3.2 Wittig-Horner Reactions

The Wittig-Horner reaction is a variant of the Wittig reaction and occasionally called the Wadsworth-Emmons reaction. It involves the condensation of an aldehyde or ketone **1** with a phosphonate **2** to afford alkenes **3**.

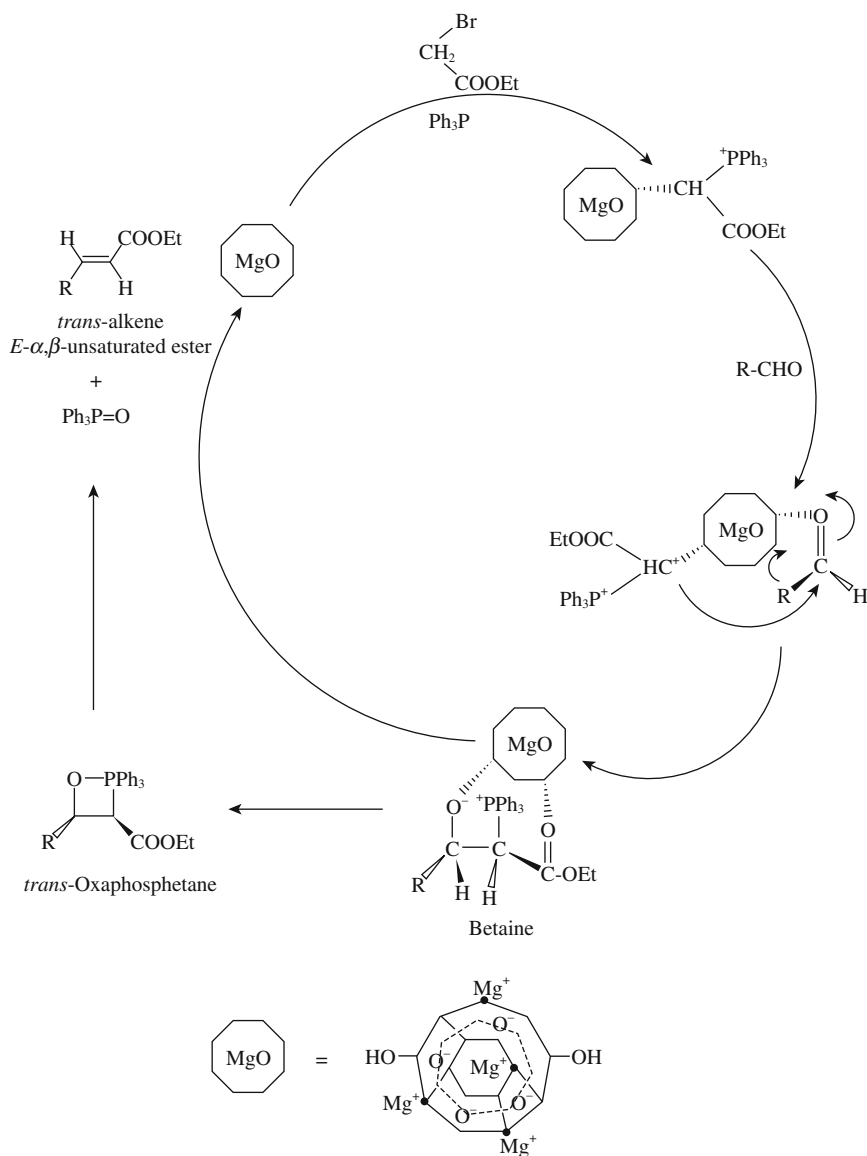
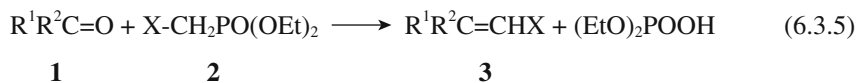


Fig. 6.3.1 Mechanism of the one-pot Wittig reaction by MgO. Reprinted with permission from B. M. Choudary, K. Mahendar, M. L. Kantam, V. S. Ranganath, T. Athar, *Adv. Synth. Catal.*, **348**, 1981 (2006) p. 1981, Scheme 3.



Here. $\text{R}^1\text{R}^2\text{C}=\text{O}$ can be benzaldehyde, benzophenone, alkanal, cyclohexanone,

2-furfurylaldehyde, etc. and X can be CN(**2a**), COOEt(**2b**), COO^tBu(**2c**), or Ph(**2d**).

Wittig-Horner reactions proceed in the presence of KF/alumina¹⁾ or barium hydroxide.^{7,8)} In both cases, the reaction rates are enhanced by a small amount of water and a rather large amount of the catalyst was required.

Catalytic Wittig-Horner reactions can be achieved with the use of hydrotalcite having ^tBuO⁻ ions in the interlayer.⁹⁾ The yield of the product is proportional to the content of ^tBuO⁻. Hydrotalcites having NO₃⁻, OH⁻ and F⁻ show poor activity. This demonstrates that the ^tBuO⁻ ions are the active sites for the Wittig-Horner reactions. Table 6.3.1 shows the results of the reactions with hydrotalcite contain-

Table 6.3.1 The Wittig-Horner reaction of carbonyl compounds with various phosphonates catalyzed by hydrotalcite with ^tBuO⁻ ions

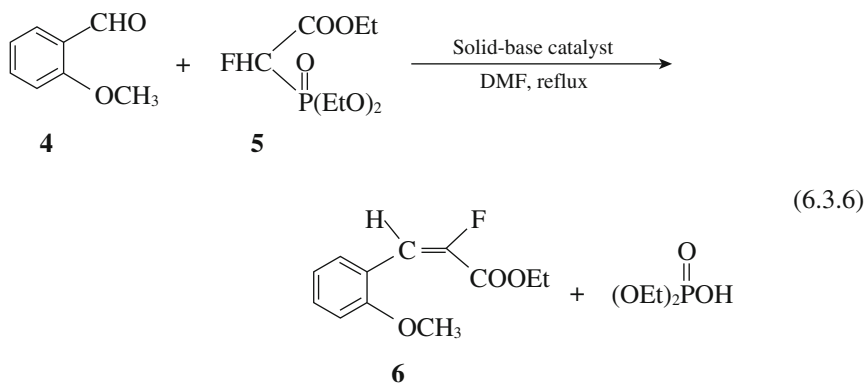
$$R^1R^2C=O + X-CH_2PO(OEt)_2 \longrightarrow R^1R^2C=CHX + (EtO)_2POOH$$

Entry	Carbonyl compound		X	Time /h	Isolated yield (E/Z)
	R ¹	R ²			
1	C ₆ H ₅	H	2a	2.0	96 (75/25)
2	C ₆ H ₅	H	2b	2.5	76 (99/1)
3	C ₆ H ₅	H	2c	2.0	61 (94/6)
4	<i>o</i> -OMeC ₆ H ₄	H	2a	2.0	96 (74/26)
5	<i>o</i> -OMeC ₆ H ₄	H	2b	2.5	62 (99/1)
6	<i>p</i> -ClC ₆ H ₄	H	2a	2.5	93 (55/45)
7	<i>p</i> -ClC ₆ H ₄	H	2b	3.0	98 (99/1)
8	<i>p</i> -NO ₂ C ₆ H ₄	H	2a	2.0	98 (78/22) 92 (76/24) ^{c)}
9	<i>p</i> -NO ₂ C ₆ H ₄	H	2b	2.5	90 (99/1)
10	C ₄ H ₃ O	H	2a	1.5	98 (75/25)
11	C ₄ H ₃ O	H	2b	2.0	86 (99/1)
12	-cC ₆ H ₁₁ -	H	2a	2.5	95 (96/4)
13	-cC ₆ H ₁₁ -	H	2b	3.0	80 (99/1)
14	C ₆ H ₄ CH=CHCH ₂	H	2a	2.5	88 (66/34)
15	C ₆ H ₄ CH=CHCH ₂	H	2b	3.0	50 (99/1)
16	-cC ₅ H ₁₀ -	H	2a	2.5	98
17	-cC ₅ H ₁₀ -	H	2b	3.0	90
18	C ₆ H ₅	CH ₃	2a	6.0	27 (67/33)
19	C ₆ H ₅	CH ₃	2b	10.0	NR ^{b)}

X = CN **2a**, COOEt **2b**, COO^tBu **2c**.

Reprinted with permission from B. M. Choudary, M. L. Kantam, C. V. Reddy, B. Bharathi, F. Figueras, *J. Catal.*, **218**, 191 (2003) p. 197, Table 2.

ing $t\text{BuO}^-$ ions. The reactions were carried out with the carbonyl compound (1 mmol), and phosphonate (1 mmol) and the catalyst (0.025 g for **2a** and 0.050g for **2b**, **2c**) in DMF under reflux. The reactions are truly catalytic and selective. No by-product prompted by aldolization or Knoevenagel reaction is noted. However, the reactions with ketones exhibit poor yields or no reaction (entries 18 and 19). The condensation of carbonyl compounds with triphenylphosphonoacetate **2b** offers *E/Z* ratios of >99, whereas diethyl cyanomethylphosphonate **2a** gives a 75 : 25 to 50 : 50 ratio. The synthesis of ethyl 2-fluoro-3-(2-methoxyphenyl)-2-propenoate, a useful class of intermediate compound **6** in the synthesis of several biologically active fluorinated molecules, is also performed. Thus, the reaction of **4** and **5** gives **6** in a 90% yield with an *E/Z* ratio of 1/99.



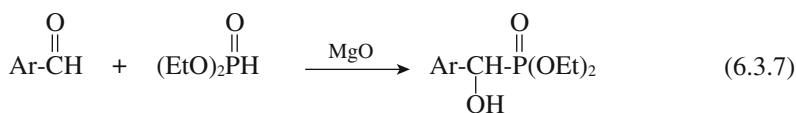
MgO can also work as a catalyst for a variety of Wittig-Horner reactions of aldehydes including aliphatic, aromatic, cyclic, heterocyclic with various phosphonates ($X = \text{COOMe}$, COOEt , COO^tBu , CN and Cl).¹⁰ Among MgO samples examined, nanocrystalline MgO ($590 \text{ m}^2 \text{ g}^{-1}$) showed the highest activity. The reactions were carried out in toluene at reflux temperature.

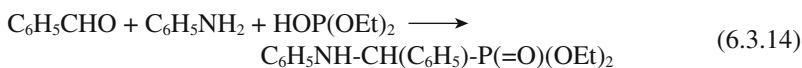
MgO- La_2O_3 mixed oxide was also reported to be active for Wittig-Horner reactions.¹¹⁾

6.3.3 Pudovik Reactions

The Pudovik reaction is one of the most versatile pathways for the formation of carbon-phosphorous bonds and involves the addition of compounds containing a labile P-H bond with unsaturated systems.

The synthesis of diethyl 1-hydroxyarylmethylphosphonates from aldehydes and diethyl hydrogen phosphonate on MgO proceeds without solvent at room temperature, the reaction time being 2 min–4 h.¹²⁾





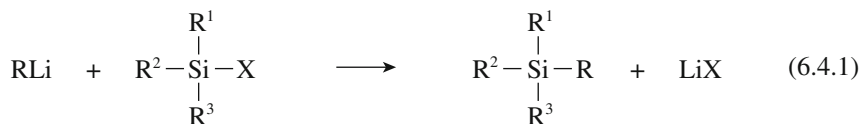
References

1. F. Texier-Boullet, D. Villemin, M. Richard, H. Moison, A. Foucaud, *Tetrahedron*, **41**, 1259 (1985).
2. H. Moison, F. Texier-Boullet, A. Foucaud, *Tetrahedron*, **43**, 537 (1987).
3. M. S. Climent, J. M. Narinas, Z. Moulougui, Y. Le Bigot, M. Delmas, A. Gaset, J. V. Sinisterra, *J. Org. Chem.*, **54**, 3695 (1989).
4. M. Sychev, R. Prihod'ko, K. Erdmann, A. Mangel, R. A. van Santen, *Appl. Clay Sci.*, **18**, 119 (2001).
5. D. D. Dhavale, M. D. Sindkhedkar, R. S. Mali, *J. Chem. Res. (S)*, **1995**, 414.
6. B. M. Choudary, K. Mahendar, M. L. Kantam, V. S. Ranganath, T. Athar, *Adv. Synth. Catal.*, **348**, 1977 (2006).
7. J. V. Sinisterra, Z. Moulougui, M. Delmas, A. Gaset, *Synthesis*, **1985**, 1097.
8. J. V. Sinisterra Gago, A. A. Leon, J. M. Marinas Rubio, *J. Colloid Interface Sci.*, **115**, 520 (1987).
9. B. M. Choudary, M. L. Kantam, C. V. Reddy, B. Bharathi, F. Fgueras, *J. Catal.*, **218**, 191 (2003).
10. B. M. Choudary, K. Mahendar, K. V. S. Ranganth, *J. Mol. Catal., A*, **234**, 25 (2005).
11. M. L. Kantam, H. Kochkar, J. -M. Clacens, B. Veldurthy, A. Garcia-Ruiz, F. Figueras, *Appl. Catal., B*, **55**, 177 (2005).
12. A. R. Sadarian, B. Kaboudin, *Synth. Commun.*, **27**, 543 (1997).
13. D. Semenzin, G. Etenma-Moghadam, D. Albouy, Q. Diallo, M. Koenig, *J. Org. Chem.*, **69**, 2414 (1997).
14. A. Smahi, A. Solhy, R. Tahir, S. Sebti, J. A. Mayoral, J. L. Garcia, *Catal. Commun.*, **9**, 2503 (2008).
15. M. Zahouily, A. Elmakssoudi, A. Mezdar, A. Rayadi, S. Sebti, *Catal. Commun.*, **8**, 225 (2007).

6.4 Reactions of Silicon Compounds

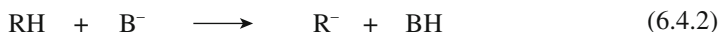
6.4.1 Substitution Reactions at Silicon

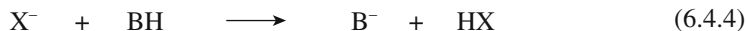
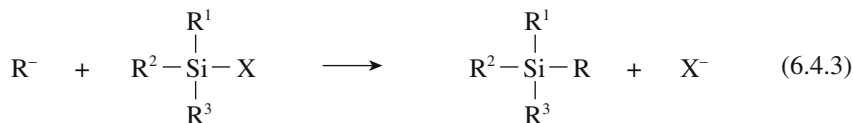
The reactions of carbanions with silanes are one of the most important methods for achieving Si-C bond forming synthetic sequences. The most common sources of 'carbanions' are alkyl lithium and Grignard reagents. These reactions can be expressed as follows.



In many cases, the leaving group X is a halide ion such as Cl⁻. The reactions are noncatalytic, organometallic compounds being required in stoichiometric quantities.

Carbanion can be generated from various sources by the action of bases, but this method has rarely been used for Si-C bond formation. The general scheme for the reaction over solid base catalysts is expressed by the following.





Here, B^- and X^- denote the basic sites of catalysts and the leaving group from the Si atom, respectively. The mechanism of the catalytic nucleophilic substitution has been described.¹⁾ In the following examples, the leaving groups are hydride or an alkynide ion. The above scheme offers novel catalytic routes for the synthesis of organosilicon compounds.

A. Metathesis of trimethylsilylacetylene

The reaction of trimethylsilylacetylene over various solid bases leads to the metathesis of the alkyne, the product being bis(trimethylsilyl)acetylene and acetylene.²⁾



As shown in Table 6.4.1, $\text{KF}/\text{Al}_2\text{O}_3$, $\text{KNH}_2/\text{Al}_2\text{O}_3$, MgO and $\text{CsOH}/\text{Al}_2\text{O}_3$ show high catalytic activities. The activity of $\text{KF}/\text{Al}_2\text{O}_3$ depends sharply on the pretreatment temperature under vacuum; the best performance was shown when the catalyst was pretreated at about 670 K. The reaction is very selective, no other products being formed. The yield is limited by the equilibrium. The partial removal of acetylene from the system during the reaction gave a higher yield of $\text{Me}_3\text{SiC}\equiv\text{CSiMe}_3$ (87%) over $\text{KF}/\text{Al}_2\text{O}_3$ at 273 K. Furthermore, the reaction of $\text{Me}_3\text{SiC}\equiv\text{CSiMe}_3$ with $\text{HC}\equiv\text{CH}$ gave $\text{Me}_3\text{SiC}\equiv\text{CH}$.

The plausible mechanism is as follows. The basic sites abstract a proton from $\text{Me}_3\text{SiC}\equiv\text{CH}$ to form the alkynide ion $\text{Me}_3\text{SiC}\equiv\text{C}^-$, which attacks at the silicon

Table 6.4.1 Catalytic activities of various solid base catalysts for the metathesis of $\text{Me}_3\text{SiC}\equiv\text{CH}$ [eq. (6.4.5)]^{a)}

Catalyst	Pretreatment	Alkaline compound supported on Al_2O_3 /mmol g-alumina ⁻¹	Yield of $\text{Me}_3\text{SiC}\equiv\text{CSiMe}_3$ ^{b)} /%
$\text{KF}/\text{Al}_2\text{O}_3$	673 K, 3 h	5	77
$\text{KNH}_2/\text{Al}_2\text{O}_3$	573 K, 1 h	2.6	76
MgO	773 K, 3 h		74
$\text{CsOH}/\text{Al}_2\text{O}_3$	673 K, 3 h	5	74
$\text{KOH}/\text{Al}_2\text{O}_3$	673 K, 3 h	5	64
$\text{K}_2\text{CO}_3/\text{Al}_2\text{O}_3$	673 K, 3 h	5	11
Cao	998 K, 3 h		2

^{a)} Reaction conditions: 293 K, 30 min, catalyst weight: 0.25 g, $\text{Me}_3\text{SiC}\equiv\text{CH}$: 13.5 mmol.

^{b)} The yields were calculated on the basis of $\text{Me}_3\text{SiC}\equiv\text{CH}$.

Reprinted with permission from T. Baba, A. Kato, H. Takahashi, F. Toriyama, H. Handa, Y. Ono, H. Sugisawa, *J. Catal.*, **176**, 488 (1998) p.490, Table 1.

atom of another molecule of the reactant. Here, the alkynide ion $\text{HC}\equiv\text{C}^-$ is a leaving group.

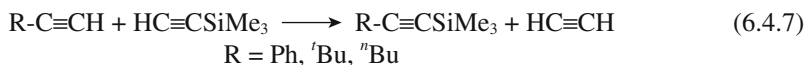
Metathesis of $\text{Et}_3\text{SiC}\equiv\text{CH}$ also proceeds to selectively afford $\text{Et}_3\text{SiC}\equiv\text{CSiEt}_3$. The yields of the product were 84% and 47% over $\text{KF}/\text{Al}_2\text{O}_3$ and $\text{KNH}_2/\text{Al}_2\text{O}_3$, respectively, at 333 K in 2 h.^{2,3)}



$\text{Me}_2(\text{EtO})\text{SiC}\equiv\text{CH}$ also undergoes metathesis. The yields of $\text{Me}_2(\text{EtO})\text{SiC}\equiv\text{CSi}(\text{OEt})\text{Me}_2$ were 77% and 61% in the presence of $\text{KNH}_2/\text{Al}_2\text{O}_3$ and $\text{KF}/\text{Al}_2\text{O}_3$, respectively.²⁾

B. Cross metathesis of alkynes

Alkynes react with trimethylsilylacetylene to give the metathesis products in the presence of solid base catalysts, as shown Table 6.4.2.^{2,3)}



$\text{KF}/\text{Al}_2\text{O}_3$ and $\text{K}_2\text{CO}_3/\text{Al}_2\text{O}_3$ are the most active to afford high yields of $\text{R-C}\equiv\text{CSiMe}_3$.

Table 6.4.2 Cross-metathesis of 1-alkyne with $\text{Me}_3\text{SiC}\equiv\text{CH}$ ^{a)}
 $\text{R-C}\equiv\text{CH} + \text{Me}_3\text{SiC}\equiv\text{CH} \longrightarrow \text{R-C}\equiv\text{SiMe}_3 + \text{HC}\equiv\text{CH}$

Reactant	Conc./mmol	Catalyst	Reaction temp./K	Yield of $\text{R-C}\equiv\text{SiMe}_3$ ^{b)} /%
$\text{Ph-C}\equiv\text{CH}$	9.0	$\text{KF}/\text{Al}_2\text{O}_3$	318	93
$\text{Ph-C}\equiv\text{CH}$	9.0	$\text{K}_2\text{CO}_3/\text{Al}_2\text{O}_3$	318	91
$\text{Ph-C}\equiv\text{CH}$	9.0	$\text{KNH}_2/\text{Al}_2\text{O}_3$	318	75
$\text{Ph-C}\equiv\text{CH}$ ^{c)}	4.5	$\text{KF}/\text{Al}_2\text{O}_3$	318	81
$t\text{-Bu-C}\equiv\text{CH}$	8.0	$\text{KF}/\text{Al}_2\text{O}_3$	303	91
$n\text{-Bu-C}\equiv\text{CH}$	8.7	$\text{KF}/\text{Al}_2\text{O}_3$	318	87

^{a)} Conditions: catalyst = 0.125 g, $\text{R-C}\equiv\text{CH}/\text{Me}_3\text{SiC}\equiv\text{CH} = 2 : 1$, reaction time = 2 h.

^{b)} The yield of $\text{R-C}\equiv\text{CSiMe}_3$ was calculated on the basis of $\text{Me}_3\text{SiC}\equiv\text{CH}$.

^{c)} $\text{R-C}\equiv\text{CH}/\text{Me}_3\text{SiC}\equiv\text{CH} = 1 : 1$.

Reprinted with permission from Y. Ono, in *Catalysis*, **Vol.15** p. 1, Royal Society of Chemistry (2000) p. 30, Table 1.7.

C. Reaction of trimethylsilylacetylene with amines

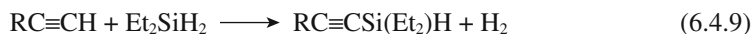
Solid base catalysts are effective in the Si-N bond formation by the reaction of amine with trimethylsilylacetylene.⁴⁾ Thus the reaction of aniline with trimethylsilylacetylene in the presence of MgO gives *N*-trimethylsilylaniline in a 92% yield in 20 h at 318 K. $\text{K}_2\text{CO}_3/\text{Al}_2\text{O}_3$, $\text{KNH}_2/\text{Al}_2\text{O}_3$ and $\text{KF}/\text{Al}_2\text{O}_3$ also show activities for this reaction.



The reaction of butylamine with trimethylsilylacetylene gives a 45% yield of the substitution product.

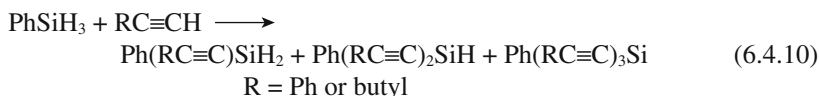
D. Dehydrogenative coupling of alkynes with silane

The dehydrogenative coupling of alkynes with diethylsilane proceeds in the presence of $\text{KNH}_2/\text{Al}_2\text{O}_3$ or $\text{KF}/\text{Al}_2\text{O}_3$.^{3,5)} In this case, the leaving group from the silane is a hydride ion.



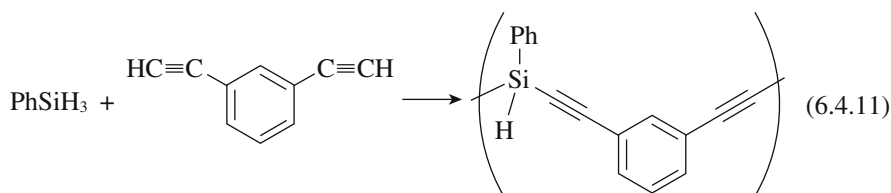
The reaction of 3,3-dimethyl-1-butyne (3.0 mmol) and Et_2SiH_2 (1.5 mmol) in hexane in the presence of $\text{KF}/\text{Al}_2\text{O}_3$ for 2 h afforded the corresponding coupling product $[\text{CH}_3\text{C}(\text{CH}_3)_2\text{C}\equiv\text{CSi}(\text{Et})_2\text{H}]$ in 83% yield (based on silane) at 303 K. Similarly, the reaction of 1-hexyne with Et_2SiH_2 afforded the $\text{C}_4\text{H}_9\text{-C}\equiv\text{CSi}(\text{Et})_2\text{H}$ at 293 K.

Phenylsilane reacts with alkynes to produce monoalkenylphenylsilane, dialkynylphenylsilane and trialkynylsilane with evolution of hydrogen gas in the presence of MgO .⁶⁾ No hydrosilylation products such as alkenylphenylsilanes are formed.



High initial activity was observed, but the activity decreased rapidly. The order of conversion of silanes was $\text{Ph}_2\text{SiH}_2 > \text{PhMeSiH}_2 > \text{PhSiH}_3$. The reaction of PhSiH_3 (5.3 mmol) and 1-hexyne (13.7 mmol) at room temperature gave a PhSiH_3 conversion of 93% to give a mixture of the three dehydrogenative coupling products, while the reaction of PhSiH_3 with phenylacetylene at 363 K gave a conversion of PhSiH_3 of 88%.

When *m*-diethynylbenzene is reacted with phenylsilane in the presence of MgO , polymerization proceeds.⁷⁾



The polymer is soluble in benzene and THF and shows very little weight loss in thermal treatment under argon. The high heat-resistance property of the polymer is attributed to a crosslinking reaction involving Si-H and $\text{C}\equiv\text{C}$ bonds.

E. Dehydrogenative coupling of alkenes with silane

$\text{KNH}_2/\text{Al}_2\text{O}_3$ catalyzes the reaction of 1-hexene with diethylsilane.³⁾

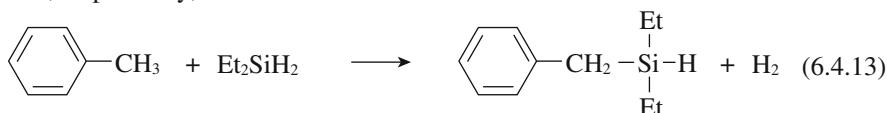


The reaction of 1-hexene (24 mmol) and Et_2SiH_2 (1.5 mmol) in the presence of $\text{KNH}_2/\text{Al}_2\text{O}_3$ (0.2 g) gave the coupling product in 22% yield (based on the

silane) in 20 h at 329 K. The ratio of *Z* : *E* in the product alkene was 77 : 23. The isomerization of 1-hexene also proceeded.

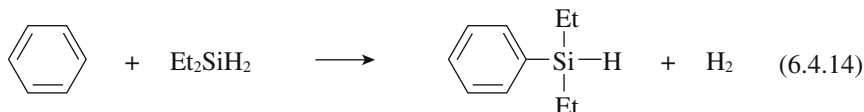
F. Dehydrogenative coupling of alkylbenzenes with silane

Because of strong basicity of $\text{KNH}_2/\text{Al}_2\text{O}_3$, the catalyst can activate toluene whose $\text{p}K_{\text{a}}$ value is 35. The reaction of diethylsilane with excess toluene in the presence of $\text{KNH}_2/\text{Al}_2\text{O}_3$ affords diethylbenzylsilane in 74% and 85% yields after 20 h and 40 h, respectively, at 329 K.⁸⁾



Other alkylbenzenes also react with diethylsilane in the presence of $\text{KNH}_2/\text{Al}_2\text{O}_3$ to selectively afford the corresponding benzylsilanes. The reactivity decreases in the order; toluene (74%) > ethylbenzene (23%) > propylbenzene (7.0%) > isopropylbenzene (2.0%), where the percentage in parentheses indicates the yields of the products. Alkylbenzenes with more acidic protons show higher reactivity towards Et_2SiH_2 , indicating that the abstraction of a proton from alkylbenzenes by basic sites on the solid base is the rate-determining step.

Benzene has a $\text{p}K_{\text{a}}$ value of 37, comparable to isopropylbenzene and is therefore expected to undergo a similar reaction. When Et_2SiH_2 (3.1 mmol) was reacted with excess benzene (68 mmol) in the presence of $\text{KNH}_2/\text{Al}_2\text{O}_3$, diethylphenylsilane was obtained in 7.5% yield in 20 h at 329 K.



G. Dehydrogenative silylation of alcohols

Baba et al. reported that the reaction of alcohols with diethylsilane proceeds in the presence of $\text{KF}/\text{Al}_2\text{O}_3$ at 329 K in tetrahydrofuran, as shown in Table 6.4.3.⁴⁾ Prior to the reaction, $\text{KF}/\text{Al}_2\text{O}_3$ was heated under vacuum at 673 K.



Table 6.4.3 Reaction of Et_2SiH_2 with alcohols with $\text{KF}/\text{Al}_2\text{O}_3$

Alcohol (ROH)	Yield of $\text{Et}_2\text{Si}(\text{OR})_2/\%$
$\text{CH}_3\text{CH}_2\text{CH}_2\text{OH}$	89
$\text{CH}_2=\text{CHCH}_2\text{OH}$	78
$\text{HC}\equiv\text{CCH}_2\text{OH}$	66

Reaction temperature : 329 K, reaction time 20 h.

Alcohol: 3 mmol, Et_2SiH_2 : 3 mmol, solvent: THF 2 mL.

Reprinted with permission from T. Baba, Y. Kawanami, H. Yuasa, S. Yoshida, *Catal. Lett.*, **91**, 31 (2003) p. 32, Table 1.

The reaction of Et_2SiH_2 with 1-propanol selectively afforded diethyldipropoxysilane in 89% yield in 20 h. Dehydrogenate silylation of allyl alcohol and 2-propyn-1-ol with Et_2SiH_2 gave diethyldi(2-propenyloxy)silane and diethyldi(2-propynyloxy)silane in 78% and 66% yields, respectively. 1,1,3,3-Tetraethyl-1,3-diprop-2-enyloxydisiloxane was formed as a by-product in the former case.

H. Disproportionation of alkoxysilanes

Silane, SiH_4 , is one of the most important chemicals in the semiconductor industry, since highly pure silicon is obtained by thermally decomposing SiH_4 . Disproportionation of chlorosilanes and alkoxysilanes can afford SiH_4 . The disproportionation of alkoxysilanes is usually performed using homogeneous base catalysts such as sodium ethoxide.

Suzuki et al. reported that as-synthesized hydrotalcite containing Cl^- or CH_3O^- in the interlayers is an effective catalyst for the disproportionation of trimethoxysilane.⁹⁾

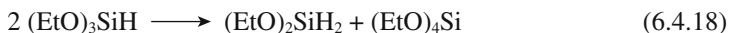


The hydrotalcite catalysts are dried at 453 K under vacuum for 2 h to remove water molecules in the interlayers. Using hydrotalcite with Cl^- , the conversion of trimethoxysilane reached 92% in 6 h at 323 K. The reaction can be performed in a fixed-bed continuous reactor. The reaction of trimethoxysilane over $\text{KF}/\text{Al}_2\text{O}_3$ gave 76% conversion at 393 K.¹⁰⁾ Only silane and tetramethoxysilanes were formed. Mixed oxides prepared from hydrotalcite were also active, but the activity was lower than that of $\text{KF}/\text{Al}_2\text{O}_3$.

Disproportionation of triethoxysilane in vapor phase also proceeds over $\text{KF}/\text{Al}_2\text{O}_3$ and $\text{MgO}-\text{Al}_2\text{O}_3$ mixed oxide (calcined hydrotalcite).¹¹⁾ In the reaction of triethoxysilane, a small amount of dialkoxysilane is also formed.



Selective formation of $(\text{EtO})_2\text{SiH}_2$ is possible using partially dehydrated calcium hydroxide.¹²⁾ Calcium hydroxide was dehydrated by treating $\text{Ca}(\text{OH})_2$ under an inert gas stream at 573 K. The catalyst has a main profile of $\text{Ca}(\text{OH})_2$ in the XRD pattern. The yields of $(\text{EtO})_4\text{Si}$ and $(\text{EtO})_2\text{SiH}_2$ are 6% and 5%, respectively, and the yield of SiH_4 is very small (0.3%) at 393 K. This shows that the reaction is practically expressed as follows.

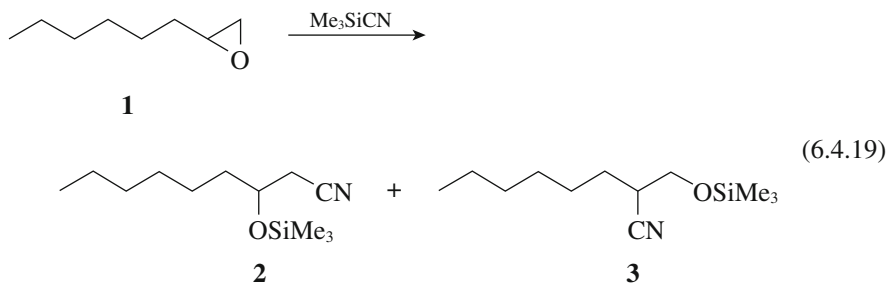


When the heating temperature is higher than 673 K, CaO is formed. In this case, SiH_4 and $(\text{EtO})_4\text{Si}$ are the main products with much higher $(\text{EtO})_3\text{SiH}$ conversion.

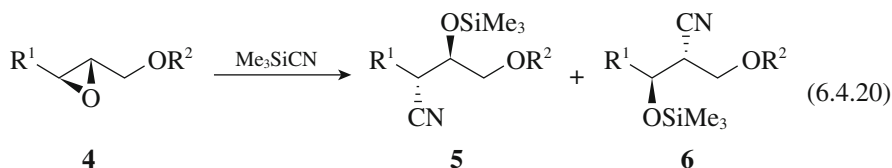
6.4.2 Ring Opening of Epoxides with Trimethylsilyl Cyanide

CaO and MgO are effective for nucleophilic ring opening of epoxides with Me_3SiCN (TMSCN).^{13,14)} Epoxides are quantitatively converted into β -trimethylsiloxynitriles by a highly regioselective attack of cyanide on the least

substituted carbon of epoxides. For example, the reaction of 1,2-epoxyoctane **1** with TMSiCN affords 3-(trimethylsilyloxy)nonanenitrile **2** in over 97% regioselectivity over CaO.



2,3-Epoxyhexan-1-ol ($R^1 = C_3H_7$, $R^2 = H$) reacts with TMSiCN to afford products **5** and **6** in good yields and good regioselectivity (**5** \gg **6**) in the presence of CaO. The regioselectivity is enhanced when 2,3-epoxy-1-ol is acetylated, as shown in Table 6.4.4.



Calcined hydrotalcite is also an efficient catalyst for ring opening of epoxides with TMSiCN.¹⁵⁾

Table 6.4.4 Reactions of *trans*-2,3-epoxy-1-alkanol and its derivative with MeSiCN

R^1	R^2	Temperature	Time/h	Yield/%	5 : 6
C_3H_7	H	room temp	4	86	89 : 11
C_3H_7	Ac	room temp	4	91	96 : 4
C_3H_7	Ac	333 K	1	75	96 : 4
Cyclohexyl	Ac	333 K	2	84	97 : 3

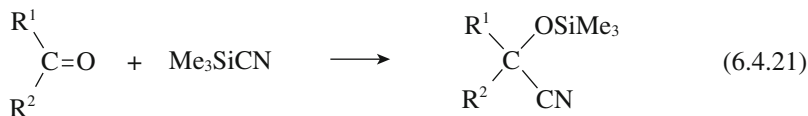
CaO(0.5 g), epoxides (0.5 mmol) and Me₃SiCN (1 mmol) in hexane.

Reprinted with permission from K. Sugita, A. Ohta, M. Onaka, Y. Izumi, *Bull. Chem. Soc. Jpn.*, **64**, 1792 (1991) p.1794, Table 3.

6.4.3 Addition of Silanes to Double Bonds

A. Cyanosilylation of carbonyl compounds

Nucleophilic addition of cyanotrimethylsilane (Me₃SiCN) to carbonyl compounds is useful in the synthesis of organic compounds such as cyanohydrins and β -aminoalcohols. The addition reactions are catalyzed by solid base catalysts.^{16,17)}



Active catalysts include CaF_2 , CaSiO_3 , hydroxyapatite, K_3PO_4 , CaO and MgO . These catalysts gave high yields in the cyanosilylation of benzaldehyde, heptanal, 2-octanone, acetophenone and benzophenone in CH_2Cl_2 at 273 K. In the case of the reaction of benzoquinone with Me_3SiCN , the mono-adduct is obtained exclusively.¹⁶⁾ In the cyanosilylation of α,β -unsaturated ketones such as cyclohexen-3-one and 4-methyl-3-penten-2-one in the presence of solid base catalysts gave 1,2-addition products in a highly regioselective manner. On the other hand, the use of solid acid catalysts such as Fe-montmorillonite selectively gives 1,4 adducts.

$\text{MgO-Al}_2\text{O}_3$ mixed oxides prepared by calcinations of hydrotalcite are also highly active for the cyanosilylation of aldehydes, ketones and enones with Me_3SiCN in hexane at room temperature.¹⁵⁾ As shown in Table 6.4.5, excellent yields of the products were obtained.

The high reactivity of Me_3SiCN in the presence of bases is ascribed to the strong affinities of the basic sites (e.g., oxide ions) to silicon, resulting in an increase in the coordination number of silicon from a normal value of 4 to 5 or 6 giving penta or hexa coordinate silicon compounds.^{15,16,19)} The penta and hexa coordinate silicon compounds have higher reactivities than the ordinary tetra-coordinate silicon compounds.¹⁾

Diamino-functionalized MCM-41 and *N*-octyldihydroimidazolium hydroxide anchored on silica is active for the cyanosilylation of a variety of carbonyl compounds.^{20,21)}

B. Reactions of aldimines and ketodimines with trimethylsilyl cyanide

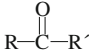
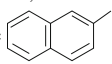
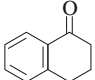
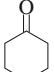
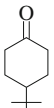
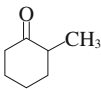
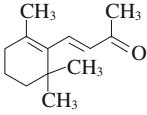
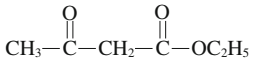
The reaction of various aldimines ($\text{R}^1 = \text{H}$) and ketodimines ($\text{R}^1, \text{R}^2 \neq \text{H}$) with trimethylsilyl cyanide (TMSCN) proceeds smoothly under mild conditions to give the corresponding α,α -disubstituted α -amino nitriles in the presence of nanocrystalline MgO ($590 \text{ m}^2 \text{ g}^{-1}$).²²⁾



Table 6.4.6 shows the results of the reactions of ketodimines with TMSCN in DMF. In every case, the corresponding α,α -disubstituted α -amino nitriles are produced in high yield. Since non-dried DMF was a better solvent than dried DMF, a small amount of moisture was suggested to be important to accelerate the reaction.

The authors suggest that the reaction proceeds through a hypervalent silicate species by coordination to O^{2-}/O^- (Lewis basic site) of MgO , proved by ^{29}Si NMR.

Table 6.4.5 Cyanosilylation of carbonyl compounds with Me₃SiCN using MgO-Al₂O₃

Entry	Substrate	Time/min	Yield/%
			
1.	R = Ph, R' = Me	5	97
2.	R = <i>p</i> -MeOC ₆ H ₄ , R' = Me	5	95
3.	R = <i>p</i> -MeC ₆ H ₄ , R' = Me	5	99
4.	R = Ph, R' = Ph	5	99
5.	R =  , R' = Me	5	97
6.	R = Me, R' = <i>n</i> -C ₆ H ₁₃	5	99
7.	R = Ph, R' = H	5	99
8.	R = <i>o</i> -NO ₂ C ₆ H ₄ , R' = H	5	90
9.	R = <i>o</i> -MeOCH ₂ C ₆ H ₄ , R' = H	5	98
10.	R = PhCH=CH, R' = H	60	90
11.	R = Ph, R' = PhCH=CH	120	92
12.		5	95
13.		5	99
14.		5	95
15.		5	94
16.		30	98
17.		300	90

Reaction conditions: carbonyl compound (4 mmol), trimethylsilyl cyanide (6 mmol), catalyst (200 mg), solvent; heptane, room temperature.

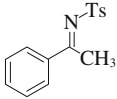
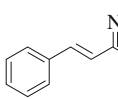
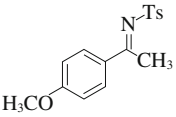
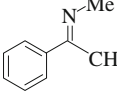
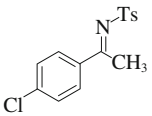
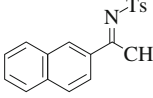
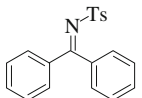
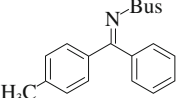
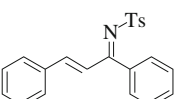
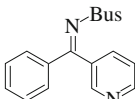
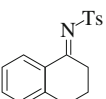
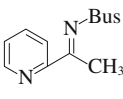
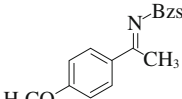
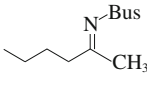
Reprinted with permission from B. M. Choudary, N. Narender, V. Bhuma, *Synth. Commun.*, **25**, 2829 (1995) p. 2832, Table 1.

Most of the products from aldimine and ketoimines can be directly subjected to acid hydrolysis to produce the corresponding amino acids.

C. Hydrosilylation of carbonyl compounds

Hydrosilylation of ketones, aldehydes and esters with triethoxysilane in the pres-

Table 6.4.6 Reaction of various aldimines with Me₃SiCN catalyzed by nanoporous MgO

Ketoimine	Time/min	Yield ^{b)} /%	Ketoimine	Time/min	Yield ^{b)} /%
	45	97		60	96
	60	97		40	95
	55	93		30	96
	45	92		45	91
	90	97		30	94
	60	94		30	96
	30	96		15	91

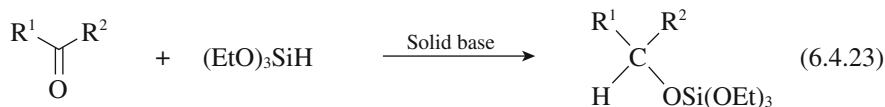
Ts = *p*-toluenesulfonyl, Bzs = benzenesulfonyl, Me = methanesulfonyl, Bus = *t*-butylsulfonyl.

^{a)} Reaction condition: ketoimine (1 mmol), (CH₃)₃SiCN (1.5 mmol), catalyat (0.05 g), DMF (3 mL) at room temperature.

^{b)} Isolated yield.

Reprinted with permission from M. L. Kantam K. Mahender, B. Sreedhar, B. M. Choudary, *Tetrahedron*, **64**, 3551 (2008) p. 3254, Table 4.

ence of hydroxyapatite was reported by Izumi and coworkers.^{19,23)}



The reactions were carried out in heptane at 363 K. The results are shown in Table 6.4.7. Silylation of enones such as cinnamaldehyde and benzylideneacetone afforded the corresponding 1,2-addition products selectively. CaO and MgO are

Table 6.4.7 Solid base-catalyzed hydrosilylation of various carbonyl compounds with silanes^{a)}

Run	Substrate	Solid base ^{b)}	Silane	Temp/°C (Time/h)	Yield/%
1	Heptanal	HAp (hydroxyapatite)	(EtO) ₃ SiH	90 (4)	81
2	Benzaldehyde	HAp	(EtO) ₃ SiH	90 (2)	72
3		CaO	(EtO) ₃ SiH	90 (1)	59
4		HAp	(EtO) ₃ SiH	90 (1)	93
5	2-Octanone	CaO	(EtO) ₃ SiH	90 (2)	71
6		HAp	(EtO) ₃ SiH	90 (1)	90
7		CaO	(EtO) ₃ SiH	90 (2)	61
8	Cyclohexanone	CaO	PhMe ₂ SiH	90 (8)	0 ^{c)}
9		CaO	Et ₃ SiH	90 (8)	0 ^{c)}
10		CaO	(EtO) ₃ SiH	90 (2)	24 ^{d)}
11	Acetophenone	CaO	(EtO) ₃ SiH	40 (2)	0 ^{e)}
12		HAp	(EtO) ₃ SiH	90 (5)	72
13		HAp	PhMe ₂ SiH	90 (20)	0
14		HAp	Et ₃ SiH	90 (23)	0
15		CaO	(EtO) ₃ SiH	90 (7)	70
16		Ca(OH) ₂	(EtO) ₃ SiH	90 (21)	0
17	Benzophene	CaF ₂	(EtO) ₃ SiH	90 (21)	0
18		HAp	(EtO) ₃ SiH	90 (1)	82 ^{f)}
19		CaO	(EtO) ₃ SiH	90 (1)	72 ^{f)}
20	Ethyl benzoate	HAp	(EtO) ₃ SiH	90 (20)	97 ^{g)}
21	Methyl hexanoate	HAp	(EtO) ₃ SiH	90 (24)	44 ^{g)}
22	Cinnamaldehyde	HAp	(EtO) ₃ SiH	90 (2)	70 ^{h)}
23	Benzylideneacetone	HAp	(EtO) ₃ SiH	90 (3)	94 ^{h)}

^{a)} Substrate (1 mmol) and silane (1.5 mmol) were mixed with a catalyst (0.5 g) in heptane (6 mL).

^{b)} HAp and CaF₂ were dried at 500°C and 0.5 Torr for 2 h. CaO was prepared from Ca(OH)₂ by calcination at 500°C and 0.5 Torr for 2 h. Ca(OH)₂ was an untreated sample.

^{c)} Condensation (aldol) reactions were observed.

^{d)} Toluene as solvent.

^{e)} CH₂Cl₂ as solvent.

^{f)} Obtained as an alcohol form.

^{g)} 3 mmol of (EtO)₃SiH was used.

^{h)} 1,2-Reduction product (100%).

Reprinted with permission from M. Onaka, K. Higuchi, H. Nanami, Y. Izumi, *Bull. Chem. Soc. Jpn.*, **66**, 2638 (1993) p. 2642, Table 5.

also active, but their activities are lower than that of hydroxyapatite. Ca(OH)₂, Mg(OH)₂, and CaF are totally inactive.

The reaction of aldehyde and ketones with alkylsilanes in the presence of a solid base catalyst proceeds to afford alkoxyasilanes, as shown in Table 6.4.8.^{4,24)} For example, the reaction of benzaldehyde with triethylsilane in DMF gives benzyltriethylsilane in high yield in the presence of KF/Al₂O₃, K₂CO₃/Al₂O₃, KNO₃/Al₂O₃ and KHCO₃/Al₂O₃.

Table 6.4.8 Alkoxysilanes synthesis through the reaction of alkylsilanes with aldehydes or ketones over solid base catalysts

Aldehyde or ketone	Silane	Catalyst	Reaction temperature/K	Reaction time/h	Yield of alkylsilane/%
PhCHO	Et ₃ SiH	KF/Al ₂ O ₃	303	1	>99
PhCHO	Et ₃ SiH	K ₂ CO ₃ /Al ₂ O ₃	303	1	99
PhCHO	Et ₃ SiH	KNO ₃ /Al ₂ O ₃	303	1	96
PhCHO	Et ₃ SiH	KHCO ₃ /Al ₂ O ₃	303	1	90
PhCHO	Et ₃ SiH	KNH ₂ /Al ₂ O ₃	303	1	60
PhCHO	Et ₃ SiH	MgO	303	20	37
PhCHO	Et ₃ SiH	CaO	303	20	7
PhCHO	Me ₂ PhSiH	KF/Al ₂ O ₃	303	1	97
PhCHO	(EtO) ₃ SiH	KF/Al ₂ O ₃	303	20	31
PhCOMe	Me ₂ PhSiH	KF/Al ₂ O ₃	353	1	74
<i>n</i> -C ₆ H ₁₃ COMe	Me ₂ PhSiH	KF/Al ₂ O ₃	353	1	32

Note: Catalyst: 0.25 g, supported amount of K in potassium, salt: 2.6 mmol g⁻¹, aldehyde or ketone: 2.5 mmol, silane: 2.5 mmol, solvent: DMF 2.5 mL.

Reprinted with permission from T. Baba, Y. Kawanami, H. Yuasa, S. Yoshida, *Catal. Lett.*, **91**, 31 (2003) p. 32, Table 2.

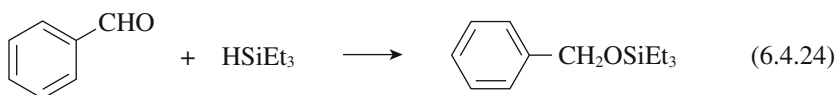
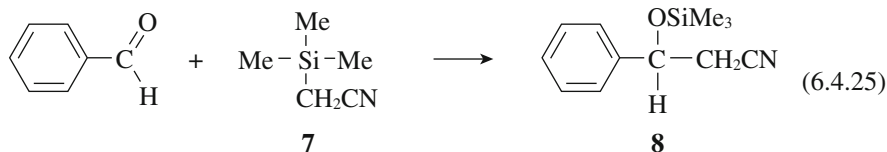


Table 6.4.8 also shows that the reaction of benzaldehyde with diethylphenylsilane gives diethylphenylbenzyloxysilane in 97% yield in the presence of KF/Al₂O₃. When the reaction was carried out in hexane or without solvent, the addition reaction did not proceed, and instead, the Tishchenko reaction of benzaldehyde occurred to give benzyl benzoate in high yields.

Hydroxyapatite and CaO are inactive for hydrosilylation of ketones with alkylsilanes (Table 6.4.7).^{19,23)}

D. Reaction of benzaldehyde with trimethylsilylacetonitrile

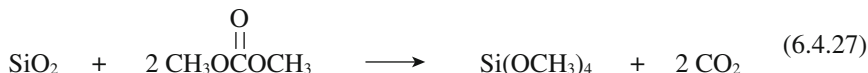
The reaction of benzaldehyde with trimethylsilylacetonitrile **7** in THF affords the addition product 3-phenyl-3-(trimethylsilyloxy)-propionitrile **8** in 81% yield.⁴⁾ Cinnamitrile **9** is also obtained as a by-product in 15% yield.



When $\text{KNH}_2/\text{Al}_2\text{O}_3$ is used as a catalyst, **9** is obtained as the sole product (49% yield), the *E/Z* ratio being 94/6.

6.4.4 Reaction of Silica with Dimethyl Carbonate

Silica is a very stable oxide and therefore the reactions with silica to afford useful chemicals are very limited. Ono and coworkers revealed that silica gel reacts with dimethyl carbonate (DMC) at 500–600 K to yield tetramethoxysilane with a catalyst supported on the reactant, silica.^{25,26)}



A typical experiment was carried out as follows. Silica gel was stirred in an aqueous solution of a catalytic material (e.g., KOH) and dried at 353 K in an evaporator. The silica loaded with the catalyst (131 mg) was packed in a fixed-bed flow reactor and heated to reaction temperature. DMC was fed with a flow rate of 43 mmol h^{-1} into a preheating zone of the reactor and the rate of formation of the product, $(\text{CH}_3\text{O})_4\text{Si}$, was monitored automatically every 3.5 min by a gas chromatograph.

Figure 6.4.1 (a) shows the change in the rate of $(\text{CH}_3\text{O})_4\text{Si}$ with reaction time at various temperatures. The catalyst was potassium hydroxide, the supported amount being 5 wt% of the reactant silica gel. In every case, the rate first increased rapidly and then decreased gradually to zero. The rapid increase of the rate at the beginning suggests that the interaction of the catalyst and silica occurs at the first stage of the reaction. Fig. 6.4.1 (b) shows the conversion of silica gel as calculated from the rate curve shown in Fig. 6.4.1 (a). It is clear that silica gel is completely converted into $(\text{CH}_3\text{O})_4\text{Si}$. The reaction is completed within 1 h at temperatures

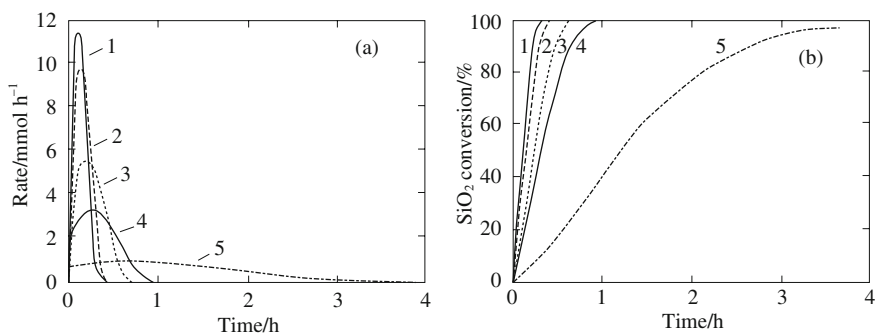


Fig. 6.4.1 Dependence of the rate of $(\text{MeO})_4\text{Si}$ formation and the conversion of silica gel on reaction temperature.

Reaction temperature: 600 K (1), 575 K (2), 550 K (3), 525 K (4) 500 K (5). DMC: 96 KPa, (43 mmol h^{-1}) .

(a) Rate of $(\text{MeO})_4\text{Si}$ formation, (b) SiO_2 conversion.

Reprinted with permission from Y. Ono, M. Akiyama, E. Suzuki, *Chem. Mater.*, **5**, 442 (1993) p. 443, Fig. 1.

higher than 525 K. Besides KOH, RbOH and CsOH were also useful. In the case of NaOH, the reaction was slower and required about 3 h to obtain complete conversion of the silica gel. Alkali halides are also effective as the catalyst. CsF was as active as CsOH. Even NaCl is active though the activity was much lower.

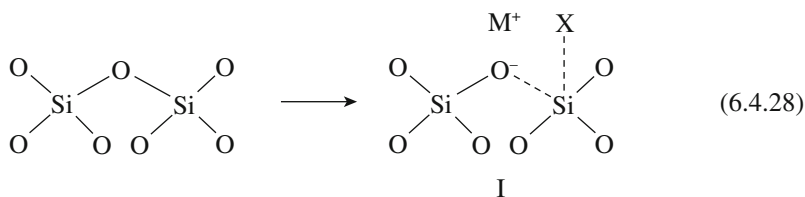
The reaction rate is greatly enhanced by heating the silica loaded with a catalyst at 775 or 1025 K prior to the reaction, indicating strong interaction between the silica and the alkali component.

Silica sources other than silica gel also react with DMC.²⁷⁾ A mesoporous silica, MCM-41, is as reactive as silica gel, indicating that the chemical properties of the mesoporous silica are close to those of amorphous silica. Mordenite (Si/Al = 110) and silicalite also react with DMC completely. However, zeolites with a low SiO₂/Al₂O₃ ratio react very slowly with DMC, indicating that Si-O-Si bonds are much more easily cleaved than Si-O-Al bonds.

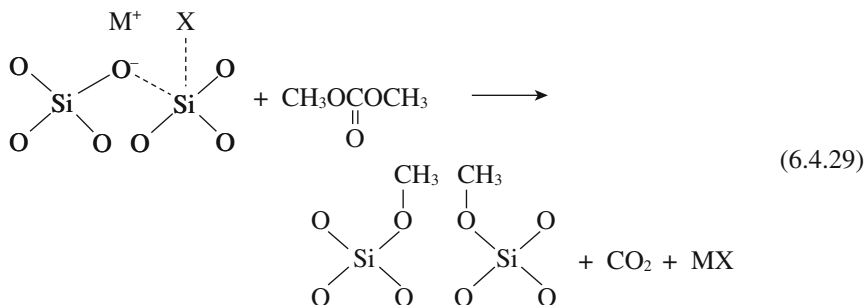
Rice hull ash obtained by burning rice hull is a highly silicic material, which is amorphous and highly reactive. Rice hull ash (SiO₂ content: 91.7%) loaded with KOH reacts with DMC.²⁸⁾ At 623 K, about 95% of the SiO₂ component reacted in 1 h. Thus most of the SiO₂ component in the ash can be extracted as (CH₃O)₄Si, other metal oxides components being left behind in the reactor. The reaction provides a convenient way to produce pure (CH₃O)₄Si from low-grade silica sources other than rice hull ash.

Silica gel also reacts with diethyl carbonate. In this case, sodium chloride was most effective as the catalyst.²⁶⁾ The complete conversion of silica gel into (C₂H₅O)₄Si was attained in 4 h at 700 K.

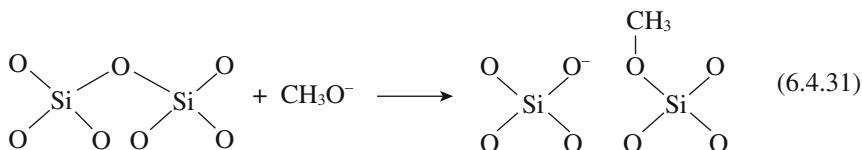
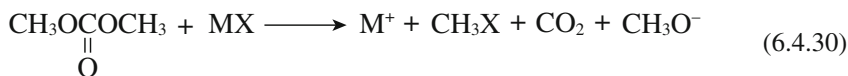
A plausible mechanism of the reaction of silica with DMC is as follows.²⁶⁾ The surface of silica may be activated in two ways. The activation occurs by a cleavage of the Si-O-Si bond by its interaction with a catalyst (MX).



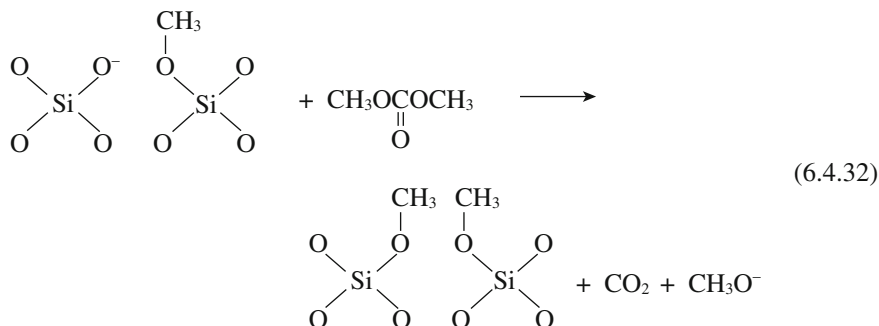
The surface species I may react with DMC to regenerate MX.



The activation may also occur through interaction with DMC. DMC may directly interact with the catalyst to form a reactive species (CH_3O^-), which in turn reacts with the Si-O-Si bond.



Once a reactive surface site containing SiO^- is formed by the reaction (6.4.31), this surface species directly reacts with DMC to afford Si-OCH₃ and cleavage of the Si-O-Si bond is completed.



Since reaction (6.4.32) regenerates CH_3O^- , the cleavage of Si-O-Si can continue by the repetition of reactions (6.4.31) and (6.4.32).

Once several layers are removed from the silica surface, the newly exposed surface may be more reactive than the original surface. Then the reaction can proceed simply by repetition of (6.4.31) and (6.4.32). This may explain the acceleration of the rate at the early stage.

Hydrous titanium dioxide ($\text{TiO}_2 \cdot n\text{H}_2\text{O}$, $n = 0.15\text{--}1.23$) loaded with NaOH reacts with dialkyl carbonates to give titanium tetraalkoxides, which are free from chlorine-containing impurities.²⁹⁾ Titanium tetraethoxide and titanium tetrapropoxide were obtained in high yields by the reaction at 473–573 K in an autoclave.

References

1. R. Corriu, *Pure Appl. Catal.*, **60**, 99 (1988).
2. T. Baba, A. Kato, H. Takahashi, F. Toriyama, H. Handa, Y. Ono, H. Sugisawa, *J. Catal.*, **176**, 488 (1988).
3. Y. Ono, T. Baba, in: *Catalysis*, Vol. 15, p.1, Royal Society of Chemistry (2000).
4. T. Baba, Y. Kawanami, H. Yuasa, S. Yoshida, *Catal. Lett.*, **91**, 31 (2003).

5. T. Baba, A. Kato, H. Yuasa, F. Toriyama, H. Handa, Y. Ono, *Catal. Today*, **44**, 271 (1998).
6. M. Itoh, M. Mitsuzuka, T. Utsumi, K. Iwata, K. Inoue, *J. Organometal. Chem.*, **476**, C30 (1994).
7. M. Itoh, M. Mitsuzuka, K. Iwata, K. Inoue, *Macromolecules*, **27**, 7917 (1994).
8. T. Baba, H. Yuasa, H. Honda, Y. Ono, *Catal. Lett.*, **50**, 83 (1998).
9. E. Suzuki, M. Okamoto, Y. Ono, *Chem. Lett.*, **18**, 1487 (1989).
10. E. Suzuki, Y. Nomoto, Y. Ono, *Catal. Lett.*, **43**, 155 (1997).
11. E. Suzuki, Y. Nomoto, M. Okamoto, Y. Ono, *Appl. Catal., A*, **167**, 7 (1998).
12. E. Suzuki, Y. Nomoto, M. Okamoto, Y. Ono, *Catal. Lett.*, **48**, 75 (1997).
13. K. Sugita, A. Ohta, M. Onaka, Y. Izumi, *Chem. Lett.*, **19**, 481 (1990).
14. K. Sugita, A. Ohta, M. Onaka, Y. Izumi, *Bull. Chem. Soc. Jpn.*, **64**, 1792 (1991).
15. B. M. Choudary, N. Narender, V. Bhuma, *Synth. Commun.*, **25**, 2829 (1995).
16. M. Onaka, K. Higuchi, K. Sugita, Y. Izumi, *Chem. Lett.*, **18**, 393 (1989).
17. K. Higuchi, M. Onaka, Y. Izumi, *J. Chem. Soc., Chem. Commun.*, **1991**, 1035.
18. K. Higuchi, M. Onaka, Y. Izumi, *Bull. Chem. Soc. Jpn.*, **66**, 2016 (1993).
19. Y. Izumi, H. Nanami, K. Higuchi, M. Onaka, *Tetrahedron Lett.*, **32**, 4741 (1993).
20. M. L. Kantam, F. Sreekanth, P. L. Santhi, *Green Chem.*, **2**, 47 (2000).
21. K. Yamaguchi, T. Imago, Y. Ogasawara, J. Kasai, M. Kotani, N. Mizuno, *Adv. Synth. Catal.*, **148**, 1516 (2000).
22. M. L. Kantam, K. Mahendar, B. Sreedhar, B. M. Choudary, *Tetrahedron*, **64**, 3351 (2008).
23. M. Onaka, K. Higuchi, H. Nanami, Y. Izumi, *Bull. Chem. Soc. Jpn.*, **66**, 2638 (1993).
24. Y. Kawakami, H. Yuasa, F. Toriyama, S. Yoshida, T. Baba, *Catal. Commun.*, **4**, 455 (2003).
25. E. Suzuki, M. Akiyama, Y. Ono, *J. Chem. Soc., Chem. Commun.*, **1992**, 136.
26. Y. Ono, M. Akiyama, E. Suzuki, *Chem. Mater.*, **5**, 442 (1993).
27. Y. Ono, *Appl. Catal., A*, **155**, 133 (1997).
28. M. Akiyama, E. Suzuki, Y. Ono, *Inorg. Chim. Acta*, **207**, 259 (1991).
29. E. Suzuki, S. Kusano, H. Hatayama, M. Okamoto, Y. Ono, *J. Mater. Chem.*, **7**, 2049 (1997).

6.5 Asymmetric Synthesis by Solid Base Catalysts

6.5.1 Asymmetric Synthesis by Metal Oxide in the Presence of Chiral Auxiliaries

Choudary and coworkers found that nanocrystalline MgO catalyzes the highly enantioselective reactions in the presence of an auxiliary chiral ligand.¹⁻⁴⁾ The catalytic activity and the ee of the products depend on the source of MgO, a chiral compound, temperature and solvent. Nanocrystalline MgO prepared by aero-sol method (NAP-MgO, ~ 600 m² g⁻¹) was found most effective with respect to both activity and enantioselectivity. The ee values are higher at lower temperatures.

Chiral nitroaldol reactions between substituted benzaldehyde and nitromethane proceed over NAP-MgO in the presence of (*S*)-(-)-1,1-bi-2-naphthol [*S*-BINOL].¹⁾ The results of the reactions of nitromethane with aromatic or aliphatic aldehydes are given in Table 6.5.1.

Chiral β -nitro- α -hydroxyesters with quaternary carbon centers are also obtained from α -ketoesters and nitromethane in the presence of NAP-MgO and *S*-BINOL.

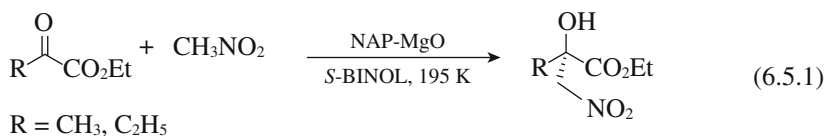
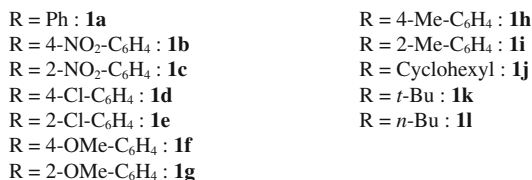
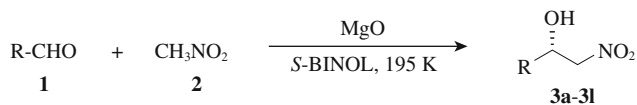


Table 6.5.1 Asymmetric Henry reaction catalyzed by MgO with substituted benzaldehyde and nitromethane at 195 K^{a)}

Entry	Substrate	Time/h	Product	Yield/% ^{b)}	ee/% ^{c)}
1	1a	12	3a	95	90
2	1b	18	3b	95	98
3	1c	15	3c	95	80
4	1d	16	3d	90	98
5	1e	15	3e	90	77
6	1f	20	3f	80	85
7	1g	20	3g	95	70
8	1h	15	3h	90	70
9	1i	15	3i	90	60
10	1j	18	3j	80	86
11	1k	18	3k	70	70
12	1l	15	3l	70	60

^{a)} Conditions: benzaldehyde (1.0 mmol), nitromethane (5.0 mmol), NAP-MgO (0.125 g), dry THF (5 mL), S-BINOL (0.040 g).

^{b)} Isolated yields.

^{c)} Absolute configurations were determined to be *S*.

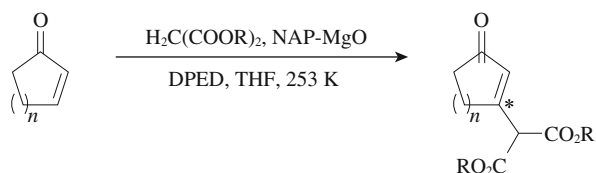
Reprinted with permission from B. M. Choudary, K. V. S. Ranganath, U. Pal, M. L. Kantam, B. Sreedhar, *J. Am. Chem. Soc.*, **127**, 13167 (2005) p. 13169, Table 5.

For asymmetric Michael addition between chalcones and nitromethane/2-nitropropane, (1*R*, 2*R*)-(–)-1,2-diaminocyclohexane in THF was most effective as the chiral auxiliary.¹⁾ For example, the reaction between chalcone and nitromethane at 253 K for 12 h gave 95% yield of the Michael adduct with an ee value of 96%. Absolute configuration was found to be *R*. For the asymmetric Michael addition between chalcone and malonates, (1*R*, 2*R*)-(+)-1,2-diphenylethylene diamine (DPED) was most effective.²⁾ An 82% ee was obtained at 93% yield in the reaction between chalcone and dimethyl malonate. DPED is also effective for Michael addition between cyclic enones with malonates as shown in Table 6.5.2.²⁾

For asymmetric aldol condensation between substituted benzaldehyde and acetone, (1*S*, 2*S*)-(+)-1,2-diaminocyclohexane was useful.³⁾ At 253 K ee values of 15–60% were obtained.

The high activity of the nanocrystalline MgO was ascribed to the high concentration of corners/edges. When the surface OH groups on MgO were silylated no

Table 6.5.2 Asymmetric Michael addition between cyclic enones and malonates catalyzed by nanoporous MgO in the presence of DPED



Entry	<i>n</i>	R	Time/h	Yield ^{a)} /%	ee ^{b)} /%
1	1	Me	12	94	84
2	1	Et	12	93	86
3	2	Me	16	95	90
4	2	Et	16	90	90
5	3	Me	24	96	94
6	3	Et	24	90	96

Reaction conditions: enone (1.0 mmol), malonate (5.0 mmol), NAP-MgO (1.25 g), dry THF (5 mL). In all cases 25 mol% of ligand was used.

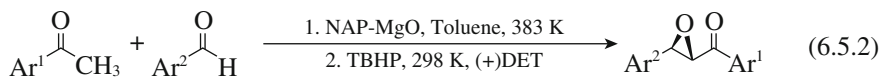
^{a)} Isolated yields.

^{b)} Ee was determined by HPLC analysis using a Chiralcel AS column (2-propanol-hexane (1 : 9), 0.5 mL/min, λ_{\max} = 210 nm).

Reprinted with permission from M. L. Kantam, K. V. S. Ranganath, K. Mahendar, L. Chakrapani, B. M. Choudary, *Tetrahedron Lett.*, **48**, 7646 (2007) p. 7648, Table 3.

ee was observed, indicating that the hydroxyl groups are involved in the development of the enantioselectivity.¹⁾

The synthesis of chiral epoxy ketones through a two-pot reaction of Claisen-Schmidt condensation and asymmetric epoxidation with *t*-butyl hydroperoxide (TBHP) has been reported.⁴⁾



Both reactions are catalyzed by MgO. Only nanocrystalline MgO showed high enantioselectivity for the epoxidation in the presence of (+)-diethyl tartarate (DET). The reaction of benzophenone and benzaldehyde gave the corresponding epoxide in 70% yield with an ee of 90%. 2-Furyl methyl ketone and 2-thienyl methyl ketone react with benzaldehyde to give the corresponding products in 70% and 68% yields with 84% and 68% ee, respectively.

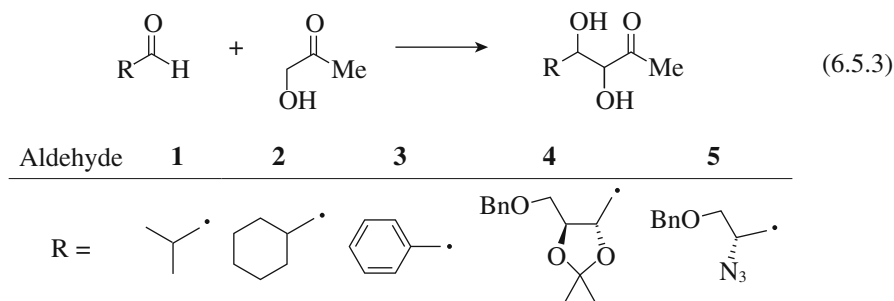
When L-proline is adsorbed on Al₂O₃ and used as a catalyst for aldol condensation of *p*-nitrobenzaldehyde and acetone, the configuration of the product switches from *R* (68% ee) for free L-proline product to the *S* configuration (21% ee).⁵⁾ The hydroxyl group on Al₂O₃ is supposed to be involved in the inversion of enantioselectivity. Actually, over silylated Al₂O₃ and α -Al₂O₃, the reaction gave 64% ee, rich in *R* configuration.

6.5.2 Asymmetric Synthesis by Supported Chiral Compounds

Heterogenized chiral amines have been tested for Michael addition reactions. Cinchonidine and chinchonine were grafted onto MCM-41 and tested for the Michael addition of ethyl 2-oxocyclopentanecarboxylate and methyl vinyl ketone.⁶⁾ Chinconidine grafted onto MCM-41 gave 80% yield of the addition product with ee of 47%. Chinconine grafted onto MCM-41 gave much lower enantioselectivity than the grafted chinconidine.

Several kinds of heterogenized chiral amines on silica, MCM-41 and ITQ-2 were prepared and tested in the Michael addition of ethyl 2-oxocycloalkane-carboxylate to acrolein.⁷⁾ The heterogenized amines presented higher rates than reference homogeneous counterparts. However, enantioselectivity was low to moderate (5-60%), depending on the support.

Asymmetric aldol reaction between hydroxyacetone and different aldehydes using L-proline immobilized on MCM-41 by post-grafting method (MCM-Pro) was reported by Calderón et al.⁸⁾



The condensations with different aldehydes proceeded in the presence of L-proline and L-proline tethered to MCM-41 (MCM-Pro) at room temperature and at 363 K, respectively. While the proline-catalyzed reactions require highly polar solvents, the reactions with heterogenized catalysts proceed also in non-polar solvents. The stereoselectivity depends on the reactions as well as the catalyst. For aldehydes **1** and **2** both L-proline and MCM41-Pro gave the very high diastereo- and enantioselectivity, the *anti*-(1*S*,2*S*)-diol being the main product. However, aldehydes **3–5** afforded different stereoselectivities depending on the catalyst. Benzaldehyde **3** in the presence of L-proline gave *anti*-(1*S*,2*S*)-diol in a 2.5 : 1 *anti/syn* ratio. On the other hand, with MCM41-Pro a mixture was obtained in which the *syn*-(1*S*, 2*S*)-diol slightly predominated. In the case of L-threonine derivative **4**, the diastereoselectivity of the reaction reversed upon changing from L-proline to MCM-Pro. For azide aldehyde **5**, MCM-Pro gave poor results. The reaction time was significantly shortened by microwave irradiation. Furthermore, yields were improved with most of the aldehydes. The results under microwave irradiation are listed in Table 6.5.3 where the results with proline-catalyst are also cited.

Table 6.5.3 Asymmetric aldol reaction [eq. (6.5.3)] catalyzed by L-proline and L-proline tethered to MCM-41 in DMSO under microwave heating

Aldehyde	Catalyst ^{a)}	Time/min	Yield/%	d.r. ^{b)}	ee/% ^{c)}
1	A	10	60	>20 : 1	>99
1	B	10	60	>20 : 1	>99
2	A	10	90	>20 : 1	>99
2	B	10	90	>20 : 1	>99
3	A	10	65	2.2 : 1	75
3	B	30	70	1 : 1.4	80
4	A	10	60	2.1 : 1	—
4	B	25	60	1 : 1.6	—
5	A	10	65	3 : 1	—
5	B	15	55	1 : 1.3	—

^{a)} A = L-proline; B = MCM41-Pro (0.52 mmol g⁻¹).

^{b)} d.r. = *anti/syn*. The ratio was determined by ¹H NMR or GC.

^{c)} The ee values were determined by chiral phase GC. All values are referred to the major diastereomer.

Reprinted with permission from F. Calderón, R. Fernández, F. Sánchez, A. Fernández-Mayoralas, *Adv. Synth. Catal.*, **347**, 1395 (2005) p. 1397, Table 4.

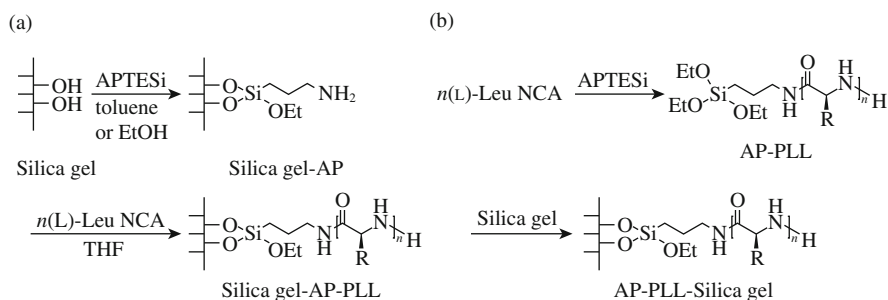
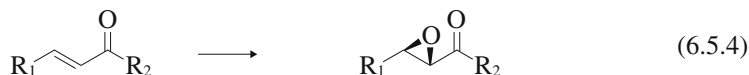


Fig. 6.5.1 Preparation scheme for Silica gel-AP-PLL (a) and AP-PLL-Silica gel (b).

Reprinted with permission from F. Yang, L.-M. He, G. Zou, J. Tang, M.-Y. He, *J. Mol. Catal., A*, **273**, 1 (2007) p. 2, Figs. 1 and 2.

Asymmetric epoxidation of α, β -unsaturated ketones (the Juliá-Colonna reaction) was attempted using silica-grafted poly-(L)-leucine (PLL).^{9,10)}



Grafting of poly-(L)-leucine to silica was achieved by two different methods, as shown in Fig 6.5.1. In the first method [Fig. 6.5.1(a)], silica was functionalized through the treatment with (3-aminopropyl)triethoxysilane (APTESi), and then the polymerization of (L)-leucine *N*-carboxyanhydride (NCA) was conducted using the functionalized silica as initiator to give the silica-grafted poly-(L)-leucine catalyst, Silica-AP-PLL. In the second method [Fig. 6.5.1 (b)], first, the polymerization of L-leucine NCA was initiated by APTPSi which led to the formation of AP-

PLL, then the AP-PLL was covalently grafted on silica gel surface by the reaction of the surface OH group with the terminal $(\text{EtO})_3\text{Si}$ group to give the catalyst AP-PLL-Silica gel. The degree of polymerization, n , can be varied.

In the epoxidation of benzalacetophenone (1.0 mmol) with sodium percarbonate ($\text{Na}_2\text{CO}_3 \cdot 3/2 \text{H}_2\text{O}_2$, 1.6 mmol), the reactants and 0.1 mmol of catalyst were stirred for 4 h in dimethyl ether (5 mL) and water (5 mL) at room temperature.¹⁰⁾ The yield and ee were 92% and 91%, respectively, for Silica gel-AP-PLL, while they were 91% and 95%, respectively, for AP-PLL-Silica gel. Furthermore, in the case of Silica gel-AP-PLL catalyst both activity and enantioselectivity gradually decreased by repeated use. On the other hand, the AP-PLL-Silica gel catalyst can be regenerated; the catalytic activity and enantioselectivity were not notably decreased after recycling six times.

Choudary et al. incorporated chiral organic molecules, viz., L-proline and S-BINOL into hydrotalcite by anion exchange or direct synthesis method.¹¹⁾ The catalysts were employed as catalysts for aldol condensation and Michael addition reactions. The products were obtained with good to excellent yields, but their ee values were low.

L-Proline anion can be intercalated into hydrotalcite by using the memory effect and used for the asymmetric aldol condensation¹²⁾ and Michael addition.¹³⁾ For aldol condensation of benzaldehyde and acetone, L-proline-loaded hydrotalcite gave a good yield (90%) and high enantiometric excess (94%).¹²⁾ An inversion in the asymmetric induction was observed in the case of Michael addition reactions such as addition of acetone to β -nitrostyrenes and addition of nitromethane to benzylideneacetone or cyclic enones. In the Michael addition of nitromethane to 2-cyclohexen-1-one, an ee. value of 61% was achieved at 100% conversion. It was suggested that hydrotalcite acts as a cocatalyst in the asymmetric reactions.¹³⁾

L-Prolinamide functionalized mesoporous silicas exhibit high enantioselectivity (91%) in asymmetric aldol reaction of cyclohexanone with 4-nitrobenzaldehyde¹⁴⁾ The L-prolinamide functionalized mesoporous silicas were prepared either by a co-condensation method or grafting method.

Enantiometrically enriched α -fluorotropinone immobilized on mesoporous MCM-41 and amorphous silica gel promotes the stereochemical epoxidation of several *trans*-substituted and trisubstituted alkenes such as 1-phenylcyclohexene with Oxone ($2\text{KHSO}_3 \cdot \text{KHSO}_4 \cdot \text{K}_2\text{SO}_4$) with ee values of up to 80%.¹⁵⁾ The catalyst is perfectly reusable with the same performance for at least three catalytic cycles.

Immobilization of (1*R*, 2*S*)-(-)-ephedrine on the surface of MCM-41-type aluminosilicate leads to chiral auxiliaries for enantioselective addition of diethylzinc to benzaldehyde.¹⁶⁾ The rate and ee (64%) are close to those obtained in homogeneous catalysis. This reaction was also studied using SBA-15 functionalized with proline derivatives.¹⁷⁾ The catalyst is very active and selective to form (*S*)-1-phenylpropanol with ca. 66% ee.

Many more examples of supported chiral organic catalysts are found in a recent review.¹⁸⁾

6.5.3 Asymmetric Synthesis by Chiral Zeotype Materials

The chiral germanium zeotype material $\text{Ge}_9\text{O}_{19}(\text{OH})_2(\text{N}_2\text{C}_4\text{H}_{10})_2(\text{N}_2\text{C}_2\text{H}_8)0.5\text{H}_2\text{O}$, ICM6 was synthesized.¹⁹⁾ Three kinds of interconnected helical 8-, 11-, and 11-ring channels are present in the 3D framework. The material was found to be an active chiral catalyst for the Michael addition and acetalization of aldehydes.

In the case of the Michael addition between benzenethiol and 5-methoxy-2,5(*H*)-furanone with a molar ratio of 1, the conversion was 100% in 1.2 h with enantiometric excess of 30%.

References

1. B. M. Choudary, K. V. S. Ranganath, U. Pal, M. L. Kantam, B. Sreedhar, *J. Am. Chem. Soc.*, **127**, 13167 (2005).
2. M. L. Kantam, K. V. S. Ranganath, K. Mahendar, L. Chakrapani, B. M. Choudary, *Tetrahedron Lett.*, **48**, 7646 (2007).
3. B. M. Choudary, L. Chakrapani, T. Ramani, K. V. Kumar, M. L. Kantam, *Tetrahedron*, **62**, 9571 (2006).
4. B. M. Choudary, M. L. Kantam, V. S. Ranganath, K. Mahendar, B. Sreedhar, *J. Am. Chem. Soc.*, **126**, 3396 (2004).
5. L. Zhong, J. Xiao, C. Li, *J. Catal.*, **243**, 442 (2006).
6. A. Corma, S. Iborra, I. Rodriguez, M. Iglesia, F. Sánchez, *Catal. Lett.*, **82**, 237 (2002).
7. A. Fuerte, A. Corma, F. Sánchez, *Catal. Today*, **107/108**, 404 (2005).
8. F. Calderón, R. Fernández, F. Sánchez, A. Fernández-Mayoralas, *Adv. Synth. Catal.*, **347**, 1395 (2005).
9. H. Yi, G. Zou, Q. Li, Q. Chen, J. Tang, M. -Y. He, *Tetrahedron Lett.*, **46**, 5665 (2005).
10. F. Yang, L. -M. He, H. Yi, G. Zou, J. Tang, M. -Y. He, *J. Mol. Catal.*, **273**, 1 (2007).
11. B. M. Choudary, B. Kavita, N. S. Chowdari, B. Sreedhar, M. L. Kantam, *Catal. Lett.*, **78**, 373 (2002).
12. Z. An, W. Zhang, H. Shi, J. He, *J. Catal.*, **241**, 319 (2006).
13. S. Vijakumar, A. Dhakshinamoorthy, K. Pitchumani, *Appl. Catal., A*, **340**, 25 (2008).
14. J. Gao, J. Lin, D. Jjiang, B. Xiao, Q. Yang, *J. Mol. Catal., A*, **313**, 79 (2009).
15. G. Sartori, A. Armstrong, R. Maggi, A. Mazzacani, R. Sartorio, F. Bigi, B. Dominguez-Fernandez, *J. Org. Chem.*, **68**, 3232 (2003).
16. S. Abramson, M. Laspéras, A. Galarneau, D. Desplandier-Giscard, D. Brunell, *Chem. Commun.*, **2000**, 1773.
17. L. -H. Hsiao, S. -Y. Chen, S. -J. Huang, S. -B. Liu, P. -H. Chen, J. C. -C. Chan, S. Chen, *Appl. Catal. A*, **159**, 96 (2009).
18. M. Benaglia, *New J. Chem.*, **30**, 1525 (2006).
19. M. E. Medina, M. Iglesias, N. Snejko, E. Gutiérrez-Puebla, M. A. Monge, *Chem. Mater.*, **16**, 594 (2004).

6.6 Solid Bases as Catalyst Support

6.6.1 Enhancing Effect of Solid Bases on Metal Catalysts

A. Ammonia synthesis over Ru catalyst

Ruthenium catalysts are known to be most active for nitrogen activation or ammonia synthesis. The activity is remarkably increased with the addition of alkali metal promoters.

Aika et al. studied the effect of the support on the ammonia synthesis by Ru

Table 6.6.1 Support effect in ammonia synthesis over 2 wt% Ru catalysts under 80 kPa of (N₂ + 3H₂) at 673 K

Support	Rate/ $\mu\text{mol NH}_3 \text{ h}^{-1} \text{ g}^{-1}$
MgO (16 m ² g ⁻¹)	379
MgO (90 m ² g ⁻¹)	364
CaO	176
Al ₂ O ₃	62
TiO ₂	5
Nb ₂ O ₅	7

Supports were heated at 773 K and impregnated with Ru₃(CO)₁₂.

All Catalysts were treated with hydrogen at 673 K for 4 h before reaction.

Reprinted with permission from K. Aika, T. Takano, S. Murata, *J. Catal.*, **136**, 126 (1992) p.128, Table 1.

catalysts.^{1,2)} Table 6.6.1 shows the turnover frequency (TOF) of NH₃ synthesis over various supported Ru catalysts.¹⁾ Ru supported on alkaline earth oxides showed much higher TOF than Ru supported on Al₂O₃ or TiO₂. XPS study showed that Ru receives an electron from the alkaline earth oxide. The TOF of Ru catalysts are further promoted by the loading of alkaline compounds such as CsOH. It was concluded that the N₂ dissociation, which is the rate-determining step of NH₃ synthesis, is promoted by electron donation from the support or promoter to Ru. The rate of ¹⁴N₂-¹⁵N₂ exchange also follows the order Ru-Cs/MgO > Ru/MgO > Ru/Al₂O₃.³⁾

Effects of the supports and promoters are also evidenced by infrared spectra of adsorbed nitrogen.⁴⁾ Infrared absorption due to side-on adsorption of nitrogen on Ru metals supported on Al₂O₃ and MgO is observed at 2214 cm⁻¹ and 2158 cm⁻¹, respectively. Upon Cs doping, the bands further shift to a lower frequency such as 2095 cm⁻¹ for Ru-Cs/Al₂O₃ and 1910 cm⁻¹ for Ru-Cs/MgO. The wavenumber reflects the N-N bond strength. The catalysts with a lower wavenumber (electron-rich Ru surface) are more active catalysts.

Ammonia synthesis has also been studied with Ru supported on zeolites. A series of alkali cation-exchanged X and Y zeolites are found to be active for NH₃ synthesis at temperatures between 573 and 723 K.⁵⁾ Ru supported on KX was more active than Ru on NaX and KY, indicating the importance of the basicity of the zeolite framework. A Ru supported on HY was the least active. In this work, CsX was less active than KX. This was ascribed to the low content of Cs ions and the presence of remaining protons.

Fishel et al. also studied the catalytic activities of Ru supported on zeolites for NH₃ synthesis.^{6,7)} In this work, Ru/CsX was more active than Ru/KX, probably because of higher exchange degree with Cs⁺. The activity of Ru/CsX was similar to that of Ru/MgO. They also found that the activities of Ru supported on alkaline earth cation-exchanged zeolites (BaX, CaX) were far greater than that of CsX, though the reason for the higher activities was not fully clarified.

B. Reactions of hydrocarbons over transition metals supported on zeolites

Pt supported on alkali cation-exchanged L zeolites exhibits high activity and selectivity for conversion of hexane to benzene. The remarkable catalytic performance of L zeolite for aromatization has been proposed to be related to the effect of cations on the Pt electronic state, to the structural geometry of the zeolite pores, or to the metal cluster size.

The conversion and selectivity for benzene over Pt supported L zeolites at 773 K increase in the order $\text{LiL} < \text{NaL} < \text{RhL} < \text{CsL}$.⁸⁾ The activity for benzene hydrogenation at 383 K changes in the same order. These orders suggest the strong influence of the basicity of zeolites on the catalytic activity of Pt particles in zeolites. Davis and Derouane reported that the activity and selectivity over $\text{MgO-Al}_2\text{O}_3$ mixed oxide ($\text{Mg/Al} = 5$) in the conversion of hexane were comparable to those over KL zeolites and claimed that the high aromatization selectivity of L zeolites could not be ascribed to the geometry of zeolite pores and stressed the importance of the basic nature of the supports in the aromatization.^{9,10)}

The effect of metal cations on the conversion of hexane over Pt supported on alkali cation-exchanged beta zeolites was studied.^{11,12)} While the selectivity for aromatics was 30–45% on $\text{Pt/Cs}\beta$, it was only 10 to 12% over $\text{Pt/K}\beta$ and less than 8% over $\text{Pt/Rb}\beta$ and $\text{Pt/Na}\beta$. In contrast, $\text{Pt/K}\beta$, $\text{Pt/Rb}\beta$ and $\text{Pt/Na}\beta$ strongly favor hexane isomerization to 2- and 3-methylpentane.

Besoukhanova et al. observed the infrared band at 2060–2065 cm^{-1} of linearly adsorbed CO in addition to ordinary linear and bridged adsorption of CO on Pt/K-L and suggested the electron enrichment of Pt particles.⁸⁾ A similar observation was also reported in several cases. Besides ordinary linear and bridged adsorption, the third band appeared at 1970 cm^{-1} and at 1965 cm^{-1} on NaX and $\text{Pt/MgO-Al}_2\text{O}_3$ ($\text{Mg/Al} = 5$) respectively.¹³⁻¹⁵⁾ These bands were assigned to linear adsorption of CO on Pt sites strongly interacting with the basic sites. The bands was observed at 1930 cm^{-1} for $\text{Pt/MgO-Al}_2\text{O}_3$ ($\text{Mg/Al} = 3$)¹⁶⁾ and 1985 cm^{-1} on $\text{Pt/Cs}\beta$.¹²⁾ The negative shift was also observed for $\text{Pd/MgO-Al}_2\text{O}_3$.¹⁷⁾

Lane et al. also observed the third band for Pt/KL , Pt/K-MFI , Pt/K-SiO_2 , Pd/KL and Pd/BaL .¹⁸⁾ The authors, however, attributed this band to linearly adsorbed CO, the O atom of which interacts with alkali cations.

ETS-10, a microporous titanosilicate, has basic property. Pt supported on ETS-10 [$\text{Na/K} = 3.4$] also shows high selectivity for the dehydrocyclization of hexane to benzene.¹⁹⁾ Both conversion of hexane and selectivity for benzene over Pt supported on alkali cation-exchanged ETS-10 at 773 K increase in the order $\text{Li} < \text{Na} < \text{K} < \text{Rb} < \text{Cs}$.²⁰⁾ The benzene yield increases from 1.3% for Pt/Li-ETS-10 to 39.5% for Pt/Cs-ETS-10 . Ba-ETS-10 shows basic property comparable to Cs-ETS-10 as observed by TPD of CO_2 and XPS of oxygen ions, and Pt/Ba-ETS-10 shows higher activity and selectivity than Pt/Cs-ETS-10 . The benzene yield was 52.1% with conversion of 85.9%.

Hydrogenation of benzene over Pt supported on Y zeolites is also greatly influenced by the counter cations.²¹⁾ The turnover frequency decreases and the apparent activation energy increases as the zeolite basicity increases. The wave-

number of adsorbed CO molecules also changes in parallel with the catalytic activity. These facts are explained in terms of an electron transfer from the basic zeolite framework to the Pt particles.

The conversion of methylcyclopentane over Pd supported on alkali cation-exchanged Y zeolites was studied by Bai and Sachtler.²²⁾ Methylcyclopentane undergoes three types of reactions: ring opening to hexane and methypentanes, ring enlargement to cyclohexane and benzene, and cracking. The rates of ring opening decrease in the order Pd/KY > Pd/NaY > Pd/LiY, while the rates of ring enlargement display the opposite sequence, i.e., Pd/LiY > Pd/NaY > Pd/KY. The decrease in ring enlargement with zeolite basicity was ascribed to the weakening of the acidic strength of protons by the presence of alkali metals, while the enhancement of the ring opening with zeolite basicity was attributed to the electron donation to small Pd clusters.

X-ray photoelectron spectroscopy of Pt supported on H β , Na β and Cs β showed that the platinum binding energy decreases when the basicity increases, indicating an electronic shift from zeolite to Pt particles.²³⁾

Mojet et al. prepared Pt and Pd supported on L zeolites of different K content and studied neopentane hydrogenolysis.²⁴⁾ The catalytic activity for the hydrogenolysis drastically increased with increasing K content. They explained the results of IR, XPS and XANES shape resonance by the change in energy of the metal ionization potential, which is caused by a Coulomb attraction between the metal particle and support oxygen ions. This model excludes the need for electron transfer.

The acid-base properties of the support show a profound effect on the combustion of C₃H₆ and C₃H₈ over Pt and Pd metals which are supported on γ -Al₂O₃ and ZrO₂.²⁵⁾ The acid-base properties of the supports were modified by impregnation of the supports with aqueous solutions of NaOH or H₂SO₄. Table 6.6.2 shows the light-off temperature of Pt catalysts for oxidation of C₃H₆ and C₃H₈. For C₃H₆, basic supports gave lower light-off temperatures (higher activity), while for C₃H₈, acidic supports gave lower light-off temperatures. In the case of C₃H₆, adsorption of C₃H₆ is stronger on more acidic supports and the rate is decreased by the self-

Table 6.6.2 Light-off temperatures of Pt catalysts for C₃H₆ and C₃H₈ oxidation

Catalysts	Light-off temperature/K	
	C ₃ H ₆	C ₃ H ₈
Pt/H ₂ SO ₄ /ZrO ₂	533	458
Pt/ZrO ₂	518	528
Pt/NaOH/ZrO ₂	463	>773
Pt/H ₂ SO ₄ /Al ₂ O ₃	528	483
Pt/Al ₂ O ₃	493	538
Pt/NaOH/Al ₂ O ₃	453	>773

Reprinted with permission from H.-C. Wu, L. -C. Liu, S. -M. Yang, *Appl. Catal.*, **211**, 159 (2001) p. 163, Table 5.

inhibition effect of C_3H_6 . On the other hand, in the oxidation of C_3H_8 , adsorption of the substrate is the rate-determining step, and the adsorption is facilitated by electron density on the Pt metal surface. This causes the higher activity of Pt metal on the more basic supports. Pd supported on Al_2O_3 and ZrO_2 showed a similar trend.

6.6.2 Bifunctional Catalysis

A. Methyl isobutyl ketone synthesis from acetone

Methyl isobutyl ketone (MIBK) is mainly used as a solvent for inks and resins, and is an important reagent in dewaxing mineral oils. MIBK is produced commercially in three steps from acetone: liquid phase aldol addition of acetone to diacetone alcohol (DAA), acid catalyzed dehydration to DAA to mesityl oxide (MO) and selective hydrogenation of MO to MIBK. A problem associated with this three-step method is the unfavorable thermodynamic equilibrium of the first addition step.

A one step process operating at 373–433 K and 10–100 atm has been developed employing bifunctional catalysts such as Pd or Pt supported on metal oxides, cation exchange resins and zirconium phosphate.²⁶⁻²⁹⁾ For example, an MIBK selectivity of 82% with acetone conversion of 38% was obtained by the reaction over Pd/MgO- Al_2O_3 mixed oxide under 400 psig at 391 K for 5 h.²⁶⁾ Although very high selectivity to MIBK (>90%) with acetone conversion (~40%) was attained, the high pressure system and its complicated operation are disadvantages.

Extensive work on low-pressure one-step synthesis of MIBK has been reported. The catalysts used are metals supported on solid bases. The reaction was performed in a flow reactor operating at ordinary pressure. Table 6.6.3 lists the recent reports on one-step synthesis of MIBK.

The reaction scheme for the synthesis of MIBK by bifunctional catalysts is shown in Fig. 6.6.1.⁴²⁾ Acetone undergoes self-condensation over basic sites to give DAA. Dehydration of DAA yields MO, which in turn can be selectively hydrogenated over metal sites to finally give MIBK. The balance of basicity and hydrogenation activity is most important. By-products depend on the balance of basicity/hydrogenation activity, the nature of the metals used and reaction conditions, such as H_2 /acetone ratio. In the case of Pd/Na/MgO, the main by-product was diisobutyl ketone (DIBK) which was formed by further condensation of MIBK with acetone.²⁹⁾ In the case of Ni/MgO, the high hydrogenation activity of Ni for C=O hydrogenation results in direct hydrogenation of acetone to 2-propanol. The other by-products are MO and methylisobutylcarbinol (MIBC). Mesitylene and isophorone are also observed in minor amounts. To avoid excess formation of 2-propanol and MIBC, the hydrogenation catalysts must be more selective for C=C bond hydrogenation than for C=O bond hydrogenation.

Acetone is obtained by dehydrogenation of 2-propanol. One-step synthesis of MIBK from 2-propanol was explored.^{41,42)} The catalyst was Cu on MgO- Al_2O_3 mixed oxide, which was obtained from Cu-Mg-Al mixed oxides obtained by coprecipitation. The oxide was reduced in flowing H_2 at 573 K to obtain metallic

Table 6.6.3 One-step synthesis of methyl isobutyl ketone over bifunctional catalysts

Metal	Support	Acetone conversion/%	Selectivity for MIBK/%	Temperature/K	Reference
Pd (0.5 wt%)	Na (0.47 wt%)-MgO	64–47	50–65	473	30
Pd (0.2 wt%)	HT, calcined	37	68	413	31
Pd (0.9 wt%)	SAPO-11	12.0	51.9	473	32
Pd (0.2 wt%)	HT, calcined	35	67	423	33
Pd (0.2 wt%)	HT calcined	27	74	423	34
Pd (2 wt%)	Hydroxyapatite	17	66.4	423	35
Pt (0.98 wt%)	NaX	7.2	80	613	36
Ni (7.1 wt%)	MgO	10–20	60–80	473	37
Ni (10 wt%)	Al ₂ O ₃	36	96	373	38
Ni (10 wt%) + Co (1 wt%)	Al ₂ O ₃	43	97	373	38
Ni (2 wt%)	CaO	70–80	60	473	39
Ni (3 wt%)	HT, calcined	44	61	413	31
Ni (10 wt%)	HT, calcined	48	78	373	40
Cu (3.46 wt%)	MgO	60–80	60–75	553	41

HT denotes hydrotalcite.

Cu. An MIBK yield of 27% was reached with 2-propanol conversion of ca. 95% at 533 K, the other products being acetone, DIBK and MIBC. Since H₂ is formed by dehydrogenation of 2-propanol, H₂ is not required as a reactant.

B. 2-Ethylhexanal from butanal

As in the case of MIBK, 2-ethylhexanal can be synthesized from butanal and hydrogen over bifunctional catalysts. Minachev et al. studied the reaction of butanal over metals (Pt, Pd, Rh, Ni, Co, Cu) on alkali cation-exchanged X zeolites.⁴⁵⁾ Among the metals, Pd was the most selective. Over 0.5% Pd/NaX, the yield of 2-ethylhexanal was 85–95% with selectivity of 94–97% at 398–423 K. Ko et al. also reported one-step synthesis of 2-ethylhexanal over K⁺-added KX zeolite loaded with Pd.⁴⁶⁾ High selectivity (>93%) was obtained at 423 K, but the catalytic activity decays with time on stream. 2-Ethylhexanal and 1-butanol were the main by-products. A Pd supported on Na(4 wt%)/SiO₂ was also tested for the reaction of butanal.⁴⁷⁾ 2-Ethylhexanal was obtained in high selectivity at 523 K, but the activity decayed with time on stream in this case as well.

C. One-pot synthesis of α -alkylated nitriles with hydrotalcite-supported metal species

Ru-loaded hydrotalcite is an effective catalyst for direct α -alkylation of nitriles with primary alcohols under an argon atmosphere.^{48,49)}

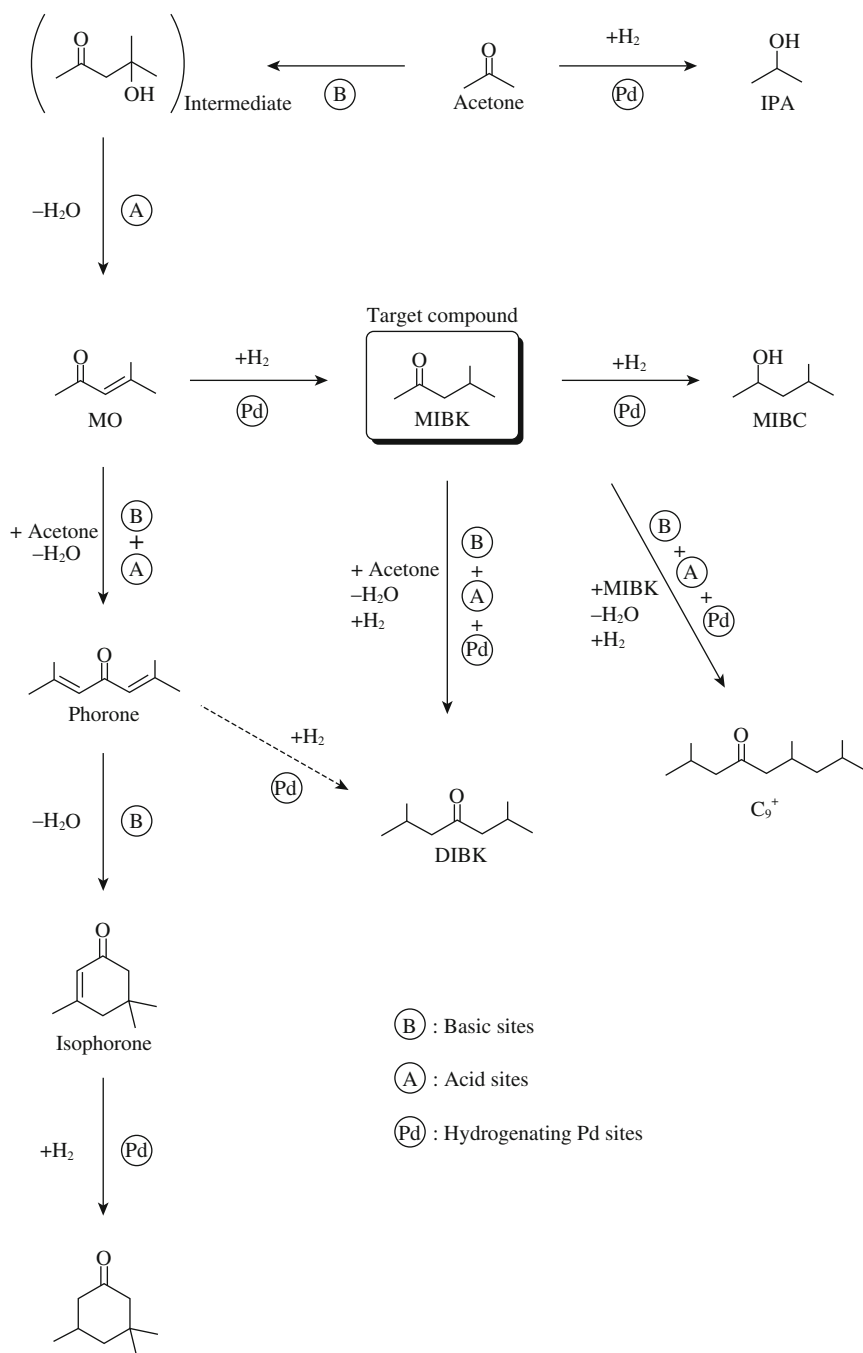
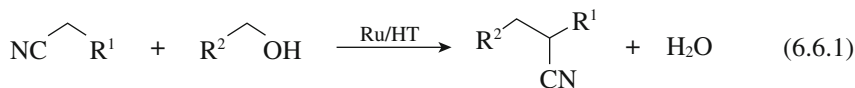


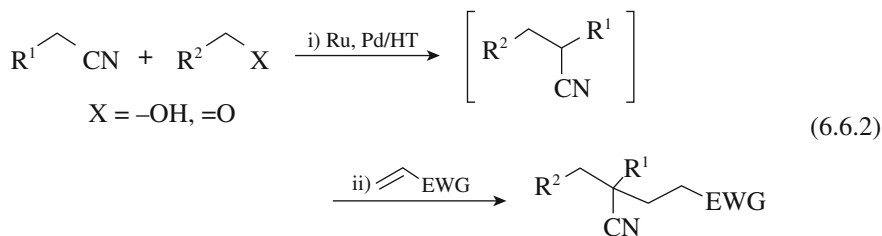
Fig. 6.6.1 Scheme of the reaction of acetone with hydrogen on bifunctional catalysts. Reprinted with permission from N. Das, D. Ticht, R. Durand, P. Graffin, B. Coq, *Catal. Lett.*, **71**, 181 (2001), p. 184, Fig. 3.



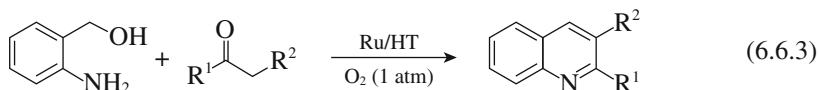
The catalyst was prepared by treatment of hydrotalcite, $\text{Mg}_6\text{Al}_2(\text{OH})_{16}\text{CO}_3$, with $\text{RuCl}_3 \cdot n\text{H}_2\text{O}$ at room temperature. Chlorine was absent in the catalyst and Ru species is in the +4 oxidation state. A wide variety of arylacetonitrile reacted with alcohols, affording the α -alkylated nitriles in excellent yields without formation of dialkylated products, as listed in Table 6.6.4.

The reaction scheme proposed is shown in Fig. 6.6.2. The α -alkylation consists of the following consecutive reactions: (i) oxidative dehydrogenation of alcohols to aldehyde with Ru(IV), (ii) base-catalyzed aldol condensation of nitriles with aldehydes, (iii) hydrogenation of α,β -unsaturated nitriles with Ru-species and (iv) formation of α,β -unsaturated nitriles.

One-pot synthesis of α,α' -dialkylated phenylacetonitrile is possible using this system.^{48,49} After completion of the alkylation of phenylacetonitrile with ethanol, acrylonitrile was added and allowed to further react at 423 K for 1 h. The base-catalyzed Michael addition occurred to afford 2-ethyl-2-phenylglutro-nitrile in 93% yield. Methyl acrylate and acrylamide were also good Michael acceptors. Pd metal supported on hydrotalcite is also useful.

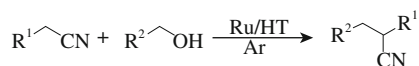


One-pot synthesis of quinoline from 2-aminobenzyl alcohol and carbonyl compounds has also been reported.⁵⁰



The reactions are assumed to proceed by oxidation of 2-aminobenzylalcohol to 2-aminobenzaldehyde with Ru species on hydrotalcite under an O_2 atmosphere, followed by aldol condensation with ketones catalyzed by basic sites of the hydrotalcite to yield quinolines.

Pd metal loaded on hydrotalcite is very effective for the alkylation of nitrile with aldehydes or ketones under hydrogen.^{49,51} The reaction is carried out in two steps. In the first step, Knoevenagel condensation of a nitrile and a carbonyl compound is carried out. Here, the hydrotalcite works as the basic catalyst. In the

Table 6.6.4 Alkylation of nitriles with primary alcohols over Ru-hydroxalcite^{a)}

Entry	Nitrile	Alcohol	Product	Isolated yield/% ^{b)}
1	R = H 1a	EtOH 2a	R = H	94
2	R = Me	2a	R = Me	99
3 ^{c)}	R = OMe	2a	R = OMe	92
4	R = Cl	2a	R = Cl	77
5		2a		89
6 ^{c)}		2a		86 ^{d)}
7		2a		37
8		2a		trace
9		2a		trace
10	1a	MeOH		65 ^{d)}
11	1a			86
12 ^{c)}	1a			85 ^{d)}
13 ^{d)}	1a			77
14 ^{e), f)}	1b			trace ^{e)}

^{a)} Reaction conditions: nitrile (1 mmol), alcohol (2 mL), Ru/HT (0.15 g, Ru: 0.0075 mmol), 180°C, 20 h, Ar. ^{b)} Based on nitrile used. ^{c)} Ru/HT (0.3 g, Ru: 0.015 mmol) was used. ^{d)} Determined by GC using internal standard. ^{e)} 2 mL of toluene and 1.5 mmol of alcohol were used. ^{f)} At 100°C.

^{g)} Benzyl cyanoacetate was formed in a 37% yield.

Reprinted with permission from K. Motokura, N. Fujita, T. Mizugaki, K. Ebirani, K. Jitsukawa, K. Kaneda, *Chem. Eur. J.*, **12**, 8228 (2006) p. 8232, Table 5.

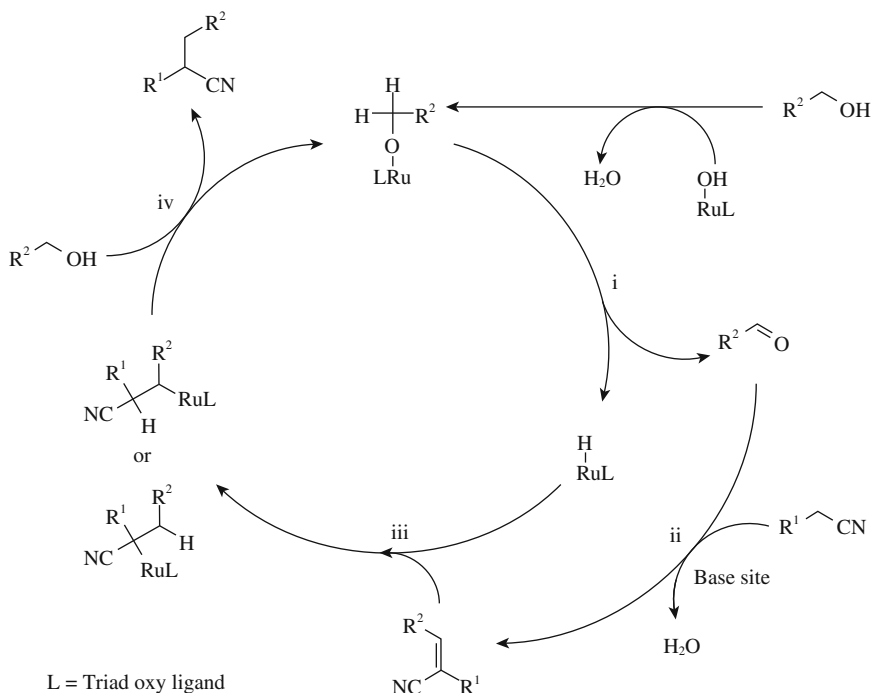
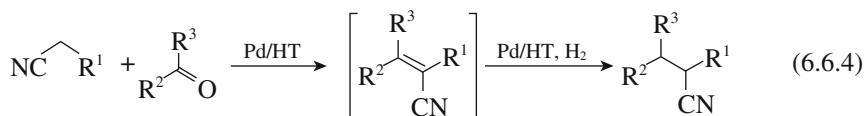


Fig. 6.6.2 Reaction scheme for the synthesis of α -alkylated nitriles from nitriles and primary alcohol. Reprinted with permission from K. Motokura N. Fujita, T. Mizugaki, K. Ebitani, K. Jitsukawa, K. Kaneda, *Chem. Eur. J.*, **12**, 8228 (2006) p.8233, Scheme 4.

second step, the product of the condensation is hydrogenated under hydrogen. The Pd component serves as a hydrogenation catalyst.



A wide variety of nitriles and carbonyl groups react to give excellent yields of α -alkylated nitriles, as shown in Table 6.6.5.

The anti-inflammatory agent nabumetone [4-(6-methoxy-2-naphthyl)-2-butanone] is synthesized from 6-methoxy-2-naphthaldehyde and methyl vinyl ketone under hydrogen with use of Pd supported on MgO.⁵²⁾ The reaction is considered to proceed by aldol condensation of 6-methoxy-2-naphthaldehyde and methyl vinyl ketone, followed by the hydrogenation of the condensation product to nabumetone. A 98% yield of nabumetone was obtained at 333 K with 100% selectivity after 60 min. The catalyst was more active when MgO of small crystalline size (3 nm, 670 m² g⁻¹) was used. Pd supported on mixed oxides derived from hydrotalcite also showed catalytic activity, but was less active and less selective compared with Pd/MgO.

Table 6.6.5 α -Alkylation of nitriles with carbonyl compounds with Pd/hydroxalcite
$$\text{NC}-\text{CH}_2-\text{R}^1 + \text{R}^2-\overset{\text{R}^3}{\text{C}}=\text{O} \xrightarrow[\text{(i)}]{\text{Pd/HT}} \left[\text{R}^2-\overset{\text{R}^3}{\text{C}}=\text{C}(\text{R}^1)-\text{CN} \right] \xrightarrow[\text{(ii)}]{\text{Pd/HT, H}_2} \text{R}^2-\overset{\text{R}^3}{\text{C}}-\text{CH}(\text{R}^1)-\text{CN}$$

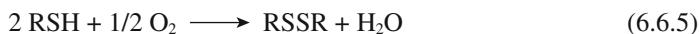
Entry	Nitrile	Acceptor	Time of (ii)/h	Product	yield/% ^{b)}
1			1		98
2		2	5		82
3 ^{c), d)}		2	4		95 ^{e)}
4		2	1		99
5		2	2.5		99
6 ^{f)}			23		84
7 ^{c)}	1		4		87
8	1		1		99
9	1		2		98
10	1		24		19
11	1		3		82
12 ^{c), g)}	1	HCHO	1		91
13	1		1		85 (81)
14			6.5		97 (92)

^{a)} (i); Nitrile(1 mmol), carbonyl compounds (1 mmol), Pd/HT (0.1 g; Pd; 0.01 mmol), toluene (3 mL), 2 h, 80°C, Ar. (ii): 60°C, H₂(1 atm). ^{b)} Determined by GC using an internal standard. Values in parentheses are isolated yield. ^{c)} DMF (3 mL) was used as solvent. ^{d)} (i); 18 h. ^{e)} Determined by ¹H NMR analysis. ^{f)} (i); 120°C. ^{g)} 30% aqueous HCHO was used, (i): 3 h.

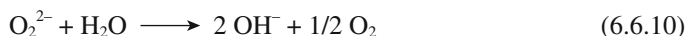
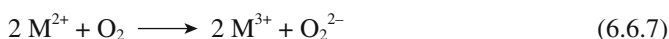
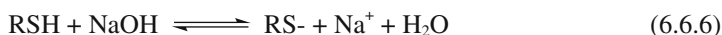
Reprinted from K. Motokuma, N. Fujita, K. Mori, T. Mizugugaki, K. Ebitani, K. Kaneda, *Tetrahedron Lett.*, **46**, 5507 (2005) p.5508, Table 2.

D. Mercaptan oxidation

Mercaptans are widely distributed in petroleum products. They cause foul odors and deteriorate the finished products. Due to their acidity, mercaptans are corrosive to metals, which is harmful in the storage and usage of oil products. To remove mercaptans, the Mercox process developed by UOP is the most widely used.⁵³⁾ The process is based on the ability of sulfonated cobalt phthalocyanine (S-CoPc) to catalyze the oxidation of mercaptan to disulfide by molecular oxygen. The overall reaction of the oxidation is



The mechanism of the oxidation can be summarized as follows.⁵⁴⁾



The first step, the formation of mercaptide ion from the mercaptan, is promoted by an aqueous base such as NaOH. However, the use of NaOH involves many problems such as the cost of handling and disposal of spent alkaline solution

Replacement of aqueous alkali with solid bases has been attempted. Alcaraz et al. used S-CoPc supported on MgO-Al₂O₃ mixed oxide (Mg/Al = 3) prepared by calcining hydrotalcite.⁵⁵⁾ For the gasoline containing a mercaptan of 149 ppm, more than 99% of the mercaptan was converted to disulfides using S-CoPc (318 ppm Co) supported on MgO-Al₂O₃ mixed oxide under the flow condition of LHSV = 3 and 5.

For kerosene treatment, however, the same catalyst deactivated significantly over 120 h. Three deactivation mechanisms were identified: rehydration of the Mg-Al oxide back to hydrotalcite, poisoning of the basic sites by the acids (primarily naphthenic acid) present in kerosene, and fouling caused by heavy components in the kerosene. Solutions were sought for these problems. Rehydration of the oxide support could be avoided by using Mg-Ni-Al oxide instead of the Mg-Al oxide. The kerosene was washed with a sodium hydroxide solution to remove all acidic poisons. A quaternary ammonium salt was continuously injected with the aqueous stream to solubilize any heavy species that would accumulate on the surface. As a result of all these procedures, the catalytic stability improved significantly.

Zhao and coworkers also reported mercaptan oxidation with S-CoPc supported on metal oxides.^{56,57)} In the first 24 h, S-CoPc supported on MgO-ZrO₂ (0.23 : 1 in weight) converted 99% of mercaptan in jet fuel to disulfide (102 ppm S). In the next 48 h, the activity decreased slowly to a conversion of 88%. With

use of S-CoPc supported on MgO-Al₂O₃ (MgO 15 wt%) as a catalyst, the mercaptan conversion started at 98% and remained at 98% during the first 200 h then slowly decreased to 90% at 575 h and to 80% at 878 h. MgO-Al₂O₃ was prepared by impregnating γ -Al₂O₃ with magnesium nitrate, followed by drying and calcination at 773 K. This MgO-Al₂O₃ was superior than MgO-Al₂O₃ prepared by calcination of hydrotalcite. In these works, the jet fuel had been washed with 2% NaOH solution to remove acidic materials which decrease the sulfur content to 102 ppm before being pumped into the reactor.

References

1. K. Aika, A. Ohya, A. Ozaki, Y. Inoue, I. Yasumori, *J. Catal.*, **92**, 305 (1985).
2. K. Aika, T. Takano, S. Murata, *J. Catal.*, **136**, 126 (1992).
3. O. Hinrichsen, F. Rosowski, A. Hornung, M. Muhler, G. Ertl, *J. Catal.*, **165**, 33 (1997).
4. J. Kubota, K. Aika, *J. Phys. Chem.*, **98**, 11293 (1994).
5. M. D. Cisneros, J. H. Lunsford, *J. Catal.*, **141**, 191 (1993).
6. C. Fishel, R. J. Davis, J. M. Garces, *J. Catal.*, **163**, 148 (1996).
7. T. Bécue, R. J. Davis, J. M. Garces, *J. Catal.*, **179**, 129 (1998).
8. C. Besoukhanova, J. Guidot, D. Barthomeuf, M. Breyse, J. B. Bernard, *J. Chem. Soc., Faraday Trans. 1*, **77**, 1595 (1981).
9. R. J. Davis, E. G. Derouane, *Nature*, **349**, 313 (1991).
10. R. J. Davis, E. G. Derouane, *J. Catal.*, **132**, 269 (1991).
11. T. Bécue, F. J. Maldonado-Hodar, A. P. Antunes, J. M. Ribeiro, P. Massiani, M. Kermarec, *J. Catal.*, **181**, 244 (1999).
12. F. J. Maldonado, T. Bécue, J. M. Silva, M. F. Ribeiro, P. Massiani, M. Kermarec, *J. Catal.*, **195**, 342 (2000).
13. A. de Mallmann, D. Barthomeuf, *Stud. Surf. Sci. Catal.*, **46**, 429 (1989).
14. V. B. Kazanki, V. Yu. Borovkov, *Stud. Surf. Sci. Catal.*, **92**, 275 (1995).
15. V. B. Kazanski, V. Yu. Borovkov, A. J. Serykh, *Catal. Lett.*, **49**, 35 (1993).
16. Z. Gandao, B. Coq, L. C. de Ménorval, D. Ticht, *Appl. Catal., A*, **147**, 395 (1996).
17. D. Ticht, M. J. Martínez-Ortiz, D. Francová, C. Gérardin, B. Coq, R. Durand, F. Prinetto, G. Ghiotti, *Appl. Catal., A*, **318**, 170 (2007).
18. G. S. Lane, J. T. Miller, F. S. Modica, M. K. Barr, *J. Catal.*, **141**, 465 (1993).
19. A. Phillipou, M. Naderi, N. Pervaiz, J. Rocha, M. W. Anderson, *J. Catal.*, **178**, 174 (1998).
20. S. B. Waghmode, R. Vetrivel, S. G. Hegde, C. S. Gopinath, S. Sivasanker, *J. Phys. Chem. B*, **107**, 8517 (2003).
21. A. de Mallmann, D. Barthomeuf, *J. Chim. Phys.*, **87**, 535 (1990).
22. X. Bai, W. M. H. Sachtler, *Catal. Lett.*, **4**, 319 (1990).
23. S. Siffert, J. -L. Schmidt, J. Sommer, F. Garin, *J. Catal.*, **184**, 19 (1999).
24. B. L. Mojet, J. T. Miller, D. E. Ramaker, D. C. Koningsberger, *J. Catal.*, **186**, 373 (1999).
25. H. -C. Wu, L. -C. Liu, S. -M. Yang, *Appl. Catal.*, **211**, 159 (2001).
26. A. A. Nikolopoulos, B. W. -L. Jang, J. J. Spivey, *Appl. Catal., A*, **296**, 128 (2005).
27. A. Mitschker, R. Wagner, P. M. Lange, *Stud. Surf. Sci. Catal.*, **41**, 61 (1988).
28. S. Talwalker, S. Mahajani, *Appl. Catal. A.*, **302**, 140 (2006).
29. Y. Onue, Y. Mitsui, S. Akiyama, Y. Izumi, Y. Watanabe, *CHEMTECH*, Jan., p. 36 (1977).
30. K. -H. Lin, A. -N. Ko, *Appl. Catal., A*, **147**, L259 (1996).
31. Y. Z. Chen, C. M. Hwang, C. W. Liaw, *Appl. Catal., A*, **169**, 207 (1998).
32. A. -M. Yang, Y. M. Wu, *Appl. Catal., A*, **192**, 211 (2000).
33. M. Matrínez-Ortiz, D. Ticht, P. Gonzalez, B. Coq, *J. Mol. Catal., A*, **201**, 199 (2003).
34. F. Prinetto, G. Ghiotti, N. Das, D. Ticht, B. Coq, *Stud. Surf. Sci. Catal.*, **140**, 391 (2001).
35. N. Cheikhi, M. Kacimi, M. Rouimi, M. Ziyad, L. F. Liotta, G. Pantaleo, G. Deganello, *J. Catal.*, **232**, 257 (2005).
36. L. V. Mattos, F. B. Noronha, J. L. E. Monteiro, *J. Catal.*, **209**, 166 (2002).
37. L. M. Gandia, M. Montes, *Appl. Catal.*, **101**, L1 (1993).
38. S. Narayana, R. Unikrishnan, *Appl. Catal. A*, **145**, 231 (1996).
39. B. -Y. Coh, J. M. Hur, H. -I., Lee, *Chem. Lett.*, **18**, 583 (1998).

40. R. Unnikrishnan, S. Narayanan, *J. Mol. Catal., A*, **144**, 173 (1999).
41. C. Chikán, Á. Molnár, K. Balázsik, *J. Catal.*, **184**, 134 (1999).
42. N. Das, D. Ticht, R. Drand, P. Graffin, B. Coq, *Catal. Lett.*, **71**, 181 (2001).
43. J. I. Di Cosimo, G. Torres, C. R. Apesteguía, *J. Catal.*, **208**, 114 (2002).
44. G. Torres, C. R. Apesteguía, J. L. Di Cosimo, *Appl. Catal.*, **317**, 161 (2007).
45. Kh. M. Minachev, Yu. I. Isakov, T. A. Isakova, N. ya. Usachev, *Izv. Akad. Nauk SSR, Ser. Khim.*, 299 (1986); (274).
46. A.-N. Ko, C. H. Hu, Y. T. Yeh, *Catal. Lett.*, **54**, 207 (1998).
47. F. King, G. J. Kelly, *Catal. Today*, **73**, 75 (2002).
48. K. Motokura, D. Nishimura, K. Mori, T. Mizugaki, K. Ebitani, K. Kaneda, *J. Am. Chem. Soc.*, **126**, 5662 (2004).
49. K. Motokura, N. Fujita, T. Mizugaki, K. Ebitani, K. Jitsukawa, K. Kaneda, *Chem. Eur. J.*, **12**, 8228 (2006).
50. K. Motokura, T. Mizugaki, K. Ebitani, K. Kaneda, *Tetrahedron Lett.*, **45**, 6029 (2004).
51. K. Motokura, N. Fujita, K. Mori, T. Mizugaki, K. Ebitani, K. Kaneda, *Tetrahedron Lett.*, **46**, 5507 (2005).
52. M. J. Climent, A. Corma, S. Ibbora, M. Mifsud, *J. Catal.*, **247**, 223 (2007).
53. B. Basu, S. Satapathy, A. K. Bhatnagar, *Catal. Rev., Sci. Eng.*, **35**, 571 (1993).
54. T. Wallace, A. Schriesheim, H. Hurwitz, M. Glaser, *Ind. Eng. Chem. Prod. Des. Dev.*, **3**, 237 (1964).
55. J. J. Alcaraz, B. J. Arena, R. D. Gillespie, J. S. Holmgren, *Catal. Today*, **43**, 89 (1998).
56. D. Jiang, G. Pan, B. Zhao, G. Ran, Y. Xie, E. Min, *Appl. Catal., A*, **201**, 169 (2000).
57. D. Jiang, B. Zhao, Y. Xie, G. Pan, G. Ran, E. Min, *Appl. Catal., A*, **219**, 69 (2001).

Subject Index

A

- acetylacetone cyclization 65, 184
- acid-base bifunctional catalysis 213
- acid-base concerted mechanism 7, 114
- addition
 - of 1-alkyne to aldehyde 296
 - of alkyne to ketone 296
 - of amine butadiene 153
 - of silane 381
 - to epoxide 291
- adsorption
 - of 2,6-di-*t*-butyl-4-methylphenol 17
 - of acrylic acid 16
 - of benzoic acid 16
 - of boron trifluoride 17
 - of carbon dioxide 17
 - of methyl iodide 37
 - of nitromethane 36
 - of NO 84
 - of phenol 16
 - of propyne 34
 - of pyrrole 29
 - of SO₂ 18, 350
 - dissociative — of H₂S 350, 366
- alcohol dehydration 24, 47, 94, 105, 190
- alcohol dehydrogenation 27, 47, 105, 190
- aldehyde from aromatic carboxylic acid 106
- aldol condensation of aldehyde 140
- aldol addition 94, 223
 - of acetone 202, 223
 - of butanal 223
- aldol condensation 6, 7, 137, 166, 202, 207, 212, 214, 216, 223, 297, 356
 - of acetaldehyde 114, 230
 - of acetone 156, 177, 226, 230
 - of aldehyde 140, 223
 - of benzaldehyde 226
 - of butanal 140, 223
 - of citral with acetone 352
 - of formaldehyde with acetone 230, 231
 - of formaldehyde with acetaldehyde 230
 - of formaldehyde with methylpropionate 231
 - of formaldehyde with propionic acid 231
 - of glyceraldehyde acetonide with acetone 225
 - of heptanal 140
 - of methyl propionate 231
 - of propanal 223
 - asymmetric — 391, 393
- AlGaPON 196, 200
- alkali cation
 - -doped silica 231
 - -exchanged carbon 287
 - -exchanged faujasite 16, 284, 286
 - -exchanged zeolite 36, 366, 399
 - -loaded MgO 281
 - MCM-41 loaded with — 66
- alkali-loaded silica 271, 276
- alkali hydroxide
 - CsX containing excess — 278
 - KX containing excess — 278
- alkali metal compound
 - -loaded Al₂O₃ 134, 154
 - -loaded alkaline earth oxide 136
 - -loaded carbon 141, 155
 - -loaded catalyst 134
 - -loaded SiO₂ 138
 - -loaded TiO₂ 140
 - -loaded ZrO₂ 140
- alkali metal oxide-loaded zeolite 178
- alkaline earth hydroxide 261
- alkaline earth oxide 13, 20, 27, 51, 63, 69, 221, 223, 261, 263, 265, 292, 294, 303, 304, 397
- alkaline metal-doped MgO 17
- alkyl carbonate
 - reaction of — with acid 324
 - reaction of — with alcohol 324
 - reaction of — with amine 326
- alkylammonium hydroxide 243
- alkylation
 - of aniline 284
 - of dihydroxybenzene 273
 - of *m*-cresol 270
 - of methylpyridine 278
 - of nitrile 283, 284
 - of phenol 114, 131, 269, 272
 - of toluene 19, 42, 276
 - N*- — of aniline with alkyl carbonate 286, 287
 - N*- — of imidazole 288
 - O*- — of naphthol 139
 - O*- — of phenol 271
 - ortho*- — of phenol 269
 - ortho*- — of phenol with methanol 269
- alkylsilylation of ZnO 118
- allylic anion 115
- π -allylic carbanion 95
- AlPO₄(amorphous) 356
- AlPO₄-5 200
- AlPON 62, 195, 197, 237, 242
- alumina \rightarrow Al₂O₃

- amine tethered to silica 210, 292, 302
 amine-functionalized silica 206, 210, 227, 233, 240, 242, 252, 293, 294, 302, 320, 355, 395
 ammonia synthesis 396
 ammonium group/SiO₂ 205, 206, 240, 242
 amorphous aluminum phosphate 7
 anatase 111
 1,6-anhydroglucose from glucose 114
 anion exchange resin 64, 201, 232, 243, 250, 261, 294, 348
 asymmetric epoxidation 394
 asymmetric aldol reaction 393, 395
 asymmetric Michael addition 395
 asymmetric synthesis 390, 393, 396
 aza-Michael addition 258
- B**
- Baeyer-Villiger oxidation 330, 338
 barium hydroxide 226, 372
 base strength
 — of alkali and alkaline earth phosphate 189
 — of oxygen ion 37
 — of solid base 3, 14
 basic site
 — strength of distribution 15
H-scale of — 12
 model of — 153
 bayerite 119
 Baylis-Hillman reaction 300
 bidentate carbonate 20, 25, 113, 123, 181
 bifunctional catalysis 104, 400
 acid-base — 213
 S-BINOL 390, 395
 biodiesel synthesis 343
 boehmite 119
 bridged carbonate 25, 123
 Brønsted acid 5
 Brønsted base 5
 brookite 111
 brucite 72
 1-butene isomerization 70, 94, 105, 114, 117, 126, 155, 182, 190
cis-2-butene isomerization 117, 135
- C**
- carbonylation
 — of hexanol 204
 — of methanol 203
 chitosan 228, 242
 choline hydroxide 349
 Claisen-Schmidt condensation 210, 213, 225, 226, 354, 392
 Claus process 350
 Claus reaction 135
 cobalt phthalocyanine 407
 co-condensation method 210, 395
 co-isomerization of 1-butene *d₀/d₈* 45, 95, 114, 126
 combustion
 — of C₃H₆ over Pd metal 399
 — of C₃H₈ over Pd metal 399
 condensation
 — of alcohol 142, 282
 — of 1-phenylethanol with dimethyl carbonate 142
 coprecipitation method → hydrotalcite synthesis 158
 corundum 119
 COS hydrolysis 27, 132
 cross metathesis of alkyne 377
 cyano-ethoxycarbonylation 214
 cyanoethylation
 — of alcohol 166, 202, 261
 — of acrylonitrile 167
 cyanosilylation 190, 210
 cyano-*O*-ethoxycarbonylation 302
 cyclization of acetylacetone 65, 184
 cycloaddition of carbon dioxide 293
- D**
- decomposition
 — of 2-propanol 51, 132, 138, 182
 — of alkylamine 107
 dehydration
 — of alcohol 47, 94, 105, 124, 190
 — of 2-alkanol 105, 131
 — of 1,4-butanediol 108
 — of 1-butanol 48
 — of 2-butanol 48, 53, 105, 198
 — of *t*-butyl alcohol 177
 — of 1-cyclohexylethanol 97
 — of 2-ethoxyethanol 139
 — of glucose 114
 — of glycol ether 139
 — of *N*-(2-hydroxyethyl)-2-pyrrolidinone 139
 — of 4-methyl-2-pentanol 23, 94, 105, 131, 140
 — of monoethanolamine 139
 — of propylamine-2-ol 97
 — over TiO₂ 114
 E1 mechanism alcohol — 47
 E1cB mechanism alcohol — 48
 E2 mechanism alcohol — 48
 intermolecular — 125
 dehydrogenation 108
 — of alcohol 24, 47, 105, 117, 190
 — of 1-butanol 198
 — of 2-butanol 137, 198
 — of 2-propanol 50, 117, 175, 177
 dehydrogenative coupling
 — of alcohol with silane 379
 — of alkene with silane 378

— of alkylbenzene with silane 379
 density functional theory (DFT) 81, 122
 diaspore 119
 dielectric outer-sphere effect 214
 diethylbenzylsilane 148
 diisopropyl ketone from isobutyraldehyde 97,
 108
 dimerization of phenylacetylene 148, 295
 dimethyl carbonate
 reaction of — with acid 324
 reaction of — with amine 326
 reaction of — with ethanol 324
 reaction of — with phenol 324
 reaction of — with silica 387
 synthesis of — 106, 294, 347, 349
 disproportionation
 — of alkoxy silane 380
 — of trimethylsilylacetylene 144, 148
 double hydroxide 157

E

E1cB mechanism 24, 48, 54, 105, 131, 199
 E1-like mechanism 190
 E2-like mechanism 105
 E1 mechanism 24, 47, 51, 199
 E2 mechanism 24, 48, 52, 53, 125, 199
 epoxidation of alkene 207, 332, 333
 epoxide
 addition to — 28, 291
 esterification 94, 319
 ethylene carbonate
 reaction of — with methanol 204, 348
 synthesis of — 294
 ethylene oxide
 reaction of — with CO₂ 294, 347, 349
 ethyl vinyl ether synthesis 139
 ethyleneimine synthesis 140
 2-ethylhexanal synthesis 401
 ETS-10 → zeolite

F

faujasite 16, 286, 284
 F center 153
 flavanone synthesis 210, 213, 354
 fluoroapatite 189, 239, 243
 α -fluorotropinene on MCM-41 395
 formic acid decomposition 117
 fructose by glucose isomerization 115

G

gibbsite 119
 glucose 114
 glycol ether, dehydration of 139
 grafting method 205, 212, 213, 250
 Guerbert reaction 282

H

H-acidity function 11, 12, 15
 H₂/D₂ equilibration 124
 H-D exchange 94, 124, 127
 heat of adsorption (CO₂) 22, 134, 185
 Henry reaction → nitroaldol reaction
 heterocycle synthesis 369
H-scale 12
H-value 13, 14, 15, 41
 Hofmann orientation 48
 hydrargillite 119
 hydration of nitrile 143
 hydrocalmite 165
 hydrogen transfer reaction → transfer hydroge-
 nation
 hydrogenation 105
 — of alkene 94
 — of aromatic carboxylic acid 97
 — of benzoic acid 306
 — of 1,3-butadiene 44, 105, 304
 — of carbon oxide 108
 — of carboxylic acid 306
 — of ethylene 95, 104, 303, 304
 — of ketone 310
 — of 2-methyl-1,3-butadiene 105
 hydrogencarbonate 20, 25, 26, 104, 113, 123
 hydrolysis 27, 108, 123
 hydrosilylation
 — of carbonyl compound 190, 383
 hydrotalcite 57, 131, 157, 258, 330, 338
 — thermal decomposition 159
 — with diisopropylamide anion 167
 — with ^tBuO⁻ 167, 227, 239, 250, 263, 320,
 324, 334, 337, 339, 372
 — with F⁻ 167, 239, 250
 as-synthesized — 162, 263, 324, 333, 335,
 339, 347, 351, 357, 362, 380
 calcined — 157, 160, 164, 168, 269, 317,
 320, 324, 329, 336, 353, 357
 Pd metal supported on — 403
 rehydrated — 64, 158, 160, 165, 224, 227,
 236, 237, 250, 257, 263, 329, 333, 336,
 353, 356, 362
 Ru- and Pd-loaded — 284
 Ru species on — 403
 Ru-loaded — 284, 401
 hydrotalcite structure 157
 hydrotalcite synthesis 158
 hydrous zirconia 311, 313, 315, 318, 319
 hydroxyapatite 14, 18, 49, 54, 189, 239, 255,
 283, 309, 382, 384

I

indicator method 11, 13, 15, 76, 164, 188,
 211, 237
 infrared → IR

intramolecular H transfer 95, 126

IR

- of alkyne 33
- of CDCl_3 31
- of CHCl_3 31
- of CH_3OH 82
- of CH_4 83
- of C_2H_2 33, 35
- of CO_2 20, 25, 85, 93, 103, 115, 123, 138
- of H_2 78, 104
- of propyne 33, 36
- of pyrrole 29, 171
- of surface OH group 80, 93, 103, 121

isomerization 42, 219, 351

- of alkene 13, 94, 124, 163, 219
- of alkyne 219, 222
- of allylamine 147, 221
- of 1-butene 18, 42, 44, 46, 70, 94, 105, 114, 182, 190, 219
- of citronellal 176
- of 2,3-dimethyl-1-butene 144, 146, 155, 211
- of estragole 163
- of eugenol 163, 351
- of 1-hexyne 222
- of isophorone 142
- of 3-methyl-1-butene 135, 147, 173
- of olefin 135
- of *cis*-pentadiene 118
- of 1-pentene 118, 154
- of α -pinene 155
- of safrole 163, 352
- of 5-vinylbicyclo[2,2,1]-2-heptene 155, 221

J

jasminealdehyde synthesis 210, 356

Julia-Colonna reaction 394

K

K-EMT \rightarrow zeolite

- Knoevenagel condensation 6, 60, 143, 163, 166, 175, 189, 190, 197, 202, 205, 207, 210, 212, 216, 237, 242, 365, 403
- of benzaldehyde with ethyl cyanoacetate 182, 237
- of benzaldehyde with malononitrile 167, 191, 199, 237

L

Lewis acid 5, 7

Lewis base 5

M

Madelung potential 76, 85

magnesium organo-silicate(MOS) 210, 224, 357

magnesium oxide fluoride 247

magnesium phosphate 285

MAS NMR

- of CDCl_3 33
- of CHCl_3 33
- of methyl iodide 37
- of nitromethane 36, 131, 144
- of OH 86
- of pyrrole 29
- ^{27}Al — 159
- ^{13}C — of adsorbed methyl iodide 37
- ^{133}Cs — 178
- ^{19}F — 141
- ^1H — 86, 172
- ^{23}Na — 155
- ^{29}Si — 194

MBOH 55, 82, 104, 117, 124, 130, 162, 177, 183, 187

MCM-41 66, 210, 233, 242, 284, 293, 348, 382, 395

Cs/— 278, 328

MgO/— 357

TBD/— 207, 252, 293, 320, 326

MCM-48 237, 242, 324

Meerwein-Ponndorf-Verley reaction 74, 94, 108, 175, 308

memory effect 160, 161, 167

mercaptan oxidation 407

Merox process 407

metal oxynitride 192, 237

metal-organic framework(MOF) 210, 211

metathesis of trimethylsilylacetylene 376

methane

- -D_2 exchange 94
- oxidative coupling of — 136

methanol

alkylation with —

- of aniline 284
- of cresol 270
- of dihydroxybenzene 273
- of phenol 269, 271
- of methylpyridine 278
- of toluene 189, 276

carbonylation of — 203

cyanoethylation of acrylonitrile with — 167

methylation of naphthol with — 276

reaction with —

- of propylene oxide 292
- of toluene 42

methyl isobutyl ketone synthesis 400

4-methyl thiazole synthesis 183

methylation

- of phenol 138, 188
- of 2-naphthol 276
- of thiol 289
- oxidative — of toluene 138

2-methyl-3-buten-2-ol \rightarrow MBOH

- Michael addition 131, 143, 183, 189, 190, 202, 207, 212, 213, 216, 246, 365, 396, 403
 — of acetone to ethyl acrylate 186
 — of H₂S methyl acrylate 255
 — of phorone 138
 — of thiol 255
 regioselectivity of — 183
 asymmetric — 391
 mixed oxide 128
 — derived from hydrotalcite→hydrotalcite (calcined)
 Miyaura-Suzuki coupling 145
 MOF 210
 mordenite 30
 MOS 210, 224, 357
 Mukaiyama aldol reaction 228
- N**
- natural phosphate 191, 239, 335, 374
 nitroaldol reaction 143, 176, 202, 212, 213, 232, 390
 NMR→MAS NMR
 nordstrandite 119
- O**
- Oppenauer oxidation 108, 308, 315
 oxidation
 — of alcohol 338
 — of amine 339
 — of propane 399
 — of propene 399
 — of pyridine 338
 — of thioether 338
 — of thiol 338
 — with alkylperoxide 331
 — with H₂O₂ 333, 338, 339
 — with molecular oxygen 330
 liquid-phase — 330
 oxidative coupling of methane 136
 oxynitride→metal oxynitride
- P**
- 2-pentylidene-cyclopentanone synthesis 354
 periclastase 72
 pH swing method 120
 phenol
 alkylation of — 114, 131, 269
 methylation of — 138, 188
 phenylacetylene
 dimerization of — 147, 295
 reaction of — with trimethylsilyl acetylene 377
 phosphorous compound, reaction of 369
 photoluminescence 76
 poisoning 18, 126
 polyoxyglycol ester 329
 post synthesis 205, 212, 250
- L-proline 392, 395
 — grafted to MCM-41 210
 — in hydrotalcite 161, 395
- 2-propanol
 alkylation of phenol with — 272
 — decomposition 50, 113, 117, 132, 137, 175, 182, 186
- propylene carbonate
 reaction of — with methanol 348
 synthesis of — 294
- propylene oxide 292
 reaction of — with alcohol 292
 reaction of — with CO₂ 294, 347, 349
 reaction of — with methanol 211
- pseudoionone synthesis 352
 Pudovik reaction 373
 pyridine, oxidation of 338
 pyrrole
 adsorption of — 29
 IR of — 29, 171
 MAS NMR of — 29, 172
 XPS of — 29, 171
- R**
- rare earth oxide 91, 303
 retro-aldol reaction 17, 65, 188
 ring opening of epoxide 292, 380
 ring transformation
 — of γ -butyrolactone 19, 365
 — of heterocycle 365
 — of tetrahydrofuran 366
- rutile 111
- S**
- safrol, isomerization of 155, 163, 352
 Sanderson's electronegativity equalization principle 30, 33, 38, 170
 SAPO-11 nitrated 200
 Saytzev orientation 48
 sepiolite 62
 side-chain alkylation 153
 — — of alkylaromatics 276, 279
 — — of *o*-xylene 186
 — — of toluene 1, 13, 155, 186, 276, 278
- silane 378, 381
 addition of — 381
 dehydrogenative coupling of — 378, 379
 disproportionation of — 387
- silica, reaction with dimethylcarbonate 387
 silicon compound, reaction of 375
 silicon oxynitride 193, 197, 237
 smectite 294
 sol-gel method 74, 120, 138, 212, 247
 solvent effect 4
 substitution reaction at silicon 375
 superbase 13
 synergetic effect 7, 8, 214

synthesis

- of carbamate 326
- of dimethyl carbonate 106, 294, 326, 347, 349
- of 2-ethylhexanal 401
- of flavanone 210, 354
- of heterocycle 360
- of jasminealdehyde 210, 356
- of methyl isobutyl ketone 400
- of monoglyceride 328
- of 2-pentylidene-cyclopentanone 354
- of phytosterol ester 357
- of pseudoionone 352
- of vesidryl 355

T

TBD

- MCM-41 252, 293, 320, 325
- SBA-15 228, 253

test reaction 41, 237

tetrahydrofuran, reaction with H₂S 366

Tishchenko reaction 108

- of benzaldehyde 144, 265, 266

titration method 13

toluene

- alkylation of — 19, 189, 276
- oxidative methylation of — 138
- side-chain alkylation of — 1, 13, 155, 186, 276, 278

TPD

- of CH₄ 83
- of CO₂ 19, 85, 102, 138, 151, 180
- of H₂ 20, 79
- of NH₃ 102
- of ¹⁸O₂ 180

transesterification 131, 207, 212, 213, 319, 343, 357, 367

- of dialkyl carbonate with alcohol 324
- of diethyl carbonate with alcohol 142, 145, 324, 325
- of diethyl carbonate with 1-phenylethanol 145, 324
- of dimethyl carbonate with ethanol 324
- of dimethyl carbonate with 1-propanol 324
- of ethylene carbonate with methanol 204, 348
- of propylene carbonate with methanol 348
- of triglyceride with methanol 343

transfer hydrogenation 6, 8, 94, 105, 131, 190, 308

- of aldehyde 310
- of citronellal 176
- of ketone 310
- of nitrile 315
- of nitro compound 315

mechanism of — 308

trimethylsilylacetylene

cross methathesis of — 377

methathesis of — 376

reaction of — with amine 377

U

unidentate carbonate 20, 25, 104, 113, 123, 181

 α,β -unsaturated compound, synthesis of 279

urea method→hydrotalcite synthesis 158

V

VAION 195, 199

vesidryl synthesis 355

vinyl ether synthesis 139

5-vinylbicyclo[2,2,1]-2-heptene synthesis 155, 221

N-vinyl-2-pyrrolidone synthesis 139

W

Wadsworth-Emmons reaction→Wittig-Horner reaction

Witting reaction 369

Witting-Horner reaction 167, 370

X

XPS 173

- of alkali modified Al₂O₃ 152
- of O_{1s} 153
- of pyrrole 29, 171

Z

zeolite 30, 37, 65, 257, 291, 398

alkali cation-exchanged — 19, 30, 35, 38, 41, 57, 170, 176, 256, 271, 276, 312, 343, 366

metal supported on — — 397, 398

alkali cation-exchanged L — 30, 398

alkali cation-exchanged mordenite 30

alkali cation-exchanged X — 1, 30, 32, 53, 60, 271, 397

alkali cation-exchanged Y — 1, 30, 32, 36, 53, 60, 397, 399

alkali metal-loaded — 184

alkali metal oxide loaded — 178, 271

 β — 250

CaX — 312

CsHZSM-5 — 285

CsOH/NaY — 38

Cs₂O/ZSM-5 — 285, 360

CsX — 37, 236, 312, 397

Cs-loaded — 37

CsY — 35, 38, 352

EST-10 62, 177, 320, 339, 343, 398

K-EMT 286

Na mordenite 35, 294

NaX — 35, 37
NaY — 35, 38, 291
NaZSM-5 — 65, 285, 326
Pt supported on — 398
X — 30, 292

Y — 30, 32, 250, 292
ZSM-5 285
Cs- — 285, 360
Na- — 65, 285, 326

Chemical Formula Index

A

- Al₂O₃ 7, 17, 18, 20, 22, 25, 29, 31, 46, 48, 56, 65, 118, 232, 243, 247, 258, 273, 288, 291, 292, 309, 333, 338, 350, 353, 369, 380, 392
 - loaded with KNO₃ 273
 - modified with Na⁺ ion 18
- alkali metal compound-loaded — 134
- alkali metal-loaded — 154
- Cs oxide supported on — 13
- K₂O-doped — 360
- KF — 264, 266, 372
- Na⁺ — 310
- OH group on — 25
- sol-gel preparation of — 120
- transition — 119
- γ- — 37, 326, 399
- Li₂O 157, 329

B

- BaO 45, 63, 69, 263, 265, 304, 320
 - ZnO 14
- Ba(OH)₂ 233, 369
- Ba(OH)₂·8H₂O 246, 263
- BeO 31
- ^tBuO⁻, hydrocalcite with 167, 239, 250, 263, 324, 334, 337, 339, 372

C

- CaF₂ 382
- CaO 14, 18, 28, 37, 63, 69, 85, 219, 222, 233, 261, 263, 266, 292, 304, 320, 326, 326, 348, 382
 - /C 348
 - SiO₂ 51
 - ZrO₂ 348
- K on — 279
- Na on — 279
- Ca(OH)₂ 14
- Ca₃(PO₄)₂ 188, 269
- CaSiO₃ 382
- CaX 312
- Cd₃(PO₄)₂ 51
- CeO₂ 23, 30, 46, 50, 91, 318, 328, 349
 - MgO 273
 - ZrO₂ 131
- CeOH/Al₂O₃ 275
- C₃H₆ oxidation 399
- C₃H₈ oxidation 399
- CH₃I 37
- CO hydrogenation 108

CO₂

- heat of adsorption of — 22, 134
- IR of — 20, 85, 93, 103, 113, 115, 123
- reaction of — 106, 293, 347, 349
- TPD of — 19, 85, 102, 151, 180

Cs

- loaded SiO₂ 232
- exchanged MCM-41 328
- exchanged MgO 328
- exchanged MgO-Al₂O₃ 328
- exchanged X-zeolite 236, 352
- loaded CsX 37
- loaded MCM-41 276
- loaded ZSM-5 360
- /carbon 279
- /Cs-beta 254
- /TiO₂ 140

Cs₂CO₃/Al₂O₃ 222, 297

CsF 292

- /Al₂O₃ 141, 247
- /α-Al₂O₃ 143, 249, 324
- /γ-Al₂O₃ 143

CsH-ZSM-5 285

CsL 277

Cs₂O 13, 15

- loaded Na-ZSM-5 285
- /Al₂O₃ 14
- /AMgO 14
- /CsX 320
- /SiO₂ 139, 271

CsO_x/CsX 14

Cs_xO/Al₂O₃ 221

CsOH/Al₂O₃ 59, 297, 376

CsOH/CsNaY 38, 285

CsOH/SiO₂ 40

CsO_x/NaX 14

CsX 37, 42, 62, 273, 278, 284, 312

- containing alkali hydroxide 278
- borate-promoted — 277
- Cs-loaded — 37

CsY 278

CuO-Al₂O₃ 270

CuO-MgO-Al₂O₃ 283

H

HO₂O₃ 93

H₃PO₄

- /MgO 310
- /ZrO₂ 350

H₂S

- reaction with γ-butyrolactone 365
- reaction with SO₂ 350

- reaction with tetrahydrofuran 366
- K**
- K**
- /CaO 279
 - /MgO 14, 276, 349
 - /TiO₂ 140
 - -exchanged TS-1 347
- K₂CO₃ 346, 349
- /Al₂O₃ 58, 328, 377, 384
 - /KCl 349
 - /MgO 349
 - /ZnO 349
- KF**
- /Al₂O₃ 5, 14, 131, 141, 146, 232, 233, 247, 261, 263, 266, 320, 325, 330, 332, 360, 369, 372, 376, 384
 - /hydroxyapatite 239
 - /phosphate 374
- KHCO₃/Al₂O₃ 58, 384
- KI**
- /Al₂O₃ 14
 - /ZnO 349
- KL₂O₂/MCM-41 357
- KNH₂/Al₂O₃ 5, 146, 221, 222, 266, 296, 376, 385
- KNO₃**
- /MCM-48 324
 - /Al₂O₃ 14, 58, 273, 384
- K₂O**
- /Al₂O₃ 134, 360
 - /MgO 14
 - /SiO₂ 139
- KOH**
- /Al₂O₃ 233, 249, 261, 263, 320, 352, 374
 - /KY 231
 - /NaA 294
 - /SiO₂ 40
- K₃PO₄ 14, 188, 382
- KX** 278, 324, 349
- KY** 286
- L**
- La₂O₃ 23, 28, 46, 50, 64, 91, 222, 261, 304, 305, 320, 328, 357
- Li**
- /MgO 137
 - /TiO₂ 140
 - X 283, 312
- Li₂O**
- /Al₂O₃ 157, 329
 - /MgO 14, 326
 - /SiO₂ 139, 231
- LiOH/Al₂O₃ 275
- M**
- MgO 6, 8, 11, 14, 17, 20, 22, 27, 29, 31, 33, 36, 51, 55, 62, 69, 78, 151, 219, 225, 226, 229, 230, 233, 237, 242, 247, 255, 258, 263, 266, 269, 282, 292, 293, 304, 308, 310, 315, 318, 320, 325, 328, 329, 346, 347, 355, 364, 369, 373, 376, 382, 392
- -Al₂O₃ 14, 17, 20, 22, 26, 51, 58, 62, 130, 164, 227, 230, 231, 242, 247, 258, 270, 288, 292, 311, 315, 322, 332, 333, 338, 346, 352, 355, 369, 380, 382, 398, 407
 - — -SnO 338
 - — -ZrO₂ 312
 - by sol-gel method 78
 - -CaO 346
 - -CeO₂ 131, 348
 - -Cr₂O₃ 270
 - -Fe₂O₃ 270
 - -Ga₂O₃ 37
 - -La₂O₃ 130, 229, 250, 325, 373
 - loaded Al-MCM-41 357
 - — by aerosol method 390
 - — by sol gel method 78
 - -SiO₂ 130, 231
 - -smoke 78
 - -TiO₂ 14, 130
 - with metal ion 279
 - -ZrO₂ 130
- alkali ion-loaded — 17, 230, 255, 281
- alkaline earth ion-loaded — 230, 255
- Cs — 328
- K⁺ — 276
- mesoporous — 75
- Mg(OH)₂ 14, 338
- Mg(OH)_{2-x}F_x 247
- N**
- Na**
- /K₂CO₃ 279
 - /MgO 14, 151
 - /NaOH/Al₂O₃ 14, 150, 154, 221, 279, 352
 - /NaX 254
- Na⁺**
- /Al₂O₃ 310
 - doped MgO 353
 - exchanged zeolite 35
 - /TiO₂ 140
- Na₂CaP₂O₇ 189, 239, 243
- NaN₃/zeolite 279
- Na₂O**
- /MgO 14
 - /SiO₂ 139, 231
- NaOH**
- /MgO 151
 - /SiO₂ 40
- Na₃PO₄ 188
- NaX 14, 37, 312, 320, 324, 349, 350

NaY 284, 286, 289, 291, 324

Nb₂O₅ 65

Nd₂O₃ 94

Ni/MgO 400

NiO-Fe₂O₃ 269

NO 83, 85

O

OH

— on Al₂O₃ 25

bridged — 103

IR of — 80, 93, 103, 121

MAS NMR of — 86,

terminal — 103

tribridged — 103

P

Pd

—-hydrotalcite 284, 399, 403

—-KF/Al₂O₃ 146

—-MgO 405

—/Na/MgO 400

—/NaX 401

—/zeolite 399

Pr₆O₁₁ 91

Pt

—/Al₂O₃ 399

—/Cs-ETS-10 398

—/K-L 398

—/L zeolite 398

—/MgO-Al₂O₃ 398, 400

—/zeolite 399

—/ZrO₂ 399

R

Rb⁺

—/LiX 283

—/TiO₂ 140

Rb₂O 15

RbOH

—/Al₂O₃ 59

—/SiO₂ 40

RbX 42

Ru

— catalyst 396

— hydrotalcite 284, 401

S

SiO₂ 206, 239, 300, 302

— Al₂O₃ 236, 302

— MgO 8

alkali ion-doped — 231

alkali metal oxide-loaded — 138

alkali oxide-loaded — 271

amine-functionalized — 206, 210, 227, 233,
240, 242, 250, 252, 292, 294, 302, 320,
355, 395

ammonium ion functionalized — 205, 240,
242

Cs- — 232

Sm₂O₃ 94

SO₂ 18, 135, 350

adsorption of — 18, 135, 350

reaction of — with H₂S 18, 350

SrO 63, 69, 222, 261, 263, 266, 303, 304, 320

Sr(OH)₂·8H₂O 263

T

Tb₄O₇ 91

TiO₂ 27, 46, 53, 111, 113, 140, 258, 269, 292

— Al₂O₃ 132

— SiO₂ 324

— ZrO₂ 52

alkali metal compound/ — 140

mesoporous — 112

Y

Y₂O₃ 46

Z

ZnO/SiO₂ 45

ZnO 35, 46, 56, 115, 219, 306, 307, 322, 328,
357, 362, 369

— Al₂O₃ 360

— Fe₂O₃ 269

— SiO₂ 231

Zr(KPO₄)₂ 189, 239, 243, 253

ZrO₂ 17, 23, 26, 46, 50, 54, 55, 96, 304, 305,
306, 309, 310, 318, 349

— Al₂O₃ 132

— CeO₂ 349

alkali metal-loaded — 140

monoclinic — 104

tetragonal — 104

ZrPON 196, 199, 354